

LIBO P-111021

DYNAMIC ANALYSIS TO ESTABLISH NORMAL SHOCK AND VIBRATION OF RADIOACTIVE MATERIAL SHIPPING PACKAGES

FINAL SUMMARY REPORT

Hanford Engineering Development Laboratory

S.R. Fields

NOTICE

This report was prepared as an account of work sponsored by an agency of the United States Government. Neither the United States Government nor any agency thereof, or any of their employees, makes any warranty, expressed or implied, or assumes any legal liability of responsibility for any third party's use, or the results of such use, of any information, apparatus, product or process disclosed in this report, or represents that its use by such third party would not infringe privately owned rights.

Availability of Reference Materials Cited in NRC Publications

Most documents cited in NRC publications will be available from one of the following sources:

1. The NRC Public Document Room, 1717 H Street, N.W.
Washington, DC 20555
2. The NRC/GPO Sales Program, U.S. Nuclear Regulatory Commission,
Washington, DC 20555
3. The National Technical Information Service, Springfield, VA 22161

Although the listing that follows represents the majority of documents cited in NRC publications, it is not intended to be exhaustive.

Referenced documents available for inspection and copying for a fee from the NRC Public Document Room include NRC correspondence and internal NRC memoranda; NRC Office of Inspection and Enforcement bulletins, circulars, information notices, inspection and investigation notices; Licensee Event Reports; vendor reports and correspondence; Commission papers; and applicant and licensee documents and correspondence.

The following documents in the NUREG series are available for purchase from the NRC/GPO Sales Program: formal NRC staff and contractor reports, NRC-sponsored conference proceedings, and NRC booklets and brochures. Also available are Regulatory Guides, NRC regulations in the *Code of Federal Regulations*, and *Nuclear Regulatory Commission Issuances*.

Documents available from the National Technical Information Service include NUREG series reports and technical reports prepared by other federal agencies and reports prepared by the Atomic Energy Commission, forerunner agency to the Nuclear Regulatory Commission.

Documents available from public and special technical libraries include all open literature items, such as books, journal and periodical articles, and transactions. *Federal Register* notices, federal and state legislation, and congressional reports can usually be obtained from these libraries.

Documents such as theses, dissertations, foreign reports and translations, and non-NRC conference proceedings are available for purchase from the organization sponsoring the publication cited.

Single copies of NRC draft reports are available free upon written request to the Division of Technical Information and Document Control, U.S. Nuclear Regulatory Commission, Washington, DC 20555.

Copies of industry codes and standards used in a substantive manner in the NRC regulatory process are maintained at the NRC Library, 7920 Norfolk Avenue, Bethesda, Maryland, and are available there for reference use by the public. Codes and standards are usually copyrighted and may be purchased from the originating organization or, if they are American National Standards, from the American National Standards Institute, 1430 Broadway, New York, NY 10018.

**NUREG/CR-2146, Vol. 3
HEDL-TME 83-18
RT**

**DYNAMIC ANALYSIS TO ESTABLISH NORMAL
SHOCK AND VIBRATION OF RADIOACTIVE
MATERIAL SHIPPING PACKAGES**

FINAL SUMMARY REPORT

Hanford Engineering Development Laboratory

**Operated by Westinghouse Hanford Company
P.O. Box 1970 Richland, WA 99352
A Subsidiary of Westinghouse Electric Corporation**

S. R. Fields

Manuscript completed: June 1983
Date published: October 1983

**Prepared for Division of Engineering Technology
Office of Nuclear Regulatory Research
U.S. Nuclear Regulatory Commission
Washington, D.C. 20555
NRC Fin No. B2263**

DYNAMIC ANALYSIS TO ESTABLISH
NORMAL SHOCK AND VIBRATION
OF RADIOACTIVE
MATERIAL SHIPPING PACKAGES
FINAL SUMMARY REPORT

S. R. Fields

ABSTRACT

A model to simulate the dynamic behavior of shipping packages (casks) and their rail car transporters during normal transport conditions was developed. This model, CARDS (Cask-Rail Car Dynamic Simulator), was used to simulate the cask-rail car systems used in Tests 3, 10, 11, 13, 16 and 18 of the series of rail car coupling tests conducted at the Savannah River Laboratories in 1978. On the basis of good agreement between calculated and measured results for these tests, it was concluded that the model has been validated as an acceptable tool for the simulation of similar systems.

A companion model, CARRS (Cask-Rail Car Response Spectrum Generator), consisting of single-degree-of-freedom representations of the equations of motion in CARDS, was developed to generate frequency response spectra.

A parametric and sensitivity analysis was conducted that identified the most influential of a selected set of parameters and the response variables that are the most sensitive to changes in the parameters.

ACKNOWLEDGMENTS

I would like to acknowledge the specialized technical support provided by S. J. Mech prior to, during, and after the coupling tests conducted at the Savannah River Laboratory in July and August of 1978. His leadership and hard work in the data acquisition and reduction task were instrumental in the successful completion of this study. He wrote the section on TEST DATA COLLECTION AND REDUCTION in eight of the fifteen quarterly progress reports published during the course of the study. Section 2.0, TEST DATA COLLECTION AND REDUCTION, of this report is an edited version of his contributions. His work was supplemented by excellent contributions from M. S. Nutter and C. Bromley (Boeing Computer Services Richland, Inc.), and H. A. Carlson (Hanford Engineering Development Laboratory). The FFT (Fast Fourier Transform) program algorithm was written by G. Ray under his direction.

I would also like to thank H. A. Carlson and P. D. Charles (Hanford Engineering Development Laboratory), who were responsible for most of the computer-generated plots presented in this report.

CONTENTS

	<u>Page</u>
Abstract	iii
Acknowledgments	iv
Figures	vii
Tables	xix
SUMMARY	1
INTRODUCTION	3
TECHNICAL APPROACH AND RESULTS	7
1.0 MODEL DEVELOPMENT	7
1.1 CASK-RAIL CAR DYNAMIC SIMULATOR (CARDS)	7
1.1.1 Rail Car Coupler and Draft Gear Subsystem Submodel	16
1.1.2 Suspension Subsystem Submodel	37
1.1.3 Pitching Moment Caused by the Offset of the Coupler and the Center of Gravity of the Rail Car	39
1.1.4 Cask-Rail Car Bending Submodel	40
1.1.5 Modeling the Anvil Train	42
1.2 CASK-RAIL CAR RESPONSE SPECTRUM GENERATOR (CARRS)	44
2.0 TEST DATA COLLECTION AND REDUCTION	67
3.0 COLLECT PARAMETER DATA	77
4.0 MODEL VALIDATION	79
4.1 THEIL'S INEQUALITY COEFFICIENTS	79
4.2 FAST FOURIER TRANSFORMS	83
4.3 VISUAL COMPARISON OF RESPONSE VARIABLES	83
4.4 FREQUENCY RESPONSE SPECTRA	83
4.5 MODEL VALIDATION AND RESULTS	84

CONTENTS (Cont'd)

	<u>Page</u>
4.5.1 Comparison of Measured and Calculated Results for Test 3	85
4.5.2 Comparison of Measured and Calculated Results for Tests 10 and 11	87
4.5.3 Comparison of Measured and Calculated Results for Tests 13, 16 and 18	89
5.0 PARAMETRIC AND SENSITIVITY ANALYSIS	97
CONCLUSIONS AND RECOMMENDATIONS	111
REFERENCES	113
APPENDIX I NOMENCLATURE OF TERMS	I-1
APPENDIX II FIGURES	II-1
APPENDIX III TABLES	III-1
APPENDIX IV LISTING OF CARDS MODEL	IV-1
APPENDIX V LISTING OF CARRS MODEL	V-1
APPENDIX VI LISTING OF FFT PROGRAM	VI-1

FIGURES

<u>Figure</u>		<u>Page</u>
1	Spent Fuel Shipping Cask-Rail Car System Modeled	II-3
2	Spring-Mass Model of Cask-Rail Car System	II-3
3	One Possible Orientation of Cask-Rail Car System After Impact	II-4
4	Comparison of Orientation of Cask-Rail Car System After Impact with Initial State	II-4
5	Rail Car-Coupler Subsystem Model	II-5
6	Coupler Force vs Time During Impact of Two Hopper Cars Loaded with Gravel (Spring Constant of "Solid" Draft Gears = 5×10^5 lbs(force)/inch)	II-5
7	Coupler Force vs Time During Impact of Two Hopper Cars Loaded with Gravel (Spring Constant of "Solid" Draft Gears = 1×10^6 lbs(force)/inch)	II-6
8	Coupler Force vs Time During Impact of Two Hopper Cars Loaded with Gravel ("Solid" Draft Gear Spring Constant a Function of Draft Gear Travel, X_T)	II-6
9	Ratio of "Solid" Draft Gear Spring Constant to a Base Value	II-7
10	Coupler Force vs Time During Impact of Two Hopper Cars Loaded with Gravel	II-7
11	Relative Displacement of Two Gravel-Filled Hopper Cars vs Time During Impact	II-8
12	Relative Velocity of Two Gravel-Filled Hopper Cars vs Time During Impact	II-8
13	Relative Acceleration of Two Gravel-Filled Hopper Cars vs Time During Impact	II-9
14	Calculated Coupler Force vs Calculated Relative Displacement of Two Gravel-Filled Hopper Cars During Impact	II-9
15	Relative Velocity of Two Gravel-Filled Hopper Cars vs Time During Impact	II-10

FIGURES (Cont'd)

<u>Figure</u>		<u>Page</u>
16	Coupler Force vs Time During Impact of Two Gravel-Filled Hopper Cars	II-10
17	Relative Displacement of Two Gravel-Filled Hopper Cars vs Time During Impact	II-11
18	Relative Velocity of Two Gravel-Filled Hopper Cars vs Time During Impact	II-11
19	Relative Acceleration of Two Gravel-Filled Hopper Cars vs Time During Impact	II-12
20	Calculated Coupler Force vs Calculated Relative Displacement of Two Gravel-Filled Hopper Cars During Impact	II-12
21	Measured Coupler Force vs Measured Relative Displacement of Two Gravel-Filled Hopper Cars During Impact	II-13
22	Arrangement of Springs and Dampers Simulating Rail Car Coupler and Suspension Subsystems	II-13
23	Effect of Coupler Offset on Rail Car Rotation	II-14
24	Deflection Diagrams for Rail Car Beam with Restraints to Define Force-Reaction System	II-14
25	Spring-Mass Submodel Representing Bending of Rail Car	II-15
26	Deflection Diagrams for Rail Car Beam to Determine Deflections and Influence Coefficients	II-15
27	Dynamic Model of Cask-Rail Car System with Bending Submodel	II-16
28	Cask-Rail Car and Anvil Train	II-16
29	Cask-Rail Car and Anvil Train	II-17
30	Coupler Force Between Cars in the Cask-Rail Car and Anvil Train System	II-17
31	Horizontal Displacement of Centers of Gravity of Cars in the Cask-Rail Car and Anvil Train System	II-18

FIGURES (Cont'd)

<u>Figure</u>		<u>Page</u>
32	Morphological Space Representation of Cask-Rail Car Coupling Tests	II-18
33	Horizontal Acceleration of the Cask-Rail Car During Impact with Four Hopper Cars Loaded with Ballast. (Test 3 - Instrument 12: Filtered at 100 Hz) (Case 1: Measured Coupler Force)	II-19
34	Shock/Vibration Data Flow for Data Reduction Model Verification	II-19
35a	Acceleration Wave Shape and Corresponding Frequency Spectrum Obtained by Fast Fourier Transform (Horizontal Center Acceleration)	II-20
35b	Acceleration Wave Shape and Corresponding Frequency Spectrum Obtained by Fast Fourier Transform (Vertical, Struck End Acceleration)	II-20
35c	Acceleration Wave Shape and Corresponding Frequency Spectrum Obtained by Fast Fourier Transform (Vertical, Far End Acceleration)	II-21
36a	Filtering of Acceleration Data Employing Inverse FFT (Power Spectra and Time Domain Image)	II-21
36b	Filtering of Acceleration Data Employing Inverse FFT (Time Domain Images)	II-22
37a	Hanning Window Effect on Power Spectra When Applied to Time Domain Data (Horizontal, Center Acceleration with Hanning Window)	II-22
37b	Hanning Window Effect on Power Spectra When Applied to Time Domain Data (Vertical, Struck End Acceleration with Hanning Window)	II-23
38	Tiedown Configuration and Instrument Location for Cask-Rail Car-Tiedown Tests (Tiedown Configuration "A")	II-23
39	Tiedown Configuration and Instrument Location for Cask-Rail Car-Tiedown Tests (Tiedown Configuration "B")	II-24

FIGURES (Cont'd)

<u>Figure</u>		<u>Page</u>
40	Tiedown Configuration and Instrument Location for Cask-Rail Car-Tiedown Tests (Tiedown Configuration "C")	II-24
41	Tiedown Configuration and Instrument Location for Cask-Rail Car-Tiedown Tests (Tiedown Configuration "D")	II-25
42	Horizontal or Longitudinal Acceleration of Car at Car/Cask Interface vs Time (Instrument No. 12 - Unfiltered)	II-25
43	Horizontal Displacement of the Car at the Struck End vs Time (Instrument No. 4 - Unfiltered)	II-26
44	Horizontal Acceleration Response of Cask/Car Interface vs Frequency (Instrument No. 12 - Unfiltered)	II-26
45	Transfer Function Magnitude vs Frequency (Vertical Energy Transfer from Instrument No. 22 to Instrument No. 11)	II-27
46	Transfer Function Magnitude vs Frequency (Vertical Energy Transfer from Instrument No. 11 to Instrument No. 9)	II-27
47	Transfer Function Magnitude vs Frequency (Horizontal Energy Transfer from Instrument No. 12 to Instrument No. 10)	II-28
48	Transfer Function Magnitude vs Frequency (Horizontal Energy Transfer from Instrument No. 10 to Instrument No. 8)	II-28
49	Comparison of Calculated and Measured Coupler Forces Using Theil's Inequality Coefficient as a Figure of Merit	II-29
50	Comparison of Calculated and Measured Relative Displacements of Rail Car Centers of Gravity in the Time Domain Using Theil's Inequality Coefficient as a Figure of Merit	II-29
51	Comparison of Calculated and Measured Relative Velocities in the Time Domain Using Theil's Inequality Coefficient as a Figure of Merit	II-30

FIGURES (Cont'd)

<u>Figure</u>		<u>Page</u>
52	Comparison of Calculated and Measured Relative Accelerations in the Time Domain using Theil's Inequality Coefficient as a Figure of Merit	II-30
53	Simultaneous Comparison of Calculated and Measured Response Variables in the Time Domain Using Theil's <u>Multiple</u> Inequality Coefficient as an Overall Figure of Merit	II-31
54	Coupler Force vs Time During Impact of Cask-Rail Car with Four Hopper Cars Loaded with Ballast (Test 3 - Instrument 3) (Case 1: Measured Coupler Force)	II-31
55	Horizontal Force of Interaction Between Cask and Rail Car vs Time During Impact with Four Hopper Cars Loaded with Ballast (Test 3 - Instrument 27) (Case 1: Measured Coupler Force)	II-32
56	Horizontal Acceleration of the Cask-Rail Car During Impact with Four Hopper Cars Loaded with Ballast (Test 3 - Instrument 12: Filtered at 100 Hz) (Case 1: Measured Coupler Force)	II-32
57	Horizontal Acceleration of the Cask During Impact with Four Hopper Cars Loaded with Ballast (Test 3 - Instrument 8: Filtered at 100 Hz) (Case 1: Measured Coupler Force)	II-33
58	Vertical Acceleration of the Cask at the Far End During Impact with Four Hopper Cars Loaded with Ballast (Test 3 - Instrument 11: Filtered at 50 Hz) (Case 1: Measured Coupler Force)	II-33
59	Vertical Acceleration of the Cask at the Struck End During Impact with Four Hopper Cars Loaded with Ballast (Test 3 - Instrument 9: Filtered at 50 Hz) (Case 1: Measured Coupler Force)	II-34
60	Vertical Displacements of the Cask During Impact with Four Hopper Cars Loaded with Ballast (Test 3) (Case 1: Measured Coupler Force)	II-34
61	Vertical Tiedown Forces During Impact with Four Hopper Cars Loaded with Ballast (Test 3) (Case 1: Measured Coupler Force)	II-35

FIGURES (Cont'd)

<u>Figure</u>		<u>Page</u>
62	Coupler Force vs Time During Impact of Cask-Rail Car with Four Hopper Cars Loaded with Ballast (Test 3 - Instrument 3) (Case 2: Calculated Coupler Force)	II-35
63	Horizontal Force of Interaction Between Cask and Rail Car vs Time During Impact with Four Hopper Cars Loaded with Ballast (Test 3 - Instrument 27) (Case 2: Calculated Coupler Force)	II-36
64	Horizontal Acceleration of the Cask-Rail Car During Impact with Four Hopper Cars Loaded with Ballast (Test 3 - Instrument 12: Filtered at 100 Hz) (Case 2: Calculated Coupler Force)	II-36
65	Horizontal Acceleration of the Cask During Impact with Four Hopper Cars Loaded with Ballast (Test 3 - Instrument 8: Filtered at 100 Hz) (Case 2: Calculated Coupler Force)	II-37
66	Vertical Acceleration of the Cask at the Far End During Impact with Four Hopper Cars Loaded with Ballast (Test 3 - Instrument 11: Filtered at 50 Hz) (Case 2: Calculated Coupler Force)	II-37
67	Vertical Acceleration of the Cask at the Struck End During Impact with Four Hopper Cars Loaded with Ballast (Test 3 - Instrument 9: Filtered at 50 Hz) (Case 2: Calculated Coupler Force)	II-38
68	Vertical Displacements of the Cask During Impact with Four Hopper Cars Loaded with Ballast (Test 3) (Case 2: Calculated Coupler Force)	II-38
69	Vertical Tiedown Forces During Impact with Four Hopper Cars Loaded with Ballast (Test 3) (Case 2: Calculated Coupler Force)	II-39
70	Coupler Force vs Time During Impact of Cask-Rail Car with Four Hopper Cars Loaded with Ballast (Test 10 - Instrument 3)	II-39
71	Horizontal Force of Interaction Between Cask and Rail Car vs Time During Impact with Four Hopper Cars Loaded with Ballast (Test 10 - Instruments 27 and 28)	II-40

FIGURES (Cont'd)

<u>Figure</u>		<u>Page</u>
72	Horizontal Acceleration of the Cask-Rail Car During Impact with Four Hopper Cars Loaded with Ballast (Test 10 - Instrument 12: Filtered at 100 Hz)	II-40
73	Horizontal Acceleration of the Cask During Impact with Four Hopper Cars Loaded with Ballast (Test 10 - Instrument 8: Filtered at 100 Hz)	II-41
74	Vertical Acceleration of the Cask at the Far End During Impact with Four Hopper Cars Loaded with Ballast (Test 10 - Instrument 11: Filtered at 50 Hz)	II-41
75	Stiffness Coefficient of Horizontal Component of Tiedowns vs Relative Displacement Between Cask and Rail Car (Tests 10 and 11)	II-42
76	Coupler Force vs Time During Impact of Cask-Rail Car with Four Hopper Cars Loaded with Ballast (Test 11 - Instrument 3)	II-42
77	Horizontal Force of Interaction Between Cask and Rail Car vs Time During Impact with Four Hopper Cars Loaded with Ballast (Test 11 - Instruments 27 and 28)	II-43
78	Horizontal Acceleration of the Cask-Rail Car During Impact with Four Hopper Cars Loaded with Ballast (Test 11 - Instrument 12: Filtered at 100 Hz)	II-43
79	Horizontal Acceleration of the Cask During Impact with Four Hopper Cars Loaded with Ballast (Test 11 - Instrument 8: Filtered at 100 Hz)	II-44
80	Vertical Acceleration of the Cask at the Far End During Impact with Four Hopper Cars Loaded with Ballast (Test 11 - Instrument 11: Filtered at 50 Hz)	II-44
81	Cask-Rail Car Configuration Used in Tests 3 and 18	II-45
82	Cask-Rail Car Configuration Used in Tests 10 and 11	II-45
83	Cask-Rail Car Configuration Used in Test 13	II-46
84	Cask-Rail Car Configuration Used in Test 16	II-46

FIGURES (Cont'd)

<u>Figure</u>		<u>Page</u>
85	Coupler Force vs Time During Impact of Cask-Rail Car with Four Hopper Cars Loaded with Ballast (Test 16 - Instrument 3)	II-47
86	Horizontal Force of Interaction Between Cask and Rail Car vs Time During Impact with Four Hopper Cars Loaded with Ballast (Test 16 - Instruments 27 and 28)	II-47
87	Horizontal Acceleration of the Cask-Rail Car During Impact with Four Hopper Cars Loaded with Ballast (Test 16 - Instrument 7: Filtered at 100 Hz)	II-48
88	Horizontal Acceleration of the Cask During Impact with Four Hopper Cars Loaded with Ballast (Test 16 - Instrument 8: Filtered at 100 Hz)	II-48
89	Vertical Acceleration of the Cask at the Far End During Impact with Four Hopper Cars Loaded with Ballast (Test 16 - Instrument 11: Filtered at 50 Hz)	II-49
90	Vertical Acceleration of the Cask at the Struck End During Impact with Four Hopper Cars Loaded with Ballast (Test 16 - Instrument 9: Filtered at 50 Hz)	II-49
91	Horizontal Tiedown Force vs Relative Displacement Between Cask and Rail Car (Test 16)	II-50
92	Stiffness Coefficient of Horizontal Component of Tiedowns vs Relative Displacement Between Cask and Rail Car (Test 16)	II-50
93	Coupler Force vs Time During Impact of Cask-Rail Car with Four Hopper Cars Loaded with Ballast (Test 13 - Instrument 3)	II-51
94	Horizontal Force of Interaction Between Cask and Rail Car vs Time During Impact with Four Hopper Cars Loaded with Ballast (Test 13 - Instruments 27 and 28)	II-51
95	Horizontal Acceleration of the Cask-Rail Car During Impact with Four Hopper Cars Loaded with Ballast (Test 13 - Instrument 7: Filtered at 50 Hz)	II-52

FIGURES (Cont'd)

<u>Figure</u>		<u>Page</u>
96	Horizontal Acceleration of the Cask During Impact with Four Hopper Cars Loaded with Ballast (Test 13 - Instrument 8: Filtered at 100 Hz)	II-52
97	Vertical Acceleration of the Cask at the Far End During Impact with Four Hopper Cars Loaded with Ballast (Test 13 - Instrument 11: Filtered at 50 Hz)	II-53
98	Vertical Acceleration of the Cask at the Struck End During Impact with Four Hopper Cars Loaded with Ballast (Test 13 - Instrument 9: Filtered at 50 Hz)	II-53
99	Coupler Force vs Time During Impact of Cask-Rail Car with Four Hopper Cars Loaded with Ballast (Test 18 - Instrument 3)	II-54
100	Horizontal Force of Interaction Between Cask and Rail Car vs Time During Impact with Four Hopper Cars Loaded with Ballast (Test 18 - Instruments 27 and 28)	II-54
101	Horizontal Acceleration of the Cask-Rail Car During Impact with Four Hopper Cars Loaded with Ballast (Test 18 - Instrument 12: Filtered at 50 Hz)	II-55
102	Horizontal Acceleration of the Cask During Impact with Four Hopper Cars Loaded with Ballast (Test 18 - Instrument 8: Filtered at 100 Hz)	II-55
103	Vertical Acceleration of the Cask at the Far End During Impact with Four Hopper Cars Loaded with Ballast (Test 18 - Instrument 11: Filtered at 50 Hz)	II-56
104	Vertical Acceleration of the Cask at the Struck End During Impact with Four Hopper Cars Loaded with Ballast (Test 18 - Instrument 9: Filtered at 50 Hz)	II-56
105	Horizontal Acceleration of the Support for an Equivalent Single-Degree-of-Freedom System (Preliminary Cases 2, 3 and 4)	II-57
106	Vertical Acceleration of the Support for an Equivalent Single-Degree-of-Freedom System (Preliminary Cases 2, 3 and 4)	II-57

FIGURES (Cont'd)

<u>Figure</u>		<u>Page</u>
107	Rotational Acceleration of the Support for an Equivalent Single-Degree-of-Freedom System (Preliminary Cases 2, 3 and 4)	II-58
108	Response Spectrum: Maximum Absolute Relative Horizontal Acceleration vs Frequency (Preliminary Cases 1 through 5)	II-58
109	Response Spectrum: Maximum Absolute Relative Vertical Acceleration vs Frequency (Preliminary Cases 1 through 5)	II-59
110	Response Spectrum: Maximum Absolute Relative Rotational Acceleration vs Frequency (Preliminary Cases 1 through 5)	II-59
111	Horizontal Acceleration of the Support for an Equivalent Single-Degree-of-Freedom System (Requested Base Case and Cases 7 and 8)	II-60
112	Vertical Acceleration of the Support for an Equivalent Single-Degree-of-Freedom System (Requested Base Case and Cases 7 and 8)	II-60
113	Rotational Acceleration of the Support for an Equivalent Single-Degree-of-Freedom System (Requested Base Case and Cases 7 and 8)	II-61
114	Force on the Horizontal Component of the Tiedown at the Struck End (Requested Base Case and Cases 7 and 8)	II-61
115	Force on the Horizontal Component of the Tiedown at the Far End (Requested Base Case and Cases 7 and 8)	II-62
116	Force on the Vertical Component of the Tiedown at the Struck End (Requested Base Case and Cases 7 and 8)	II-62
117	Force on the Vertical Component of the Tiedown at the Far End (Requested Base Case and Cases 7 and 8)	II-63
118	Response Spectrum: Maximum Absolute Relative Horizontal Acceleration vs Frequency (Requested Base Case and Cases 7 and 8)	II-63

FIGURES (Cont'd)

<u>Figure</u>		<u>Page</u>
119	Response Spectrum: Maximum Absolute Relative Vertical Acceleration vs Frequency (Requested Base Case and Cases 7 and 8)	II-64
120	Response Spectrum: Maximum Absolute Relative Rotational Acceleration vs Frequency (Requested Base Case and Cases 7 and 8)	II-64
121	Response Spectrum: Maximum Absolute Relative Horizontal Accelerations vs Frequency (Base Case, + 50% Base Case, and Cases 1, 2, C, D, and 3 through 21)	II-65
122	Response Spectrum: Maximum Absolute Relative Vertical Accelerations vs Frequency (Base Case, + 50% Base Case, and Cases 1, 2, C, D, and 3 through 21)	II-65
123	Response Spectrum: Maximum Absolute Relative Rotational Accelerations vs Frequency (Base Case, + 50% Base Case, and Cases 1, 2, C, D, and 3 Through 21)	II-66
124	Ranking of Parameters by Absolute Percent Difference of Absolute Peak Horizontal Support Acceleration from Base Case Value	II-66
125	Ranking of Parameters by Absolute Percent Difference of Absolute Peak Vertical Support Acceleration from Base Case Value	II-67
126	Ranking of Parameters by Absolute Percent Difference of Absolute Peak Rotational Support Acceleration from Base Case Value	II-67
127	Ranking of Parameters by Absolute Percent Difference of Maximum Absolute Relative Horizontal Acceleration from Base Case Value	II-68
128	Ranking of Parameters by Absolute Percent Difference of Maximum Absolute Relative Vertical Acceleration from Base Case Value	II-68
129	Ranking of Parameters by Absolute Percent Difference of Maximum Absolute Relative Rotational Acceleration from Base Case Value	II-69

FIGURES (Cont'd)

<u>Figure</u>		<u>Page</u>
130	Ranking of Parameters by Absolute Percent Difference of Maximum Absolute Horizontal Tiedown Force (Struck End) from Base Case Value	II-69
131	Ranking of Parameters by Absolute Percent Difference of Maximum Absolute Horizontal Tiedown Force (Far End) from Base Case Value	II-70
132	Ranking of Parameters by Absolute Percent Difference of Maximum Absolute Vertical Tiedown Force (Struck End) from Base Case Value	II-70
133	Ranking of Parameters by Absolute Percent Difference of Maximum Absolute Vertical Tiedown Force (Far End) from Base Case Value	II-71
134	Sensitivity of Absolute Peak Support Accelerations to Changes in the Stiffness Coefficients of the Vertical Components of the Tiedowns (Requested Base Case and Cases 7 and 8)	II-71
135	Sensitivity of Maximax Absolute Relative Accelerations to Changes in the Stiffness Coefficients of the Vertical Components of the Tiedowns (Base Case and Cases 7 and 8)	II-72
136	Sensitivity of Absolute Tiedown Forces to Changes in the Stiffness Coefficients of the Vertical Components of the Tiedowns (Requested Base Case and Cases 7 and 8)	II-72

TABLES

<u>Table</u>		<u>Page</u>
1	Parameters Used in the CARDT Model for Simulation of Impact Between Two Hopper Cars Loaded with Gravel	III-3
2	Summary of Configurations and Conditions of Completed Cask-Rail Car-Tiedown Tests	III-3
3	Force Terms from the CARDS Test 3 Simulation Run Measured at the Time (0.116 second) When the Vertical Acceleration of the Rail Car (Support) Is a Maximum	III-4
4	Force Terms from the CARDS Test 3 Simulation Run Measured at the Time (0.057 second) When the Horizontal Acceleration of the Rail Car (Support) Is a Maximum	III-4
5	Input Data and Results from the CARDS Test 3 Simulation Run. Results Measured at the Time (0.116 second) When the Vertical Acceleration of the Rail Car (Support) Is a Maximum	III-5
6	Input Data and Results from the CARDS Test 3 Simulation Run. Results Measured at the Time (0.057 second) When the Horizontal Acceleration of the Rail Car (Support) Is a Maximum	III-5
7	Instrument Configuration for Cask-Rail Car-Tiedown Tests	III-6
8	Measured and Reduced Parameter Values from Rail Car Humping Tests (Test No. 1: 40-Ton Cask, 70-Ton Seaboard Coastline Rail Car, Impact Velocity 8.3 mph)	III-7
9	Theil's Inequality Coefficients for Response Variables Determined Using Calculated and Measured Coupler Force	III-8
10	Definitions of Cases Used for Generation of Preliminary Response Spectra	III-8
11	Conditions Imposed on Cases Requested for Parametric and Sensitivity Analysis and Generation of Response Spectra	III-9

TABLES

<u>Table</u>		<u>Page</u>
12	Definitions of "Pure" Parameters and Their Cases	III-10
13	Definitions of "Composite" Parameters and Their Cases	III-10
14	Parameter Values Used in Cases Requested for Parametric/Sensitivity Analysis	III-11
15	Parametric and Sensitivity Analysis - Sensitivity of Response Variables to Parameter Changes	III-13
16	Parametric and Sensitivity Analysis - Ranking of Parameters by Absolute Percent Difference of Response Variables from Base Case Values	III-18
17	Parametric and Sensitivity Analysis - Sensitivity of Response Variables in Terms of Percent Difference from Base Case Values	III-23
18	Parametric and Sensitivity Analysis - Ranking of "Pure" Parameters by Influence Coefficient and Sensitivity	III-25
19	Parametric and Sensitivity Analysis - Ranking of Parameters by Parameter Ratio-Based Influence Coefficient and Sensitivity	III-27

DYNAMIC ANALYSIS TO ESTABLISH NORMAL SHOCK AND VIBRATION

OF RADIOACTIVE MATERIAL SHIPPING PACKAGES

FINAL SUMMARY REPORT

SUMMARY

A computer model CARDS (Cask-Rail Car Dynamic Simulator) was developed for the U.S. Nuclear Regulatory Commission to provide input data for a broad range of radioactive material package-tiedown structural assessments.

CARDS simulates the dynamic behavior of shipping packages and their rail car transporters during normal transport conditions. The model was used to identify parameters that significantly affect the normal shock and vibration environments that, in turn, provide the basis for determining the forces transmitted to the packages. The determination of these forces is necessary for the package-tiedown structural assessments. The objective was to determine the extent to which the shocks and vibrations experienced by the shipping packages during normal transport are influenced by, or are sensitive to, various structural parameters of the transport system (i.e., package, package supports, vehicle characteristics, etc.).

It was assumed that the greatest shock suffered by the cask-rail car in its normal (not accident) transport environment will be that experienced during coupling operations in a "humping" or classification yard. An earlier study by the Sandia Laboratories showed that 99.8% of all train coupling operations occurred at speeds of 11.05 mph or less. Eighteen tests were conducted at the Savannah River Laboratory in 1978 during which coupling velocities as high as 11.2 mph were recorded. The CARDS model was used to simulate six of these tests. On the basis of the good agreement obtained between the calculated and experimental results, it was concluded that CARDS is an acceptable tool for subsequent simulation of cask-rail car system behavior during coupling operations.

CARDS is a complex two-dimensional, multi-degree-of-freedom model that determines the horizontal, vertical, and rotational motion of both the package and its transporter following impact with an anvil train during coupling operations. It also determines the horizontal motion of each of the cars in the anvil train. For the simulation of the Savannah River tests, the current version of CARDS has an anvil train that consists of four hopper cars filled with ballast. However, the formulation of CARDS provides flexibility for the simulation of a broad range of package-car, and package-car-anvil train configurations.

The CARDS model consists of twelve equations of motion, one derived for each degree of freedom (generalized coordinate), and supplementary auxiliary equations. The equations of motion were derived from an energy balance on the system (expressed in generalized coordinates). The entire model definition was written in the Advanced Continuous Simulation Language (ACSL).

A companion model CARRS (Cask-Rail Car Response Spectrum Generator), a model to generate frequency response spectra using calculated results from CARDS, was also developed. The equations of motion of the cask-rail car system were transformed into equivalent single-degree-of-freedom (1-DOF) representation of the relative vertical, horizontal and rotational motions between the cask and its rail car platform or support. These equations of motion were then used to construct CARRS. The right-hand sides of each of these equivalent 1-DOF equations of motion represent the time-varying accelerations of a platform (rail car) supporting 1-DOF devices defined by the left-hand sides of the respective equations of motion. The definition of CARRS was also written in the ACSL language.

Frequency response spectra were generated by the spectrum generator, CARRS, using the time-varying support accelerations obtained from the simulator, CARDS. Response spectra for a base-case cask-rail car system are presented in Figures 118 through 123.

A parametric and sensitivity analysis was conducted to identify those parameters that significantly affect the normal shock and vibration environment and the response of the cask-rail car system. The response of the system was defined by the absolute values of the maximum support accelerations, the maximum relative accelerations between the cask and its support, and the vertical and horizontal tiedown forces. The sensitivities of these response variables to changes in various parameters were determined (see Table 18). For all the response variables except the vertical accelerations, the most influential parameter is the vertical distance Z_p (see Appendix I, NOMENCLATURE OF TERMS). The parameter that has the most influence on the vertical accelerations is l_{OCR} , the horizontal distance between the centers-of-gravity of the cask and rail car. The parameter that contributes most to the sensitivities (total changes) of the horizontal accelerations is W_p , the package or cask weight. The vertical accelerations are the most sensitive to l_{OCR} ; and the rotational accelerations are the most sensitive to $\{k_y\}$, the set of stiffness coefficients of the vertical components of the tiedowns. The tiedown forces $DUS1_{MAX}$, $DUS4_{MAX}$, $DUS2_{MAX}$, and $DUS3_{MAX}$ are the most sensitive to the parameters W_p , $\{k_x\}$, Z_p and Z_p , respectively. The ranges of parameters used to arrive at the sensitivities were specified at the outset in the definition of the cases requested by Nuclear Regulatory Commission personnel. More meaningful values of the sensitivities are obtained if these ranges represent the uncertainties in the parameters.

INTRODUCTION

The objective of this study was to determine the extent to which the shocks and vibrations experienced by radioactive material shipping packages during normal transport conditions are influenced by, or are sensitive to, various structural parameters of the transport system (i.e., package, package supports and vehicle). The purpose of this effort was to identify those parameters that significantly affect the normal shock and vibration environments so as to provide the basis for determining the forces transmitted to radioactive material packages. Determination of these forces will provide the input data necessary for a broad range of package-tiedown structural assessments.

A computer model CARDS (Cask-Rail Car Dynamic Simulator) was developed to provide the data for these assessments. A companion model CARRS (Cask Rail Car Response Spectrum Generator) was also developed to generate frequency response spectra using results from CARDS. These two models were used to identify parameters that significantly affect the shock and vibration environments and, in turn, the forces transmitted to the packages.

It was assumed that the greatest shock suffered by the cask-rail car in its normal (not accident) transport environment will be that experienced during coupling operations in a "humping" or classification yard. An earlier study by the Sandia Laboratories showed that 99.8% of all train coupling operations occurred at speeds of 11.05 mph or less. Eighteen tests were conducted at the Savannah River Laboratory in 1978 during which coupling velocities as high as 11.2 mph were recorded. The validity of the CARDS model as an acceptable tool for the simulation of cask-rail car systems was established by comparison of calculated results with results obtained from six of these tests.

The CARDS and CARRS models were used together to generate frequency response spectra, to determine the sensitivity of selected response variables to changes in parameters, and to rank the parameters according to their influence and their contribution to the sensitivity of the response variables.

This report interprets, supplements, consolidates, and summarizes information previously published in the following quarterly progress reports:

1. S. R. Fields, Dynamic Analysis to Establish Normal Shock and Vibration Environments Experienced by Radioactive Material Shipping Packages, NUREG/CR-0071, (HEDL-TME 78-19), Quarterly Progress Report (October 1 - December 31, 1977), Hanford Engineering Development Laboratory, May 1978.
2. S. R. Fields and S. J. Mech, Dynamic Analysis to Establish Normal Shock and Vibration of Radioactive Material Shipping Packages, NUREG/CR-0161, (HEDL-TME 78-41), Quarterly Progress Report (January 1 - March 31, 1978), Hanford Engineering Development Laboratory, July 1978.

3. S. R. Fields and S. J. Mech, Dynamic Analysis to Establish Normal Shock and Vibration of Radioactive Material Shipping Packages, NUREG/CR-0448, (HEDL-TME 78-74), Quarterly Progress Report (April 1 - June 30, 1978), Hanford Engineering Development Laboratory, December 1978.
4. S. R. Fields and S. J. Mech, Dynamic Analysis to Establish Normal Shock and Vibration of Radioactive Material Shipping Packages, NUREG/CR-0589, (HEDL-TME 78-102), Quarterly Progress Report (July 2 - September 30, 1978), Hanford Engineering Development Laboratory, March 1979.
5. S. R. Fields and S. J. Mech, Dynamic Analysis to Establish Normal Shock and Vibration of Radioactive Material Shipping Packages, NUREG/CR-0766, (HEDL-TME 79-3), Quarterly Progress Report (October 1 - December 31, 1978), Hanford Engineering Development Laboratory, June 1979.
6. S. R. Fields and S. J. Mech, Dynamic Analysis to Establish Normal Shock and Vibration of Radioactive Material Shipping Packages, NUREG/CR-0880, (HEDL-TME 79-29), Quarterly Progress Report (January 1 - March 31, 1979), Hanford Engineering Development Laboratory, July 1979.
7. S. R. Fields and S. J. Mech, Dynamic Analysis to Establish Normal Shock and Vibration and Radioactive Material Shipping Packages, NUREG/CR-1066, (HEDL-TME 79-43), Quarterly Progress Report (April 1 - June 30, 1979), Hanford Engineering Development Laboratory, October 1979.
8. S. R. Fields and S. J. Mech, Dynamic Analysis to Establish Normal Shock and Vibration of Radioactive Material Shipping Packages, NUREG/CR-1265, (HEDL-TME 79-71), Quarterly Progress Report (July 1 - September 30, 1979), Hanford Engineering Development Laboratory, March 1980.
9. S. R. Fields and S. J. Mech, Dynamic Analysis to Establish Normal Shock and Vibration of Radioactive Material Shipping Packages, NUREG/CR-1484, (HEDL-TME 80-24), Quarterly Progress Report (October 1 - December 31, 1979), Hanford Engineering Development Laboratory, August 1980.
10. S. R. Fields, Dynamic Analysis to Establish Normal Shock and Vibration of Radioactive Material Shipping Packages, NUREG/CR-1685, Volume 1, (HEDL-TME 80-51), Quarterly Progress Report (January 1 - March 31, 1980), Hanford Engineering Development Laboratory, January 1981.
11. S. R. Fields, Dynamic Analysis to Establish Normal Shock and Vibration of Radioactive Material Shipping Packages, NUREG/CR-1685, Volume 2, (HEDL-TME 80-72), Quarterly Progress Report (April 1 - June 30, 1980), Hanford Engineering Development Laboratory, April 1981.
12. S. R. Fields, Dynamic Analysis to Establish Normal Shock and Vibration of Radioactive Material Shipping Packages, NUREG/CR-1685, Volume 3, (HEDL-TME 80-91), Quarterly Progress Report (July 1 - September 30, 1980), Hanford Engineering Development Laboratory, April 1981.

13. S. R. Fields, Dynamic Analysis to Establish Normal Shock and Vibration of Radioactive Material Shipping Packages, NUREG/CR-1685, Volume 4, (HEDL-TME 80-92), Quarterly Progress Report (October 1 - December 31, 1980), Hanford Engineering Development Laboratory, July 1981.
14. S. R. Fields, Dynamic Analysis to Establish Normal Shock and Vibration of Radioactive Material Shipping Packages, NUREG/CR-2146, Volume 1, (HEDL-TME 81-15), Quarterly Progress Report (January 1 - March 31, 1981), Hanford Engineering Development Laboratory, November 1981.
15. S. R. Fields, Dynamic Analysis to Establish Normal Shock and Vibration of Radioactive Material Shipping Packages, NUREG/CR-2146, Volume 2, (HEDL-TME 83-8), Quarterly Progress Report (April 1 - June 30, 1981), Hanford Engineering Development Laboratory, July 1983.

NOTICE OF ERRORS IN PREVIOUS REPORTS

Errors were found in three of the above previously published quarterly reports. These reports are Volumes 2, 3 and 4 of NUREG/CR-1685 (HEDL-TME 80-72, HEDL-TME 80-91 and HEDL-TME 80-92, respectively). In these reports, all frequencies are angular frequencies and should be reported in units of radians/second rather than in units of Hz. This applies to all figures with frequency as the abscissa, and to all references to frequency in the texts of the reports.

1. The first part of the document is a list of names and addresses of the members of the committee. The names are listed in alphabetical order, and the addresses are given in full. The list is as follows:

2. The second part of the document is a list of the names and addresses of the members of the committee who have been elected to the office of Secretary. The names are listed in alphabetical order, and the addresses are given in full. The list is as follows:

3. The third part of the document is a list of the names and addresses of the members of the committee who have been elected to the office of Treasurer. The names are listed in alphabetical order, and the addresses are given in full. The list is as follows:

MEMBERS OF THE COMMITTEE

4. The fourth part of the document is a list of the names and addresses of the members of the committee who have been elected to the office of Chairman. The names are listed in alphabetical order, and the addresses are given in full. The list is as follows:

TECHNICAL APPROACH AND RESULTS

1.0 MODEL DEVELOPMENT

1.1 CASK-RAIL CAR DYNAMIC SIMULATOR (CARDS)

A two-dimensional, multi-degree-of-freedom model of a spent fuel shipping cask-rail car system was developed. A sketch of the idealized cask-rail car system modeled is shown in Figure 1, and the spring-mass model of this system is shown in Figure 2. This model was given the name CARDS: An acronym for Cask-Rail Car Dynamic Simulator.

Each of the masses in the cask-rail car model of Figure 1 is free to translate horizontally (front to back) and vertically, and to rotate about its axis normal to the plane of the illustration. The system is excited by impact with one or more cars (mass M_F) at the front coupler. One possible orientation of the system after impact is shown in Figure 3, and a comparison with the initial state is illustrated in Figure 4. Figure 5 is obtained by superimposing Figures 2 and 3. (See Appendix I NOMENCLATURE OF TERMS for definition of terms used in this report.)

The model consists of twelve equations of motion, one derived for each degree of freedom (generalized coordinate), and supplementary auxiliary equations. There are two general approaches that could have been used to derive the equations of motion for this dynamic system. The first is known as the force-acceleration method and the second is known as the energy method. The first method is also sometimes referred to as the method of dynamic equilibrium, while the second method may be referred to as the Lagrange-equation method. The force-acceleration method consists of analyzing the forces and the torques applied to the system and relating them to the accelerations. In the energy method one sets up the energy expressions for the system and applies Lagrange's equation to get the equations of motion. The energy or Lagrange-equation method was used for this study.

The equations of motion were derived from an energy balance (expressed in generalized coordinates) on the system. This energy balance is sometimes known as the law of virtual work, which states that the work done on the system by the external forces (virtual work) during a virtual distortion (a small change in one of the generalized coordinates) must equal the change in internal strain energy. The work done by external forces includes the work done by external loads, by inertia forces, and by damping or dissipation forces. The energy balance on the system may be written as

$$\delta W_e + \delta W_{in} + \delta W_c = \delta U \quad (1)$$

where:

δW_e = Work done by external loads

δW_{in} = Work done by inertia forces

δW_c = Work done by damping forces

δU = Change in internal strain energy (potential energy)

For a generalized coordinate q_i

$$\delta W_e = \frac{\partial W_e}{\partial q_i} \delta q_i \quad (2)$$

$$\delta W_c = \frac{\partial W_c}{\partial q_i} \delta q_i \quad (3)$$

$$\delta U = \frac{\partial U}{\partial q_i} \delta q_i \quad (4)$$

and

$$\delta W_{in} = - \frac{d}{dt} \left(\frac{\partial K}{\partial \dot{q}_i} \right) \delta q_i + \left(\frac{\partial K}{\partial q_i} \right) \delta q_i \quad (5)$$

where:

$$K = \sum_{r=1}^j \frac{1}{2} M_r \dot{\chi}_r^2 \quad (6)$$

$$\frac{\partial K}{\partial \dot{q}_i} = \sum_{r=1}^j M_r \dot{\chi}_r \frac{\partial \dot{\chi}_r}{\partial \dot{q}_i} \quad (7)$$

$$\frac{\partial K}{\partial q_i} = \sum_{r=1}^j M_r \dot{x}_r \frac{\partial \dot{x}_r}{\partial q_i} \quad (8)$$

Substituting (2), (3), (4) and (5) into (1) gives

$$\frac{\partial W_e}{\partial q_i} - \frac{d}{dt} \left(\frac{\partial K}{\partial \dot{q}_i} \right) + \frac{\partial K}{\partial q_i} + \frac{\partial W_c}{\partial q_i} = \frac{\partial U}{\partial q_i} \quad (9)$$

or

$$\frac{d}{dt} \left(\frac{\partial K}{\partial \dot{q}_i} \right) - \frac{\partial K}{\partial q_i} + \frac{\partial U}{\partial q_i} - \frac{\partial W_c}{\partial q_i} = \frac{\partial W_e}{\partial q_i} \quad (10)$$

where:

t = Time

q_i = A generalized coordinate

\dot{q}_i = Time rate of change of q_i

K = Kinetic energy

U = Strain energy

W_c = Work done by damping forces

W_e = Work done by external loads

This equation is one form of Lagrange's equation. When appropriate expressions are written for K, U, W_c and W_e, all in terms of the generalized coordinates q₁, q₂, ..., q_n, differentiated as indicated and substituted into the above expression, equations of motion are obtained. There will be one equation of motion for each of the n coordinates or degrees of freedom. In all cases considered, $\partial K / \partial q_i$ is zero, since kinetic energy is a function of velocity rather than displacement. For example, consider an energy balance on the cask (i.e., the mass M_p), and let the generalized coordinate be the vertical displacement Y_p, i.e.,

$$q_i = Y_p \quad (11)$$

therefore

$$\frac{\partial K}{\partial Y_p} = 0 \quad (12)$$

$$\frac{\partial \dot{K}}{\partial \dot{Y}_p} = \frac{\partial}{\partial \dot{Y}_p} \left(\frac{1}{2} M_p \dot{X}_p^2 + \frac{1}{2} M_p \dot{Y}_p^2 + \dots \right) = M_p \dot{Y}_p \quad (13)$$

and

$$\frac{d}{dt} \left(\frac{\partial \dot{K}}{\partial \dot{Y}_p} \right) = \frac{d}{dt} (M_p \dot{Y}_p) = M_p \ddot{Y}_p \quad (14)$$

Also

$$\frac{\partial U}{\partial Y_p} = \frac{\partial}{\partial Y_p} (US2Y + US3Y) \quad (15)$$

where:

$$US2Y = \frac{k_{S2}}{2} [(Y_{RC} - \epsilon_{CR} \theta_{RC}) - (Y_p - \epsilon_{PR} \theta_p)]^2 \quad (16)$$

and

$$US3Y = \frac{k_{S3}}{2} [(Y_{RC} + \epsilon_{CF} \theta_{RC}) - (Y_p + \epsilon_{PF} \theta_p)]^2 \quad (17)$$

Therefore

$$\frac{\partial (US2Y)}{\partial Y_p} = -k_{S2} [(Y_{RC} - \epsilon_{CR} \theta_{RC}) - (Y_p - \epsilon_{PR} \theta_p)] = DUS2 \quad (18)$$

and

$$\frac{\partial (US3Y)}{\partial Y_p} = -k_{S3} [(Y_{RC} - \epsilon_{CF} \theta_{RC}) - (Y_p + \epsilon_{PF} \theta_p)] = DUS3 \quad (19)$$

Finally,

$$\frac{\partial W_c}{\partial Y_p} = \frac{\partial}{\partial Y_p} (WCS2Y + WCS3Y) \quad (20)$$

where:

$$\begin{aligned} WCS2Y &= -C_{S2} \left[\frac{d}{dt} (Y_{RC} - \epsilon_{CR} \theta_{RC}) - \frac{d}{dt} (Y_p - \epsilon_{PR} \theta_p) \right] \\ &\quad \times [(Y_{RC} - \epsilon_{CR} \theta_{RC}) - (Y_p - \epsilon_{PR} \theta_p)] \end{aligned} \quad (21)$$

$$\begin{aligned} WCS3Y &= -C_{S3} \left[\frac{d}{dt} (Y_{RC} + \epsilon_{CF} \theta_{RC}) - \frac{d}{dt} (Y_p + \epsilon_{PF} \theta_p) \right] \\ &\quad \times [(Y_{RC} + \epsilon_{CF} \theta_{RC}) - (Y_p + \epsilon_{PF} \theta_p)] \end{aligned} \quad (22)$$

and

$$\frac{\partial (WCS2Y)}{\partial Y_p} = C_{S2} \left[\frac{d}{dt} (Y_{RC} - \epsilon_{CR} \theta_{RC}) - \frac{d}{dt} (Y_p - \epsilon_{PR} \theta_p) \right] = DWS2 \quad (23)$$

$$\frac{\partial (WCS3Y)}{\partial Y_p} = C_{S3} \left[\frac{d}{dt} (Y_{RC} + \epsilon_{CF} \theta_{RC}) - \frac{d}{dt} (Y_p + \epsilon_{PF} \theta_p) \right] = DWS3 \quad (24)$$

There is no work done by external loads, so

$$\frac{\partial W_e}{\partial Y_p} = 0 \quad (25)$$

The equation of motion for the cask is then obtained by substitution of the above terms in Lagrange's Equation [Eq. (10)] to give

$$M_p \frac{d^2 Y_p}{dt^2} - 0 + DUS2 + DUS3 - DWS2 - DWS3 = 0 \quad (26)$$

The twelve derived equations of motion are:

(1) The Package or Cask

$$\begin{aligned} M_p \ddot{X}_p &= (k_{S1} + k_{S4})[(X_{RC} + Z_{RC}\theta_{RC}) - (X_p - Z_p\theta_p)] \\ &+ (c_{S1} + c_{S4})[\dot{X}_{RC} + Z_{RC}\dot{\theta}_{RC}) - (\dot{X}_p - Z_p\dot{\theta}_p)] \\ &- (W_{P1} + W_{P4})\mu_{PR}\text{sgn}(\dot{X}_p - \dot{X}_{RC}) \end{aligned} \quad (27)$$

$$\begin{aligned} M_p \ddot{Y}_p &= k_{S2} [(Y_{RC} + \ell_{CR}\theta_{RC}) - (Y_p + \ell_{PR}\theta_p)] + k_{S3} [(Y_{RC} - \ell_{CF}\theta_{RC}) \\ &- (Y_p - \ell_{PF}\theta_p)] + c_{S2} [(\dot{Y}_{RC} + \ell_{CR}\dot{\theta}_{RC}) - (\dot{Y}_p + \ell_{PR}\dot{\theta}_p)] \\ &+ c_{S3} [(\dot{Y}_{RC} - \ell_{CF}\dot{\theta}_{RC}) - (\dot{Y}_p - \ell_{PF}\dot{\theta}_p)] \end{aligned} \quad (28)$$

$$\begin{aligned} I_p \ddot{\theta}_p &= - (k_{S1} + k_{S4})Z_p [(X_{RC} + Z_{RC}\theta_{RC}) - (X_p - Z_p\theta_p)] \\ &+ k_{S2}\ell_{PR} [(Y_{RC} + \ell_{CR}\theta_{RC}) - (Y_p + \ell_{PR}\theta_p)] \\ &- k_{S3}\ell_{PF} [(Y_{RC} - \ell_{CF}\theta_{RC}) - (Y_p - \ell_{PF}\theta_p)] \\ &- (c_{S1} + c_{S4})Z_p [(\dot{X}_{RC} + Z_{RC}\dot{\theta}_{RC}) - (\dot{X}_p - Z_p\dot{\theta}_p)] \\ &+ c_{S2}\ell_{PR} [(\dot{Y}_{RC} + \ell_{CR}\dot{\theta}_{RC}) - (\dot{Y}_p + \ell_{PR}\dot{\theta}_p)] \\ &- c_{S3}\ell_{PF} [(\dot{Y}_{RC} - \ell_{CF}\dot{\theta}_{RC}) - (\dot{Y}_p - \ell_{PF}\dot{\theta}_p)] \end{aligned} \quad (29)$$

(2) The Rail Car

$$\begin{aligned}
 M_{RC} \ddot{X}_{RC} = & - (k_{S1} + k_{S4}) [(X_{RC} + Z_{RC} \theta_{RC}) - (X_P - Z_P \theta_P)] \\
 & - k_{S5} [(X_{RC} - Z_{RC} \theta_{RC}) - X_{TR}] - k_{S8} [(X_{RC} - Z_{RC} \theta_{RC}) - X_{TF}] \\
 & - k_{SCARS} (X_{RC} - X_F) - (C_{S1} + C_{S4}) [(\dot{X}_{RC} + Z_{RC} \dot{\theta}_{RC}) - (\dot{X}_P - Z_P \dot{\theta}_P)] \\
 & - C_{S5} [(\dot{X}_{RC} - Z_{RC} \dot{\theta}_{RC}) - \dot{X}_{TR}] - C_{S8} [(\dot{X}_{RC} - Z_{RC} \dot{\theta}_{RC}) - \dot{X}_{TF}] \\
 & + (W_{P1} + W_{P4}) \mu_{PR} \text{sgn}(\dot{X}_P - \dot{X}_{RC}) \quad (30)
 \end{aligned}$$

$$\begin{aligned}
 M_{RC} \ddot{Y}_{RC} = & - k_{S2} [(Y_{RC} + \ell_{CR} \theta_{RC}) - (Y_P + \ell_{PR} \theta_P)] - k_{S3} [(Y_{RC} - \ell_{CF} \theta_{RC}) \\
 & - (Y_P - \ell_{PF} \theta_P)] - k_{S6} (Y_{RC} + \ell_{RC} \theta_{RC}) - k_{S7} (Y_{RC} - \ell_{RC} \theta_{RC}) \\
 & - C_{S2} [(\dot{Y}_{RC} + \ell_{CR} \dot{\theta}_{RC}) - (\dot{Y}_P + \ell_{PR} \dot{\theta}_P)] - C_{S3} [(\dot{Y}_{RC} - \ell_{CF} \dot{\theta}_{RC}) \\
 & - (\dot{Y}_P - \ell_{PF} \dot{\theta}_P)] - C_{S6} (\dot{Y}_{RC} + \ell_{RC} \dot{\theta}_{RC}) - C_{S7} (\dot{Y}_{RC} - \ell_{RC} \dot{\theta}_{RC}) \\
 & - \mu_{CPL} \beta_{CPL} \text{sgn}(\dot{Y}_{RC} - \ell_{CPL} \dot{\theta}_{RC}) \left| k_{SCARS} (X_{RC} - X_F) \right|^{\alpha_{CPL}} \quad (31)
 \end{aligned}$$

$$\begin{aligned}
 I_{RC} \ddot{\theta}_{RC} = & - (k_{S1} + k_{S4}) Z_{RC} [(X_{RC} + Z_{RC} \theta_{RC}) - (X_P - Z_P \theta_P)] \\
 & - k_{S2} \ell_{CR} [(Y_{RC} + \ell_{CR} \theta_{RC}) - (Y_P + \ell_{PR} \theta_P)] + k_{S3} \ell_{CF} [(Y_{RC} - \ell_{CF} \theta_{RC}) \\
 & - (Y_P - \ell_{PF} \theta_P)] + k_{S5} Z_{RC} [(X_{RC} - Z_{RC} \theta_{RC}) - X_{TR}] - k_{S6} \ell_{RC} (Y_{RC} + \ell_{RC} \theta_{RC}) \\
 & + k_{S7} \ell_{RC} (Y_{RC} - \ell_{RC} \theta_{RC}) + k_{S8} Z_{RC} [(X_{RC} - Z_{RC} \theta_{RC}) - X_{TF}] \\
 & - (C_{S1} + C_{S4}) Z_{RC} [(\dot{X}_{RC} + Z_{RC} \dot{\theta}_{RC}) - (\dot{X}_P - Z_P \dot{\theta}_P)] \\
 & - C_{S2} \ell_{CR} [(\dot{Y}_{RC} + \ell_{CR} \dot{\theta}_{RC}) - (\dot{Y}_P + \ell_{PR} \dot{\theta}_P)] + C_{S3} \ell_{CF} [(\dot{Y}_{RC} - \ell_{CF} \dot{\theta}_{RC}) \\
 & - (\dot{Y}_P - \ell_{PF} \dot{\theta}_P)] + C_{S5} Z_{RC} [(\dot{X}_{RC} - Z_{RC} \dot{\theta}_{RC}) - \dot{X}_{TR}]
 \end{aligned}$$

$$\begin{aligned}
& - C_{S6} \dot{\rho}_{RC} (\dot{Y}_{RC} - \dot{\rho}_{RC} \dot{\theta}_{RC}) + C_{S7} \dot{\rho}_{RC} (\dot{Y}_{RC} - \dot{\rho}_{RC} \dot{\theta}_{RC}) \\
& + C_{S8} Z_{RC} [(\dot{X}_{RC} - Z_{RC} \dot{\theta}_{RC}) - \dot{X}_{TF}] \\
& + \mu_{CPL} \dot{\rho}_{CPL} \operatorname{sgn}(\dot{Y}_{RC} - \dot{\rho}_{CPL} \dot{\theta}_{RC}) \beta_{CPL} \left| k_{SCARS} (X_{RC} - X_F) \right|^{\alpha_{CPL}} \\
& + (Z_{CDGO} + \dot{\rho}_{CPL} \dot{\theta}_{RC}) k_{SCARS} (X_{RC} - X_F)
\end{aligned} \tag{32}$$

(3) The Front and Rear Trucks

$$\begin{aligned}
M_{TR} \ddot{X}_{TR} &= k_{S5} [(X_{RC} - Z_{RC} \dot{\theta}_{RC}) - X_{TR}] + C_{S5} [(\dot{X}_{RC} - Z_{RC} \dot{\theta}_{RC}) - \dot{X}_{TR}] \\
& - \mu_{TR} W_{XTR} \operatorname{sgn}(\dot{X}_{TR}) \cdot \text{BRAKER}
\end{aligned} \tag{33}$$

$$\begin{aligned}
M_{TF} \ddot{X}_{TF} &= k_{S8} [(X_{RC} - Z_{RC} \dot{\theta}_{RC}) - X_{TF}] + C_{S8} [(\dot{X}_{RC} - Z_{RC} \dot{\theta}_{RC}) - \dot{X}_{TF}] \\
& - \mu_{TF} W_{XTF} \operatorname{sgn}(\dot{X}_{TF}) \cdot \text{BRAKEF}
\end{aligned} \tag{34}$$

(4) The Anvil Train (Four Loaded Hopper Cars)

$$M_F \ddot{X}_F = k_{SCARS} (X_{RC} - X_F) - k_{FF2} (X_F - X_{F2}) - \mu_F W_F \operatorname{sgn}(\dot{X}_F) \cdot \text{BRKIRC} \tag{35}$$

$$M_{F2} \ddot{X}_{F2} = k_{FF2} (X_F - X_{F2}) - k_{F2F3} (X_{F2} - X_{F3}) - \mu_{F2} W_{F2} \operatorname{sgn}(\dot{X}_{F2}) \cdot \text{BRKF2} \tag{36}$$

$$M_{F3} \ddot{X}_{F3} = k_{F2F3} (X_{F2} - X_{F3}) - k_{F3F4} (X_{F3} - X_{F4}) - \mu_{F3} W_{F3} \operatorname{sgn}(\dot{X}_{F3}) \cdot \text{BRKF3} \tag{37}$$

$$M_{F4} \ddot{X}_{F4} = k_{F3F4} (X_{F3} - X_{F4}) - \mu_{F4} W_{F4} \operatorname{sgn}(\dot{X}_{F4}) \cdot \text{BRKF4} \tag{38}$$

See Appendix I, NOMENCLATURE OF TERMS, for definitions of the terms used in these equations.

The energy method was used in this study because it is a convenient and efficient process for deriving the equations of motion of the cask-rail car system. Specifically, several reasons for its selection are:

- (1) It has the advantage that, for a multi-degree-of-freedom system, the equations that describe the motion of the system are simplified and reduced in number because all the internal forces that do no work will not appear in the equations.
- (2) To express the results of the study as acceleration response spectra, it is necessary to relate maximum system response to system frequency. One way of accomplishing this is to use the modal method of analysis, which is considered to be an energy method because the modal equations are derived using the method outlined above. In the modal method, responses in the normal modes are determined separately and then superimposed to provide the total response. It can be shown that, by the use of this approach, each normal mode may be treated as an independent one-degree system. However the modal method was not used in this study. Independent one-degree-of-freedom (1-DOF) systems were used to relate system response to system frequency, but the technique used was not the modal method. [See Section 1.2, CASK-RAIL CAR RESPONSE SPECTRUM GENERATOR MODEL (CARRS)].
- (3) Common practice associates matrix formulation (stiffness matrices, etc.) with the alternate method. This is not always necessary; nevertheless, it is common to set up a problem in matrix notation when using the force-acceleration method. This is not the case with the energy method, although each method produces a system of differential equations of motion that can be expressed in this form. The formulation of the equations of motion using the energy method requires more mathematical manipulation, which might be considered by some to be a disadvantage; however, in this study, this was felt to be a small price to pay to maintain a close feel for the system attributes and to be able to subdivide the equations of motion into their various energy components.
- (4) The system simulation model is set up in terms of the equations of motion, which are subdivided into the various energy terms. This facilitates modification of the model at any time with a minimum of effort. This provides extreme flexibility in model construction.

Both the energy method and the force-acceleration method are only alternate methods of formulating the equations of motion of the cask-rail car system. They are not methods for solving the system of differential equations obtained. Because of the complexity of the system of equations and the fact that the equations are non-linear, a numerical method of integration was used in this study.

The entire model definition was written in the Advanced Continuous Simulation Language (ACSL).⁽¹⁾ ACSL was developed for the purpose of modeling systems described by time-dependent, non-linear differential equations and/or transfer functions. Program preparation can either be from block diagram interconnection, conventional FORTRAN statements, or a mixture of both. The ACSL program is intended to provide a simple method of representing complex mathematical models on a digital computer. Working from a system of equations describing the problem or from a block diagram, the user writes ACSL statements to describe the system under investigation. Statements describing the model do not need to be ordered, since the ACSL processor will sort the equations so that no values are used before they have been calculated. This operation of the language is in contrast to the usual digital programming languages like FORTRAN, where program execution depends critically on statement order.

All integration in an ACSL program is handled by a centralized integration routine. The user has a choice of four numerical integration algorithms:

- (1) The Adam's-Moulton variable-step, variable-order,
- (2) The Gears-Stiff variable-step, variable-order,
- (3) The Runge-Kutta second-order, and
- (4) The Runge-Kutta fourth-order.

The Runge-Kutta fourth-order algorithm was used in the model developed for this study.

A listing of the CARDS Model is presented in Appendix IV.

1.1.1 Rail Car Coupler and Draft Gear Subsystem Submodel

The rail car coupler and draft gear subsystem affects the response of the cask-rail car system more than any other component because the shock of impact is attenuated and transmitted to the cask-rail car system through this device.

A calculation sequence was developed to simulate the behavior of the coupler subsystem for the cask-rail car and the lead car in the group it impacts during humping operations. This coupler submodel determines the displacements of the springs and dampers (dashpots) during normal operating conditions, and the displacements and other conditions when one or more of these components bottom out at their limits of travel. The submodel was developed as a simplified preliminary model to develop and test the simulation of a coupler with a friction draft gear. It was given the name CARDT, which is an acronym for Cask-Rail Car Dynamic Test model. Later, after validation of CARDT by comparing calculated results with some experimental data, the basic features of the submodel were incorporated into CARDS.

Friction draft gears consist of springs and dampers in parallel; therefore, CARDT is based on the spring and damper arrangement shown in Figure 5(a). The equations of motion for the simple rail car-coupler subsystem model of Figure 5 are

$$M_{RC} \frac{d^2 X_{RC}}{dt^2} = -k_T (X_{RC} - X_F) \quad (39)$$

and

$$M_F \frac{d^2 X_F}{dt^2} = k_T (X_{RC} - X_F) \quad (40)$$

where:

X_{RC} = Displacement of the hammer car (in.)

X_F = Displacement of the struck car (in.)

M_{RC} = Mass of the hammer car, including lading [lb(force)-s²/in.]

M_F = Mass of the struck car, including lading [lb(force)-s²/in.]

k_T = Total equivalent spring constant of the combined draft gears [lb(force)/in.]

An equivalent spring representing the draft gears separating the cars is obtained by combining the spring and damper of each draft gear into a single equivalent spring [Figure 5(b)] and then reducing these series-connected springs to a single spring [Figure 5(c)].

When a force is applied to a parallel arrangement of a spring and damper, such as that representing the draft gear on the hammer car in Figure 5(a), the forces and displacements are defined, respectively, by

$$F_{T1} = F_1 + F_{D1} \quad (41)$$

and

$$X = X_1 = X_{D1} \quad (42)$$

where:

F_{T1} = Total force applied to the draft gear on the hammer car
[lb(force)]

F_1 = Force causing displacement of the spring [lb(force)]

F_{D1} = Force causing displacement of the damper [lb(force)]

X = Total travel or displacement of the draft gear on the
hammer car (in.)

X_1 = Displacement of the spring (in.)

X_{1D} = Displacement of the damper (in.)

The force on the spring is

$$F_1 = k_1 X_1 \quad (43)$$

or, since $X = X_1$

$$F_1 = k_1 X \quad (44)$$

where: k_1 = Spring constant of the spring in the hammer car draft gear
[lb(force)/in.]

According to Roggeveen, (2) in a friction draft gear the friction force is caused by the spring force and is, therefore, proportional to it. With this in mind, the friction force or force on the damper was defined as

$$F_{D1} = \mu_D F_1 \text{sgn}(\dot{X}) \quad (45)$$

where:

μ_D = A multiplying factor corresponding to a coefficient of friction

$\text{sgn}(X)$ = Signum function or sign function

The signum function is defined as

$$\text{sgn}(\dot{X}) = \begin{cases} +1, & \dot{X} > 0 \\ 0, & \dot{X} = 0 \\ -1, & \dot{X} < 0 \end{cases} \quad (46)$$

where: \dot{X} = Total relative velocity of displacement or travel of the draft gear (in./s)

Equation (45) implies that frictional damping in the draft gear is due to the sliding of two surfaces with a friction coefficient of μ_D , pressed together by the spring force F_1 . Equation (41), which defines the total force applied to the draft gear, may now be written as

$$F_{T1} = F_1 + \mu_D F_1 \text{sgn}(\dot{X}) \quad (47)$$

or
$$F_{T1} = F_1 [1 + \mu_D \text{sgn}(\dot{X})] \quad (48)$$

Using the definition of F_1 from Equation (44), the equation for the total force becomes

$$F_{T1} = k_1 X [1 + \mu_D \text{sgn}(\dot{X})] \quad (49)$$

Corresponding equations for the draft gear on the struck car are

$$F_{T2} = F_2 + F_{D2} \quad (50)$$

$$X' = X_2 = X_{D2} \quad (51)$$

$$F_2 = k_2 X_2 \quad (52)$$

or
$$F_2 = k_2 X' \quad (53)$$

and
$$F_{T2} = k_2 X' [1 + \mu_D \text{sgn}(\dot{X}')] \quad (54)$$

where:

F_{T2} = Total force applied to the draft gear on the struck car
[lb(force)]

F_2 = Force causing displacement of the spring in the struck
car draft gear [lb(force)]

F_{D2} = Force causing displacement of the damper in the struck
car draft gear [lb(force)]

X' = Total displacement or travel of the draft gear on the
struck car (in.)

X_2 = Displacement of the spring in the struck car draft gear
(in.)

X_{D2} = Displacement of the damper in the struck car draft gear
(in.)

The coupler subsystem of Figure 5(a) can now be reduced to the equivalent arrangement shown in Figure 5(b). The total forces acting on the draft gears may now be expressed in terms of the spring constants of the equivalent springs

$$F_{T1} = k_{RCDG} X \quad (55)$$

and
$$F_{T2} = k_{FDG} X' \quad (56)$$

where:

$$k_{RCDG} = k_1 [1 + \mu_D \text{sgn}(\dot{X})] \quad (57)$$

$$k_{FDG} = k_1 [1 + \mu_D \text{sgn}(\dot{X})] \quad (58)$$

For two springs in series, the total force applied is the same as that on each spring,

$$F_T = F_{T1} = F_{T2} \quad (59)$$

and the total relative displacement or travel of the two springs is equal to the sum of the relative displacements of each of the springs,

$$X_T = X + X' \quad (60)$$

For a single equivalent spring, the total force may be defined as

$$F_T = k_T X_T \quad (61)$$

where:

X_T = Total relative displacement of a single spring representing both draft gears (in.)

k_T = Spring constant of the single equivalent spring
[lb(force)/in.]

Solving Equations (55), (56) and (61) for the displacements and substituting into Equation (60) gives

$$\frac{F_T}{k_T} = \frac{F_{T1}}{k_{RCDG}} + \frac{F_{T2}}{k_{FDG}} \quad (62)$$

but since Equation (59) is true, Equation (62) may be reduced to

$$\frac{1}{k_T} = \frac{1}{k_{RCDG}} + \frac{1}{k_{FDG}} \quad (63)$$

or

$$k_T = \frac{k_{RCDG} k_{FDG}}{k_{RCDG} + k_{FDG}} \quad (64)$$

Before this definition of k_T can be used for the submodel of Figure 5(c), both k_{RCDG} and k_{FDG} must be expressed in terms of \dot{X}_T rather than as functions of \dot{X} and \dot{X}' . The total travel of the combined draft gears may be expressed as

$$X_T = X_{RC} - X_F \quad (65)$$

and the velocity as

$$\dot{X}_T = \dot{X}_{RC} - \dot{X}_F \quad (66)$$

Combining Equations (55) and (61) gives the relationship between X and X_T ,

$$X = \frac{k_T}{k_{RCDG}} X_T \quad (67)$$

and combining Equations (56) and (61) gives the corresponding relationship between X' and X_T ,

$$X' = \frac{k_T}{k_{FDG}} X_T \quad (68)$$

Differentiating Equations (67) and (68) with respect to time gives

$$\dot{X} = \frac{k_T}{k_{RCDG}} \dot{X}_T \quad (69)$$

and

$$\dot{X}' = \frac{k_T}{k_{FDG}} \dot{X}_T \quad (70)$$

Substituting from Equations (69) and (70) into Equations (57) and (58) makes both k_{RCDG} and k_{FDG} functions of \dot{X}_T ,

$$k_{RCDG} = k_1 [1 + \mu_D \text{sgn}(k_T \dot{X}_T / k_{RCDG})] \quad (71)$$

$$k_{FDG} = k_2 [1 + \mu_D \text{sgn}(k_T \dot{X}_T / k_{FDG})] \quad (72)$$

but, since only the sign and not the magnitude of \dot{X}_T is of interest and since k_T , k_{RCDG} and k_{FDG} are always positive,

$$k_{RCDG} = k_1 [1 + \mu_D \text{sgn}(\dot{X}_T)] \quad (73)$$

and

$$k_{FDG} = k_2 [1 + \mu_D \text{sgn}(\dot{X}_T)] \quad (74)$$

Equations (73) and (74) define the equivalent spring constants of the draft gears in their "active" state, i.e., when the total displacement lies between its upper and lower limits. When these limits are reached, the draft gears go "solid", i.e., they behave like a solid beam with properties consistent with the structural characteristics of the draft gears and rail cars. Consequently, the definitions of k_{RCDG} and k_{FDG} must be modified to represent the transition from the "active" to "solid" states. This is accomplished by branching within the submodel equivalent to the following:

$$\left. \begin{aligned} k_{RCDG} &= k_1 [1 + \mu_D \text{sgn}(\dot{X}_T)] \\ k_{FDG} &= k_2 [1 + \mu_D \text{sgn}(\dot{X}_T)] \end{aligned} \right\} X_{TL} < X_T < X_{TU} \quad (75)$$

and

$$\left. \begin{aligned} k_{RCDG} &= k_{SDG1} \\ k_{FDG} &= k_{SDG2} \end{aligned} \right\} X_T \leq X_{TL} \text{ or } X_T \geq X_{TU} \quad (76)$$

where:

X_{TL}, X_{TU} = Lower and upper limits, respectively, on the travel of the combined draft gears (in.)

k_{SDG1}, k_{SDG2} = Spring constants of the "solid" draft gears on the hammer car and struck cars, respectively [lb(force)/in.]

In the submodel, this branching is accomplished by the use of switching functions. In Fortran notation,

$$KRCDG = RSW(XT.LT.XTU.AND.XT.GT.XTL, K1*(1.+MUD*SGNF(DXT)), KSDG1) \quad (77)$$

and

$$KFDDG = RSW(XT.LT.XTU.AND.XT.GT.XTL, K2*(1.+MUD*SGNF(DXT)), KSDG2) \quad (78)$$

where:

$RSW ()$ = A "real switch" function in ACSL (Advanced Continuous Simulation Language)

and $SGNF ()$ = A specially constructed "signum function"

As a simple general example of how the real switch function works in ACSL, let

$$R = RSW (A, B, C).$$

If A is TRUE, $R = B$,

Otherwise $R = C$.

The foregoing has been a presentation of the development of the coupler subsystem submodel. The same general approach was applied to the suspension subsystem submodel since a Barber stabilized truck⁽³⁾ utilizes friction damping where friction is proportional to the load. (See Section 1.1.2, Suspension Subsystem Submodels.)

The coupler submodel described here was used to simulate an actual impact between two loaded 70-ton cars at ~6 mph. The calculated results are

presented in Figures 6 and 7 as coupler force as a function of time during impact. Results from the impact test, as reported by Baillie,⁽⁴⁾ are also presented in Figures 6 and 7 for comparison.

The results obtained from the model agreed reasonably well with the actual results for the periods when the draft gears were "active", but deviated considerably for the period when the draft gears became "solid" after bottoming out. Roggeveen⁽⁵⁾ simulated the same test using an analogue computer and obtained the same general trend of results. He concluded that the lower peak force during the actual test could be attributed to energy dissipation due to lading slip or cargo shift, and developed a model that divided the masses of each car into two masses, one for the car and one for the lading. This "two lump" approach of Roggeveen's was not used. In its place, an approach was used in which car-to-car characterization functions were developed to characterize the behavior of rail cars and their draft gears during the "solid" state of the draft gears. The "solid" state of a draft gear refers to that state after bottoming out when the draft gear behaves as a solid beam. This is in contrast to the draft gear's "active" state which is the normal condition before the draft gear spring has reached its limit of travel. A characterization function defines a pseudo spring constant or resistance function for the draft gear for its "solid" state, which accounts for dissipation of a portion of the total kinetic energy of the system due to cargo shifting and/or deformation of the cargo or rail car during this state. The spring constant defined is unique in that it increases gradually at first while the cargo shifts or deforms easily, but then rises sharply as the cargo compresses or stiffens. An upper limit is imposed on the spring constant during compression which represents near total compaction of the cargo. Energy dissipation due to crushing and deformation of the cargo during the "solid" state is simulated by removing a large fraction of the potential energy stored in the spring before the draft gear rebounds or recovers at zero relative kinetic energy of the two coupled cars. A car-to-car characterization function was first developed for CARDT and then expanded and installed in CARDS. This function was developed to avoid having to model each car in a train in detail.

The first step in the development of a car-to-car characterization function was linked to the development and application of a model validation algorithm based on Theil's inequality coefficients. (See Section 4.0, MODEL VALIDATION). A Theil's inequality coefficient (TIC) is a figure of merit computed from comparisons of predicted and measured time-varying (series) values of a response variable. A TIC ranges in value from 0 (indicating equality or perfect agreement) to 1 (indicating maximum inequality or poorest agreement).

Simulation runs were made to define a spring constant for a draft gear in its "solid" state. This spring constant was developed by varying certain parameters and conditions to minimize a Theil's inequality coefficient for comparison of calculated and measured time-varying values of coupler force. The system simulated was the impact test where two gravel-filled 70-ton hopper cars collided at 26 miles per hour.⁽⁴⁾ The simulation runs were

based on "solid" draft gear spring constants that were allowed to vary as functions of the relative displacement

$$X_T = X_{RC} - X_F \quad (79)$$

beyond the maximum value of X_T for the "active" state. The spring constants increased in magnitude as X_T increased beyond this "active" limit. The spring constants were expressed as the products of pre-selected base values and a multiplying factor that varied as a function of X_T beyond its active limit, as shown in Equations (80) and (81), and conditions (82).

$$k_{SDG1} = k_{SDG10} \phi(X_T) \quad (80)$$

$$k_{SDG2} = k_{SDG20} \phi(X_T) \quad (81)$$

where:

k_{SDG10} , k_{SDG20} = base spring constants corresponding to k_{SDG1} and k_{SDG2} , respectively [lb(force)/in.]

$\phi(X_T)$ = a multiplying factor, where

$$\left. \begin{aligned} \phi(X_T) &= 1.0, \text{ when } X_T = 5.6 \text{ in.} \\ \phi(X_T) &> 1.0, \text{ when } X_T > 5.6 \text{ in.} \end{aligned} \right\} \quad (82)$$

The lower limit on the base "solid" state spring constants was set at the value of the "active" state spring constant. The lower limit on the multiplying factor was 1.0, and the upper limit was an extrapolation from an arbitrary upper value of 6.35 in. set for X_T .

The time-varying coupler force, calculated using Equations (80) and (81), was compared with Baillie's data in Figure 8. The calculated coupler force vs time curve had the characteristic shape of the experimental curve, but both its magnitude and duration were substantially larger than those of the experimental curve. It was determined that, if the "solid" draft gear spring constants were bounded at some upper value less than that reached at zero relative velocity (i.e., $dX_T/dt = 0$), the peak coupler force would be reduced, but the duration would be increased. It was further determined that the duration could then be reduced by extracting a suitable fraction of

the potential energy stored in the springs. To accomplish these two effects, Equations (80) and (81), and conditions (82), were modified as follows:

$$k_{SDG1} = k_{SDG10} \phi(X_T) [1 + \mu_{XT} \text{sgn}(\dot{X}_T)] \quad (83)$$

$$k_{SDG2} = k_{SDG20} \phi(X_T) [1 + \mu_{XT} \text{sgn}(\dot{X}_T)] \quad (84)$$

and

$$\left. \begin{aligned} \phi(X_T) &= \phi(X_T)_L && \text{when } X_T \leq 5.6 \text{ in.} \\ \phi(X_T) &= \phi(X_T) && \text{when } 5.6 < X_T < 6.35 \text{ in.} \\ \phi(X_T) &= \phi(X_T)_U && \text{when } X_T \geq 6.35 \text{ in.} \end{aligned} \right\} \quad (85)$$

where: μ_{XT} = A multiplying factor representing the extent of energy dissipation ($0 \leq \mu_{XT} \leq 1$).

When the draft gears bottom out and enter their "solid" state, the relative displacement X_T no longer represents the travel of the combined draft gears. The terms X_{RC} and X_F are the horizontal displacements of the centers of gravity (cg) of the hammer car and anvil car, respectively. During the "solid" state of the draft gears, the cargo shifts or displaces, causing a shift or change in these displacements even though the actual travel of the draft gears during this period may be very slight. Consequently, the coupler force between the cars becomes a function of the resistance of the cargo to shift or deformation. A load-deflection curve for the cargo during this period would be based on cargo displacement relative to that of the rail car (i.e., displacement of the cg) and would produce a pseudo spring constant with the characteristics of the "solid" draft gear spring constants described in the previous paragraph. It is assumed that no cargo shifting or deformation occurs during the "active" state of the draft gears. This pseudo spring constant or "solid" draft gear spring constant also contains a term that accounts for the dissipation of a large portion of the energy required to shift or deform the cargo. Normally, a spring would restore to the system its energy of compression. In cargo shifting and deformation, energy is dissipated due to friction and due to permanent deformation of the cargo. Therefore, in the model, when the cargo is no longer compelled to move in the direction of greater compaction, the energy stored in the spring is discarded from the system by a substantial reduction in the spring constant for the recovery phase. This is accomplished by adjusting the parameter μ_{XT} . During the compaction or shifting

of the cargo, when the relative velocity \dot{X}_T is positive, μ_{XT} is set at 0 or some small fraction. At the end of compaction, when the spring would normally restore the energy of compaction to the system and when \dot{X}_T is negative, μ_{XT} is set at some large fraction. μ_{XT} is defined by

$$\left. \begin{aligned} \mu_{XT} &= \mu_{XTC} && \text{when } \dot{X}_T > 0 \text{ (Compaction)} \\ \mu_{XT} &= \mu_{XTE} && \text{when } \dot{X}_T \leq 0 \text{ (Recovery)} \end{aligned} \right\} \quad (86)$$

where:

μ_{XTC} = An energy dissipation coefficient for cargo compaction

μ_{XTE} = An energy dissipation coefficient for the cargo recovery phase

The equivalent spring constants of the draft gears in both their "active" and "solid" states may be summarized by restating Equation (75) and combining Equations (76), (83) and (84) to give

$$\left. \begin{aligned} k_{RCDG} &= k_1 [1 + \mu_D \text{sgn}(\dot{X}_T)] \\ k_{FDG} &= k_2 [1 + \mu_D \text{sgn}(\dot{X}_T)] \end{aligned} \right\} \quad X_{TL} < X_T < X_{TU} \quad (75)$$

for the "active" state, and

$$\left. \begin{aligned} k_{RCDG} &= k_{SDG10} \phi(X_T) [1 + \mu_{XT} \text{sgn}(\dot{X}_T)] \\ k_{FDG} &= k_{SDG20} \phi(X_T) [1 + \mu_{XT} \text{sgn}(\dot{X}_T)] \end{aligned} \right\} \quad X_T \leq X_{TL} \text{ or } X_T \geq X_{TU} \quad (87)$$

for the "solid" state.

Using the above expressions for the spring constants of the draft gears in the CARDT model, additional runs were made to simulate the 6 mph impact between the two gravel-loaded 70-ton hopper cars discussed earlier. During these runs, values of the parameters k_{SDG10} , k_{SDG20} , $\phi(\dot{X}_T)$, μ_{XTC} and μ_{XTE} were adjusted to obtain a coupler force vs time curve that compared reasonably well with the actual data reported by Baillie⁽⁴⁾ for this experiment. Final values of these and other pertinent parameters are summarized in Table 1. The parameter $\phi(\dot{X}_T)$ is presented in Figure 9. Results of these simulation runs are compared with experimental results in Figures 10 through 13. Coupler forces, relative displacements of the centers of gravity of the cars, relative velocities and relative accelerations are compared in Figures 10, 11, 12 and 13, respectively. Good comparisons were obtained up to ~ 0.076 second after impact. Beyond this time the response variables deviate as shown, indicating that further adjustments in the parameters are required. The experimental coupler force peaks at about 0.07 second while the calculated force peaks at ~ 0.085 second. The calculated coupler force as a function of calculated relative displacement is presented in Figure 14. This load-deflection curve for the single equivalent spring separating the rail cars encompasses both the "active" and "solid" states of the draft gears. The shape of the cyclic curve of Figure 14 is not unlike the curves presented by Kasbekar⁽⁶⁾ and Scales⁽⁷⁾ for standard draft gears.

It was noted that a lower value of the spring constant for the "solid" draft gear lowers the peak coupler force and increases its duration (i.e., broadens the peak), while a higher spring constant increases the peak force and decreases the duration. The calculated coupler force curve may be "shaped" to approach that of the experimental curve by the judicious adjustment of the parameters k_{SDG10} , k_{SDG20} , $\phi(\dot{X}_T)$, μ_{XTC} and μ_{XTE} . The first three parameters tend to raise and lower the peak force with a corresponding narrowing and broadening of its duration. The last two parameters, when used with the sign function $\text{sgn}(\dot{X}_T)$, cause the coupler force to drop to a level consistent with the dissipation of energy due to cargo shifting and deformation. The width of the pulse then depends upon the time at which \dot{X}_T goes negative.

After a careful study of the differences between the calculated and measured values of coupler force, relative displacement, relative velocity, and relative acceleration compared in Figures 10, 11, 12 and 13, respectively, it was determined that two adjustments were necessary to obtain better agreement.

The first adjustment made was to the energy dissipation coefficient, μ_{XTE} . μ_{XTE} was changed from a value of 0.9 to 0.95 (see Table 1). This drops the coupler force to a lower value after the velocity \dot{X}_T goes negative (cargo recovery phase).

The second adjustment made was in the argument of the sign functions in Equations (87) and to the control variable for Equations (86). As stated earlier, the width of the coupler force pulse depends upon the time at which \dot{X}_T goes negative. The velocity \dot{X}_T cannot be altered since it is determined from the equations of motion of the system; however, the argument of

the sign functions and the control variable for Equation (86) can be re-defined to produce the desired results. For this purpose, an "adjusted" relative velocity of displacement or travel of the centers of gravity of the two rail cars, \dot{X}_{TA} , was used and Equations (87) and (86) changed to

$$\left. \begin{aligned} k_{RCDG} &= k_{SDG10} \phi(X_T) [1 + \mu_{XT} \operatorname{sgn}(\dot{X}_{TA})] \\ k_{FDG} &= k_{SDG20} \phi(X_T) [1 + \mu_{XT} \operatorname{sgn}(\dot{X}_{TA})] \end{aligned} \right\} \begin{array}{l} X_T \leq X_{TL} \\ \text{or} \\ X_T \geq X_{TU} \end{array} \quad (88)$$

and

$$\left. \begin{aligned} \mu_{XT} &= \mu_{XTC} && \text{when } \dot{X}_{TA} > 0 \text{ (Compaction)} \\ \mu_{XT} &= \mu_{XTE} && \text{when } \dot{X}_{TA} \leq 0 \text{ (Recovery)} \end{aligned} \right\} \quad (89)$$

where: \dot{X}_{TA} = Adjusted relative velocity of displacement or travel of the cgs of the two rail cars (in./s)

The adjusted relative velocity is defined as

$$\frac{dX_{TA}}{dt} = \frac{dX_T}{dt} - \frac{dX_{LA}}{dt} \quad (90)$$

or

$$\dot{X}_{TA} = \dot{X}_T - \dot{X}_{LA} \quad (91)$$

where: \dot{X}_{LA} = An adjustment factor or relative velocity to regulate the relative velocity \dot{X}_T (in./s)

The function of \dot{X}_{LA} is to make the argument and control variable, \dot{X}_{TA} , go negative before \dot{X}_T . A constant value of \dot{X}_{LA} would give a time plot of \dot{X}_{TA} similar to that shown in Figure 15. Therefore, \dot{X}_{LA} becomes an additional control variable that can be used to vary the size of the pulse of the coupler force curve by "shaving" slices from its back side. Increasing the magnitude of \dot{X}_{LA} would result in larger slices being removed from the pulse. A negative value of \dot{X}_{LA} would add slices to the pulse.

The adjusted relative velocities, \dot{X}_{TA} and \dot{X}_{LA} , may be related to the velocities of the rail cars (not the cg's) and the velocities of the cargos on the rail cars, respectively, as follows. The velocity of the cg of the hammer car is defined as

$$\dot{X}_{RC} = \frac{M_{RC}\dot{X}_{CRC} + M_{LRC}\dot{X}_{LRC}}{M_{TRC}} \quad (92)$$

and the velocity of the center of gravity of the anvil car as

$$\dot{X}_F = \frac{M_F\dot{X}_{CF} + M_{LF}\dot{X}_{LF}}{M_{TF}} \quad (93)$$

where:

$$\begin{aligned} M_F &= \text{Mass of the anvil car (M)} \\ M_{RC} &= \text{Mass of the hammer car (M)} \\ M_{LF} &= \text{Mass of the lading or cargo on the anvil car (M)} \\ M_{LRC} &= \text{Mass of the lading or cargo on the hammer car (M)} \\ \dot{X}_{RC} &= \text{Velocity of the cg of the hammer car and its cargo (L/\theta)} \\ \dot{X}_F &= \text{Velocity of the cg of the anvil car and its cargo (L/\theta)} \\ \dot{X}_{CRC} &= \text{Velocity of the cg of the empty hammer car (L/\theta)} \\ \dot{X}_{CF} &= \text{Velocity of the cg of the empty anvil car (L/\theta)} \\ M_{TF} &= \text{Total mass of the anvil car and its cargo (M)} \\ &= M_F + M_{LF} \end{aligned} \quad (94)$$

$$\begin{aligned} M_{TRC} &= \text{Total mass of the hammer car and its cargo (M)} \\ &= M_{RC} + M_{LRC} \end{aligned} \quad (95)$$

The relative velocity of displacement or travel of the centers of gravity of the two loaded rail cars is defined by

$$\dot{x}_T = \dot{x}_{RC} - \dot{x}_F \quad (96)$$

Substitution from Equations (92) and (93) into Equation (96) gives

$$\dot{x}_T = \frac{M_{RC}\dot{x}_{CRC} + M_{LRC}\dot{x}_{LRC}}{M_{TRC}} - \frac{M_F\dot{x}_{CF} + M_{LF}\dot{x}_{LF}}{M_{TF}} \quad (97)$$

Replacing \dot{x}_T in Equation (91) with the above gives

$$\dot{x}_{TA} = \frac{M_{RC}\dot{x}_{CRC} + M_{LRC}\dot{x}_{LRC}}{M_{TRC}} - \frac{M_F\dot{x}_{CF} + M_{LF}\dot{x}_{LF}}{M_{TF}} - \dot{x}_{LA} \quad (98)$$

Assuming that \dot{x}_{LA} may be expressed in terms of the velocities of the cargos and their mass fractions as

$$\dot{x}_{LA} = \frac{M_{LRC}\dot{x}_{LRC}}{M_{TRC}} - \frac{M_{LF}\dot{x}_{LF}}{M_{TF}} \quad (99)$$

Then Equation (98) may be rewritten as

$$\dot{x}_{TA} = \frac{M_{RC}\dot{x}_{CRC}}{M_{TRC}} + \frac{M_{LRC}\dot{x}_{LRC}}{M_{TRC}} - \frac{M_F\dot{x}_{CF}}{M_{TF}} - \frac{M_{LF}\dot{x}_{LF}}{M_{TF}} - \frac{M_{LRC}\dot{x}_{LRC}}{M_{TRC}} + \frac{M_{LF}\dot{x}_{LF}}{M_{TF}} \quad (100)$$

or

$$\dot{x}_{TA} = \frac{M_{RC}\dot{x}_{CRC}}{M_{TRC}} - \frac{M_F\dot{x}_{CF}}{M_{TF}} \quad (101)$$

Equation (101) states that the adjusted relative velocity of the centers of gravity of the two rail cars is equal to the difference between the products of the mass fractions of the cars and their absolute velocities, if the adjustment factor or relative velocity \dot{X}_{LA} is defined as the difference between the products of the mass fractions of the cargos and their absolute velocities. The velocity \dot{X}_{LA} may be considered to be the adjusted relative velocity of the cargos on the two rail cars.

The expressions for the spring constants of the draft gears in the CARDT model were replaced by Equations (88) and (89), and the simulation of the 6 mph impact between the two gravel-loaded 70-ton hopper cars was repeated. A constant value of 30 in./s was assumed for \dot{X}_{LA} . Results of this simulation run are compared with the results reported by Baillie⁽⁴⁾ in Figures 16 through 19.

Coupler forces, relative displacements of the centers of gravity of the cars, relative velocities and relative accelerations as functions of time are compared in Figures 16, 17, 18 and 19, respectively. The calculated coupler force as a function of calculated relative displacement is presented in Figure 20, and the experimental coupler force as a function of the experimental relative displacement is presented in Figure 21. The comparisons between the calculated and experimental response variables show some improvement over those shown in Figures 10 through 13. The "goodness" of the comparisons has been expressed in terms of Theil's inequality coefficients for each response variable and Theil's multiple inequality coefficient for the simultaneous comparison of all the response variables (see Section 4, MODEL VALIDATION).

The CARDS model was modified to include equations equivalent to Equations (75), (88) and (89), and the function presented in Figure 9. Sets of equations were written to represent the linkage between the cask-rail car (hammer car) and the first ballast-filled anvil car, and the linkages between the remaining three ballast-filled anvil cars. However, an additional control variable was required since the cargo of the cask-rail car (the cask) is considered as a separate mass with its own equations of motion. Also, the trucks on the rail car are considered as separate masses with their own equations of motion. Consequently since the character of the cask-rail car is known and modeled accordingly, that portion of the car characterization function for the hammer car-anvil car linkage need not include the effects of cargo compaction and energy dissipation. To accomplish this, the control variable RCOR was introduced to provide control over the draft gear spring constant during the "solid" state. RCOR was added as a restriction on Equation set (88) as follows:

$$\left. \begin{aligned} k_{RCDG} &= k_{SDG10} \phi(\dot{X}_T) [1 + \mu_{XT} \text{sgn}(\dot{X}_{TA})] \\ k_{FDG} &= k_{SDG20} \phi(\dot{X}_T) [1 + \mu_{XT} \text{sgn}(\dot{X}_{TA})] \end{aligned} \right\} \quad (102)$$

when

$$x_T \leq x_{TL} \text{ or } x_T \geq x_{TU}$$

and

$$RCOR = 0$$

and

$$k_{RCDG} = k_{SDG10}$$

$$k_{FDG} = k_{SDG20} \phi(\dot{x}_T) [1 + \mu_{XT} \text{sgn}(\dot{x}_{TA})]$$

}

(103)

when

$$x_T \leq x_{TL} \text{ or } x_T \geq x_{TU}$$

and

$$RCOR = 1$$

where:

RCOR = cask-rail car override variable, with the control function

RCOR = 1.0, to override rail car characterization function

RCOR = 0, to activate rail car characterization function

RCOR is a control variable that is set at 1 since the cargo on the cask-rail car (the cask) is considered as a separate mass with its own equations of motion. The adjustment factor λ_{LA} is an input parameter. Similar equations and conditions were defined for the linkages between the other anvil cars in the train; however, the control variables equivalent to RCOR were set equal to 0.

When the cask-rail car strikes one or more anvil cars, it will tend to rotate about its center of gravity such that the striking or front end will tend to move downward and the far or rear end will move upward. This rotational or pitching motion is opposed by the damping in the suspension subsystems, and by frictional damping due to the vertical sliding motion of the coupler face on the cask-rail car against the coupler face on the adjacent anvil car. The frictional force at the coupler faces is represented as a vertical dash-pot in Figure 22.

The energy dissipated as frictional work at the coupler faces was defined as

$$W_{CRF} = F_{YRF} Y_{CPL} \quad (104)$$

where:

W_{CRF} = Energy dissipated as frictional work, [lb(force)-in.]

F_{YRF} = Frictional force opposing movement of sliding coupler faces [lb(force)]

Y_{CPL} = Vertical displacement of coupler face on cask-rail car, (in.)

The frictional force F_{YRF} was defined by the expression

$$F_{YRF} = -\mu_{CPL} \left| F_{CPL} \right|^{\alpha_{CPL}} \text{sgn}(\dot{Y}_{CPL})^{\beta_{CPL}} \quad (105)$$

where:

$\left| F_{CPL} \right|$ = Absolute value of force applied to coupler faces perpendicular to the sliding surfaces [lb(force)]

\dot{Y}_{CPL} = Vertical velocity of coupler face on cask-rail car (in./s)
(Coupler on anvil car is assumed to be stationary.)

β_{CPL} = A multiplying factor representing the fraction of F_{CPL} actually applied to the moving coupler faces

μ_{CPL} = Coefficient of friction for the sliding of the two coupler faces against each other

$\text{sgn}(\dot{Y}_{CPL})$ = Signum function or sign function of \dot{Y}_{CPL}

α_{CPL} = A factor to allow the damping term to vary as a function of the absolute value of F_{CPL} raised to the factor power

The force applied to the coupler, F_{CPL} , is the coupler force, i.e.,

$$F_{CPL} = k_{SCARS}(X_{RC} - X_F) \quad (106)$$

where:

k_{SCARS} = Spring constant of an equivalent single spring representing the draft gears on cask-rail car and first anvil car [lb(force)/in.]

X_{RC} = Horizontal displacement of cask-rail car (in.)

X_F = Horizontal displacement of first anvil car (in.)

The equivalent spring constant, k_{SCARS} , is actually k_T , the spring constant defined by Equation (64) as a function of the equivalent spring constants representing the draft gears on each car.

By combining Equations (104) and (105), the energy dissipated as work may be expressed as

$$W_{CRF} = - \mu_{CPL} \left| F_{CPL} \right|^{\alpha_{CPL}} \text{sgn}(\dot{Y}_{CPL})^{\beta_{CPL}} Y_{CPL} \quad (107)$$

or

$$W_{CRF} = - \mu_{CPL} \left| F_{CPL} \right|^{\alpha_{CPL}} \text{sgn}(\dot{Y}_{RC} - l_{CPL} \dot{\theta}_{RC})^{\beta_{CPL}} (Y_{RC} - l_{CPL} \theta_{RC}) \quad (108)$$

where:

Y_{RC} = Vertical displacement of the cg of the cask-rail car (in.)

θ_{RC} = Angle of rotation of the X_{RC} and Y_{RC} axes about an axis perpendicular to the $X_{RC} - Y_{RC}$ plane through the cg of the rail car (rad)

l_{CPL} = Horizontal distance from vertical centerline of cask-rail car to coupler face (in.)

Differentiating Equation (108) with respect to each of the generalized coordinates of the system yields

$$\frac{\partial W_{CRF}}{\partial Y_{RC}} = -\mu_{CPL} |F_{CPL}| \operatorname{sgn}(\dot{Y}_{RC} - \ell_{CPL} \dot{\theta}_{RC})^{\beta_{CPL}} \quad (109)$$

and

$$\frac{\partial W_{CRF}}{\partial \theta_{RC}} = \ell_{CPL} \mu_{CPL} |F_{CPL}| \operatorname{sgn}(\dot{Y}_{RC} - \ell_{CPL} \dot{\theta}_{RC})^{\beta_{CPL}} \quad (110)$$

These terms were included as energy dissipation terms in those equations of motion of the system that define the vertical and angular accelerations, \ddot{Y}_{RC} and $\ddot{\theta}_{RC}$, respectively. Although the coupler force, F_{CPL} , is a function of X_{RC} and X_F , similar dissipation terms were not derived from Equation (108) for these coordinates since it was felt that an energy dissipation term for vertical motion in the equations of motion defining the horizontal accelerations did not seem appropriate. However, since the existence of these dissipation terms is indicated by the use of the energy method, further study should be made to determine if these terms are significant.

1.1.2 Suspension Subsystem Submodel

The rail car suspension subsystem is important since it controls the vertical and rotational movement of the car during and after impact. Like the coupler subsystem, suspension subsystems consist of springs and dampers in parallel, as illustrated in Figure 22. In a Barber stabilized truck,⁽³⁾ the stabilizing or damping friction force is proportional to the load on the truck. Therefore, the spring constants for the equivalent springs shown in Figure 22 are defined by equations similar to those for the draft gears, i.e.,

$$k_{S6} = k_6 \left[1 - \mu_{D6}^{\beta_6} \left| \dot{Y}_{RC56} \right|^{\alpha_6} \operatorname{sgn}(\dot{Y}_{RC56}) \right] \quad Y_{RC56} > Y_{RCMAX} \quad (111)$$

or
$$k_{S6} = k_{6S} \quad Y_{RC56} \leq Y_{RCMAX} \quad (112)$$

and
$$k_{S7} = k_7 \left[1 - \mu_{D7}^{\beta_7} \left| \dot{Y}_{RC78} \right|^{\alpha_7} \operatorname{sgn}(\dot{Y}_{RC78}) \right] \quad Y_{RC78} > Y_{RCMAX} \quad (113)$$

or
$$k_{S7} = k_{7S} \quad Y_{RC78} \leq Y_{RCMAX} \quad (114)$$

where:

- α_6, α_7 = Factors that allow the damping term to vary as a function of the absolute value of the velocity raised to the factor power
- k_{S6}, k_{S7} = Spring constants for the equivalent springs representing the rear and front suspensions, respectively [lb(force)/in.]
- k_6, k_7 = Spring constants of the combined springs in the rear and front suspensions, respectively, in their "active" state [lb(force)/in.]
- k_{6S}, k_{7S} = Spring constants of the combined springs in the rear and front suspensions, respectively, in their "solid" state, i.e., after they have bottomed out [lb(force)/in.]
- $\dot{Y}_{RC56}, \dot{Y}_{RC78}$ = Vertical displacement velocities of the rail car at the rear and front suspensions, respectively (in./s)
- Y_{RCMAX} = Maximum downward vertical displacement of the rail car (the point at which the suspension springs bottom out or go "solid") (in.)
- Y_{RC56}, Y_{RC78} = Vertical displacements of the rail car at the rear and front suspensions, respectively (in.)
- μ_{D6}, μ_{D7} = Multiplying factors corresponding to coefficients of friction for the dampers in the rear and front suspensions, respectively
- β_6, β_7 = Multiplying factors representing the fraction of the load on the respective suspensions that is applied perpendicular to the sliding surfaces of the damper
- $\text{sgn}(\dot{Y}_{RC56}), \text{sgn}(\dot{Y}_{RC78})$ = Signum functions or sign functions of \dot{Y}_{RC56} and \dot{Y}_{RC78} , respectively.

The signum function is defined as follows for an argument \dot{Y}

$$\text{sgn}(\dot{Y}) = \begin{cases} +1, & \dot{Y} > 0 \\ -1, & \dot{Y} = 0 \\ -1, & \dot{Y} < 0 \end{cases} \quad (115)$$

Equations (111) and (113) differ from those of the draft gears in two ways. First, the sign of the second term is opposite to that of the draft gear equations. This is necessary since the sign convention used for the model is positive horizontal displacement to the right and positive vertical displacement upward. With this convention, the velocity of the vertical displacement is negative downward in the direction of the load compressing the suspension subsystem. A negative value of this velocity in Equations (111) and (113) will result in the addition of the terms in the brackets. The net result is that the equivalent springs for the suspension subsystems will be stiffer during compression than during relaxation or lifting. The second way in which Equations (111) and (113) differ from those of the draft gears is due to the multiplying factors β_6 and β_7 . These factors are related to the action of the so-called "side springs" that apply the force perpendicular to the sliding surfaces of the damping device. These factors represent fractions of the force on the respective suspension subsystems which are actually applied to the sliding surfaces for damping. The action of the velocity terms in Equations (111) and (113) is to augment the friction factors μ_{D6} and μ_{D7} . They act in conjunction with the load fractions β_6 and β_7 and the friction factors to regulate the amount of energy lost due to the forces exerted on the friction surfaces by the sidesprings. The absolute value of the velocity multiplied by a sign function with the velocity as the argument is equivalent to the vertical velocity; therefore, the second term in Equations (111) and (113) is equivalent to a viscous damping term. However, due to the presence of the factors α_6 and α_7 , greater latitude than either pure viscous or pure frictional damping is possible.

1.1.3 Pitching Moment Caused by the Offset of the Coupler and the Center of Gravity of the Rail Car

The CARDS model contains a term representing the pitching moment caused by the offset of the coupler and the center of gravity of the rail car. This term is part of the equation of motion defining the angle of rotation of the car.

Figure 23 is a simplified sketch of the rail car portion of the CARDS model that shows how the rotation of the rail car about a lateral axis passing through its center of gravity is enhanced by the moment of the coupler force about the axis. The moment about the center of gravity is

$$M_{RCCG} = Z_{CDG} DUSCAR \quad (116)$$

where:

Z_{CDG} = Vertical distance between the line of force and the cg of the rail car (in.)

DUSCAR = Coupler force [lb(force)]

The coupler force is defined by

$$DUSCAR = K_{SCARS}(X_{RC} - X_F) \quad (117)$$

The vertical distance, Z_{CDG} , is defined by

$$Z_{CDG} = Z_{CDGO} + \ell_{CPL}\theta_{RC} \quad (118)$$

where:

Z_{CDGO} = Distance between the centerline of the draft gear and the cg of the cask-rail car (in.)

ℓ_{CPL} = Horizontal distance from the vertical centerline of the cask-rail car to the coupler face (in.)

θ_{RC} = Angle of rotation of the cask-rail car about the lateral axis through its cg (rad)

The pitching moment, M_{RCCG} , was added to the equation of motion that defines the angle of rotation of the cask-rail car, i.e.,

$$\frac{d^2\theta_{RC}}{dt^2} = \frac{\left\{ \sum_i^N [(DUS_i) (\ell_i)] + M_{RCCG} \right\}}{I_{RC}} \quad (119)$$

where:

DUS_i = i-th force on the rail car [lb(force)]

ℓ_i = Distance from the rail car cg to the line of the applied i-th force (in.)

1.1.4 Cask-Rail Car Bending Submodel

The CARDS model contains a submodel to simulate bending of the cask-rail car (hammer car); however, although a spring arrangement to represent bending of the car was developed and incorporated into the model, it has never been

used or tested. At present, the bending submodel is isolated from the rest of the model by the use of switching functions that are in the deactivate mode.

The bending submodel remains isolated since time did not permit a study of some potential problems affecting superposition. The system of equations that define the present rail car model is based on the rotation (front to back pitching) of a rigid, nonbending rail car. The displacement at all support points on the rail car (cask to rail car and rail car to trucks) are functions of the vertical displacement of the center of mass of the rail car, angle of rotation, and a constant (nonbending) distance from the center of mass to the support points. When bending of the rail car occurs, the center of mass and, therefore, the vertical displacement are no longer located on a straight line and can no longer be related to the support points simply as a function of the distance and angle of rotation. If the increment of displacement due to bending is small, the present bending submodel may be used with little error. If the effect of bending is large, modifications will be necessary to assure that the displacements of the support points are correctly represented.

It was felt from the start that bending of the cask-rail car would be slight and that the effect on system response would be small. Subsequent comparisons of measured and calculated response variables have tended to re-enforce this belief. However, a bending submodel was developed and, although it has never been used or tested, the approach to its development is presented here for the record.

The approach used is based on the representation of a beam with lumped masses as a far-coupled spring-mass system.⁽⁸⁾ The proper spring arrangement to represent bending of the rail car was established by considering the rail car as a beam, and defining a stiffness coefficient k_{ij} to be a force applied at point j to produce a deflection equal to unity in the direction of the force, while point i is restrained against translation (zero deflection at i). The coefficients k_{ij} represent a force system that is capable of translating point j a unit amount while preventing the translation of point i . For example, in Figure 24, application of the force k_{11} at position 1 to give a deflection $y_1 = 1$, while preventing translation or deflections at the other load positions, causes the reactions k_{R1} , k_{31} , k_{21} , and k_{F1} at the rear support R, positions 3 and 2, and the front support F, respectively. Similar application of forces k_{33} and k_{22} yields the reactions shown. Because of Maxwell's reciprocal law

$$k_{12} = k_{21} \quad (120)$$

and

$$k_{23} = k_{32} \quad (121)$$

Relating the mass or load positions to the reactions, the bending submodel of the beam (rail car) may be represented by the far-coupled spring-mass

system shown in Figure 25(a). If the front and rear supports are mounted on springs (suspension system), the bending submodel is represented by the spring-mass arrangement of Figure 25(b).

The stiffness coefficients or spring constants, k_{ij} , for the bending submodel are obtained from a determination of flexibility influence coefficients. The influence coefficients are determined, as shown in Figure 26, by placing a unit load at one load position at a time (positions 1, 2 and 3 in Figure 26) and making use of the area-moment method to determine the deflections D_{ij} . These deflections are superimposed and then combined with the actual loads (F_i) at the positions to obtain the total deflections

$$y_1 = F_1 D_{11} + F_2 D_{12} + F_3 D_{13} \quad (122)$$

$$y_2 = F_1 D_{21} + F_2 D_{22} + F_3 D_{23} \quad (123)$$

and
$$y_3 = F_1 D_{31} + F_2 D_{32} + F_3 D_{33} \quad (124)$$

When this system of equations is solved for the loads, three equations of motion are obtained. The coefficients of y_1 , y_2 and y_3 in these equations of motion are combinations of the D_{ij} , and can be shown to be equal to the appropriate k_{ij} . Equations for the D_{ij} and the k_{ij} , in terms of the locations of the support points and other rail car parameters, have been programmed into the model.

The springs representing bending have been incorporated into the cask-rail car model, as shown in Figure 27.

1.1.5 Modeling the Anvil Train

During humping operations, the cask-rail car may impact "n" loaded cars making up a train. The CARDS model consists of the cask-rail car (hammer car) and four "anvil" cars in an "anvil train" as shown in Figures 28 and 29. Although any number of anvil cars may be considered in the anvil train, only four are in the model at present to be consistent with the make-up of the train used in the humping tests conducted at the Savannah River Laboratories from June 8, 1978 to August 3, 1978.

The model of the anvil train consists of the four masses, M_F , M_{F2} , M_{F3} and M_{F4} , each representing a single loaded car and each separated from the other by a coupler. The equations of motion for the four anvil cars are:

$$M_F \ddot{X}_F = k_{SCARS}(X_{RC} - X_F) - k_{FF2}(X_F - X_{F2}) - \mu_F W_F \text{sgn}(\dot{X}_F) \cdot \text{BRKIRC} \quad (125)$$

$$M_{F2} \ddot{X}_{F2} = k_{FF2}(X_F - X_{F2}) - k_{F2F3}(X_{F2} - X_{F3}) - \mu_{F2} W_{F2} \text{sgn}(\dot{X}_{F2}) \cdot \text{BRKF2} \quad (126)$$

$$M_{F3} \ddot{X}_{F3} = k_{F2F3}(X_{F2} - X_{F3}) - k_{F3F4}(X_{F3} - X_{F4}) - \mu_{F3} W_{F3} \text{sgn}(\dot{X}_{F3}) \cdot \text{BRKF3} \quad (127)$$

$$M_{F4} \ddot{X}_{F4} = k_{F3F4}(X_{F3} - X_{F4}) - k_{F4} W_{F4} \text{sgn}(\dot{X}_{F4}) \cdot \text{BRKF4} \quad (128)$$

The terms in Equations (125) through (128) are defined as follows:

M_F, M_{F2}, M_{F3} and M_{F4} = Masses of anvil cars 1 through 4, respectively

$\text{BRKIRC}, \text{BRKF2}, \text{BRKF3}$ and BRKF4 = Brake switches for anvil cars 1 through 4, respectively. (Brakes are on and locked when equal to 1 and off when equal to 0.)

$k_{SCARS}, k_{FF2}, k_{F2F3}$ and k_{F3F4} = Spring constants of equivalent springs representing the draft gear combinations between cars [lb(force)/in.]

X_F, X_{F2}, X_{F3} and X_{F4} = Horizontal displacement of anvil cars 1 through 4, respectively (in.)

W_F, W_{F2}, W_{F3} and W_{F4} = Weights of loaded anvil cars 1 through 4, respectively [lb(force)]

$\mu_F, \mu_{F2}, \mu_{F3}$ and μ_{F4} = Coefficients of friction for sliding contact between the tracks and the wheels of anvil cars 1 through 4, respectively

The size of the anvil train may be increased by adding additional equations between the equations for the first anvil car [Equation (125)] and the last anvil car [Equation (128)]. Also, appropriate auxiliary equations for the spring constants, etc. must be added to the model. The size of the anvil train may be easily varied by using switches as multipliers of the spring constants of the equivalent springs representing the couplers separating the cars. Cars may be switched into or out of the train, as desired, by simply setting these switches either to 1 or to 0, respectively.

Some results of a simulation of Test 3 of the humping tests at Savannah River Laboratories are presented in Figures 30 and 31 to illustrate how the shock of impact is propagated through the train. The coupler force between cars as a function of time after impact is presented in Figure 30, and Figure 31 shows the corresponding horizontal displacements or travel of each car along the track. Rebounding and multiple collisions of the cars in the train, with energy dissipation, are illustrated in these two figures. Figure 30 shows four force peaks in rapid succession initially, due to successive bottoming of the draft gears at impact. Friction in the draft gears and at the sliding contacts between the wheels and the track continually dissipates the energy in the system, resulting in a weakening of the force peaks after the first cycle. Some rebounding of the cars due to release of potential energy stored in the draft gears appears to occur during the first cycle, which accounts for the dips in the displacement curves in Figure 31. The dip in the displacement curve for the hammer car is more prominent than those for the other cars because it was the only car that did not have its brakes on and locked.

This simulation of Test 3 was conducted prior to final validation of the cask-rail car portion of the CARDS model. The validation was carried out using the coupler forces recorded during each of the tests as the shock forces causing vibration of the respective systems. (See Section 4.0, MODEL VALIDATION.) Time did not permit a repetition of this simulation after validation in which the coupler force for Test 3 would be calculated along with other variables that describe the response of both the cask-rail car and the anvil train.

1.2 CASK-RAIL CAR RESPONSE SPECTRUM GENERATOR (CARRS)

Equations of motion were derived for equivalent single degree-of-freedom (1-DOF) representations of the relative horizontal, vertical and rotational motion between a radioactive material shipping package and its rail car (support). These equations of motion (EOMs) were used to construct CARRS (Cask Rail Car Response Spectrum Generator), a model to generate frequency response spectra using calculated results obtained from the CARDS (Cask Rail Car Dynamic Simulator) model.

Response spectra for the cask-rail car system are obtained by converting the coupled EOMs for the cask in the CARDS model into EOMs for equivalent independent 1-DOF systems. The procedure for making this conversion is patterned after that of Harris and Crede.⁽⁹⁾ Equivalent independent 1-DOF equations describing the relative horizontal, vertical and rotational motion between the cask and rail car will now be derived using this procedure.

In the CARDS model, the equation of motion for vertical motion of the cask is expressed as

$$M_p \ddot{Y}_p = -DUS2 - DUS3 + DWS2 + DWS3 \quad (129)$$

where:

$$DUS2 = -k_{S2}[(Y_{RC} + l_{CR}\theta_{RC}) - (Y_P + l_{PR}\theta_P)] \quad (130)$$

$$DUS3 = -k_{S3}[(Y_{RC} - l_{CF}\theta_{RC}) - (Y_P - l_{PF}\theta_P)] \quad (131)$$

$$DWS2 = C_{S2}[(\dot{Y}_{RC} + l_{CR}\dot{\theta}_{RC}) - (\dot{Y}_P + l_{PR}\dot{\theta}_P)] \quad (132)$$

$$DWS3 = C_{S3}[(\dot{Y}_{RC} - l_{CF}\dot{\theta}_{RC}) - (\dot{Y}_P - l_{PF}\dot{\theta}_P)] \quad (133)$$

A sketch of the spring-mass model of the cask-rail car system is shown in Figure 2. A nomenclature of terms used in all the equations is presented in Appendix I. Combining Equations (129) through (133) gives

$$\begin{aligned} M_P \ddot{Y}_P = & k_{S2}[(Y_{RC} + l_{CR}\theta_{RC}) - (Y_P + l_{PR}\theta_P)] + k_{S3}[(Y_{RC} - l_{CF}\theta_{RC}) \\ & - (Y_P - l_{PF}\theta_P)] + C_{S2}[(\dot{Y}_{RC} + l_{CR}\dot{\theta}_{RC}) - (\dot{Y}_P + l_{PR}\dot{\theta}_P)] \\ & + C_{S3}[(\dot{Y}_{RC} - l_{CF}\dot{\theta}_{RC}) - (\dot{Y}_P - l_{PF}\dot{\theta}_P)] \end{aligned} \quad (28)$$

Let the relative vertical displacement be defined as

$$Y_d = Y_{RC} - Y_P \quad (134)$$

The relative vertical velocity and acceleration are

$$\dot{Y}_d = \dot{Y}_{RC} - \dot{Y}_P \quad (135)$$

and

$$\ddot{Y}_d = \ddot{Y}_{RC} - \ddot{Y}_P \quad (136)$$

Substituting from Equations (134) through (136) into Equation (28) and rearranging gives

$$M_P \ddot{Y}_{RC} - M_P \ddot{Y}_d = k_{S2} [Y_d + (l_{CR} \theta_{RC} - l_{PR} \theta_P)] + k_{S3} [Y_d - (l_{CP} \theta_{RC} - l_{PF} \theta_P)] \\ + C_{S2} [\dot{Y}_d + (l_{CR} \dot{\theta}_{RC} - l_{PR} \dot{\theta}_P)] + C_{S3} [\dot{Y}_d - (l_{CP} \dot{\theta}_{RC} - l_{PF} \dot{\theta}_P)] \quad (137)$$

Further rearrangement of Equation (137) yields an EOM in terms of the relative displacement Y_d

$$M_P \ddot{Y}_d + (k_{S2} + k_{S3}) Y_d + (C_{S2} + C_{S3}) \dot{Y}_d = M_P \ddot{Y}_{RC} + (k_{S3} l_{CF} - k_{S2} l_{CR}) \theta_{RC} \\ + (k_{S2} l_{PR} - k_{S3} l_{PF}) \theta_P \\ + (C_{S3} l_{CF} - C_{S2} l_{CR}) \dot{\theta}_{RC} \\ + (C_{S2} l_{PR} - C_{S3} l_{PF}) \dot{\theta}_P \quad (138)$$

The cask-rail car configuration used in Tests 1 and 4 conducted at the Savannah River Laboratories (SRL) is defined in Table 2 and Figure 32. Measurements before the tests show that, for this configuration, the cask is not centered on the rail car (along its length) (see Figure 2), i.e.,

$$l_{CR} > l_{CF} \quad (139)$$

However, the lengths l_{PR} and l_{PF} are equal. Using this information, Equation (138) may be rewritten as

$$M_P \ddot{Y}_d + (k_{S2} + k_{S3}) Y_d + (C_{S2} + C_{S3}) \dot{Y}_d = M_P \ddot{Y}_{RC} + (k_{S3} l_{CF} - k_{S2} l_{CR}) \theta_{RC} \\ + (k_{S2} - k_{S3}) l_{PR} \theta_P \\ + (C_{S3} l_{CF} - C_{S2} l_{CR}) \dot{\theta}_{RC} \\ + (C_{S2} - C_{S3}) l_{PR} \dot{\theta}_P \quad (140)$$

If it is assumed that

$$k_{S2} = k_{S3} \quad (141)$$

and

$$c_{S2} = c_{S3} \quad (142)$$

then Equation (140) may be expressed as

$$M_P \ddot{Y}_d + (k_{S2} + k_{S3})Y_d + (c_{S2} + c_{S3})\dot{Y}_d = M_P \ddot{Y}_{RC} + k_{S2}(l_{CF} - l_{CR})\theta_{RC} + 0 + c_{S2}(l_{CF} - l_{CR})\dot{\theta}_{RC} + 0 \quad (143)$$

Dividing Equation (143) by M_P and introducing the frequency

$$\omega_Y^2 = \frac{(k_{S2} + k_{S3})}{M_P} \quad (144)$$

gives

$$\ddot{Y}_d + \omega_Y^2 Y_d + \frac{(c_{S2} + c_{S3})}{M_P} \dot{Y}_d = \ddot{Y}_{RC} + \frac{\omega_Y^2}{2}(l_{CF} - l_{CR})\theta_{RC} + \frac{c_{S2}}{M_P}(l_{CF} - l_{CR})\dot{\theta}_{RC} \quad (145)$$

If the cask had been mounted at the center of the rail car (i.e., if the center of gravity of the cask had been placed to coincide with that of the rail car), then l_{CF} would have been equal to l_{CR} and Equation (145) would be reduced to

$$\ddot{Y}_d + \omega_Y^2 Y_d + \frac{(c_{S2} + c_{S3})}{M_P} \dot{Y}_d = \ddot{Y}_{RC} \quad (146)$$

Equation (146) is an EOM for an equivalent single-degree-of-freedom (1-DOF) representation of the cask-rail car system with support (rail car) motion \ddot{Y}_{RC} .

When $l_{CF} = l_{CR}$, the EOM for vertical motion is uncoupled from that for rotational motion of the rail car. However, since the cask was not centered on the rail car in Tests 1 through 4, Equation (145) must be used to determine the response spectra for these tests.

The CARDS model equation for horizontal motion of the cask is

$$M_p \ddot{X}_p = -DUS1 - DUS4 + DWS1 + DWS4 + DWP1 + DWP4 \quad (147)$$

where:

$$DUS1 = -k_{S1}[(X_{RC} + Z_{RC}\theta_{RC}) - (X_p - Z_p\theta_p)] \quad (148)$$

$$DUS4 = -k_{S4}[(X_{RC} + Z_{RC}\theta_{RC}) - (X_p - Z_p\theta_p)] \quad (149)$$

$$DWS1 = C_{S1}[(\dot{X}_{RC} + Z_{RC}\dot{\theta}_{RC}) - (\dot{X}_p - Z_p\dot{\theta}_p)] \quad (150)$$

$$DWS4 = C_{S4}[(\dot{X}_{RC} + Z_{RC}\dot{\theta}_{RC}) - (\dot{X}_p - Z_p\dot{\theta}_p)] \quad (151)$$

$$DWP1 = -\mu_{PR}W_{P1}\text{sgn}(\dot{X}_p - \dot{X}_{RC}) \quad (152)$$

$$DWP4 = -\mu_{PR}W_{P4}\text{sgn}(\dot{X}_p - \dot{X}_{RC}) \quad (153)$$

Combining Equations (147) through (153) gives

$$\begin{aligned} M_p \ddot{X}_p = & (k_{S1} + k_{S4})[(X_{RC} + Z_{RC}\theta_{RC}) - (X_p - Z_p\theta_p)] \\ & + (C_{S1} + C_{S4})[(\dot{X}_{RC} + Z_{RC}\dot{\theta}_{RC}) - (\dot{X}_p - Z_p\dot{\theta}_p)] \\ & - \mu_{PR}(W_{P1} + W_{P4})\text{sgn}(\dot{X}_p - \dot{X}_{RC}) \end{aligned} \quad (154)$$

Let the relative horizontal displacement be defined as

$$X_d = X_{RC} - X_p \quad (155)$$

The relative horizontal velocity and acceleration are then

$$\dot{X}_d = \dot{X}_{RC} - \dot{X}_p \quad (156)$$

and

$$\ddot{X}_d = \ddot{X}_{RC} - \ddot{X}_P \quad (157)$$

Substituting from Equations (156) through (157) into Equation (154) and rearranging gives

$$\begin{aligned} M_P \ddot{X}_{RC} - M_P \ddot{X}_d &= (k_{S1} + k_{S4})X_d + (C_{S1} + C_{S4})\dot{X}_d + \mu_{PR}(W_{P1} + W_{P4})\text{sgn}(\dot{X}_d) \\ &+ (k_{S1} + k_{S4})(Z_{RC}\theta_{RC} + Z_P\theta_P) + (C_{S1} + C_{S4})(Z_{RC}\dot{\theta}_{RC} + Z_P\dot{\theta}_P) \end{aligned} \quad (158)$$

Additional rearrangement of Equation (158) yields an EOM in terms of the relative displacement X_d

$$\begin{aligned} M_P \ddot{X}_d + (k_{S1} + k_{S4})X_d + (C_{S1} + C_{S4})\dot{X}_d + \mu_{PR}(W_{P1} + W_{P4})\text{sgn}(\dot{X}_d) \\ = M_P \ddot{X}_{RC} - (k_{S1} + k_{S4})(Z_{RC}\theta_{RC} + Z_P\theta_P) \\ - (C_{S1} + C_{S4})(Z_{RC}\dot{\theta}_{RC} + Z_P\dot{\theta}_P) \end{aligned} \quad (159)$$

Dividing Equation (159) by M_P and introducing the frequency

$$\omega_X^2 = \frac{(k_{S1} + k_{S4})}{M_P} \quad (160)$$

gives

$$\begin{aligned} \ddot{X}_d + \omega_X^2 X_d + \frac{(C_{S1} + C_{S4})}{M_P} \dot{X}_d + \frac{\mu_{PR}}{M_P}(W_{P1} + W_{P4})\text{sgn}(\dot{X}_d) \\ = \ddot{X}_{RC} - \omega_X^2(Z_{RC}\theta_{RC} + Z_P\theta_P) - \frac{(C_{S1} + C_{S4})}{M_P}(Z_{RC}\dot{\theta}_{RC} + Z_P\dot{\theta}_P) \end{aligned} \quad (161)$$

Now, if

$$Z_{RC} = Z_p = 0 \quad (\text{see Figure 2}) \quad (162)$$

that is, if the tiedown attachment points on the cask and rail car are located on horizontal lines through their respective cg's, then Equation (161) would reduce to

$$\ddot{X}_d + \omega_X^2 X_d + \frac{(C_{S1} + C_{S4})}{M_p} \dot{X}_d + \frac{\mu_{PR}}{M_p} (W_{P1} + W_{P4}) \text{sgn}(\dot{X}_d) = \ddot{X}_{RC} \quad (163)$$

Equation (163) is an EOM for an equivalent 1-DOF representation of the cask-rail car system with support (rail car) motion \ddot{X}_{RC} . When both Z_{RC} and Z_p are equal to zero, the EOM for horizontal motion is uncoupled from those for rotational motion of the cask and rail car. Since part of the tiedown configuration for the cask-rail car system used in the experiments is embodied in the cask base, framework, chocks and horizontal load cells, it does not seem likely that Z_{RC} and Z_p are zero; therefore, Equation (161) probably should be used to determine the response spectra for horizontal motion.

Under certain special conditions, and if

$$k_{CR} = k_{CF} \quad (164)$$

and

$$Z_{RC} = Z_p = 0, \quad (162)$$

the vertical response spectra may be obtained from the solution of Equation (146) and the horizontal response spectra from Equation (163). This is accomplished by determining the support motions, \ddot{Y}_{RC} and \ddot{X}_{RC} , either from measurements from experiments or from simulations using a model such as CARDS. If the support motions are in no way influenced by the package motion, as in the case of earthquake analysis where the ground motion is not significantly influenced by structure motion, then \ddot{Y}_{RC} and \ddot{X}_{RC} may be input input to Equations (146) and (163), respectively, and the equations solved for the maximum values of \dot{Y}_d and \dot{X}_d at various values of the frequencies ω_X and ω_Y . One plot of maximum response vs frequency is generated for each level of damping defined by the last term on the left-hand side (LHS) of Equation (146) and the last two terms on the LHS of Equation (163), respectively.

For the cask-rail car configurations being considered, the support or rail car motion is strongly influenced by the motion of the cask. Results from the CARDS simulation of Test 3 will now be used to justify this statement. This simulation run produced results as functions of time which agreed very well with experimental measurements, in terms of both shape and magnitude of the time plots. The equations in the CARDS model that define the vertical motion of the cask and rail car are

$$M_P \ddot{Y}_P = -DUS2 - DUS3 + DWS2 + DWS3 \quad (129)$$

and

$$M_{RC} \ddot{Y}_{RC} = DUS2 + DUS3 - DUS6 - DUS7 - DWS2 - DWS3 - DWS6 - DWS7 + DWCRF \quad (165)$$

respectively. Combining Equations (129) and (165) gives

$$M_{RC} \ddot{Y}_{RC} = -M_P \ddot{Y}_P - DUS6 - DUS7 - DWS6 - DWS7 + DWCRF \quad (166)$$

where:

$$DUS6 = k_{S6}(Y_{RC} + l_{RC}\theta_{RC}) \quad (167)$$

$$DUS7 = k_{S7}(Y_{RC} - l_{RC}\theta_{RC}) \quad (168)$$

$$DWS6 = c_{S6}(\dot{Y}_{RC} + l_{RC}\dot{\theta}_{RC}) \quad (169)$$

$$DWS7 = c_{S7}(\dot{Y}_{RC} - l_{RC}\dot{\theta}_{RC}) \quad (170)$$

$$DWCRF = -\mu_{CPL} \beta_{CPL} |DUSCAR|^\alpha_{CPL} \text{sgn}(\dot{Y}_{RC} - l_{CPL}\dot{\theta}_{RC}) \quad (171)$$

DUSCAR = Coupler force

The terms DUS2, DUS3, DWS2 and DWS3 are defined by Equations (130) through (133), respectively.

In the Test 3 simulation run, at the time when the vertical acceleration of the rail car (support) \ddot{Y}_{RC} is a maximum (0.116 s), these force terms have the numerical values shown in Table 3. Using these values in Equations (129) and (166) gives

$$\begin{aligned}
 -DUS2 &= -44754.6 \\
 -DUS3 &= 54094.7 \\
 +DWS2 &= 17889.5 \\
 +DWS3 &= 4904.6
 \end{aligned}$$

$$M_p \ddot{Y}_p = 76285.6 = \sum F_{Yp} \quad (172)$$

and

$$\begin{aligned}
 -M_p \ddot{Y}_p &= -76285.6 \\
 -DUS6 &= -74418.0 \\
 -DUS7 &= 51971.8 \\
 -DWS6 &= 0.0 \\
 -DWS7 &= 0.0 \\
 +DWCRF &= 0.0
 \end{aligned}$$

$$M_{RC} \ddot{Y}_{RC} = -98731.8 = \sum F_{YRC} \quad (173)$$

It is clear that, if the force $M_p \ddot{Y}_p$ were not included in the summation of Equation (173) (i.e., if the cask were cut loose or isolated from the rail car), the deceleration of M_{RC} (the rail car or support) would be substantially reduced. The force $M_p \ddot{Y}_p$ is the following fraction of the sum of the absolute values of all the vertical forces acting on the rail car.

$$\frac{|M_p \ddot{Y}_p|}{\sum |\text{Vertical Forces}|} = \frac{76285.6}{202675.4} = 0.376 \quad (174)$$

This shows that the vertical motion of the cask strongly influences the vertical motion of the rail car (support).

The influence of the horizontal motion of the cask on the horizontal motion of the rail car may be determined in the same way. The equations in the CARDS model that define the horizontal motion of the cask and rail car are

$$M_p \ddot{X}_p = -DUS1 - DUS4 + DWS1 + DWS4 + DWP1 + DWP4 \quad (147)$$

and

$$\begin{aligned}
 M_{RC} \ddot{X}_{RC} &= DUS1 + DUS4 - DUS5 - DUS8 - DUSCAR - DWS1 - DWS4 \\
 &\quad + DWS5 + DWS8 - DWP1 - DWPR
 \end{aligned} \quad (175)$$

respectively. Combining Equations (147) and (175) gives

$$M_{RC} \ddot{X}_{RC} = -M_P \ddot{X}_P - DUS5 - DUS8 - DUSCAR + DWS5 + DWS8 \quad (176)$$

where:

$$DUS5 = k_{S5} [(X_{RC} - Z_{RC} \theta_{RC}) - X_{TR}] \quad (177)$$

$$DUS8 = k_{S8} [(X_{RC} - Z_{RC} \theta_{RC}) - X_{TF}] \quad (178)$$

$$DWS5 = -C_{S5} [\dot{X}_{RC} - Z_{RC} \dot{\theta}_{RC}] - \dot{X}_{TR} \quad (179)$$

$$DWS8 = -C_{S8} [\dot{X}_{RC} - Z_{RC} \dot{\theta}_{RC}] - \dot{X}_{TF} \quad (180)$$

$$DUSCAR = k_{SCARS} (X_{RC} - X_F) \quad (\text{If calculated coupler force is used.}) \quad (181)$$

$$= DUSX4 \quad (\text{If measured coupler force is used.}) \quad (182)$$

The terms DUS1, DUS4, DWS1, DWS4, DWP1 and DWP4 are defined by Equations (148) through (153), respectively.

In the Test 3 simulation run, at the time when the horizontal acceleration of the rail car \ddot{X}_{RC} is a maximum (0.057 s), these force terms have the values shown in Table 4. Using these values in Equations (147) and (176) gives

$$\begin{aligned} -DUS1 &= -221589.0 \\ -DUS4 &= 0.0 \\ +DWS1 &= -57230.0 \\ +DWS4 &= -57230.0 \\ +DWP1 &= -23200.0 \\ +DWP4 &= -23200.0 \\ \hline M_P \ddot{X}_P &= -382449.0 = \Sigma F_{XP} \end{aligned} \quad (183)$$

and

$$\begin{aligned} -M_P \ddot{X}_P &= 382449.0 \\ -DUS5 &= 31802.7 \\ -DUS8 &= 31802.7 \\ -DUSCAR &= -1160000.0 \\ +DWS5 &= 34563.8 \\ +DWS8 &= 34563.8 \\ \hline M_{RC} \ddot{X}_{RC} &= -644818.0 = \Sigma F_{XRC} \end{aligned} \quad (184)$$

From this it appears that, if the force $M_p \ddot{X}_p$ were removed from the summation of Equation (184) (i.e., if the cask were cut loose or isolated from the rail car), the deceleration of M_{RC} (the rail car or support) would be substantially increased. The force $M_p \ddot{X}_p$ is the following fraction of the sum of the absolute values of all horizontal forces acting on the rail car

$$\frac{|M_p \ddot{X}_p|}{\sum |\text{Horizontal Forces}|} = \frac{382449}{1644182} = \underline{0.233} \quad (185)$$

This shows that the horizontal motion of the cask strongly influences the horizontal motion of the rail car (support); however, since this fraction is smaller than that of Equation (174), it appears that the cask affects the vertical motion of the support to a greater degree.

To confirm this conclusion, the CARDS model was adjusted to disconnect all components that tend to decrease the magnitude of the deceleration of the rail car (i.e., the cask and trucks), and a simulation run was made to determine the horizontal acceleration of the rail car. The experimentally measured coupler force was used in this simulation. The results of this simulation are compared, in Figure 33, to the calculated and experimental results for the complete cask-rail car system. It is evident that the calculated and experimental results for the full system compare well, but the deceleration of the "isolated" rail car is substantially greater. The deceleration of the "isolated" car, as might be expected, follows the coupler force curve. The experimental data used in this comparison contained high frequency noise that had to be filtered out before comparisons could be made. Filtering of these high frequency noise (>100 Hz) components from the experimental data was accomplished using the Fast Fourier Transform (FFT) program. (See Section 4.0, MODEL VALIDATION.)

Earlier in this section, EOMs were derived for 1-DOF representations of the cask-rail car system for determination of the response spectra in terms of the relative motion between the cask and rail car in both the vertical and horizontal directions. It was shown that, for special orientation of the cask on the rail car, the EOMs could be uncoupled from the rotational or pitching components of motion. Unfortunately, the cask-rail car configurations used in the tests at SRL were not arranged to provide for this uncoupling. Consequently, the EOMs that must be used to generate the desired response spectra are Equation (145),

$$\ddot{Y}_d + \omega_Y^2 Y_d + \frac{(C_{S2} + C_{S3})}{M_p} \dot{Y}_d = \ddot{Y}_{RC} + \frac{\omega_Y^2}{2} (\ell_{CF} - \ell_{CR}) \theta_{RC} + \frac{C_{S2}}{M_p} (\ell_{CF} - \ell_{CR}) \dot{\theta}_{RC} \quad (145)$$

for the relative vertical motion [or Equation (140) if $k_{S2} \neq k_{S3}$], and Equation (161)

$$\begin{aligned} \ddot{x}_d + \omega_X^2 x_d + \frac{(C_{S1} + C_{S4})}{M_p} \dot{x}_d + \frac{\mu_{PR}}{M_p} (W_{P1} + W_{P4}) \operatorname{sgn}(\dot{x}_d) \\ = \ddot{x}_{RC} - \omega_X^2 (Z_{RC} \theta_{RC} + Z_P \theta_P) - \frac{(C_{S1} + C_{S4})}{M_p} (Z_{RC} \dot{\theta}_{RC} + Z_P \dot{\theta}_P) \end{aligned} \quad (161)$$

for the relative horizontal motion. The uncoupled equivalent of Equation (145) is Equation (145) without the last two terms on the right hand side (RHS) [see Equation (146)]. The uncoupled equivalent of Equation (161) is Equation (161) without the last two terms on its RHS [see Equation (163)].

How important are the rotational terms in Equations (145) and (161)? To answer this, the RHSs of each equation were evaluated using input data and results from the same simulation run (using the CARDS model) from which the results of Tables 3 and 4 were obtained. The RHS of Equation (145) may be expressed as

$$\text{RHS(145)} = \ddot{y}_{RC} + \frac{\omega_Y^2}{2} (\ell_{CF} - \ell_{CR}) \theta_{RC} + \frac{C_{S2}}{M_p} (\ell_{CF} - \ell_{CR}) \dot{\theta}_{RC} \quad (186)$$

and that of Equation (161) as

$$\text{RHS(161)} = \ddot{x}_{RC} - \omega_X^2 (Z_{RC} \theta_{RC} + Z_P \theta_P) - \frac{(C_{S1} + C_{S4})}{M_p} (Z_{RC} \dot{\theta}_{RC} + Z_P \dot{\theta}_P) \quad (187)$$

The frequencies are defined by

$$\omega_Y^2 = \frac{(k_{S2} + k_{S3})}{M_p} \quad (144)$$

and

$$\omega_X^2 = \frac{(k_{S1} + k_{S4})}{M_p} \quad (160)$$

Using the values given in Table 5,

$$\omega_Y^2 = 966.2 \text{ s}^{-2}$$

$$\omega_X^2 = 31.08 \text{ s}^{-1}$$

and

$$\begin{aligned}\text{RHS}(145) &= -353.9 \text{ in./s}^2 + 131.3 \text{ in./s}^2 - 120.5 \text{ in./s}^2 \\ &= -353.9 \text{ in./s}^2 + 10.8 \text{ in./s}^2\end{aligned}$$

The last two terms of RHS(145) only contribute about 3% of the total. Similarly, using the values given in Table 6

$$\omega_X^2 = 5072.5 \text{ s}^{-2}$$

$$\omega_X = 71.22 \text{ s}^{-1}$$

and

$$\begin{aligned}\text{RHS}(161) &= -4180.5 \text{ in./s}^2 - 110.9 \text{ in./s}^2 - 47.9 \text{ in./s}^2 \\ &= -4180.5 \text{ in./s}^2 - 158.8 \text{ in./s}^2\end{aligned}$$

The last two terms of RHS(161) contribute about 4% of the total. Since maximum displacement occurs at zero velocity and maximum velocity occurs at zero displacement, the net magnitudes of the last two terms in the RHSs of Equations (145) and (161) should remain nearly constant. Consequently, the percentages of the contributions should increase as the magnitudes of the vertical and horizontal accelerations of the support decrease from their maximum values. At this time, it is not clear how the variation of the rotational components would affect the values of \ddot{Y}_d and \ddot{X}_d .

The vertical motion of the cg of the rail car was never measured during the experiments; however, measurements of the vertical acceleration were made for the car structure at the struck end, far end, and above the truck center at the struck end, using two piezoelectric (PE) accelerometers and one piezoresistive (PR) accelerometer. Apparently the vertical rail car motion at these locations was at a frequency that was outside the range that could be recorded by a PE accelerometer, so the data recorded could not be used. However, piezoresistive accelerometers are capable of measurements at these frequencies. The only PR accelerometer was located on the car structure at the struck end; however, the data recorded by this accelerometer was useless due to a considerable amount of noise that could not be filtered out. The output of this instrument was processed using the Fast Fourier Transform (FFT) program to filter out the high noise components, but to no avail. It was thought that, if these data were judged to be valid, they might be used to replace \ddot{Y}_{RC} in a modified version of Equation (186). To accomplish this, the vertical displacement of the rail car at the struck end (see Figures 2 through 4) is defined as

$$Y_{RC78} = Y_{RC} - l_{RC}\theta_{RC} \quad (188)$$

and the acceleration as

$$\ddot{Y}_{RC78} = \ddot{Y}_{RC} - l_{RC}\ddot{\theta}_{RC} \quad (189)$$

Solving Equation (189) for \ddot{Y}_{RC} gives

$$\ddot{Y}_{RC} = \ddot{Y}_{RC78} + l_{RC}\ddot{\theta}_{RC} \quad (190)$$

Substitution from Equation (190) into Equation (186) gives

$$\text{RHS(145)} = \ddot{Y}_{RC78} + l_{RC}\ddot{\theta}_{RC} + \frac{\omega_Y^2}{2}(l_{CF} - l_{CR})\theta_{RC} + \frac{C_{S2}}{M_p}(l_{CF} - l_{CR})\theta_{RC} \quad (191)$$

Since the data from the PR accelerometer were not valid, then response spectra could not be obtained from Equation (145), using the experimentally measured support motion \ddot{Y}_{RC78} . However, if these data had been valid and if the rotational terms are small compared to \ddot{Y}_{RC78} , then Equation (191) could have been reduced to the approximation

$$\text{RHS(145)} = \ddot{Y}_{RC78} \quad (192)$$

It was established earlier that the last two terms of RHS(145) [Equation (191)] are quite small, but from Table 5,

$$l_{RC} = 264 \text{ in.}$$

$$\ddot{\theta}_{RC} = -6.89 \text{ rad/s}^2$$

and

$$\ddot{Y}_{RC78} = 1465.5 \text{ in./s}^2$$

The product $x_{RC}\ddot{\theta}_{RC}$ is

$$x_{RC}\ddot{\theta}_{RC} = (264)(-6.89) = -1819 \text{ in./s}^2$$

The magnitude of this product is larger than that of \ddot{Y}_{RC78} , therefore, if a measured value of \ddot{Y}_{RC78} had been used to generate the response spectra, it would have had to be accompanied by a measurement of $\ddot{\theta}_{RC}$. No such measurement was made, so Equation (192) still would not have been valid.

The horizontal acceleration of the cg of the rail car also was not measured during the experiments, but measurements were made using both a PE and a PR accelerometer at the struck end, and a PE accelerometer at the far end. Only the PE accelerometer at the struck end appears to have failed to provide good data. Since the data from the other two accelerometers appeared to be valid, they were used for \ddot{x}_{RC} in Equation (187). The horizontal displacement of the rail car at the struck end is defined by

$$x_{RC78} = x_{RC} - z_{RC}\theta_{RC} \quad (193)$$

and the acceleration by

$$\ddot{x}_{RC78} = \ddot{x}_{RC} - z_{RC}\ddot{\theta}_{RC} \quad (194)$$

Solving Equation (194) for \ddot{x}_{RC} gives

$$\ddot{x}_{RC} = \ddot{x}_{RC78} + z_{RC}\ddot{\theta}_{RC} \quad (195)$$

Substituting \ddot{x}_{RC} from Equation (195) into Equation (187) gives

$$\begin{aligned} \text{RHS(161)} = & \ddot{x}_{RC78} + z_{RC}\ddot{\theta}_{RC} - \omega_X^2(z_{RC}\theta_{RC} + z_P\theta_P) \\ & - \frac{(C_{S1} + C_{S4})}{M_P}(z_{RC}\dot{\theta}_{RC} + z_P\dot{\theta}_P) \end{aligned} \quad (196)$$

Earlier, it was determined that the last two terms of this equation are small compared to \ddot{x}_{RC} . If it can be shown that the second term is small compared to \ddot{x}_{RC78} , then it would justify the use of \ddot{x}_{RC78} as an approximation of \ddot{x}_{RC} . From Table 6, $Z_{RC} = 18.0$ inches. The output from the CARDS simulation of Test 3 shows that the maximum value of $\ddot{\theta}_{RC}$ occurs at 0.104 second. At this time,

$$\ddot{\theta}_{RC} = -11.4 \text{ rad/s}^2$$

and

$$\ddot{x}_{RC} = -2036 \text{ in./s}^2$$

The product $Z_{RC}\ddot{\theta}_{RC}$ is

$$\begin{aligned} Z_{RC}\ddot{\theta}_{RC} &= (18)(-11.4) \\ &= -205.2 \text{ in./s}^2 \end{aligned}$$

Substituting these values into Equation (194) gives

$$\begin{aligned} \ddot{x}_{RC78} &= 2036 + 205.2 \\ &= -1830.8 \text{ in./s}^2 \end{aligned}$$

The second term is ~11% of the absolute value of \ddot{x}_{RC78} . If this percentage is deemed small enough then the measurements of \ddot{x}_{RC78} may be used as an approximation of \ddot{x}_{RC} , and Equation (196) may be reduced to

$$\text{RHS(161)} = \ddot{x}_{RC78} \tag{197}$$

The horizontal displacement and acceleration of the far end of the rail car are defined by

$$x_{RC56} = x_{RC} - Z_{RC}\theta_{RC} \tag{198}$$

and

$$\ddot{X}_{RC56} = \ddot{X}_{RC} - Z_{RC}\ddot{\theta}_{RC} \quad (199)$$

respectively. Since the RHSs of these equations are the same as those of Equations (193) and (194), \ddot{X}_{RC56} is equal to \ddot{X}_{RC78} and the same conclusions apply.

Finally, to determine response spectra using Equations (145) and/or (161), a special compatibility condition must exist between the RHS and left hand side (LHS) of each equation. This compatibility condition requires that if the RHS is determined at a particular frequency, then the relative response may be determined from the LHS only at that same frequency. In other words, the relative response cannot be determined from the LHS for various frequencies while using a RHS determined from a different frequency. This is supported by the previous discussion of the influence of the cask and trucks on the rail car (support) motion. Changes in the tiedown spring constants change the frequencies and the response of the rail car to cask motion. Isolation of the car from the cask and trucks may be accomplished by setting the appropriate spring constants equal to zero. The effect of this is illustrated in Figure 33.

The RHS forcing functions obtained from CARDS contain frequencies, or variables that are contained in the frequencies, corresponding to the frequencies on the LHSs of the respective 1-DOF EOMs. Therefore, when the frequencies on the LHSs are set at successively different values and runs made using the time-varying RHSs determined for a specific frequency, it would seem that an incompatibility exists. However, if it is assumed that a shaker table in a vibration testing facility is given motion matching the appropriate RHS forcing function, then the response of a device described by the respective 1-DOF EOMs may be studied. The shaker table (support) would be given time-varying accelerations or motions equal to the RHSs, i.e.

$$\ddot{Y}_S = \text{RHS}(145) \quad (200)$$

$$\ddot{X}_S = \text{RHS}(161) \quad (201)$$

where:

\ddot{Y}_S = Vertical acceleration of the support or shaker table (L/θ^2)

\ddot{X}_S = Horizontal acceleration of the support or shaker table (L/θ^2)

Comparing Equations (186) and (200), \ddot{Y}_S may be expressed as

$$\ddot{Y}_S = \ddot{Y}_{RC} + \frac{\omega_Y^2}{2} (\ell_{CF} - \ell_{CR}) \theta_{RC} + \frac{C_{S2}}{M_p} (\ell_{CF} - \ell_{CR}) \dot{\theta}_{RC} \quad (202)$$

Similarly, comparison of Equations (187) and (201) yields

$$\ddot{X}_S = \ddot{X}_{RC} - \omega_X^2 (Z_{RC} \theta_{RC} + Z_P \theta_P) - \frac{(C_{S1} + C_{S4})}{M_p} (Z_{RC} \dot{\theta}_{RC} + Z_P \dot{\theta}_P) \quad (203)$$

Since k_{S2} might not be the same as k_{S3} , and C_{S2} may be different than C_{S3} , a more general equation of motion may be obtained from Equation (140), i.e.,

$$\begin{aligned} \ddot{Y}_d + \omega_Y^2 Y_d + \frac{(C_{S2} + C_{S3})}{M_p} \dot{Y}_d = \ddot{Y}_{RC} + \frac{(k_{S3} \ell_{CF} - k_{S2} \ell_{CR})}{M_p} \theta_{RC} \\ + \frac{(k_{S2} - k_{S3})}{M_p} \ell_{PR} \theta_P \\ + \frac{(C_{S3} \ell_{CF} - C_{S2} \ell_{CR})}{M_p} \dot{\theta}_{RC} \\ + \frac{(C_{S2} - C_{S3})}{M_p} \ell_{PR} \dot{\theta}_P \end{aligned} \quad (204)$$

or

$$\ddot{Y}_d + \omega_Y^2 Y_d + \frac{(C_{S2} + C_{S3})}{M_p} \dot{Y}_d = \ddot{Y}_S \quad (205)$$

where, in this case,

$$\begin{aligned} \ddot{Y}_S = \ddot{Y}_{RC} + \frac{(k_{S3} \ell_{CF} - k_{S2} \ell_{CR})}{M_p} \theta_{RC} + \frac{(k_{S2} - k_{S3})}{M_p} \ell_{PR} \theta_P \\ + \frac{(C_{S3} \ell_{CF} - C_{S2} \ell_{CR})}{M_p} \dot{\theta}_{RC} + \frac{(C_{S2} - C_{S3})}{M_p} \ell_{PR} \dot{\theta}_P \end{aligned} \quad (206)$$

Assuming \ddot{X}_S and \ddot{Y}_S to be the motion of a support not influenced by the device attached to it, the response spectra of the device may be determined by varying the frequencies on the LHSs of Equations (161) and (205).

The experiments at SRL were run with two casks and four tiedown configurations (see Figure 32). Experiments or tests may be identified according to particular combinations of these masses and "springs," and frequencies determined. The maximum relative responses may be determined from Equations (145) and (161) using these frequencies and the appropriate measurements available for their respective RHSs. These could then be compared to the corresponding calculated maximum responses at the same frequencies, using calculated response data for the RHSs of Equations (145) and (161).

An equivalent independent 1-DOF equation describing the relative rotational motion between the cask and rail car was also derived using the same procedure used to get Equations (145) and (161). In the CARDS model, the equation of motion for rotational motion of the cask is expressed as

$$\begin{aligned} I_P \ddot{\theta}_P = & Z_P(DUS1 + DUS4 - DWS1 - DWS4) - \epsilon_{PR}(DUS2 - DWS2) \\ & + \epsilon_{PF}(DUS3 - DWS3) \end{aligned} \quad (207)$$

The terms DUS1, DUS4, DWS1 and DWS4 are defined by Equations (148) through (151), respectively, and the terms DUS2, DUS3, DWS2 and DWS3 are defined by Equations (130) through (133), respectively. Combining these Equations with Equation (207) gives

$$\begin{aligned} I_P \ddot{\theta}_P = & - Z_P(k_{S1} + k_{S4})[(X_{RC} + Z_{RC}\theta_{RC}) - (X_P - Z_P\theta_P)] \\ & + k_{S2}\epsilon_{PR}[(Y_{RC} + \epsilon_{CR}\theta_{RC}) - (Y_P + \epsilon_{PR}\theta_P)] \\ & - k_{S3}\epsilon_{PF}[(Y_{RC} - \epsilon_{CF}\theta_{RC}) - (Y_P - \epsilon_{PF}\theta_P)] \\ & - Z_P(c_{S1} + c_{S4})[(\dot{X}_{RC} + Z_{RC}\dot{\theta}_{RC}) - (\dot{X}_P - Z_P\dot{\theta}_P)] \\ & + c_{S2}\epsilon_{PR}[(\dot{Y}_{RC} + \epsilon_{CR}\dot{\theta}_{RC}) - (\dot{Y}_P + \epsilon_{PR}\dot{\theta}_P)] \\ & - c_{S3}\epsilon_{PF}[(\dot{Y}_{RC} - \epsilon_{CF}\dot{\theta}_{RC}) - (\dot{Y}_P - \epsilon_{PF}\dot{\theta}_P)] \end{aligned} \quad (208)$$

Let the relative horizontal displacement be defined as

$$\theta_d = \theta_{RC} - \theta_P \quad (209)$$

The relative rotational velocity and acceleration are then

$$\dot{\theta}_d = \dot{\theta}_{RC} - \dot{\theta}_p \quad (210)$$

and

$$\ddot{\theta}_d = \ddot{\theta}_{RC} - \ddot{\theta}_p \quad (211)$$

Combining Equations (208) through (211) gives, after much algebra, the following EOM in terms of the relative displacement θ_d

$$\ddot{\theta}_d + \omega_\theta^2 \theta_d + \xi_\theta \dot{\theta}_d = \ddot{\theta}_{RC} + \omega_\theta^2 \theta_{RC} + \xi_\theta \dot{\theta}_{RC} - \psi_\theta \quad (212)$$

The frequency ω_θ is defined by

$$\omega_\theta^2 = \frac{Z_P^2(k_{S1} + k_{S4}) + k_{S2}^2 l_{PR}^2 + k_{S3}^2 l_{PF}^2}{I_p} \quad (213)$$

The term ξ_θ is a damping coefficient defined as

$$\xi_\theta = \frac{Z_P^2 (C_{S1} + C_{S4}) + C_{S2}^2 l_{PR}^2 + C_{S3}^2 l_{PF}^2}{I_p} \quad (214)$$

The remaining term, ψ_θ , is a coupling term. It is expressed in terms of the coordinates X_{RC} , Y_{RC} , and θ_{RC} describing the motion of the rail car, and the two remaining coordinates X_p and Y_p describing the horizontal and vertical motion of the cask. This coupling term is defined as

$$\begin{aligned}
\psi_{\theta} = & \left\{ -Z_P(k_{S1} + k_{S4})[(X_{RC} + Z_{RC}\theta_{RC}) - X_P] \right. \\
& + k_{S2}l_{PR}[(Y_{RC} + l_{RC}\theta_{RC}) - Y_P] \\
& - k_{S3}l_{PF}[(Y_{RC} - l_{CF}\theta_{RC}) - Y_P] \\
& - Z_P(c_{S1} + c_{S4})[(\dot{X}_{RC} + Z_{RC}\dot{\theta}_{RC}) - \dot{X}_P] \\
& + c_{S2}l_{PR}[(\dot{Y}_{RC} + l_{CR}\dot{\theta}_{RC}) - \dot{Y}_P] \\
& \left. - c_{S3}l_{PF}[(\dot{Y}_{RC} - l_{CF}\dot{\theta}_{RC}) - \dot{Y}_P] \right\} / I_P \quad (215)
\end{aligned}$$

Equations (161), (204) and (212) are independent 1-DOF EOMs with forcing functions defined by the right hand sides (RHSs) of the respective equations. As stated earlier, if it is assumed that the RHS of each 1-DOF EOM represents the time-varying acceleration of a platform supporting a 1-DOF device defined by the left hand side (LHS) of the respective EOM, then the response of the device to various platform or support motions may be studied. The RHSs of Equations (161) and (204) are defined by Equations (203) and (206), respectively. The RHS of Equation (212) is defined by

$$\ddot{\theta}_S = \ddot{\theta}_{RC} + \omega_{\theta}^2 \theta_{RC} + \xi_{\theta} \dot{\theta}_{RC} - \psi_{\theta} \quad (216)$$

The 1-DOF EOMs of the cask-rail car system may now be summarized as follows:

$$\ddot{Y}_d + \omega_Y^2 Y_d + \frac{(c_{S2} + c_{S3})}{M_P} \dot{Y}_d = \ddot{Y}_S \quad (205)$$

$$\ddot{X}_d + \omega_X^2 X_d + \frac{(c_{S1} + c_{S4})}{M_P} \dot{X}_d + \frac{\mu_{PR}}{M_P} (W_{P1} + W_{P4}) \text{sgn}(\dot{X}_d) = \ddot{X}_S \quad (217)$$

and

$$\ddot{\theta}_d + \omega_{\theta}^2 \theta_d + \xi_{\theta} \dot{\theta}_d = \ddot{\theta}_S \quad (218)$$

where: $\ddot{\theta}_S$ = Rotational acceleration of support or shaker table ($1/\theta^2$)

Assuming that the motion of a support is not influenced by the device attached to it, the response spectra of the device may be determined by varying the frequencies on the LHSs of Equations (205), (217) and (218).

Equations (205), (217) and (218) were used to construct the response spectrum generator model CARRS. The support accelerations, defined by Equations (203), (206) and (216), are determined as functions of time by the CARDS model during a simulation and are written on a file to be read later by the CARRS model to generate the response spectra.

Response spectra are generated by the CARRS model in the following manner. Time-varying support accelerations (the RHSs of the 1-DOF EOMs in CARRS) are read from the file created by CARDS until arrays are filled. These arrays are then accessed at each time interval as the transient progresses. A common frequency is then set for the LHSs of the 1-DOF EOMs. The support accelerations are then traversed over the complete transient and the relative horizontal, vertical and rotational accelerations computed. The frequency on the LHSs of the 1-DOF EOMs is then set at a different value, the integrators are re-initialized, and the transient traversed again to obtain new values of the relative accelerations. This procedure was repeated for frequencies of 2, 5 and 10 through 260 rad/s in 10 rad/s increments. The entire frequency range was covered, for a particular set of support accelerations, by successive CARRS runs chained together as one run. A set of maximum or peak relative accelerations for each frequency was automatically determined by CARRS. Response spectra were then obtained by plotting the absolute values of these maximum accelerations against the frequency.

A listing of the CARRS model is presented in Appendix V.

Shock and vibration data gathered from the cask-rail car humping tests conducted at the Savannah River Laboratories in July and August of 1978 were reduced and analyzed to be used for validation of the CARDS model.

A summary of the configurations and conditions of these completed tests is presented as Table 2. For convenience, this summary has been transformed into a 4-dimensional morphological space as shown in Figure 32. The four dimensions are rail car design, cask design, tiedown configuration and type of coupler. Entries at each of these levels or dimensions are linked together, if they are related, by lines representing the tests identified by test numbers.

To collect and reduce data for model validation, transducers sensitive to force, displacement, and acceleration were mounted on the shipping container, tiedowns, and rail car in positions that corresponded to those in the analytical model. Following data reduction, the empirical data, together with the corresponding analytical data, were analyzed to allow modification and verification of the model. A simplified flow diagram of the procedure from data collection through model verification is shown in Figure 34.

The locations, types, and ranges of selected transducers were based on preliminary analytical results. Since the dynamic model described in the previous section simulates the longitudinal, vertical and rotational motion of the cask-rail car system, four additional data locations were required. These locations, on each set of trucks and on the car bed immediately above those trucks, were expected to produce accelerations in the ranges of ± 120 g and ± 150 g, respectively, within a frequency band of 3 to 1100 Hz. These requirements fell within the scope of previously planned instrumentation support.

The test plan specified 26 data channels plus a voice channel and timing channel with a FM-multiplexed into two channels of information on the test vehicle. The two channels were transmitted via a radio frequency link to a Sandia-supplied ground station, where they were recorded on both magnetic tape and oscillograph.

Oscillographic data give on-line quick-look data for test data verification. The magnetic tape recordings, because they represented the only reproducible form of all the test data, were reproduced under laboratory conditions at Sandia following the tests. Once copies of the original data tapes were made, they were demodulated to their original analog form and remodulated and recorded in a wide-band FM format compatible with equipment at the Hanford Engineering Development Laboratory (HEDL). Following this re-recording, the tapes containing all the experimental data and timing information were sent to HEDL for data reduction and analysis.

Data reduction consisted of reducing all data channels, with the aid of the appropriate calibration information and timing tracks, to a set of time-amplitude digital records of the experimental data. This step was performed on an existing Time-Data system, producing digital records compatible with Digital Equipment Corporation PDP-11 series computers.

Digital data flowed between the Time-Data system and the existing PDP-11/34 for various forms of data analysis, and between the PDP-11/34 and Boeing Computer Service's (BCS) Cyber 74 and Univac 1140/44 for model verification.

Initial data reduction consisted of conventional normalization of data amplitude with respect to calibration information. Digital and analog recordings of the time domain record were prepared for comparison with the original on-line oscillographic recordings. Simultaneously, the power spectra of each information channel were generated.

Data analysis and model verification, where practical, employed existing software. Software systems available included:

Time-Data: TSL (Time Series Language) - Time-Data proprietary analysis software system.

PDP-11/34: SPS-Basic (Scientific Programming System) - Tektronix operating system with graphical as well as analysis capabilities.

SPARTA: DEC RT-11 buffer oriented interactive system.

SSP: (Scientific Subroutine Package) DEC RT-11 Fortran subroutines.

RT-11: DEC operating system; digital information transfer to BCS.

RSX-11M: DEC operating system; multi-user operating system for special verification and analysis software.

These software systems, together with the communications link to the analytical model at BCS, processed the data to be used later for model validation.

Early in the study, it was decided to exercise the data reduction and model verification techniques to be used. For this purpose, data were synthesized employing a preliminary version of the CARDS model. (See Section 1.0, MODEL DEVELOPMENT, and Figures 2, 3 and 4.) Arbitrary values were used for some of the spring constants, damping factors, masses and dimensions. The model (shown in Figures 2, 3 and 4) produced instantaneous acceleration, velocity and displacement of three locations at 0.01-s intervals for a total interval of 2 seconds.

The parameters employed in this exercise were:

- XRC - Horizontal displacement at center of rail car
- YRC56 - Vertical displacement at rear of car above support (rear truck)
- YRC78 - Vertical displacement at front of car above support (front truck)
- DXRC - Derivative of XRC, or velocity
- DYRC56 - Derivative of YRC56, or velocity
- D2XRC - Second derivative of XRC, or acceleration
- D2YR56 - Second derivative of YRC56, or acceleration
- D2YR78 - Second derivative of YRC78, or acceleration

Impact was assumed to be at the "front-end" of the car.

Data obtained experimentally are generally acceleration, but by employing the proper boundary conditions to establish the constants of integration, both the velocity and displacement data can be derived. Because of this, the displacement, velocity and acceleration data derived from the model are assumed equivalent to that obtained experimentally.

Initially, the acceleration data for the three positions were operated on by Fast Fourier Transforms (FFT)⁽¹⁰⁾ producing the frequency domain equivalent of original time-domain data. The results of this process (shown in Figure 35) are the same as those derived from a spectrum analyzer--power spectral density.

The inverse FFT, which transforms the frequency domain data to its time-domain equivalent, offers an ideal filtering ability. If the bandwidth of the information is reduced, the time-domain information is altered, as shown in Figure 36.

The example given is where the vertical acceleration on the struck end (D2YR56) is limited to 75% and 50% of the total bandwidth of 50 Hz. It should be noted that, as the higher frequency information is deleted (as in the 50% bandwidth case), the instantaneous peak acceleration value is altered. This process, if improperly used, could misrepresent the instantaneous peak forces in a system. Similarly, if one were to attempt to find similarities between filtered time-domain waveforms, the nature of the filtering would have to be comparable.

Discrete Fourier transform methods assume a repetitive function of time convolved with a rectangular window that covers the interval of the time-domain sample. The results of this assumption are both beneficial and detrimental. The benefit is that a non-recurrent wave, such as the response to impact, may be objectively analyzed. The detriment is that an artifact-leakage⁽¹⁰⁾ may occur if the time-domain constituents are not harmonically related to the sample window.

A method of minimizing this "leakage" is to shape the time-domain information with a cosine or Hanning window, as illustrated in Figure 37. The Hanning weighting,

$$A = 0.5(1 - 2\pi t/T) \quad \text{for } t = 0 \text{ to } T,$$

while reducing the leakage, preserves the amplitude information in the frequency domain. The amplitude of frequency domain parameters, when shaped with the Hanning window, is scaled by 0.5 if the information is uniform in the sample interval.

The example shown in Figure 37 illustrates that the spectral information for both the weighted and original data are similar, while their corresponding time-domain representations are quite different.

These simple exercises in data analysis illustrate some of the fundamental techniques used for the analysis of the experimental data and, ultimately, for model verification.

Because of the restrictions of the data analysis techniques, it would be pure chance that data generated analytically and that obtained experimentally would be comparable in their time-domain form. The technique that was initially employed to reduce the experimental data is as follows:

- Digitize all acceleration information with attention given to a consistent time scale with respect to impact
- Assure that the time sample t for each digital representation conforms to $t < 1/2f_h$, where f_h is the highest frequency of interest in the measurement
- Scale the time-domain information with the Hanning window
- Repeat the operation for data generated from the analytical model

Once the power spectra are in the same form, the model's parameters may be adjusted to force agreement.

Instrumentation configurations were developed to be compatible with the rail car-cask tiedown system being tested. The instruments, together with the mechanical configuration they support, are illustrated in Figures 38 through 41. A brief description of this instrumentation is given in Table 7. The data acquisition techniques described in the opening paragraphs of this section were employed.

As during the "preliminary tests", high-speed photogrametric instrumentation (high-speed movies) recorded the coupling action of the rail car under test, as well as the interactions of the rail car, shipping cask, and the tiedown mechanism. In addition, still photographic records were made of the instrumentation, rail car, shipping cask, and tiedown assembly.

During these impact tests, the velocity of the rail car under test was accurately measured just prior to impact. The technique employed was to break glass wands with a protrusion extending from the moving rail car. Since the wands were of known separation, the elapsed time between the rods allowed accurate velocity measurements. These values agreed with those from radar measurements.

As expected, some data acquisition channels failed during tests. Also, some estimated peak amplitudes (used during calibration of the systems) were too large or too small producing either data that was on the same order of magnitude as the background noise or was clipped off at the saturation level of the system. Although these problems voided the data on the affected channels and reduced the amount and variety of data available for model validation, the model validation task was successfully completed. (See Section 4.0, MODEL VALIDATION.)

A further shakedown of the data reduction methods used was undertaken by analyzing representative data derived from Test 1, an 8.3 mph impact of a 70-ton SCL (Seaboard Coastline) rail car with a standard coupler, a 40-ton shipping cask, and tiedown configuration "A". This configuration and the location of the instruments are shown in Figure 38.

Initial analysis consisted of digitizing the analog signals at 5.12 kHz* which, according to the Nyquist sampling theorem,⁽¹⁰⁾ will accurately define and preserve frequencies up to 2.56 kHz. This is consistent with the 2.5 kHz band width of information obtainable from the employed wide-band FM analog recordings made at 7-1/2 IPS (IRIG intermediate band). Further, the maximum frequency of information was estimated by specialists at the Sandia Laboratories to be no greater than 1100 Hz (with instrument 7 the single exception at 2.56 kHz).

*kHz = kilohertz

For this initial effort, every second data point from the digitized time-domain record was employed for analysis and presentation. This data selection process results in an effective sampling rate of 2.56 kHz, which preserves information content up to 1.28 kHz.

The data reduction effort produced the following results:

- Raw time-domain data and their peak excursion values
- Filtered time-domain data and their peak excursion values
- Instant Fast Fourier Transform (FFT) for both unfiltered and filtered data
- Relative spectral energy content of filtered and raw data
- Example transfer functions

Table 8 summarizes the measured and reduced parameter values from the time-domain information.

Raw time-domain data (one example is illustrated in Figure 42) are the first 400 ms* (1024 samples of 0.39 ms/sample) following initial displacement as measured on instrument No. 4, Figure 43. These data were transformed into their frequency domain equivalent using the Fast Fourier Transforms (FFT) discussed earlier. The resulting spectra, corresponding to the time-domain waveform of Figure 42, is a measure of the frequency content of the waveform. These spectra are shown in Figure 44.

The representation of spectra content covers a range from DC (0th harmonic) to 1.28 kHz (512th harmonic), where a harmonic division is 2.5 Hz. The units of measure of these instant FFTs are g's/ $\sqrt{\text{Hz}}$ for acceleration or k-lb/ $\sqrt{\text{Hz}}$.** As in an electronic spectrum analyzer, the total harmonic content over a finite band width (2.5 Hz) must be reported at a single point; therefore, a normalizing factor K is applied. To permit the magnitudes presented here to be compared with those derived by other methods of analysis, a test was developed around Parseval's formula: (11)

$$\int_{-\infty}^{\infty} |f^2(t)| dt = K \int_{-\infty}^{\infty} |F^2(\omega)| d\omega$$

*ms = milliseconds

**k-lb/ $\sqrt{\text{Hz}}$ = kilopounds per square root of hertz.

where:

$f(t)$ = Time-domain information
 $F(\omega)$ = Fourier Transform of $f(t)$
 K = Applied scale factor (previously mentioned)

A unity magnitude sine wave was synthesized such that the sample window was equal to an integral number of periods. The resulting integral of the squared instant FFT, when compared to the integral of the original input wave square, revealed that:

$$K = \frac{1}{\text{No. of Harmonics}} = \frac{2}{\text{No. of Input Samples}}$$

Since K is associated with $F^2(\omega)$ or average power spectras, the employed instant FFTs have an applied scale factor of $1/\sqrt{K}$. In the presented example of 512 harmonics of instant FFTs, a scale factor of $1/\sqrt{512}$, or 0.0442, has been incorporated.

One of the objectives of this empirical data analysis was to provide information to validate the analytical model. It was determined that, by analyzing a narrow band of frequencies rather than the entire spectrum, a first-order solution would be more easily obtained. Further, if the energy content of that narrow band represented the major portion of the total energy, further analysis might be minimized. Using the symmetric properties of the FFT, ideal filtering was performed by truncating the frequency at the 100th harmonic (250 Hz) and performing an inverse FFT.

Table 9 compares the energy in the band-width limited spectra to the energy of the entire spectra, for a selected example of acceleration data. These data are shown as unfiltered time-domain information in Figure 42, and as filtered time-domain data in Figure 44. It is apparent that the time-domain peak values may be significantly reduced when the eliminated high frequency energy represented an appreciable portion of the entire spectrum. Note that this energy relationship is a necessary but not sufficient condition to cause the peak value variations.

Also related to the limited band width energy distribution is the range of effectiveness of a transfer function $\bar{H}(\omega)$. Transfer functions are essentially ratios of corresponding instant FFTs derived from the input and output of the system. For a linear, time-invariant system:

$$\bar{H}(f) = \frac{\bar{Y}(f)}{\bar{X}(f)} = \text{Transfer function}$$

where:

$X(f)$ = Complex frequency domain input function
 $Y(f)$ = Complex frequency domain output function

This function represents the system's output response to an input stimuli of a single frequency. If incomplete parameters are employed to represent the system's response, the response is incompletely characterized. However, the system is accurately characterized over that limited range. The data presented here consider the band of frequencies DC to 250 Hz. The assumption was made that system noise was above 250 Hz, but no attempt has been made to characterize or to quantify that noise.

The above transfer function obviously is dependent on the input and output spectra being over the same range; hence, windowing or filtering may be necessary. It is conceivable that a matrix of transfer functions, appropriately windowed, will permit the data to verify the model in a piece-wise linear fashion. At the minimum, it should give insight into the nature of the required model modification.

Figures 45 and 46 illustrate the transfer function magnitude relating the energy transfer from instrument 22 to 11 and from instrument 11 to 9 over the frequency range DC to 250 Hz. This corresponds to the vertical transfer of energy from the far end of the car on its structure, to the far end of the cask; then to the struck end of the cask. These figures show that $|\bar{H}| > 1$. Therefore, the energy is transferred from 9 to 11 (from the struck end to the far end) rather than the direction shown (11 to 9).

In a similar fashion, Figures 47 and 48 illustrate the longitudinal energy transfer characteristics from Instruments 12 to 10 and 10 to 8. Again observing the value of $|\bar{H}|$ relative to 1, general characteristics of energy couplings directions are revealed. In this case the direction is related to frequency in a complicated manner relative to the simple paths assumed.

The results of these efforts illustrate the techniques that were employed for data reduction. They show the applicability of analyzing the band width limited data as a first step towards model verification.

A meeting to discuss the quality of the data obtained from the SRL rail car impact tests was held at the Sandia Laboratories in Albuquerque, New Mexico on December 4, 1979. It was learned that data on the vertical acceleration of points on the rail car, and on the horizontal acceleration of the trucks, were lost due to the use of piezoelectric (PE) accelerometers. These accelerometers were not functional at the frequency range of the rail car and truck responses to be measured.

Measurements of vertical acceleration were made for points on the car structure at the struck end, far end, and above the truck center at the struck end using two PE accelerometers and one piezoresistive (PR) accelerometer.

Apparently the frequency of the vertical rail car motion at these locations was outside the range of the PE accelerometers, so the data recorded could not be used. A PR accelerometer is capable of measurements at these frequencies. The vertical acceleration of the rail car structure at the struck end was monitored using a PR accelerometer, but these data were lost due to either "clipping" (over-ranging) or substructure "noise".

The horizontal accelerations of the rail car and cask and the vertical accelerations of the cask were recorded without difficulty. These data were adequate for the successful validation of the CARDS model. (See Section 4.0, MODEL VALIDATION.)

Approximately the number of the vertical wall can be found in the
was found in the wall of the PE. The data recorded in the
not be used. A 20% reduction in the number of vertical wall
was found. The vertical wall of the wall is shown in the
who was not used in the wall. The data recorded in the
of the wall is shown in the wall.

The horizontal wall of the wall is shown in the wall. The data
was found in the wall. The data recorded in the wall is shown
the data for the vertical wall of the wall. The data recorded
the wall is shown in the wall.

3.0 COLLECT PARAMETER DATA

A literature search was made to collect data on key parameters to be used in the CARDS model for model validation (see Section 4.0, MODEL VALIDATION) and for the parametric and sensitivity analysis (see Section 5.0, PARAMETRIC AND SENSITIVITY ANALYSIS). Data collected included characteristics of flat bulkhead rail cars (i.e., dimensions, weights, etc.), data on rail car suspension systems, data on draft gears (couplers), and data on heavy shielded spent-fuel shipping casks and their tiedown systems.

Dimensions, weights and other data that make up specifications for the design, fabrication and construction of a 50-ton flat bulkhead car were obtained from the Association of American Railroads (AAR).⁽¹²⁾ These data were supplemented by drawings supplied by Savannah River Laboratories of the flat bulkhead car used in the coupling tests.

Load-deflection characteristics and the arrangement of springs in rail car suspension systems were obtained from AAR specifications (References 13 and 14, respectively). The load-deflection characteristics are given for helical springs, in terms of spring diameter and number of turns. These must be related to the proper height, number and grouping for a suspension system before they can be translated into a spring constant for that particular system.

Kasbekar et al.,⁽⁶⁾ present a piece-wise linear load-deflection curve for an M-901E draft gear obtained from tests performed by the AAR.⁽¹⁵⁾ Roggeveen⁽²⁾ implies that a spring constant of $\sim 6.25 \times 10^4$ lb(force)/in. may be acceptable for a draft gear in a coupling situation.

Weights, dimensions and other data on some heavy shielded spent fuel shipping casks and their tiedown systems are available in Reference 16 and in safety analysis reports for the National Lead Industries NLI 1/2, and Nuclear Fuel Services NFS-4 shipping casks.

It was noted that the sources of parameter data in the literature, in turn, usually refer to publications of the Association of American Railroads (AAR) as the source of their information. Therefore, several individuals in the AAR were contacted to obtain information on rail car suspension subsystem and coupler subsystem components. In particular, information was sought on the damping devices in these subsystems, including the side-springs in the suspension subsystem spring groups. Also, AAR specifications were obtained that contained a broad spectrum of pertinent information on flat bulkhead cars and other types of cars suitable for hauling heavy radioactive material packages.

ENSCO, Inc. was retained to provide parameter data on the railway equipment used in the coupling tests conducted at the Savannah River Laboratories, and on equipment that may be encountered in future studies. In addition, ENSCO supplied data from similar independent experiments conducted in the past to supplement the SRL data for model validation. Information on draft gear modeling, cargo shifting, and on the mix of rail car types present in an anvil train were also provided.

The parameter data supplied by ENSCO were used in the CARDS model to establish a base case to be used in model validation and in the parametric and sensitivity analyses. These data are clearly presented in the listing of the CARDS model in Appendix IV. It should be pointed out here that some of these data required adjustment during the subsequent model validation runs, as the model was being tuned to the particular test analyzed. The adjusted data are also clearly noted in the model listing.

4.0 MODEL VALIDATION

Three model validation techniques or algorithms were used, at various points throughout the study, to assess the "goodness" of agreement between time-varying response variables measured during humping or coupling experiments and their counterparts calculated using the CARDT and CARDS models. These techniques are:

- 1) A statistical technique for comparing, in the time domain, the differences between predicted and measured values of a time varying response variable
- 2) A spectral analysis technique that maps the predicted and measured values of a response variable into the frequency domain for comparison
- 3) A straightforward visual comparison of the time-varying response variables in the time domain

4.1 THEIL'S INEQUALITY COEFFICIENTS

The first model validation algorithm used is a statistical technique for computing a figure of merit from comparisons of time-varying values (series) of predicted and actual outputs. Statistical techniques available for testing the "goodness" of fit of models to actual system behavior include analysis of variance, the Chi-square test, factor analysis, Kolmogorov-Smirnov tests, nonparametric test, regression analysis, spectral analysis, and Theil's inequality coefficients.⁽¹⁷⁾ The technique based on Theil's inequality coefficients was selected. It was first programmed into the CARDT model and demonstrated successfully, and then included in the CARDS model. This technique was chosen as one of the three validation algorithms considered for three reasons:

- 1) It represents a simple addition to the dynamic model
- 2) It produces one number or figure of merit (the inequality coefficient) that reflects the degree of agreement between the model and the system modeled
- 3) It may be expanded to measure the degree of agreement based on "n" output variables by using Theil's multiple inequality coefficient

Theil's inequality coefficient is defined as

$$TIC = \frac{\left[\frac{1}{n} \sum_i^n (Y_{Pi} - Y_{Ai})^2 \right]^{0.5}}{\left(\frac{1}{n} \sum_i^n Y_{Pi}^2 \right)^{0.5} + \left(\frac{1}{n} \sum_i^n Y_{Ai}^2 \right)^{0.5}} \quad (219)$$

where: n = Number of sampling points, and

$$Y_{P1}, Y_{P2}, Y_{P3}, \dots, Y_{Pi}, \dots, Y_{Pn}$$

$$Y_{A1}, Y_{A2}, Y_{A3}, \dots, Y_{Ai}, \dots, Y_{An}$$

are the values of output variable Y at discrete points in time (a time series). Y_{Pi} and Y_{Ai} are the corresponding predicted and actual values, respectively, of the output variable Y . The values of TIC from Equation (219) will vary between the following two extremes:

TIC = 0 when $Y_{Pi} = Y_{Ai}$ for all i (The case of equality or perfect agreement)

TIC = 1 (The case of maximum inequality or poor agreement)

Theil's multiple or overall inequality coefficient (TMIC) is a figure of merit based on the number of observations or data points, the values of several output or response variables selected at discrete points, and the two-variable inequality coefficients (TICs) defined by Equation (219). The two-variable (calculated and experimental variable values) inequality coefficients are combined to generate the TMIC.⁽¹⁷⁾ The TMIC is defined by

$$TMIC = \frac{(PPD+PXD)TICD+(PPV+PXV)TICV+(PPA+PXA)TICA+(PPF+PXF)TIC}{(PPD+PXD+PPV+PXV+PPA+PXA+PPF+PXF)} \quad (220)$$

where:

$$PPD = \sqrt{\frac{x_T^2}{n}} \quad (221)$$

$$PXD = \sqrt{\frac{x_{TX}^2}{n}} \quad (222)$$

$$PPV = \sqrt{\frac{\dot{x}_T^2}{n}} \quad (223)$$

$$PXV = \sqrt{\frac{\dot{x}_{TX}^2}{n}} \quad (224)$$

$$PPA = \sqrt{\frac{\ddot{x}_T^2}{n}} \quad (225)$$

$$PXA = \sqrt{\frac{\ddot{x}_{TX}^2}{n}} \quad (226)$$

$$PPF = \sqrt{\frac{F_{CPL}^2}{n}} \quad (227)$$

$$PXF = \sqrt{\frac{F_{CPLX}^2}{n}} \quad (228)$$

The terms in these equations are

TMIC = Theil's multiple inequality coefficient

TIC, TICD, TICV, TICA = Theil's two-variable inequality coefficients for comparison of calculated and experimental values of coupler force, relative displacement, relative velocity, and relative acceleration, respectively

F_{CPL}, F_{CPLX} = Calculated and experimental coupler forces, respectively [lb(force)]

x_T, x_{TX} = Calculated and experimental relative displacements, respectively (in.)

\dot{x}_T , \dot{x}_{TX} = Calculated and experimental relative velocities, respectively (in./s)

$\ddot{X}_T, \ddot{X}_{TX}$ = Calculated and experimental relative accelerations, respectively (in./s/s)

n = Number of observations or sampling points

Equation (220) is a corrected version of the equation presented in Reference 17. A correction was made to this equation when it was discovered, after an evaluation, that a factor of 2 in the denominator was a mistake. This factor was removed. Equations (220) through (228) were added to the CARDT model for calculation of the TMIC during the simulation discussed in Section 1.0, MODEL DEVELOPMENT. The values of TMIC from Equation (220) will vary between the following two extremes:

TMIC = 0 (The case of equality or perfect agreement)

TMIC = 1 (The case of maximum inequality or poor agreement)

The model validation algorithm based on Theil's inequality coefficients (TIC) was tested by comparing actual values of some time-varying response variables, recorded following a 6-mph impact between the two 70-ton hopper cars loaded with gravel,⁽⁴⁾ with values calculated using the CARDT model. (See Section 1.1.1, Rail Car Coupler and Draft Gear Subsystem Submodel.) Theil's inequality coefficients for the response variables of Figures 16, 17, 18 and 19, in the time domain, are presented as Figures 49, 50, 51 and 52, respectively. Theil's multiple inequality coefficient for the time domain is presented in Figure 53. The final value of the multiple coefficient of Figure 53 is ~0.106, which indicates that the model accomplishes a reasonably good simulation of the experiment. However, it is also an indication that further refinements and adjustments are possible to drive TMIC as close to 0 as possible. The values of TMIC presented in Figure 53 are low by a factor of 2. This is due to the factor of 2 error discovered in the literature version of Equation (216). This error was not discovered until after the CARDT simulation was completed. The final value of TMIC in Figure 53 should be about 0.212 rather than 0.106.

The shape of the TIC vs time curve of Figure 49 may be explained as follows. The maximum value of TIC of about 0.74 is due to a perturbation in the experimental data during the first 0.002 second after impact (see Figure 16). During this time period, the measured coupler force rises from 0 to ~50,000 lb(force) at 0.002 second after impact, and then drops back to 0 during the following 0.001 second. The calculated coupler force varies gradually during this period. Consequently, due to the differences between the values of the calculated and measured coupler forces and the small number of data points for comparison, the TIC calculated for this period amplifies the poor initial agreement between the model output and experimental data. Further examination of Figures 16 and 49 reveals a quick recovery by TIC as it drops to its lowest value (best agreement) of about 0.0684 just before the next major perturbation in the measured coupler force at about 0.053 second.

This perturbation causes a short sharp rise in TIC followed by a short recovery period. The draft gears then bottom out, and large differences between measured and calculated values of coupler force during the draft gears' "solid" state result in an increase in TIC to about 0.25. TIC then recovers to some extent at rebound to a value of about 0.12, and then levels off at a final value of about 0.212 when the draft gears re-enter their "active" state.

4.2 FAST FOURIER TRANSFORMS

The second model validation algorithm chosen for use with the CARDS model is based on spectral analysis. This algorithm was transformed into the computer program FFT (Fast Fourier Transform) as part of the data collection and reduction task. (A listing of FFT is presented in Appendix VI). FFT converts the displacement, velocity and acceleration response of a cask-rail car system from the time domain to the frequency domain and allows the response spectra to be determined directly from either model output or from test data. An example of response spectra produced by FFT from test data is presented as Figure 44. Additional examples may be found in References 18 and 19.

Originally, it was intended that FFT would be used as a subroutine in the CARDS model; but, due to certain incompatibilities with ACSL (Advanced Continuous Simulation Language), it was used instead as a separate program for processing model output as if it were the recorded output from an experiment. FFT was used only to a limited extent for model validation. Its primary uses were to map response variables from the time domain into the frequency domain and to filter out the high frequency noise in the test data. [See Section 1.2, CASK-RAIL CAR RESPONSE SPECTRUM GENERATOR (CARRS)].

4.3 VISUAL COMPARISON OF RESPONSE VARIABLES

The third technique used to assess the "goodness" of agreement between measured and calculated response variables was a straightforward visual comparison of plots of the response variables in the time domain.

As the study progressed, after the CARDS model had been modified and tuned to account for flaws in some of the test configurations, this technique was found to be adequate and was used exclusively for the comparison of measured and calculated response variables.

4.4 FREQUENCY RESPONSE SPECTRA

A fourth technique was developed for both model validation and for the parametric and sensitivity analysis discussed in Section 5.0. However, for reasons stated in Section 1.2, this technique was not used for model validation. This technique is based on the transformation of the multi-degree-of-freedom representation of the cask-rail car system into an equivalent single-degree-of-freedom representation. [See Section 1.2, CASK-RAIL CAR

RESPONSE SPECTRUM GENERATOR (CARRS)]. Theoretically, the single degree-of-freedom (1-DOF) representation of the system (CARRS model) may be used to generate frequency response spectra for both the test configurations and their simulations (using the CARDS model). The "goodness" of agreement of these spectra would be a measure of how well the CARDS model simulates the tests. Horizontal and vertical accelerations measured at various points on the cask-rail car systems of the tests would be used as the forcing functions in the CARRS model to generate "measured or experimentally derived" frequency response spectra. Calculated accelerations (forcing functions) obtained from the CARDS model simulations of the tests would then be used to generate the corresponding "calculated" spectra to be compared to the "measured or experimentally derived" spectra. However, for the reasons discussed in Section 1.2, the "experimentally derived" spectra for relative vertical motion could not be generated. Specifically, these spectra could not be generated because all measurements of the vertical accelerations of the rail car structure were lost. The "experimentally derived" spectra for relative horizontal motion could have been generated but, since visual comparisons of the horizontal accelerations for Test 3 were good, it was decided that these visual comparisons would be sufficient.

4.5 MODEL VALIDATION AND RESULTS

During the development of the CARDS model it was noted that, although the time-domain plots of some measured and calculated response variables were similar in appearance, they were offset sufficiently to yield values of their inequality coefficients (TICs) that suggested poor agreement. In some cases, the model was "tuned" to identify the parameter or parameters causing the offset and to determine the values of these parameters that would bring the plots closer together. This "tuning" process consisted of varying the values of selected parameters one at a time while holding the others constant at their base case values, and computing values of Theil's multiple inequality coefficient (TMIC). A minimum value of TMIC would be obtained for the "best" value of a given parameter. One of the first parameters investigated was the time shift required to obtain the best fit when values of calculated and experimental response variables were superimposed. Early in the study, an initial comparison of the time-varying calculated and experimental coupler forces showed that the ramps and peaks of the experimental curve lagged considerably behind those of the calculated curve. Since the starting time for the CARDS simulation is the time at which the coupler begins to travel, this suggested that perhaps the recording device installed for the experiment was activated by almost imperceptible movements of the coupler mechanism prior to significant compression. Frame by frame examination of the high speed film of this portion of Test 3 showed that, from the instant of initial contact between the couplers to the first sign of draft gear travel, 9 frames were exposed. At 400 frames per second, this meant that 0.0225 second had elapsed over this interval. A shift of the results by this amount of time produced much better agreement between the times at which the various events occurred. This time shift represents a suspected lag between the time the recording device was activated and the time at which the coupler actually begins to travel. A final value of this time lag was established by trying

a number of values while evaluating Theil's two-variable inequality coefficient for the coupler force, and Theil's multiple inequality coefficient. Minimum values of these coefficients (indicating the best agreement) occurred for a time shift of 0.038 second. The time shift of 0.038 second fixed the common zero point on the time traces of the experimental data for further comparisons.

4.5.1 Comparison of Measured and Calculated Results for Test 3

In Reference 20 it was shown that results obtained from a CARDS simulation of Test 3 of the SRL coupling tests were in good agreement with experimental results except for the vertical accelerations of the cask. In the following reporting period,⁽²¹⁾ ENSCO, Inc. completed a study to provide parameter data on the railway equipment used in the coupling tests at SRL. These data were inserted in the CARDS model to establish a base case for model validation and for planned parametric and sensitivity analyses. Additional simulation runs were made to obtain new calculated results to be compared with the experimental results.

At first, the new data resulted in less agreement between the calculated and experimental results than had been obtained previously. The calculated and experimental values of the vertical acceleration of the cask at the far end did not show acceptable agreement when compared both visually and quantitatively. After modifications were made to the model, based on a review of high speed films of the tests and of system structural features, a dramatic improvement in the agreement was realized (especially in the visual comparisons). The high speed films of Test 3 showed that water was ejected from the collar around the cask at the far end at impact (rain water had collected under the collar during a rain storm the night before the test). It was also recalled that a rubber gasket or shim was used under the collar. This suggested that the rubber, or a gap, or both, could cause both an increase in the magnitude and frequency of the acceleration readings at the far end, precisely the characteristics needed to achieve agreement. Double integration of the measured accelerations gave displacements that confirmed this conclusion. Therefore, a nonlinear stiffness coefficient was devised for the rear tiedowns that was assumed to consist of a series combination of an initial gap between the cask and its collar, a rubber shim, and then the intended tiedown structure. A corresponding damping coefficient was also devised.

As in the preliminary assessment of Reference 20, the latest assessment of how well the CARDS model simulated the behavior of the cask-rail car system for the conditions of Test 3 of the SRL experiments was made by comparing, for two cases, both visually and quantitatively, the calculated and experimental values of coupler force, the longitudinal force of interaction between the cask and rail car, the horizontal acceleration of the rail car, the horizontal acceleration of the cask, the vertical acceleration of the cask at the far end, and the vertical acceleration of the cask at the struck end. Also, in this latest assessment, the calculated vertical displacements of the cask were compared to those obtained by double integration of the

measured vertical accelerations of the cask. In both cases, the coupler force was the force of excitation causing the system to vibrate. In the first case (Case 1), the experimentally measured coupler force was used. In the second case (Case 2), the coupler force used was that calculated by the CARDS model. Visual comparisons are presented in Figures 54 through 60 for Case 1, and in Figures 62 through 68 for Case 2. To supplement these comparisons, calculated vertical tiedown forces are presented in Figure 61 for Case 1, and in Figure 69 for Case 2. Quantitative comparisons of each pair of individual response variables were made using Theil's two-variable inequality coefficients. A simultaneous quantitative comparison of all the response variables was made using Theil's multiple inequality coefficient. The quantitative comparisons are summarized in Table 9. Theil's two-variable inequality coefficients and Theil's multiple inequality coefficient are discussed in Section 4.1.

The Theil's inequality coefficients in Table 9 show that good agreement between calculated and experimental results was obtained for all but the vertical accelerations. The vertical accelerations of the cask produced two-variable inequality coefficients above 0.5 (Theil's inequality coefficients are zero at perfect agreement and 1 at the poorest agreement). However, Figures 58, 59, 66 and 67 show that good visual agreement exists between the vertical accelerations. Both the magnitude and frequency of these plots are in good agreement. It appears, however, that better quantitative agreement could be obtained if the calculated vertical acceleration at the far end (Figures 58 and 66) could be made to shift ~ 0.025 second forward on the time scale, and if the calculated vertical acceleration at the struck end (Figures 59 and 67) could be shifted ~ 0.02 second backward on the time scale. Theil's multiple inequality coefficient for Case 1 is 0.059, and that for Case 2 is 0.214.

The plots of calculated vertical acceleration of the cask at the far end in Figures 58 and 66 are shaped by the nonlinear stiffness coefficient devised for the rear tiedowns. Initially, then the cask accelerates freely upward due to the loose fit of the collar, but then it soon encounters the rubber-cushioned collar and decelerates rapidly. The stiffness coefficient of the rubber shim varies with relative displacement; therefore, the frequency varies. The structural damping of the collar varies in a manner similar to that of the stiffness coefficient.

The vertical displacements of the cask are presented in Figures 60 and 68. These figures compare the calculated vertical displacements with those obtained by double integration of the measured vertical accelerations of the cask. Figure 60 presents the comparisons of Case 1 results, and Figure 68 the comparisons of Case 2 results. Both of these figures show good agreement up to about 0.1 second, and then the calculated and "experimental" displacement curves show substantial separation.

4.5.2 Comparison of Measured and Calculated Results for Tests 10 and 11

An assessment of how well the CARDS model simulates the behavior of the cask-rail car system for the conditions of Tests 10 and 11 was made by comparing the calculated and experimental values of the longitudinal force of interaction between the cask and rail car, the horizontal acceleration of the rail car, the horizontal acceleration of the cask, and the vertical acceleration of the cask at the far end. The coupler force measured during these tests was used as the force of excitation causing the system simulated by CARDS to vibrate. This coupler force is shown in Figures 70 and 76 for Tests 10 and 11, respectively.

The cask-rail car system used in Tests 10 and 11 consisted of a 70-ton cask mounted on a flat bulkhead rail car with standard couplers. (For test configurations and conditions, see Table 2 and Figure 32.) The cask used in these tests was a rectangular box-shaped 70-ton cask used for onsite shipments at SRL. The rail car was the same one used in Test 3. When the base of the cask was placed in contact with the bumper beams between the cask and the load cells, its vertical centerline (fore and aft) fell almost 8.0 feet forward [toward the struck end (SE)] of the rail car centerline. This offset placed the far end (FE) of the cask almost directly over the center of gravity of the rail car.

For Test 10, the calculated longitudinal force of interaction between the cask and rail car, the horizontal acceleration of the rail car, the horizontal acceleration of the cask, and the vertical acceleration of the cask at the far end are compared with corresponding experimental data in Figures 71, 72, 73 and 74, respectively. All of these response variables compare well with their experimental counterparts, except for the vertical acceleration of the cask at the far end. The peak values of the calculated vertical acceleration of the cask in Figure 74 are substantially lower than the peaks on the plot of the experimental data. There is evidence indicating that the experimental data may be in error. First, these vertical accelerations of the cask are compared, in Figure 74, to the calculated vertical acceleration of a point on the rail car over the trucks at the far end. The agreement between this calculated vertical rail car acceleration and the experimental data for the vertical acceleration of the cask is better than that between the calculated and experimental values of the vertical accelerations of the cask. This would mean that the far end of the cask was pitching as much as the far end of the rail car. This does not seem reasonable in view of the statement made earlier that the far end of the cask was located almost directly above the center of gravity (cg) of the rail car. There is rotation about the cg of the rail car, but the vertical motion of the rail car at this point is substantially less than that of the rail car over the trucks at the struck and far ends. The second piece of evidence which indicates that the experimental data from Test 10 may be in error is found by moving forward in the text to Figure 80 where the vertical acceleration of the cask at the far end, calculated for Test 11 conditions, is compared to the same vertical acceleration measured during Test 11. Figure 80 shows that very good agreement exists between the calculated and experimental values of this acceleration, and that they both differ substantially from a superimposed plot of

the vertical acceleration of a point on the rail car over the trucks at the far end. The only changes made to CARDS in proceeding from the simulation of Test 10 to the simulation of Test 11 were 1) the impact velocity was increased from 8.0 miles per hour to 11.2 miles per hour, and 2) the coupler force recorded during Test 11 (Figure 76) replaced that from Test 10 (Figure 70) as the force of excitation applied at the coupler. None of the structural parameters of the cask-rail car system were changed.

Two key assumptions were made when the parameters were prepared for insertion into CARDS for the simulation of Tests 10 and 11. First of all, it was assumed that the vertical components of the tiedowns were tight. This is in contrast to the simulation of the cask-rail car system of Test 3 where some looseness, and the installation of rubber bushings in the collar at the far end of the 40-ton Hallam cask, required the use of a nonlinear stiffness coefficient to represent the vertical component of the tiedown structure (see Section 4.5.1). The 70-ton cask used in Tests 10 and 11, unlike the 40-ton Hallam cask used in the rest of the tests, did not require a cradle structure that became part of the tiedown structure. The 70-ton cask was bolted directly to the rail car structure. The assumption of tight vertical tiedowns for Tests 10 and 11 appears to be justified by the good agreement between the calculated and experimental values of the vertical acceleration of the far end of the cask, for Test 11, as shown in Figure 80.

The horizontal component of the tiedowns, in Tests 10 and 11, consisted of a rigid welded stop to restrain the cask from moving longitudinally. Initially, it was assumed that the stiffness coefficient of this horizontal component was constant. Several values, ranging up to 5×10^6 lb/in., were tried; however, none of these trial simulations produced results that matched the experimental data. These simulations suggested that a nonlinear stiffness coefficient was required for the horizontal component of the tiedowns. Consequently, this was the second assumption made for the simulation of Tests 10 and 11. It was assumed that a constant stiffness coefficient of 1.0×10^5 lb(force)/in. was valid up to a relative displacement between the cask and rail car of ~ 0.2 in. and that, after this initial movement, the tiedowns yielded and could be represented by the nonlinear stiffness coefficient shown in Figure 75. This stiffness coefficient was established for Test 10 and used, without change, for the simulation of Test 11.

For Test 11, the calculated longitudinal force of interaction between the cask and rail car, the horizontal acceleration of the cask, and the vertical acceleration of the cask at the far end are compared with experimental data in Figures 77, 79 and 80, respectively. The calculated horizontal acceleration of the rail car is presented in Figure 78. In the comparisons for Test 10, this acceleration was compared to data from instrument 12. However, in Test 11 the data from instrument 12, and from all other instruments measuring the horizontal acceleration of the car, were not suitable for use, so no experimental data are shown in Figure 78. Except for the horizontal acceleration of the car, all of the response variables listed above compare well with the corresponding experimental data.

There is some uncertainty with regard to the measured coupler force shown in Figure 76. The experimental traces show that, from ~ 0.2 s to ~ 0.5 s, this coupler force leveled off at a value of $\sim 200,000$ lb(force) rather than 0. In contrast, the coupler force measured for Test 10 dropped to zero force after ~ 0.25 s. It is not known whether or not this failure to drop to zero, as would be expected, is due to a faulty instrument and, if so, at what point along the trace the instrument went awry. A comparison of the coupler force plots in Figures 70 and 76 suggests that the instrument for Test 11 might have experienced some difficulty at ~ 0.2 s.

The experimental acceleration data used in the above comparisons contained high frequency noise that had to be filtered out before the comparisons could be made. As indicated in Figures 72 through 74, and Figures 78 through 80, the horizontal acceleration data were filtered at 100 Hz and the vertical acceleration data at 50 Hz. Filtering of the high frequency noise components from these data was accomplished using the FFT (Fast Fourier Transform) program. (See Section 4.2.)

4.5.3 Comparison of Measured and Calculated Results for Tests 13, 16 and 18

The validation of the CARDS model was completed with the comparison of measured results from Tests 13, 16 and 18 with corresponding results calculated using the CARDS model.

An assessment of how well the CARDS model simulates the behavior of the cask-rail car systems used in these tests was made by comparing calculated and measured values of the horizontal force of interaction between the cask and rail car, the horizontal acceleration of the rail car, the horizontal acceleration of the cask, the vertical acceleration of the cask at the far end, and the vertical acceleration of the cask at the struck end. The coupler force measured during these tests was used as the force of excitation causing the system simulated by CARDS to vibrate. This coupler force is shown in Figures 85, 93 and 99 for Tests 16, 13 and 18, respectively.

The cask used in Tests 13, 16 and 18 was the 40-ton Hallam cask used in Test 3 (see Figure 32 and Table 2). Unlike the box-shaped 70-ton cask used in Tests 10 and 11, this cylindrical cask was mounted on and secured to a cradle structure that served as part of the tiedown structure. In Test 3, this cradle structure was fastened to a rail car with bolts, but in Tests 13, 16 and 18, it was fastened to a different rail car (a different one for each of these three tests) with cables. As reported in Section 4.5.1, good agreement between the calculated and experimental results for Test 3 was obtained only after allowance was made for slack in the vertical tiedown structure at the far end (opposite the struck end of the car). This slack, or looseness, in the tiedowns was evident in high speed films of Test 3. The films showed rain water being ejected from the collar at the far end of the cask at impact. Also, it was recalled that a rubber shim had been installed between the collar and the cask. When this gap and rubber shim combination was considered as part of the tiedown structure, and an appropriate nonlinear stiffness coefficient devised, good agreement between the

calculated and experimental results was obtained. This same nonlinear representation of the stiffness coefficient for the vertical component of the rear tiedowns was used, without change, in the simulations of Tests 13, 16 and 18.

In Tests 10 and 11, the 70-ton cask was bolted directly to the rail car. As shown in Figure 32 and Table 2, the same rail car was used in Tests 3, 10 and 11. This rail car was a Seaboard Coastline (SCL) flat, bulkhead car with standard couplers. For Tests 13 and 16, an 80-ton flat rail car with three-wheeled trucks was used. The 80-ton rail car was equipped with a standard coupler on one end for use in Test 16, and a 15-in. travel end-of-car (EOC) cushion device on the opposite end for use in Test 13. This latter car is referred to as the 80-ton Union Carbide car because the Union Carbide Corporation converted it for transporting canisters placed in a welded, "saw-toothed" rack superstructure added to the top of the car.⁽²²⁾ For Test 18, a SCL flat bulkhead car with a cushion underframe coupling mechanism was used. The principal difference between this car and the one used in Tests 3, 10 and 11 was in the coupling mechanism used.⁽²²⁾

The CARDS model is a complex two-dimensional, multi-degree-of-freedom model that determines the horizontal, vertical and rotational motion of both the cask and its rail car following impact with an anvil train during coupling operations. Results of a parametric and sensitivity analysis, using CARDS and the cask-rail car configuration of Test 3, showed that the relative vertical and rotational accelerations (of the cask relative to the rail car) are highly sensitive and sensitive, respectively, to the horizontal distance between the cgs of the cask and rail car. (See Section 5.0, PARAMETRIC AND SENSITIVITY ANALYSIS.) This horizontal distance, given the parameter name l_{OCR} in Section 5.0, is highlighted in Figures 2 and 81 through 84. Figures 81, 82, 83 and 84 are sketches of the cask-rail car configurations used in Tests 3 and 18, 10 and 11, 13, and 16, respectively. These figures identify not only l_{OCR} and the casks and rail cars used in the tests, but also the types of couplers and tiedowns used.

The simulations of Tests 13, 16 and 18 were initially guided by comparisons of measured and calculated values of the horizontal force of interaction between the cask and the rail car. In the CARDS model, this force is defined by the equation,

$$DUSLF = -(k_{S1} + k_{S4}) [(X_{RC} + Z_{RC} \theta_{RC}) - (X_p - Z_p \theta_p)] \quad (229)$$

where:

$$DUSLF = \text{Horizontal interaction force [lb(force)]}$$

k_{S1} and k_{S4} = Stiffnesses of the horizontal components of the rear and front tiedowns, respectively, between the cask and rail car [lb(force)/in.]

X_{RC} = Horizontal displacement of the cg of the cask-rail car (in.)

X_p = Horizontal displacement of the cg of the cask or package (in.)

Z_{RC} = Vertical distance from the horizontal centerline of the cask-rail car to its top and bottom surfaces (in.)

Z_p = Vertical distance from the horizontal centerline of the cask to its top and bottom surfaces (in.)

θ_{RC} = Angle of rotation of the X_{RC} and Y_{RC} axes about an axis perpendicular to the $X_{RC} - Y_{RC}$ plane through the cg of the rail car (rad)

θ_p = Angle of rotation of the X_p and Y_p axes about an axis perpendicular to the $X_p - Y_p$ plane through the cg of the cask or package (rad)

Initial comparisons revealed poor agreement between the calculated and measured values of this force. Specifically, after the peak forces following the impact pulses of Tests 13 and 16, the calculated results included some substantial negative values of this force while the measured results included only a few small negative values.

Of the three tests, Test 16 was the most similar to Test 3, a test simulated successfully earlier in the study (see Section 4.5.1). The horizontal interaction force calculated for Test 3 did not show this tendency to negative values, so it was concluded that reasons for the differences in the results might be found by examining the differences in the cask-rail car systems used in these two tests. The primary differences between the cask-rail car systems of Test 3 and Test 16 are (see Figures 32, 81 and 84 and Table 2):

- 1) A 70-ton SCL flat, bulkhead rail car was used in Test 3. In Test 16 the 80-ton Union Carbide rail car was used. Both of these tests were conducted with standard couplers.
- 2) In Test 3, the cg of the cask was located 49.0 in. forward of the cg of the rail car. In Test 16, the cg of the cask was located 18.25 inches aft of the cg of the rail car (see Figures 81 and 84)
- 3) Bolted tiedowns were used for vertical restraint in Test 3. In Test 16, cable tiedowns were used.

The major difference between the cars used was in the car weights. The average weight of the loaded 80-ton Union Carbide car (designated as OROX805), based on weights measured prior to Tests 6 through 9 and Tests 12 through 16, is 160,105 lb. Only the 40-ton cask was used with this car, so subtracting the weight of this cask gives a car weight (which includes the cask cradle) of about 80,105 lb. The 70-ton SCL rail car used in Tests 1 through 5 and in Tests 10 and 11 was designated as ACL78498. The loaded weight of this car, measured prior to Tests 10 and 11, was 222,920 lb. Subtracting the weight of the 70-ton cask gives a car weight of about 82,920 lb. This means that the rail car used in Test 16 was about 3.4% lighter than the rail car used in Test 3. A lighter car would decelerate faster, resulting in less horizontal displacement of the car (i.e., X_{RC} in Equation (229) would be smaller). This would produce a greater tendency toward negative values of the horizontal interaction force; however, it was felt that the difference in the car weights was too small to account for the large negative values obtained from the model.

The location of the cask along the length of the rail car has little effect on the horizontal force of interaction. This is evident from the results of the parametric and sensitivity analysis reported in Section 5.0. In Figures 130 and 131, the horizontal distance between the vertical centerlines of the cask and rail car, l_{OCR} , is listed in the eighth and tenth positions, respectively, out of ten parameters ranked according to their influence on the horizontal tiedown force. The only parameters ranked below l_{OCR} (that is, in positions indicating less influence) are the stiffness coefficients of the vertical components of the tiedowns, and two composite parameters representing variations of these coefficients.

The remaining difference between the cask-rail car systems of Tests 3 and 16 that might account for the differences in the calculated values of the horizontal interaction force is in the type of tiedowns used. The effect of the type of tiedowns used on the horizontal interaction force is primarily due to the stiffness coefficients of the horizontal components of the tiedowns [see Equation (229)]. It was reasoned that, because cables instead of bolts were used for vertical restraint in Test 16, the cask (and its cradle) apparently tended to shift longitudinally during impact and did not return to its original position. This was because the restoring "spring" action or "chocking" effect of the vertically oriented bolts was missing. Instead, energy was dissipated during the shifting of the cask.

The equations in the CARDS model that define the stiffness coefficients of the horizontal components of the tiedowns were modified to account for this loss of energy due to shifting of the cask. Previously, these stiffness coefficients were computed in a calculation sequence that set the coefficients either to their high or low values, or to the sum of their high and low values, depending upon conditions related to the movement of the cask (and its cradle). This procedure was retained, but the values computed were modified as follows. Let the unmodified values be expressed as

$$k_{S1} = f_1[k_{S1}(\text{low}), k_{S1}(\text{high})] \quad (230)$$

and

$$k_{S4} = f_4[k_{S4}(\text{low}), k_{S4}(\text{high})] \quad (231)$$

These coefficients were modified using the expressions

$$k_{S1}(\text{new}) = k_{S1}(\text{old}) \left[1 + M_{kS1} \text{sgn} \left(\frac{dx_{RPRC}}{dt} \right) \right] \quad (232)$$

and

$$k_{S4}(\text{new}) = k_{S4}(\text{old}) \left[1 + M_{kS4} \text{sgn} \left(\frac{dx_{RPRC}}{dt} \right) \right] \quad (233)$$

where:

$$\frac{dx_{RPRC}}{dt} = \text{Relative velocity of cask-rail car combination (in./s)}$$

$$= \frac{dx_P}{dt} - \frac{dx_{RC}}{dt}$$

$$\frac{dx_P}{dt} = \text{Velocity of the cask (in./s)}$$

$$\frac{dx_{RC}}{dt} = \text{Velocity of the rail car (in./s)}$$

M_{kS1} and M_{kS4} = Energy dissipation factors for k_{S1} and k_{S4} , respectively

$\text{sgn}(A)$ = Sign function

$$= \begin{cases} +1, & A > 0 \\ -1, & A = 0 \\ -1, & A < 0 \end{cases} \text{ where } A = \frac{dx_{RPRC}}{dt}$$

The values of the energy dissipation factors used depend upon the conditions encountered and imposed, i.e.,

$$\begin{aligned}
 M_{kS1} &= M_{kS1F} \left[\text{if } \frac{dx_{RPRC}}{dt} < 0 \text{ and cable tiedowns used} \right] \\
 M_{kS1} &= 0 \quad \text{[otherwise]}
 \end{aligned} \tag{234}$$

Similarly,

$$\begin{aligned}
 M_{kS4} &= M_{kS4F} \left[\text{if } \frac{dx_{RPRC}}{dt} < 0 \text{ and cable tiedowns used} \right] \\
 M_{kS4} &= 0 \quad \text{[otherwise]}
 \end{aligned} \tag{235}$$

M_{kS1F} and M_{kS4F} = Arbitrary factors currently set at 0.5

The above representation of the stiffness coefficients in CARDS produced a good comparison of the calculated and measured values of the horizontal force of interaction between the cask and rail car of Test 16 (see Figure 86), and reasonable agreement in comparisons of four additional response variables (see Figures 87, 88, 89 and 90).

When the above equations and factors were used, without change, to determine the stiffness coefficients k_{S1} and k_{S4} for Tests 13 and 18, improvements in the comparisons of the calculated and measured results for these tests were also realized (see Figures 93 through 104).

The stiffness coefficients defined by Equations (232) and (233) generate hysteresis-type curves. Figure 91 is a load-deflection curve generated for the horizontal component of the tiedown at the far end during the simulation of Test 16, and Figure 92 is the corresponding plot of the stiffness coefficient k_{S1} as a function of the relative displacement, $X_p - X_{RC}$.

Figure 87 shows three plots of the horizontal acceleration of the rail car during Test 16. The solid line is a plot of the calculated acceleration, the dashed line is a plot of the measured acceleration, and the dash-dot line is a plot of the calculated acceleration of the rail car with no cask. The calculated and measured values of the acceleration of the loaded rail car show poor agreement. During the peak pulse, the calculated acceleration is only about one-fourth of the measured acceleration. The peak acceleration of the unloaded rail car is about one-half that of the measured acceleration during the same time period. There is strong evidence that suggests that the measured values of the acceleration may be in error. In Figure 33, values of the horizontal acceleration of the loaded rail car, measured during Test 3, were compared with calculated values for both the loaded and unloaded

rail car (an unloaded rail car is defined as one without both the cask and the trucks). The purpose of this earlier comparison of results was to show that the horizontal motion of the cask strongly influences the horizontal motion of the rail car. These earlier comparisons showed that the calculated and measured results for the "loaded" system compare very well, and that the deceleration of the "isolated" or "unloaded" rail car is substantially greater. It was also shown that the deceleration of the unloaded car follows the coupler force curve. When the results in Figure 87 are compared with those of Figure 33, the following facts may be noted:

- 1) The measured and calculated accelerations in Figure 33 are in very close agreement
- 2) The peak calculated accelerations of both the loaded and unloaded rail cars in Figure 87 are consistent with those in Figure 33
- 3) The calculated accelerations of the unloaded rail car in Figures 87 and 33 follow the respective coupler force curves for Tests 16 and 3
- 4) The coupler force curves for Test 3 (see Figure 54) and for Test 16 (see Figure 85) are not identical, but they are very similar and their peak values are in the neighborhood of 1.1×10^6 lb(force).

In addition to these facts, further evidence is suggested by the comparison of the measured and calculated values of the horizontal acceleration of the cask in Figure 88. This figure shows that very good agreement between the measured and calculated values was realized. It seems doubtful that such good agreement could be obtained for the horizontal acceleration of the cask while the measured and calculated values of the horizontal acceleration of the rail car show such poor agreement. It was shown earlier, in Section 1.2, CASK-RAIL CAR RESPONSE SPECTRUM GENERATOR (CARRS), that the horizontal motion of the cask strongly influences the horizontal motion of the rail car.

Measured and calculated values of the vertical acceleration of the cask at the far end are compared in Figure 89. Only fair agreement was realized since the peak values of the calculated acceleration are about 50% or 60% greater than the measured accelerations, and the frequency is lower. However, the calculated results appear to be consistent with the corresponding results for Test 3 (see Figure 58), while the measured results are about a factor of 2 less than those obtained from Test 3. The press of time ruled out an in-depth analysis of these differences that might have led to their verification or to some justification for modifications to the model that would have produced better agreement.

Figure 90 compares measured and calculated values of the vertical acceleration of the cask at the struck end. Here again, only fair agreement was realized. Comparisons with Test 3 results, in this case, do not show any

resemblance or consistency. In fact, it appears that there is better agreement between the measured and calculated values for Test 16 than there is between corresponding values from Test 16 and Test 3. For example, the frequencies of both the measured and calculated values of Test 16 are higher than those of Test 3, and are consistent with one another. However, the frequency of the calculated results is higher than that of the measured results.

Although time did not permit an in-depth analysis to find a reason for the differences in the vertical accelerations of the cask obtained for the cask-rail car systems used in Tests 3 and 16, it should be pointed out again that one of the three primary differences between the cask-rail car systems used in these tests is the parameter l_{OCR} , the horizontal distance between the vertical centerlines of the cask and rail car. In Test 3, the cg of the cask was located 49.0 in. forward of the cg of the rail car whereas, in Test 16, the cg of the cask was located 18.25 in. aft of the cg of the rail car (see Figures 81 and 84). It is not certain what effect this has on the vertical accelerations; however, the results of the parametric and sensitivity analysis show that both the maximum absolute relative vertical acceleration of an equivalent single-degree-of-freedom model of the cask-rail car system of Test 3 and the maximum vertical acceleration of its support are highly sensitive to l_{OCR} (see Table 17 and Figures 125 and 128).

It was stated earlier that when Equations (230) through (235) and the arbitrary factors M_{KS1F} and M_{KS4F} were used, without change, to determine the stiffness coefficients k_{S1} and k_{S4} for the cask-rail car systems used in Tests 13 and 18, improvements in the comparisons of the calculated and measured results for these tests were also realized. For these tests, time did not permit further analysis beyond this stage; consequently, comparisons of measured and calculated values of response variables for these tests are presented, as developed, in Figures 94 through 104. Figures 94 through 104 show that, even though no further work was done, the calculated and measured results for these tests are in reasonable agreement.

5.0 PARAMETRIC AND SENSITIVITY ANALYSIS

A parametric and sensitivity analysis was conducted to identify those parameters that significantly affect the normal shock and vibration environment and the response of the cask-rail car system. Frequency response spectra were generated for the horizontal, vertical and rotational accelerations of a radioactive material shipping package (cask) relative to the accelerations of its support (rail car). Generation of the response spectra was coupled to a parametric and sensitivity analysis to assess the effects on the response spectra (and on selected response variables) of varying certain selected parameters.

Parameters are usually varied to study the effect on one or more response variables (RV) or figures of merit (FOM). This is termed a parametric analysis. A parametric analysis is usually coupled to a sensitivity analysis. The objectives of a sensitivity analysis are to arrive at a measure of how sensitive the RVs or FOMs are to changes in the parameters, and to rank the parameters according to their influence on the RVs or FOMs. The determination of the response spectra, an assessment of the changes in these spectra due to the variation of the parameters, and the identification of the most influential parameters constitutes a parametric and sensitivity analysis. Details of the sensitivity analysis and the ranking of parameters will be presented and discussed later.

Equivalent single-degree-of-freedom (1-DOF) equations of motion (EOMs) were derived to generate the response spectra [see Section 1.2, CASK-RAIL CAR RESPONSE SPECTRUM GENERATOR (CARRS)]. These 1-DOF EOMs have forcing functions on their right-hand sides that are equivalent to the motions of a support (or shaker table in a testing facility). These support motions, and the 1-DOF EOMs, are derived from the equations of motion used in the CARDS model. (See Sections 1.1 and 1.2.)

Parameters are varied in the CARDS model to produce "support" accelerations as functions of time. These time-varying support motions are then used in the 1-DOF EOMs of the CARRS model to generate the horizontal, vertical and rotational accelerations of the cask relative to the actual acceleration of the rail car. The actual rail car acceleration is not the same as the support acceleration. Detailed derivations of the horizontal, vertical and rotational accelerations of the support, along with derivations of the 1-DOF EOMs in terms of the corresponding relative accelerations, are presented in Section 1.2.

Frequency response spectra were generated using the CARRS model (Section 1.2) and results obtained from the CARDS model (Section 1.1). Two sets of response spectra were generated. The first set, designated as "preliminary", was generated for five preliminary or exploratory cases. A second set of response spectra, designated as "requested", was generated for 23 cases (in addition to a base case) based on conditions and parameters specified or requested by the US Nuclear Regulatory Commission. The five "preliminary"

cases are defined in Table 10, and the "requested" cases are defined in Tables 11 through 13. The procedure used to generate the response spectra, using CARDS and CARRS, is described in Section 1.2.

The cask-rail car system simulated by CARDS for the parametric and sensitivity analysis was the Test 3 configuration shown in Figures 1 and 81.

The preliminary cases defined in Table 10 differ due to only three of the conditions listed. The only difference between Cases 1 and 2 is due to the condition of the rear tiedowns. Case 1 represents the actual condition of the rear tiedowns in Test 3 of the coupling tests conducted at SRL. It was stated earlier in Section 4.5.1 that ENSCO, Inc. had completed a study to provide parameter data on the railway equipment used in the coupling tests conducted at SRL. These data were used to establish the base case for the simulation of Test 3 using the CARDS model. After experiencing difficulty in matching the vertical acceleration of the cask at the far end (as determined using the CARDS model) with that measured during the test, high speed films of Test 3 were examined for some indication of the reason for the mismatch. The films showed that water (rain water collected during a rain storm the previous night) was ejected from the collar around the cask at the far end. It was also recalled that a rubber bushing or liner had been installed between the cask and the collar. These conditions indicated a possible loose fit between the cask and the collar. Because this cask and collar combination is part of the tiedown system at the far end, it was concluded that the mismatch of results was due to looseness in the rear tiedowns. This was confirmed by integrating the cask acceleration recorded during the test twice with respect to time to get cask displacement, and then comparing this displacement to the calculated displacement (see Figures 60 and 68). It was found that the calculated displacement matched the "integrated-measured" displacement reasonably well only by assuming an initial "free" or loose rear tiedown, followed by contact with a rubber bushing, and finally followed by "solid" contact with rubber compressed against the collar.

Case 2 in Table 10 represents a condition where neither slack nor a rubber bushing exists in the rear tiedowns, i.e., the rear tiedowns are as tight as the front tiedowns. This case is, in effect, the base case for Cases 1, 3, 4 and 5. Case 2 represents a set of conditions including:

- 1) No looseness in the vertical component of the rear (or front) tiedowns
- 2) The cask centerline is positioned 4 ft forward of the rail car centerline
- 3) The time-varying coupler force is that measured during the SRL tests
- 4) Damping in the equations of motion in the CARDS model includes both viscous (structural) damping and damping due to friction opposing the horizontal motion of the cask relative to the rail car

- 5) Damping in the 1-DOF EOMs in the CARRS model is the same as of Condition (4) above.

Case 3 differs from Case 2 due to a change in Condition 5) above, i.e., there is no damping of any kind in the 1-DOF EOMs in CARRS. The only difference between Case 4 and Case 2 is also due to a change in Condition 5), however, in Case 4, there is viscous (structural) damping only. Finally, Case 5 differs from Case 2 due to Condition 2), i.e., the cask is centered fore and aft on the rail car rather than being shifted 4 ft forward of this position, as in the SRL tests.

Results for the "preliminary" cases are presented in the form of "support" accelerations as functions of time, and maximum absolute relative (MAR) accelerations as functions of frequency. The MAR accelerations are the response spectra.

The support accelerations [defined by Equations (203), (206), and (216)] for the preliminary cases defined in Table 10, calculated by CARDS, are presented in Figures 105, 106 and 107. Figure 105 is a plot of the horizontal acceleration of the support for the equivalent 1-DOF system, as a function of time, for Cases 2, 3 and 4. Figures 106 and 107 are the corresponding plots for the vertical and rotational accelerations of the support, respectively. The support accelerations for Cases 1 and 5 are different than those shown in Figures 105, 106 and 107 because the differences in Conditions (1) and (2) in Table 10 required separate CARDS simulations, which produced different results. The support accelerations of Figures 105, 106 and 107 are presented as typical examples of the RHS forcing functions used in the 1-DOF EOMs in CARRS.

The response spectra generated by the CARRS model, for the "preliminary" cases defined in Table 10, are presented in Figures 108, 109 and 110. Figure 108 consists of plots of the maximum absolute relative (MAR) horizontal acceleration of the equivalent 1-DOF system as a function of frequency [see Equation (161)]. Figures 109 and 110 are the corresponding frequency plots of the maximum absolute relative vertical and rotational accelerations, respectively. In Figure 108, Cases 3 and 5 produce almost identical plots with the highest accelerations over the range of frequencies considered. These plots have a common maximum value of the maximum (maximax) absolute relative horizontal acceleration of about 8500 in./s^2 at a frequency of 250 rad/s. The significance of the identical plots produced by Cases 3 and 5 is that the only difference between these cases is the positioning of the cask on the rail car (see Table 10). Case 3 has the cask centerline positioned 4 ft forward of the rail car centerline, while Case 5 has the cask centered fore and aft. The conclusion may be drawn that this difference in the location of the cask on the rail car has little effect on the maximum absolute relative horizontal acceleration over the range of frequencies considered. However, the location of the cask on the rail car has a great effect on the maximum absolute relative vertical acceleration, as shown in Figure 109. A maximax absolute relative vertical acceleration of about

at a frequency of 50 rad/s, is obtained for Case 3, while the maximum (not maximax) absolute relative vertical acceleration obtained for Case 5 is less than 100 in./s² over the entire frequency range. It should be pointed out here that these accelerations are the relative vertical accelerations of the cg of the cask relative to the cg of the rail car. There are higher relative vertical accelerations at other locations on the cask. Results from the CARDS model show that, for the centered cask case (Case 5), the absolute relative vertical accelerations of the cask at the tiedown attachment points are ~280 in./s², while the corresponding absolute relative vertical acceleration at the cg is ~62 in./s². The absolute relative vertical accelerations at the tiedown attachment points are almost 5 times greater than the corresponding accelerations at the cg.

The plots for Cases 1 and 2 in Figure 108 are close together, which indicates that looseness in the vertical component of the rear tiedowns has little effect on the maximum absolute relative horizontal acceleration. In contrast, the plots for Cases 1 and 2 in Figure 109 are widely separated, indicating that this looseness in the rear tiedowns produces significantly higher values of the maximum absolute relative vertical acceleration at all frequencies. Vertical looseness in the rear tiedowns also produces substantially greater maximum absolute relative (MAR) rotational accelerations, as shown in Figure 110. Figure 110 shows widely separated plots for Cases 1 and 2, with Case 1 having the higher accelerations over the range of frequencies considered.

The effect of frictional damping opposing the horizontal motion of the cask relative to the rail car is illustrated by the plots for Cases 2 and 4 in Figures 108, 109 and 110. In Figure 108, separation of the plots for Cases 2 and 4 shows that frictional damping decreases the MAR horizontal acceleration over most of the frequency range. The lower plot in Figure 108 consists of the results for Case 2, the case where frictional damping is present along with viscous (structural) damping. The results of Case 4 are presented as the upper plot in Figure 108. This case has viscous damping but no frictional damping. Frictional damping has little effect on the MAR vertical acceleration and on the MAR rotational acceleration, as indicated by the superposition of points on the plots for Cases 2 and 4 in Figures 109 and 110, respectively.

The 23 cases "requested" are defined in Tables 11, 12 and 13. These cases are defined in terms of the requested conditions in Table 11, and in terms of the requested parameters in Tables 12 and 13. The parameters used in the definitions of Tables 12 and 13 are defined in NOMENCLATURE OF TERMS, Appendix I. Some of these parameters are also shown in Figure 2, 3 and 4. It should be noted that, among the conditions specified in Table 11, the coupler force used for all the cases was that measured during Test 3 of the humping tests.

Table 11 shows that the conditions are the same for all the "requested" cases and that, except for one condition, the cases would be the same as "preliminary" Case 4. The requested cases do not include frictional damping opposing the horizontal motion of the cask relative to the rail car in the EOMS in the CARDS model.

The requested parameters were divided into two groups. The first group consists of five parameters designated as "pure" parameters. The second group contains eight parameters designated as "composite" parameters. The group of pure parameters includes individual parameters, but has been extended to include sets of parameters that are closely related. The two sets included in this group are $\{k_x\}$, a set of stiffness coefficients consisting of those for the horizontal components of the rear and front tiedowns and $\{k_y\}$, a set of stiffness coefficients consisting of those for the vertical components of the rear and front tiedowns. Composite parameters consist of unrelated parameters, or related parameters that are varied by differing amounts. For example, the composite parameter CP1 defined in Table 13 consists of the stiffness coefficients of both the horizontal and vertical components of the tiedowns. The stiffness coefficients of these components are considered to be unrelated because of their differences in orientation. Pure parameters and definitions of their cases are presented in Table 12. Composite parameters and definitions of their cases are presented in Table 13.

The definitions of the cases are expanded in Table 14 in terms of the numerical values of the parameters. It should be noted that there are high and low values of the stiffness coefficients of the horizontal components of the tiedowns. The low value represents the stiffness coefficient of a tiedown consisting of such devices as cables, chains, bolts, etc, which provide constraint while the cask and frame combination is free to move between chocks. The high value represents the stiffness coefficient of a chock. The actual stiffness coefficient used when the chock is encountered is a combination of these two values.

The results for the "requested" have been presented in the form of "support" accelerations as functions of time, and MAR accelerations as functions of frequency. In addition, the forces in the horizontal and vertical components of the tiedowns at both the struck and far ends have been presented as functions of time. The horizontal, vertical and rotational accelerations of the "support" were presented as functions of time (for the base case and Cases 1, 2, C, D, and 3 through 8) in Figures 2 through 16 in Reference 23, and (for the base case and Cases 9 through 21) in Figures 2 through 19 in Reference 24. The forces in the tiedowns, for Cases 1, 2, C, D, and 3 through 21, were presented as functions of time in Figures 20 through 63 in Reference 24. The MAR accelerations were presented as functions of frequency (for the base case and Cases 1, 2, C, D, and 3 through 8) in Figures 17 through 31 in Reference 23, and (for the base case and Cases 9 through 21) in Figures 64 through 81 in Reference 24. Only those plots for the base case and Cases 7 and 8 are presented here as examples. The bulk of the results will be summarized later in some special tables and figures.

The support accelerations (for the base case and Cases 7 and 8), as functions of time, are presented in Figures 111, 112 and 113, and the corresponding tiedown forces are presented in Figures 114 through 117. The corresponding MAR accelerations as functions of frequency (the response spectra) are shown in Figures 118, 119 and 120.

In Reference 23, plots of the MAR horizontal accelerations as functions of frequency are presented in Figures 17, 20, 23, 26 and 29. Corresponding plots of the MAR vertical accelerations are presented in Figures 18, 21, 24, 27 and 30, and the corresponding MAR rotational accelerations are presented in Figures 19, 22, 25, 28, and 31.

Figure 20 in Reference 23 is almost identical to Figure 26 of the same reference, which indicates that Cases C and D produce MAR horizontal accelerations nearly equal to those produced by Cases 5 and 6. Tables 12, 13 and 14 show that, in Cases C and D, the stiffness coefficients of both the horizontal and vertical components of the tiedowns were varied and that, in Cases 5 and 6, only the stiffness coefficients of the horizontal components were varied. This indicates that the stiffness coefficients of the vertical components have little, if any, effect on the MAR horizontal acceleration. In Figure 29 of Reference 23, the plots for the base case and Cases 7 and 8 are very close together. Tables 13 and 14 show that the only parameters varied in Cases 7 and 8 were the stiffness coefficients of the vertical components of the tiedowns. Therefore, this confirms the previous conclusion that these coefficients have little effect on the MAR horizontal accelerations.

Figures 21 and 30 in Reference 23, although far from identical, are similar. These figures contain plots of the MAR vertical acceleration vs frequency for the base case and Cases C and D, and Cases 7 and 8, respectively. The similarity of these plots is an indication that a similarity exists between Cases C and D and Cases 7 and 8. Tables 12, 13 and 14 show that, in Cases C and D, the stiffness coefficients of both the horizontal and vertical components of the tiedowns were varied and that, in Cases 7 and 8, only the stiffness coefficients of the vertical components of the tiedowns were varied. It may be concluded from this that the MAR vertical acceleration is moderately affected by the stiffness coefficients of the horizontal components of the tiedowns.

Figure 28 in Reference 23 contains plots of the MAR rotational acceleration for the base case and Cases 5 and 6. These plots, although not identical, are close together compared to those in Figures 19, 22, 25 and 31 in the same reference. Recalling that, in Cases 5 and 6, only the stiffness coefficients of the horizontal components of the tiedowns were varied, this indicates that these coefficients only moderately affect the MAR rotational acceleration. This may be confirmed by comparing Figures 22 (Cases C and D) and 31 (Cases 7 and 8) of Reference 23. This comparison suggests that Cases C and D produce nearly the same results as those obtained from Cases 7 and 8. The only parameters that are not common to these two sets of cases are the stiffness coefficients of the vertical components of the tiedowns.

A crossover or change of position of the plots, over the range of frequencies considered, is evident in Figures 17, 20, 23, 26, 27 and 28 in Reference 23. This change of position also occurs over a very short frequency span at the high frequency range in Figure 21 (Reference 23). As an example of how the plots change position, consider Figure 23 (Reference 23). In this figure,

over the range of frequencies from 2 rad/s to ~ 100 rad/s, Case 3 is represented by the lower plot and Case 4 by the upper plot. Between 100 rad/s and 130 rad/s, the plot representing the base case becomes the upper plot, and the Case 4 plot becomes the middle plot. Over the frequency range between 130 rad/s and 260 rad/s, the Case 3 plot becomes the upper plot, the Case 4 plot becomes the lower plot, and the base case plot occupies the middle position again. It is not clear at this time whether this changing of position is due to the frequency used in the 1-DOF EOMs in CARRS or whether it is due to the variation in the support accelerations produced by CARDS for the various cases.

The MAR acceleration plots in References 23 and 24 are the acceleration response spectra for paired cases compared to the base case. These spectra are concentrated on three plots (presented in this report as Figures 121, 122 and 123), one for each of the three MAR accelerations, to show how the various spectra lie with respect to a band bounded by $\pm 50\%$ values of the base case spectra. The horizontal spectra are well behaved, that is, all of the spectra lie within the band; however, the vertical and rotational spectra do not conform as well. Seven cases fall outside the band for the vertical spectra, and ten cases fall outside the band for the rotational spectra. These cases, and the parameters they represent, are:

Vertical Spectra		Rotational Spectra	
Case	Parameter	Case	Parameter
C	CP1	C	CP1
7	$\{k_y\}$	D	CP1
8	$\{k_y\}$	3	CP2
11	$\&_OCR$	4	CP2
13	CP6	7	$\{k_y\}$
18	$\&_OCR$	10	CP4
19	$\&_OCR$	11	$\&_OCR$
		13	CP6
		20	CP8
		21	CP8

These cases and their parameters are defined in Tables 12 and 13. It should be noted that, for the vertical spectra, the "pure" parameters $\{k_y\}$, $\&_OCR$, $\&_{PR}$ and $\&_{PF}$ seem to be dominant since CP1 consists of $\{k_y\}$ and the less dominant $\{k_x\}$ while CP6 consists of $\&_{PR}$ and $\&_{PF}$ for a cask centered on the rail car. The same "pure" parameters appear to be dominant for the rotational spectra. The additional parameters affecting the rotational spectra are CP2, which consists of $\{k_y\}$ and the less dominant $\{k_x\}$ and W_p , CP4 which consists of the elements of $\{k_y\}$ varied individually, and CP8 which consists of $\{k_y\}$, $\{k_x\}$, W_{p_x} and the stiffness coefficients of the horizontal and vertical components of the springs between the rail car and its trucks.

In the last five paragraphs, an attempt was made to interpret the differences evident in the response spectra of Figures 17 through 31 (in Reference 23) in terms of the parameters varied. A better picture of the effects due to variation of the parameters was obtained for these and subsequent simulations from a sensitivity analysis. As stated earlier, parameters are usually varied to study the effects on one or more response variables (RV) or figures of merit (i.e., a parametric analysis). It was also stated that a parametric analysis is usually coupled to a sensitivity analysis. The objectives of a sensitivity analysis are to arrive at a measure of how sensitive the RVs are to changes in the parameters, and to rank the parameters according to their influence on the RVs.

A sensitivity analysis was used to determine the sensitivities of selected RVs to parameter variations. Results of this sensitivity analysis are presented in Tables 15 through 19 of this report, in Figures 32 through 41 in Reference 23, and in Figures 85 through 111 in Reference 24. For this sensitivity analysis, three sets of RVs were chosen:

- 1) The peak (or maximum) absolute values of the support accelerations determined by the CARDS model, i.e., $|\ddot{X}_s|_{\max}$, $|\ddot{Y}_s|_{\max}$ and $|\ddot{\theta}_s|_{\max}$
- 2) The maximum values of the maximum absolute relative accelerations (or "maximax" absolute relative accelerations)* determined by the CARRS model, i.e., $|\ddot{X}_d|_{\max}$, $|\ddot{Y}_d|_{\max}$ and $|\ddot{\theta}_d|_{\max}$
- 3) The peak or maximum values of the forces in the horizontal components of the tiedowns ($DUS1_{\max}$ and $DUS4_{\max}$) and in the vertical components of the tiedowns ($DUS3_{\max}$ and $DUS3_{\max}$), as determined by the CARDS model.

Absolute peak support accelerations were selected as RVs for the sensitivity analysis because the support accelerations are the only output variables produced by the CARDS model that are used in the CARRS model. They are, in fact, essential variables because they are the forcing functions on the RHSs of the 1-DOF EOMs of the CARRS model [see Equations (145), (161) and (212) in Section 1.2]. The effects of changes in the parameters used in CARDS are propagated through the support accelerations to the 1-DOF EOMs in CARRS. The maximax absolute relative accelerations were selected as RVs because they

*The response spectra of Figures 17 through 81 in Reference 23 and Figures 64 through 81 in Reference 24 are obtained by plotting the maximum absolute values of the relative accelerations obtained from CARRS runs for each of the frequencies shown. The maximax absolute relative accelerations are the maximum values of the maximum absolute relative accelerations plotted in Figures 17 through 31 (Reference 23) and Figures 64 through 81 (Reference 24).

represent the ultimate FOMs of the study, i.e., the response spectra of the cask-rail car system (represented as an equivalent 1-DOF system in CARRS) resting upon a support with accelerations (motions) determined by CARDS. The maximum forces in the tiedown components were selected as RVs because they represent the loads imposed on the tiedowns due to the parameter changes.

The sensitivity of a RV to changes in the parameters may be defined in a number of ways. In this study, the sensitivity is expressed as the contribution of each parameter to the total change in a RV, i.e.,

$$\Delta(RV) = \left[\frac{\partial(RV)}{\partial P_1} \right] \Delta P_1 + \left[\frac{\partial(RV)}{\partial P_2} \right] \Delta P_2 + \dots + \left[\frac{\partial(RV)}{\partial P_n} \right] \Delta P_n \quad (236)$$

where:

$\Delta(RV)$ = Total change in the RV

ΔP_n = Variation or change of the n-th parameter about its base case value

Terms in brackets = Influence coefficients (partial derivatives)

Influence coefficients are defined as the rate of change of a RV with respect to a parameter, say P_1 , obtained by varying P_1 about its base case value while holding all other parameters at their base case values, i.e.,

$$\left[\begin{array}{l} \text{Coefficient of Influence} \\ \text{of Parameter } P_1 \text{ on} \\ \text{Response Variable RV} \end{array} \right] = \left[\frac{\partial(RV)}{\partial P_1} \right]_{P_2, P_3, \dots, P_n} \quad (237)$$

The sensitivity of the RV to the parameter P_n is

$$\left[\begin{array}{l} \text{Sensitivity of RV} \\ \text{to Parameter } P_n \end{array} \right] = \left[\frac{\partial(RV)}{\partial P_n} \right] \Delta P_n \quad (238)$$

Normally, the variations in Equation (236) are taken to be very small; however, in studies of this type, extreme latitude is justified if the RV vs P plots are well-behaved and if piece-wise linear approximations are used.

In Figures 32 through 41 of Reference 23, Figures 95 through 111 in Reference 24, and in the example plots of Figures 134 through 136 in this report, the slope of a plot is an indication of the magnitude of the influence of the parameter ratio on the RV, and of the sensitivity of the RV to the parameter ratio. The greater the slope, the greater the influence of the parameter

and the greater the sensitivity. The plots in these figures are graphical representations of Table 15 since the values of the response variables plotted are those shown for the base case and the various cases defined in Tables 12, 13 and 14. The effects of the parameters on the RVs, expressed as influence coefficients and as the contribution of each parameter to the total change (sensitivity) in a RV, were determined using the results from Table 15 and the figures in References 23 and 24. In this study, influence coefficients were obtained by using a weighted average of the slopes of the straight line segments of plots equivalent to the appropriate figures in References 23 and 24 (and the example Figures 134 through 136). As an example, consider the coefficient of influence of the cask weight, W_p , on the absolute peak horizontal acceleration of the support, $|\ddot{X}_s|_{\max}$. The slope of the first line segment of an $|\ddot{X}_s|_{\max}$ plot equivalent to that in Figure 32 of Reference 23, but in terms of the cask weight rather than the ratio, is

$$\text{Slope Seg 1} \approx \left(\frac{\partial |\ddot{X}_s|_{\max}}{\partial W_p} \right) \{k_{S1}, k_{S4}\}, \{k_{S2}, k_{S3}\}, \text{ etc.} \quad (239)$$

Seg 1

$$= \frac{4189 - 4663}{(8 \times 10^4) - (4 \times 10^4)}$$

$$= -0.01185 \text{ in./[lb(force)} \cdot \text{s}^2]$$

The slope of the second line segment is

$$\text{Slope Seg 2} \approx \left(\frac{\partial |\ddot{X}_s|_{\max}}{\partial W_p} \right) \{k_{S1}, k_{S4}\}, \{k_{S2}, k_{S3}\}, \text{ etc.} \quad (240)$$

Seg 2

$$= \frac{3843 - 4189}{(1.6 \times 10^5) - (8 \times 10^4)}$$

$$= -0.004325 \text{ in./[lb(force)} \cdot \text{s}^2]$$

The approximate total influence coefficient for the combined line segments is taken to be the weighted average slope (WAS)

$$WAS = \left(\frac{\partial |\ddot{X}_s|_{\max}}{\partial W_p} \right) \{k_{S1}, k_{S4}\}, \{k_{S2}, k_{S3}\}, \text{ etc.} \quad (241)$$

WAS

$$= \frac{\left[\left(\frac{\partial |\ddot{X}_s|_{\max}}{\partial W_p} \right) \Delta W_p \right]_{\text{Seg 1}} + \left[\left(\frac{\partial |\ddot{X}_s|_{\max}}{\partial W_p} \right) \Delta W_p \right]_{\text{Seg 2}}}{(\Delta W_p)_{\text{Seg 1}} + (\Delta W_p)_{\text{Seg 2}}} \quad (242)$$

$$= \frac{(-0.01185)(4 \times 10^4) + (-0.004325)(8 \times 10^4)}{(4 \times 10^4) + (8 \times 10^4)}$$

$$= -0.006833 \text{ in./[lb(force) \cdot s}^2]$$

This same procedure was used to obtain the influence coefficients for the influence of the various parameters on the remaining absolute peak support accelerations, and on the maximax absolute relative accelerations. The influence coefficients obtained are presented in Table 18.

Table 15 is a summary of the results of the parametric and sensitivity analysis in terms of the values of the selected RVs at the base case and at the other 23 cases considered. This table shows the differences between the values of the RVs at the base case and the values of the RVs at the other cases. These differences are also presented as a percent difference from the base case (%DFB).

The parameters are ranked according to how sensitive the response variables are to the parameter changes. In Table 16, the parameters are ranked by sensitivity expressed as the absolute value of the percent difference from the base case, |%DFB|, obtained from Table 15. These rankings are graphically portrayed in bar charts, one for each of the response variables, in Figures 124 through 133.

The results presented in Tables 15 and 16, and in Figures 124 through 133, are expressed in terms of "sensitivity ranges" in Table 17. In this table, the dividing point between "sensitive" and "insensitive" was arbitrarily selected as 40%DFB. The entire sensitivity range is divided into the following five subranges:

<u> %DFB </u>	<u>Ranges</u>	<u>Subranges</u>
80 - 100 Up	Sensitive	1) Response Variable (RV) Highly Sensitive
60 - 80		2) RV Sensitive
40 - 60		3) RV Moderately Sensitive
20 - 40	Insensitive	4) RV Moderately Insensitive
0 - 20		5) RV Insensitive

Table 17 shows that, when this sensitivity scale is applied, the horizontal accelerations $|\dot{X}_s|_{\max}$ and $|\dot{X}_d|_{\max}$ fall into the insensitive range, while the vertical accelerations $|\dot{Y}_s|_{\max}$ and $|\dot{Y}_d|_{\max}$ and the rotational accelerations $|\ddot{\theta}_s|_{\max}$ and $|\ddot{\theta}_d|_{\max}$ extend into the "highly sensitive" subrange. The tiedown forces extend no higher than the "moderately sensitive" subrange. The vertical accelerations are sensitive to the parameters $\{k_y\}$, e_{OCR} , CP1 and CP6. The rotational accelerations are sensitive to the parameters $\{k_y\}$, CP1, CP2, CP8, e_{OCR} , CP6, CP4 and CP3. Seven of these parameters and their cases are the same as those identified with the response spectra that fell outside the $\pm 50\%$ band on the response spectra plots of Figures 121, 122 and 123. They have been discussed earlier. It should be noted from Table 17 that $|\ddot{\theta}_s|_{\max}$ is also moderately sensitive to W_p . The tiedown forces are moderately sensitive to the parameters CP2 and CP8. The vertical tiedown forces are also moderately sensitive to the vertical distance Z_p .

In Table 18, the "pure" parameters are ranked by influence coefficient and by sensitivity expressed as the contribution of each parameter to the total change in the response variable. Table 18 shows that, for all the response variables except the vertical accelerations, the most influential "pure" parameter is the vertical distance Z_p . The parameter that has the most influence on the vertical accelerations is e_{OCR} , the horizontal distance between the cgs of the cask and rail car. It should be noted that, for the vertical accelerations, e_{OCR} is divided into two parameters, $e_{OCR}(FE)$ when the cg of the cask is located on the far end side of the rail car cg, and $e_{OCR}(SE)$ when the cg of the cask is located on the struck end side of the rail car cg. This was necessary since the slopes (rates of change of the vertical accelerations with respect to the e_{OCR}) were nearly equal and opposite in sign. Influence coefficients derived from weighted averages of these slopes would not have reflected the true influence of e_{OCR} . Table 18 also shows that the "pure" parameter that contributes the most to the total changes in the horizontal accelerations (i.e., the sensitivities) is W_p , the package weight. This table also reveals that the parameter which most affects the total changes in the vertical accelerations is e_{OCR} , and the parameter causing the greatest changes in the rotational accelerations is

$\{k_y\}$. The parameters that most affect the total changes in the tiedown forces $DUS1_{max}$, $DUS4_{max}$, $DUS2_{max}$ and $DUS3_{max}$ are W_p , $\{k_x\}$, Z_p and Z_p , respectively. It should be remembered that the ranges of the parameters used to arrive at the sensitivities were specified at the outset in the definition of the cases. More meaningful values of the sensitivities are obtained if these ranges represent the uncertainties in the parameters.

Nine of the thirteen parameters (both "pure" and "composite") varied were varied about the base case by applying a multiplying factor to the base case values. This multiplying factor is expressed in terms of a parameter ratio, ϕ , the ratio of the parameter value to the base case parameter value. Treating these parameter ratios as parameters, influence coefficients and sensitivities were obtained. These parameter ratio-based influence coefficients and sensitivities are presented in Table 19. The sensitivities of each of the response variables to changes in the parameter ratios are illustrated in Figures 32 through 41 in Reference 23 and in Figures 95 through 111 in Reference 24. Only the plots for the base case and Cases 7 and 8 (Figures 34 and 39 in Reference 23, and Figure 107 in Reference 24) are presented in this report as examples. The sensitivities of the absolute peak support accelerations to changes in the pure parameter $\{k_y\}$ (Figure 34 in Reference 23) are presented in Figure 134. The sensitivities of the maximax absolute relative accelerations to changes in $\{k_y\}$ (Figure 39 in Reference 23) are shown in Figure 135, and the sensitivities of the absolute tiedown forces to changes in $\{k_y\}$ (Figure 107 in Reference 24) are shown in Figure 136. Four of the "composite" parameters could not be expressed in terms of parameter ratios. These parameters are CP3, CP4, CP5 and CP6, which correspond to Cases 9, 10, 12, and 13, respectively. Consequently, these cases are not included in Table 19, in Figures 32 through 41 in Reference 23, and in Figures 95 through 111 in Reference 24. The results in Table 19 may be condensed as follows:

Response Variable	Most Influential Parameter (Parameter Ratio)	Parameter Ratio to Which Response Variable Is Most Sensitive
$ \ddot{X}_s _{max}$	$\phi(CP8)$	$\phi(CP8)$
$ \ddot{Y}_s _{max}$	$\phi(\{k_y\})$	$\phi[\lambda_{OCR}(SE)]$
$ \ddot{\theta}_s _{max}$	$\phi(CP2)$	$\phi(CP2)$
$ \ddot{X}_d _{max}$	$\phi(W_p)$	$\phi(W_p)$
$ \ddot{Y}_d _{max}$	$\phi(\{k_y\})$	$\phi[\lambda_{OCR}(SE)]$
$ \ddot{\theta}_d _{max}$	$\phi(CP2)$	$\phi(CP2)$

The sensitivities presented here are consistent with those presented in Table 17.

It is the author's intention to present the results of the study in a clear and concise manner. The data presented here are consistent with the findings of other researchers in the field. The results of the study are presented in the following table.

The data presented here are consistent with the findings of other researchers in the field. The results of the study are presented in the following table.

Parameter	Value
Parameter 1	0.123
Parameter 2	0.456
Parameter 3	0.789
Parameter 4	0.101
Parameter 5	0.234
Parameter 6	0.567
Parameter 7	0.890
Parameter 8	0.112
Parameter 9	0.345
Parameter 10	0.678

The data presented here are consistent with the findings of other researchers in the field.

CONCLUSIONS AND RECOMMENDATIONS

On the basis of the good agreement obtained between the measured and calculated results for Tests 3, 10, 11, 13, 16 and 18, it is concluded that the CARDS model has been validated and, therefore, is an acceptable tool for the prediction of the dynamic response of a Cask-Rail Car System (CRS) impacting a stationary train of anvil cars at speeds up to 11 mph.

A CRS is a complex system. It is conceivable that supposedly identical CRSs may not behave the same, depending on how its subsystems and component parts are fastened to one another, on the fabrication or assembly tolerances permitted, etc. Perhaps a CRS that is thought to be well-defined might contain "surprises" that may cause the CRS to respond in a manner drastically different from the predicted response. When results obtained from CARDS were compared with the measured results from coupling Tests 3, 13, 16 and 18, some, up to that time, unsuspected situations were brought to light that significantly affected the agreement between the measured and calculated results. In Test 3, good agreement between the two sets of vertical accelerations of the cask at the far end was obtained only after allowance was made for previously unsuspected slack in the vertical tiedown structure (the cradle collar portion) at the far end. The same cask-cradle combination was used in Tests 13, 16 and 18; so this allowance was also used for these tests with good results. Also, in Tests 13, 16 and 18, the simulations were initially guided by comparisons of measured and calculated values of the horizontal force of interaction for Test 16. Differences between the measured and calculated values of this force for Test 16 were attributed to horizontal slippage between the cask and the rail car that resulted in an energy loss to the system. In these three tests, cable tiedowns were used instead of bolted tiedowns. It was assumed that when the chocking effect due to vertically oriented bolts was no longer present, some horizontal slippage occurred. When this energy loss or "slippage" was accounted for in the model by modifying the stiffnesses of the horizontal components of the cable tiedowns, good agreement between the measured and calculated values of the horizontal interaction force and four other response variables was realized. When these modifications were applied, without change, to the simulation of the cask-rail car systems used in Test 13 and 18, substantial reductions were realized in the differences between the measured and calculated values of the five response variables compared.

It is recommended that simulation models such as CARDS, that have been validated against experimental data, be used to establish standards for the preparation of a CRS before shipment.

REFERENCES

1. Advanced Continuous Simulation Language (ACSL), User Guide/Reference Manual, Mitchell and Gauthier Associates, Concord, MA, 1975.
2. R. C. Roggeveen, "Computer Predictions of Freight Train Shock Actions," ASME Paper 72-WA/RT-9, November 26-30, 1972.
3. C. L. Combes et al., 1966 Car and Locomotive Cyclopedia, 1st Ed., Simmons-Boardman Publishing Corp., New York, NY, 1966.
4. W. E. Baillie, "Impact as Related to Freight Car and Lading Damage," ASME Paper 59-A-249.
5. R. C. Roggeveen, "Analog Computer Simulations of End Impact of Railway Cars," ASME Paper 65-RR-3.
6. P. V. Kasbekar, V. K. Garg and G. C. Martin, "Dynamic Simulation of Freight Car and Lading During Impact," Journal of Engineering for Industry, Transactions of the ASME, November 1977.
7. B. T. Scales, "Longitudinal-Shock Problems in Freight Train Operation," ASME Paper 64-WA/RR-4, 1964.
8. J. M. Biggs, Introduction to Structural Dynamics. 1st Ed., McGraw-Hill Book Co., New York, NY, pp. 87-89 and 102-104, 1964.
9. C. M. Harris and C. Crede, Shock and Vibration Handbook, Volume 2 (p. 31-2) and Volume 3 (p. 50-10), McGraw-Hill, New York, NY, 1961.
10. R. W. Ramirez, The FFT: Fundamentals and Concepts, Tektronix, Inc., Beaverton, OR, 1975.
11. A. Papoulis, The Fourier Integral and Its Application, McGraw-Hill, New York, NY, p. 27, 1962.
12. Specifications for Design, Fabrication and Construction of Freight Cars (Adopted September 1, 1964), 25853, Appendix L: "Stress Analysis for 50-ton, 53-ft 6-in. Bulkhead Flat Car," Association of American Railroads, Chicago, IL, January 1966.
13. Helical Springs, Heat Treated Steel, Specifications M-114, Association of American Railroads, Operations and Maintenance Department, Mechanical Division, Chicago, IL, March 1, 1973.
14. Specifications for Testing Special Devices to Control Stability of Freight Cars, Specifications D-65 through D-76A, Association of American Railroads, Chicago, IL, January 1, 1974.

REFERENCES (Cont'd)

15. A. A. R. Test Data - Friction Draft Gear, Specifications M-901-E, Association of American Railroads, Chicago, IL.
16. Design and Analysis Report, IF-300 Shipping Cask, NEDO-10084-1, General Electric Company, Nuclear Fuel Department, February 1973.
17. N. A. Kheir and W. M. Holmes, "On Validating Simulation Models of Missile Systems," Simulation, April 1978.
18. S. R. Fields and S. J. Mech, Dynamic Analysis to Establish Normal Shock and Vibration of Radioactive Material Shipping Packages, Quarterly Progress Report (October 1, 1978 - December 31, 1978), NUREG/CR-0766 (HEDL-TME 79-3), June 1979.
19. S. R. Fields and S. J. Mech, Dynamic Analysis to Establish Normal Shock and Vibration of Radioactive Material Shipping Packages, Quarterly Progress Report (January 1, 1979 - March 31, 1979), NUREG/CR-0880 (HEDL-TME 79-29), July 1979.
20. S. R. Fields and S. J. Mech, Dynamic Analysis to Establish Normal Shock and Vibration of Radioactive Material Shipping Packages, Quarterly Progress Report (October 1, 1979 - December 31, 1979), NUREG/CR-1484, (HEDL-TME 80-24), August 1980.
21. S. R. Fields, Dynamic Analysis to Establish Normal Shock and Vibration of Radioactive Material Shipping Packages, Quarterly Progress Report (January 1, 1980 - March 31, 1980), NUREG/CR-1685, Vol. 1, (HEDL-TME 80-51), January 1981.
22. S. F. Petry, Rail Tiedown Tests with Heavy Casks for Radioactive Shipments, DP-1536, August 1980.
23. S. R. Fields, Dynamic Analysis to Establish Normal Shock and Vibration of Radioactive Material Shipping Packages, Quarterly Progress Report (July 1, 1980 - September 30, 1980), NUREG/CR-1685, Vol. 3, (HEDL-TME 80-91), April 1981.
24. S. R. Fields, Dynamic Analysis to Establish Normal Shock and Vibration of Radioactive Material Shipping Packages, Quarterly Progress Report (October 1 - December 31, 1980), NUREG/CR-1685, Vol. 4, (HEDL-TME 80-92), July 1981.

A P P E N D I X I

NOMENCLATURE OF TERMS

APPENDIX I

LIST OF TERMS

NOMENCLATURE OF TERMS

- BRAKEF, BRAKER = Brake switches applied to the front and rear rail car trucks, respectively. When switches are set at 1.0, the brakes at the trucks are on and locked; when they are set at 0, the brakes are off.
- BRKIRC, BRKF2, BRKF3, BRKF4 = Brake switches for anvil cars 1 through 4, respectively. Brakes are on and locked when set at 1.0 and off when set at 0.
- C_{S1} through C_{S8} = Damping coefficients for viscous dampers representing structural damping at springs S_1 through S_8 in Figures 2 and 3 [lb(force)·s/in.
- DTHP, $\frac{d\theta_p}{dt}$, θ_p = Angular velocity of package or cask about an axis through its cg (rad/s)
- DTHRC, $\frac{d\theta_{RC}}{dt}$, θ_{RC} = Angular velocity of rail car about an axis through its cg (rad/s)
- DUSCAR = Coupler force calculated by CARDS model [lb(force)]
- DUSLF = Horizontal interaction force [lb(force)]
- DUSX4 = Coupler force obtained from experimental measurements [lb(force)]
- DUS1 through DUS8 = Forces acting on springs S_1 through S_8 , respectively (see Figures 1 and 3) [lb(force)]
- DWCRF = Frictional force opposing vertical motion of coupler faces between hammer car (cask-rail car) and first car in anvil train [lb(force)]
- DWP1, DWP4 = Frictional forces opposing horizontal motion of cask on rail car at rear and front attachment points, respectively [lb(force)]
- DWS1 through DWS8 = Viscous damping forces representing structural damping associated with springs S_1 through S_8 , respectively [lb(force)]
- DXCF, $\frac{dx_{CF}}{dt}$, \dot{x}_{CF} = Velocity of the cg of empty anvil car (L/θ)

- $DXCRC, \frac{dx_{CRC}}{dt}, \dot{x}_{CRC}$ = Velocity of cg of the empty hammer car (L/θ)
- $DXD, \frac{dx_d}{dt}, \dot{x}_d$ = Relative horizontal velocity of 1-DOF representation of package-rail car system (in./s)
- $DXF, \frac{dx_F}{dt}, \dot{x}_F$ = Horizontal velocity of cg of anvil car and its cargo (L/θ)
- $DXLA, \frac{dx_{LA}}{dt}, \dot{x}_{LA}$ = Adjustment factor or relative velocity to regulate the relative velocity \dot{x}_T (in./s)
- $DXP, \frac{dx_p}{dt}, \dot{x}_p$ = Horizontal velocity of cg of cask or package (in./s)
- $DXRC, \frac{dx_{RC}}{dt}, \dot{x}_{RC}$ = Horizontal velocity of the cg of hammer car and its cargo (L/θ or in./s)
- $DXRPC, \frac{dx_{RPC}}{dt}$ = Relative velocity of cask-rail car combination (in./s)
- $= \frac{dx_p}{dt} - \frac{dx_{RC}}{dt}$
- $DXT, DXTX, \frac{dx_T}{dt}, \frac{dx_{TX}}{dt}, \dot{x}_T, \dot{x}_{TX}$ = Calculated and experimental total relative velocities of displacement of the cgs of two rail cars, respectively (in./s)
- $DXTA, \frac{dx_{TA}}{dt}, \dot{x}_{TA}$ = Adjusted relative velocity of displacement or travel of the cg of two impacting rail cars (in./s)
- $DYCPL, \frac{dy_{CPL}}{dt}, \dot{y}_{CPL}$ = Vertical velocity of coupler face on cask-rail car (in./s) (Coupler on anvil car is assumed to be stationary.)
- $DYD, \frac{dy_d}{dt}, \dot{y}_d$ = Relative vertical velocity of equivalent 1-DOF model of package-rail car system (in./s)

- DYP, $\frac{dY_p}{dt}, \dot{Y}_p$ = Vertical velocity of cg of cask or package (in./s)
- DYRC, $\frac{dY_{RC}}{dt}, \dot{Y}_{RC}$ = Vertical velocity of cask-rail car at its cg (in./s)
- D2THP, $\frac{d^2\theta_p}{dt^2}, \ddot{\theta}_p$ = Angular acceleration of package or cask about an axis through its cg (rad/s²)
- D2THRC, $\frac{d^2\theta_{RC}}{dt^2}, \ddot{\theta}_{RC}$ = Angular acceleration of rail car about an axis through its cg (rad/s²)
- D2THS, $\frac{d^2\theta_s}{dt^2}, \ddot{\theta}_s$ = Angular or rotational acceleration of support (1/θ²)
- D2XD, $\frac{d^2x_d}{dt^2}, \ddot{x}_d$ = Relative horizontal acceleration of 1-DOF representation of package-rail car system (in./s²)
- D2XF, $\frac{d^2x_F}{dt^2}, \ddot{x}_F$ = Horizontal acceleration of cg of car(s) (mass M_F) at front (struck end) of rail car (in./s²)
- D2XP, $\frac{d^2x_p}{dt^2}, \ddot{x}_p$ = Horizontal acceleration of cg of cask or package (M_p) (in./s²)
- D2XRC, $\frac{d^2x_{RC}}{dt^2}, \ddot{x}_{RC}$ = Horizontal acceleration of cg of cask-rail car (M_{RC}) (in./s²)
- D2XR56, $\frac{d^2x_{RC56}}{dt^2}, \ddot{x}_{RC56}$ = Horizontal acceleration of cask-rail car at support point at rear truck (in./s²)
- D2XR78, $\frac{d^2x_{RC78}}{dt^2}, \ddot{x}_{RC78}$ = Horizontal acceleration of cask-rail car at support point at front truck (in./s²)

- $D2XS, \frac{d^2x_S}{dt^2}, \ddot{x}_S$ = Horizontal acceleration of support (L/θ^2)
- $D2XTR, D2XFR, \frac{d^2x_{TR}}{dt^2}, \frac{d^2x_{TF}}{dt^2}, \ddot{x}_{TR}, \ddot{x}_{TF}$ = Horizontal accelerations of the cgs of rear (M_{TR}) and front (M_{TF}) rail car trucks, respectively ($in./s^2$)
- $D2YD, \frac{d^2y_d}{dt^2}, \ddot{y}_d$ = Relative vertical acceleration of equivalent 1-DOF model of package-rail car system ($in./s^2$)
- $D2YP, \frac{d^2y_p}{dt^2}, \ddot{y}_p$ = Vertical acceleration of cask or package at its cg ($in./s^2$)
- $D2YP12, \frac{d^2y_{P12}}{dt^2}, \ddot{y}_{P12}$ = Vertical acceleration of cask or package at rear tiedown attachment point ($in./s^2$)
- $D2YP34, \frac{d^2y_{P34}}{dt^2}, \ddot{y}_{P34}$ = Vertical acceleration of cask or package at front tiedown attachment point ($in./s^2$)
- $D2YRC, \frac{d^2y_{RC}}{dt^2}, \ddot{y}_{RC}$ = Vertical acceleration of cask-rail car at its cg ($in./s^2$)
- $D2YR12, \frac{d^2y_{RC12}}{dt^2}, \ddot{y}_{RC12}$ = Vertical acceleration of cask-rail car at rear tiedown attachment point ($in./s^2$)
- $D2YR34, \frac{d^2y_{RC34}}{dt^2}, \ddot{y}_{RC34}$ = Vertical acceleration of cask-rail car at front tiedown attachment point ($in./s^2$)
- $D2YR56, \frac{d^2y_{RC56}}{dt^2}, \ddot{y}_{RC56}$ = Vertical acceleration of cask-rail car at support point at rear truck ($in./s^2$)

- $D2YR78, \frac{d^2 y_{RC78}}{dt^2}, \ddot{y}_{RC78}$ = Vertical acceleration of cask-rail car at support point at front truck (in./s²)
- $D2YS, \frac{d^2 y_s}{dt^2}, \ddot{y}_s$ = Vertical acceleration of support (L/θ²)
- F_{CPL}, F_{CPLX} = Calculated and experimental coupler forces, respectively [lb(force)]
- $|F_{CPL}|$ = Absolute value of force applied to coupler faces, perpendicular to sliding surfaces [lb(force)]
- F_{YRF} = Frictional force opposing movement of sliding coupler faces [lb(force)]
- I_p = Mass moment of inertia of cask or package [lb(mass)-in.²] or [lb(force)-in.-s²]
- I_{RC} = Mass moment of inertia of rail car [lb(mass)-in.²] or [lb(force)-in.-s²]
- K = Kinetic energy of system [lb(force)-in.]
- k_{FDG} = Spring constant of single equivalent spring representing combined spring and fraction damper of draft gear on first anvil car [lb(force)/in.]
- $k_{SCARS}, k_{FF2}, k_{F2F3}, k_{F3F4}$ = Spring constants of equivalent springs representing draft gear combinations between cars [lb(force)/in.]
- k_{RCDG} = Spring constant of single equivalent spring representing combined spring and friction damper of draft gear on hammer car [lb(force)/in.]
- k_{SCARS}, k_{SCARS} = Total equivalent spring constant for combined draft gears of cask-rail car (hammer car) and first struck car (anvil car) [lb(force)/in.]
- k_{SDG1}, k_{SDG2} = Spring constants of "solid" draft gears on hammer and anvil cars, respectively [lb(force)/in.]
- k_{SDG10}, k_{SDG20} = Base spring constants corresponding to k_{SDG1} and k_{SDG2} , respectively [lb(force)/in.]
- k_{SF} = Stiffness of structure of car(s) (M_f) at front of cask-rail car [lb(force)/in.]

- k_{SRC} = Stiffness of structure of cask-rail car (M_{RC})
[lb(force)/in.]
- k_{S1}, K_{S1} = Stiffness of horizontal component of rear tiedown
between cask (M_p) and rail car (M_{RC})
[lb(force)/in.]
- k_{S2}, K_{S2} = Stiffness of vertical component of rear tiedown
between cask (M_p) and rail car (M_{RC})
[lb(force)/in.]
- k_{S3}, K_{S3} = Stiffness of vertical component of front tiedown
between cask (M_p) and rail car (M_{RC})
[lb(force)/in.]
- k_{S4}, K_{S4} = Stiffness of horizontal component of front tie-
down between cask (M_p) and rail car (M_{RC})
[lb(force)/in.]
- k_{S5}, K_{S5} = Stiffness of horizontal component of cask-rail
car suspension at rear truck [lb(force)/in.]
- $k_{S6}, k_{S7},$
 K_{S6}, K_{S7} = Spring constants for equivalent springs repre-
senting vertical components of rear and front
suspensions, respectively [lb(force)/in.]
- k_{S8}, K_{S8} = Stiffness of horizontal component of cask-rail
car suspension at front truck [lb(force)/in.]
- k_T = Spring constant of single equivalent spring
representing combined draft gears of hammer and
anvil rail cars [lb(force)/in.]
- k_1 = Spring constant of spring in hammer car draft
gear [lb(force)/in.]
- k_2 = Spring constant of spring in the anvil car draft
gear [lb(force)/in.]
- k_6, k_7 = Spring constants of combined springs in vertical
components of rear and front suspensions,
respectively, in their "active" state
[lb(force)/in.]
- k_{6S}, k_{7S} = Spring constants of combined springs in vertical
components of rear and front suspensions,
respectively, in their "solid" state, i.e.,
after they have bottomed out [lb(force)/in.]

- l_{CF}, LCF = Horizontal distance from vertical centerline of cask-rail car to front tiedown attachment point (in.)
- $l_{CPL}, LCPL$ = Horizontal distance from vertical centerline of cask-rail car to coupler face (in.)
- l_{CR}, LCR = Horizontal distance from vertical centerline of cask-rail car to rear tiedown attachment point (in.)
- $l_{OCR}, LOCR$ = Horizontal distance between vertical centerlines of cask and cask-rail car (in.)
- l_{PF}, LPF = Horizontal distance from vertical centerline of cask to front tiedown attachment point (in.)
- l_{PR}, LPR = Horizontal distance from vertical centerline of cask to rear tiedown attachment point (in.)
- l_{RC}, LRC = Horizontal distance from vertical centerline of cask-rail car to a suspension point at a truck (in.) ($2 * LRC$ = distance between suspension points)
- $M_F, M_{F2}, M_{F3}, M_{F4}$ = Masses of anvil cars 1 through 4, respectively, [$lb(force) \cdot s^2/in.^2$]
- M_{kS1}, M_{kS4} = Energy dissipation factors for k_{S1} and k_{S4} , respectively
- M_{kS1F}, M_{kS4F} = Arbitrary factors currently set at 0.5
- M_{LF} = Mass of lading or cargo on anvil car (M)
- M_{LRC} = Mass of lading or cargo on hammer car (M)
- M_p, MP = Mass of the cask or package [$lb(force) \cdot s^2/in.$]
- M_{RC}, MRC = Mass of the cask-rail car [$lb(force) \cdot s^2/in.$]
- M_{RCCG} = Moment about cg of cask-rail car [$lb(force) \cdot in.$]
- M_{TF} = Total mass of anvil car and its cargo (M)
- $M_F + M_{LF}$
- M_{TF}, MTF = Mass of front truck on cask-rail car [$lb(force) \cdot s^2/in.$]

- M_{TR}, M_{TR} = Mass of rear truck on cask-rail car
 [lb(force)-s²/in.]
- M_{TRC} = Total mass of hammer car and its cargo (M)
 = $M_{RC} + M_{LRC}$
- n = Number of observations or sampling points
- $NCARSF$ = Number of cars at front (struck end)
 of cask-rail car
- q_i = The i-th generalized coordinate
- $\dot{q}_i, \frac{dq_i}{dt}$ = Time rate of change of i-th generalized
 coordinate
- $RCOR$ = Cask-rail car override variable, with control
 function:
 $RCOR = 1.0$, to override rail car
 characterization function
 $RCOR = 0$, to activate rail car
 characterization function
- $SCARS$ = Composite spring connecting the cgs of cask-rail
 car (M_{RC}) and car(s) at front (struck end) of
 cask-car (M_F). (This spring is composed of
 springs representing the structures of M_{RC} and
 M_F , and is based on the assumption of rigid
 couplers.)
- $sgn(A)$ = Signum function or sign function of argument A

$$= \begin{cases} +1, & A > 0 \\ -1, & A = 0 \\ -1, & A < 0 \end{cases}$$
- $S_1, S1$ = Spring representing horizontal component of rear
 tiedown between cask (M_p) and rail car (M_{RC})
- $S_2, S2$ = Spring representing vertical component of rear
 tiedown between M_p and M_{RC}
- $S_3, S3$ = Spring representing vertical component of front
 tiedown between M_p and M_{RC}
- $S_4, S4$ = Spring representing horizontal component of front
 tiedown between M_p and M_{RC}

- S_5, S_5 = Spring representing horizontal component of cask-rail car suspension at rear truck
- S_6, S_6 = Spring representing vertical component of cask-rail car suspension at rear truck
- S_7, S_7 = Spring representing vertical component of cask-rail car suspension at front truck
- S_8, S_8 = Spring representing horizontal component of cask-rail car suspension at front truck
- S_9, S_9 = Composite spring connecting the cg of the cask-rail car to the tip of its coupler
- S_{10}, S_{10} = Composite spring connecting cg of car(s) (M_F) at front of cask-rail car to the tip of its coupler
- t, T = Time (s)
- J_{HP}, θ_p = Angle of rotation of X_p and Y_p axes about an axis perpendicular to $X_p - Y_p$ plane through cg of cask or package (rad)
- $THRC, \theta_{RC}$ = Angle of rotation of X_{RC} and Y_{RC} axes about an axis perpendicular to $X_{RC} - Y_{RC}$ plane through the cg of rail car (rad)
- $TIC, TICD, TICV, TICA$ = Theil's two-variable inequality coefficients for comparison of calculated and experimental values of coupler force, relative displacement, relative velocity, and relative acceleration, respectively
- $TMIC$ = Theil's multiple inequality coefficient
- U = Potential energy or internal strain energy of system [lb(force)·in.]
- $VXFI$ = Initial velocity of car(s) (M_F) at front of cask-rail car (in./s)
- $VXRCI$ = Initial velocity of cask-rail car (M_{RC}) (in./s)
- W_C = Work done on system by damping forces [lb(force)·in.]
- W_{CRF} = Energy dissipated as frictional work [lb(force)·in.]
- W_e = Work done on system by external forces [lb(force)·in.]

$W_F, W_{F2},$ W_{F3}, W_{F4}	= Weights of loaded anvil cars 1 through 4, respectively [lb(force)]
W_p	= Weight of cask or package [lb(force)]
W_{p1}	= That portion of package weight concentrated at rear (far end) tiedown attachment point [lb(force)]
W_{p4}	= That portion of package weight concentrated at front (struck end) tiedown attachment point [lb(force)]
W_{RC}	= Weight of cask-rail car [lb(force)]
W_{TF}	= Weight of front truck on cask-rail car [lb(force)]
W_{TR}	= Weight of rear truck on cask-rail car [lb(force)]
X_d	= Horizontal displacement of an equivalent single-degree-of-freedom (1-DOF) representation of the package-railcar system, displacement of package (cask) relative to rail car (in.)
$X_F, X_{F2},$ X_{F3}, X_{F4}	= Horizontal displacement of cg of anvil cars 1 through 4, respectively (in.)
X_p	= Horizontal displacement of cg of cask or package (in.)
X_{p12}, X_{P12}	= Horizontal displacement of cask at rear tiedown attachment point (in.)
X_{p34}, X_{P34}	= Horizontal displacement of cask at front tiedown attachment point (in.)
X_{RC}, X_{RC}	= Horizontal displacement of cask-rail car at its cg (in.)
X_{RC56}	= Horizontal displacement of cask-rail car at support point at rear truck (in.)
X_{RC78}	= Horizontal displacement of cask-rail car at support point at front truck (in.)
X_T, X_{TX}	= Calculated and experimental relative displacements of the cgs of two rail cars, respectively (in.)
X_{TL}, X_{TU}	= Lower and upper limits, respectively, on travel of combined draft gears (in.)

X_{TR}, X_{TF}	=	Horizontal displacements of cgs of rear and front trucks, respectively, on cask-rail car (in.)
Y_{CPL}	=	Vertical displacement of coupler face on cask-rail car (in.)
Y_d	=	Vertical displacement of an equivalent 1-DOF representation of package-rail car system, displacement of the package (cask) relative to rail car (in.)
Y_p	=	Vertical displacement of cg of cask or package (in.)
Y_{P12}, Y_{P12}	=	Vertical displacement of cask at rear tiedown attachment point (in.)
Y_{P34}, Y_{P34}	=	Vertical displacement of cask at front tiedown attachment point (in.)
Y_{RC}	=	Vertical displacement of cg of cask-rail car (in.)
Y_{RCMAX}	=	Maximum downward vertical displacement of rail car (the point at which suspension springs bottom out or go "solid") (in.)
Y_{RC12}, Y_{RC12}	=	Vertical displacement of cask-rail car at rear tiedown attachment point (in.)
Y_{RC34}, Y_{RC34}	=	Vertical displacement of cask-rail car at front tiedown attachment point (in.)
Y_{RC56}, Y_{RC56}	=	Vertical displacement of cask-rail car at support point at rear truck (in.)
Y_{RC78}, Y_{RC78}	=	Vertical displacement of cask-rail car at support point at front truck (in.)
Z_{CDG}	=	Vertical distance between line of force and cg of the rail car (in.)
Z_{CDG0}	=	Distance between centerline of draft gear and the cg of cask-rail car (in.)
Z_p, Z_p	=	Vertical distance from horizontal centerline of cask to its top and bottom surfaces (in.)
Z_{RC}, Z_{RC}	=	Vertical distance from horizontal centerline of cask-rail car to its top and bottom surfaces (in.)

- α_{CPL} = A factor to allow the damping term DWCRF to vary as a function of the absolute value of the coupler force $|FCPL|$ raised to the factor power
- α_6, α_7 = Factors that allow the suspension system damping term to vary as a function of the absolute value of the velocity ($\dot{Y}_{RC56}, \dot{Y}_{RC78}$) raised to the factor power
- β_{CPL} = A multiplying factor representing the fraction of the coupler force $|FCPL|$ actually applied to the moving coupler faces
- β_6, β_7 = Multiplying factors representing the fraction of the load on the respective rear and front suspensions that is applied perpendicular to the sliding surfaces of the damper
- θ_p = Angle of rotation of X_p and Y_p axes about an axis perpendicular to the $X_p - Y_p$ plane through the cg of the cask or package (rad)
- θ_{RC} = Angle of rotation of X_{RC} and Y_{RC} axes about an axis perpendicular to the $X_{RC} - Y_{RC}$ plane through the cg of the rail car (rad)
- μ_{CPL} = The coefficient of friction for the sliding of the two coupler faces against each other
- μ_D = Multiplying factor corresponding to a coefficient of friction for the damper in a draft gear
- μ_{D6}, μ_{D7} = Multiplying factors corresponding to coefficients of friction for the dampers in the rear and front suspensions, respectively
- $\mu_F, \mu_{F2}, \mu_{F3}, \mu_{F4}$ = Coefficients of friction for sliding contact between tracks and wheels of anvil cars 1 through 4, respectively
- μ_{XT} = A multiplying factor representing extent of energy dissipation ($0 \leq \mu_{XT} \leq 1$)

$$\mu_{XT} = \mu_{XTC}, \text{ when } \dot{X}_T > 0 \text{ (Compaction)}$$

$$\mu_{XT} = \mu_{XTE}, \text{ when } \dot{X}_T \leq 0 \text{ (Recovery)}$$

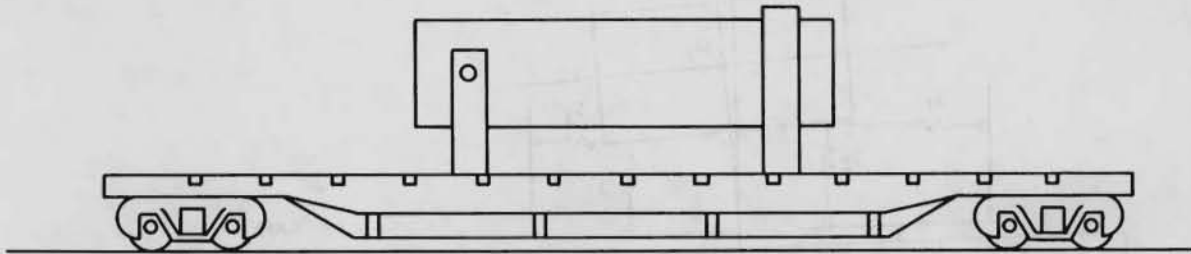
μ_{XTC}	= Energy dissipation coefficient for cargo compaction
μ_{XTE}	= Energy dissipation coefficient for cargo recovery phase
μ_{PR}	= Coefficient of friction for sliding of package or cask on rail car
$\phi(X_T)$	= Multiplying factor where: $\phi(X_T) = \phi(X_T)_L$, when $X_T \leq 5.6$ in. $\phi(X_T) = \phi(X_T)$, when $5.6 < X_T < 6.35$ in. $\phi(X_T) = \phi(X_T)_U$, when $X_T \geq 6.35$ in.
ω_X	= Frequency of vibration of the 1-DOF EOM for the relative horizontal motion of the cask-rail car system (rad/s)
ω_Y	= Frequency of vibration for the 1-DOF EOM for the relative vertical motion of the cask-rail car system (rad/s)
ΣF_{XP}	= Summation of horizontal forces acting on the cask or package [lb(force)]
ΣF_{XRC}	= Summation of horizontal forces acting on rail car [lb(force)]
ΣF_{YP}	= Summation of vertical forces acting on cask [lb(force)]
ΣF_{YRC}	= Summation of vertical forces acting on rail car [lb(force)]

A P P E N D I X I I

FIGURES

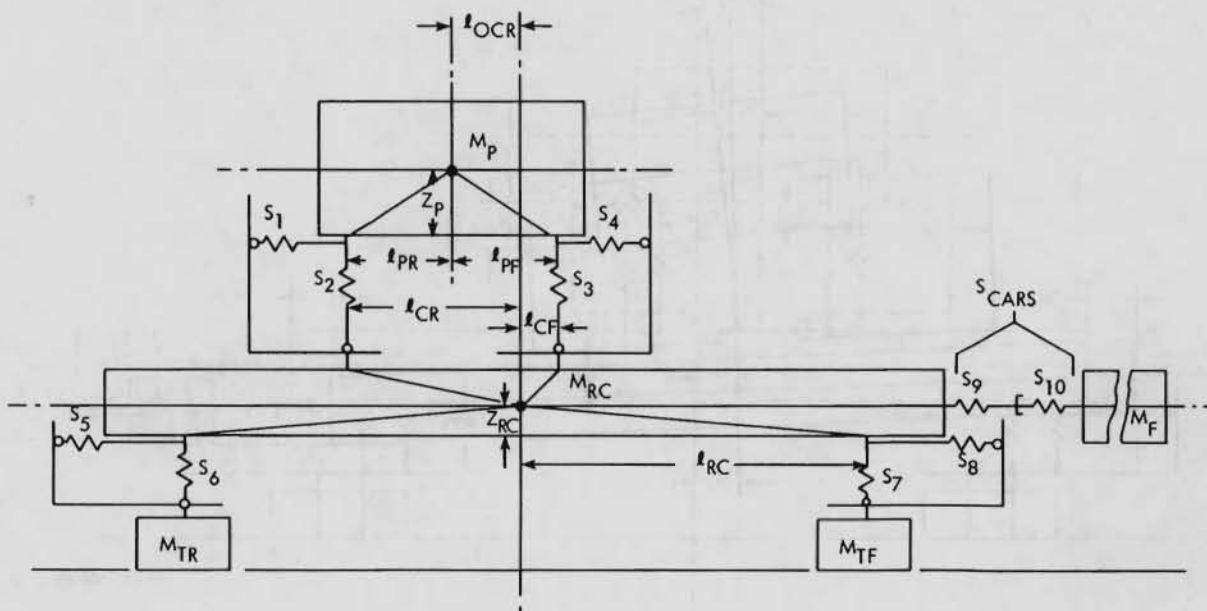
1970-1971

1971



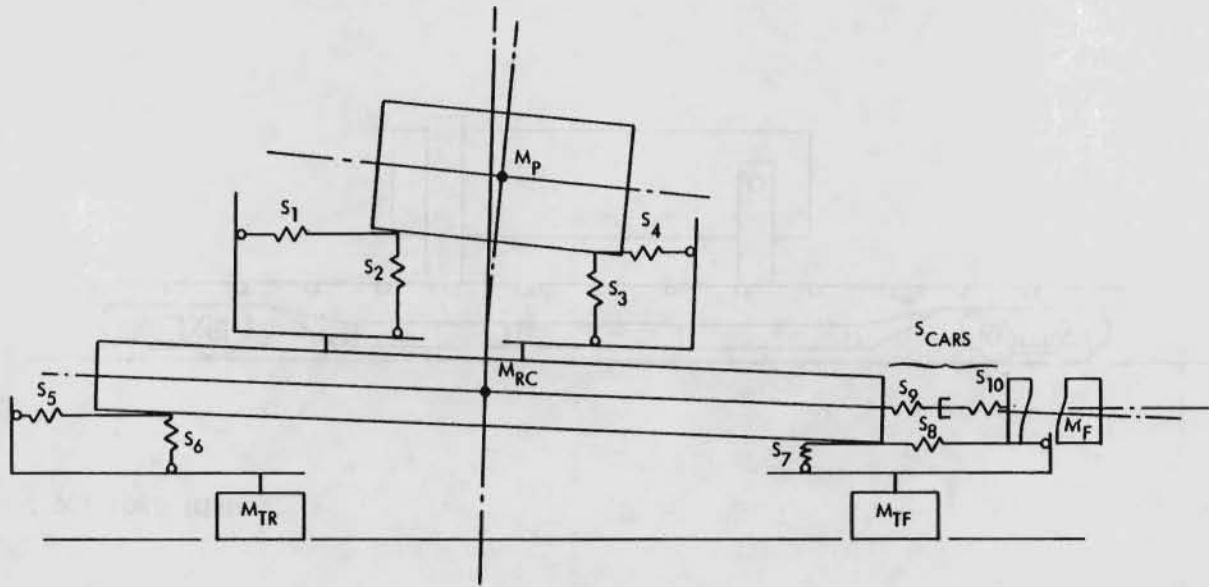
HEDL 7803-106.2

FIGURE 1. Spent Fuel Shipping Cask-Rail Car System Modeled.



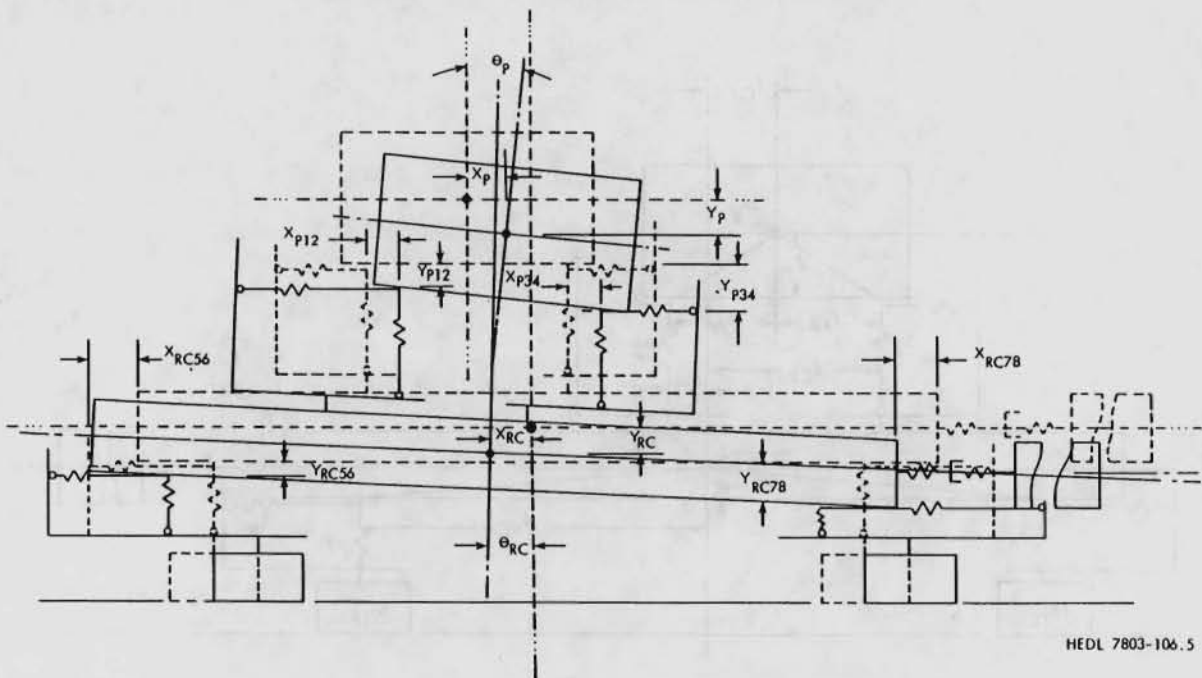
HEDL 7803-106.4

FIGURE 2. Spring-Mass Model of Cask-Rail Car System.



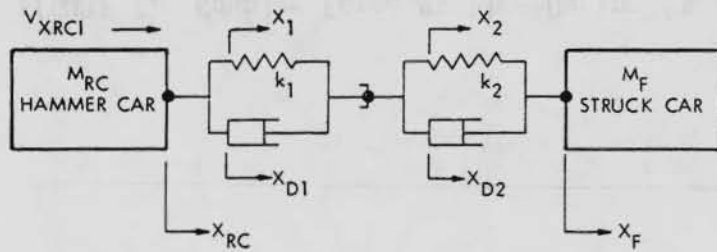
HEDL 7803-106.3

FIGURE 3. One Possible Orientation of Cask-Rail Car System After Impact.

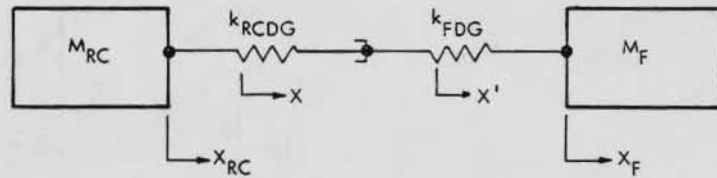


HEDL 7803-106.5

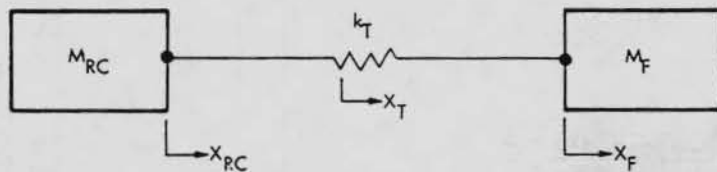
FIGURE 4. Comparison of Orientation of Cask-Rail Car System After Impact with Initial State.



(a) COUPLER SUBSYSTEM SUBMODEL

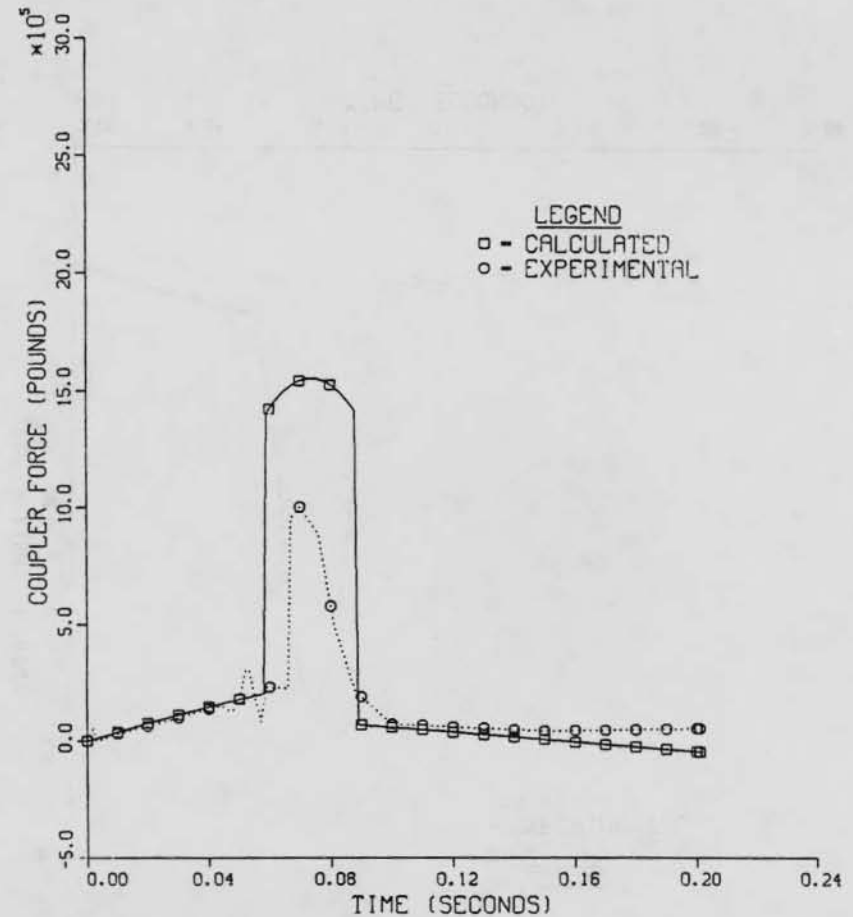


(b) COUPLER SUBSYSTEM SUBMODEL WITH EACH DRAFT GEAR REDUCED TO AN EQUIVALENT SPRING



(c) COUPLER SUBSYSTEM SUBMODEL WITH BOTH DRAFT GEARS REDUCED TO ONE EQUIVALENT SPRING

HEDL 7812-133.1

FIGURE 5. Rail Car-Coupler Subsystem Model.
Neg 7814254FIGURE 6. Coupler Force vs Time During Impact of Two Hopper Cars Loaded with Gravel (Spring Constant of "Solid" Draft Gears = 5×10^5 lbs(force)/inch).

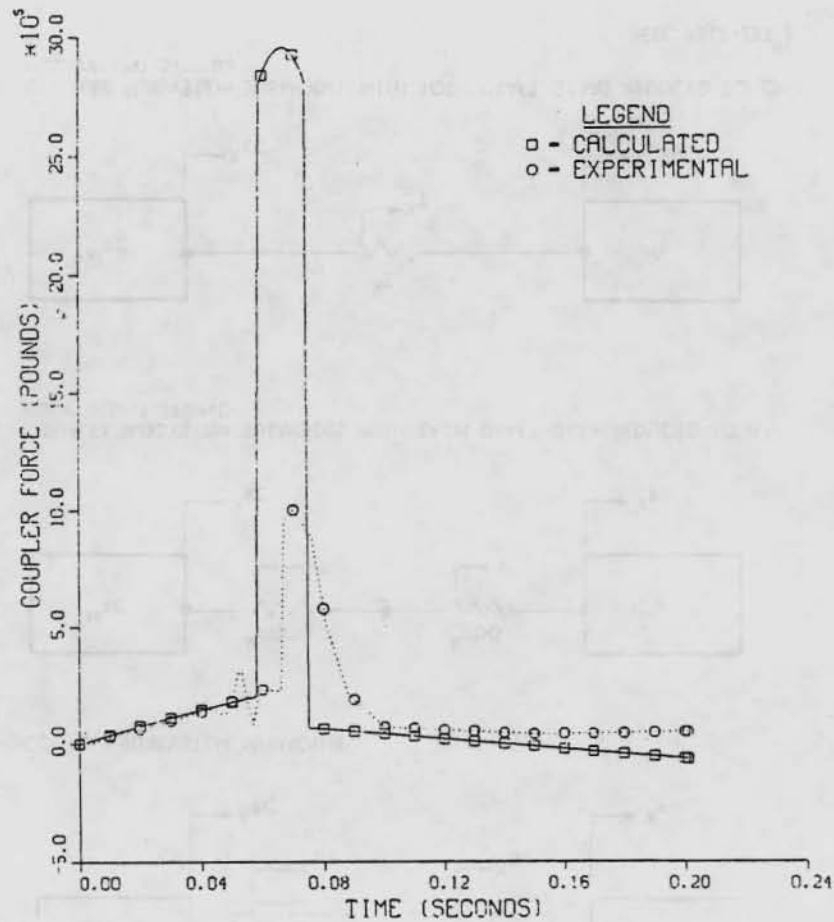


FIGURE 7. Coupler Force vs Time During Impact of Two Hopper Cars Loaded with Gravel (Spring Constant of "Solid" Draft Gears = 1×10^6 lbs(force)/inch).

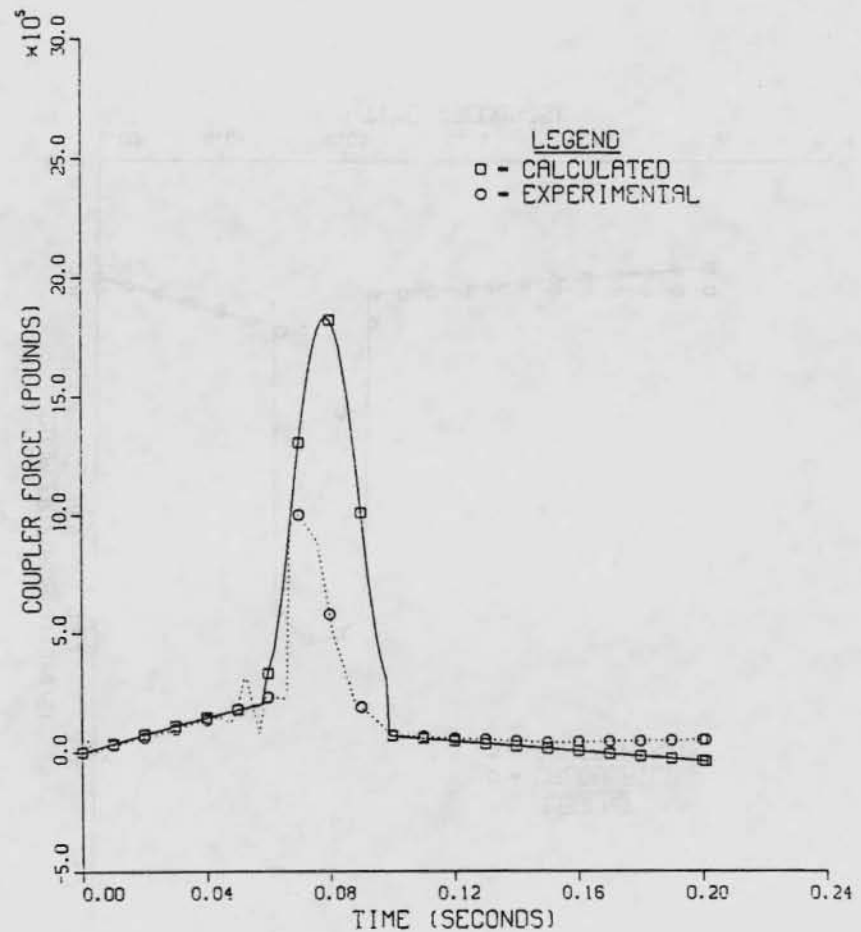


FIGURE 8. Coupler Force vs Time During Impact of Two Hopper Cars Loaded with Gravel ("Solid" Draft Gear Spring Constant a Function of Draft Gear Travel, X_T).

L-II

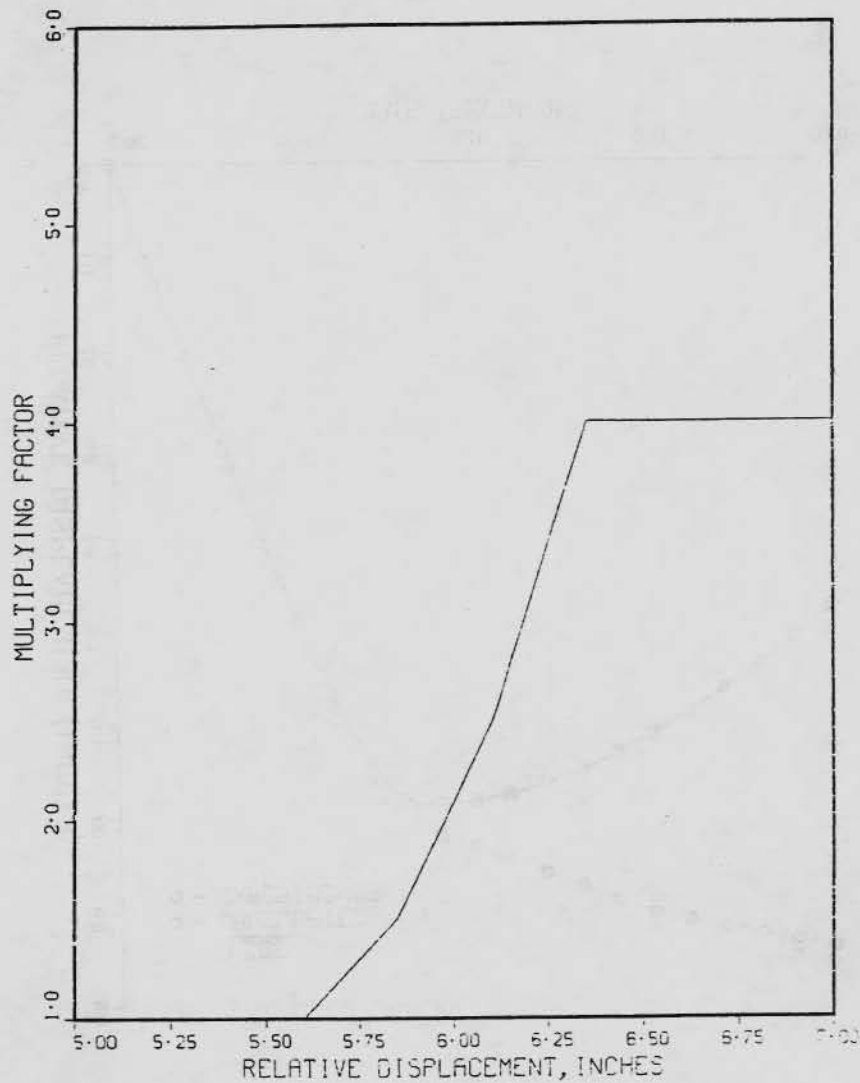


FIGURE 9. Ratio of "Solid" Draft Gear Spring Constant to a Base Value.

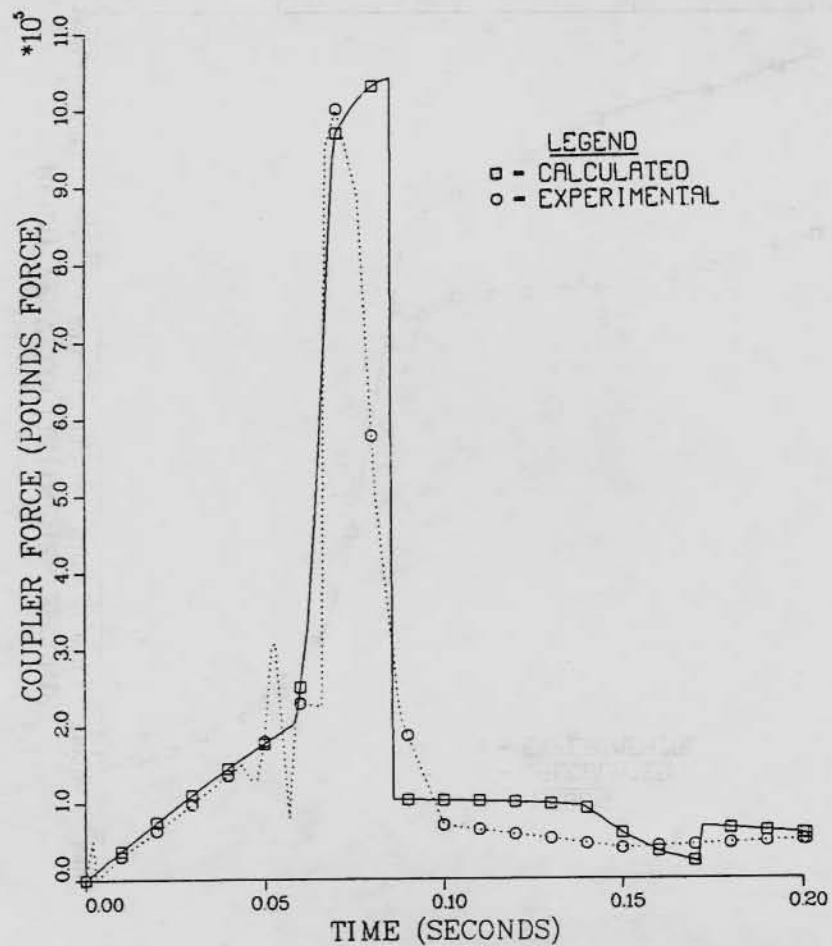


FIGURE 10. Coupler Force vs Time During Impact of Two Hopper Cars Loaded with Gravel.

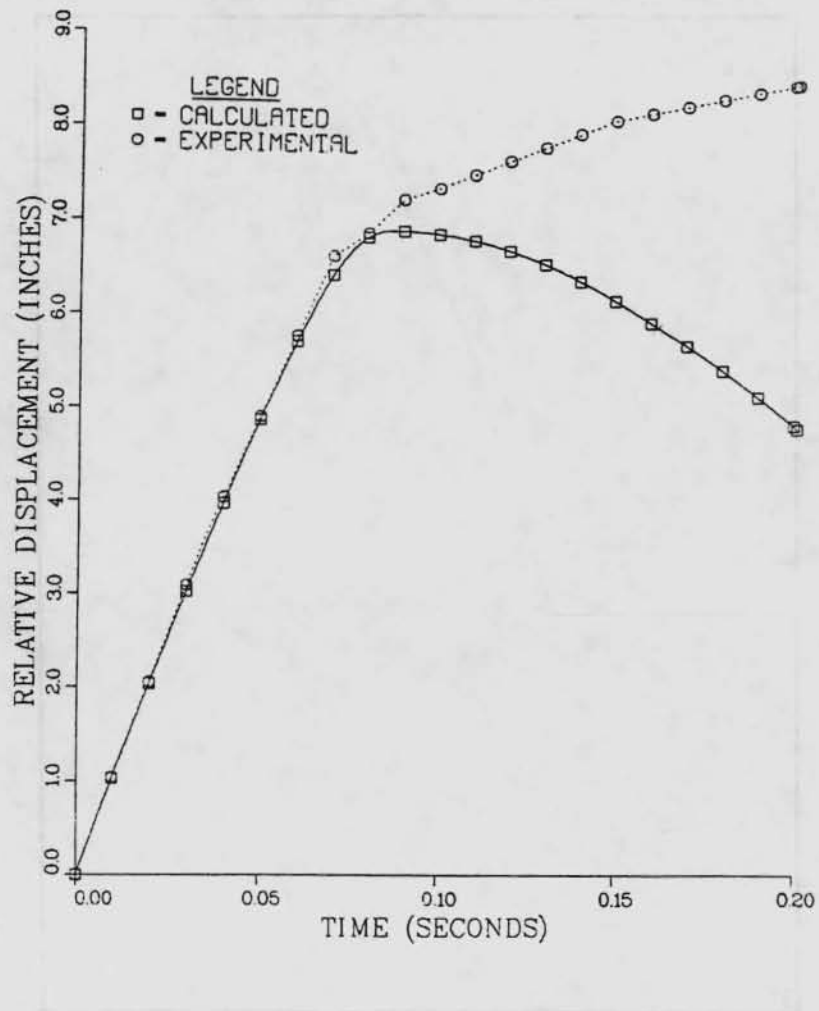


FIGURE 11. Relative Displacement of Two Gravel-Filled Hopper Cars vs Time During Impact.

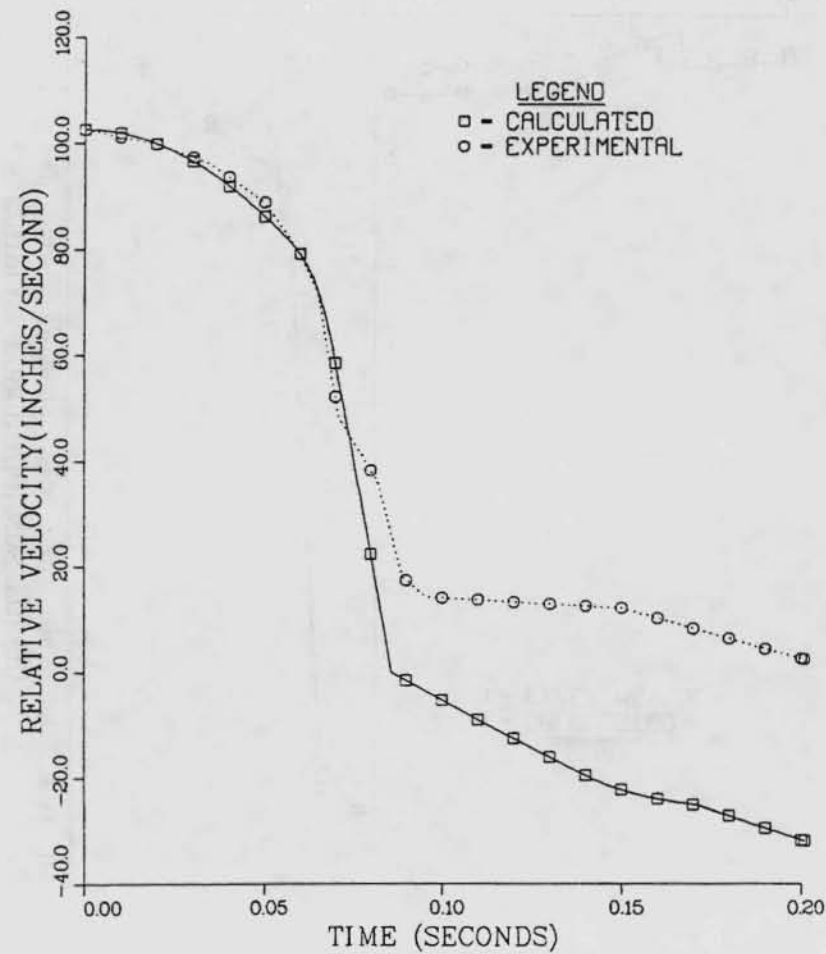


FIGURE 12. Relative Velocity of Two Gravel-Filled Hopper Cars vs Time During Impact.

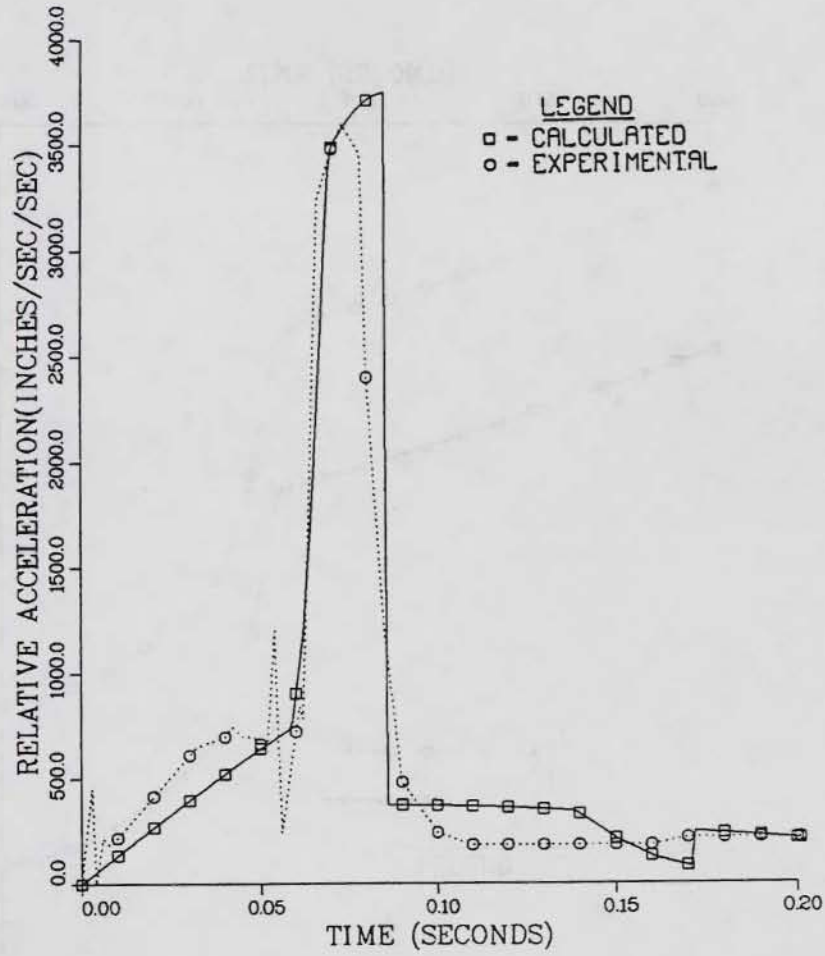


FIGURE 13. Relative Acceleration of Two Gravel-Filled Hopper Cars vs Time During Impact.

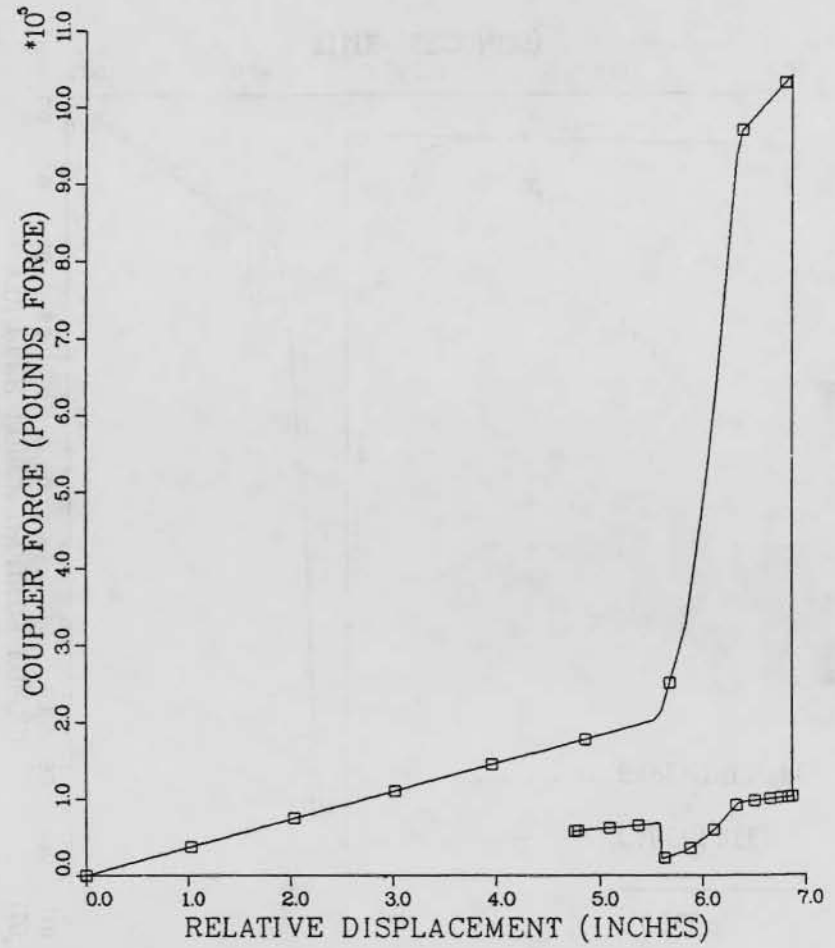


FIGURE 14. Calculated Coupler Force vs Calculated Relative Displacement of Two Gravel-Filled Hopper Cars During Impact.

01-11

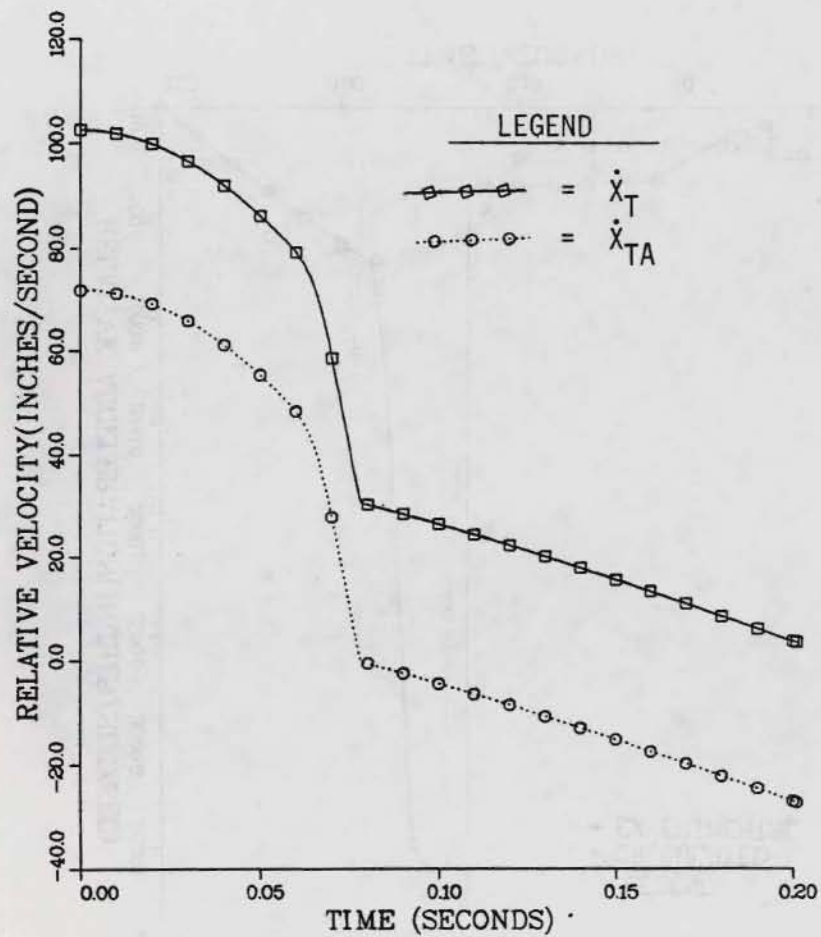


FIGURE 15. Relative Velocity of Two Gravel-Filled Hopper Cars vs Time During Impact.

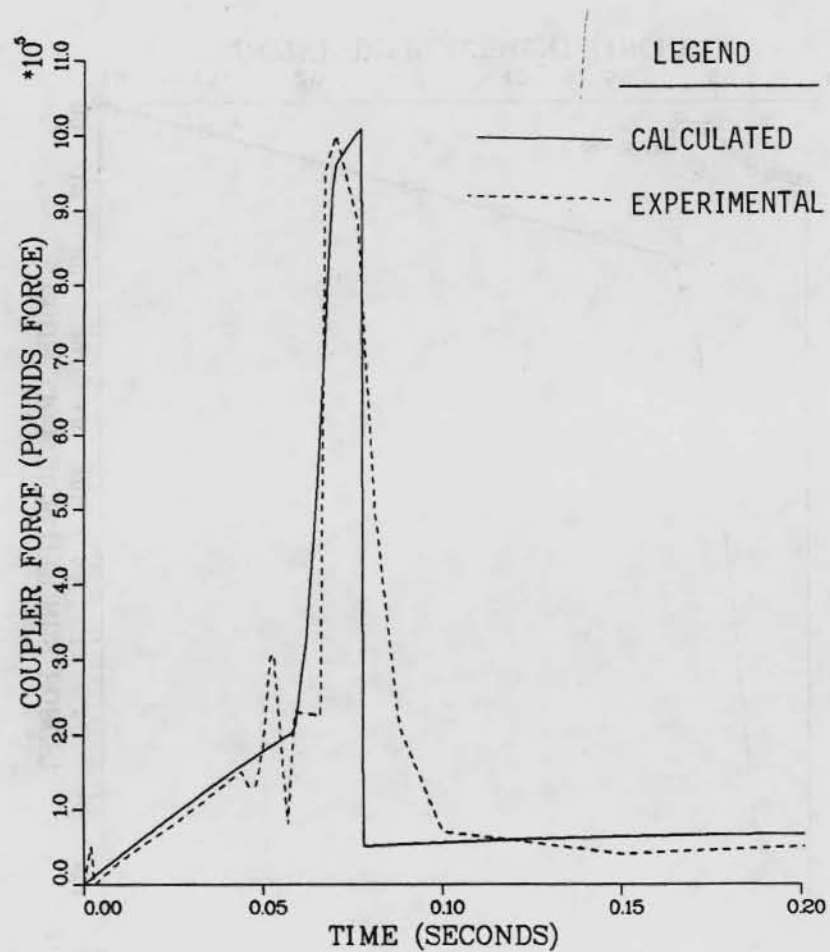


FIGURE 16. Coupler Force vs Time During Impact of Two Gravel-Filled Hopper Cars.

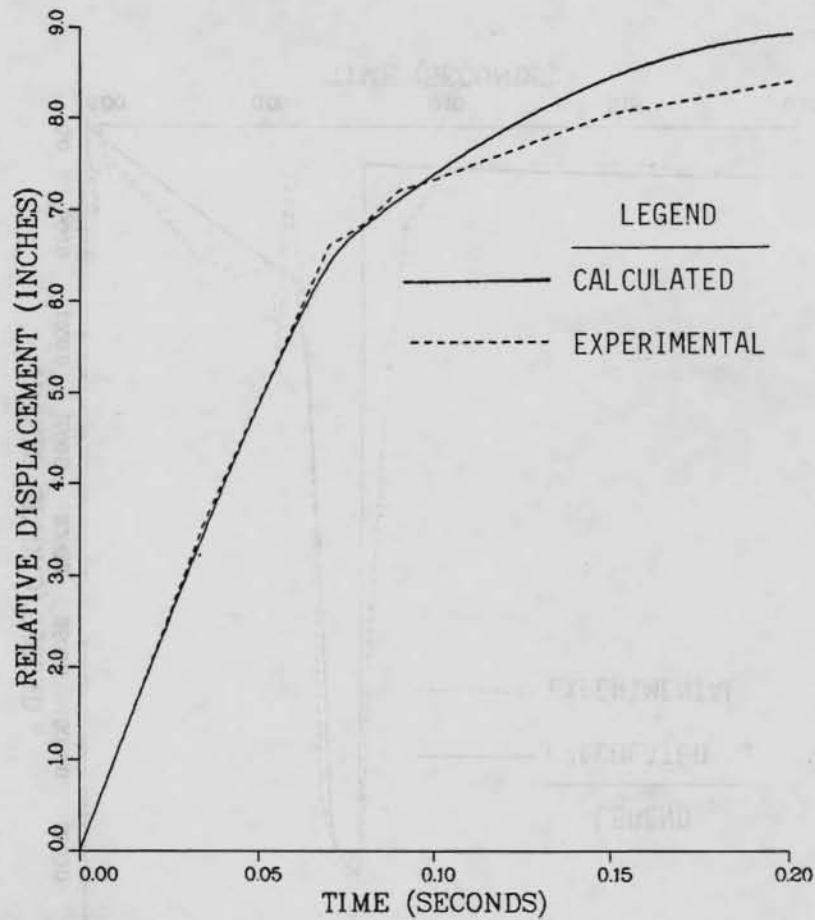


FIGURE 17. Relative Displacement of Two Gravel-Filled Hopper Cars vs Time During Impact.

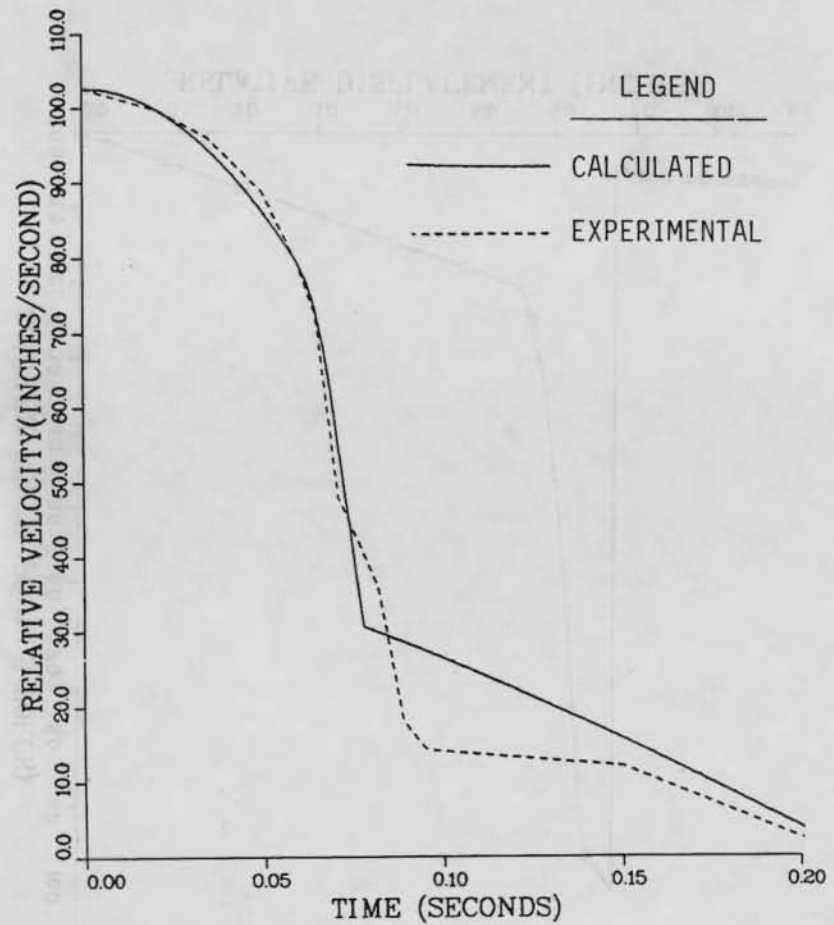


FIGURE 18. Relative Velocity of Two Gravel-Filled Hopper Cars vs Time During Impact.

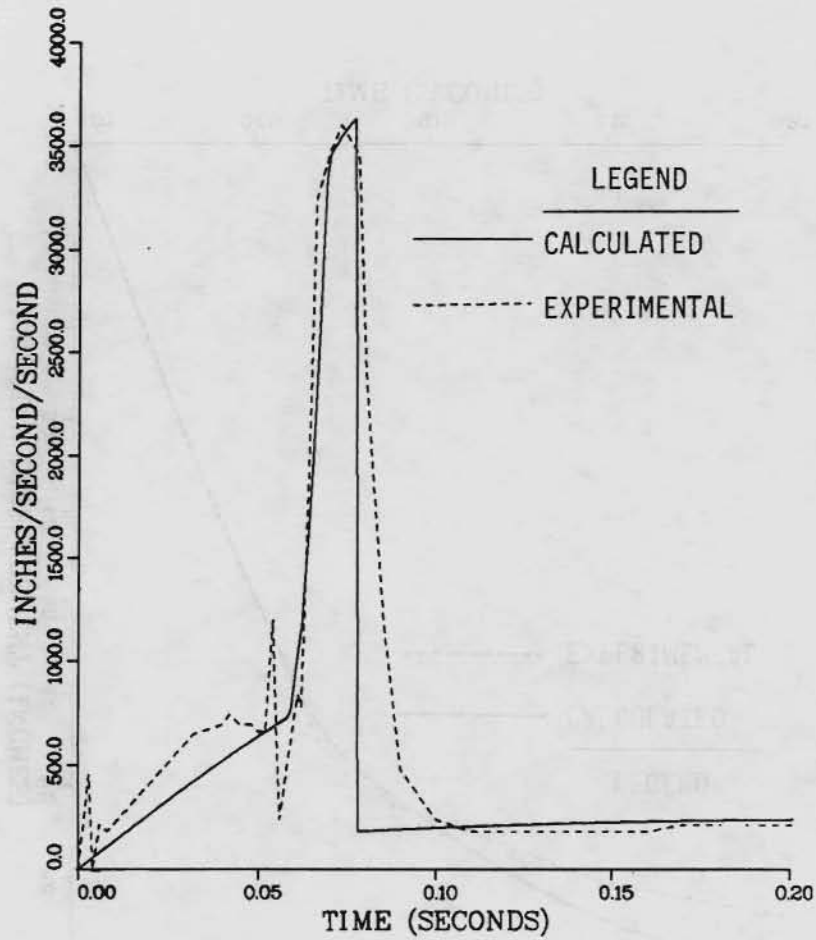


FIGURE 19. Relative Acceleration of Two Gravel-Filled Hopper Cars vs Time During Impact.

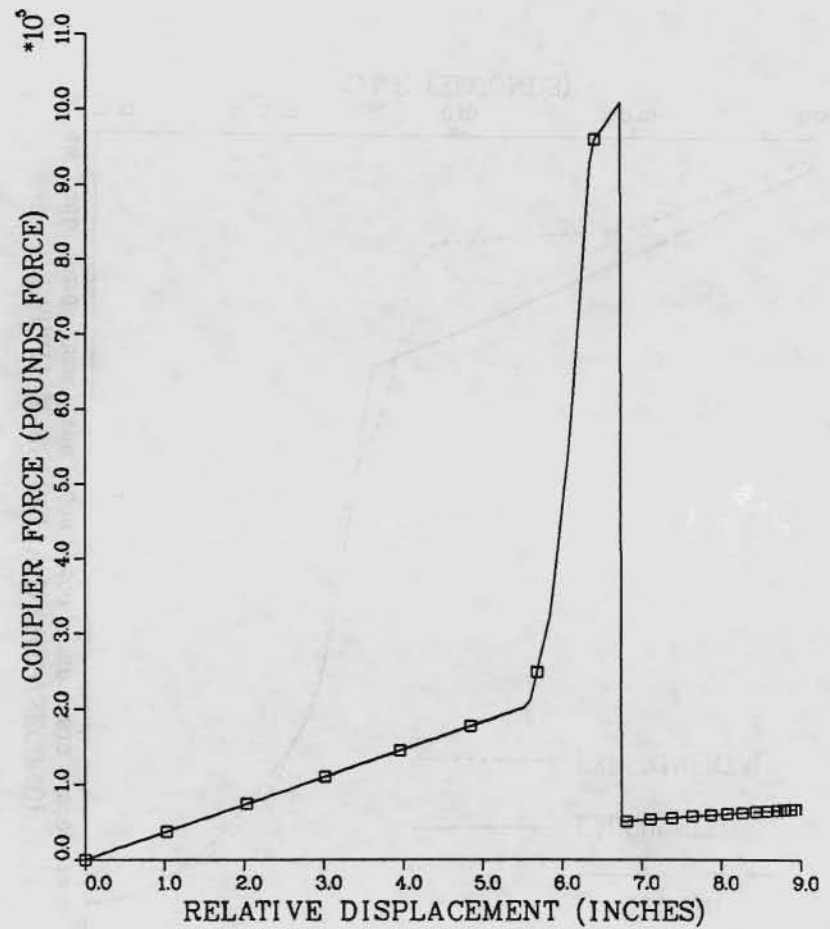


FIGURE 20. Calculated Coupler Force vs Calculated Relative Displacement of Two Gravel-Filled Hopper Cars During Impact.

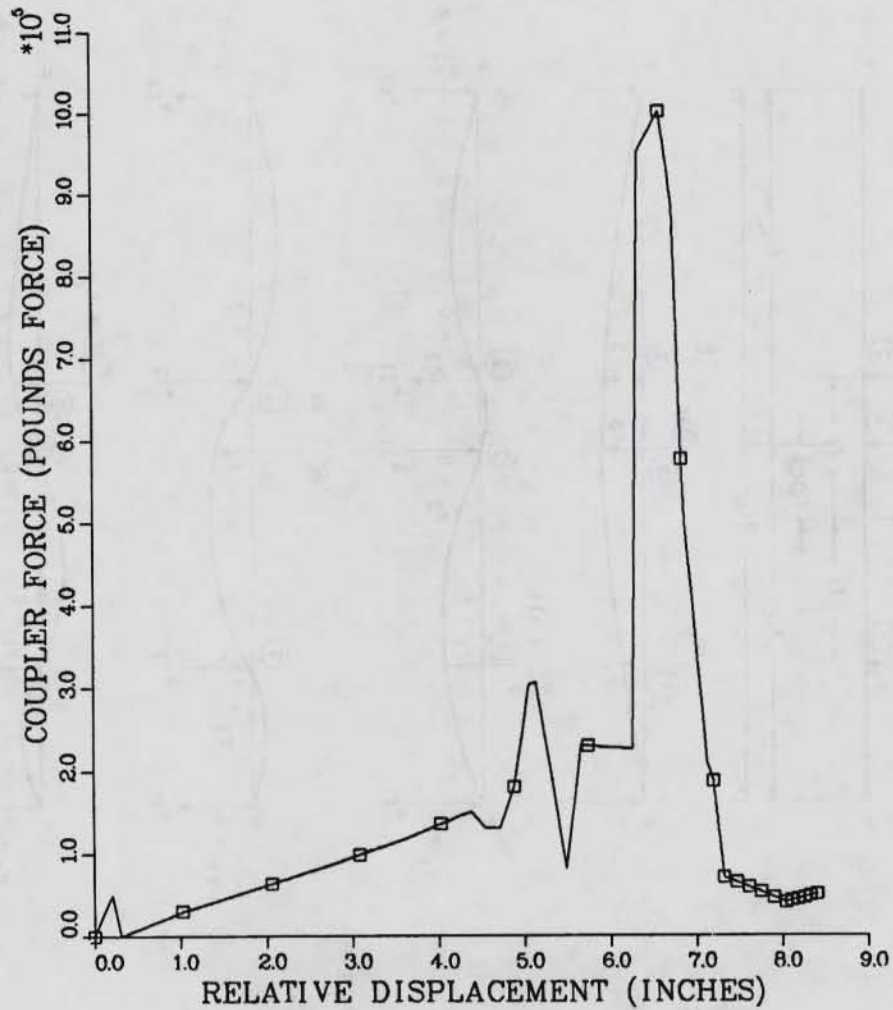
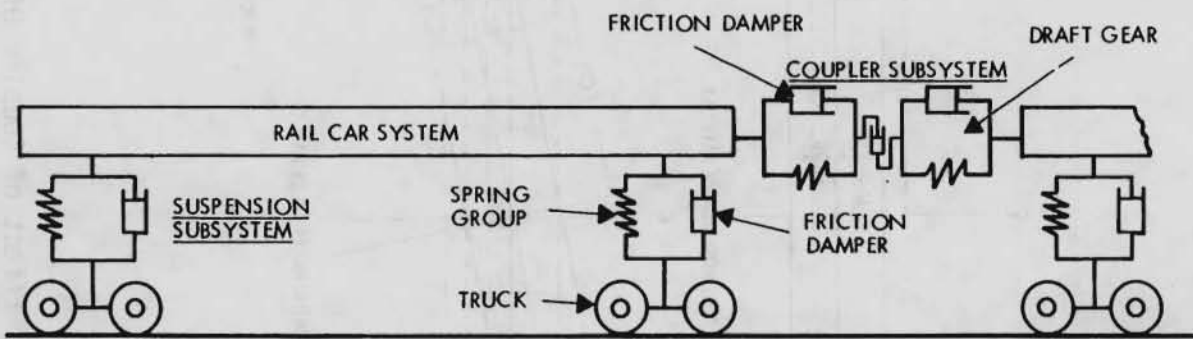


FIGURE 21. Measured Coupler Force vs Measured Relative Displacement of Two Gravel-Filled Hopper Cars During Impact.



HEDL 7904-320.1

FIGURE 22. Arrangement of Springs and Dampers Simulating Rail Car Coupler and Suspension Subsystems. Neg 7904699-1

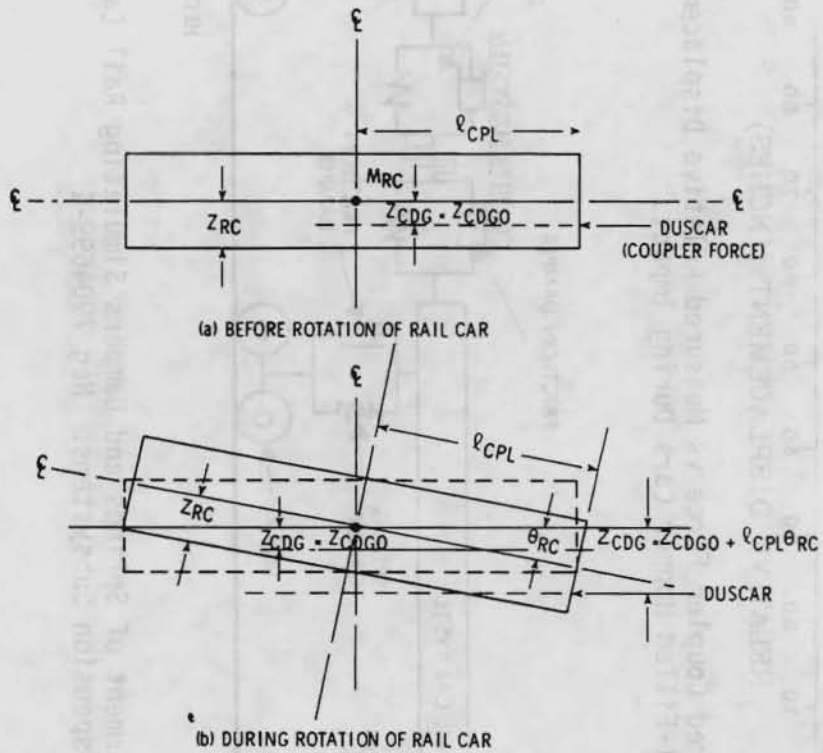


FIGURE 23. Effect of Coupler Offset on Rail Car Rotation.

HEDL 7905-163.1

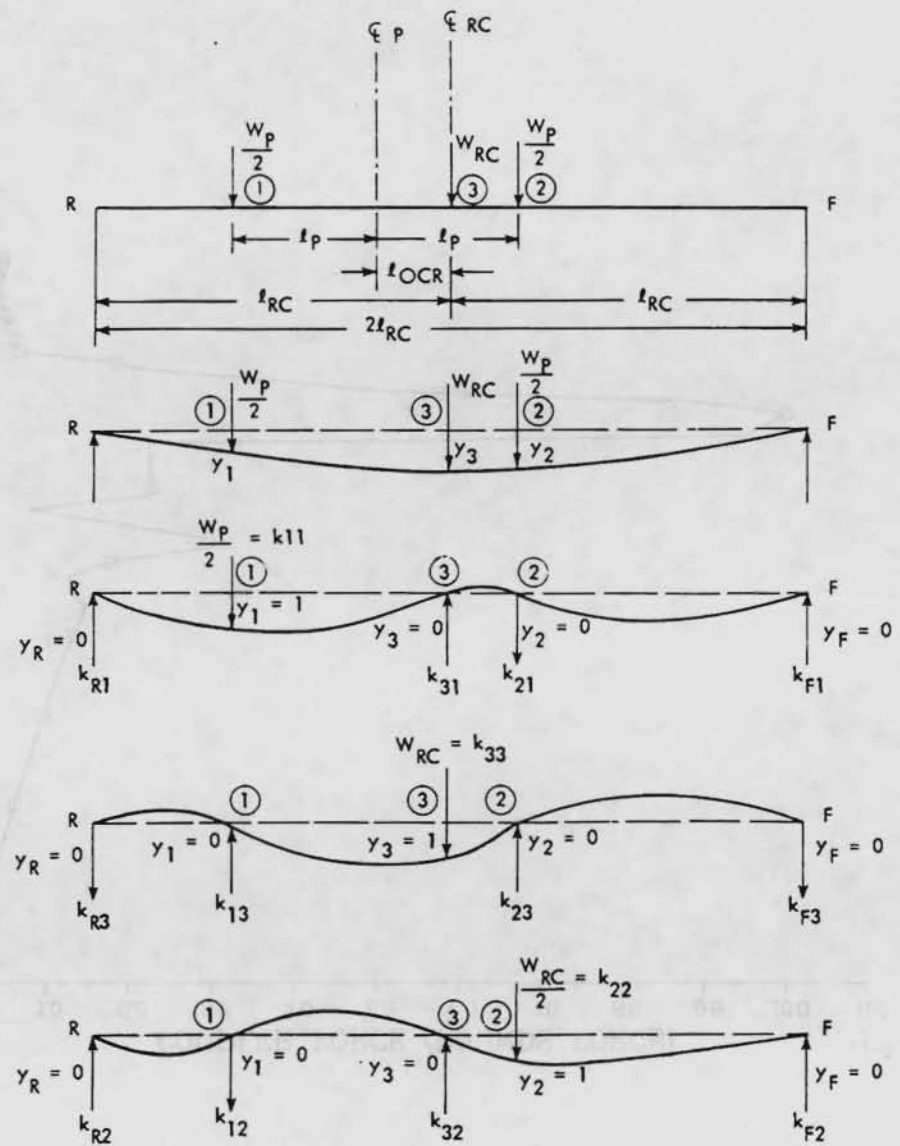
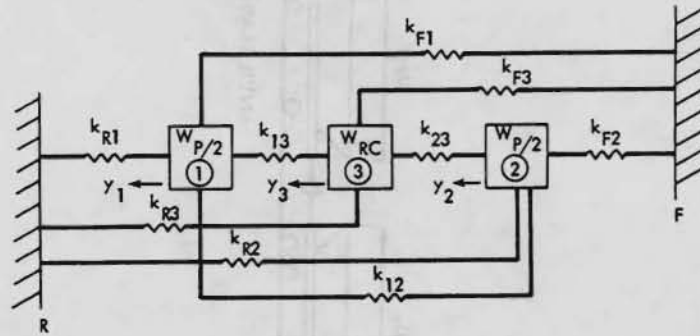
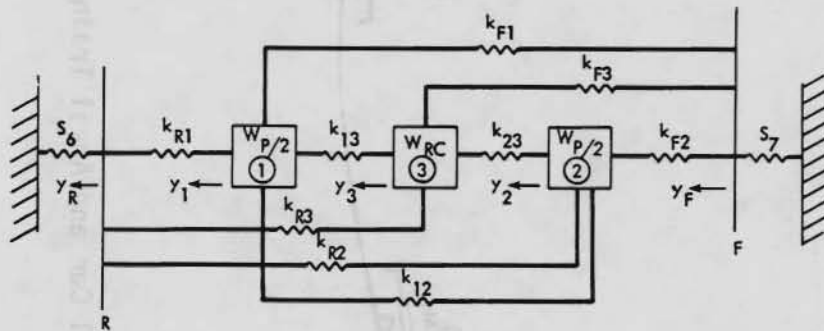


FIGURE 24. Deflection Diagrams for Rail Car Beam with Restraints to Define Force-Reaction System.



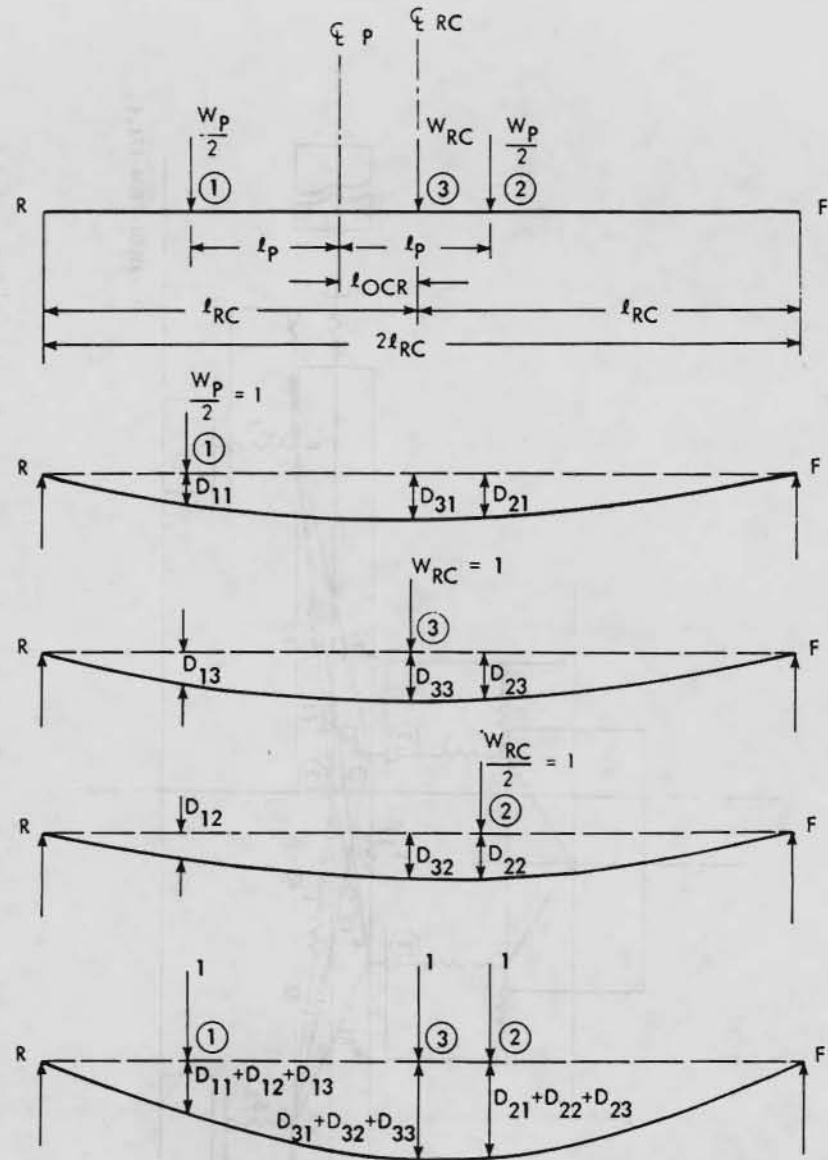
(a) Rail Car as Beam on Rigid Supports



(b) Rail Car as Beam Supported by Springs

HEDL 7804-174.5

FIGURE 25. Spring-Mass Submodel Representing Bending of Rail Car.



HEDL 7804-174.3

FIGURE 26. Deflection Diagrams for Rail Car Beam to Determine Deflections and Influence Coefficients.

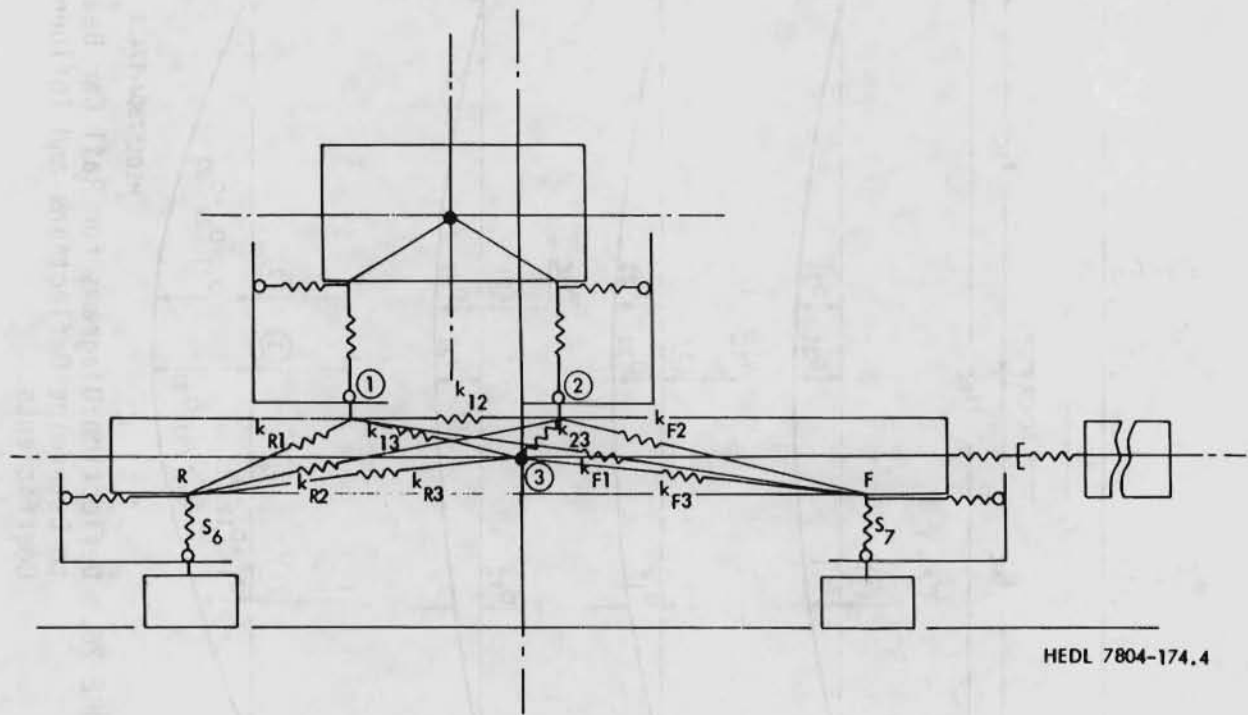


FIGURE 27. Dynamic Model of Cask-Rail Car System with Bending Submodel.

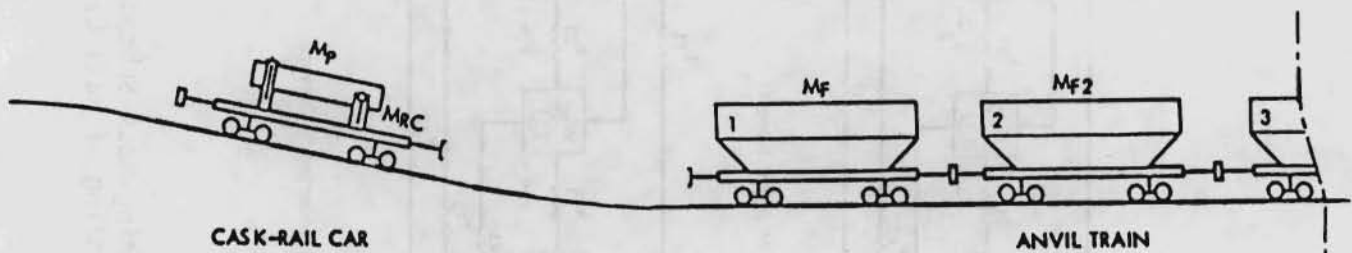
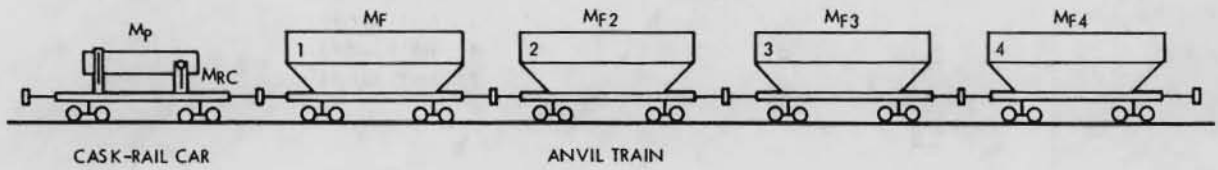


FIGURE 28. Cask-Rail Car and Anvil Train.



HEDL 7902-125.1

FIGURE 29. Cask-Rail Car and Anvil Train. Neg 7901733-1

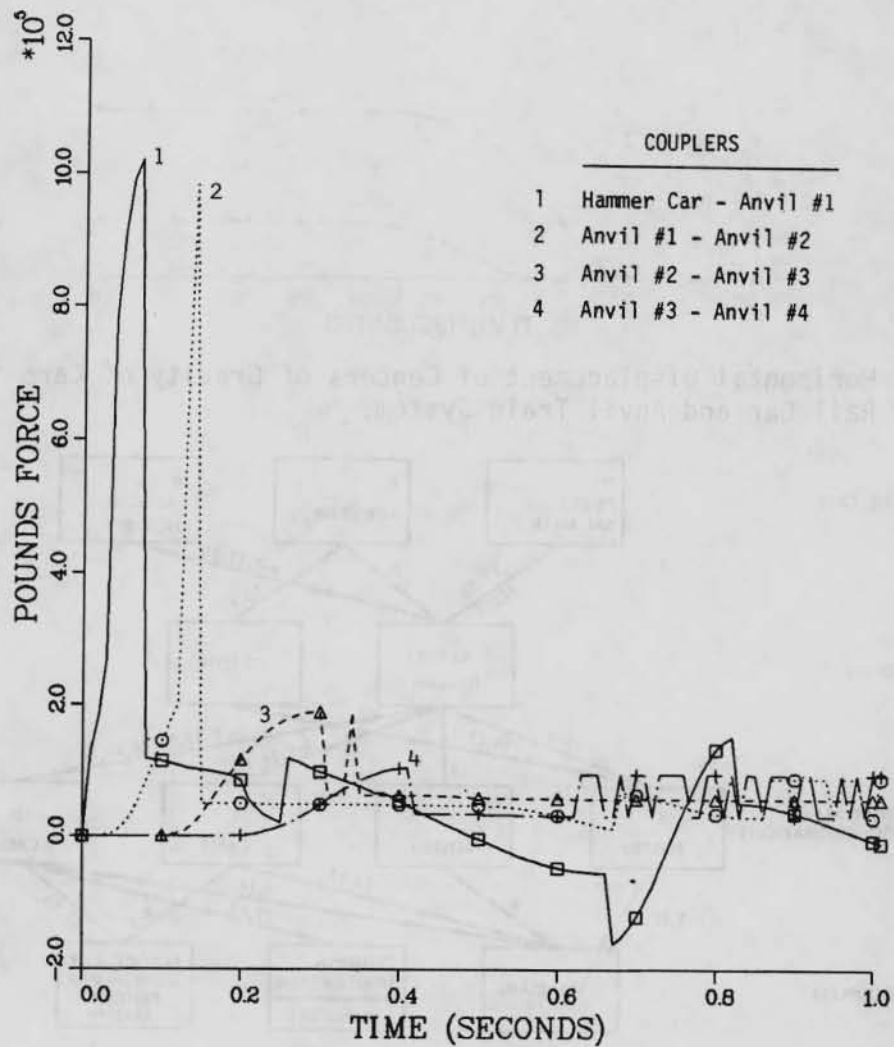


FIGURE 30. Coupler Force Between Cars in the Cask-Rail Car and Anvil Train System.

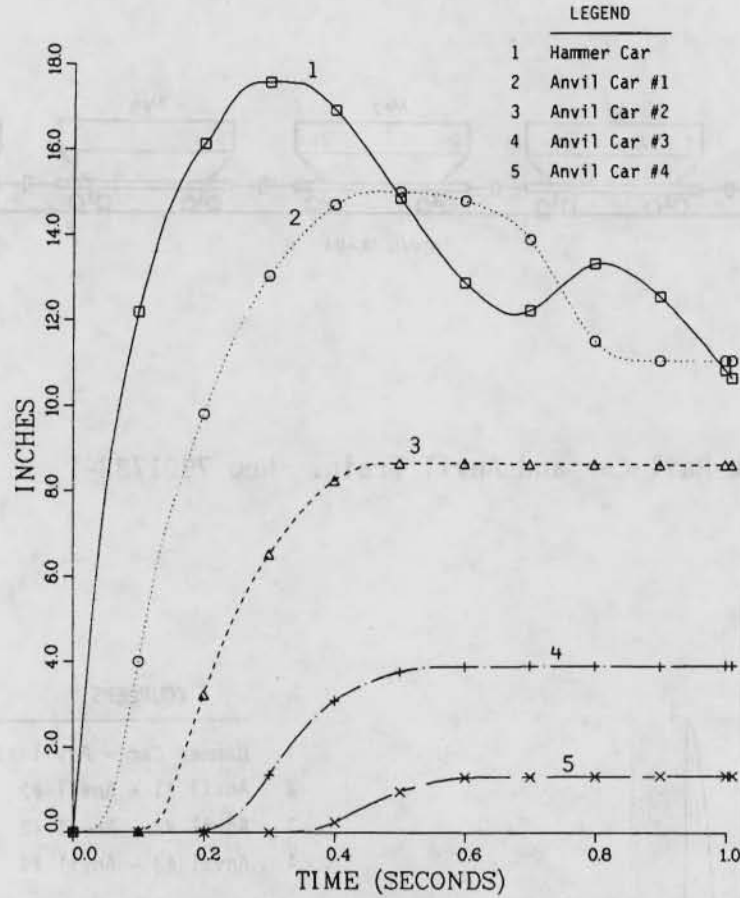
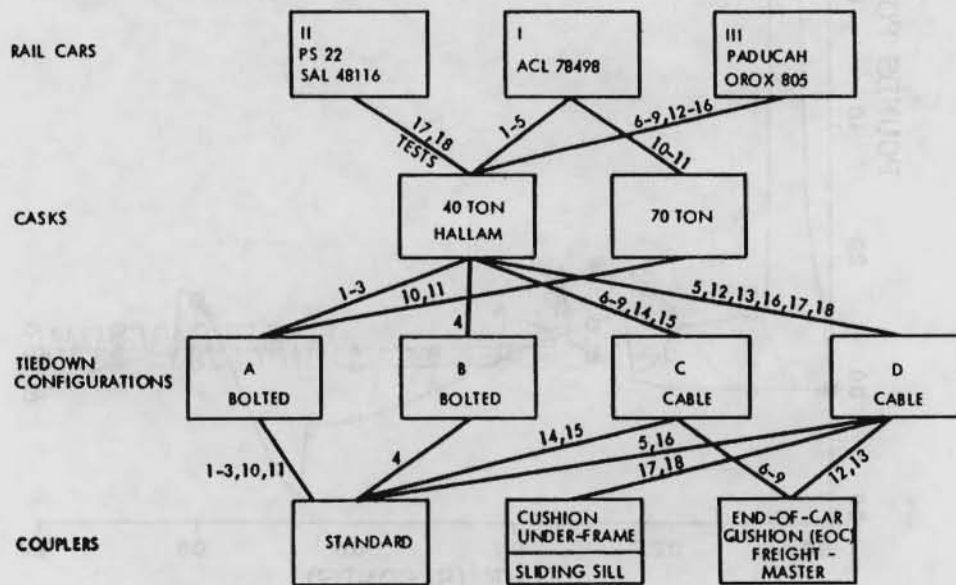


FIGURE 31. Horizontal Displacement of Centers of Gravity of Cars in the Cask-Rail Car and Anvil Train System.



HEDL 7911-198.1

FIGURE 32. Morphological Space Representation of Cask-Rail Car Coupling Tests.

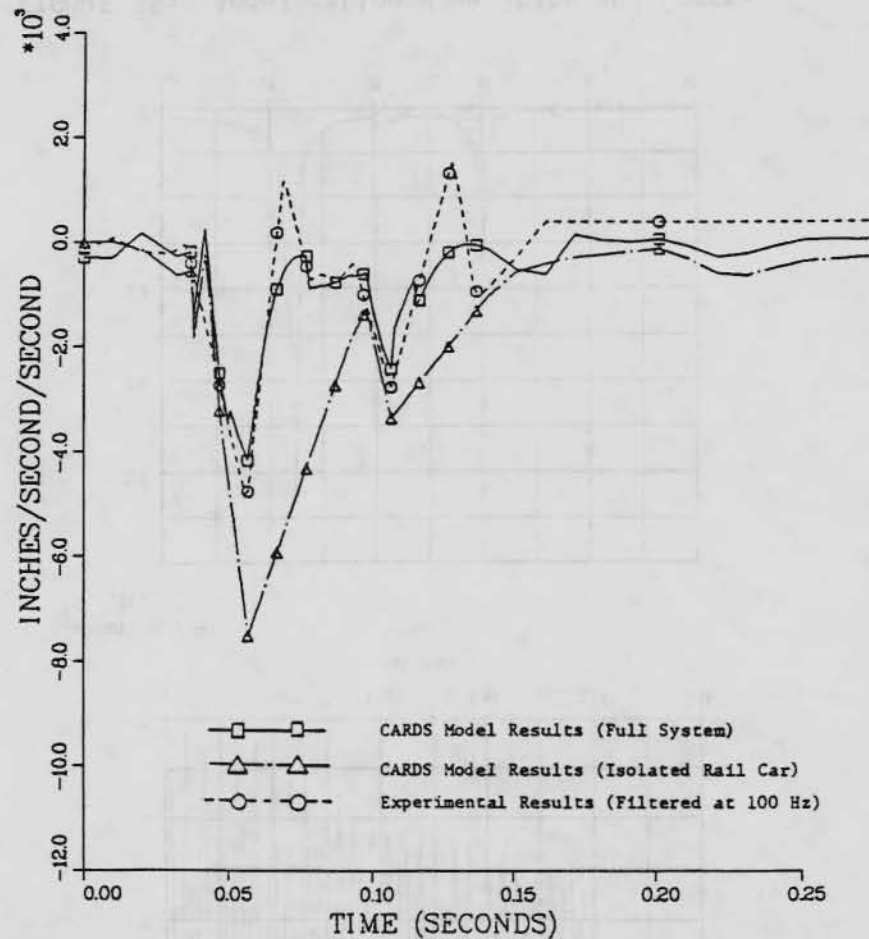


FIGURE 33. Horizontal Acceleration of the Cask-Rail Car During Impact with Four Hopper Cars Loaded with Ballast. (Test 3 - Instrument 12: Filtered at 100 Hz)(Case 1: Measured Coupler Force).

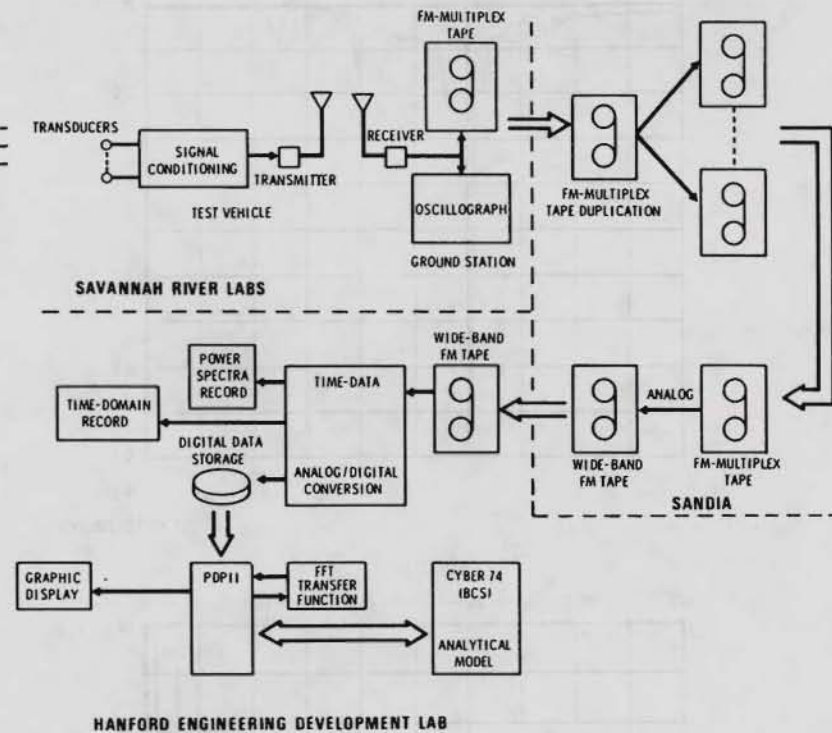


FIGURE 34. Shock/Vibration Data Flow for Data Reduction Model Verification.

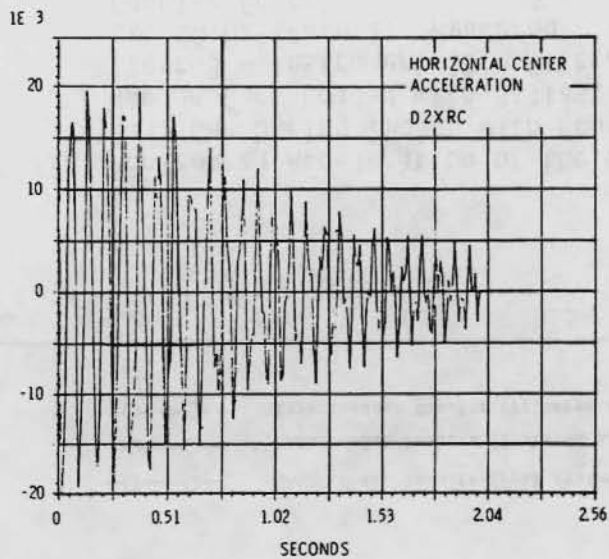


FIGURE 35a. Acceleration Wave Shape and Corresponding Frequency Spectrum Obtained by Fast Fourier Transform. (Horizontal Center Acceleration.)

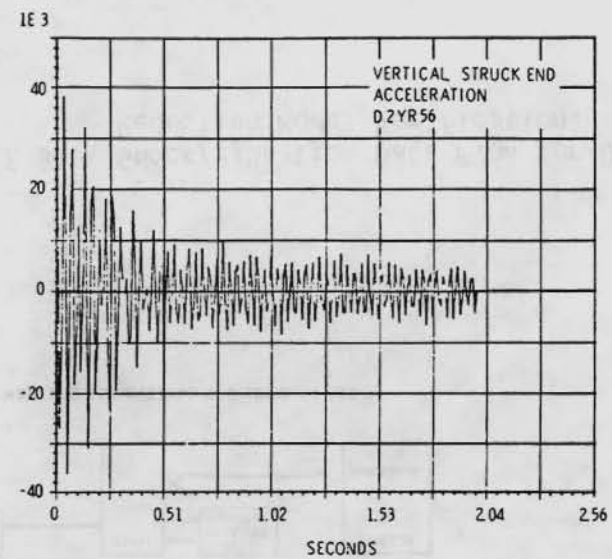
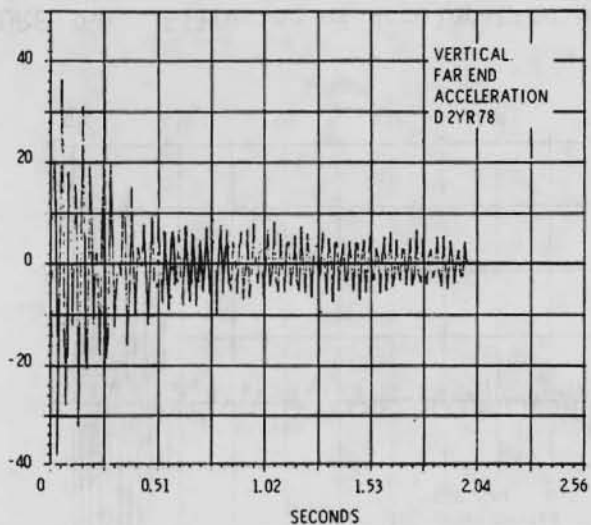
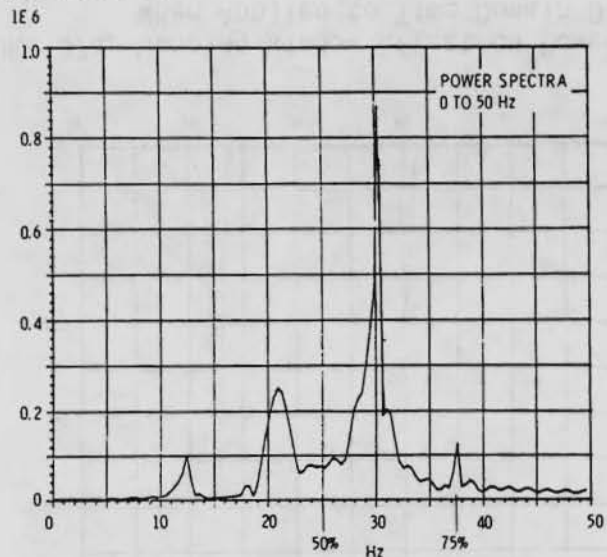


FIGURE 35b. Acceleration Wave Shape and Corresponding Frequency Spectrum Obtained by Fast Fourier Transform. (Vertical, Struck End Acceleration.)

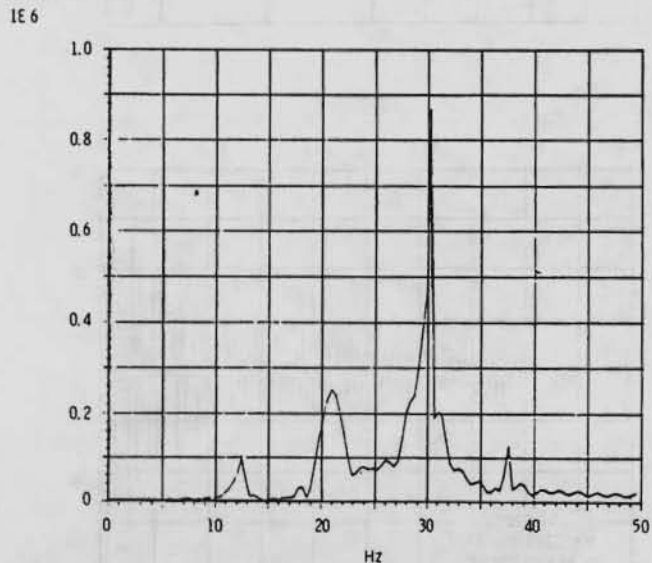
1 E 3



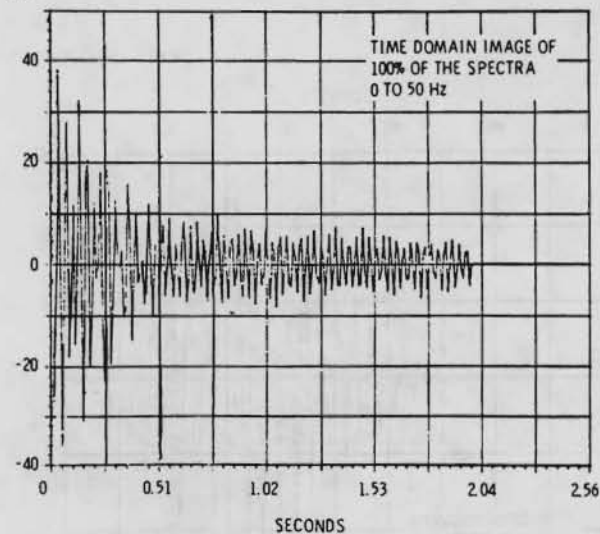
MAGNITUDE OF FFT OF D2YR56



MAGNITUDE OF FFT (X19)



1 E 3



11-21

FIGURE 35c. Acceleration Wave Shape and Corresponding Frequency Spectrum Obtained by Fast Fourier Transform. (Vertical, Far End Acceleration.)

FIGURE 36a. Filtering of Acceleration Data Employing Inverse FFT. (Power Spectra and Time Domain Image.)

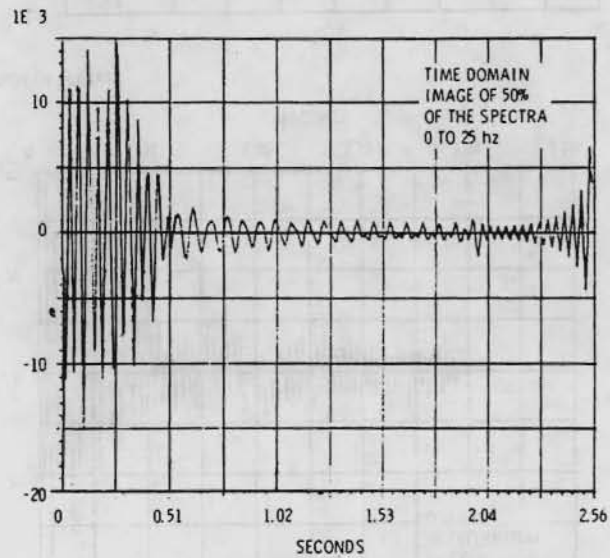
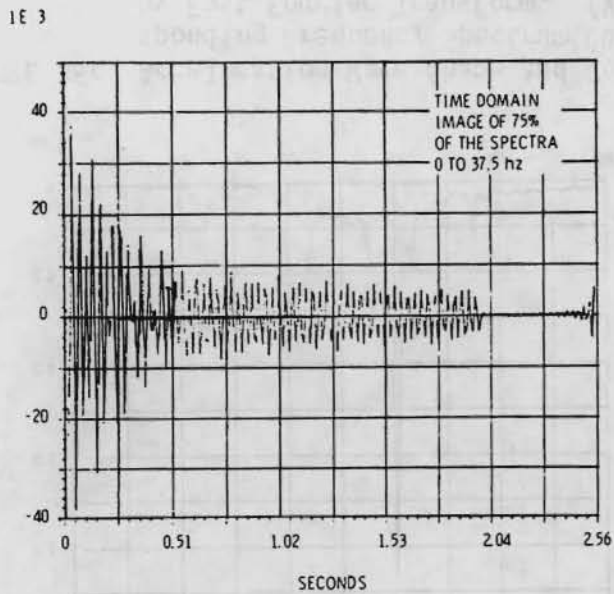


FIGURE 36b. Filtering of Acceleration Data Employing Inverse FFT. (Time Domain Images.)

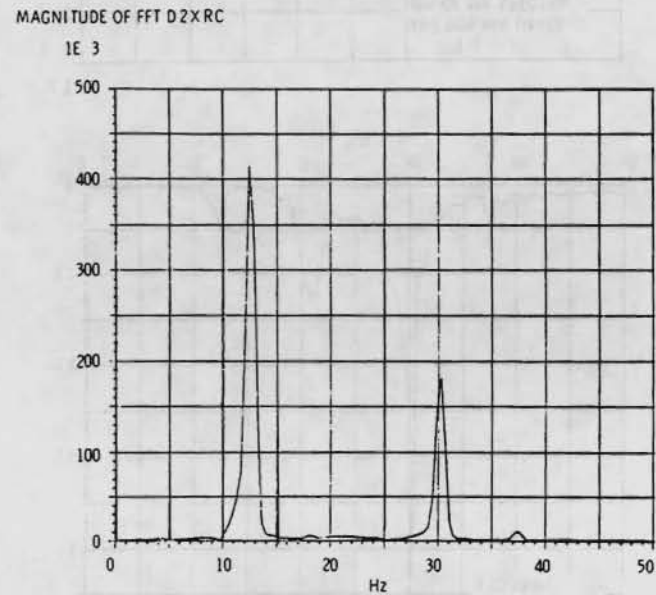
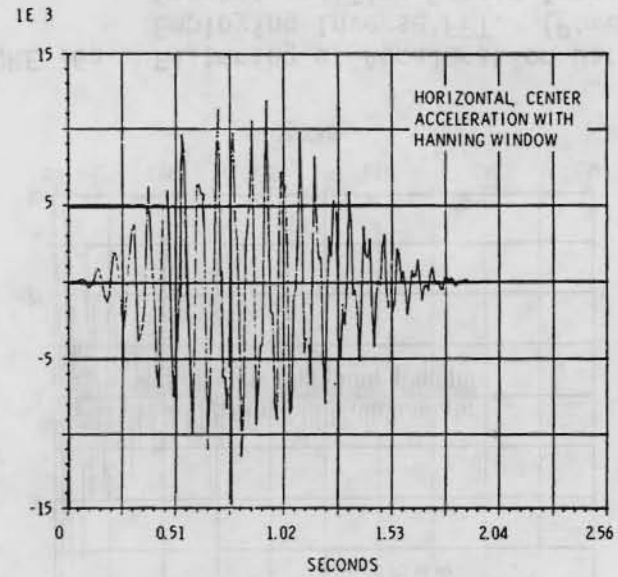
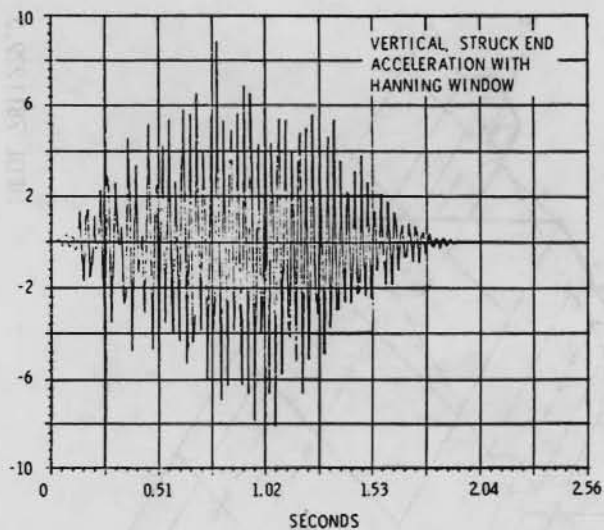


FIGURE 37a. Hanning Window Effect on Power Spectra When Applied to Time Domain Data. (Horizontal, Center Acceleration with Hanning Window.)

1E3 - D2YR56



MAGNITUDE OF FFT D2YR56

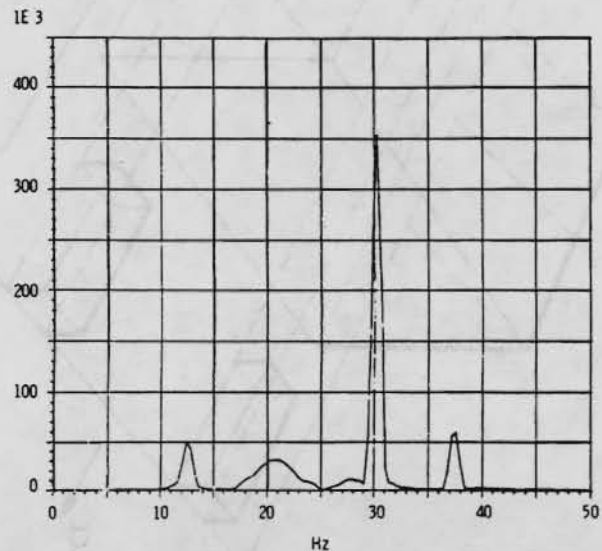


FIGURE 37b. Hanning Window Effect on Power Spectra When Applied to Time Domain Data. (Vertical, Struck End Acceleration with Hanning Window.)

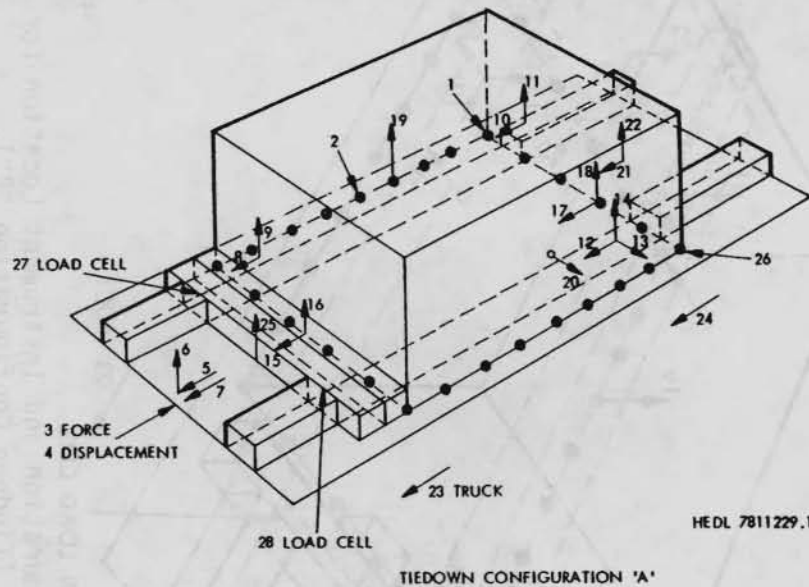
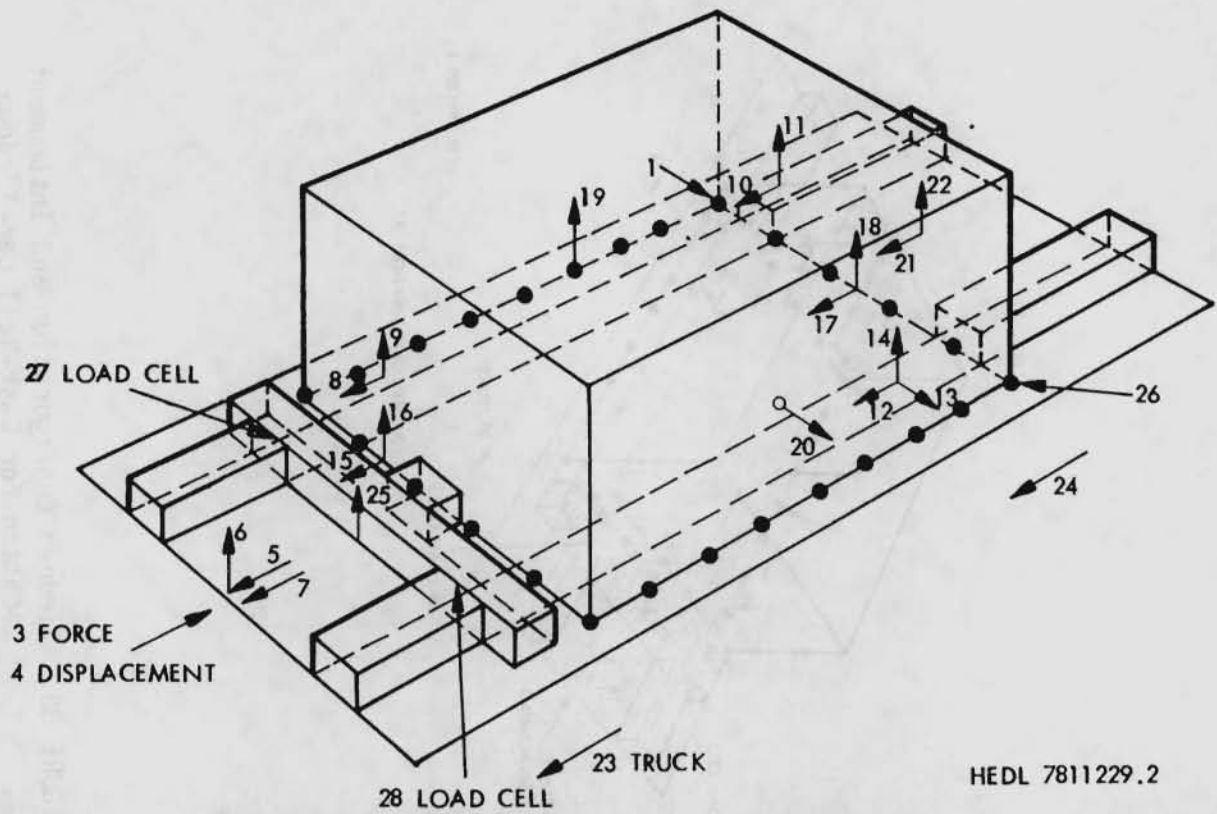
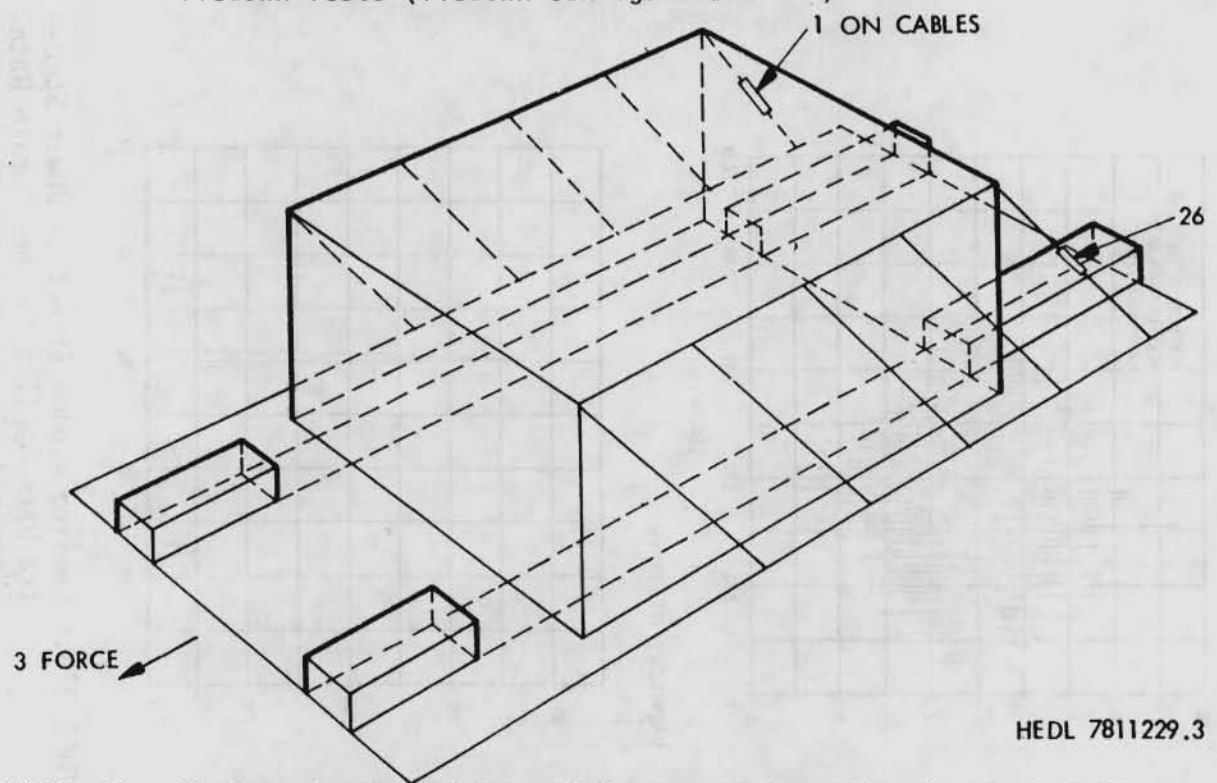


FIGURE 38. Tiedown Configuration and Instrument Location for Cask-Rail Car-Tiedown Tests (Tiedown Configuration "A").



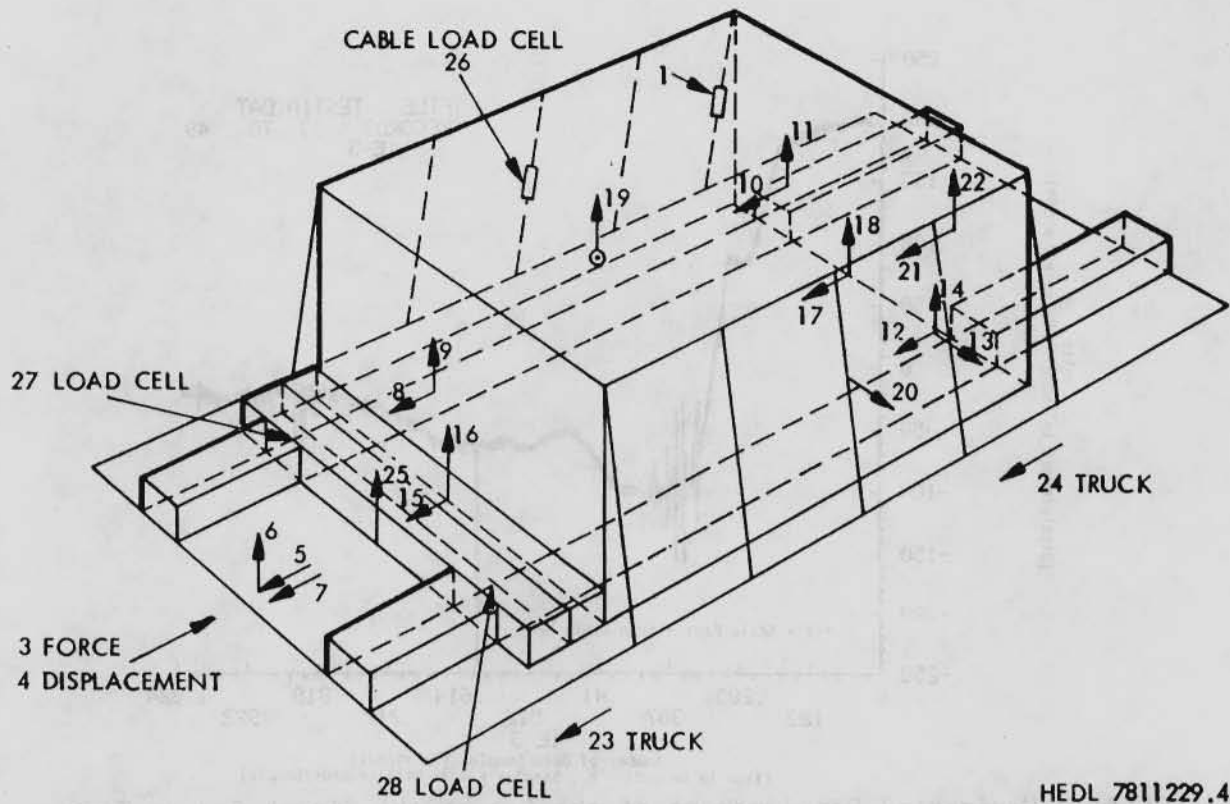
HEDL 7811229.2

FIGURE 39. Tiedown Configuration and Instrument Location for Cask-Rail Car-Tiedown Tests (Tiedown Configuration "B").



HEDL 7811229.3

FIGURE 40. Tiedown Configuration and Instrument Location for Cask-Rail Car-Tiedown Tests (Tiedown Configuration "C").



HEDL 7811229.4

FIGURE 41. Tiedown Configuration and Instrument Location for Cask-Rail Car-Tiedown Tests (Tiedown Configuration "D").

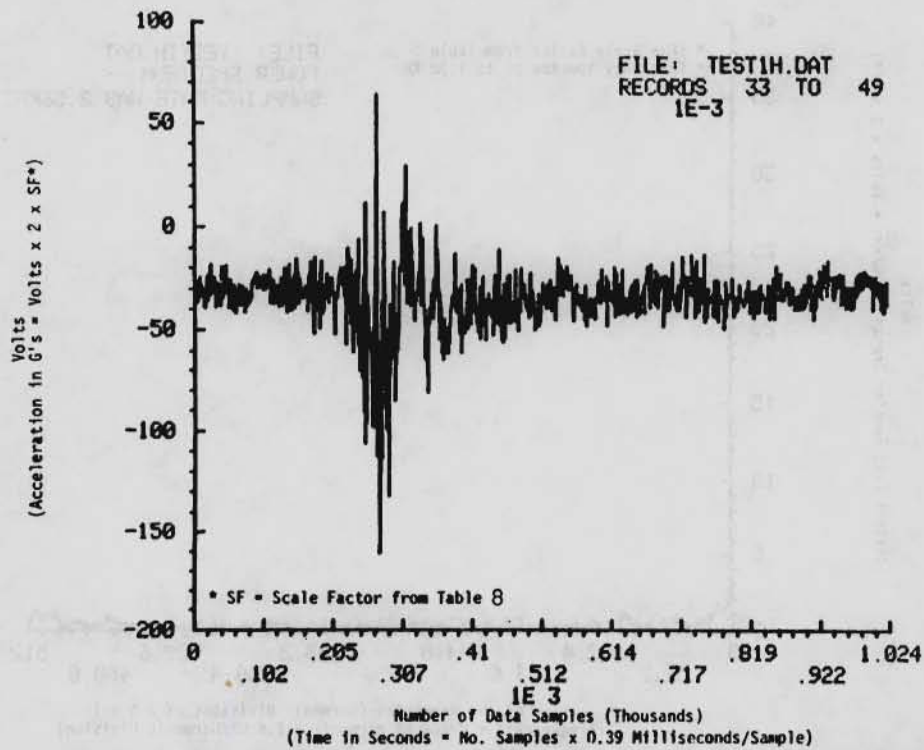


FIGURE 42. Horizontal or Longitudinal Acceleration of Car at Car/Cask Interface vs Time (Instrument No. 12 - Unfiltered).

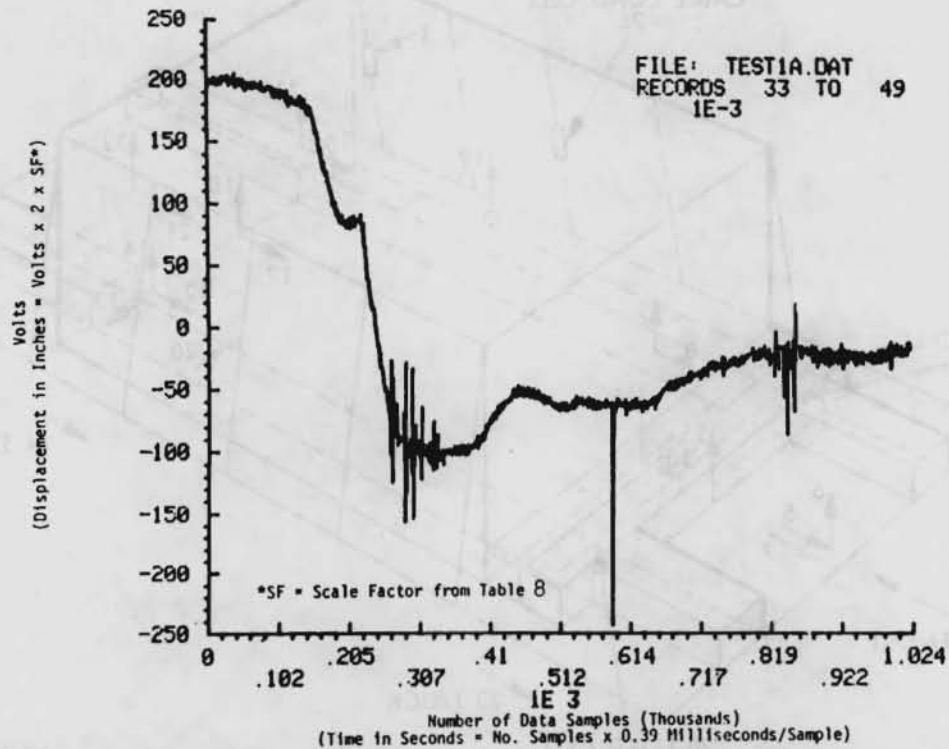


FIGURE 43. Horizontal Displacement of the Car at the Struck End vs Time (Instrument No. 4 - Unfiltered).

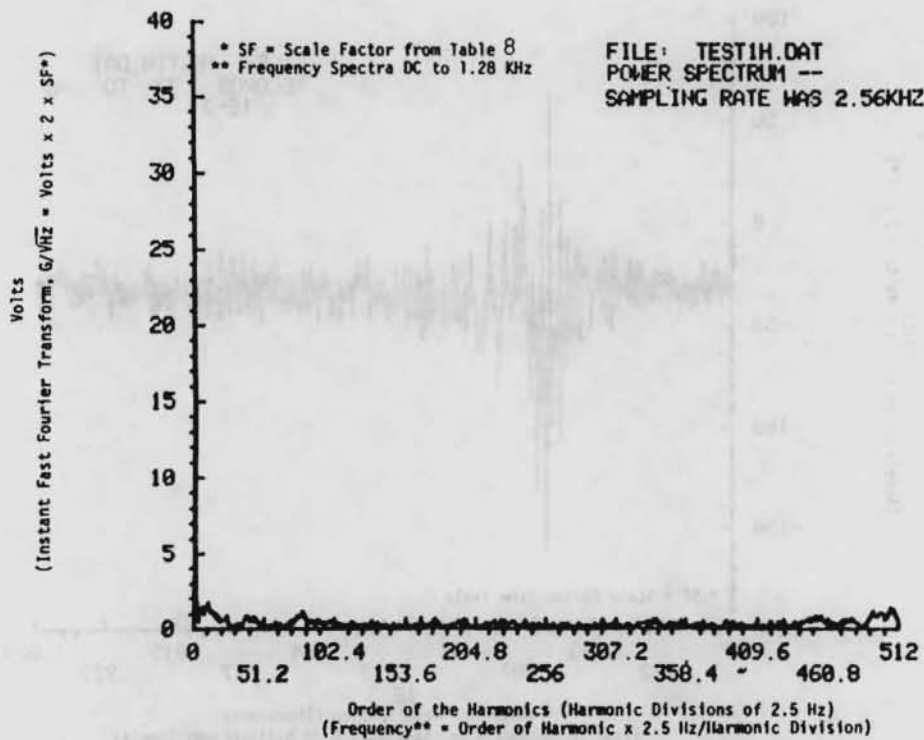


FIGURE 44. Horizontal Acceleration Response of Cask/Car Interface vs Frequency (Instrument No. 12 - Unfiltered).

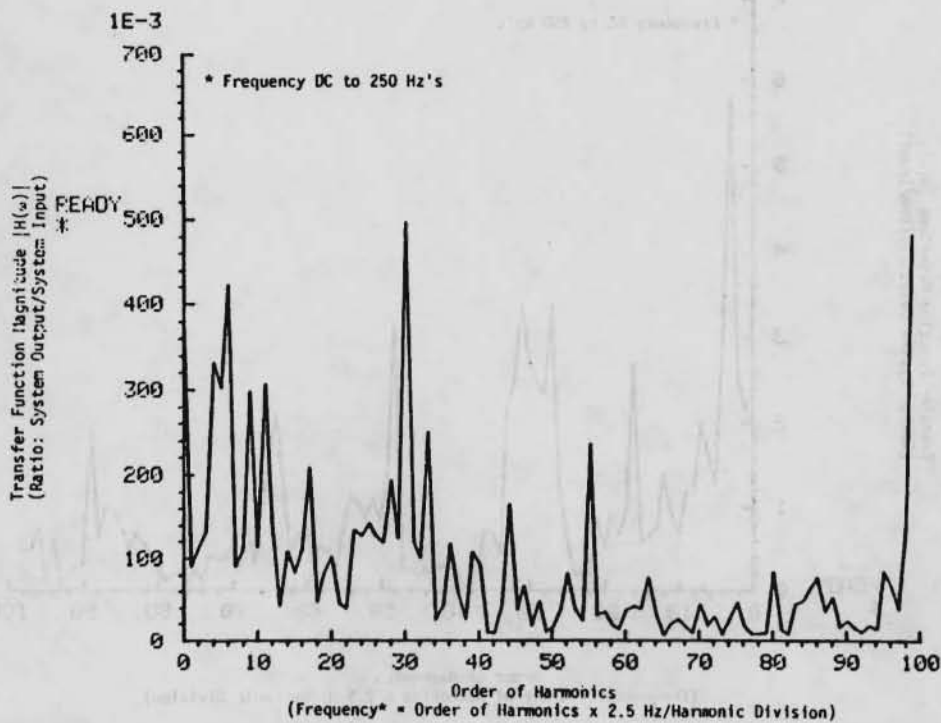


FIGURE 45. Transfer Function Magnitude vs Frequency (Vertical Energy Transfer from Instrument No. 22 to Instrument No. 11).

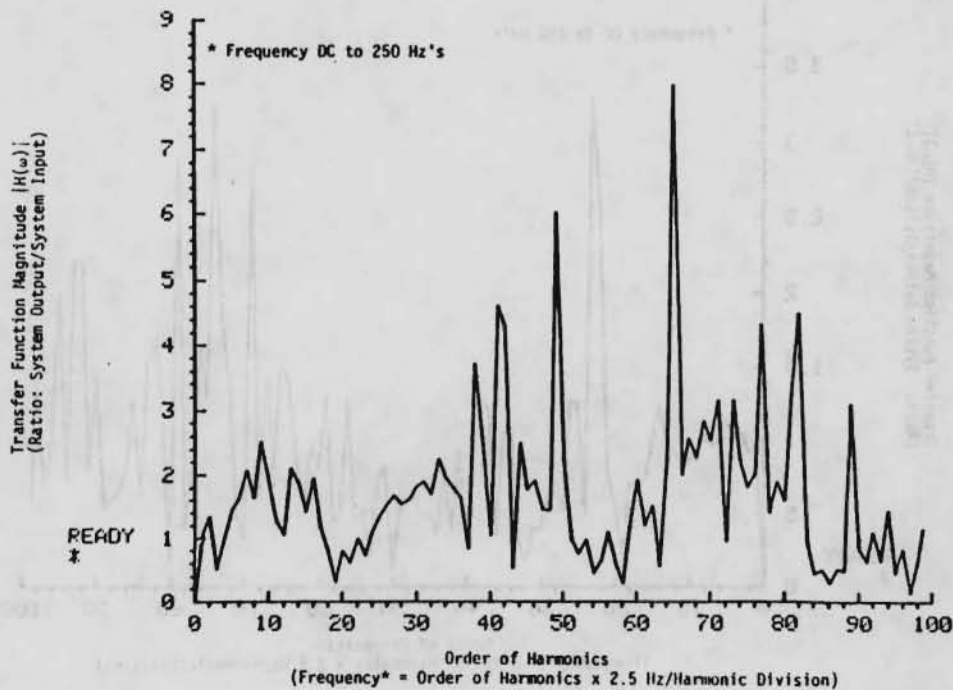


FIGURE 46. Transfer Function Magnitude vs Frequency (Vertical Energy Transfer from Instrument No. 11 to Instrument No. 9).

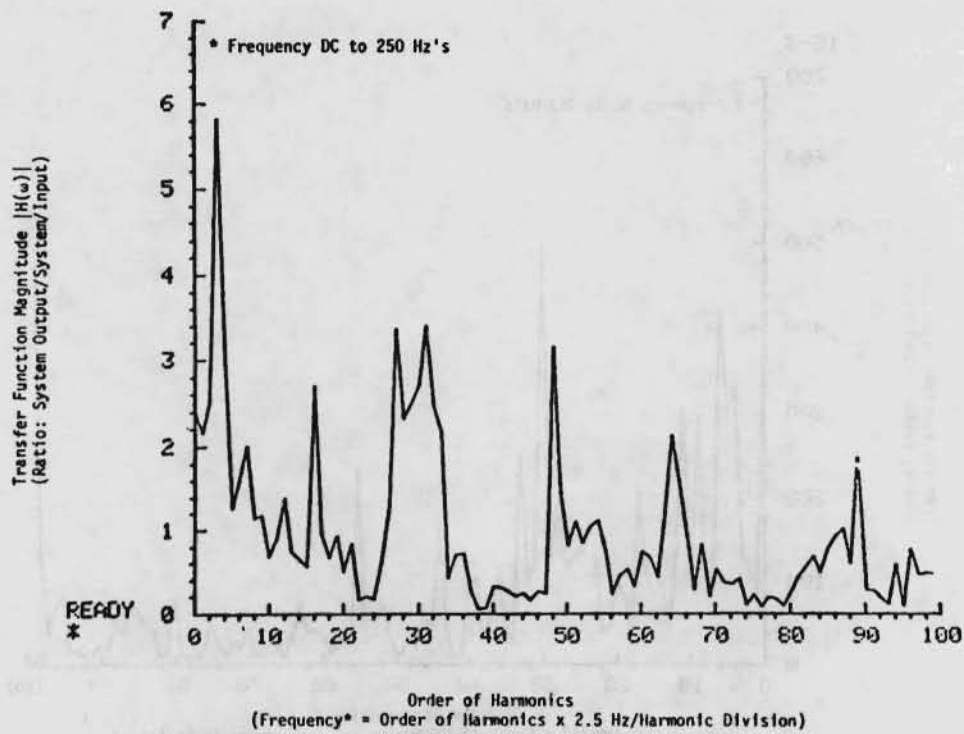


FIGURE 47. Transfer Function Magnitude vs Frequency (Horizontal Energy Transfer from Instrument No. 12 to Instrument No. 10).

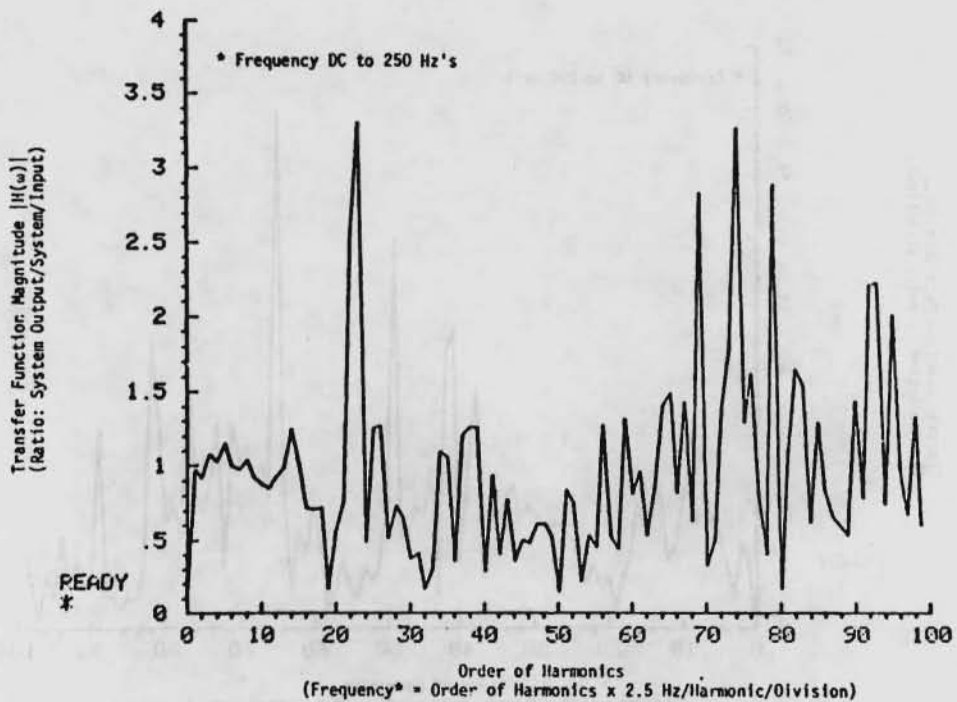


FIGURE 48. Transfer Function Magnitude vs Frequency (Horizontal Energy Transfer from Instrument No. 10 to Instrument No. 8).

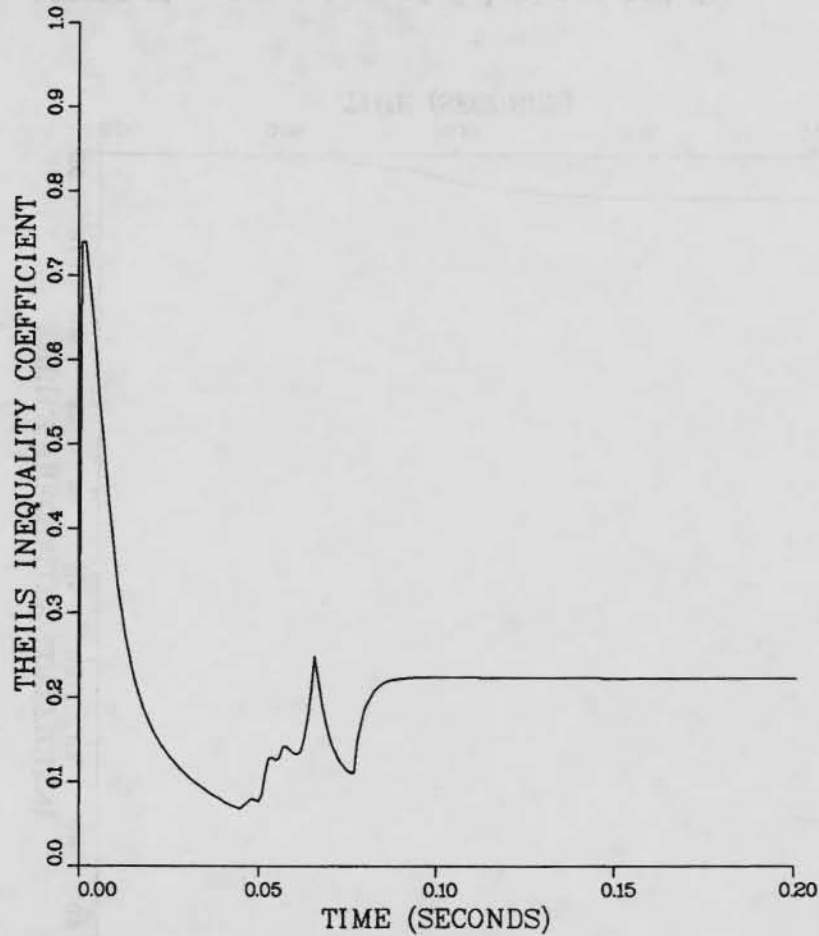


FIGURE 49. Comparison of Calculated and Measured Coupler Forces Using Theil's Inequality Coefficient as a Figure of Merit.

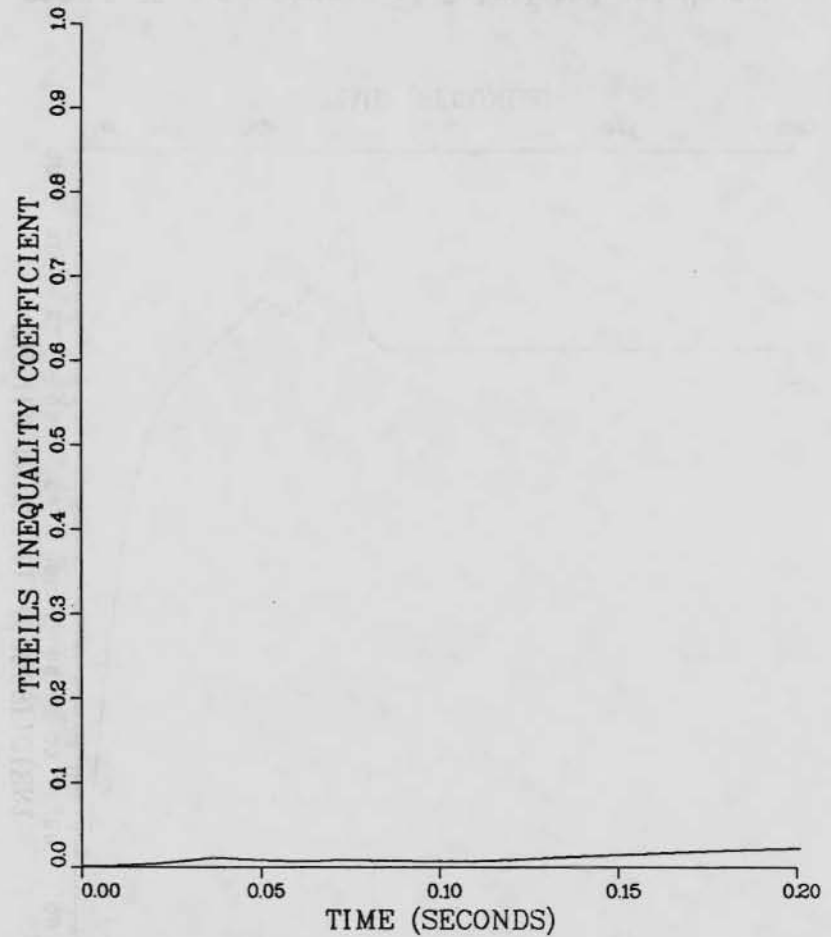


FIGURE 50. Comparison of Calculated and Measured Relative Displacements of Rail Car Centers of Gravity in the Time Domain Using Theil's Inequality Coefficient as a Figure of Merit.

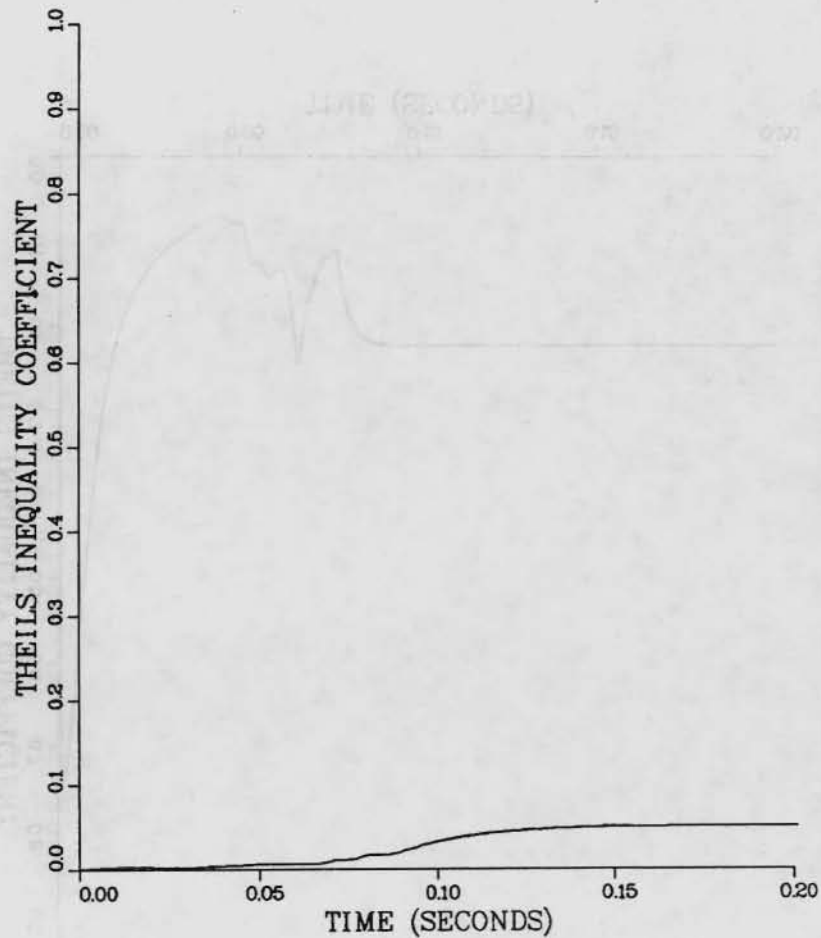


FIGURE 51. Comparison of Calculated and Measured Relative Velocities in the Time Domain Using Theil's Inequality Coefficient as a Figure of Merit.

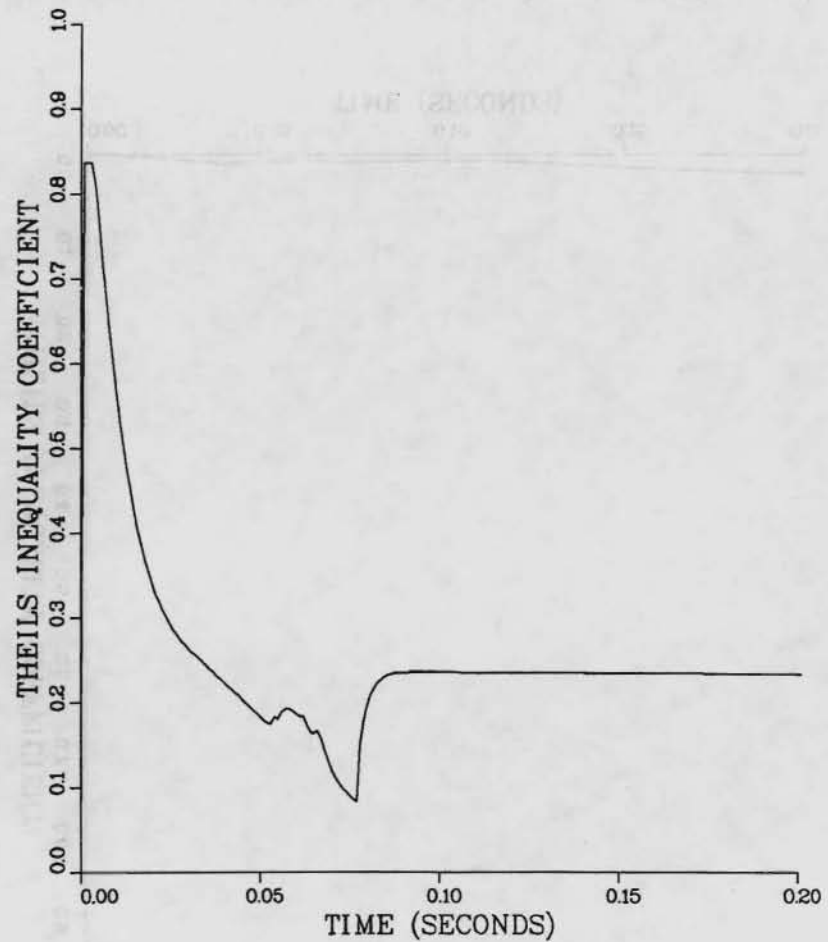


FIGURE 52. Comparison of Calculated and Measured Relative Accelerations in the Time Domain Using Theil's Inequality Coefficient as a Figure of Merit.

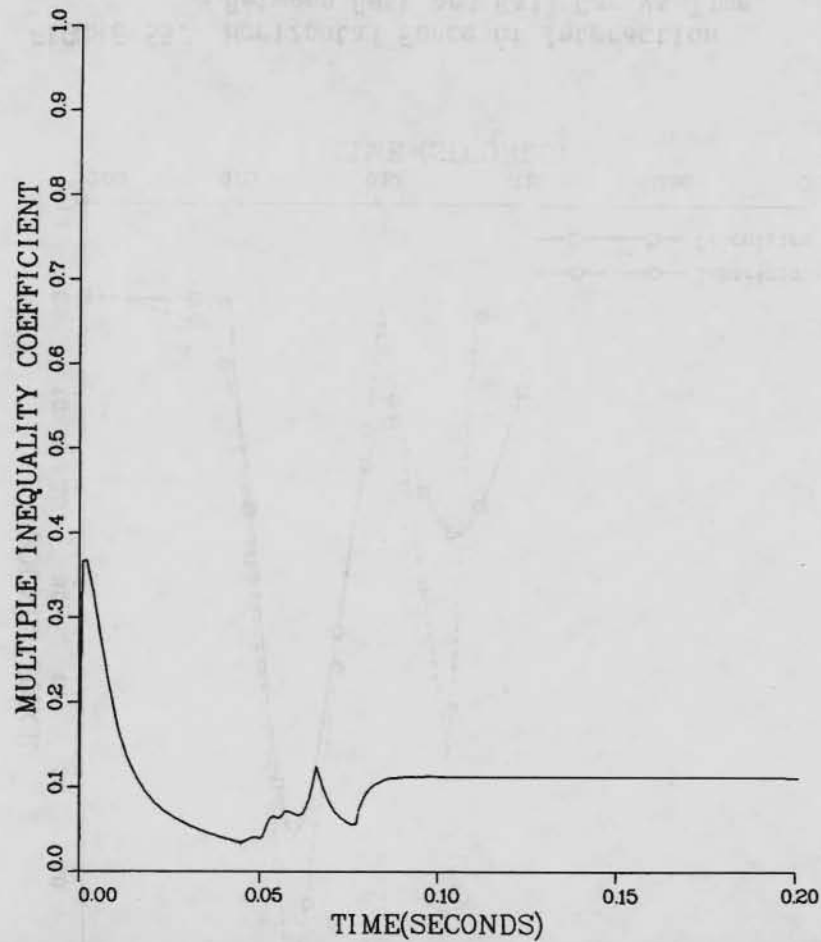


FIGURE 53. Simultaneous Comparison of Calculated and Measured Response Variables in the Time Domain Using Theil's Multiple Inequality Coefficient as an Overall Figure of Merit.

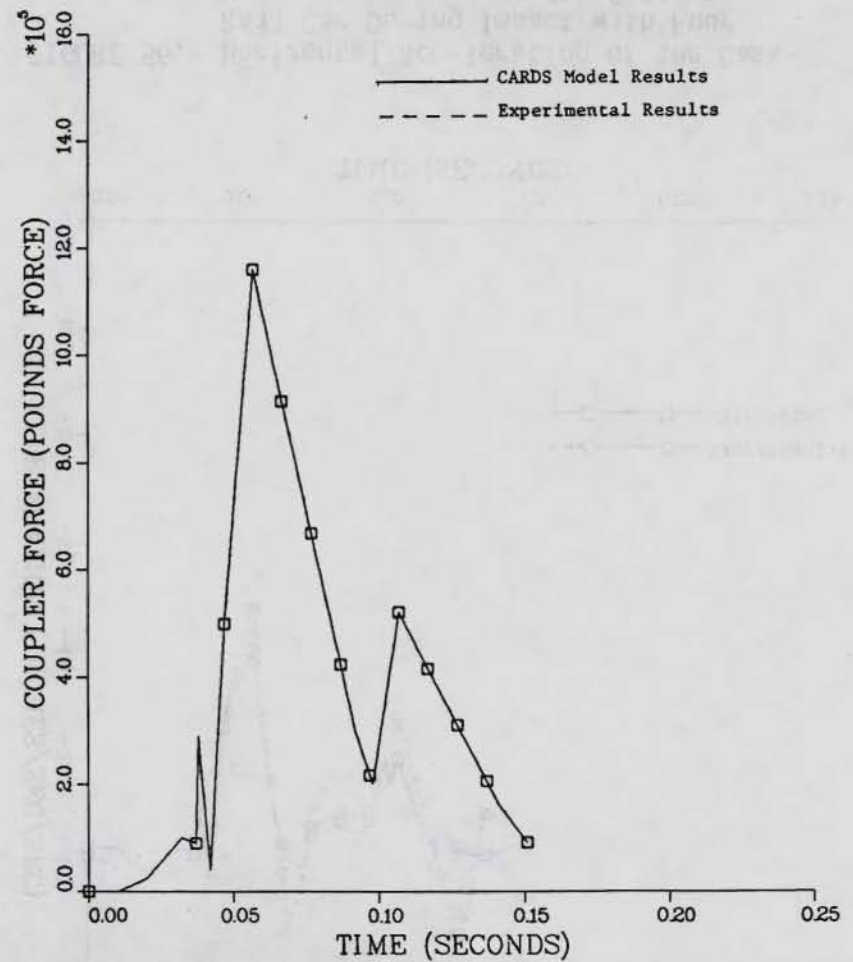


FIGURE 54. Coupler Force vs Time During Impact of Cask-Rail Car with Four Hopper Cars Loaded with Ballast (Test 3 - Instrument 3) (Case 1: Measured Coupler Force).

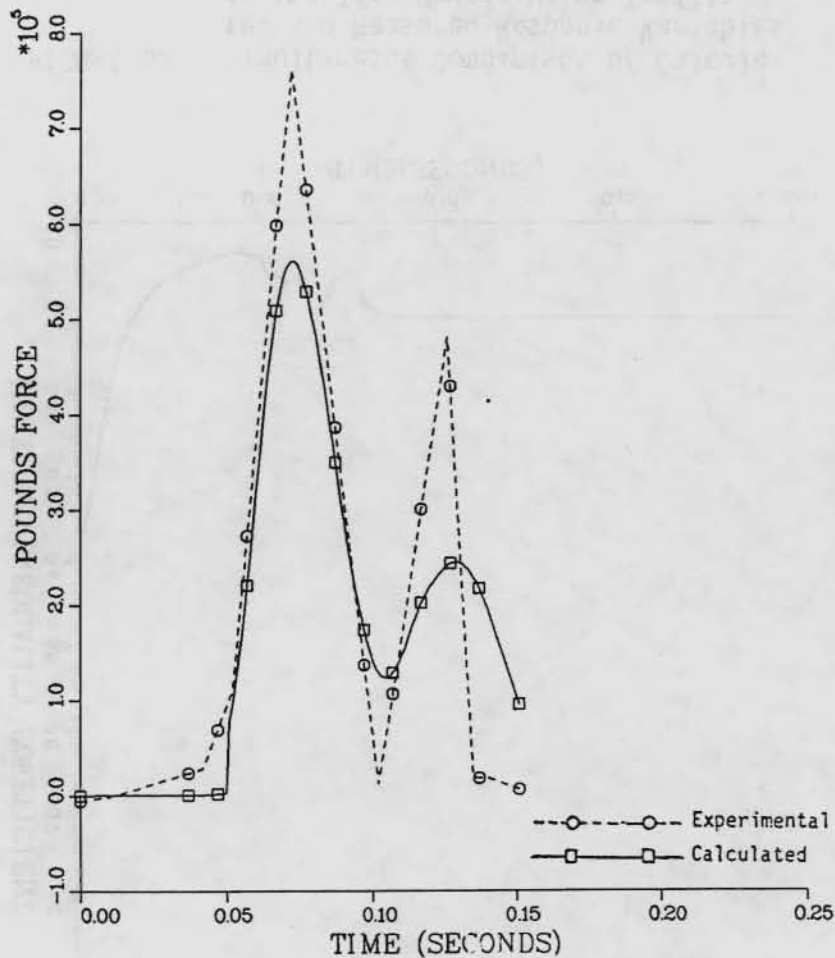


FIGURE 55. Horizontal Force of Interaction Between Cask and Rail Car vs Time During Impact with Four Hopper Cars Loaded with Ballast (Test 3 - Instrument 27) (Case 1: Measured Coupler Force).

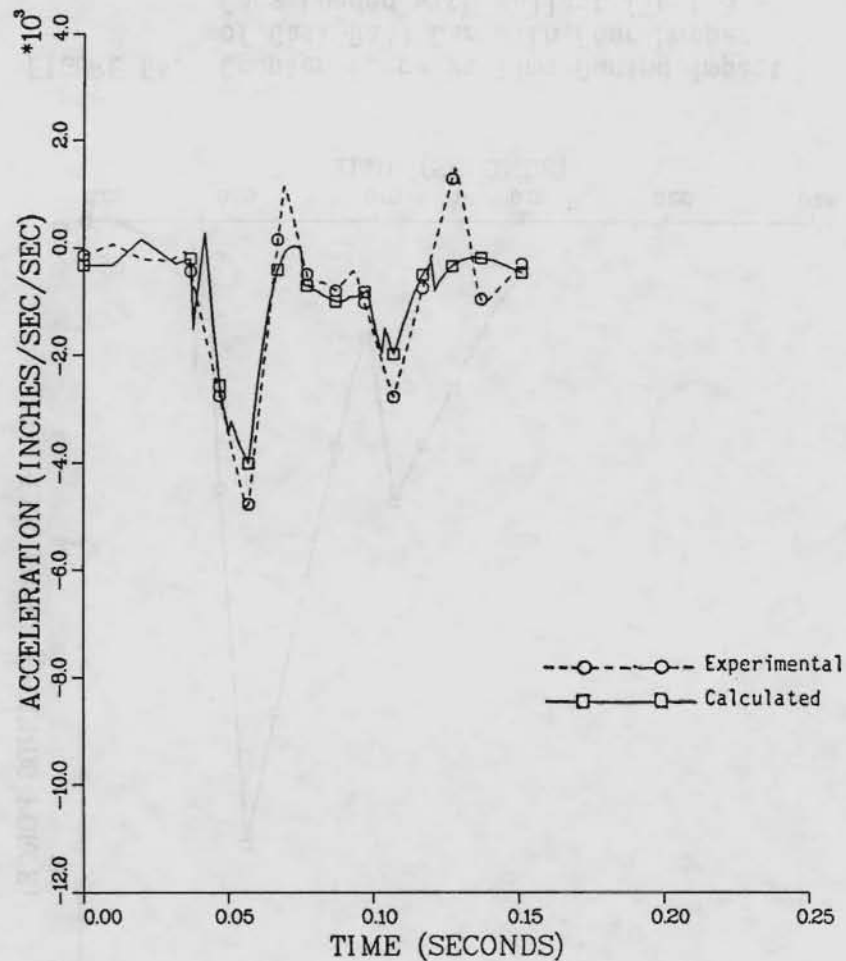


FIGURE 56. Horizontal Acceleration of the Cask-Rail Car During Impact with Four Hopper Cars Loaded with Ballast (Test 3 - Instrument 12: Filtered at 100 Hz) (Case 1: Measured Coupler Force).

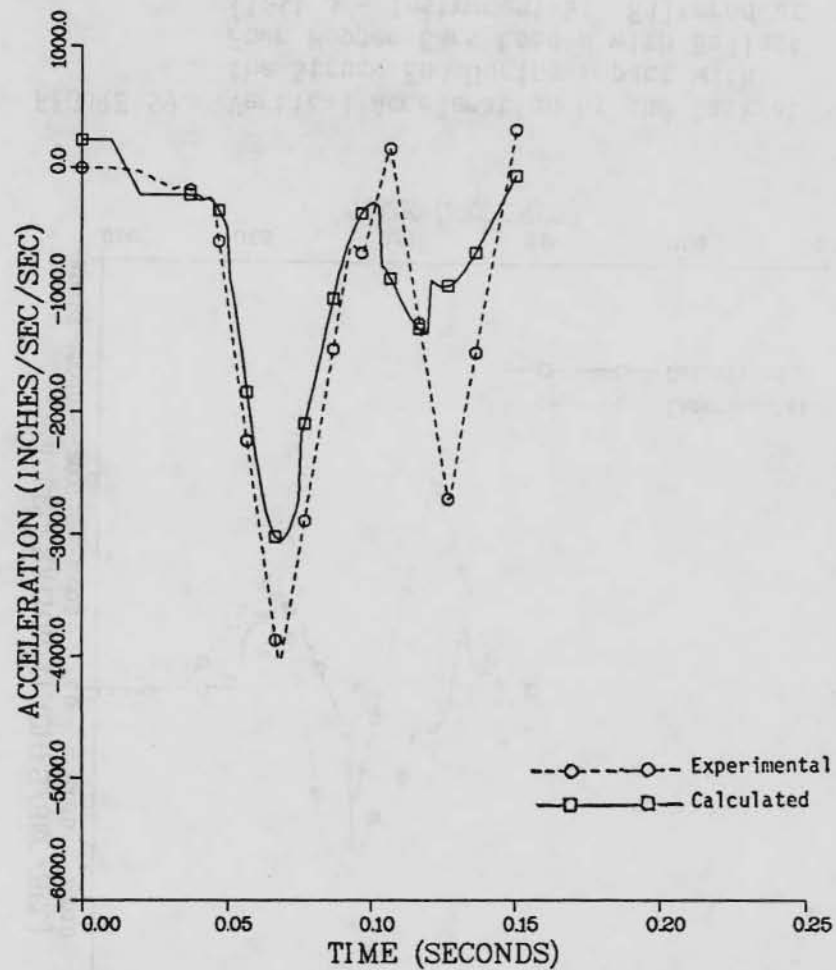


FIGURE 57. Horizontal Acceleration of the Cask During Impact with Four Hopper Cars Loaded with Ballast (Test 3 - Instrument 8: Filtered at 100 Hz) (Case 1: Measured Coupler Force).

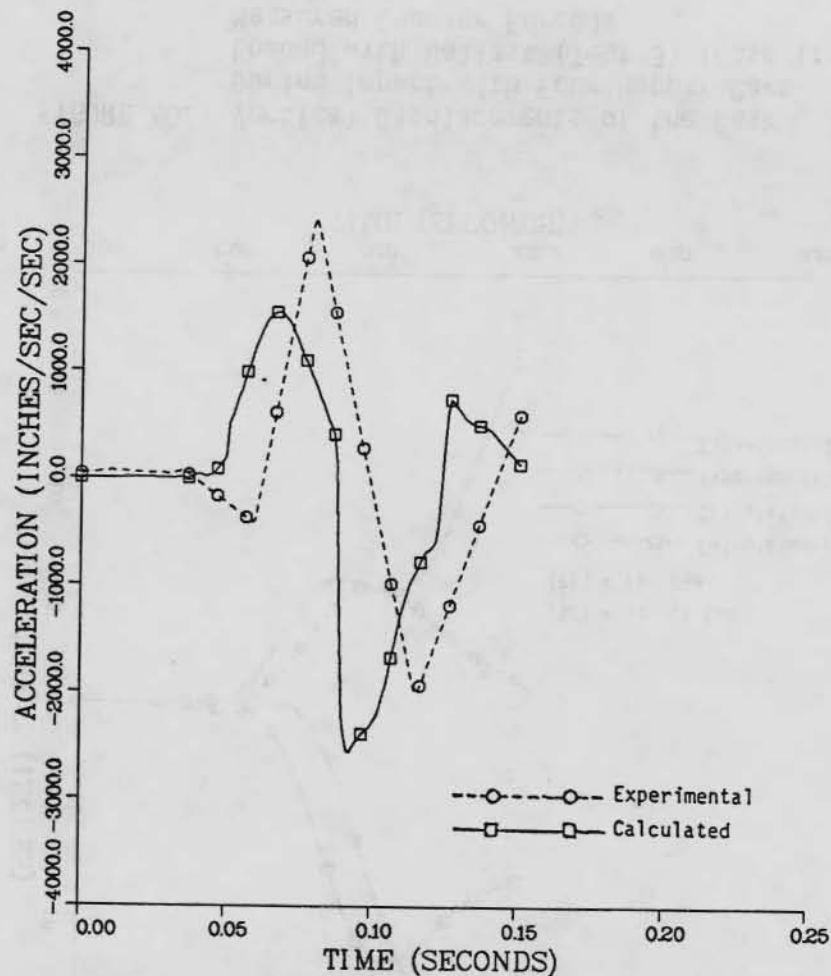


FIGURE 58. Vertical Acceleration of the Cask at the Far End During Impact with Four Hopper Cars Loaded with Ballast (Test 3 - Instrument 11: Filtered at 50 Hz) (Case 1: Measured Coupler Force.)

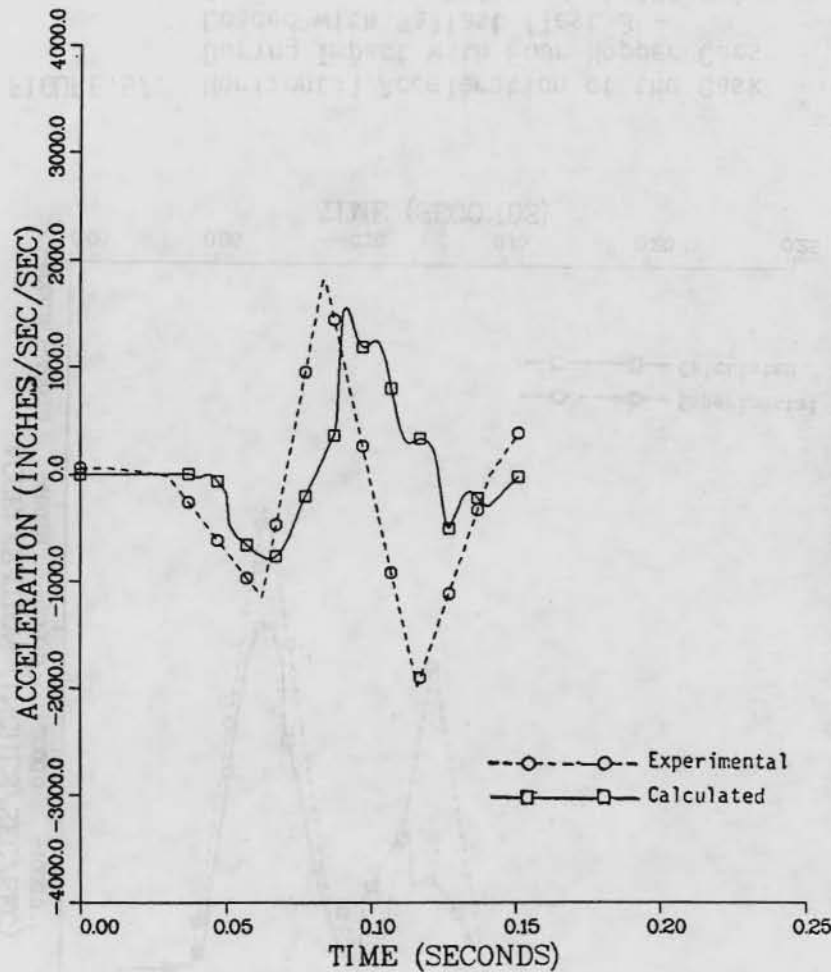


FIGURE 59. Vertical Acceleration of the Cask at the Struck End During Impact with Four Hopper Cars Loaded with Ballast (Test 3 - Instrument 9: Filtered at 50 Hz) (Case 1: Measured Coupler Force).

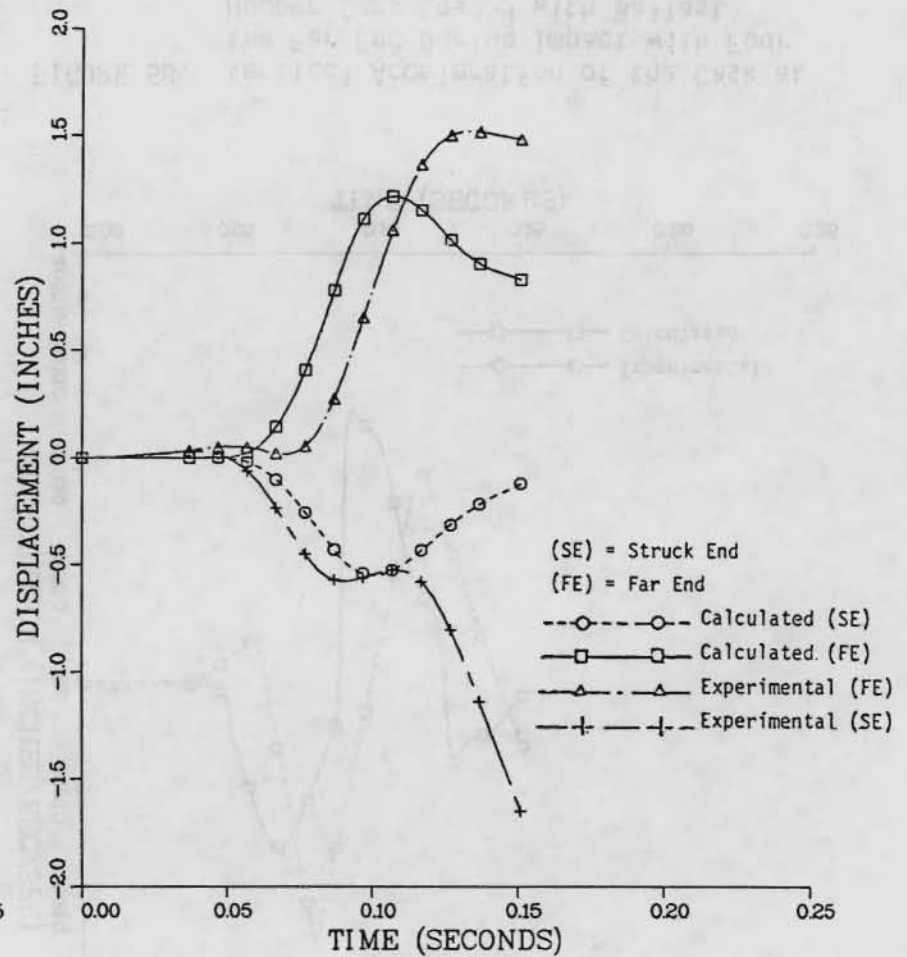


FIGURE 60. Vertical Displacements of the Cask During Impact with Four Hopper Cars Loaded with Ballast (Test 3) (Case 1: Measured Coupler Force).

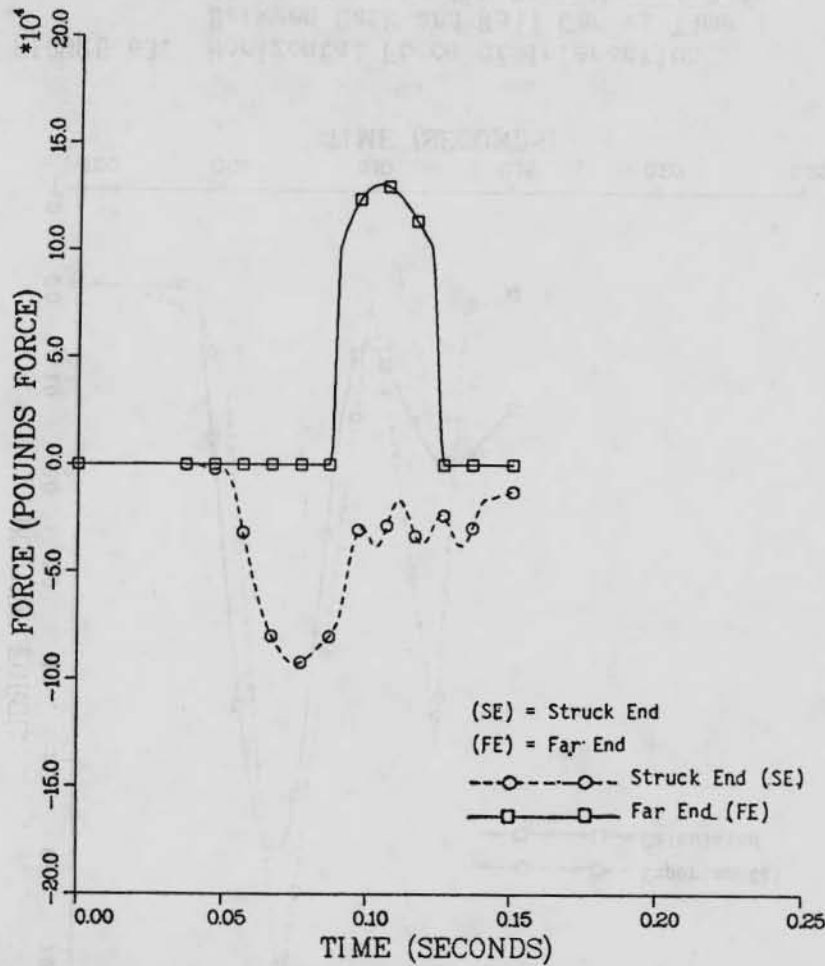


FIGURE 61. Vertical Tiedown Forces During Impact with Four Hopper Cars Loaded with Ballast (Test 3) (Case 1: Measured Coupler Force).

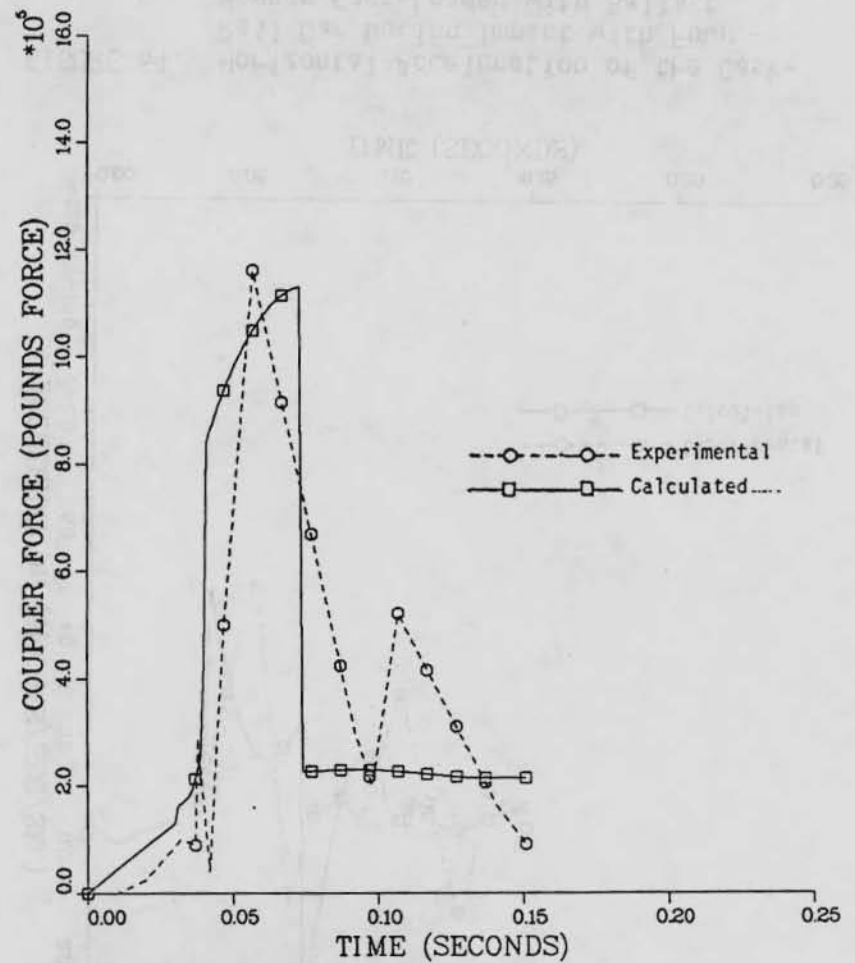


FIGURE 62. Coupler Force vs Time During Impact of Cask-Rail Car with Four Hopper Cars Loaded with Ballast (Test 3 - Instrument 3) (Case 2: Calculated Coupler Force).

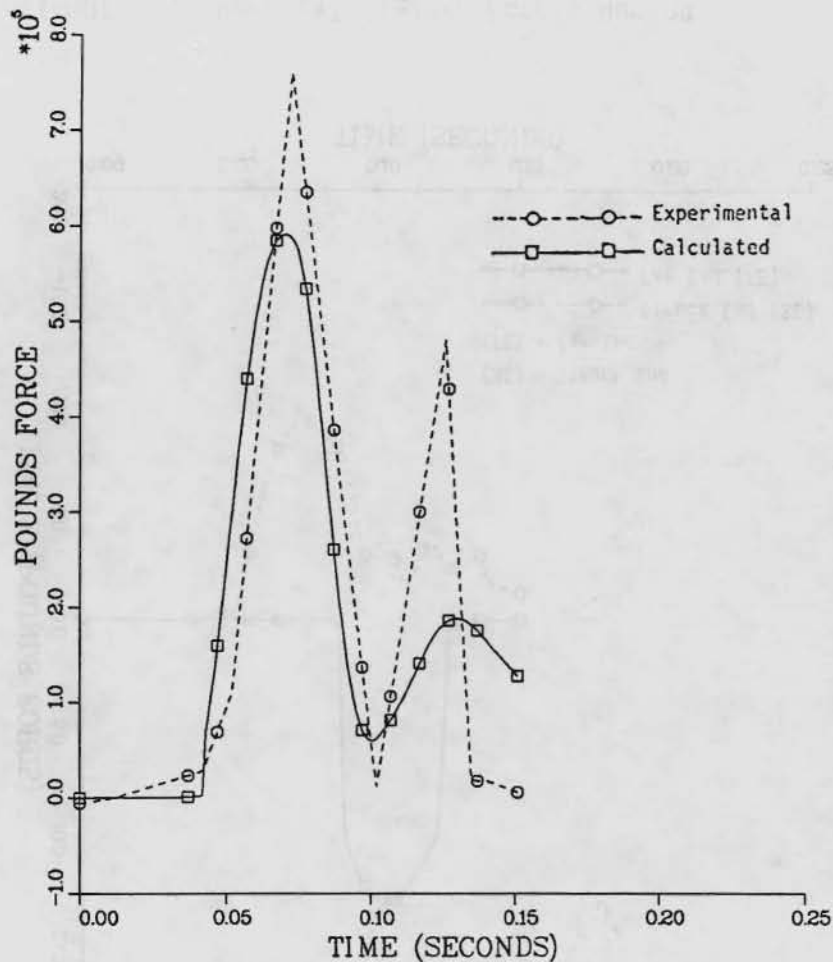


FIGURE 63. Horizontal Force of Interaction Between Cask and Rail Car vs Time During Impact with Four Hopper Cars Loaded with Ballast (Test 3 - Instrument 27) (Case 2: Calculated Coupler Force).

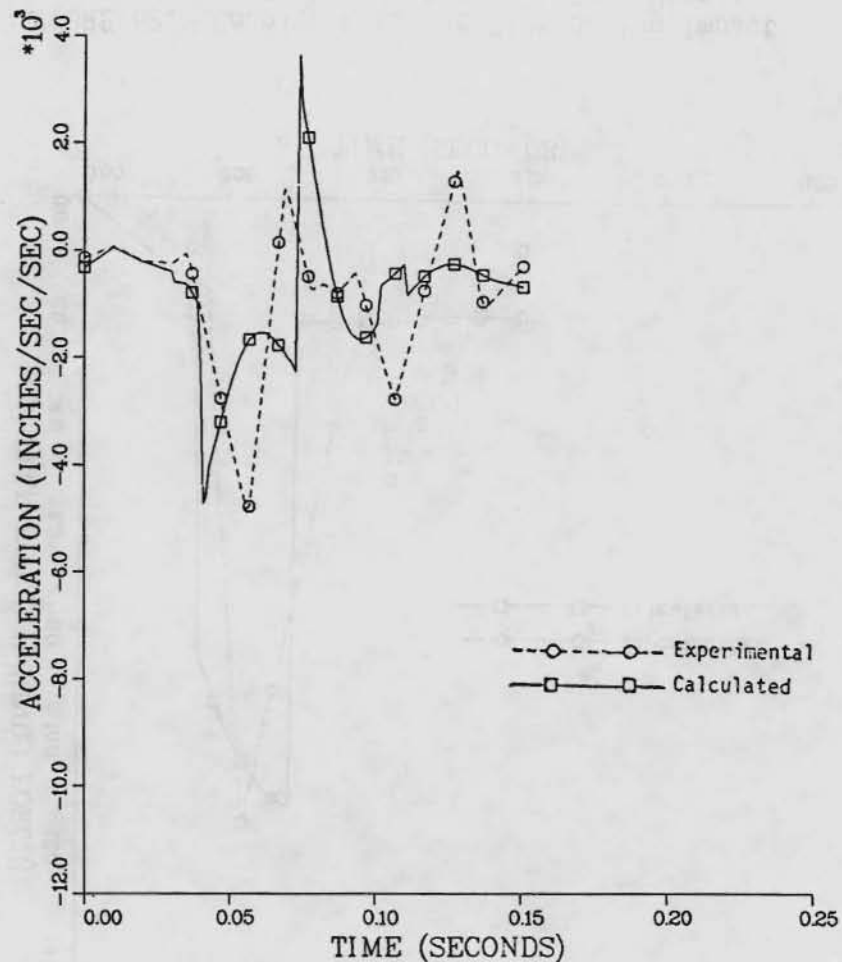


FIGURE 64. Horizontal Acceleration of the Cask-Rail Car During Impact with Four Hopper Cars Loaded with Ballast (Test 3 - Instrument 12: Filtered at 100 Hz) (Case 2: Calculated Coupler Force).

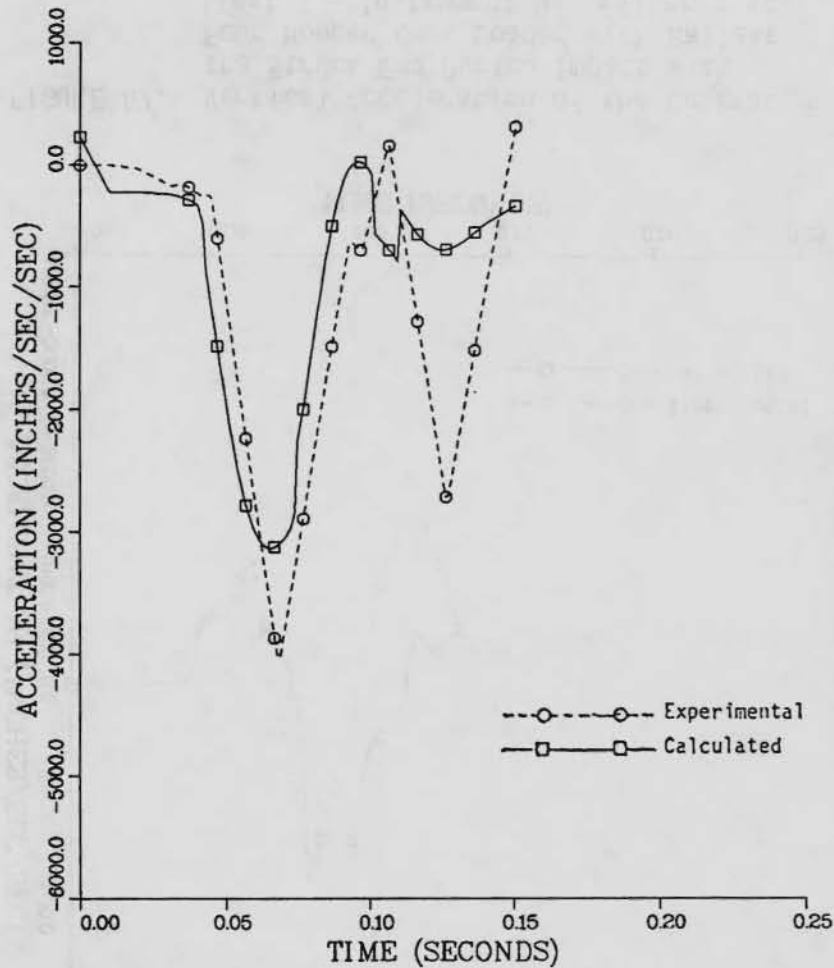


FIGURE 65. Horizontal Acceleration of the Cask During Impact with Four Hopper Cars Loaded with Ballast (Test 3 - Instrument 8: Filtered at 100 Hz) (Case 2: Calculated Coupler Force).

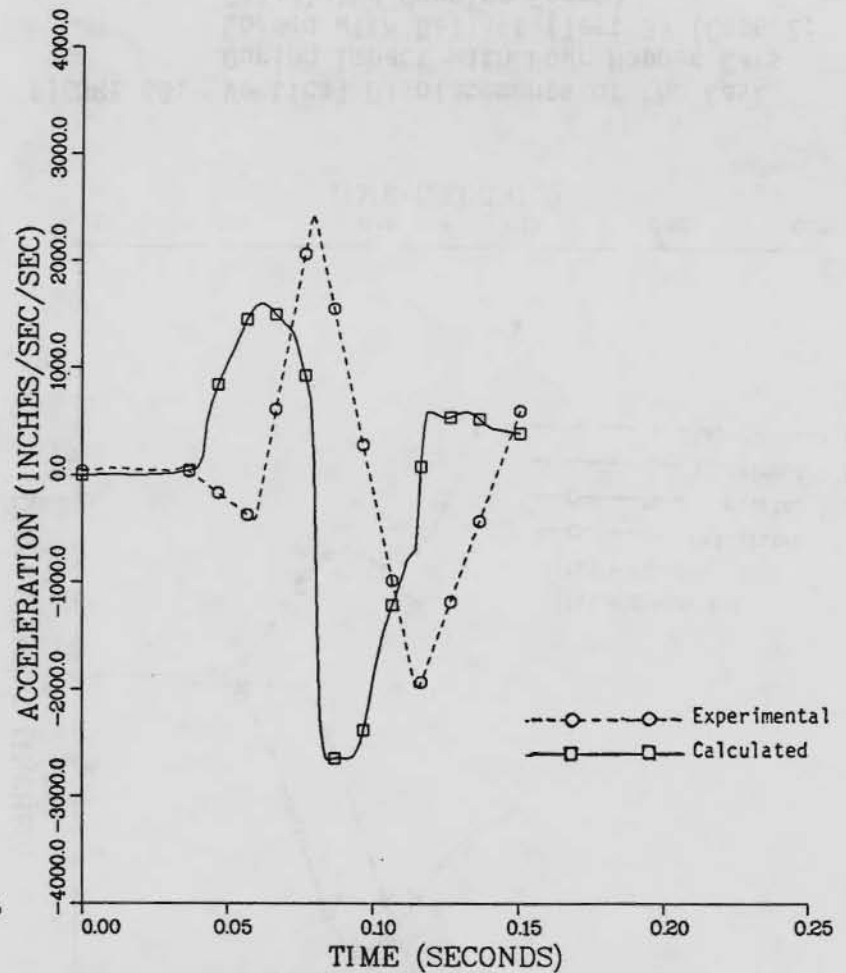


FIGURE 66. Vertical Acceleration of the Cask at the Far End During Impact with Four Hopper Cars Loaded with Ballast (Test 3 - Instrument 11: Filtered at 50 Hz) (Case 2: Calculated Coupler Force).

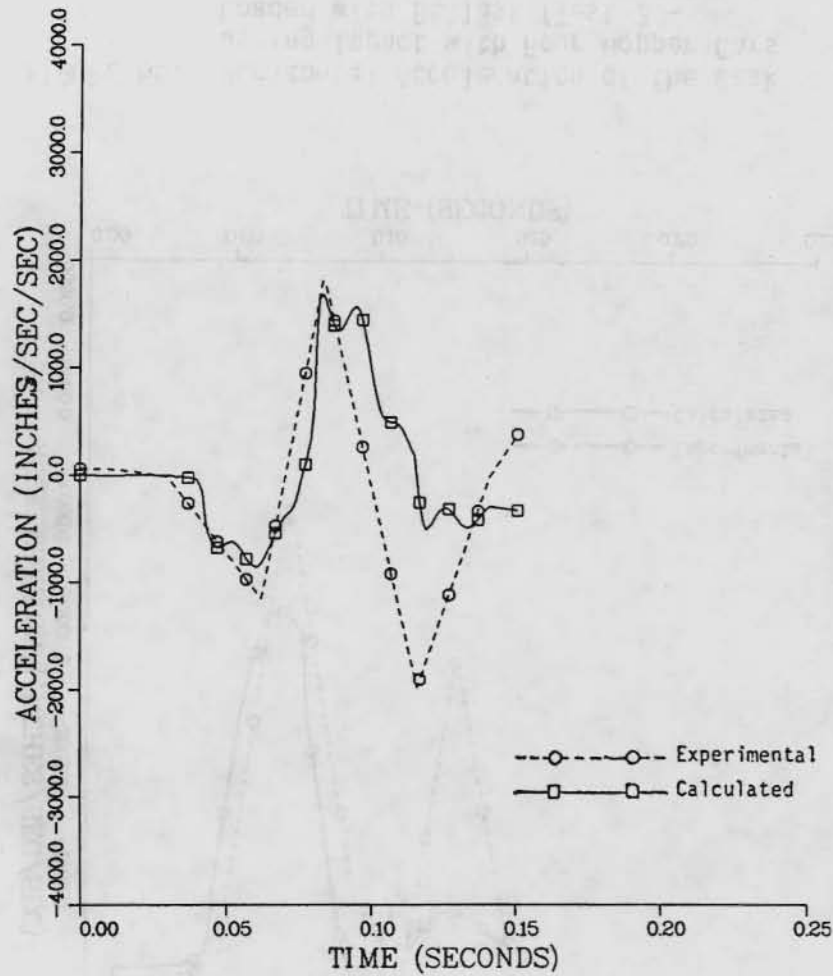


FIGURE 67. Vertical Acceleration of the Cask at the Struck End During Impact with Four Hopper Cars Loaded with Ballast (Test 3 - Instrument 9: Filtered at 50 Hz) (Case 2: Calculated Coupler Force).

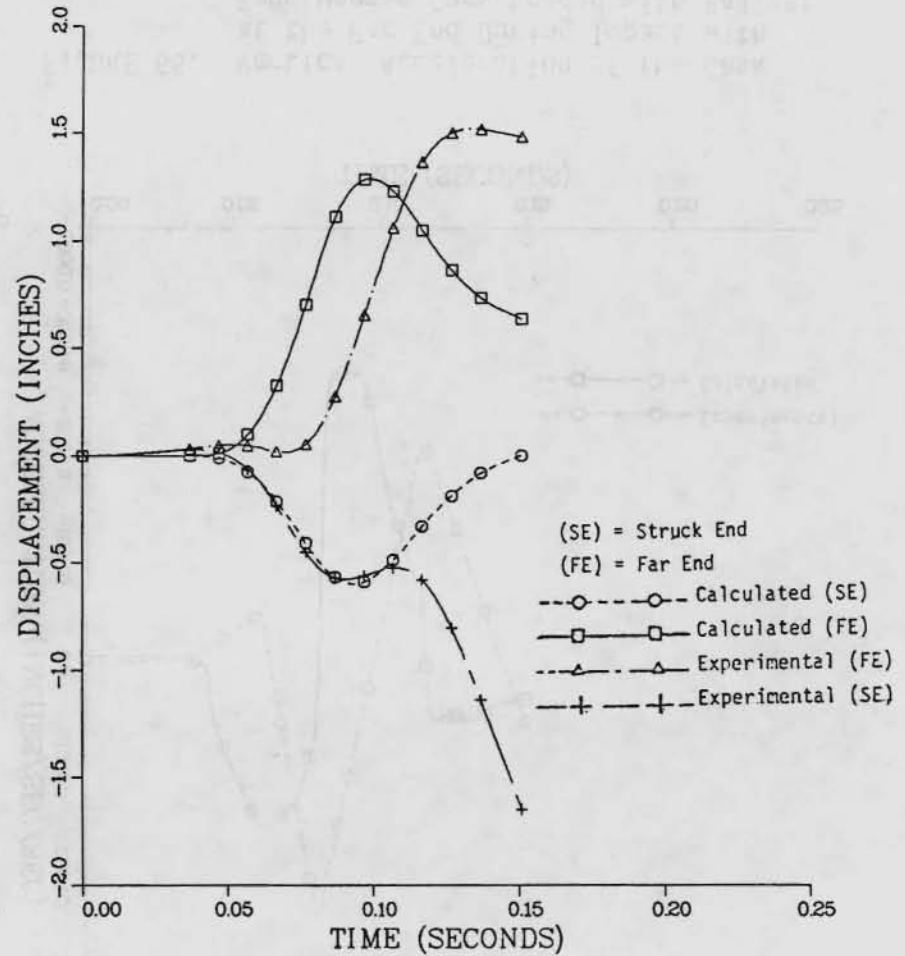


FIGURE 68. Vertical Displacements of the Cask During Impact with Four Hopper Cars Loaded with Ballast (Test 3) (Case 2: Calculated Coupler Force).

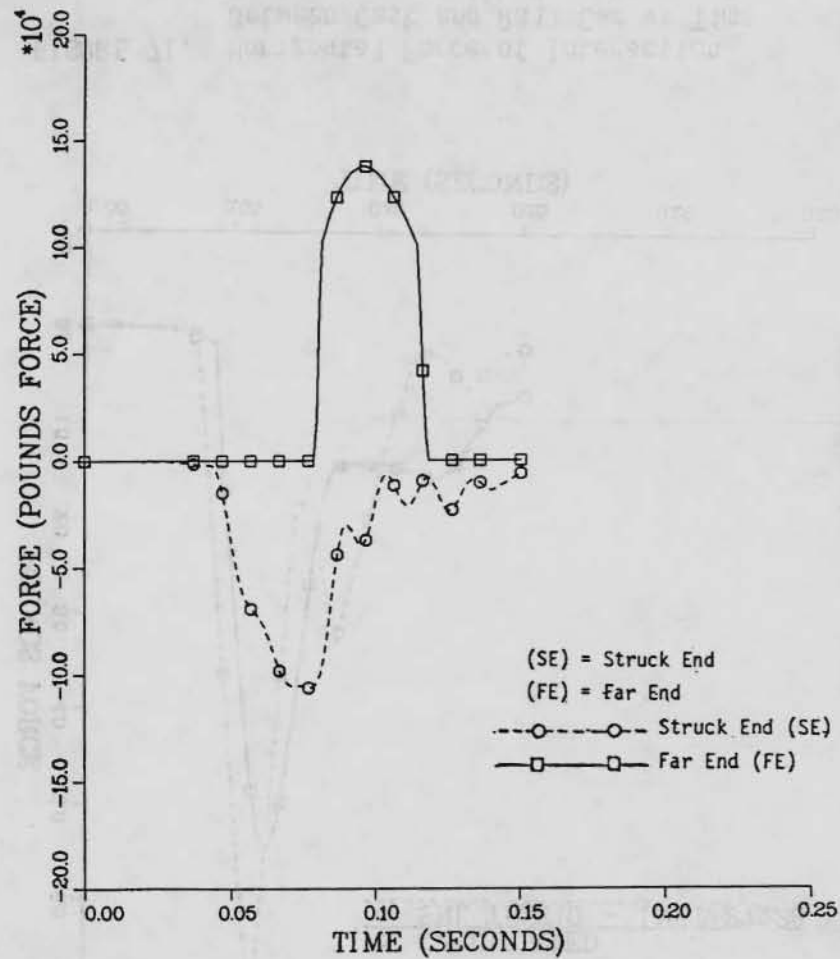


FIGURE 69. Vertical Tiedown Forces During Impact with Four Hopper Cars Loaded with Ballast (Test 3) (Case 2: Calculated Coupler Force).

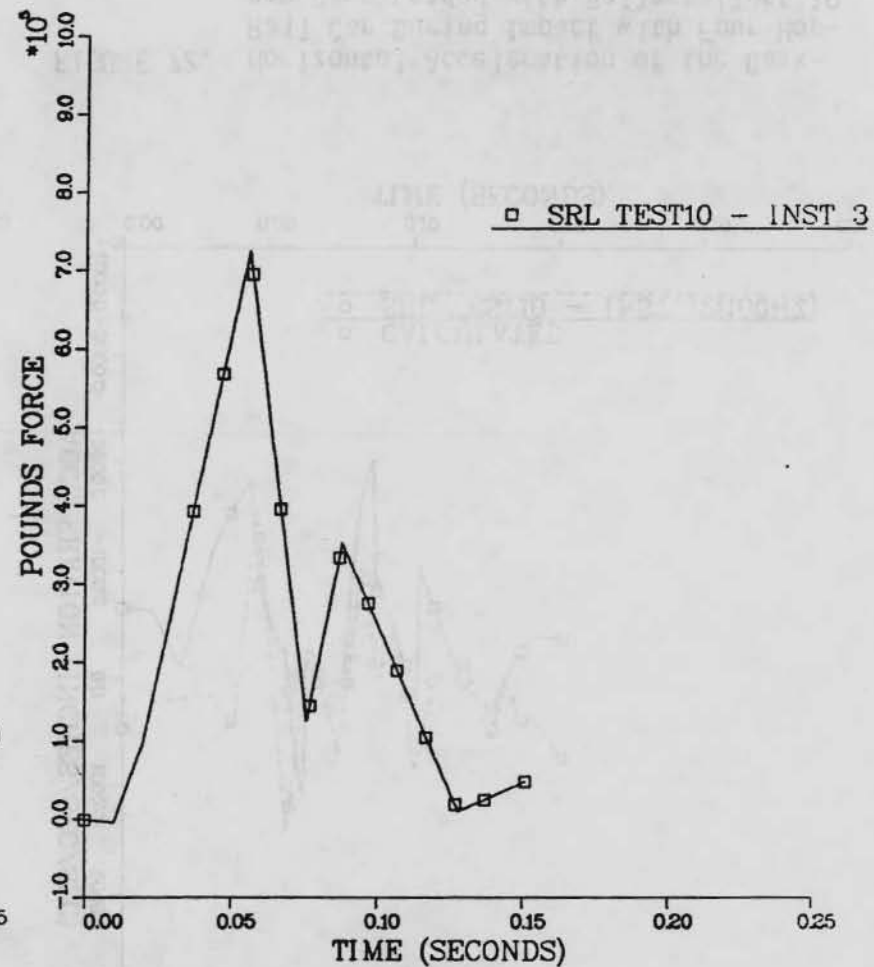


FIGURE 70. Coupler Force vs Time During Impact of Cask-Rail Car with Four Hopper Cars Loaded with Ballast (Test 10 - Instrument 3).

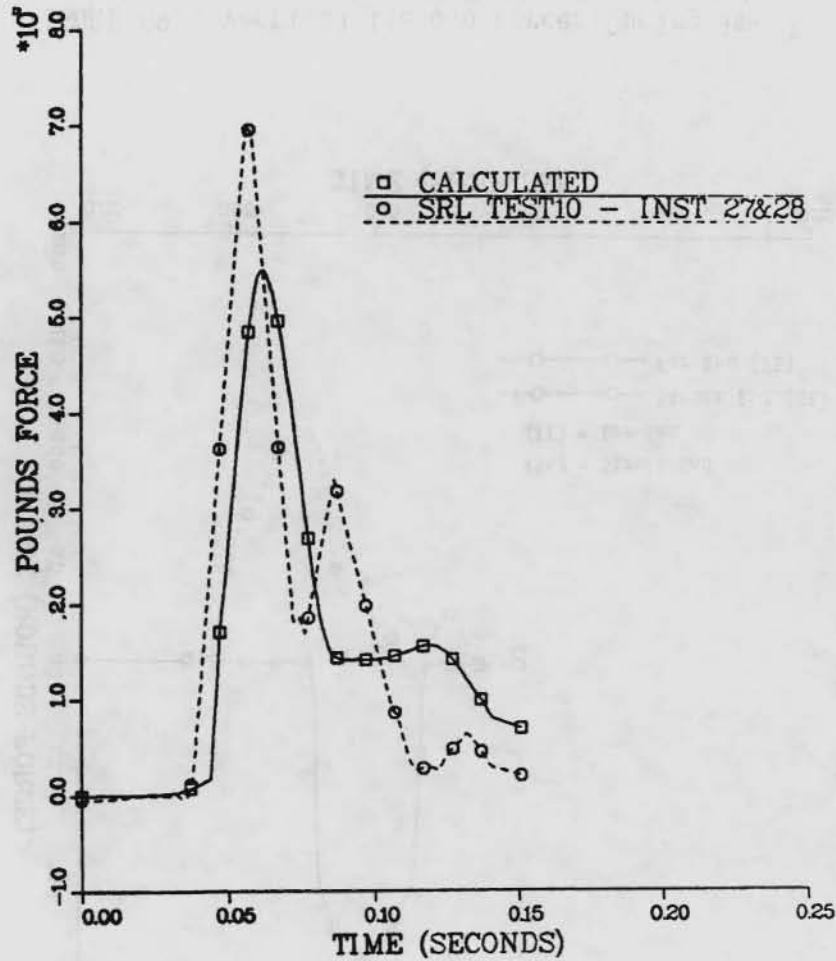


FIGURE 71. Horizontal Force of Interaction Between Cask and Rail Car vs Time During Impact with Four Hopper Cars Loaded with Ballast (Test 10 - Instruments 27 and 28).

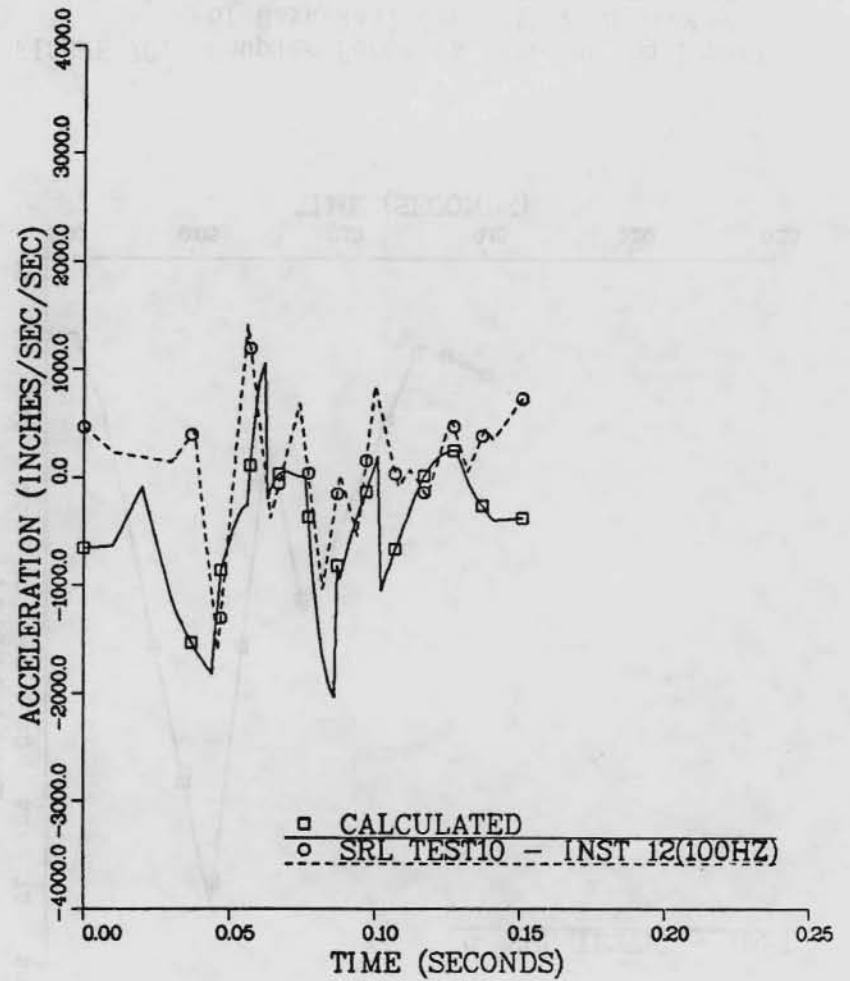


FIGURE 72. Horizontal Acceleration of the Cask-Rail Car During Impact with Four Hopper Cars Loaded with Ballast (Test 10 - Instrument 12: Filtered at 100 Hz).

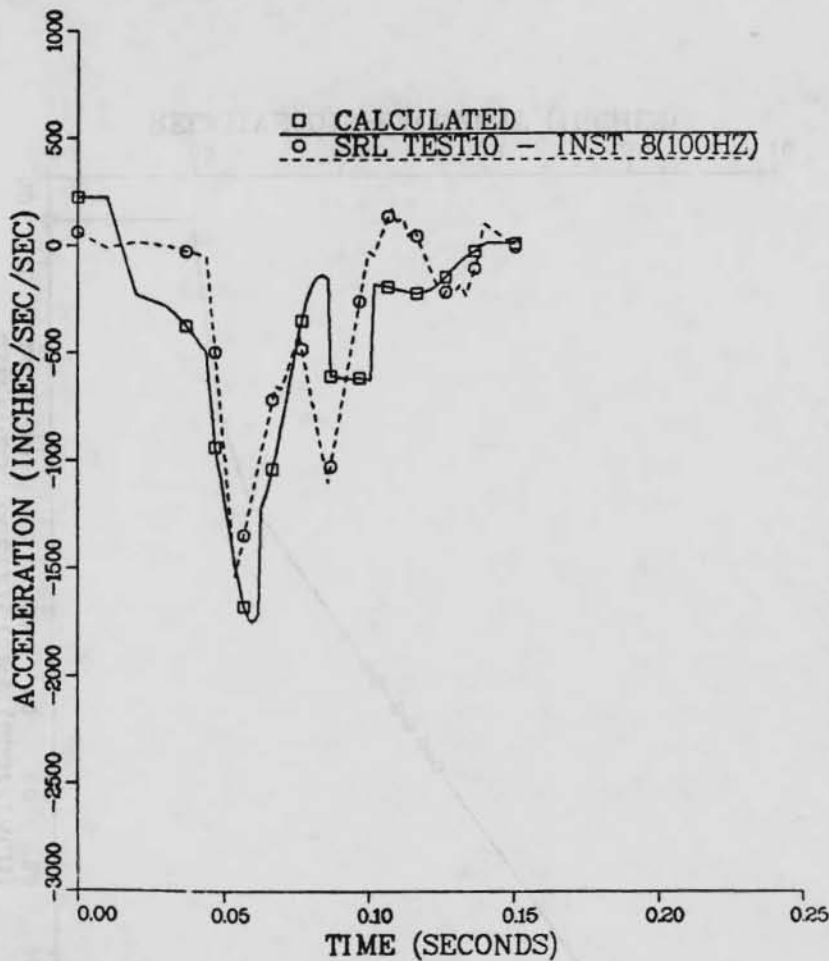


FIGURE 73. Horizontal Acceleration of the Cask During Impact with Four Hopper Cars Loaded with Ballast (Test 10 - Instrument 8: Filtered at 100 Hz).

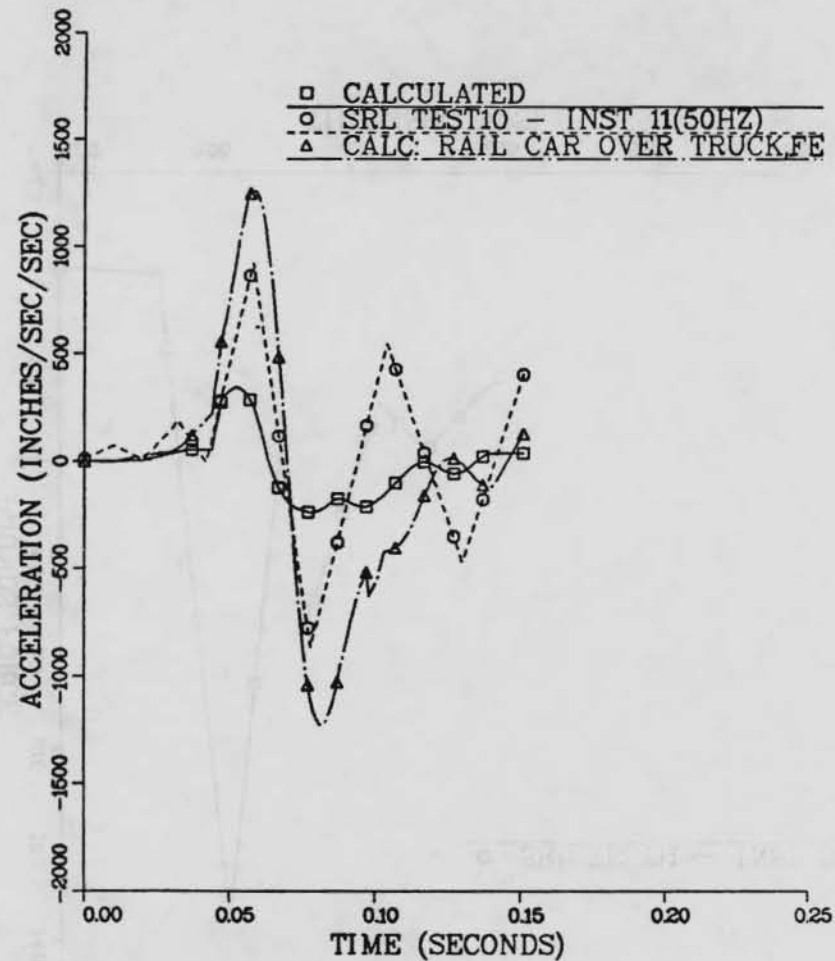


FIGURE 74. Vertical Acceleration of the Cask at the Far End During Impact with Four Hopper Cars Loaded with Ballast (Test 10 - Instrument 11: Filtered at 50 Hz).

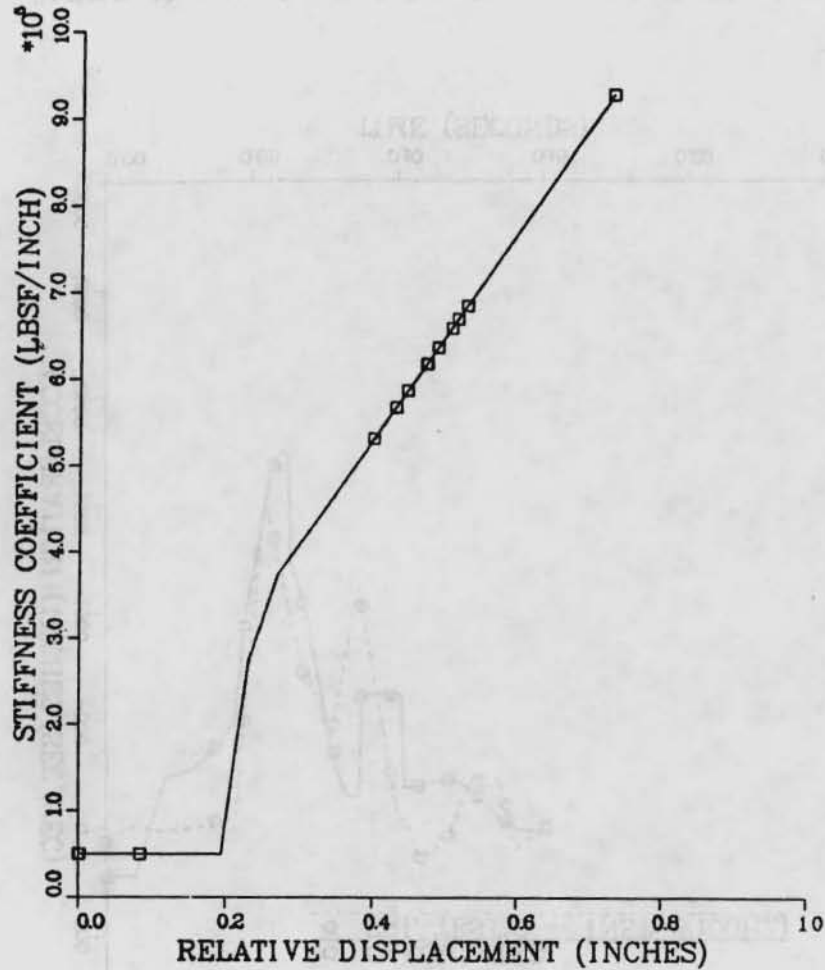


FIGURE 75. Stiffness Coefficient of Horizontal Component of Tiedowns vs Relative Displacement Between Cask and Rail Car (Tests 10 and 11).

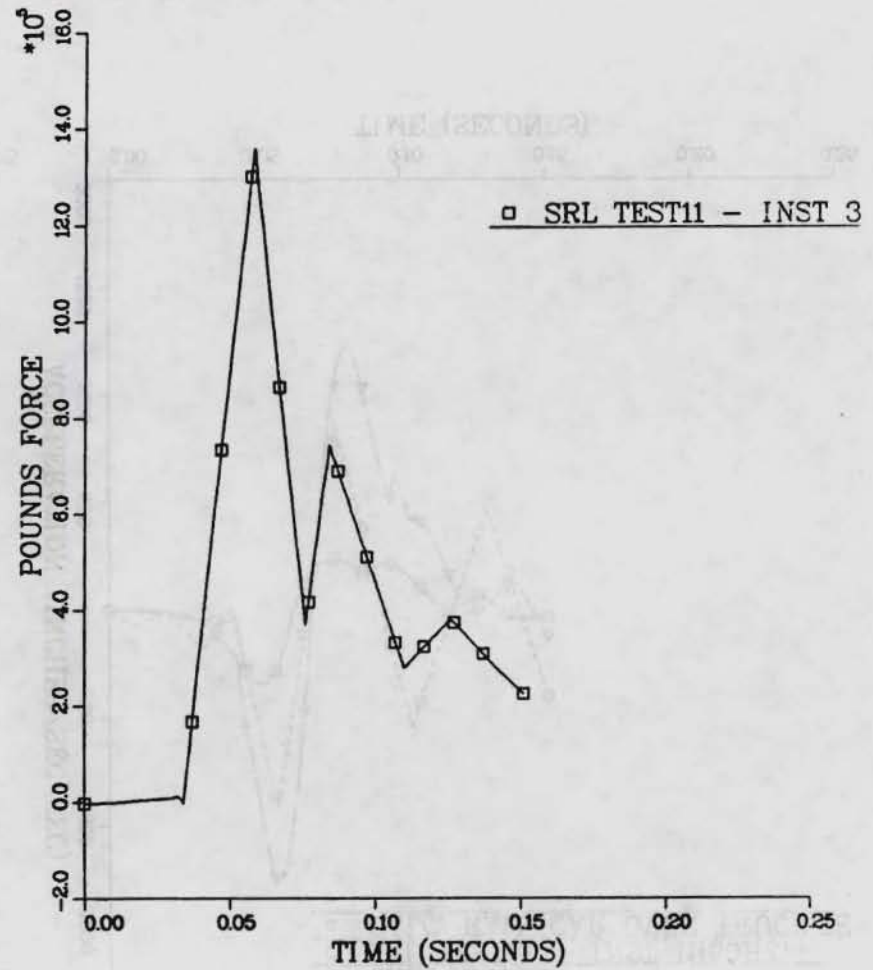


FIGURE 76. Coupler Force vs Time During Impact of Cask-Rail Car with Four Hopper Cars Loaded with Ballast (Test 11 - Instrument 3).

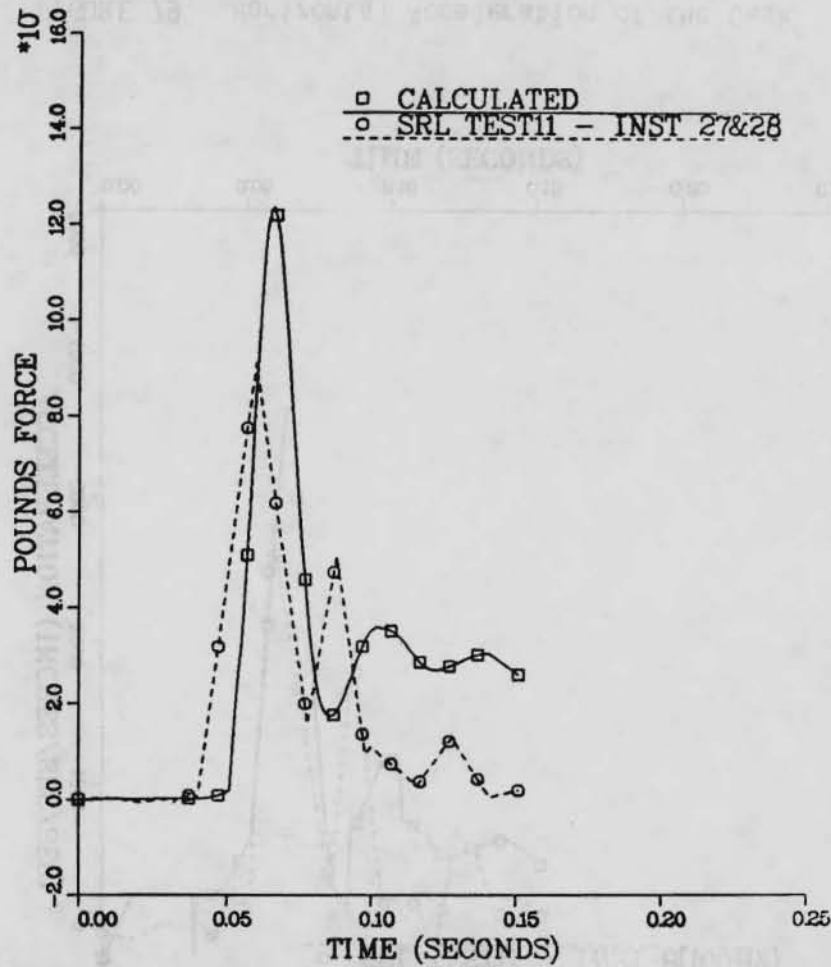


FIGURE 77. Horizontal Force of Interaction Between Cask and Rail Car vs Time During Impact with Four Hopper Cars Loaded with Ballast (Test 11 - Instruments 27 and 28).

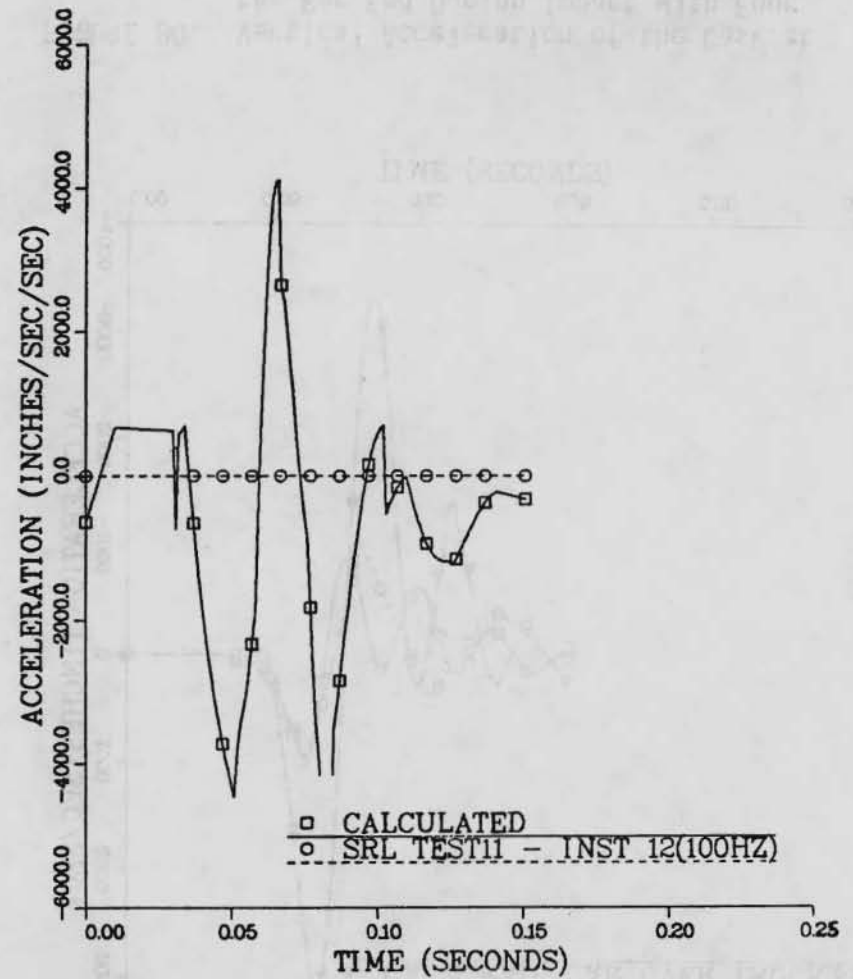


FIGURE 78. Horizontal Acceleration of the Cask-Rail Car During Impact with Four Hopper Cars Loaded with Ballast (Test 11 - Instrument 12: Filtered at 100 Hz).

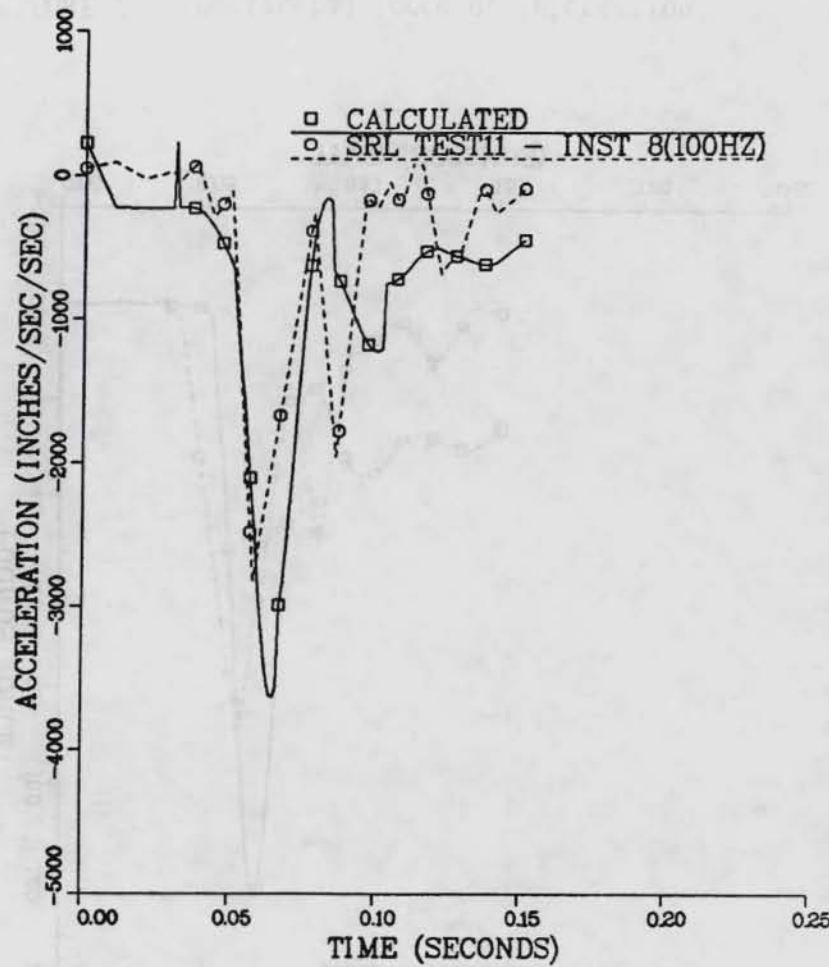


FIGURE 79. Horizontal Acceleration of the Cask During Impact with Four Hopper Cars Loaded with Ballast (Test 11 - Instrument 8: Filtered at 100 Hz).

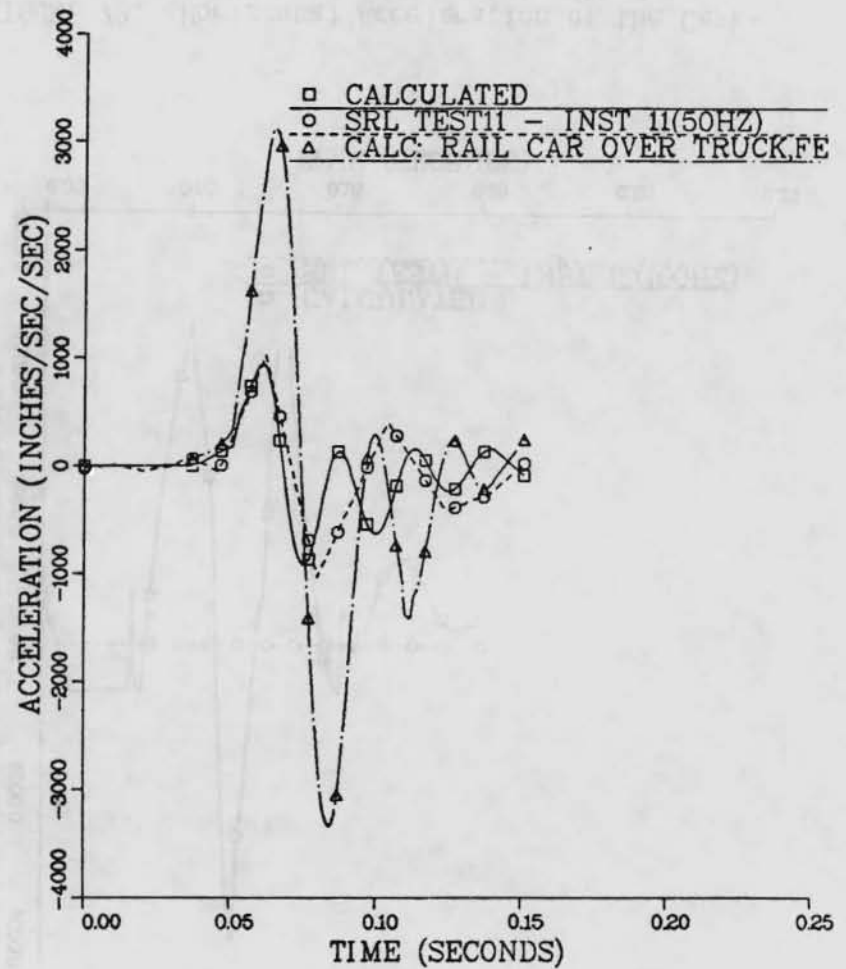
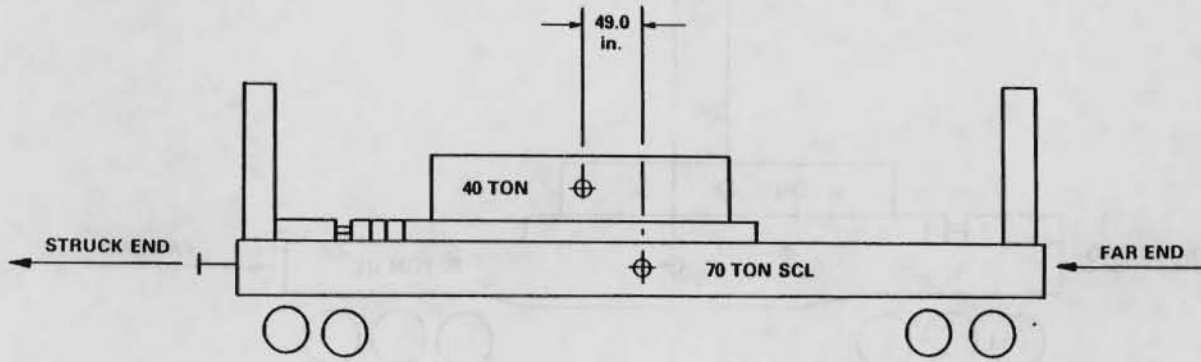


FIGURE 80. Vertical Acceleration of the Cask at the Far End During Impact with Four Hopper Cars Loaded with Ballast (Test 11 - Instrument 11: Filtered at 50 Hz).

TESTS 3 AND 18



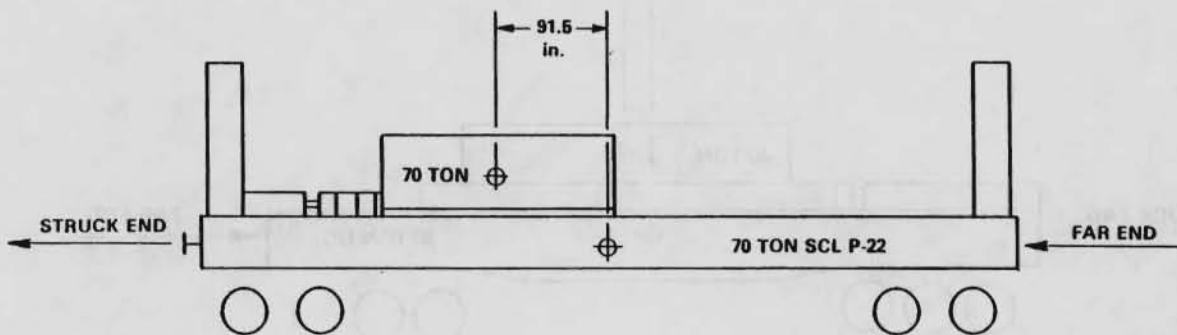
- TEST 3
- STD DRAFT GEAR
- TIEDOWNS - 6 BOLTS
- P-22 RAIL CAR

- TEST 18
- CUSHION UNDERFRAME
- TIEDOWNS - 6 CABLES
- PS-22 RAIL CAR

HEDL 8304-166.1

FIGURE 81. Cask-Rail Car Configuration Used in Tests 3 and 18.

TESTS 10 AND 11

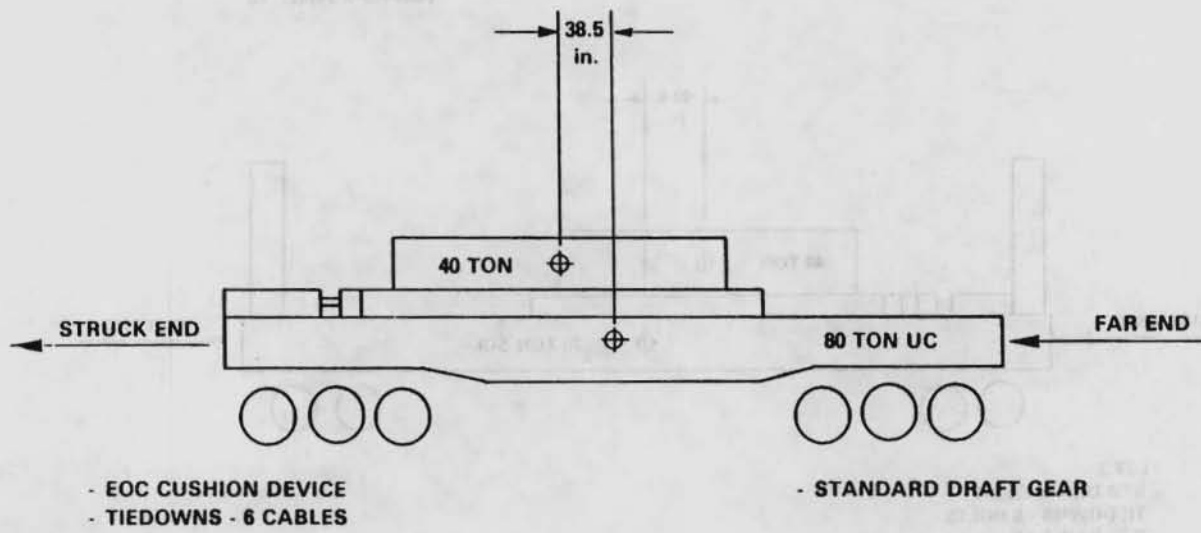


- STANDARD DRAFT GEAR
- TIEDOWNS - 6 BOLTS

HEDL 8304-166.2

FIGURE 82. Cask-Rail Car Configuration Used in Tests 10 and 11.

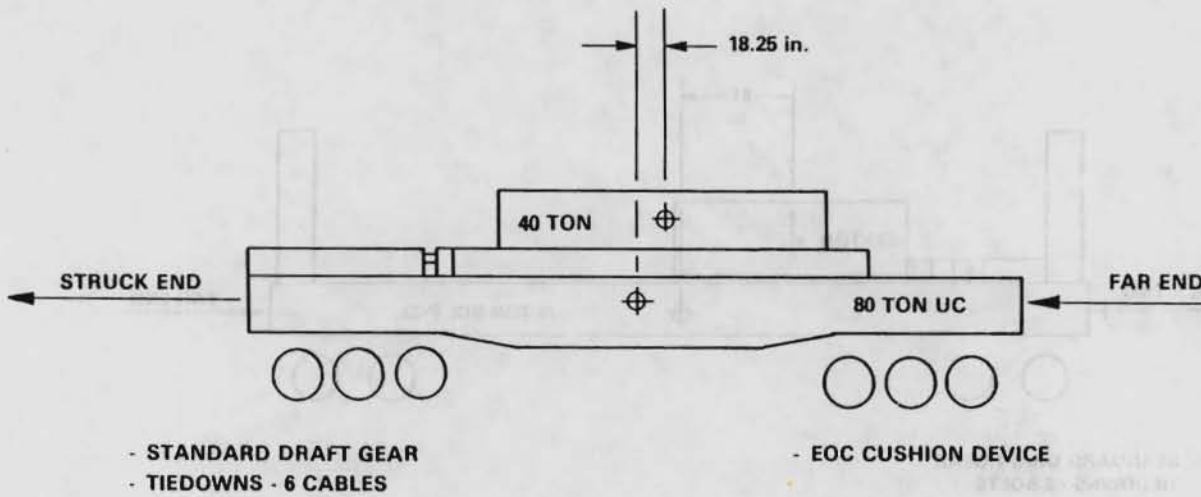
TEST 13



HEDL 8304-166.3

FIGURE 83. Cask-Rail Car Configuration Used in Tests 13.

TEST 16



HEDL 8304-166.4

FIGURE 84. Cask-Rail Car Configuration Used in Test 16.

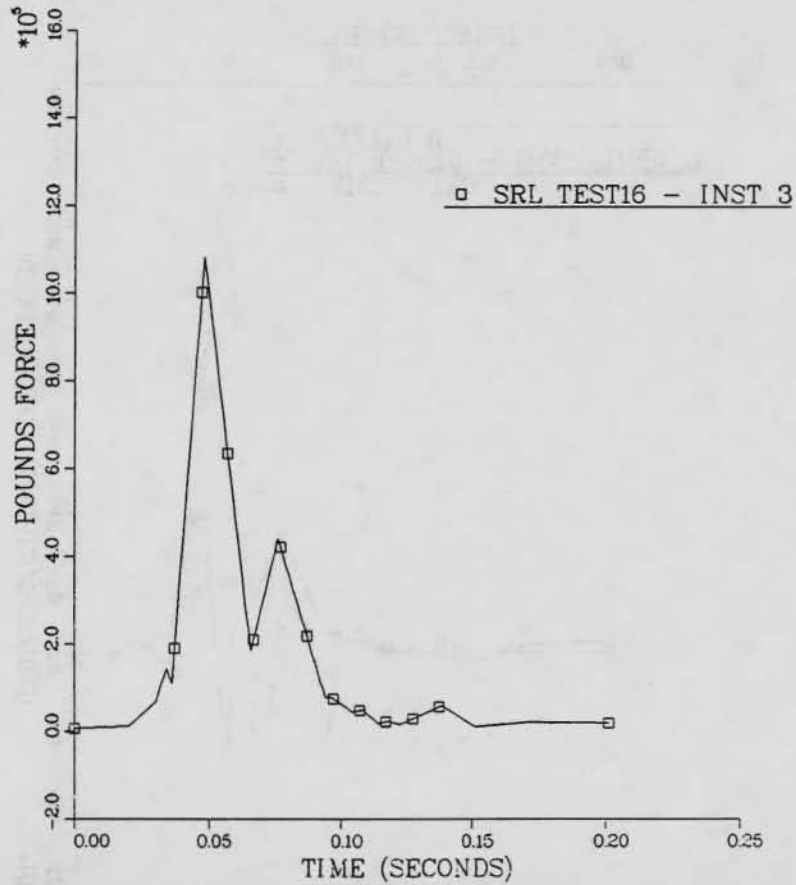


FIGURE 85. Coupler Force vs Time During Impact of Cask-Rail Car with Four Hopper Cars Loaded with Ballast (Test 16 - Instrument 3).

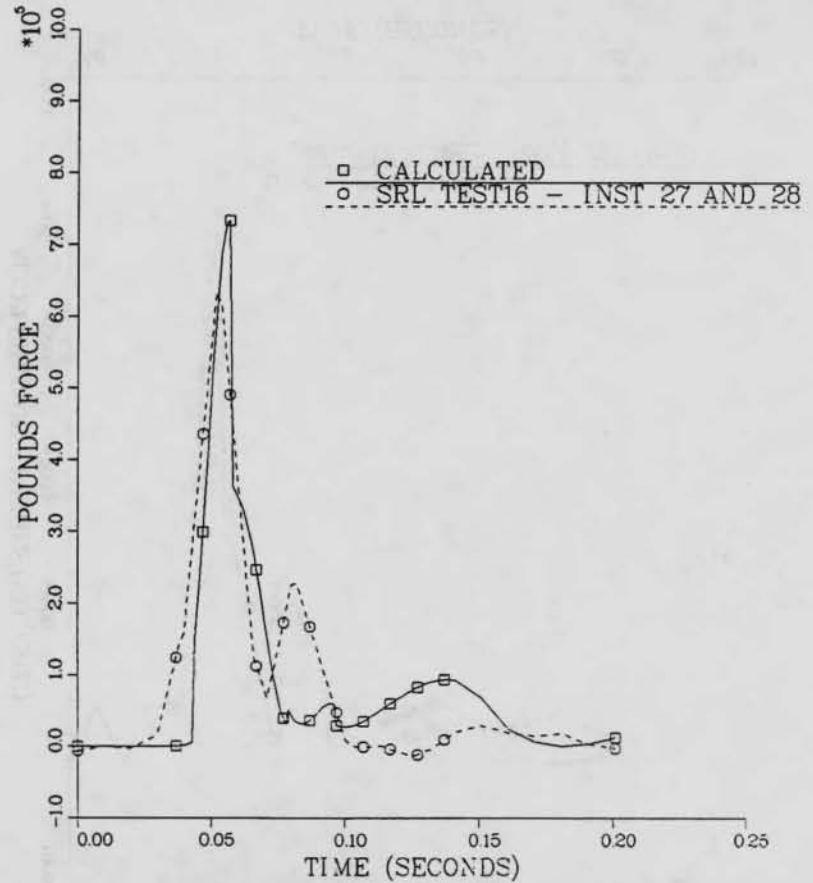


FIGURE 86. Horizontal Force of Interaction Between Cask and Rail Car vs Time During Impact with Four Hopper Cars Loaded with Ballast (Test 16 - Instruments 27 and 28).

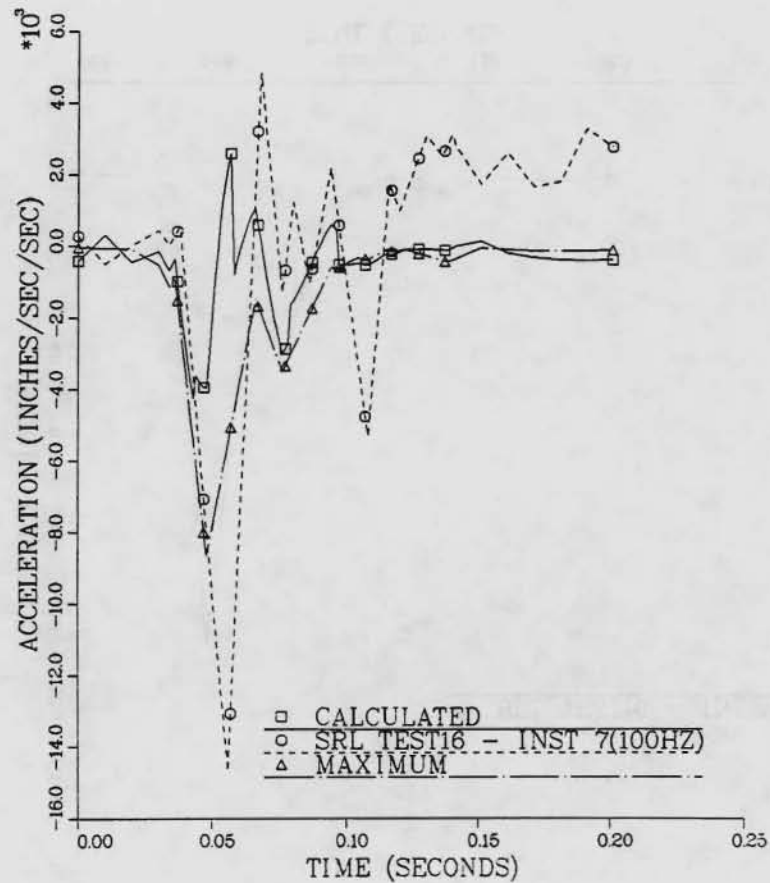


FIGURE 87. Horizontal Acceleration of the Cask-Rail Car During Impact with Four Hopper Cars Loaded with Ballast (Test 16 - Instrument 7: Filtered at 100 Hz).

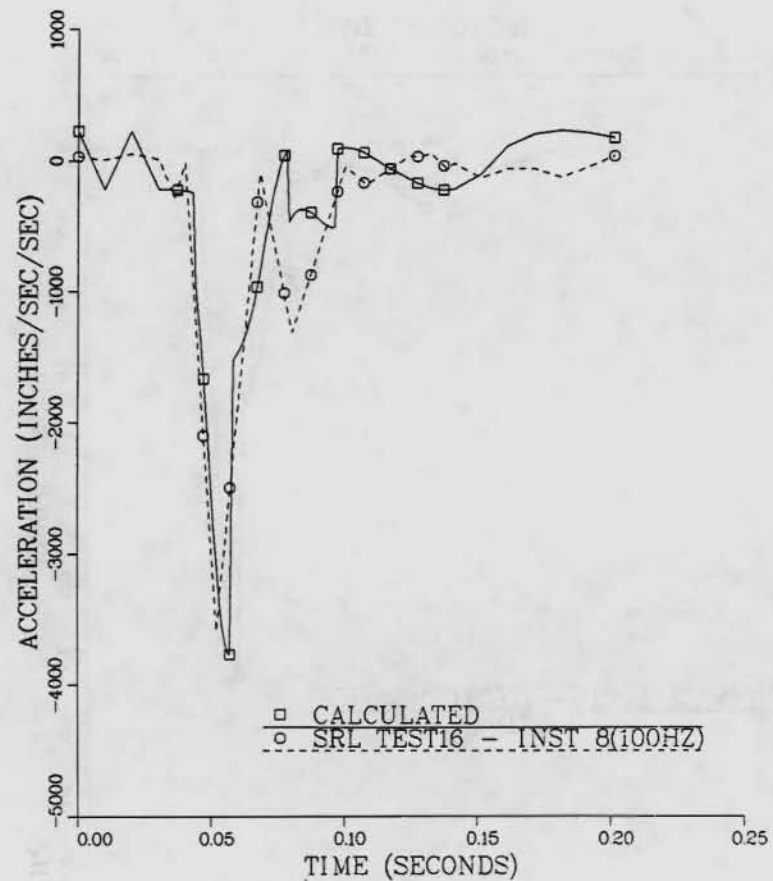


FIGURE 88. Horizontal Acceleration of the Cask During Impact with Four Hopper Cars Loaded with Ballast (Test 16 - Instrument 8: Filtered at 100 Hz).

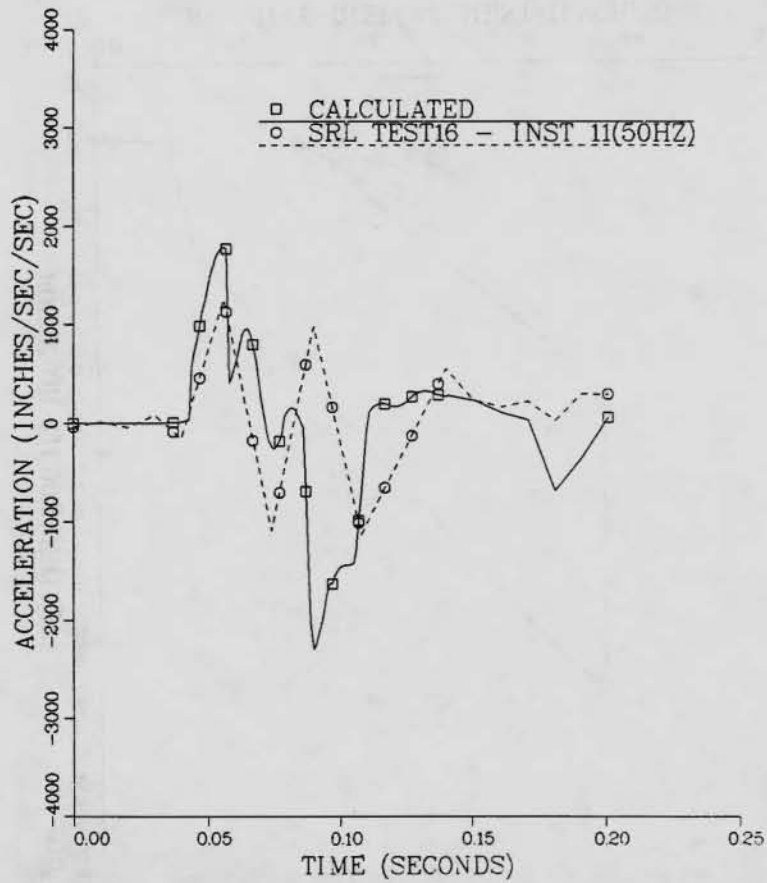


FIGURE 89. Vertical Acceleration of the Cask at the Far End During Impact with Four Hopper Cars Loaded with Ballast (Test 16 - Instrument 11: Filtered at 50 Hz).

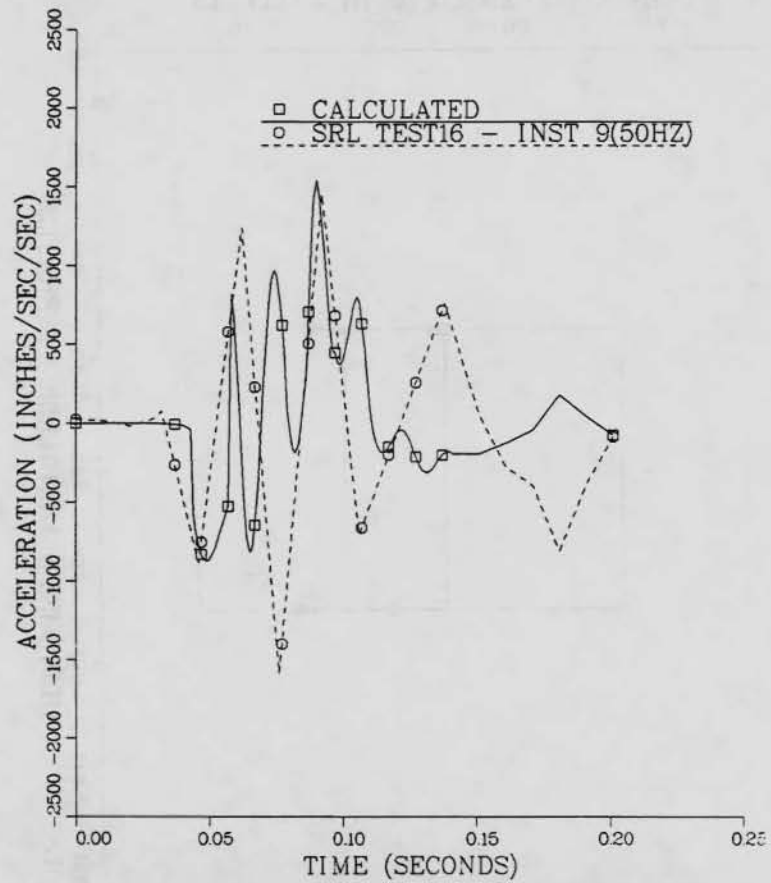


FIGURE 90. Vertical Acceleration of the Cask at the Struck End During Impact with Four Hopper Cars Loaded with Ballast (Test 16 - Instrument 9: Filtered at 50 Hz).

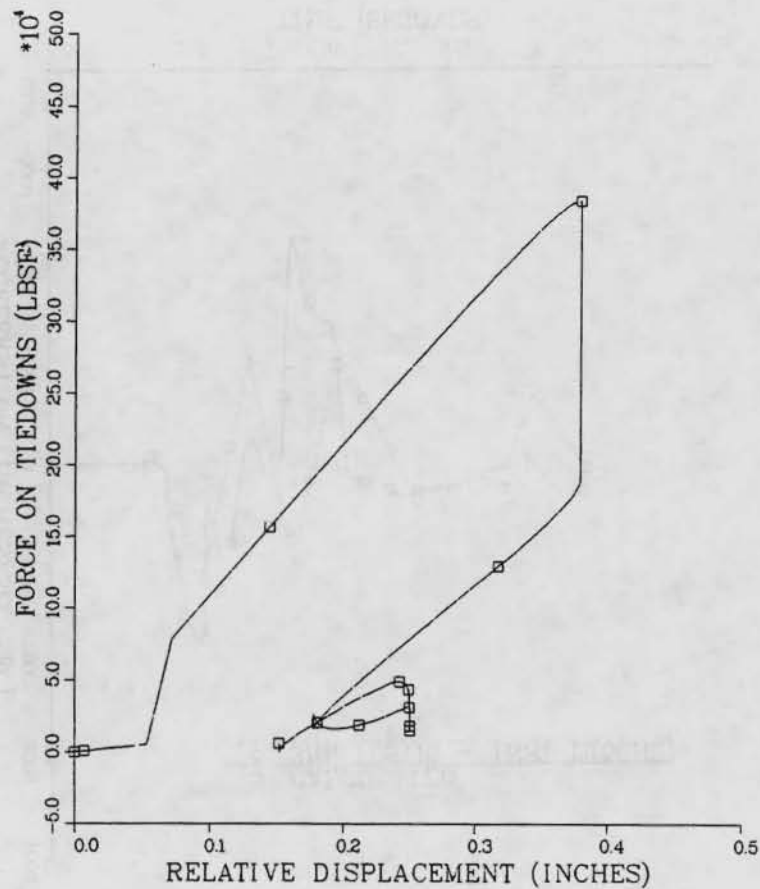


FIGURE 91. Horizontal Tiedown Force vs Relative Displacement Between Cask and Rail Car (Test 16).

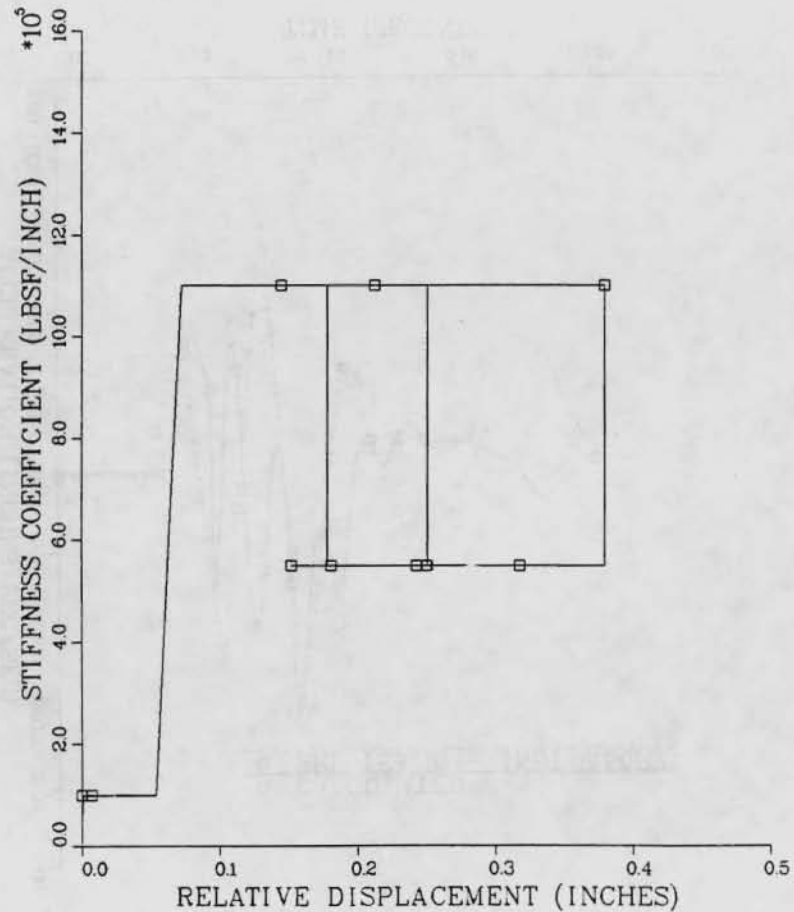


FIGURE 92. Stiffness Coefficient of Horizontal Component of Tiedowns vs Relative Displacement Between Cask and Rail Car (Test 16).

15-11

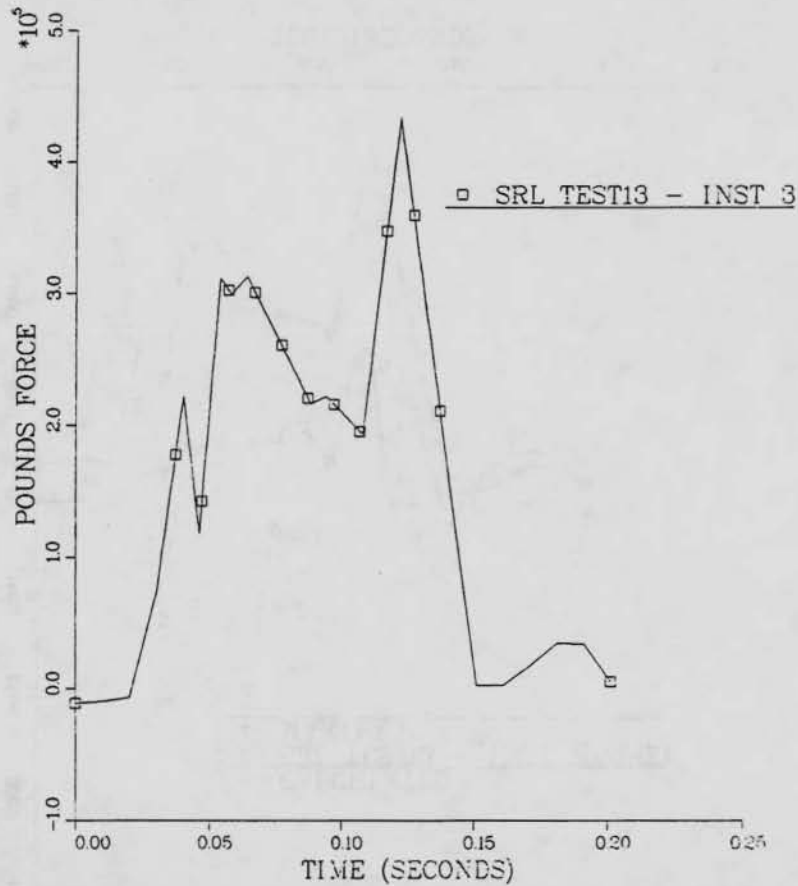


FIGURE 93. Coupler Force vs Time During Impact of Cask-Rail Car with Four Hopper Cars Loaded with Ballast (Test 13 - Instrument 3).

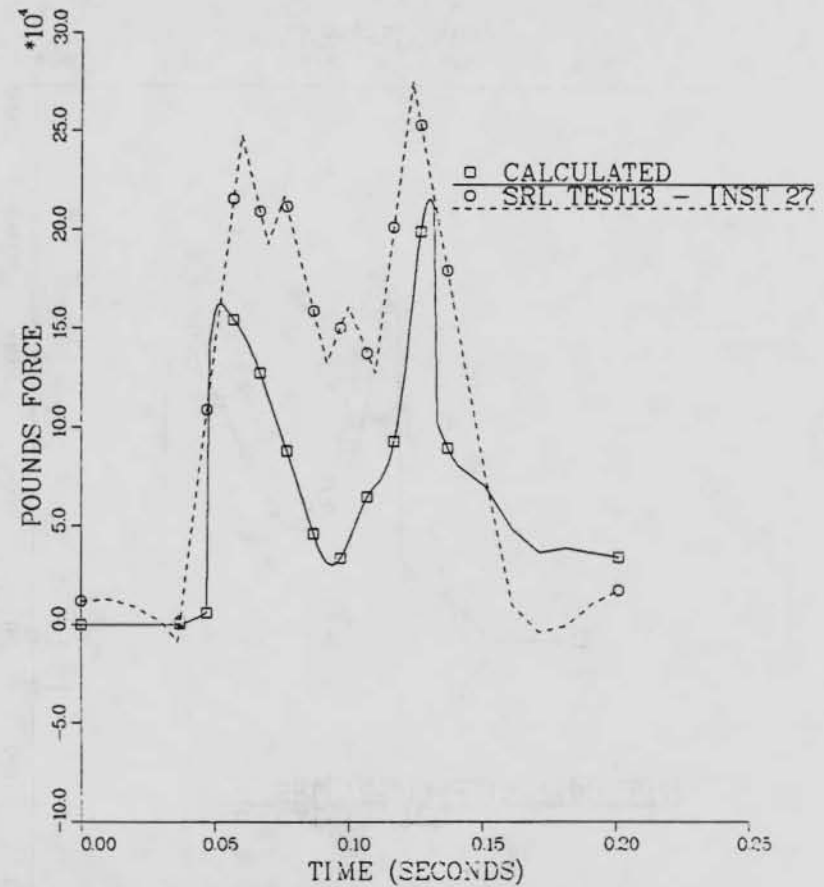


FIGURE 94. Horizontal Force of Interaction Between Cask and Rail Car vs Time During Impact with Four Hopper Cars Loaded with Ballast (Test 13 - Instruments 27 and 28).

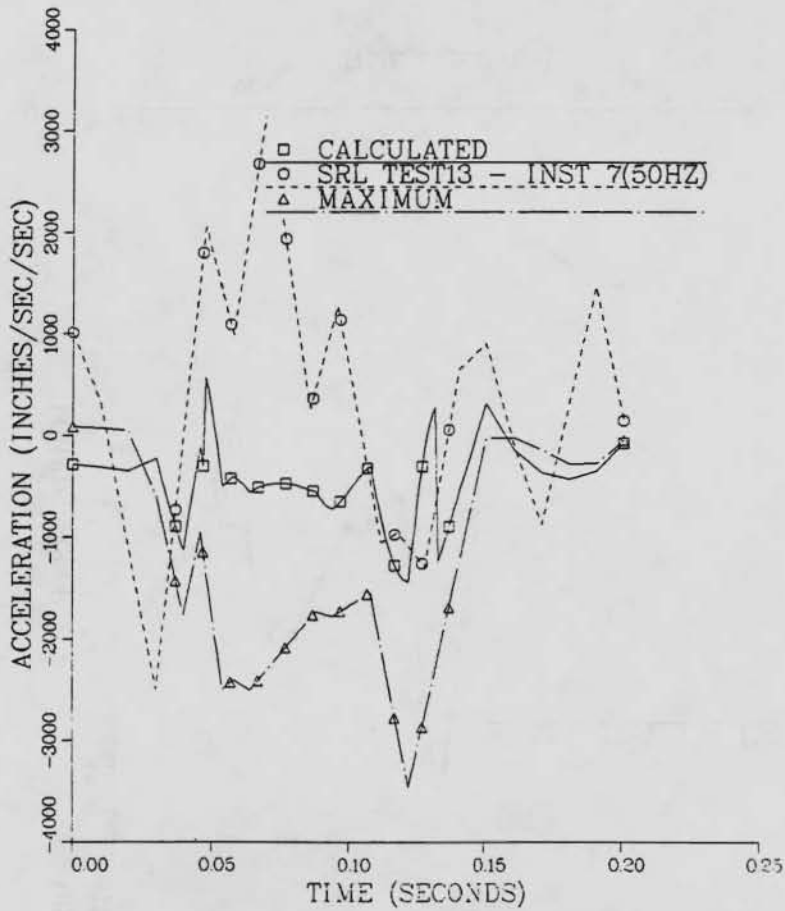


FIGURE 95. Horizontal Acceleration of the Cask-Rail Car During Impact with Four Hopper Cars Loaded with Ballast (Test 13 - Instrument 7: Filtered at 50 Hz).

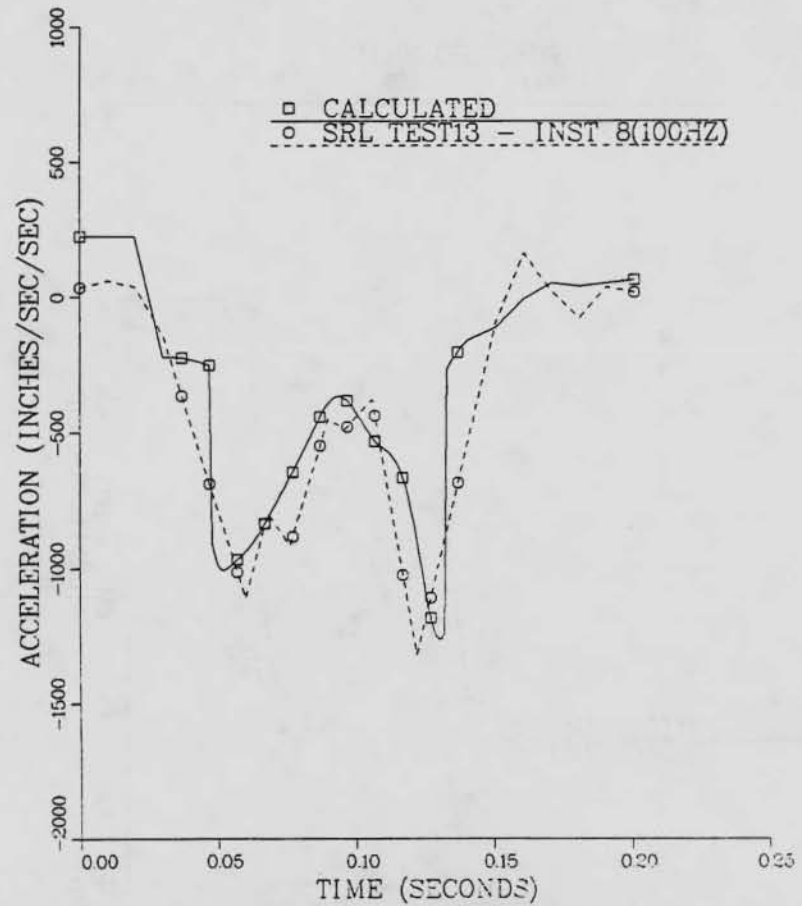


FIGURE 96. Horizontal Acceleration of the Cask During Impact with Four Hopper Cars Loaded with Ballast (Test 13 - Instrument 8: Filtered at 100 Hz).

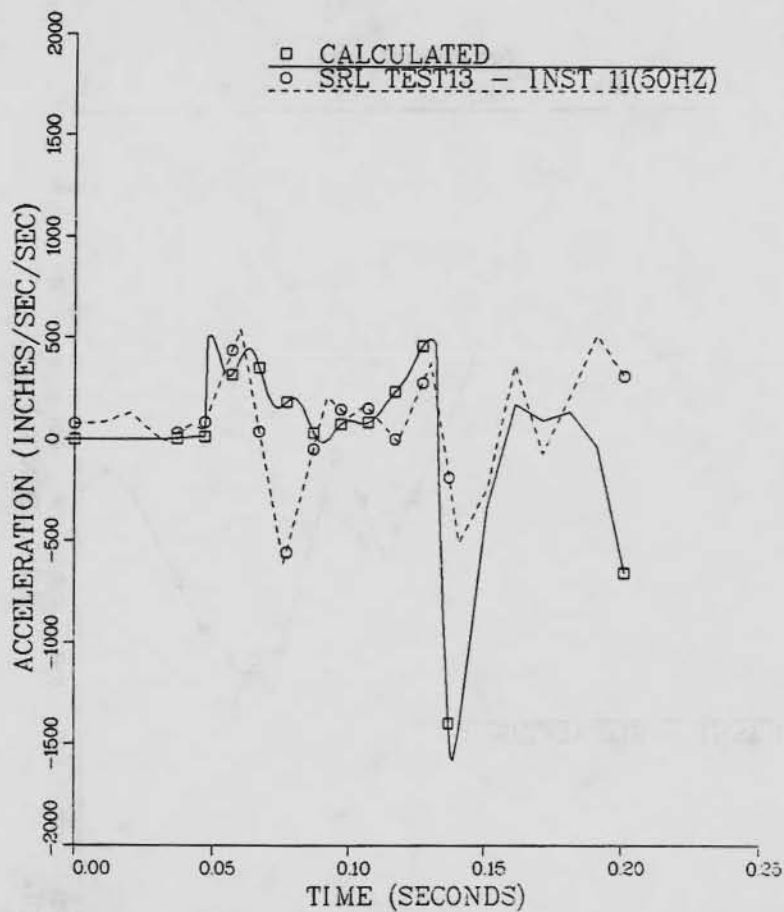


FIGURE 97. Vertical Acceleration of the Cask at the Far End During Impact with Four Hopper Cars Loaded with Ballast (Test 13 - Instrument 11: Filtered at 50 Hz).

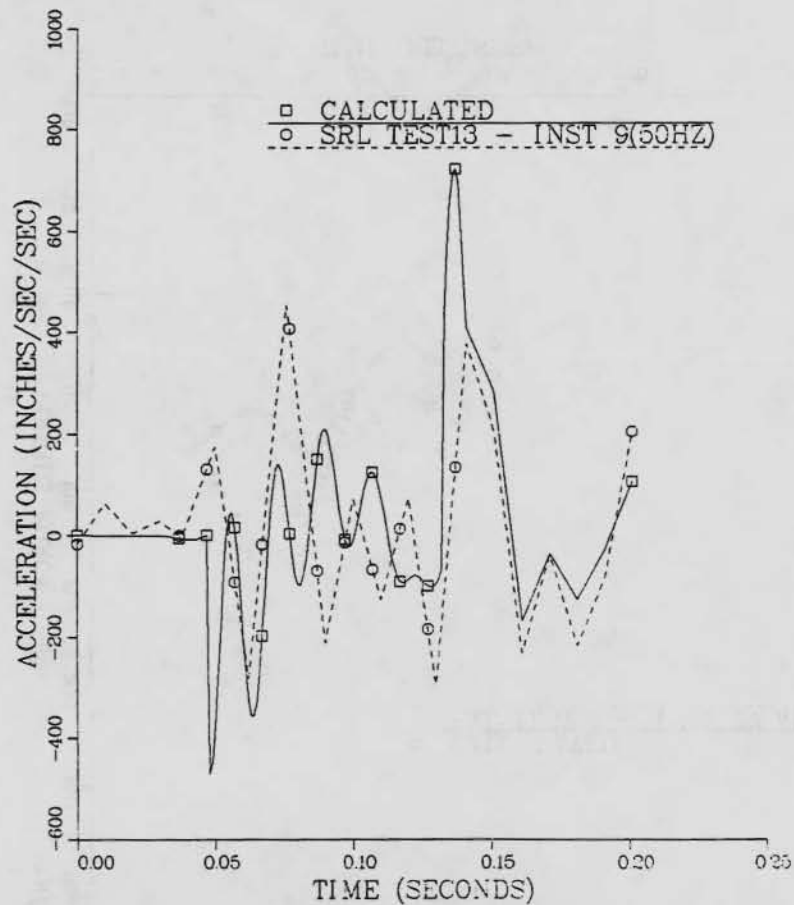


FIGURE 98. Vertical Acceleration of the Cask at the Struck End During Impact with Four Hopper Cars Loaded with Ballast (Test 13 - Instrument 9: Filtered at 50 Hz).

11-54

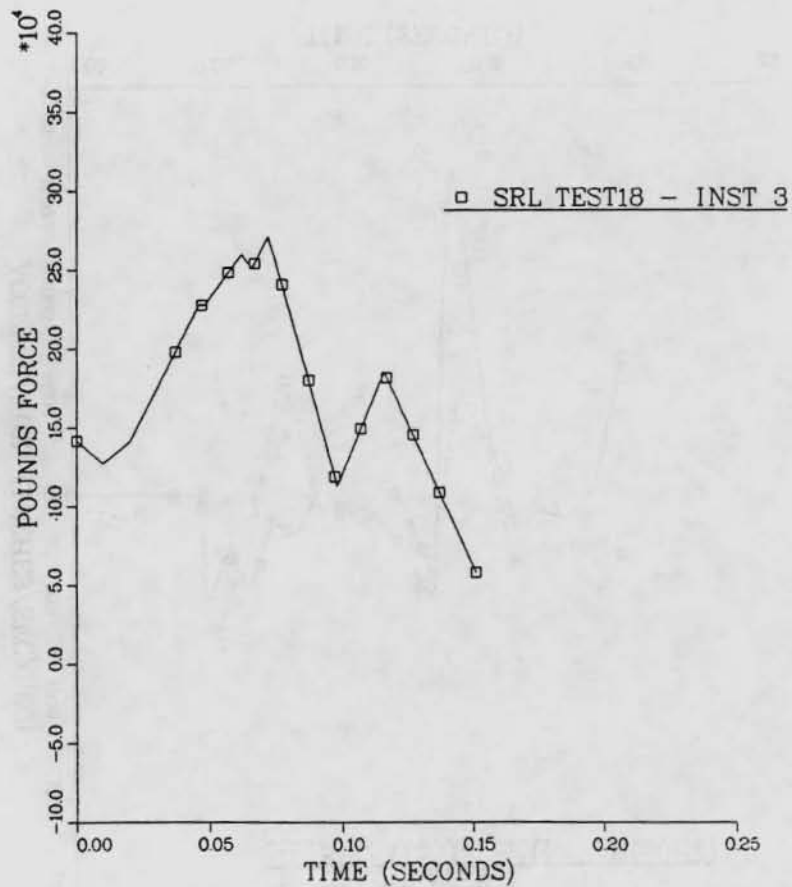


FIGURE 99. Coupler Force vs Time During Impact of Cask-Rail Car with Four Hopper Cars Loaded with Ballast (Test 18 - Instrument 3).

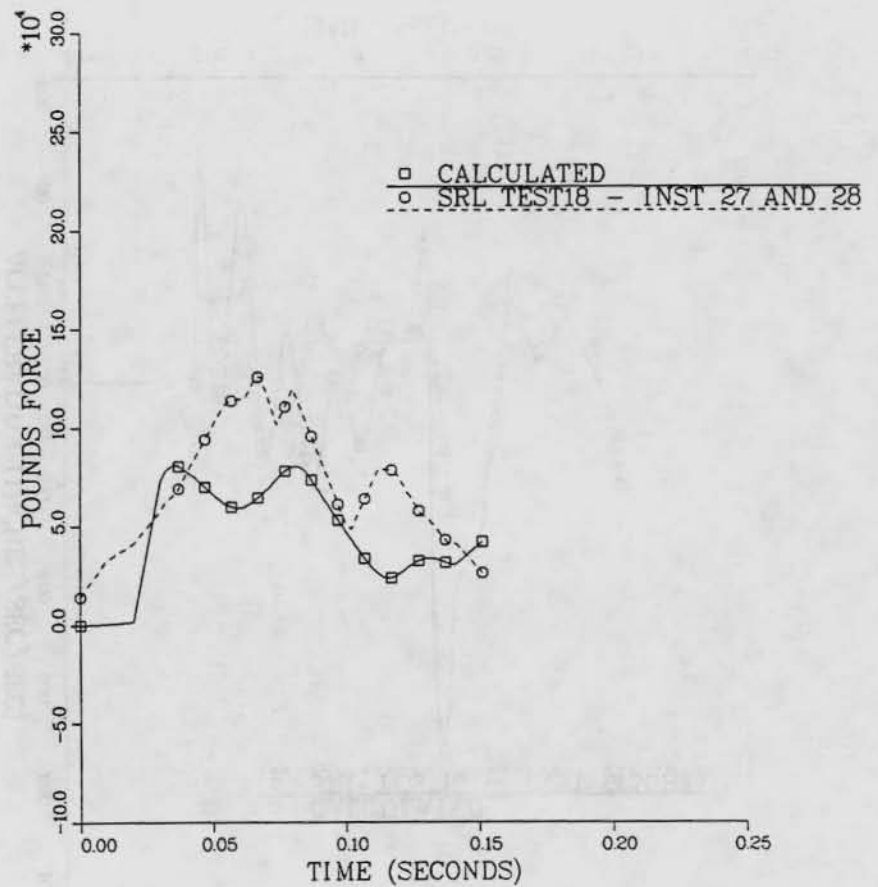


FIGURE 100. Horizontal Force of Interaction Between Cask and Rail Car vs Time During Impact with Four Hopper Cars Loaded with Ballast (Test 18 - Instruments 27 and 28).

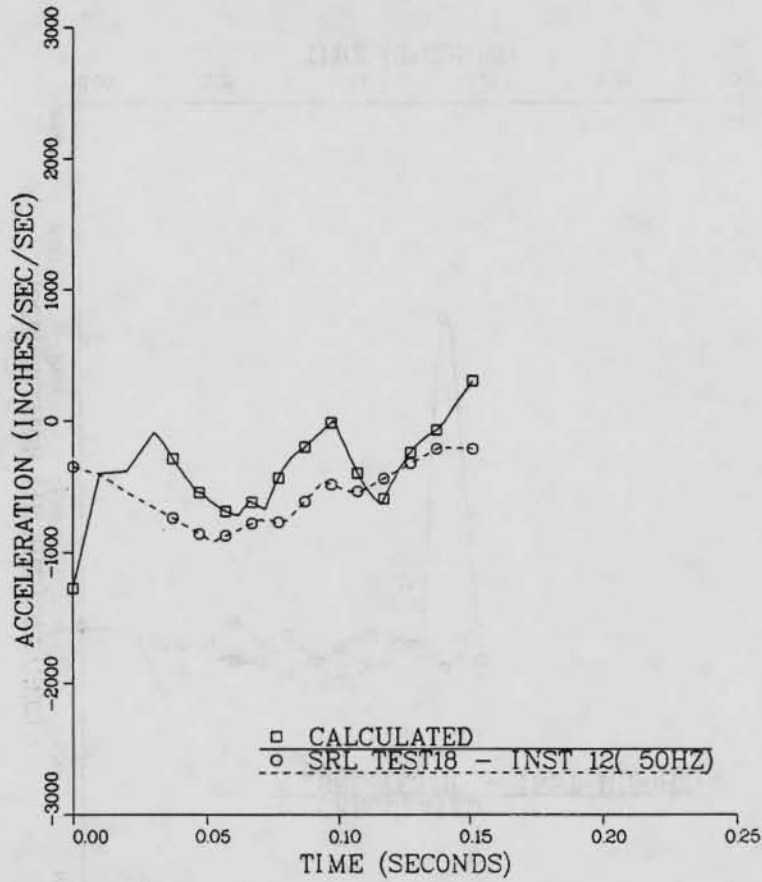


FIGURE 101. Horizontal Acceleration of the Cask-Rail Car During Impact with Four Hopper Cars Loaded with Ballast (Test 18 - Instrument 12: Filtered at 50 Hz).

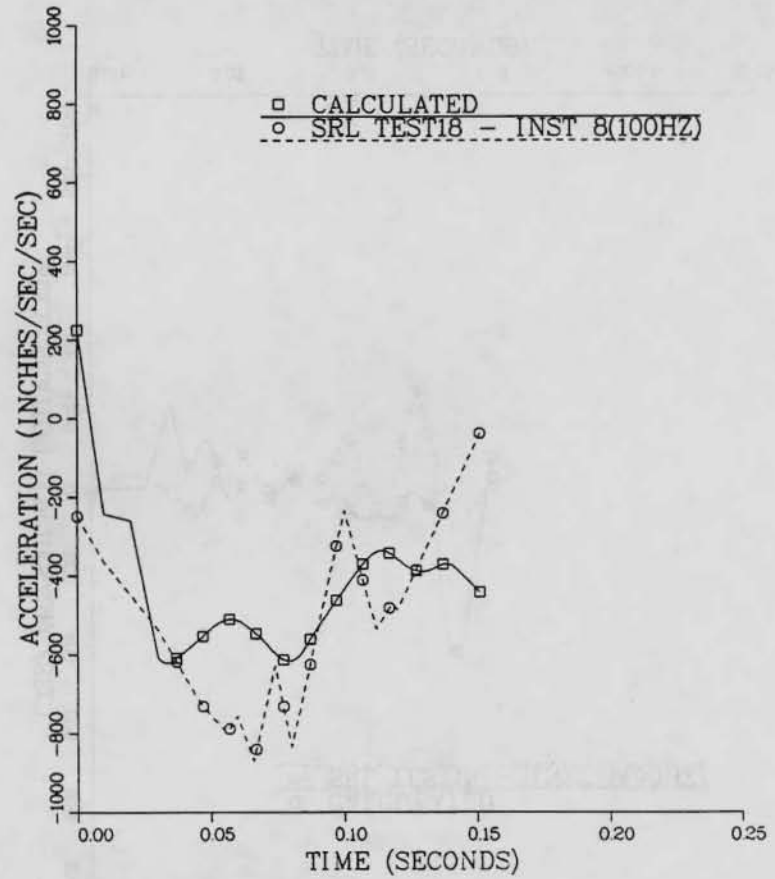


FIGURE 102. Horizontal Acceleration of the Cask During Impact with Four Hopper Cars Loaded with Ballast (Test 18 - Instrument 8: Filtered at 100 Hz).

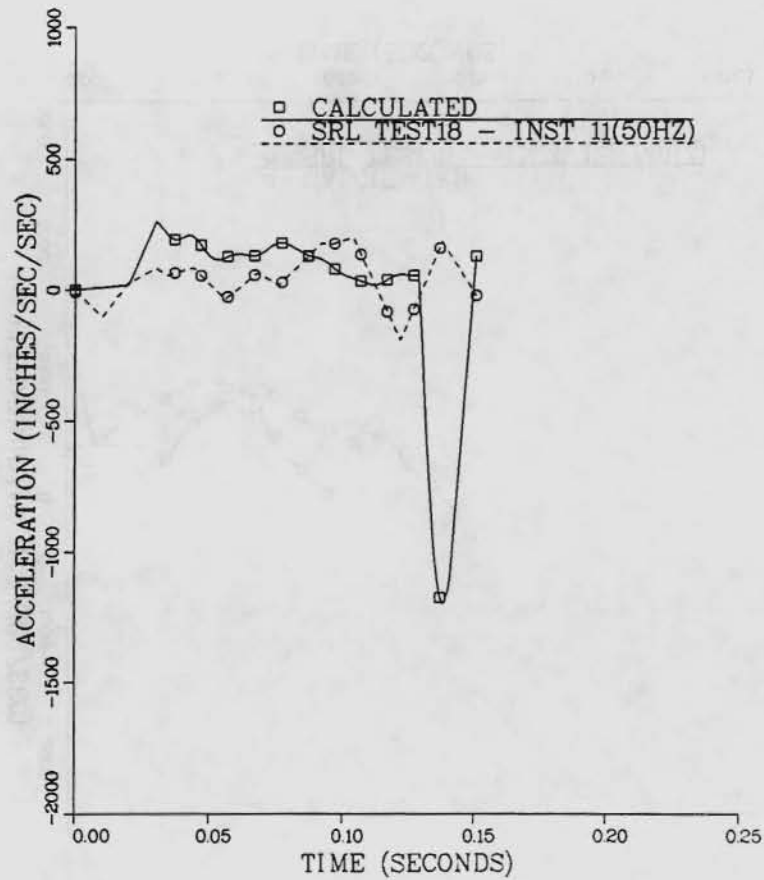


FIGURE 103. Vertical Acceleration of the Cask at the Far End During Impact with Four Hopper Cars Loaded with Ballast (Test 18 - Instrument 11: Filtered at 50 Hz.)

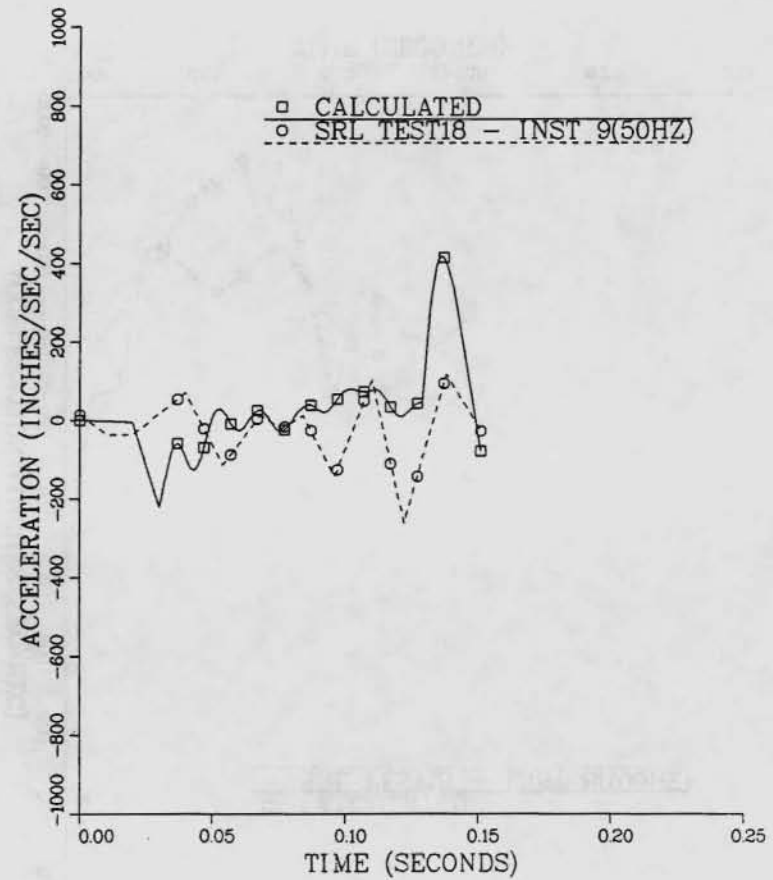


FIGURE 104. Vertical Acceleration of the Cask at the Struck End During Impact with Four Hopper Cars Loaded with Ballast (Test 18 - Instrument 9: Filtered at 50 Hz).

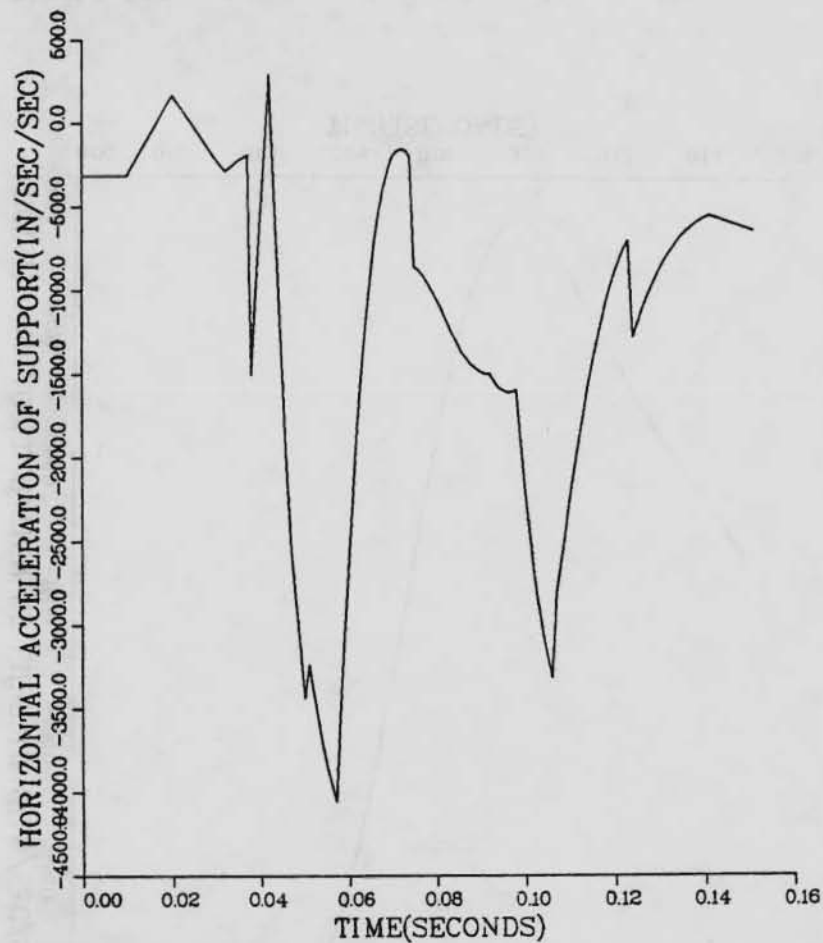


FIGURE 105. Horizontal Acceleration of the Support for an Equivalent Single-Degree-of-Freedom System (Preliminary Cases 2, 3 and 4).

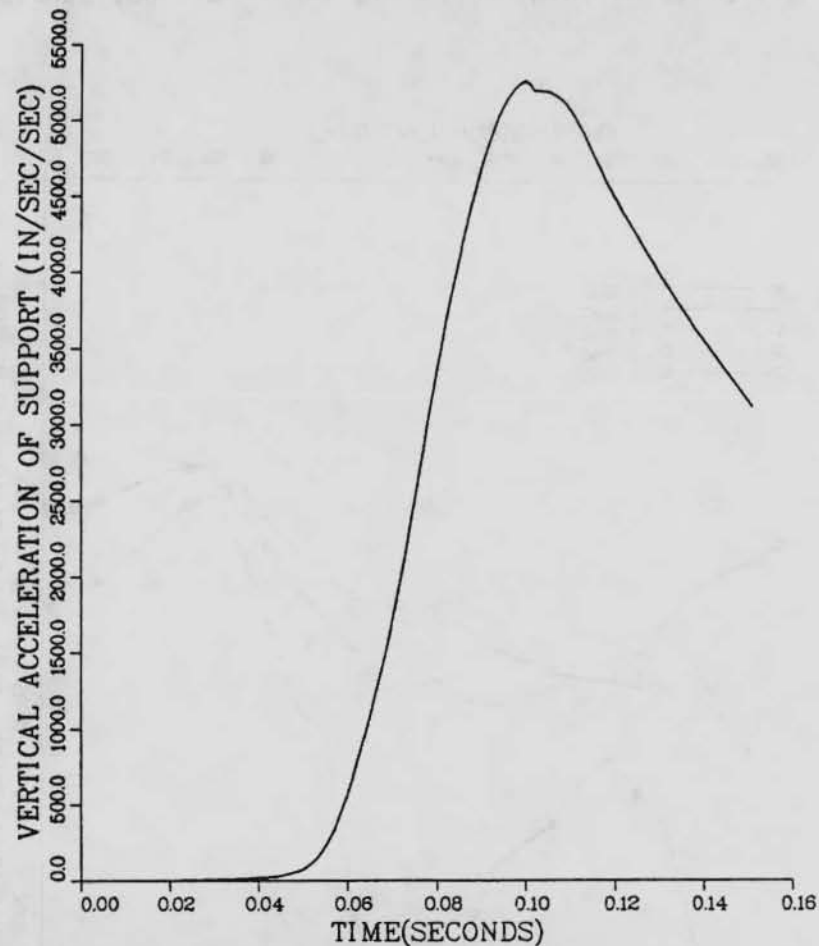


FIGURE 106. Vertical Acceleration of the Support for an Equivalent Single-Degree-of-Freedom System (Preliminary Cases 2, 3 and 4).

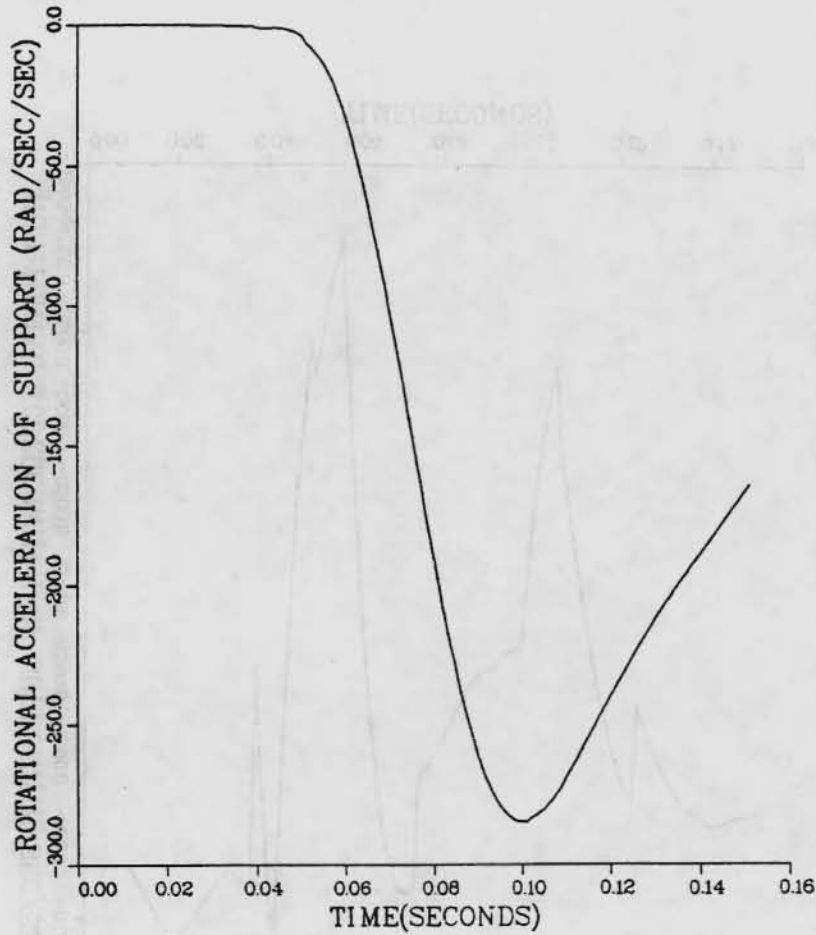


FIGURE 107. Rotational Acceleration of the Support for an Equivalent Single-Degree-of-Freedom System (Preliminary Cases 2, 3 and 4).

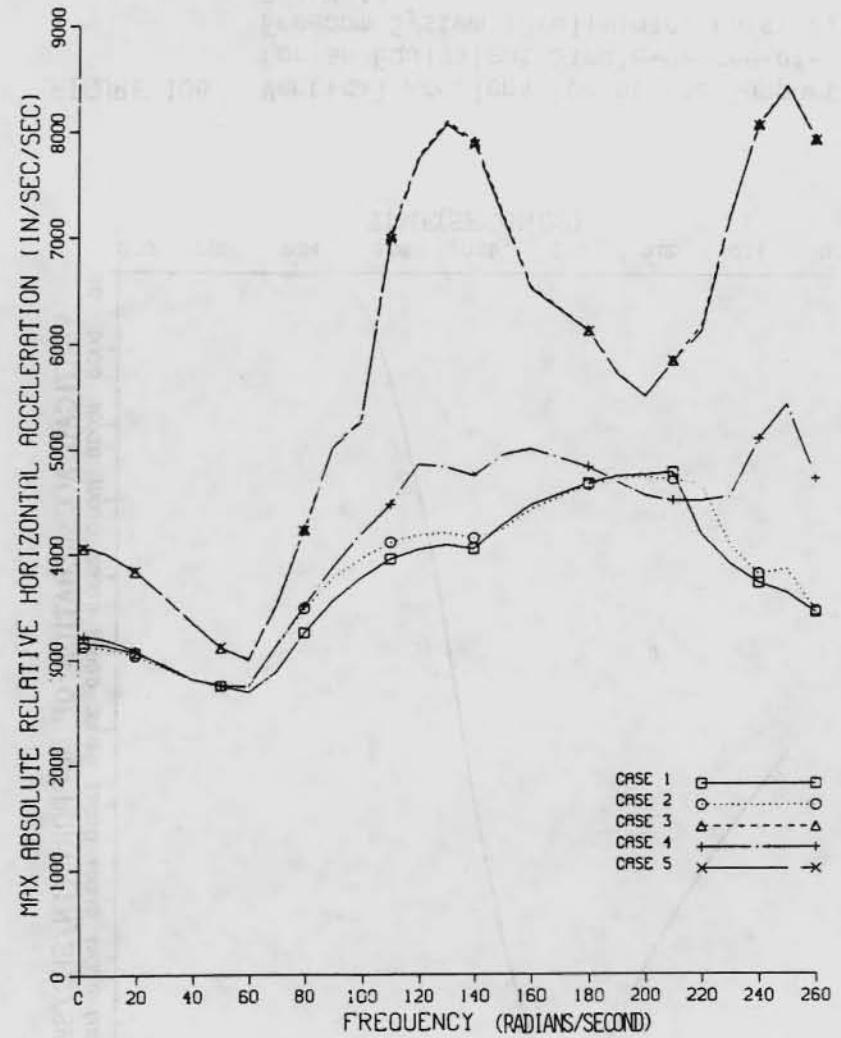


FIGURE 108. Response Spectrum: Maximum Absolute Relative Horizontal Acceleration vs Frequency (Preliminary Cases 1 through 5).

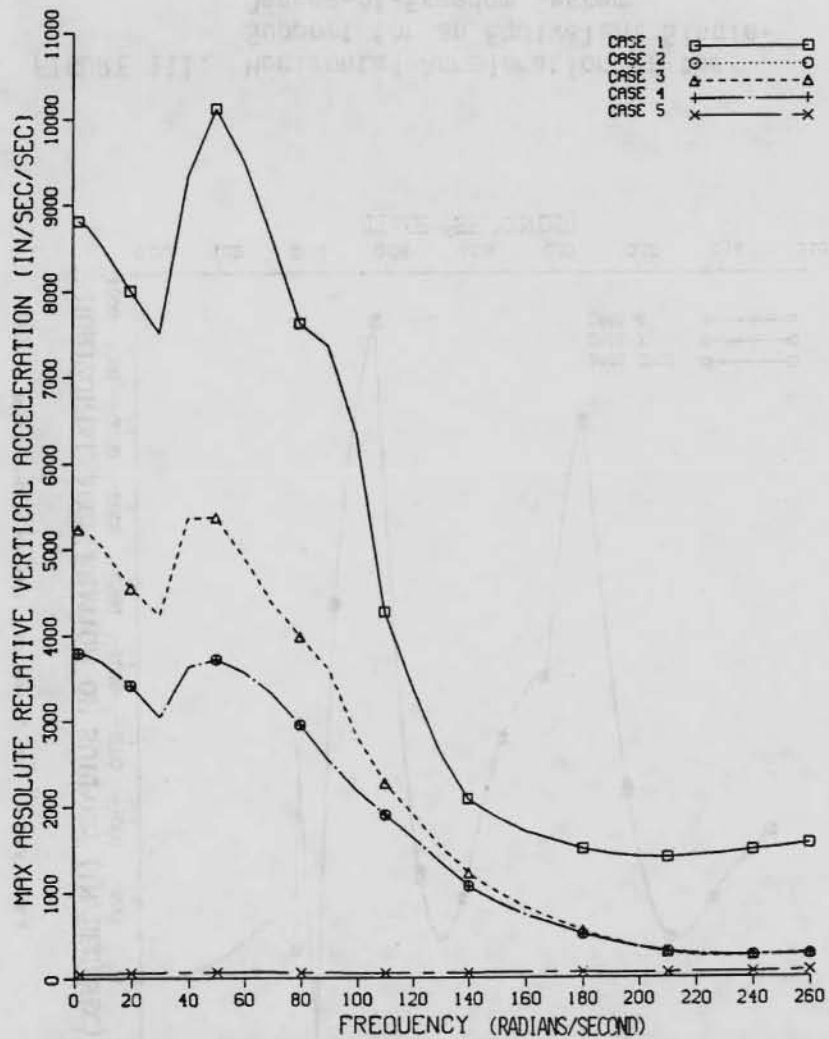


FIGURE 109. Response Spectrum: Maximum Absolute Relative Vertical Acceleration vs Frequency (Preliminary Cases 1 through 5).

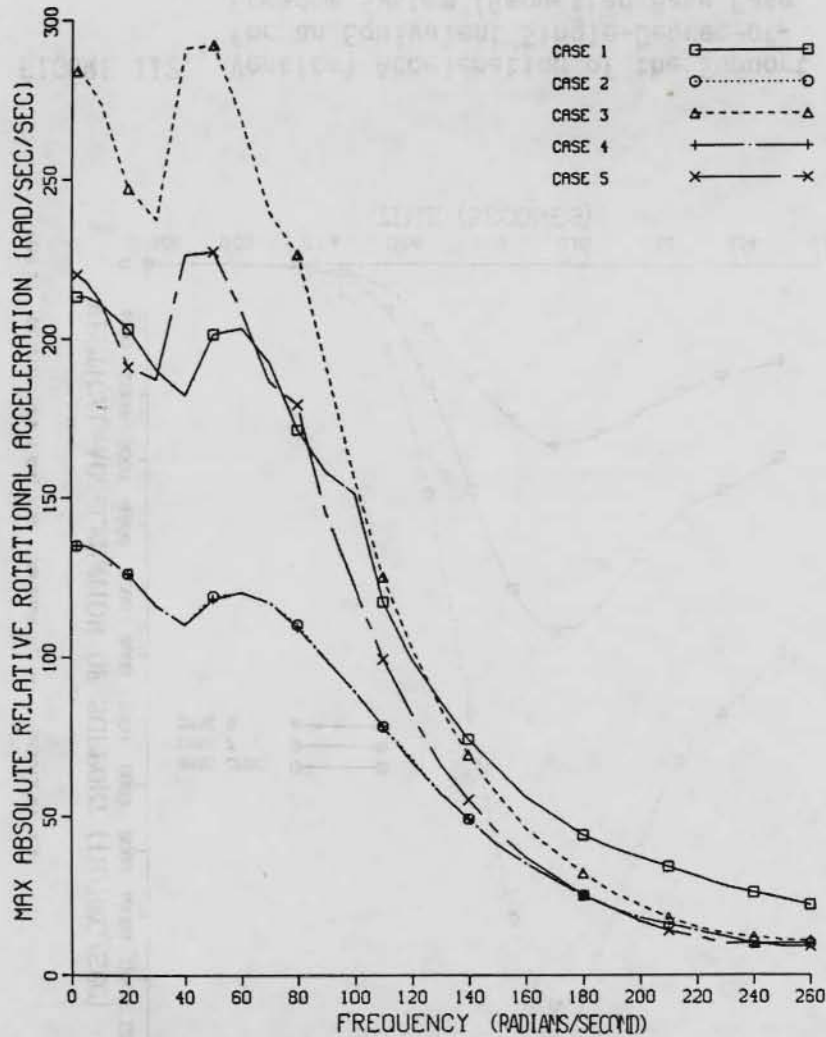


FIGURE 110. Response Spectrum: Maximum Absolute Relative Rotational Acceleration vs Frequency (Preliminary Cases 1 through 5).

09-11

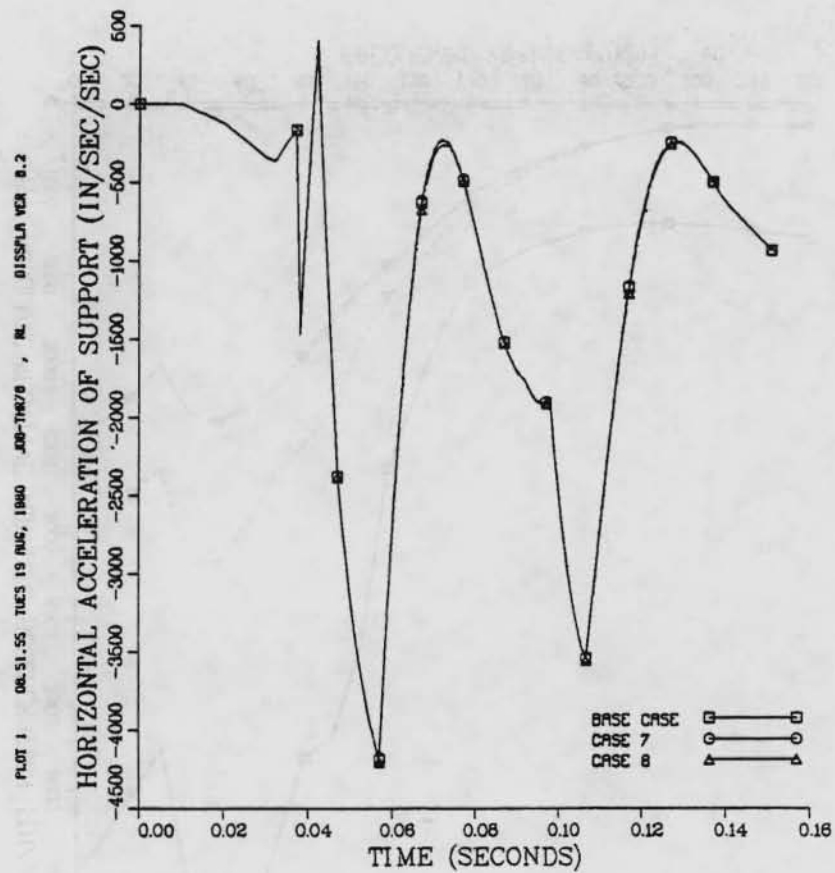


FIGURE 111. Horizontal Acceleration of the Support for an Equivalent Single-Degree-of-Freedom System (Requested Base Case and Cases 7 and 8).

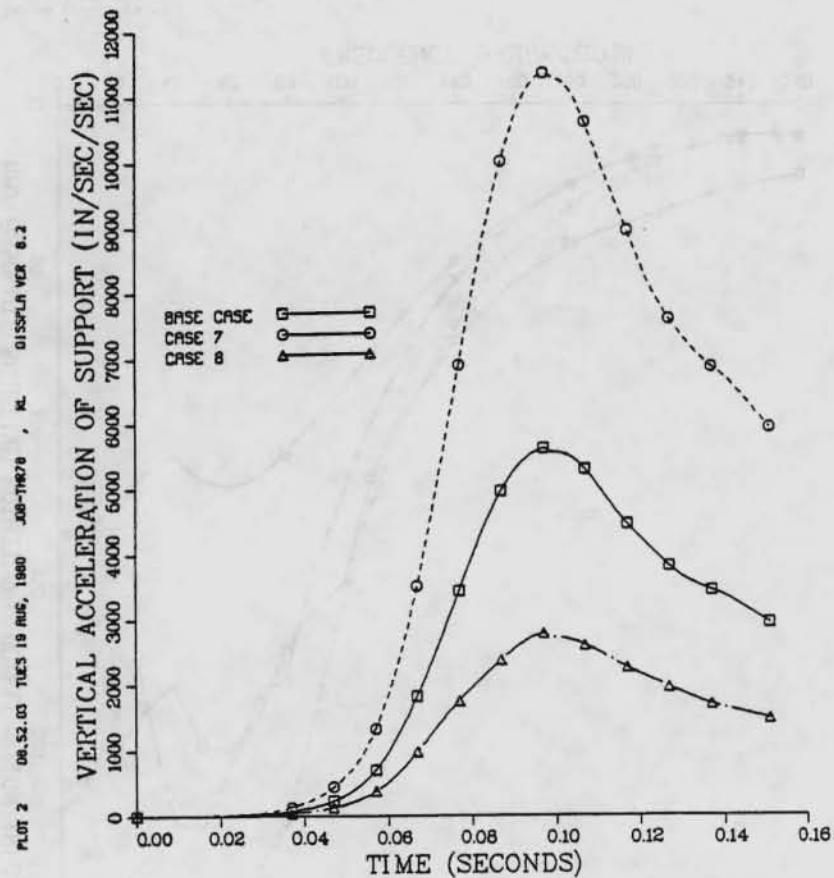


FIGURE 112. Vertical Acceleration of the Support for an Equivalent Single-Degree-of-Freedom System (Requested Base Case and Cases 7 and 8).

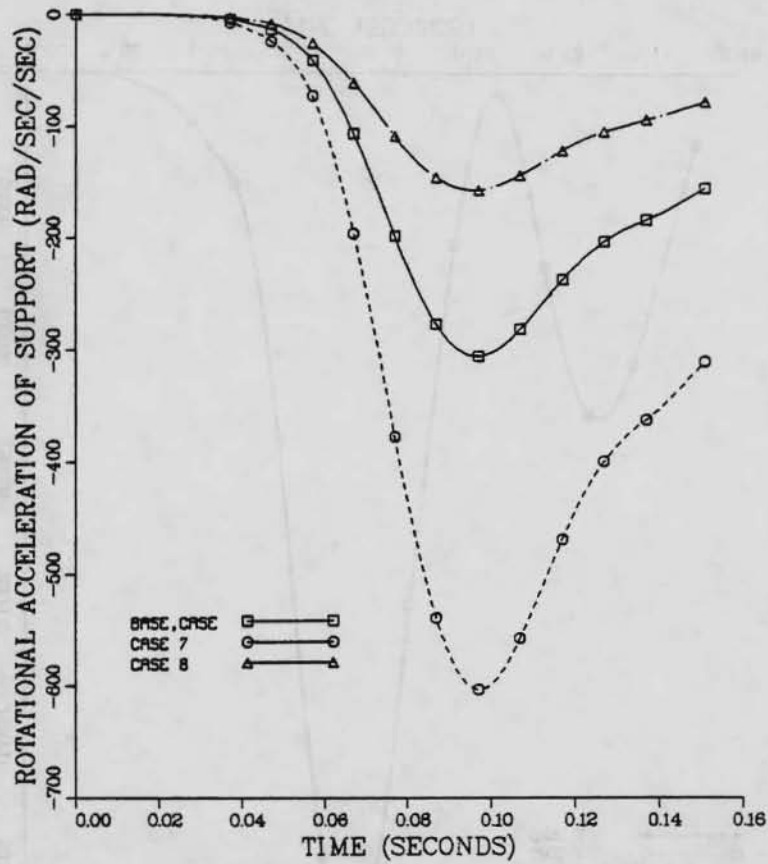


FIGURE 113. Rotational Acceleration of the Support for an Equivalent Single-Degree-of-Freedom System (Requested Base Case and Cases 7 and 8).

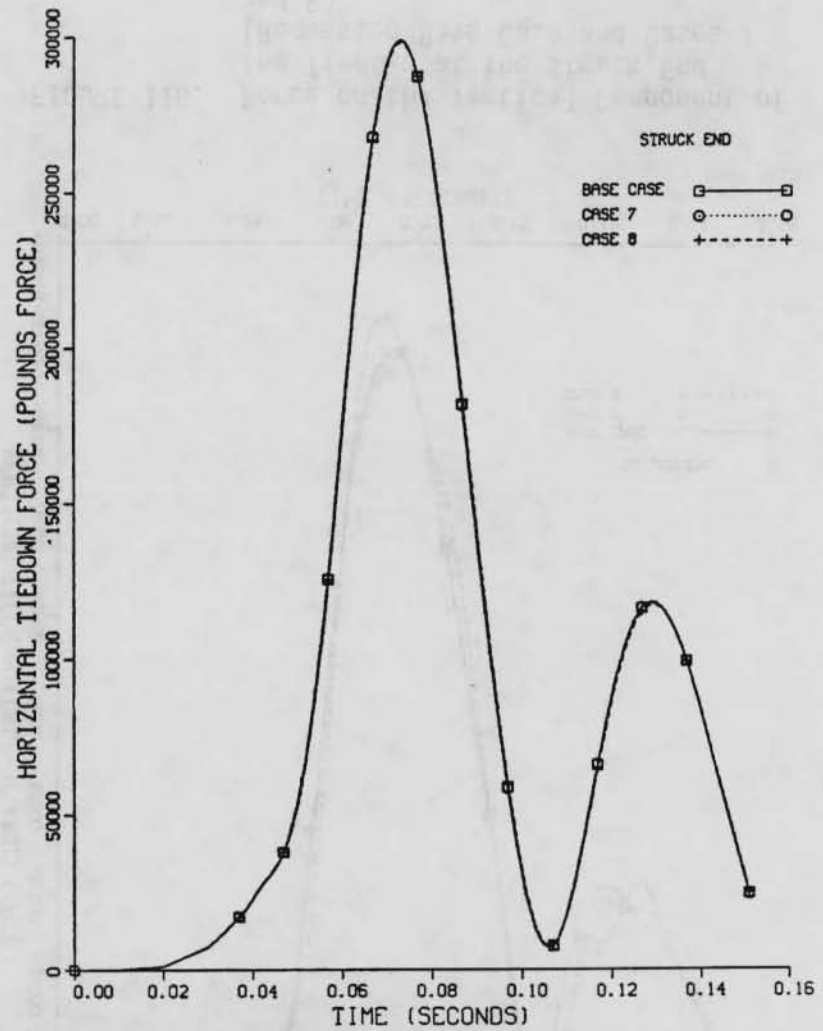


FIGURE 114. Force on the Horizontal Component of the Tiedown at the Struck End (Requested Base Case and Cases 7 and 8).

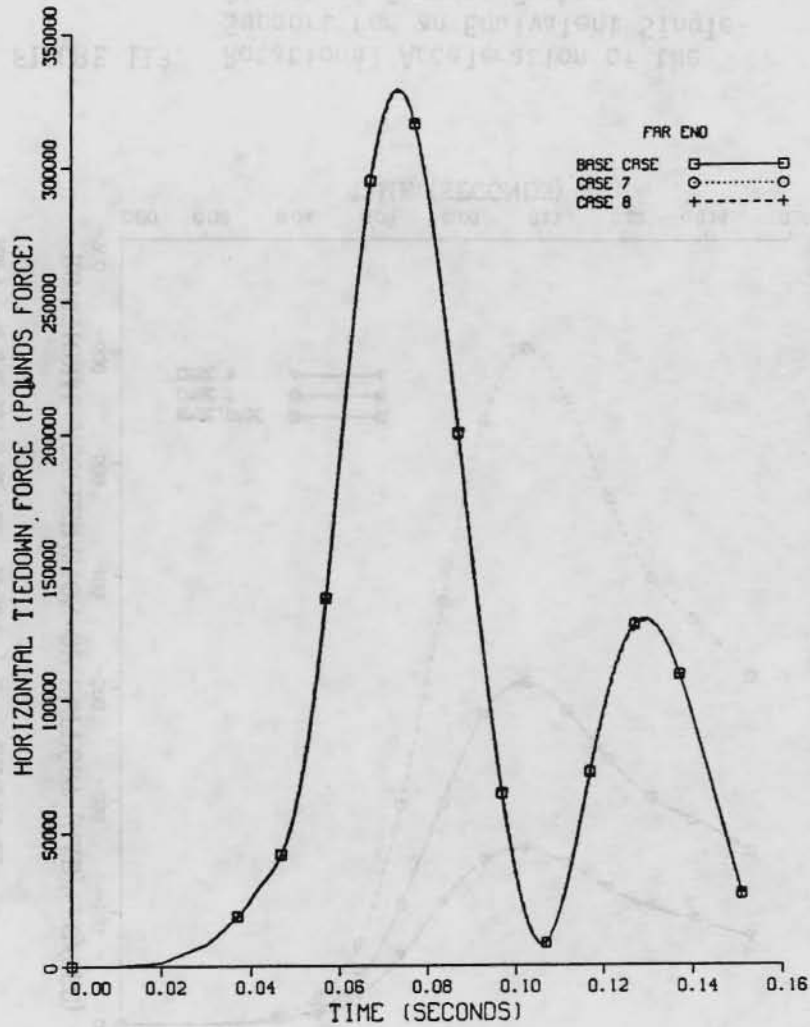


FIGURE 115. Force on the Horizontal Component of the Tiedown at the Far End (Requested Base Case and Cases 7 and 8).

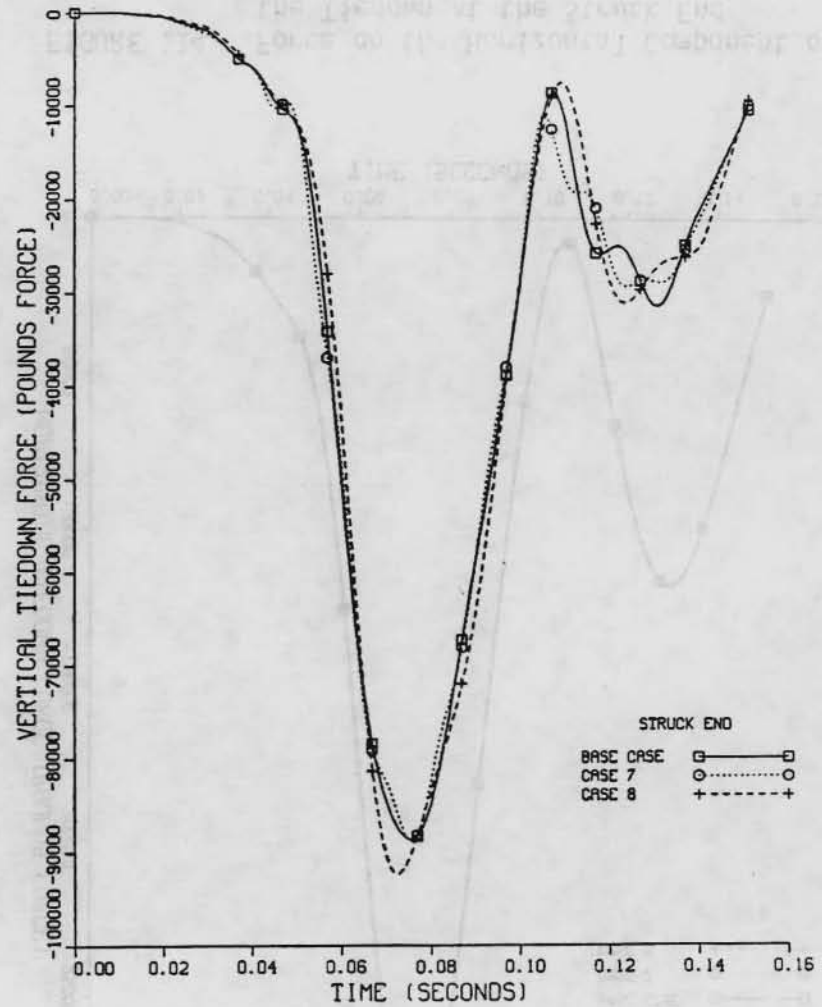


FIGURE 116. Force on the Vertical Component of the Tiedown at the Struck End (Requested Base Case and Cases 7 and 8).

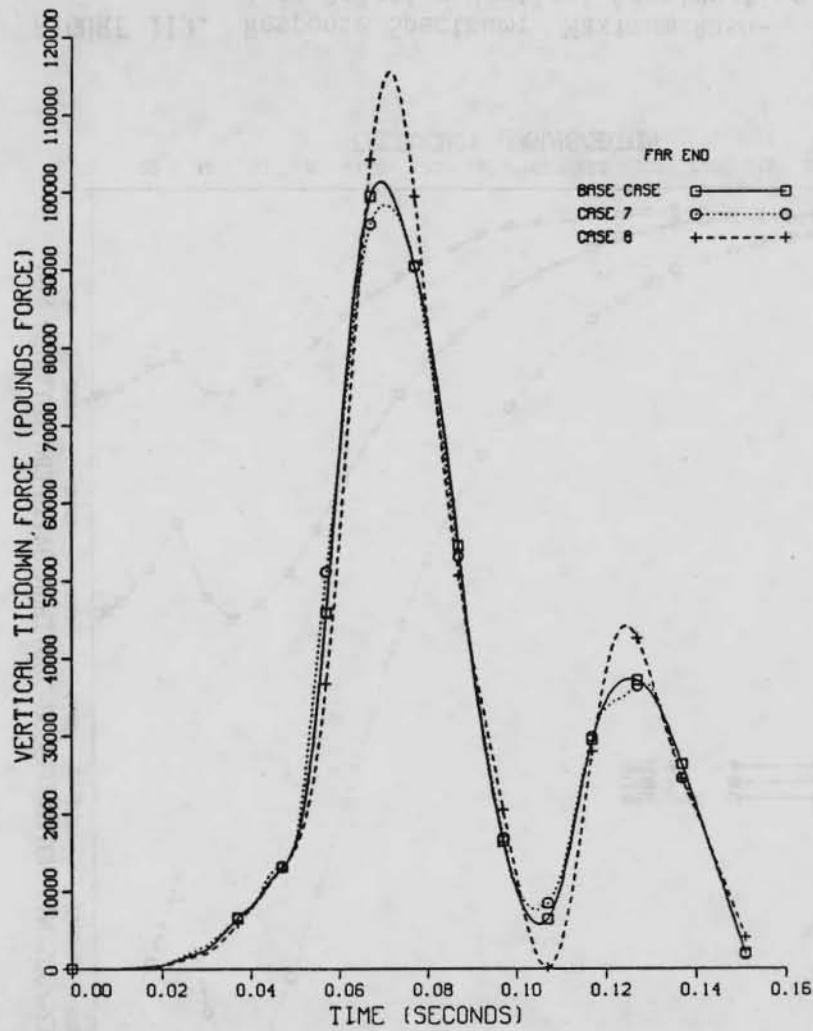


FIGURE 117. Force on the Vertical Component of the Tiedown at the Far End (Requested Base Case and Cases 7 and 8).

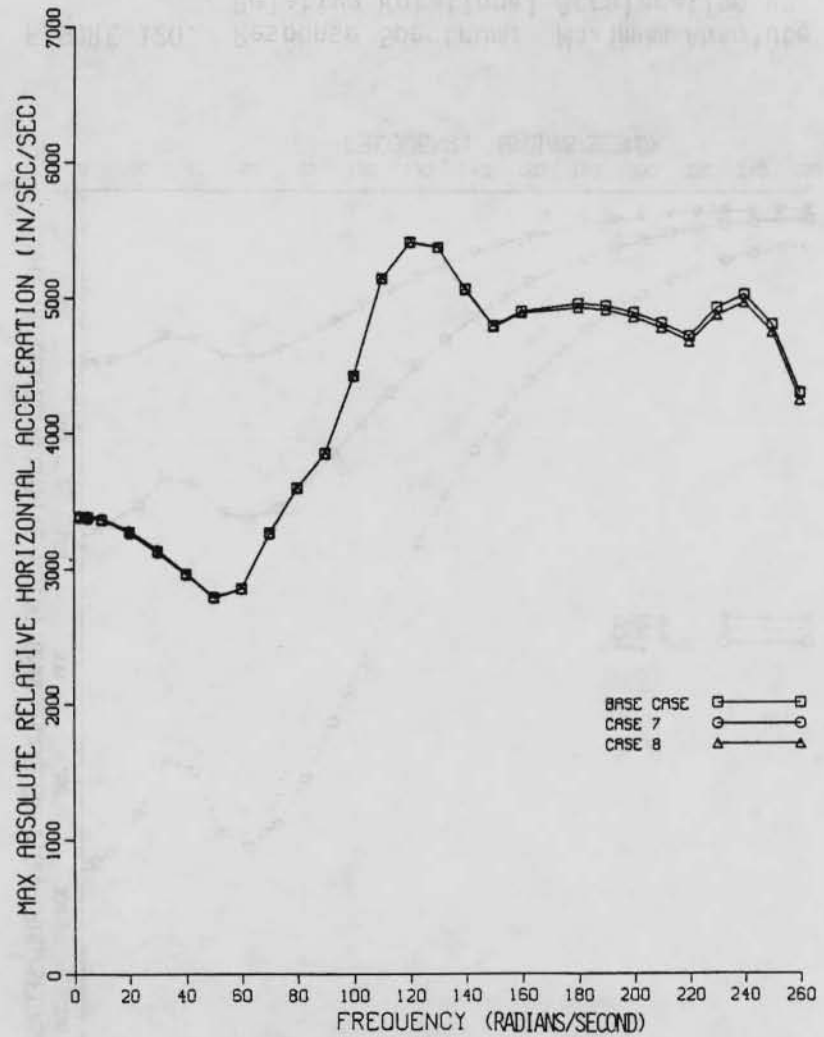


FIGURE 118. Response Spectrum: Maximum Absolute Relative Horizontal Acceleration vs Frequency (Requested Base Case and Cases 7 and 8).

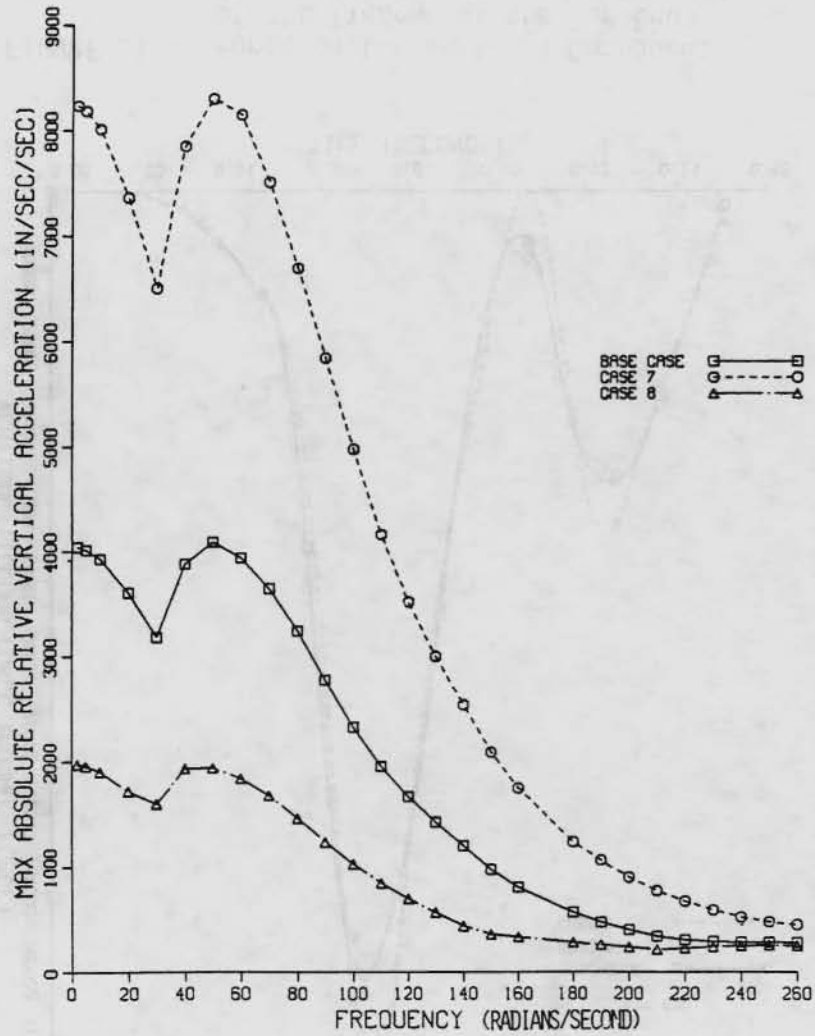


FIGURE 119. Response Spectrum: Maximum Absolute Relative Vertical Acceleration vs Frequency (Requested Base Case and Cases 7 and 8).

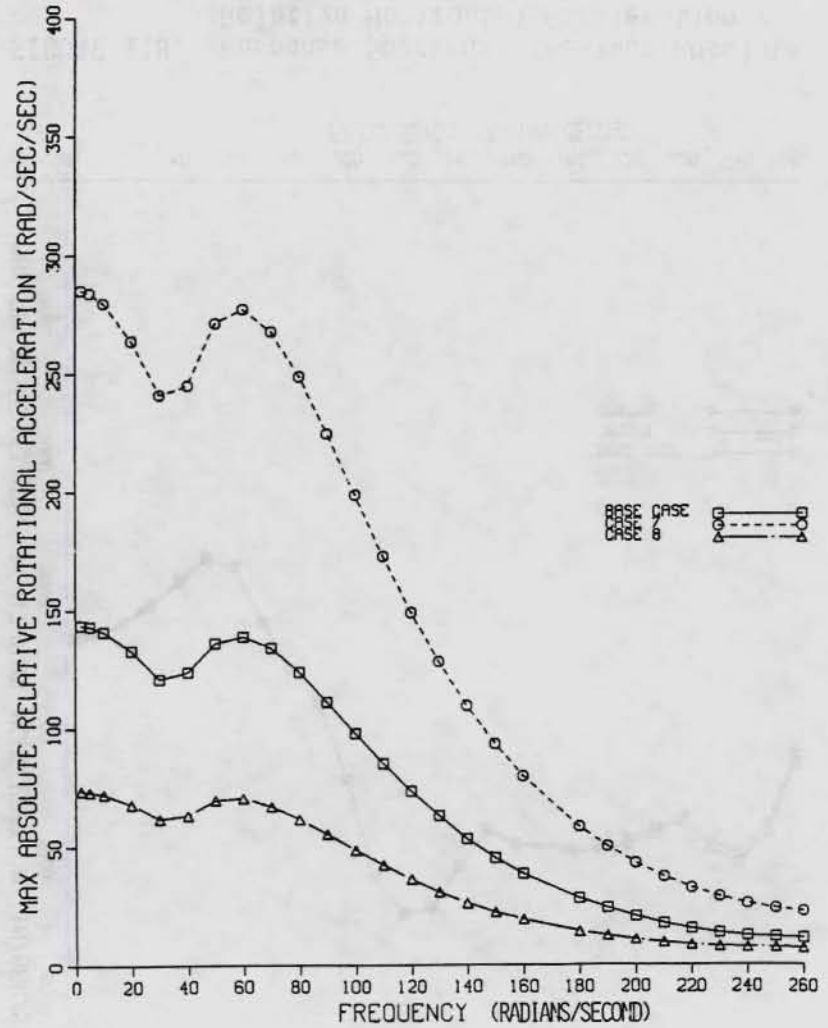


FIGURE 120. Response Spectrum: Maximum Absolute Relative Rotational Acceleration vs Frequency (Requested Base Case and Cases 7 and 8).

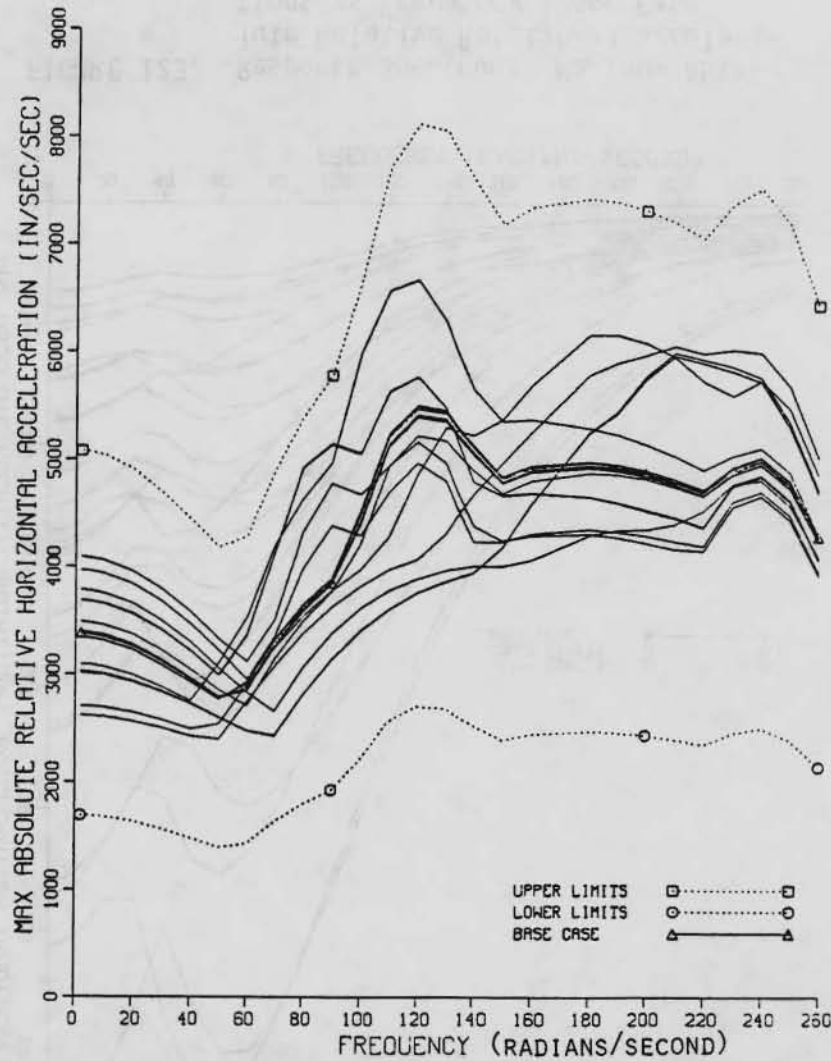


FIGURE 121. Response Spectrum: Maximum Absolute Relative Horizontal Accelerations vs Frequency (Base Case, $\pm 50\%$ Base Case, and Cases 1, 2, C, D, and 3 through 21).

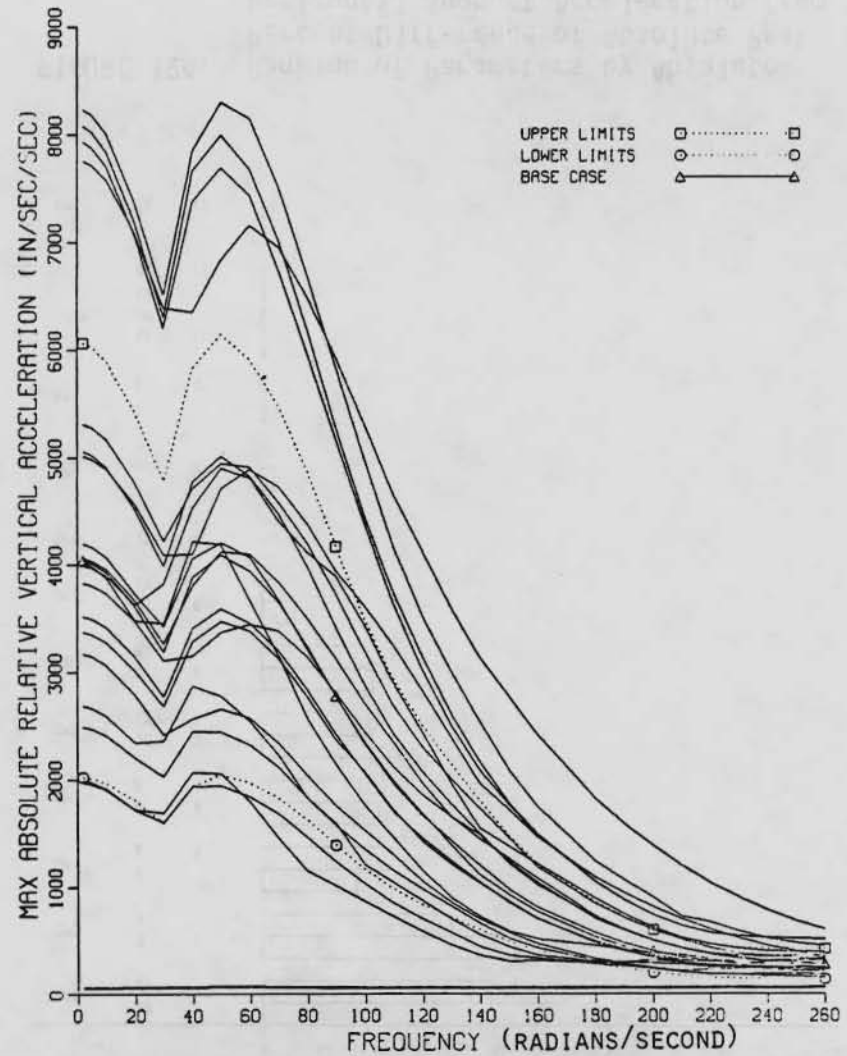


FIGURE 122. Response Spectrum: Maximum Absolute Relative Vertical Accelerations vs Frequency (Base Case, $\pm 50\%$ Base Case, and Cases 1, 2, C, D, and 3 through 21).

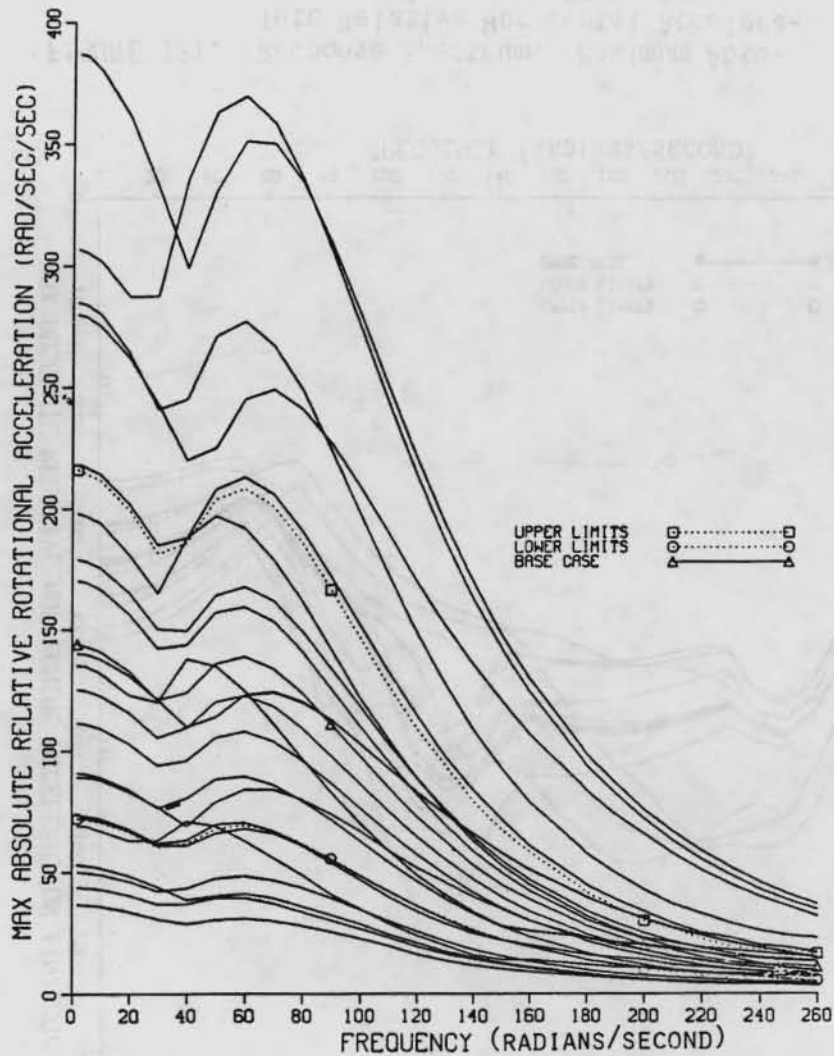


FIGURE 123. Response Spectrum: Maximum Absolute Relative Rotational Accelerations vs Frequency (Base Case, $\pm 50\%$ Base Case, and Cases 1, 2, C, D, and 3 through 21).

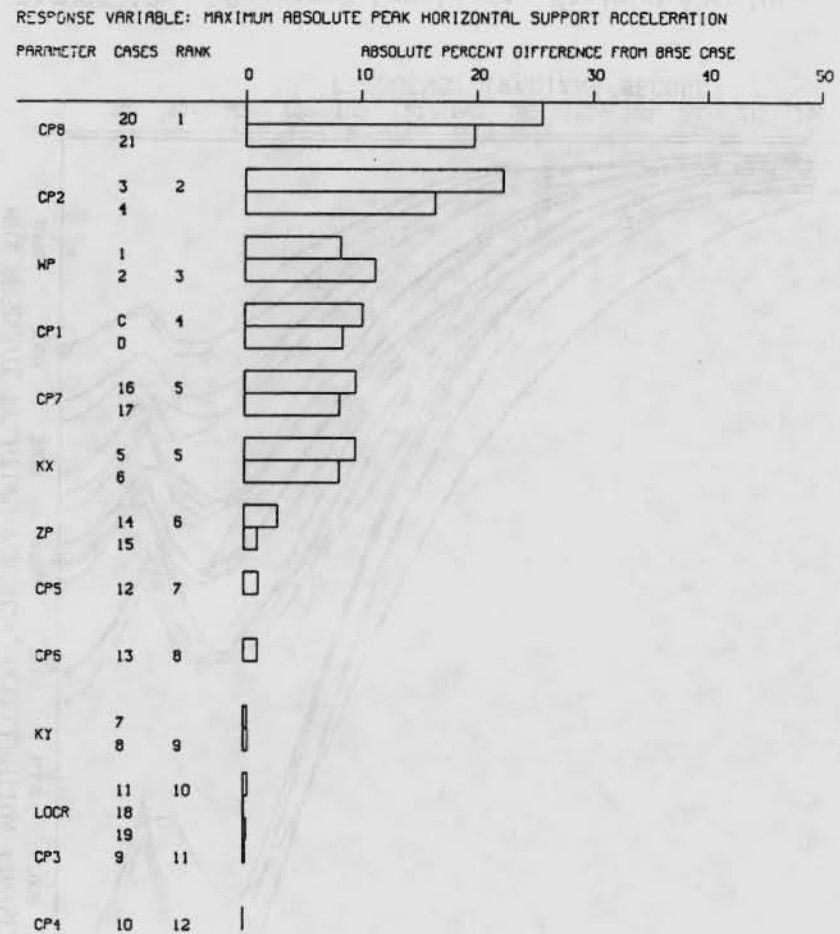


FIGURE 124. Ranking of Parameters by Absolute Percent Difference of Absolute Peak Horizontal Support Acceleration from Base Case Value.

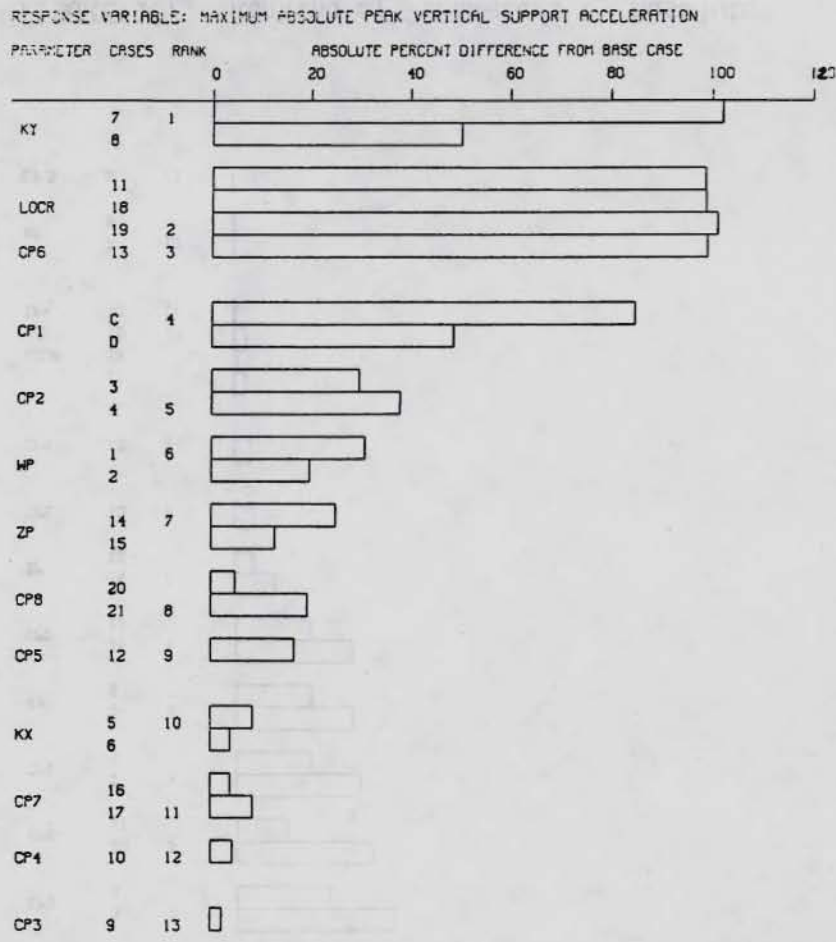


FIGURE 125. Ranking of Parameters by Absolute Percent Difference of Absolute Peak Vertical Support Acceleration from Base Case Value.

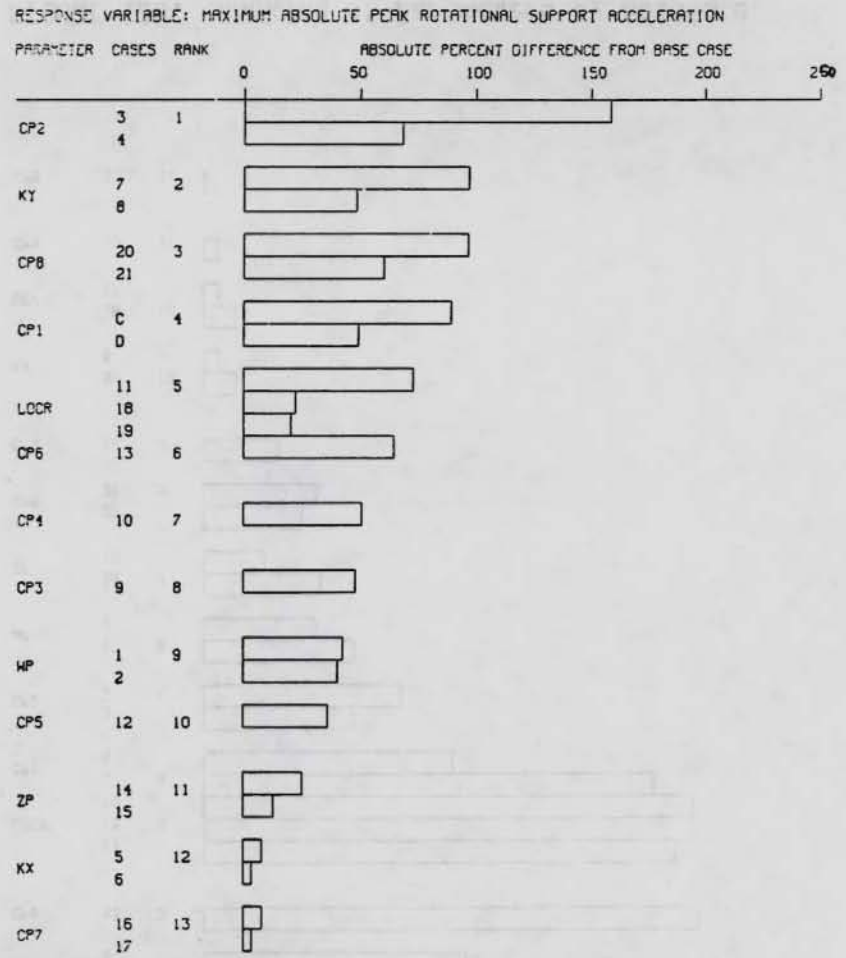


FIGURE 126. Ranking of Parameters by Absolute Percent Difference of Absolute Peak Rotational Support Acceleration from Base Case Value.

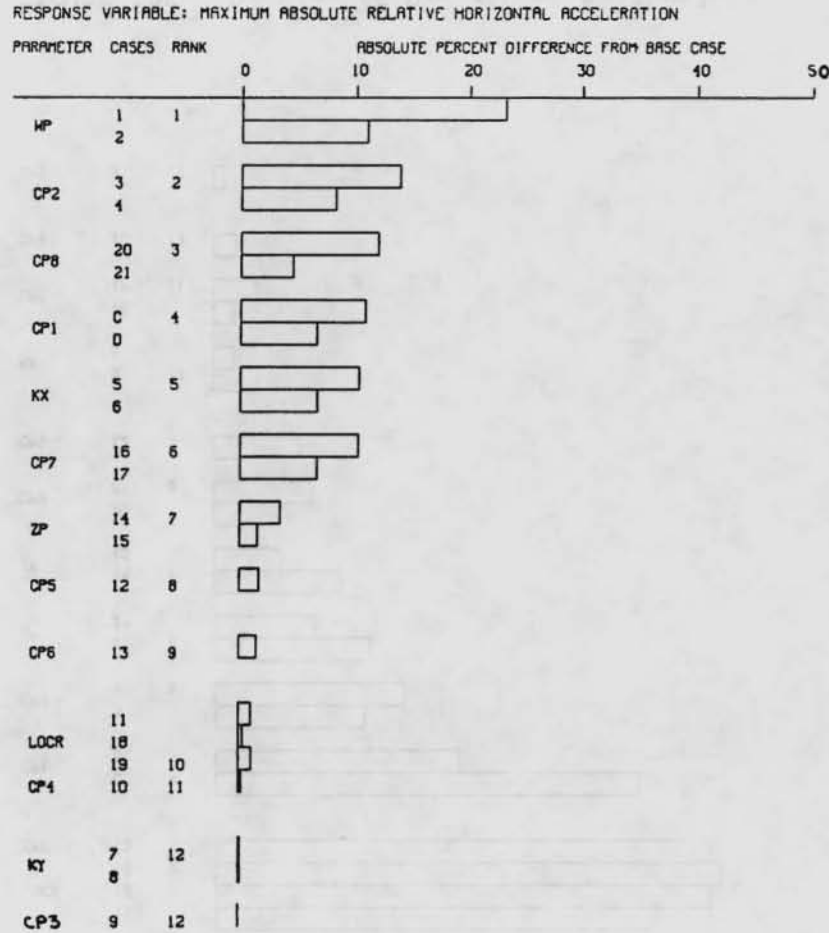


FIGURE 127. Ranking of Parameters by Absolute Percent Difference of Maximum Absolute Relative Horizontal Acceleration from Base Case Value.

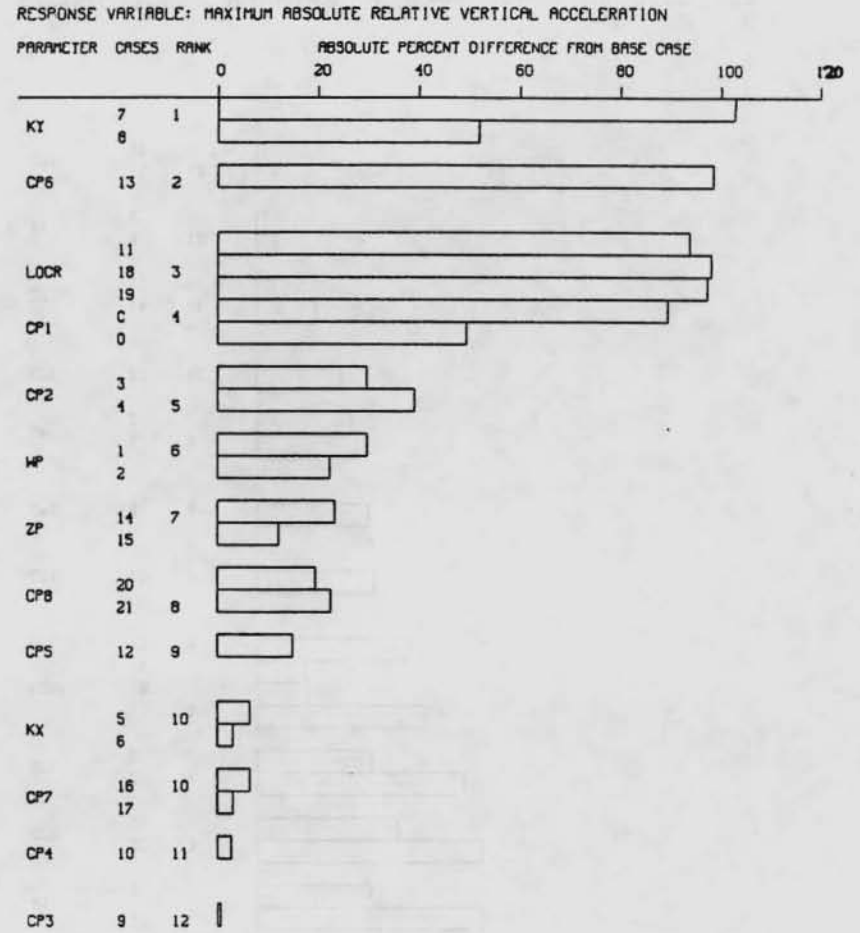


FIGURE 128. Ranking of Parameters by Absolute Percent Difference of Maximum Absolute Relative Vertical Acceleration from Base Case Value.

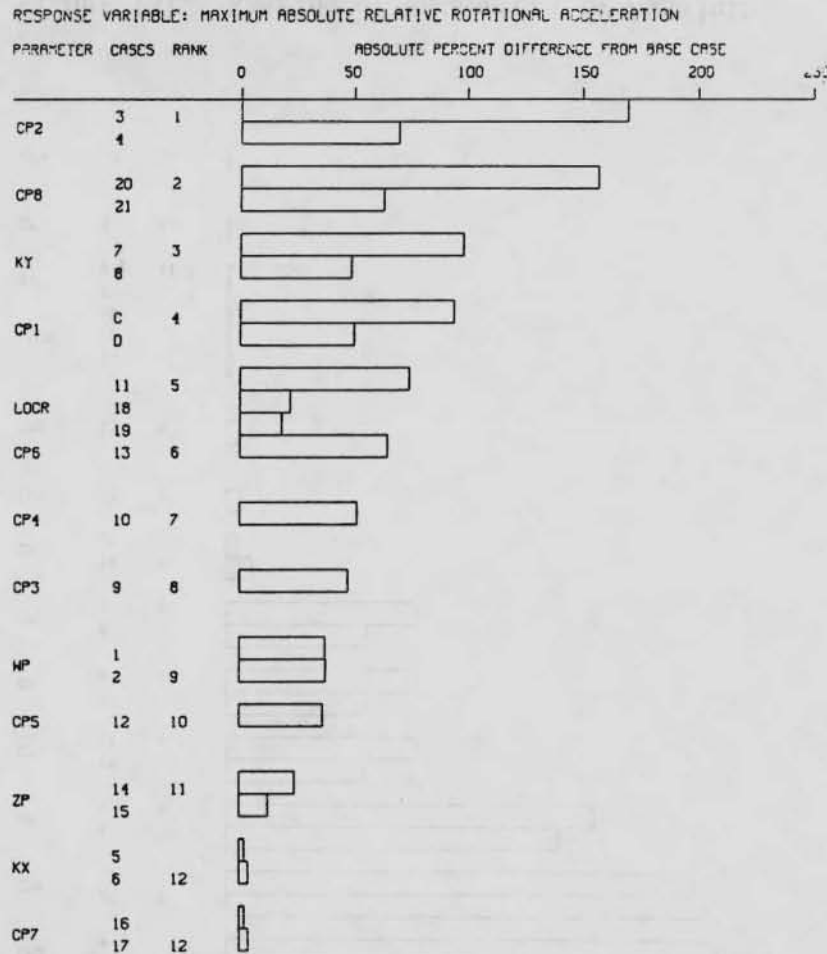


FIGURE 129. Ranking of Parameters by Absolute Percent Difference of Maximum Absolute Relative Rotational Acceleration from Base Case Value.

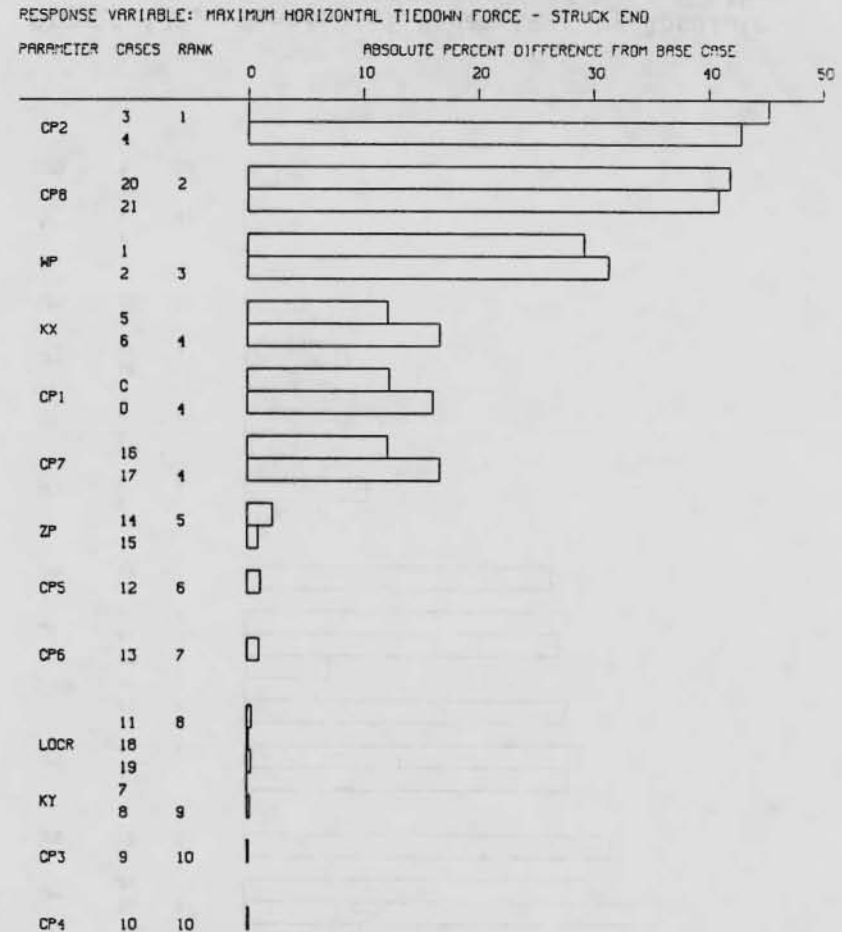


FIGURE 130. Ranking of Parameters by Absolute Percent Difference of Maximum Absolute Horizontal Tiedown Force (Struck End) from Base Case Value.



FIGURE 131. Ranking of Parameters by Absolute Percent Difference of Maximum Absolute Horizontal Tiedown Force (Far End) from Base Case Value.

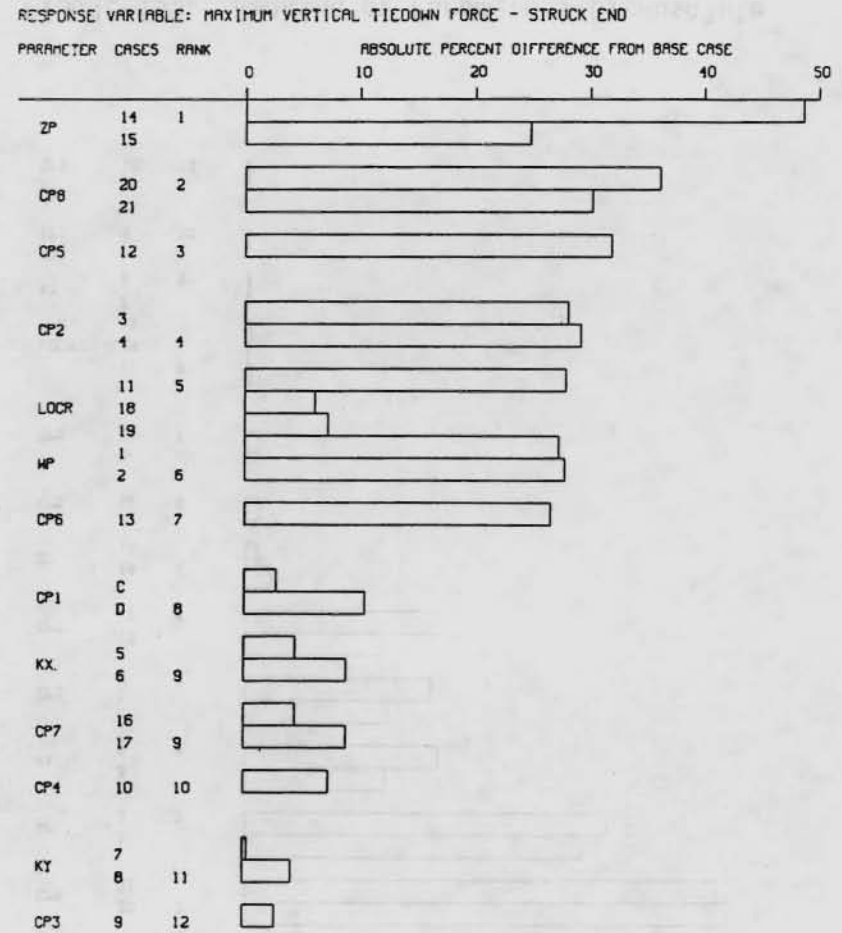


FIGURE 132. Ranking of Parameters by Absolute Percent Difference of Maximum Absolute Vertical Tiedown Force (Struck End) from Base Case Value.

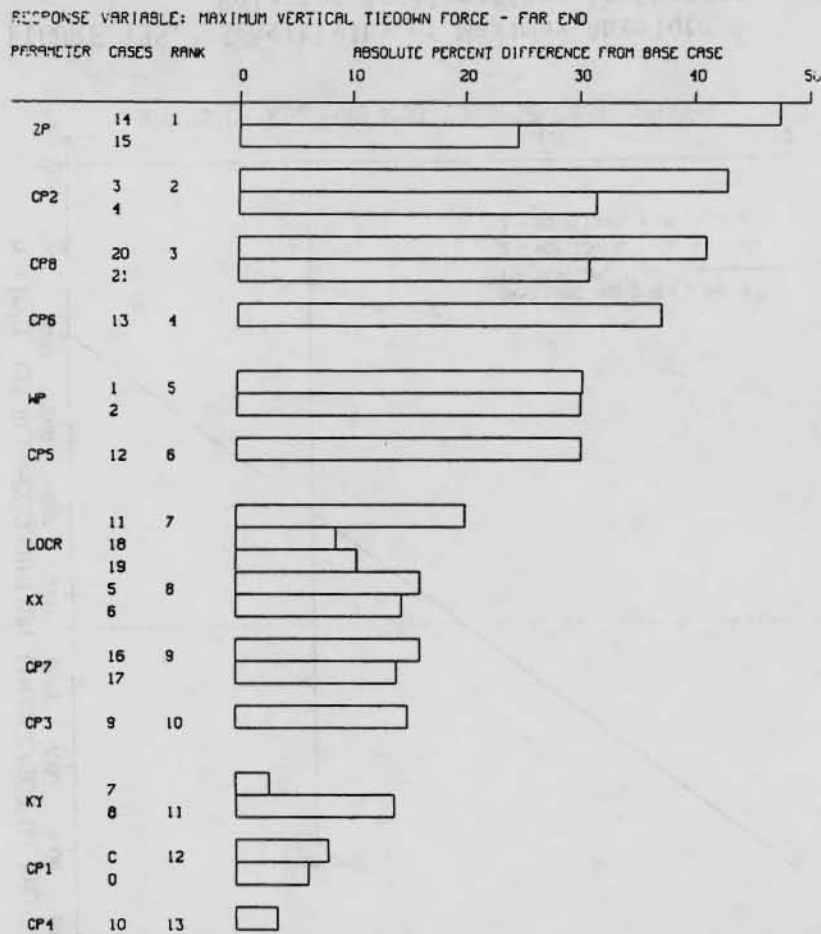


FIGURE 133. Ranking of Parameters by Absolute Percent Difference of Maximum Absolute Vertical Tiedown Force (Far End) from Base Case Value.

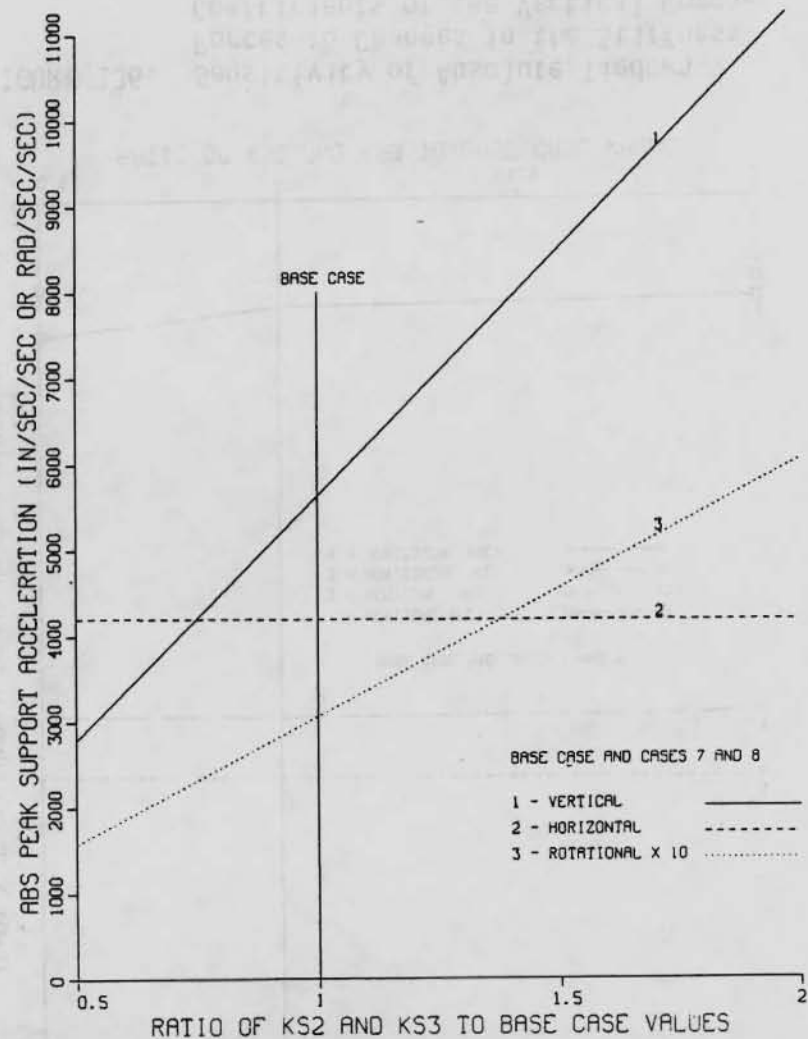


FIGURE 134. Sensitivity of Absolute Peak Support Accelerations to Changes in the Stiffness Coefficients of the Vertical Components of the Tiedowns (Requested Base Case and Cases 7 and 8).

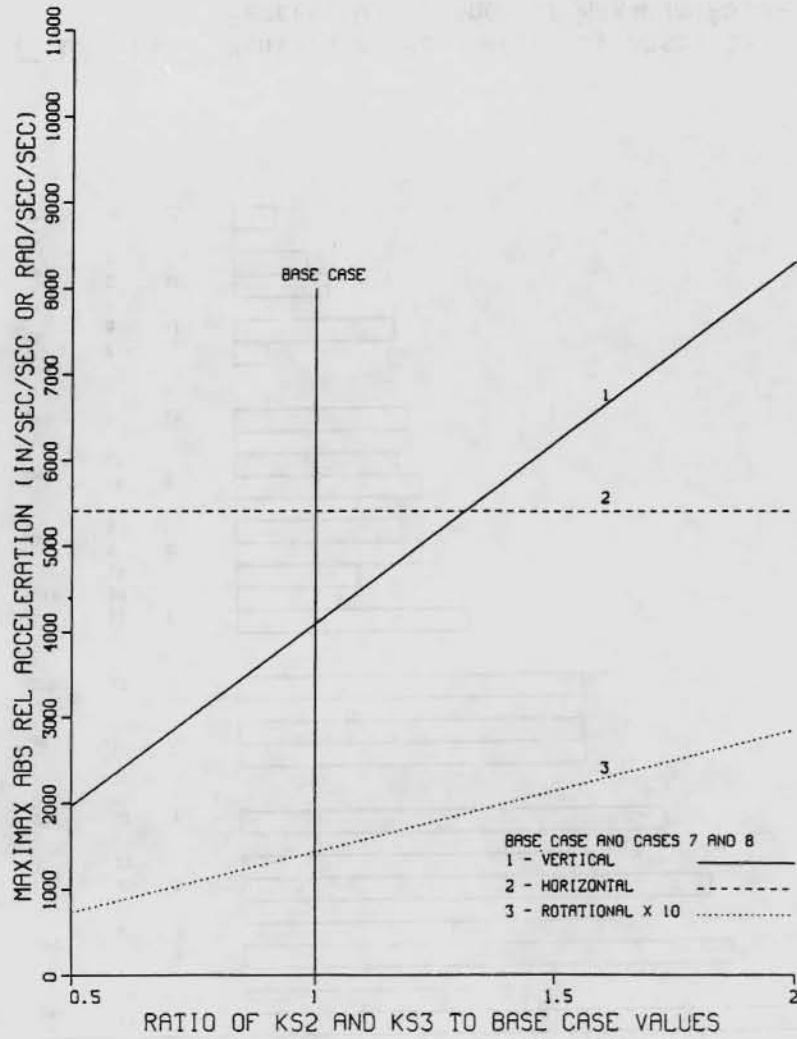


FIGURE 135. Sensitivity of Maximax Absolute Relative Accelerations to Changes in the Stiffness Coefficients of the Vertical Components of the Tiedowns (Base Case and Cases 7 and 8).

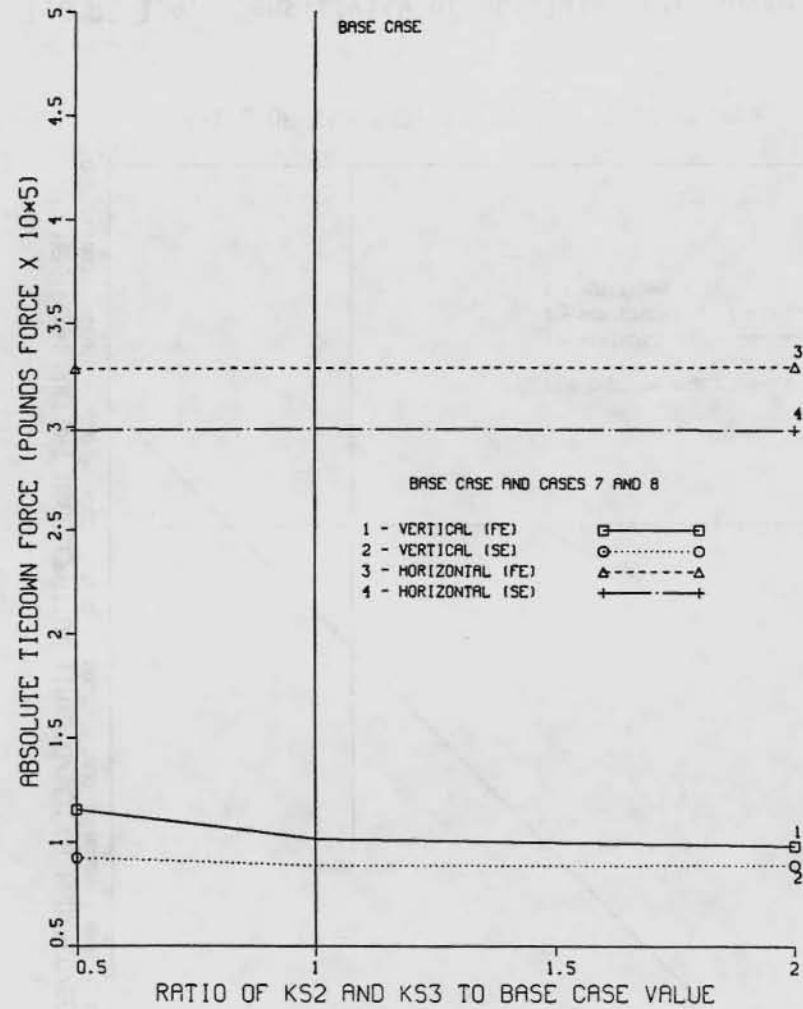


FIGURE 136. Sensitivity of Absolute Tiedown Forces to Changes in the Stiffness Coefficients of the Vertical Components of the Tiedowns (Requested Base Case and Cases 7 and 8).

A P P E N D I X I I I

TABLES

ANDERSON III

1982

111

TABLE 1

PARAMETERS USED IN THE *CARDT* MODEL FOR SIMULATION
OF IMPACT BETWEEN TWO HOPPER CARS LOADED WITH GRAVEL

Weight of Hammer Car [lb(force)]	W_{RC}	218,000
Weight of Anvil Car [lb(force)]	W_F	211,000
Upper Limit on Travel of Combined Draft Gears (in.)	X_{TU}	5.6
Lower Limit on Travel of Combined Draft Gears (in.)	X_{TL}	-5.6
Spring Constants of Draft Gears During "Active" State [lb(force)/in.]	k_1, k_2	48,666
Base Spring Constants of Draft Gears During "Solid" State [lb(force)/in.]	k_{SDG10}, k_{SDG20}	75,000
Energy Dissipation Coefficient for Cargo Compaction Phase	μ_{XTC}	0.01
Energy Dissipation Coefficient for Cargo Recovery Phase	μ_{XTE}	0.95

TABLE 2

SUMMARY OF CONFIGURATIONS AND CONDITIONS
OF COMPLETED CASK-RAIL CAR-TIEDOWN TESTS

Test No.	Date	Rail Car	Coupler	Cask Wt. Tons	Impact Speed MPH	Stop Frequency f_n	Tiedown	Remarks
Preliminary test no instrumentation								
P1	6/8	III	Std	42.5	5.5	-	-	<ul style="list-style-type: none"> - Concrete simulation - Welded Steel Stop - Cable Rigging to Restrain Weight - No structural damage
P2	6/8	III	Std	42.5	7.6			
P3	6/8	III	Std	42.5	11.8			
1	7/14	I	Std	40	8.3	Hi	A	Instrumented Coupler Faulty
2	7/18	I	Std	40	9.0	Hi	A*	Instrumented Coupler Faulty
3	7/19	I	Std	40	10.5	Hi	A	Instrumented Coupler Faulty
4	7/19	I	Std	40	10.7	Low	B	
5	7/20	I	Std	40	10.5	Hi	D	Cable Load Instruments Faulty
6	7/26	III	EOC	40	2.8	-	C	No Photography - No Data on Tape
7	7/26	III	EOC	40	5.6	-	C	No Photography - No Data on Tape
8	7/26	III	EOC	40	9.2	-	C	No Photography - No Data on Tape
9	7/26	III	EOC	40	9.2	-	C	No Photography - No Data on Tape
10	7/27	I	Std	70	8.0	-	A	One High Speed Camera Only
11	7/27	I	Std	70	11.2	-	A	One High Speed Camera Only
12	7/31	III	EOC	40	11.2	-	D	Data Questionable
13	8/1	III	EOC	40	11.2	-	D	Report of Test 12
14	8/1	III	Std	40	5.4	-	C	
15	8/1	III	Std	40	6.5	-	C	
16	8/2	III	Std	40	10.8	-	D	Some Cables Loose After Test
17	8/3	II	Cushion	40	5.9	-	D	
18	8/3	II	Cushion	40	10.7	-	D	

*Support Underbeam Reinforced (i.e., stiffened)

Key

Railcars: I 70 ton SCL - Std Couplers
 II 70 ton SCL - Cushion Underframe
 III 80 ton Union Carbide - Mixed Couplers

Tiedowns: A - 2 load cells between stop and cask bumper beams
 - 2 load bolts reproducibly snug
 B - Same as A, except f_n lowered with bumper beams
 C - Ten 1" cables at same angle - No stop
 D - Vertical Tiedown with six cables - two instrumented

TABLE 3

FORCE TERMS FROM THE *CARDS* TEST 3 SIMULATION RUN
MEASURED AT THE TIME (0.116 SECOND) WHEN THE VERTICAL
ACCELERATION OF THE RAIL CAR (SUPPORT) IS A MAXIMUM

<u>Variable</u>	<u>Value lb(Force)</u>
DUS2	44754.6
DUS3	-54094.7
DWS2	17899.5
DWS3	4904.6
DUS6	74418.0
DUS7	-51971.8
DWS6	0.0
DWS7	0.0
DWCRF	0.0

TABLE 4

FORCE TERMS FROM THE *CARDS* TEST 3 SIMULATION RUN
MEASURED AT THE TIME (0.057 SECOND) WHEN THE HORIZONTAL
ACCELERATION OF THE RAIL CAR (SUPPORT) IS A MAXIMUM

<u>Variable</u>	<u>Value lb(Force)</u>
DUS1	221589.0
DUS4	0.0
DWS1	-57230.0
DWS4	-57230.0
DUS5	-31802.7
DUS8	-31802.7
DWS5	34563.8
DWS8	34563.8
DUSCAR (Experimental)	1160000.0
DWP1	-23200.0
DWP4	-23200.0

TABLE 5

INPUT DATA AND RESULTS FROM THE *CARDS* TEST 3 SIMULATION RUN
RESULTS MEASURED AT THE TIME (0.116 SECOND) WHEN THE VERTICAL
ACCELERATION OF THE RAIL CAR (SUPPORT) IS A MAXIMUM

<u>Input Data</u>		<u>Calculated Results</u>	
M_p	= 207 lb(force)-s ² /in.	θ_{RC}	= 2.82×10^{-3} radian
$k_{S2} = k_{S3}$	= 1×10^9 lb(force)/in.	$\dot{\theta}_{RC}$	= -0.12993 radian/s
$C_{S2} = C_{S3}$	= 2×10^3 lb(force)-s/in.	$\ddot{\theta}_{RC}$	= -6.89 radians/s ²
l_{CF}	= 166.5 in.	\ddot{Y}_{RC}	= -353.9 in./s ²
l_{CR}	= 70.5 in.	\ddot{Y}_{RC78}	= 1465.5 in./s ²
l_{RC}	= 264 in.		

TABLE 6

INPUT DATA AND RESULTS FROM THE *CARDS* TEST 3 SIMULATION RUN
RESULTS MEASURED AT THE TIME (0.057 SECOND) WHEN THE HORIZONTAL
ACCELERATION OF THE RAIL CAR (SUPPORT) IS A MAXIMUM

<u>Input Data</u>		<u>Calculated Results</u>	
M_p	= 207 lb(force)-s ² /in.	θ_p	= 3.03506×10^{-4} radian
k_{S1}	= 1.05×10^6 lb(force)/in.	$\dot{\theta}_p$	= 7.25067×10^{-2} radian/s
k_{S4}	= 0 lb(force)/in.	θ_{RC}	= 3.84508×10^{-5} radian
$C_{S1} = C_{S4}$	= 2000 lb(force)-s/in.	$\dot{\theta}_{RC}$	= 1.2836×10^{-2} radian/s
Z_p	= 31 in.	$\ddot{\theta}_{RC}$	= 2.944 radians/s ²
Z_{RC}	= 18 in.	\ddot{X}_{RC}	= -4180.5 in./s ²

TABLE 7

INSTRUMENT CONFIGURATION FOR CASK-RAIL CAR-TIEDOWN TESTS

Instrument No.	CONFIGURATIONS A AND B			CONFIGURATIONS C** AND D				
	Instrument Location	Instrument Type	Measurements	Instrument Location	Instrument Type	Measurements		
1	Bolt Holddown (FE)*	Instrumented Bolt	Change in Tension	Cable (FE)*	Load Cell	Change in Tension		
2	Bolt Holddown (Side)	Instrumented Bolt	Change in Tension					
3	Coupler	Bridge Type	Force/Time	Coupler	Bridge Type	Force/Time		
4	Struck End Of Car	Displacement	Displacement/Time	Struck End Of Car	Displacement	Displacement/Time		
5	Car Structure (SE)*	PR Accelerometer	Shock	Car Structure (SE)*	PR Accelerometer	Shock		
6	Car Structure (SE)	PR Accelerometer	↓	Car Structure (SE)	PR Accelerometer	↓		
7	Car Structure (SE)	PE Accelerometer						
8	CaSk (SE)	PR Accelerometer						
9	Cask (SE)	PR Accelerometer						
10	Cask (FE)	PR Accelerometer						
11	Cask (FE)	PR Accelerometer						
12	Car/Cask Interface	PR Accelerometer						
13	Car/Cask Interface	PR Accelerometer						
14	Car/Cask Interface	PR Accelerometer						
15	Cask Base (SE)	PE Accelerometer						
16	Cask Base (SE)	PE Accelerometer						
17	Cask Base (FE)	PE Accelerometer						
18	Cask Base (FE)	PE Accelerometer						
19	Cask Top Center	PE Accelerometer						
20	Cask Side Center	PE Accelerometer						
21	Car Structure (FE)	PE Accelerometer		Shock	Car Structure (FE)		PE Accelerometer	Shock
22	Car Structure (FE)	PE Accelerometer		Shock	Rail Car Above Truck Center (FE)		PE Accelerometer	Shock
23	Truck (SE)	PE Accelerometer		Shock	Truck (SE)		PE Accelerometer	Shock
24	Truck (FE)	PE Accelerometer		Shock	Truck (FE)		PE Accelerometer	Shock
25	Rail Car Above Truck Center (SE)	PE Accelerometer	Shock	Rail Car Above Truck Center (SE)	PE Accelerometer	Shock		
26	Bolted Holddown (FE)	Instrument Bolt	Change in Tension	Cable (FE)	Load Cell	Change in Tension		
27	Base/Chock Interface (SE)	Load Cell	Change in Compression	Base/Chock Interface (SE)	Load Cell	Change in Compression		
28	Base/Chock Interface (SE)	Load Cell	Change in Compression	Base/Chock Interface (SE)	Load Cell	Change in Compression		

*SE = Struck End; FE = Far End.

**Only Instruments 1, 3 and 26 on Configuration C.

TABLE 8

MEASURED AND REDUCED PARAMETER VALUES FROM RAIL CAR HUMPING TESTS
 (Test No. 1: 40-Ton Cask, 70-Ton Seaboard Coastline Rail Car,
 Impact Velocity 8.3 mph)

DATA CHANNEL ID	INST NO.	LOCATION	MEASURED PARAMETER	RAW DATA SCALE FACTOR (SF) (FULL SCALE $\pm 2V$)	FILTERED DATA (Max/Min)	UNFILTERED DATA (Max/Min)
A	4	(SE) Car	Displacement	Timing Only	---	---
B	1	(FE) Bolt Holddown	Force	43.75 K#/V	20.21/-1.4	20.13/-2.12
C	2	(SIDE) Bolt Holddown	Force	21.88 K#/V	16.58/-2.12	16.84/-2.19
D	8	(SE) Cask	L-Acc.	$\pm 150g/V$	1.5/-13.4	3.3/-13.5
E	9	(SE) Cask	V-Acc.	$\pm 62.5g/V$	6/-5.4	6.25/-5.9
F	10	(FE) Cask	L-Acc.	$\pm 150g/V$	1.65/-10.65	3.75/-12
G	11	(FE) Cask	V-Acc.	$\pm 62.5g/V$	40/-3.69	40.63/-4.063
H	12	Car/Cask Interface	L-Acc.	$\pm 150g/V$	4.65/-9.9	14.55/-18.75
J	13	Car/Cask Interface	T-Acc.	$\pm 25g/V$	3.5/-3.92	10.75/-11.5
K	14	Car/Cask Interface	V-Acc.	$\pm 62.5g/V$	(Impulse Noise)	(Impulse Noise)
L	17	(FE) Cask Base	L-Acc.	$\pm 100g/V$	2.5/-7.9	3.5/-8.4
M	22	(FE) Car Structure	V-Acc.	$\pm 375g/V$	22.1/-58.5	76.88/-155.6
N	26	(FE) Bolt Holddown	Force	35 K#/V 43.75 K#/V	10.98/- .79 13.73/- .98	11.73/-8.8 14.66/-1.1

TABLE 9

THEIL'S INEQUALITY COEFFICIENTS FOR RESPONSE VARIABLES DETERMINED USING CALCULATED AND MEASURED COUPLER FORCE

Response Variable	Theil's Two-Variable Inequality Coefficients*	
	Case 1: Measured Coupler Force	Case 2: Calculated Coupler Force
Coupler Force	0	0.223
Longitudinal Force of Interaction Between Cask and Rail Car	0.158	0.194
Horizontal Acceleration of Cask	0.205	0.252
Horizontal Acceleration of Rail Car	0.211	0.445
Vertical Acceleration of Cask at Far End	0.600	0.776
Vertical Acceleration of Cask at Struck End	0.656	0.470
Theil's Multiple Inequality Coefficient	0.059	0.214

*A value of 0 indicates the best agreement, and a value of 1 indicates the poorest agreement.

TABLE 10

DEFINITIONS OF CASES USED FOR GENERATION OF PRELIMINARY RESPONSE SPECTRA

CONDITION *	CASE				
	1	2	3	4	5
1. Rear Tiedowns					
- Loose	X				
- Tight		X	X	X	X
2. Cask Position on Rail Car					
- Centered Fore & Aft					X
- Cask Centerline 4 ft Forward of Rail Car Centerline	X	X	X	X	
3. Coupler Force Used					
- Calculated by CARDS		X	X	X	X
- Measured During SRL Tests	X	X	X	X	X
4. Damping in CARDS Model					
- Viscous + Friction**	X	X	X	X	X
- Viscous Only					
- No Damping					
5. Damping in CARRS Model					
- Viscous + Friction**	X	X			
- Viscous Only				X	
- No Damping			X		X

*Conditions not specified here are base case conditions in the CARDS model.

**Friction opposing horizontal motion of cask relative to the rail car.

TABLE 11

CONDITIONS IMPOSED ON CASES REQUESTED FOR PARAMETRIC AND SENSITIVITY ANALYSIS
AND GENERATION OF RESPONSE SPECTRA

CONDITION	CASES																							
	Base	1	2	C	D	3	4	5	6	7	8	9	10	11	12	13	14	15	16	17	18	19	20	21
1. Rear Tiedowns																								
- Loose	X	X	X	X	X	X	X	X	X	X	X	X	X	X	X	X	X	X	X	X	X	X	X	X
- Tight																								
2. Cask Position on Rail Car																								
- Cask Centerline 4 ft. Forward of Rail Car Centerline	X	X	X	X	X	X	X	X	X	X	X	X	X		X		X	X					X	X
- Tiedown Attachment Point on Cask at Far End Located Above cg of Rail Car																						X		
- Cask Centered Fore and Aft																X		X	X	X				
- Tiedown Attachment Point on Cask at Struck End Located Above cg of Rail Car														X										
3. Coupler Force Used																								
- Calculated by CARDS																								
- Measured During SRL Tests	X	X	X	X	X	X	X	X	X	X	X	X	X	X	X	X	X	X	X	X	X	X	X	X
4. Damping in CARDS Model																								
- Viscous + Friction																								
- Viscous Only	X	X	X	X	X	X	X	X	X	X	X	X	X	X	X	X	X	X	X	X	X	X	X	X
- No Damping																								
5. Damping in CARRS Model																								
- Viscous + Friction																								
- Viscous Only	X	X	X	X	X	X	X	X	X	X	X	X	X	X	X	X	X	X	X	X	X	X	X	X
- No Damping																								

6-III

TABLE 12

DEFINITIONS OF "PURE" PARAMETERS AND THEIR CASES

PARAMETER	CASE	DEFINITION
W_p	1	1. Cask weight W_p doubled.
	2	2. Cask weight W_p halved.
$\{k_x\}$	5	1. k_{S1} and k_{S4} doubled.
	6	2. k_{S1} and k_{S4} halved.
$\{k_y\}$	7	1. k_{S2} and k_{S3} doubled.
	8	2. k_{S2} and k_{S3} halved.
z_{OCR}	11	1. $z_{CF} = 0$. This is equivalent to the tiedown attachment point on the cask at the struck end being located directly above the center or cg of the railcar, or $z_{OCR} = z_{PF}$.
	18	2. $z_{CF} = z_{PF}$. This is equivalent to the cask being centered on the railcar, i.e., the cg of the cask directly above the cg of the railcar, or $z_{OCR} = 0$.
	19	3. $z_{CR} = 0$. This is equivalent to the tiedown attachment point on the cask at the far end being located directly above the cg of the railcar, or $z_{OCR} = z_{PR}$.
Z_p	14	1. Z_p increased by 50%.
	15	2. Z_p reduced by 25%.

TABLE 13

DEFINITIONS OF "COMPOSITE" PARAMETERS AND THEIR CASES

COMPOSITE PARAMETER	CASE	DEFINITION
CP1	C	1. k_{S1} , k_{S4} , k_{S2} and k_{S3} doubled.
	D	2. k_{S1} , k_{S4} , k_{S2} and k_{S3} halved.
CP2	3	1. W_p , k_{S1} , k_{S4} , k_{S2} and k_{S3} doubled.
	4	2. W_p , k_{S1} , k_{S4} , k_{S2} and k_{S3} halved.
CP3	9	k_{S2} halved and k_{S3} changed such that their sum remains constant.
CP4	10	k_{S3} halved and k_{S2} changed such that their sum remains constant.
CP5	12	z_{PR} and z_{PF} increased by 50%.
CP6	13	z_{PR} and z_{PF} increased by 50% with $z_{CR} = z_{CF}$ (cask centered on rail car).
CP7	16	1. $z_{OCR} = 0$ and k_{S1} and k_{S4} doubled.
	17	2. $z_{OCR} = 0$ and k_{S1} and k_{S4} halved. (cask centered on rail car when $z_{OCR} = 0$)
CP8	20	1. W_p , k_{S1} , k_{S2} , k_{S3} , k_{S4} , k_{S5} , k_{S6} , k_{S7} and k_{S8} doubled.
	21	2. W_p , k_{S1} , k_{S2} , k_{S3} , k_{S4} , k_{S5} , k_{S6} , k_{S7} and k_{S8} halved.

TABLE 14

PARAMETER VALUES USED IN CASES REQUESTED FOR PARAMETRIC/SENSITIVITY ANALYSIS

VARIABLE INPUT PARAMETER	BASE CASE	CASES 1, 2		CASES C, D		CASES 3, 4		CASES 5, 6		CASES 7, 8		CASES 9, 10	
		2 CHANGE	1 CHANGE	D CHANGE	C CHANGE	4 CHANGE	3 CHANGE	6 CHANGE	5 CHANGE	8 CHANGE	7 CHANGE	10 CHANGE	9 CHANGE
11_{P_2}	8×10^4	4×10^4	1.6×10^5			4×10^4	1.6×10^5						
k_{S1} (Low)	5×10^4			2.5×10^4	1×10^5	2.5×10^4	1×10^5	2.5×10^4	1×10^5				
k_{S1} (High)	1×10^6			5×10^5	2×10^6	5×10^5	2×10^6	5×10^5	2×10^6				
k_{S4} (Low)	5×10^4			2.5×10^4	1×10^5	2.5×10^4	1×10^5	2.5×10^4	1×10^5				
k_{S4} (High)	1×10^6			5×10^5	2×10^6	5×10^5	2×10^6	5×10^5	2×10^6				
k_{S2}	5×10^6			2.5×10^6	1×10^7	2.5×10^6	1×10^7			2.5×10^6	1×10^7	7.5×10^6	2.5×10^6
k_{S3}	5×10^6			2.5×10^6	1×10^7	2.5×10^6	1×10^7			2.5×10^6	1×10^7	2.5×10^6	7.5×10^6

LL-III

TABLE 14 (Cont'd)

VARIABLE INPUT PARAMETER	BASE CASE	CASES 16, 17		CASES 20, 21		CASE 18		CASES 11, 19		CASES 12, 13		CASES 14, 15	
		17 CHANGE	16 CHANGE	21 CHANGE	20 CHANGE	18 CHANGE		19 CHANGE	11 CHANGE	13 CHANGE	CHANGE	15 CHANGE	14 CHANGE
W_p	8×10^4			4×10^4	1.6×10^5								
k_{S1} (low)	5×10^4	2.5×10^4	1×10^5	2.5×10^4	1×10^5								
k_{S1} (high)	1×10^6	5×10^5	2×10^6	5×10^5	2×10^6								
k_{S4} (low)	5×10^4	2.5×10^4	1×10^5	2.5×10^4	1×10^5								
k_{S4} (high)	1×10^6	5×10^5	2×10^6	5×10^5	2×10^6								
k_{S2}	5×10^6			2.5×10^6	1×10^7								
k_{S3}	5×10^6			2.5×10^6	1×10^7								
t_{CF}	151					102		204	0.	102			
t_{CR}	53					102		0.	204	102			
t_{PF}	102									153	153		
t_{PR}	102									153	153		
Z_p	31											23.25	46.5
t_{OCR}	-49	0	0			(0)*		(-102)	(102)	(51)	(2)		
H_{k5} **	1.			0.5	2.								
k_6 ***	6.4×10^4			3.2×10^4	1.28×10^5								
k_7	6.4×10^4			3.2×10^4	1.28×10^5								
H_{k8} **	1.			0.5	2.								

* Values of t_{OCR} derived from t_{PF} and t_{CF} , i.e., $t_{OCR} = t_{PF} - t_{CF}$.

** Multipliers of basic spring constants from which k_{S5} and k_{S8} derived.

*** k_5 , k_6 , k_7 and k_8 are basic spring constants from which k_{S5} , k_{S6} , k_{S7} and k_{S8} are derived.

TABLE 15

PARAMETRIC AND SENSITIVITY ANALYSIS - SENSITIVITY OF RESPONSE VARIABLES TO PARAMETER CHANGES

RESPONSE VARIABLE	BASE CASE	CASES 1, 2		CASES C, D		CASES 3, 4		CASES 5, 6		CASES 7, 8	
		2 CHANGE	1 CHANGE	D CHANGE	C CHANGE	4 CHANGE	3 CHANGE	6 CHANGE	5 CHANGE	8 CHANGE	7 CHANGE
$ \ddot{x}_s _{max}$	4189	4663	3843	4544	3760	4874	3256	4535	3784	4204	4176
DIFF. FROM BASE	--	474	-346	355	-429	685	-933	346	-405	15	-13
% DIFF. FROM BASE	--	11.3%	-8.3%	8.5%	-10.2%	16.4%	-22.3%	8.26%	-9.67%	0.36%	-0.31%
$ \ddot{y}_s _{max}$	5626	6748	3883	2876	10400	3487	7302	5852	5142	2786	11369.7
DIFF. FROM BASE	--	1122	-1743	-2750	4774	-2139	1676	226	-484	-2840	5743.7
% DIFF. FROM BASE	--	19.9%	-30.98%	-48.9%	84.8%	-38.0%	29.8%	4.02%	8.6%	-50.5%	102.1%
$ \ddot{\theta}_s _{max}$	306.1	181.2	437.3	163.9	554	96.5	791.7	316.8	281.8	157.96	603.2
DIFF. FROM BASE	--	-124.9	131.2	-142.2	247.9	-209.6	485.6	10.7	-24.3	-148.14	297.1
% DIFF. FROM BASE	--	-40.8%	42.9%	-46.4%	81.0%	-68.5%	158.6%	3.5%	-7.94%	-48.4%	97.1%
$ \ddot{x}_d _{max}$	5406	4812	6662	5764	5995	4964	6158	5765	5965	5405	5399
DIFF. FROM BASE	--	-594	1256	358	589	-442	752	359	559	-1	-7
% DIFF. FROM BASE	--	-11.0%	23.2%	6.62%	10.9%	-8.2%	13.9%	6.64%	10.34%	-0.02%	-0.13%
$ \ddot{y}_d _{max}$	4093	5009	2872	2069	7756	2488	5308	4218	3825	1970	8301
DIFF. FROM BASE	--	916	-1221	-2024	3663	-1605	1215	125	-268	-2123	4208
% DIFF. FROM BASE	--	22.4%	-29.8%	-49.5%	89.5%	-39.2%	29.7%	3.05%	-6.55%	-51.9%	102.8%
$ \ddot{\theta}_d _{max}$	143.7	89.1	197.9	71.4	279.6	43.9	387.4	138	140.4	73.5	285.1
DIFF. FROM BASE	--	-54.6	54.2	-72.3	135.9	-99.8	243.7	-5.7	-3.3	-70.2	141.4
% DIFF. FROM BASE	--	-38.0%	37.7%	-50.3%	94.6%	-69.5%	169.6%	-3.97%	-2.3%	-48.9%	98.4%

TABLE 15 (Cont'd)

RESPONSE VARIABLE	BASE CASE	CASES 9, 10		CASE 18		CASES 11, 19		CASES 12, 13		CASES 14, 15	
		10 CHANGE	9 CHANGE	18 CHANGE		19 CHANGE	11 CHANGE	13 CHANGE	12 CHANGE	15 CHANGE	14 CHANGE
$ \ddot{x}_s _{max}$	4189	4190	4195	4192		4178	4175	4139	4136	4141	4310
DIFF. FROM BASE	--	1	6	3		-11	-14	-50	-53	-48	121
% DIFF. FROM BASE	--	0.024%	0.143%	0.072%		0.26%	-0.33%	-1.19%	-1.27%	-1.15%	2.9%
$ \ddot{y}_s _{max}$	5626	5876	5500	62.3		11320	11180	52.2	4673	4898	7038
DIFF. FROM BASE	--	250	-126	-5564		5694	5554	-5574	-953	-728	1412
% DIFF. FROM BASE	--	4.44%	-2.24%	-98.9%		101.2%	98.7%	-99.1%	-16.9%	-12.9%	25.1%
$ \ddot{o}_s _{max}$	306.1	461.9	158.2	237.2		368.7	81.6	107.1	194.2	266.2	384
DIFF. FROM BASE	--	155.8	-147.9	-68.9		62.6	-224.5	-199.	-111.9	-39.9	77.9
% DIFF. FROM BASE	--	50.9%	-48.3%	-22.5%		20.4%	-73.3%	-65.%	-36.6%	-13.%	25.4%
$ \ddot{x}_d _{max}$	5406	5392	5413	5386		5465	5464	5480	5499	5489	5218
DIFF. FROM BASE	--	-14	7	-20		59	58	80	93	83	-188
% DIFF. FROM BASE	--	-0.26%	0.13%	-0.37%		1.09%	1.07%	1.48%	1.72%	1.54%	-3.48%
$ \ddot{y}_d _{max}$	4093	4203	4117	73.4		8081	7932	61.99	3474	3593	5052
DIFF. FROM BASE	--	110	24	-4020		3988	3839	4031	-619	-500	959
% DIFF. FROM BASE	--	2.69%	0.59%	-98.2%		97.4%	93.8%	98.5%	-15.1%	-12.2%	23.4%
$ \ddot{o}_d _{max}$	143.7	218.	75.	111.7		170.3	36.8	50.1	90.96	125.4	179.1
DIFF. FROM BASE	--	74.3	-68.7	-32.		26.6	-106.9	-93.6%	-52.7	-18.3	35.4
% DIFF. FROM BASE	--	51.7%	-47.8%	-22.3%		18.5%	-74.4%	-65.1%	-36.7%	-12.7%	24.6%

III-14

TABLE 15 (Cont'd)

RESPONSE VARIABLE	BASE CASE	CASES 16, 17		CASES 20, 21							
		17 CHANGE	16 CHANGE	21 CHANGE	20 CHANGE						
$ \bar{x}_s _{max}$	4189	4535	3784	5017	3118						
DIFF. FROM BASE	--	346	-405	828	-1071						
% DIFF. FROM BASE	--	8.26%	-9.67%	19.8%	-25.6%						
$ \bar{y}_s _{max}$	5626	5852	5144	4530	5350						
DIFF. FROM BASE	--	226	-482	-1096	-276						
% DIFF. FROM BASE	--	4.02%	-8.57%	-19.5%	-4.9%						
$ \bar{o}_s _{max}$	306.1	316.8	281.8	121.3	602						
DIFF. FROM BASE	--	10.7	-24.3	-184.8	295.9						
% DIFF. FROM BASE	--	3.5%	-7.9%	-60.4%	96.7%						
$ \bar{x}_d _{max}$	5406	5765	5965	5161	6052						
DIFF. FROM BASE	--	359	559	-245	646						
% DIFF. FROM BASE	--	6.64%	10.3%	-4.5%	12%						
$ \bar{y}_d _{max}$	4093	4218	3825	3167	4897						
DIFF. FROM BASE	--	125	-268	-926	804						
% DIFF. FROM BASE	--	3.05%	-6.55%	-22.6%	19.6%						
$ \bar{o}_d _{max}$	143.7	138.	140.4	53.	369.5						
DIFF. FROM BASE	--	-5.7	-3.3	-90.7	225.8						
% DIFF. FROM BASE	--	-3.97%	-2.3%	-63.1%	157.1%						

TABLE 15 (Cont'd)

RESPONSE VARIABLE	BASE CASE	CASES 1, 2		CASES C, D		CASES 3, 4		CASES 5, 6		CASES 7, 8		CASES 9, 10	
		2 CHANGE	1 CHANGE	D CHANGE	C CHANGE	4 CHANGE	3 CHANGE	6 CHANGE	5 CHANGE	8 CHANGE	7 CHANGE	10 CHANGE	9 CHANGE
DUS1 _{max}	328800	222900	424880	273700	369300	187900	477600	273700	368800	328000	328800	328400	328300
DIFF. FROM BASE		-105900	96080	-55100	40500	-140900	148800	-55100	40000	-800	0.	-400.	-500.
% DIFF. FROM BASE		-32.2%	29.22%	-16.75%	12.31%	-42.9%	45.3%	-16.76%	12.17%	-0.243%	0.	-0.12%	-0.15%
DUS4 _{max}	298900	205000	386260	248800	335800	170800	434200	248800	335300	298200	298900	298500	298500
DIFF. FROM BASE		-93900	87360	-50100	36900	-128100	135300	-50100	36400	-700	0.	-400.	-400.
% DIFF. FROM BASE		-31.4%	29.23%	-16.76%	12.35%	-42.86%	45.27%	-16.76%	12.18%	-0.23%	0.	-0.13%	-0.13%
DUS2 _{max}	101300	70700	132040	94840	109500	69350	144800	86500	117700	115400	98310	97580	116600
DIFF. FROM BASE		-30600	30740	-6460	8200	-31950	43500	-14800	16400	14100	-2990	-3720.	15300.
% DIFF. FROM BASE		-30.21%	30.35%	-6.38%	8.095%	-31.5%	42.9%	-14.61%	16.19%	13.92%	-2.95%	-3.67%	15.1%
DUS3 _{max}	-88580	-63920	-112800	-79260	-91060	-62680	-113500	-80700	-92500	-92300	-88880	-95120	-86120
DIFF. FROM BASE		24660	-24220	9320	-2480	25900	-24920	7880	-3920	-3720	-300	-6540	2460
% DIFF. FROM BASE		-27.8%	27.3%	-10.52%	2.8%	-29.2%	28.1%	-8.9%	4.43%	4.2%	0.34%	7.38%	-2.8%

TABLE 15 (Cont'd)

RESPONSE VARIABLE	BASE CASE	CASE 18		CASES 11, 19		CASES 12, 13		CASES 14, 15		CASES 16, 17		CASES 20, 21	
		18 CHANGE		19 CHANGE	11 CHANGE	13 CHANGE	12 CHANGE	15 CHANGE	14 CHANGE	17 CHANGE	16 CHANGE	21 CHANGE	20 CHANGE
DUS1 _{max}	328800	328400		329900	330100	332300	332600	331900	321500	273700	368800	194300	466500
DIFF. FROM BASE		-400.		1100.	1300.	3500.	3800.	3100.	-7300.	-55100	40000	-134500	137700
% DIFF. FROM BASE		-0.12%		0.335%	0.395%	1.06%	1.16%	0.943%	-2.22%	-16.8%	12.17%	-40.9%	41.9%
DUS4 _{max}	298900	298500		300000	300100	302100	302300	301700	292300	248800	335300	176600	424100
DIFF. FROM BASE		-400.		1100.	1200.	3200.	3400.	2800.	-6600.	-50100	36400	-122300	125200
% DIFF. FROM BASE		-0.13%		0.368%	0.4%	1.07%	1.14%	0.937%	-2.2%	-16.76%	12.18%	-40.9%	41.9%
DUS2 _{max}	101300	92370		112100	80800	63610	70640	76340	149300	86500	117700	70010	142900
DIFF. FROM BASE		-8930		10800	-20500	-37690	-30660	-24960	48000	-14800	16400	-31290	41600
% DIFF. FROM BASE		-8.82%		10.66%	-20.2%	-37.2%	-30.27%	-24.6%	47.38%	-14.6%	16.19%	-30.9%	41.07%
DUS3 _{max}	-88580	-94000		-82160	-113300	-65060	-60340	-66590	-131600	-80740	-92500	61850	-120600
DIFF. FROM BASE		-5420.		6420	-24720	23520	28240	21990	-43020	7840	-3920	26730	-32020
% DIFF. FROM BASE		6.1%		-7.25%	27.9%	-26.6%	-31.9%	-24.8%	48.6%	-8.9%	4.43%	-30.2%	36.15%

III-17

TABLE 16

PARAMETRIC AND SENSITIVITY ANALYSIS - RANKING OF PARAMETERS BY ABSOLUTE PERCENT DIFFERENCE OF RESPONSE VARIABLES FROM BASE CASE VALUES

RESPONSE VARIABLES (RV)	PARAMETERS (P)	CASES	ABSOLUTE PERCENT DIFFERENCE FROM BASE [% DFB]	PARAMETER RANKING BY [% DFB]
$ \ddot{x}_s $	w_p	1	8.3	
	w_p	2	11.3	3
	CP1	C	10.2	4
	CP1	D	8.5	
	CP2	3	22.3	2
	CP2	4	16.4	
	$\{k_x\}$	5	9.67	5
	$\{k_x\}$	6	8.26	
	$\{k_y\}$	7	0.31	
	$\{k_y\}$	8	0.36	9
	CP3	9	0.143	11
	CP4	10	0.024	12
	z_{OCR}	11	0.33	10
	z_{OCR}	18	0.072	
	z_{OCR}	19	0.26	
	CP5	12	1.27	7
	CP6	13	1.19	8
	z_p	14	2.9	6
	z_p	15	1.15	
	CP7	16	9.67	5
	CP7	17	8.26	
CP8	20	25.6	1	
CP8	21	19.8		

RESPONSE VARIABLES (RV)	PARAMETERS (P)	CASES	ABSOLUTE PERCENT DIFFERENCE FROM BASE [% DFB]	PARAMETER RANKING BY [% DFB]
$ \ddot{y}_s _{max}$	w_p	1	30.98	6
	w_p	2	19.9	
	CP1	C	84.8	4
	CP1	D	48.9	
	CP2	3	29.8	
	CP2	4	38.	5
	$\{k_x\}$	5	8.6	10
	$\{k_x\}$	6	4.02	
	$\{k_y\}$	7	102.1	1
	$\{k_y\}$	8	50.5	
	CP3	9	2.24	13
	CP4	10	4.44	12
	z_{OCR}	11	98.7	
	z_{OCR}	18	98.9	
	z_{OCR}	19	101.2	2
	CP5	12	16.9	9
	CP6	13	99.1	3
	z_p	14	25.1	7
	z_p	15	12.9	
	CP7	16	4.02	
	CP7	17	8.57	11
CP8	20	4.9		
CP8	21	19.5	8	

TABLE 16 (Cont'd)

RESPONSE VARIABLES (RV)	PARAMETERS (P)	CASES	ABSOLUTE PERCENT DIFFERENCE FROM BASE [% DFB]	PARAMETER RANKING BY [% DFB]
$ \bar{\delta}_s _{max}$	W_p	1	42.9	9
	W_p	2	40.8	
	CP1	C	81.	4
	CP1	D	46.4	
	CP2	3	158.6	1
	CP2	4	68.5	
	$\{k_x\}$	5	7.94	12
	$\{k_x\}$	6	3.5	
	$\{k_y\}$	7	97.1	2
	$\{k_y\}$	8	48.4	
	CP3	9	48.3	8
	CP4	10	50.9	7
	z_{OCR}	11	73.3	5
	z_{OCR}	18	22.5	
	z_{OCR}	19	20.4	
	CP5	12	36.6	10
	CP6	13	65.	6
	Z_p	14	25.4	11
	Z_p	15	13.	
	CP7	16	7.9	13
	CP7	17	3.5	
CP8	20	96.7	3	
CP8	21	60.4		

RESPONSE VARIABLES (RV)	PARAMETERS (P)	CASES	ABSOLUTE PERCENT DIFFERENCE FROM BASE [% DFB]	PARAMETER RANKING BY [% DFB]
$ \bar{x}_d _{max}$	W_p	1	23.2	1
	W_p	2	11.	
	CP1	C	10.9	4
	CP1	D	6.62	
	CP2	3	13.9	2
	CP2	4	8.2	
	$\{k_x\}$	5	10.34	5
	$\{k_x\}$	6	6.64	
	$\{k_y\}$	7	0.13	12
	$\{k_y\}$	8	0.02	
	CP3	9	0.13	12
	CP4	10	0.26	11
	z_{OCR}	11	1.07	
	z_{OCR}	18	0.37	
	z_{OCR}	19	1.09	10
	CP5	12	1.72	8
	CP6	13	1.48	9
	Z_p	14	3.48	7
	Z_p	15	1.54	
	CP7	16	10.3	6
	CP7	17	6.64	
CP8	20	12.	3	
CP8	21	4.5		

TABLE 16 (Cont'd)

RESPONSE VARIABLES (RV)	PARAMETERS (P)	CASES	ABSOLUTE PERCENT DIFFERENCE FROM BASE [% DFB]	PARAMETER RANKING BY [% DFB]
$ \ddot{y}_d _{\max}$	W_p	1	29.8	6
	W_p	2	22.4	
	CP1	C	89.5	4
	CP1	D	49.5	
	CP2	3	29.7	
	CP2	4	39.2	5
	$\{k_x\}$	5	6.55	10
	$\{k_x\}$	6	3.05	
	$\{k_y\}$	7	102.8	1
	$\{k_y\}$	8	51.9	
	CP3	9	0.59	12
	CP4	10	2.69	11
	z_{OCR}	11	93.8	
	z_{OCR}	18	98.2	3
	z_{OCR}	19	97.4	
	CP5	12	15.1	9
	CP6	13	98.5	2
	Z_p	14	23.4	7
	Z_p	15	12.2	
	CP7	16	6.55	10
	CP7	17	3.05	
CP8	20	19.6		
CP8	21	22.6	8	

RESPONSE VARIABLES (RV)	PARAMETERS (P)	CASES	ABSOLUTE PERCENT DIFFERENCE FROM BASE [% DFB]	PARAMETER RANKING BY [% DFB]
$ \ddot{y}_d _{\max}$	W_p	1	37.7	
	W_p	2	38.	9
	CP1	C	94.6	4
	CP1	D	50.3	
	CP2	3	169.6	1
	CP2	4	69.5	
	$\{k_x\}$	5	2.3	
	$\{k_x\}$	6	3.97	12
	$\{k_y\}$	7	98.4	3
	$\{k_y\}$	8	48.9	
	CP3	9	47.8	8
	CP4	10	51.7	7
	z_{OCR}	11	74.4	5
	z_{OCR}	18	22.3	
	z_{OCR}	19	18.5	
	CP5	12	36.7	10
	CP6	13	65.1	6
	Z_p	14	24.6	11
	Z_p	15	12.7	
	CP7	16	2.3	
	CP7	17	3.97	12
CP8	20	157.1	2	
CP8	21	63.1		

III-20

TABLE 16 (Cont'd)

RESPONSE VARIABLES (RV)	PARAMETERS (P)	CASES	ABSOLUTE PERCENT DIFFERENCE FROM BASE [% DFB]	PARAMETER RANKING BY [% DFB]
DUS1 _{max}	W _p	1	29.2	
	W _p	2	32.2	3
	CP1	C	12.31	
	CP1	D	16.75	6
	CP2	3	45.3	1
	CP2	4	42.9	
	{k _x }	5	12.17	
	{k _x }	6	16.76	5
	{k _y }	7	0	
	{k _y }	8	0.243	11
	CP3	9	0.15	12
	CP4	10	0.12	13
	¹ OCR	11	0.395	10
	² OCR	18	0.12	
	³ OCR	19	0.335	
	CP5	12	1.16	8
	CP6	13	1.06	9
	Z _p	14	2.22	7
	Z _p	15	0.943	
	CP7	16	12.17	
	CP7	17	16.8	4
CP8	20	41.9	2	
CP8	21	40.9		

RESPONSE VARIABLES (RV)	PARAMETERS (P)	CASES	ABSOLUTE PERCENT DIFFERENCE FROM BASE [% DFB]	PARAMETER RANKING BY [% DFB]
DUS4 _{max}	W _p	1	29.23	
	W _p	2	31.4	3
	CP1	C	12.35	
	CP1	D	16.76	4
	CP2	3	45.27	1
	CP2	4	42.86	
	{k _x }	5	12.18	
	{k _x }	6	16.76	4
	{k _y }	7	0	
	{k _y }	8	0.23	9
	CP3	9	0.13	10
	CP4	10	0.13	10
	¹ OCR	11	0.4	8
	² OCR	18	0.13	
	³ OCR	19	0.368	
	CP5	12	1.14	6
	CP6	13	1.07	7
	Z _p	14	2.2	5
	Z _p	15	0.937	
	CP7	16	12.18	
	CP7	17	16.76	4
CP8	20	41.9	2	
CP8	21	40.9		

TABLE 16 (Cont'd)

RESPONSE VARIABLES (RV)	PARAMETERS (P)	CASES	ABSOLUTE PERCENT DIFFERENCE FROM BASE [% DFB]	PARAMETER RANKING BY [% DFB]
DUS _{max} ²	W _p	1	30.35	5
	W _p	2	30.21	
	CP1	C	8.095	11
	CP1	D	6.38	
	CP2	3	42.9	2
	CP2	4	31.5	
	{k _x }	5	16.19	8
	{k _x }	6	14.61	
	{k _y }	7	2.95	
	{k _y }	8	13.92	10
	CP3	9	15.1	9
	CP4	10	3.67	12
	² OCR	11	20.2	7
	² OCR	18	8.82	
	² OCR	19	10.66	
	CP5	12	30.27	6
	CP6	13	37.2	4
	Z _p	14	47.38	1
	Z _p	15	24.6	
	CP7	16	16.19	8
	CP7	17	14.6	
CP8	20	41.07	3	
CP8	21	30.9		

RESPONSE VARIABLES (RV)	PARAMETERS (P)	CASES	ABSOLUTE PERCENT DIFFERENCE FROM BASE [% DFB]	PARAMETER RANKING BY [% DFB]
DUS _{max} ³	W _p	1	27.3	
	W _p	2	27.8	6
	CP1	C	2.8	
	CP1	D	10.52	8
	CP2	3	28.1	
	CP2	4	29.2	4
	{k _x }	5	4.43	
	{k _x }	6	8.9	9
	{k _y }	7	0.34	
	{k _y }	8	4.2	11
	CP3	9	2.8	12
	CP4	10	7.38	10
	² OCR	11	27.9	5
	² OCR	18	6.1	
	² OCR	19	7.25	
	CP5	12	31.9	3
	CP6	13	26.6	7
	Z _p	14	48.6	1
	Z _p	15	24.8	
	CP7	16	4.43	
	CP7	17	8.9	9
CP8	20	36.15	2	
CP8	21	30.2		

TABLE 17

PARAMETRIC AND SENSITIVITY ANALYSIS - SENSITIVITY OF RESPONSE VARIABLES IN TERMS OF PERCENT DIFFERENCE FROM BASE CASE VALUES

RANGE OF DFB	INSENSITIVE		SENSITIVE		
	0 - 20	20.01 - 40	40.01 - 60	60.01 - 80.	80.01 - 100 UP
RESPONSE VARIABLE (RV)	RV INSENSITIVE	RV MODERATELY INSENSITIVE	RV MODERATELY SENSITIVE	RV SENSITIVE	RV HIGHLY SENSITIVE
$\bar{x}_s _{max}$	w_p	CP8			
	CP1	CP2			
	CP7				
	(k_x)				
	z_p				
	CP5				
	CP6				
	(k_y)				
	t_{OCR}				
	CP3				
	CP4				
$\bar{y}_s _{max}$	CP8	CP2			(k_y)
	CP5	w_p			t_{OCR}
	(k_x)	z_p			CP6
	CP7				CP1
	CP4				
	CP3				
$\bar{y}_s _{max}$	(k_y)	CP5	CP4	t_{OCR}	CP2
	CP7	z_p	CP3	CP6	(k_y)
			w_p		CP8
					CP1

RANGE OF DFB	INSENSITIVE		SENSITIVE		
	0 - 20	20.01 - 40	40.01 - 60	60.01 - 80.	80.01 - 100 UP
RESPONSE VARIABLE (RV)	RV INSENSITIVE	RV MODERATELY INSENSITIVE	RV MODERATELY SENSITIVE	RV SENSITIVE	RV HIGHLY SENSITIVE
$\bar{y}_d _{max}$	CP2	w_p			
	CP8				
	CP1				
	(k_x)				
	CP7				
	z_p				
	CP5				
	CP6				
	t_{OCR}				
	CP4				
	(k_y)				
	CP3				
$\bar{y}_d _{max}$	CP5	CP2			(k_y)
	(k_x)	w_p			CP6
	CP7	z_p			t_{OCR}
	CP4	CP8			CP1
	CP3				
$\bar{y}_d _{max}$	(k_x)	w_p	CP4	t_{OCR}	CP2
	CP7	CP5	CP3	CP6	CP8
		z_p			(k_y)
					CP1

TABLE 18

PARAMETRIC AND SENSITIVITY ANALYSIS - RANKING OF "PURE" PARAMETERS
BY INFLUENCE COEFFICIENT AND SENSITIVITY

RESPONSE VARIABLES (RV)	PARAMETERS (P)	INFLUENCE COEFFICIENTS $\frac{\partial(RV)}{\partial(P)}$	SENSITIVITY $\frac{\partial(RV)}{\partial(P)} \Delta(P)$	PARAMETER RANKING BY INFLUENCE COEFFICIENT	PARAMETER RANKING BY SENSITIVITY
$ \ddot{x}_s _{max}$	W_p	-6.833×10^{-3}	-820.	3	1
	(k_x) *	-4.768×10^{-4}	-751.	4	2
	(k_y) **	-3.733×10^{-6}	-28.	5	4
	Z_p	7.3	169.7	1	3
	t_{OCR}	-0.0147	-3.	2	5
$ \ddot{y}_s _{max}$	W_p	-0.02388	-2865.	4	4
	(k_x)	-4.508×10^{-4}	-710.	6	6
	(k_y)	-1.144×10^{-3}	8580.	5	3
	Z_p	92.04	2140.	3	5
	t_{OCR}^{***} (FE)	109.	11118.	2	2
t_{OCR} (SE)	-110.	-11220.	1	1	
$ \ddot{a}_s _{max}$	W_p	2.134×10^{-3}	256.	3	3
	(k_x)	-2.222×10^{-5}	-35.	5	5
	(k_y)	5.937×10^{-5}	445	4	1
	Z_p	5.067	117.8	1	4
	t_{OCR}	-1.407	-287.	2	2

RESPONSE VARIABLES (RV)	PARAMETERS (P)	INFLUENCE COEFFICIENTS $\frac{\partial(RV)}{\partial(P)}$	SENSITIVITY $\frac{\partial(RV)}{\partial(P)} \Delta(P)$	PARAMETER RANKING BY INFLUENCE COEFFICIENT	PARAMETER RANKING BY SENSITIVITY
$ \ddot{x}_d _{max}$	W_p	0.01542	1850.	2	1
	(k_x)	1.2698×10^{-4}	200.	4	3
	(k_y)	-8.0×10^{-7}	-6.	5	4
	Z_p	-11.66	-271.	1	2
	t_{OCR}	-0.0049	-1.	3	5
$ \ddot{y}_d _{max}$	W_p	-0.01781	-2137.	4	4
	(k_x)	-2.495×10^{-4}	-393.	6	6
	(k_y)	8.441×10^{-4}	6331.	5	3
	Z_p	62.75	1459.	3	5
	t_{OCR} (FE)	77.	7854.	2	2
t_{OCR} (SE)	-78.5	-8007.	1	1	
$ \ddot{a}_d _{max}$	W_p	9.07×10^{-4}	109.	3	3
	(k_x)	1.524×10^{-6}	2.4	5	5
	(k_y)	2.821×10^{-5}	212.	4	1
	Z_p	2.31	53.7	1	4
	t_{OCR}	-0.6544	-133.5	2	2

TABLE 18 (Cont'd)

RESPONSE VARIABLES (RV)	PARAMETERS (P)	INFLUENCE COEFFICIENTS $\frac{\partial(RV)}{\partial(P)}$	SENSITIVITY $\frac{\partial(RV)}{\partial(P)} \Delta(P)$	PARAMETER RANKING BY INFLUENCE COEFFICIENT	PARAMETER RANKING BY SENSITIVITY
DUS1 _{max}	W _p	1.68	201600.	2	1
	{k _x }	0.0604	95130.	4	2
	{k _y }	1.067 x 10 ⁻⁴	800.	5	4
	Z _p	-447.3	-10400.	1	3
	t _{OCR}	0.9804	200.	3	5
DUS4 _{max}	W _p	0.51	61200.	2	2
	{k _x }	0.0549	86468.	4	1
	{k _y }	9.33 x 10 ⁻⁵	700.	5	4
	Z _p	-404.3	-9400.	1	3
	t _{OCR}	0.4902	100.	3	5
DUS2 _{max}	W _p	0.51	61200.	3	2
	{k _x }	0.0198	31185.	4	4
	{k _y }	-2.279 x 10 ⁻³	-17092.	5	5
	Z _p	3138.	72959.	1	1
	t _{OCR}	-153.4	31294.	2	3

RESPONSE VARIABLES (RV)	PARAMETERS (P)	INFLUENCE COEFFICIENTS $\frac{\partial(RV)}{\partial(P)}$	SENSITIVITY $\frac{\partial(RV)}{\partial(P)} \Delta(P)$	PARAMETER RANKING BY INFLUENCE COEFFICIENT	PARAMETER RANKING BY SENSITIVITY
DUS3 _{max}	W _p	-0.407	-48840.	3	2
	{k _x }	-0.00749	-11797.	4	4
	{k _y }	4.56 x 10 ⁻⁴	3420.	5	5
	Z _p	-2796.	-65007.	1	1
	t _{OCR}	-152.6	-31130.	2	3

- * Set of stiffness coefficients of the horizontal components of the tiedowns
- ** Set of stiffness coefficients of the vertical components of the tiedowns.
- *** t_{OCR} divided into two parameters. t_{OCR} (FE) when the cg of the cask is on the far end of the rail car cg, and t_{OCR} (SE) when the cg of the cask is on the struck end of the rail car cg.

TABLE 19

PARAMETRIC AND SENSITIVITY ANALYSIS - RANKING OF PARAMETERS BY PARAMETER RATIO-BASED INFLUENCE COEFFICIENT AND SENSITIVITY

RESPONSE VARIABLES (RV)	PARAMETERS (P)	INFLUENCE COEFFICIENTS $\frac{\partial(RV)}{\partial(P)}$	SENSITIVITY $\frac{\partial(RV)}{\partial(P)} \cdot s(P)$	PARAMETER RANKING BY INFLUENCE COEFFICIENT	PARAMETER RANKING BY SENSITIVITY
$ \bar{x}_s _{max}$	+(CP8)	-1266.	-1899.	1	1
	+(CP2)	-1078.7	-1618.	2	2
	+(Wp)	-546.7	-820.	3	3
	+(CP1)	-522.7	-784.	4	4
	+(kx)	-500.7	-751.	5	5
	+(CP7)	-500.7	-751.	5	5
	+(Zp)	225.3	169.	6	6
	+(ky)	-18.7	-28.	7	7
	+(OCR)	0.72	3.	8	8
$ \bar{y}_s _{max}$	+(CP8)	546.7	820.	8	8
	+(CP2)	2543.3	3815.	6	5
	+(Wp)	-1910.	-2865.	7	6
	+(CP1)	5016.	7524.	4	4
	+(kx)	-473.3	-710.	9	9
	+(CP7)	-472.	-708.	10	10
	+(Zp)	2853.3	2140.	5	7
	+(ky)	5722.5	8584.	1	3
	+[OCR (FE)]	-5341.	11118.	3	2
	+[OCR (SE)]	5409.	-11258.	2	1

RESPONSE VARIABLES (RV)	PARAMETERS (P)	INFLUENCE COEFFICIENTS $\frac{\partial(RV)}{\partial(P)}$	SENSITIVITY $\frac{\partial(RV)}{\partial(P)} \cdot s(P)$	PARAMETER RANKING BY INFLUENCE COEFFICIENT	PARAMETER RANKING BY SENSITIVITY
$ \bar{x}_d _{max}$	-(CP8)	320.5	481.	2	2
	-(CP2)	463.5	695.	1	1
	-(Wp)	170.7	256.	5	6
	-(CP1)	260.1	390.1	4	4
	-(kx)	-23.3	-35.	8	8
	-(CP7)	-23.3	-35.	8	8
	-(Zp)	157.1	117.8	6	7
	-(ky)	296.8	445.2	3	3
	-(OCR)	68.95	287.1	7	5
$ \bar{y}_d _{max}$	+(CP8)	594.	891.	3	3
	+(CP2)	796.	1194.	2	2
	+(Wp)	1233.	1850.	1	1
	+(CP1)	154.	231.	5	5
	+(kx)	133.3	200.	6	6
	+(CP7)	133.3	200.	6	6
	+(Zp)	-361.3	-271.	4	4
	+(ky)	-4.	-6.	7	7
	+(OCR)	0.24	1.	8	8

III-27

TABLE 19 (Cont'd)

RESPONSE VARIABLES (RV)	PARAMETERS (P)	INFLUENCE COEFFICIENTS $\frac{\partial(RV)}{\partial(P)}$	SENSITIVITY $\frac{\partial(RV)}{\partial(P)} \Delta(P)$	PARAMETER RANKING BY INFLUENCE COEFFICIENT	PARAMETER RANKING BY SENSITIVITY
$ \dot{v}_d _{max}$	$\alpha(CP8)$	1153.3	1730.	8	7
	$\alpha(CP2)$	1880.	2820.	6	5
	$\alpha(W_p)$	-1424.7	-2137.	7	6
	$\alpha(CP1)$	3791.	5687.	3	4
	$\alpha(k_x)$	-262.	-393.	9	9
	$\alpha(CP7)$	-262.	-393.	9	9
	$\alpha(Z_p)$	1945.3	1459.	5	8
	$\alpha(k_y)$	4220.7	6331.	1	3
	$\alpha(t_{OCR}(FE))$	-3775.	7858.	4	2
	$\alpha(t_{OCR}(SE))$	3847.	-8008.	2	1
	$ \dot{\delta}_d _{max}$	$\alpha(CP8)$	211.	317.	2
$\alpha(CP2)$		229.	344.	1	1
$\alpha(W_p)$		72.5	108.8	5	6
$\alpha(CP1)$		138.8	208.2	4	4
$\alpha(k_x)$		1.6	2.4	8	8
$\alpha(CP7)$		1.6	2.4	8	8
$\alpha(Z_p)$		71.6	53.7	6	7
$\alpha(k_y)$		141.1	211.6	3	3
$\alpha(t_{OCR})$		32.1	133.5	7	5

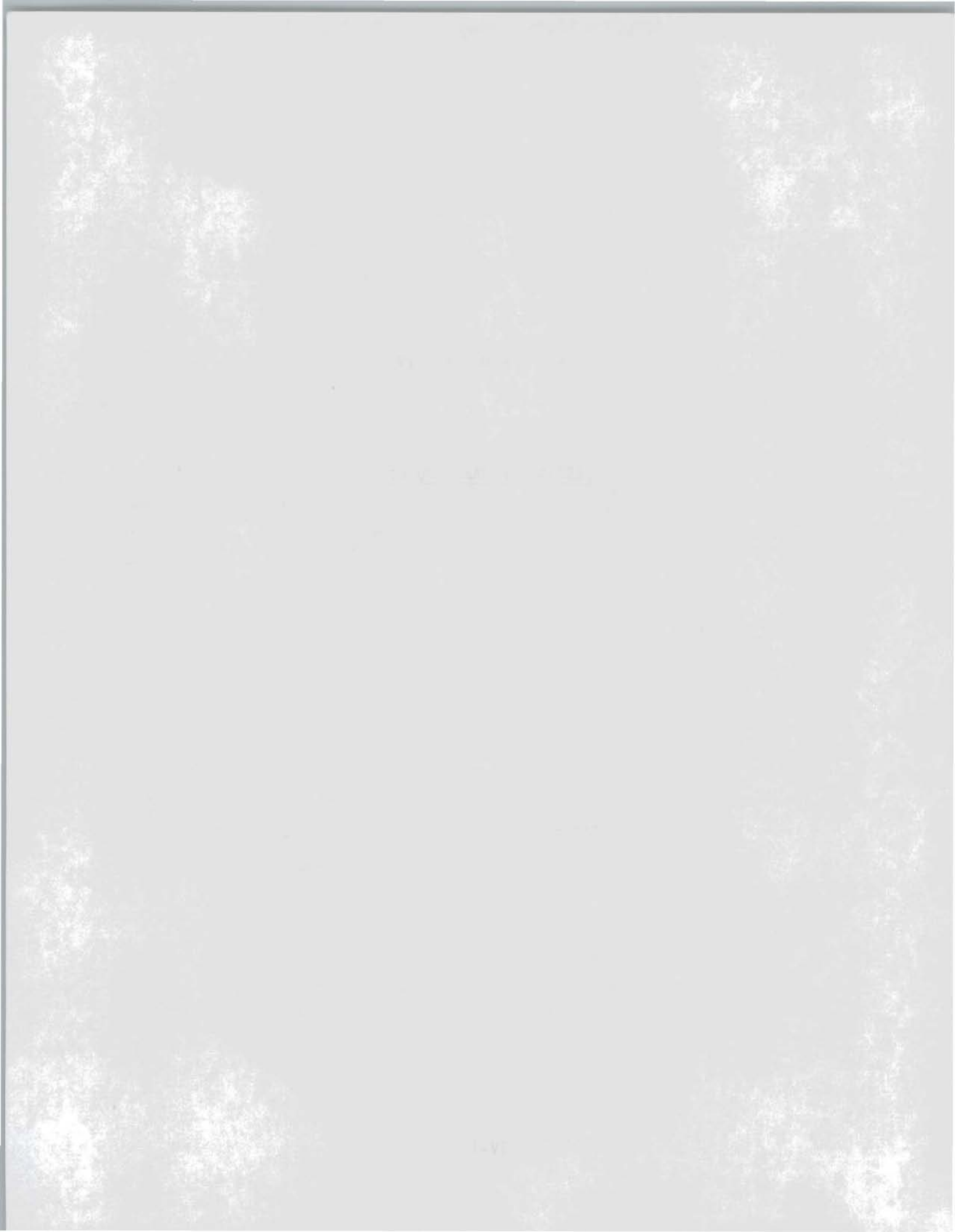
RESPONSE VARIABLES (RV)	PARAMETERS (P)	INFLUENCE COEFFICIENTS $\frac{\partial(RV)}{\partial(P)}$	SENSITIVITY $\frac{\partial(RV)}{\partial(P)} \Delta(P)$	PARAMETER RANKING BY INFLUENCE COEFFICIENT	PARAMETER RANKING BY SENSITIVITY
DUS1 _{max}	$\alpha(CP8)$	1.815×10^5	2.722×10^5	2	2
	$\alpha(CP2)$	1.931×10^5	2.897×10^5	1	1
	$\alpha(W_p)$	1.347×10^5	2.0198×10^5	3	3
	$\alpha(CP1)$	6.373×10^4	9.56×10^4	4	4
	$\alpha(k_x)$	6.34×10^4	9.51×10^4	5	5
	$\alpha(CP7)$	6.34×10^4	9.51×10^4	5	5
	$\alpha(Z_p)$	-1.3867×10^4	-1.04×10^4	6	6
	$\alpha(k_y)$	533.	800.	7	7
	$\alpha(t_{OCR})$	-48.	-200.	8	8
	DUS4 _{max}	$\alpha(CP8)$	1.65×10^5	2.475×10^5	2
$\alpha(CP2)$		1.756×10^5	2.634×10^5	1	1
$\alpha(W_p)$		1.2084×10^5	1.8126×10^5	3	3
$\alpha(CP1)$		5.8×10^4	8.7×10^4	4	4
$\alpha(k_x)$		5.77×10^4	8.65×10^4	5	5
$\alpha(CP7)$		5.77×10^4	8.65×10^4	5	5
$\alpha(Z_p)$		-1.253×10^4	-9400.	6	6
$\alpha(k_y)$		467.	700.	7	7
$\alpha(t_{OCR})$		-24.	-100.	8	8

TABLE 19 (Cont'd)

RESPONSE VARIABLES (RV)	PARAMETERS (P)	INFLUENCE COEFFICIENTS $\frac{\partial(RV)}{\partial(P)}$	SENSITIVITY $\frac{\partial(RV)}{\partial(P)} \cdot \Delta(P)$	PARAMETER RANKING BY INFLUENCE COEFFICIENT	PARAMETER RANKING BY SENSITIVITY
DUS2 _{max}	$\sigma(CP8)$	4.859×10^4	7.289×10^4	3	3
	$\sigma(CP2)$	5.03×10^4	7.545×10^4	2	1
	$\sigma(W_p)$	4.089×10^4	6.134×10^4	4	4
	$\sigma(CP1)$	9773.	14660.	7	8
	$\sigma((k_x))$	20800.	31200.	5	5
	$\sigma(CP7)$	20800.	31200.	5	5
	$\sigma(Z_p)$	97280.	72960.	1	2
	$\sigma((k_y))$	7517.	21300.	8	6
	$\sigma(t_{OCR})$	-11393.	-17090.	6	7
DUS3 _{max}	$\sigma(CP8)$	-56987.	-85480.	2	1
	$\sigma(CP2)$	-33880.	-50820.	3	3
	$\sigma(W_p)$	-32587.	-48880.	4	4
	$\sigma(CP1)$	-7867.	-11800.	5	6
	$\sigma((k_x))$	-7867.	-11800.	5	6
	$\sigma(CP7)$	-7840.	-11760.	6	7
	$\sigma(Z_p)$	-86680.	-65010.	1	2
	$\sigma((k_y))$	2280.	3420.	8	8
	$\sigma(t_{OCR})$	7478.	31140.	7	5

A P P E N D I X I V

LISTING OF CARDS MODEL



CONSTANT PAYR12 = +1.	01-08-81
CONSTANT PAYR56 = +1.	01-08-81
CONSTANT PAYCPL = +1.	01-08-81
CONSTANT PAYCPL = -1.	01-12-81
---WEIGHTS OF SYSTEM COMPONENTS	
CONSTANT WP=1.4E5,WF=1.77E5, WTR=7150., WTF=7150., WRC=5.27E4	
CONSTANT WP=6.E4 5*40 TON CASK*	7-03-79
CONSTANT WRC= 5.96E4	7-03-79
CONSTANT FRMP=0.0	8-28-79
CONSTANT WF=1.74E5,WF2=1.74E5,WF3=1.74E5,WF4=1.74E5	7-03-79
---MOMENTS OF INERTIA	
CONSTANT IP=5.18E5,IRC=2.596E6	8-30-79
---MODULUS OF ELASTICITY OF BEAM (RAIL CAR)	
CONSTANT E=3.E7	
---DIMENSIONS	
CONSTANT LRC=264.,LP=237.,LCR=70.5,LCF=166.5,LPR=118.5,LPF=118.5	01-18-80
CONSTANT PI = 3.1416	04-11-80
CONSTANT LCPL = 341.25	
CONSTANT ZRC= 18., ZP=31., WDTSRC= 2.	
CONSTANT ZCDG0=.38	
CONSTANT ZRCP=12. 5'DISTANCE BETWEEN SURFACES OF CASK AND RC*	03-27-80
---CONSTANTS	
CONSTANT G=386.4	
CONSTANT BETA6=.05,BETA7=.05	9-10-79
CONSTANT BETA6E=0.,BETA6C=.20	01-08-80
CONSTANT BETA7E=0.,BETA7C=.20	01-08-80
CONSTANT BTACPL=.000	01-09-80
CONSTANT ALFA6=.001,ALFA7=.001	04-4-80
CONSTANT ALFACP=1.0	12-14-79
---INITIAL VELOCITIES	
CONSTANT VXPI=+176.,VYPI=0.,VTHPI=0.,VXRCI=+176.,VYRCI=0., ... VTHRCI=0.,VXTRI=+176.,VXTFI=+176.,VXFI=0.	
CONSTANT VXF2I=0.,VXF3I=0.,VXF4I=0.	
---INITIAL DISPLACEMENTS	
CONSTANT XPI=0.,YPI=0.00,THPI=0.,XRCI=0.,YRCI=0.00,THRCI=0.	
CONSTANT XTRI=0.,XTFI=0.,XFI=0.	
CONSTANT XF2I=0.,XF3I=0.,XF4I=0.	
CONSTANT XTINI=-.0	02-01-80
*---INITIAL VALUES OF INFLUENCE COEFFICIENTS AND DERIVATIVES	
CONSTANT IC8I=0.,DIC8I=0.	05-15-80
CONSTANT IC9I=0.,DIC9I=0.	4-12-79
CONSTANT IC10I=0.,DIC10I=0.	4-12-79
CONSTANT IC11I=0.,DIC11I=0.	4-12-79
CONSTANT IC12I=0.,DIC12I=0.	4-12-79
CONSTANT IC13I=0.,DIC13I=0.	4-12-79
CONSTANT IC14I=0.,DIC14I=0.	4-12-79
CONSTANT IC15I=0.,DIC15I=0.	4-12-79
CONSTANT IC16I=0.,DIC16I=0.	4-12-79
CONSTANT IC17I=0.,DIC17I=0.	4-12-79
CONSTANT IC18I=0.,DIC18I=0.	4-12-79
CONSTANT IC19I=0.,DIC19I=0.	4-12-79
CONSTANT IC20I=0.,DIC20I=0.	4-12-79
CONSTANT IC21I=0.,DIC21I=0.	4-12-79
CONSTANT IC22I=0.,DIC22I=0.	4-12-79
CONSTANT IC23I=0.,DIC23I=0.	4-12-79
CONSTANT IC24I=0.,DIC24I=0.	4-12-79
CONSTANT IC25I=0.,DIC25I=0.	4-12-79

CONSTANT IC26I=0.,DIC26I=0.	4-12-79
CONSTANT IC27I=0.,DIC27I=0.	4-12-79
CONSTANT IC28I=0.,DIC28I=0.	4-12-79
---LIMITS ON DISPLACEMENTS	
CONSTANT XRPL0=-.0625,XRPHI=.0625	
CONSTANT YRCMAX = -1.125	9-08-79
CONSTANT XTU= 5.6 ,XT12U= 5.6,XT23U= 5.6,XT34U= 5.6	
CONSTANT XTL= -5.6,XT12L=-5.6,XT23L=-5.6,XT34L=-5.6	
CONSTANT XTU1 = 2.8,XTU2 = 5.6	8-6-79
CONSTANT XTL1 =-2.8,XTL2 =-5.6	
---ADJUSTMENT FACTORS FOR RELATIVE VELOCITIES	
CONSTANT ADRCF=-10.	8-15-79
CONSTANT AD12=0.	8-29-79
CONSTANT AD23=0.	9-07-79
CONSTANT AD34=0.	9-07-79
---DAMPING COEFFICIENTS	
CONSTANT CS1=2.E3,CS2=2.E3,CS3=2.E3,CS4=2.E3,CS5=2.E3,CS6=2.E3	8-28-79
CONSTANT CS7=2.E3,CS8=2.E3,CSCARS=2.E3	8-28-79
CONSTANT CS6=000.,CS7=000.	01-07-80
CONSTANT CS12=.0 ,CSR1 =.0 ,CSF1 =.0 ,CS31= .0	
CONSTANT CS23= .0 ,CSR3 =.0 ,CSF3 =.0 ,CSR2 =.0	
CONSTANT CSF2= 0.	
---SPRING CONSTANTS(STIFFNESSES)	
---SPRING CONSTANTS (NON-BENDING)	
CONSTANT KSCARS=1.045E7,KS1=1.E7,KS2=1.E7,KS3=1.E7,KS4=1.E7	
CONSTANT KS2=1.0E5,KS3=1.0E5	01-11-80
CONSTANT KS5=1.E6,KS6=6.29E4,KS7=6.29E4,KS8=1.E6	
CONSTANT KS5=1.E6,KS8=1.E6	01-24-80
CONSTANT KS6I=6.29E4,KS7I=6.29E4,KS6INF=2.E7,KS7INF=2.E7	
CONSTANT KS6INF= 1.E6,KS7INF= 1.E6	9-09-79
CONSTANT KS1L0=5.E4,KS1HI=1.E6,KS4L0=5.E4,KS4HI=1.E6	01-24-80
CONSTANT K2FF2=48666.	
CONSTANT K1=48666.,K2=48666.,K1FF2=48666.,K1F2F3=48666.	
CONSTANT K2F2F3=48666.,K1F3F4=48666.,K2F3F4=48666.	
CONSTANT KSDG1=.5E6,KSDG2=.5E6,KSFF21=.5E6,KSFF22=.5E6	
CONSTANT KSF231=.5E6,KSF232=.5E6,KSF341=.5E6,KSF342=.5E6	
CONSTANT K6=8.0E4,K7=8.0E4	01-17-80
CONSTANT KSDG10=.75E5,KSDG20=.75E5	
CONSTANT KSDG10=0.2E6	7-20-79
CONSTANT KSF210=.75E5,KSF220=.75E5	
CONSTANT KS2310=.75E5,KS2320=.75E5	
CONSTANT KS3410=.75E5,KS3420=.75E5	
CONSTANT KMRCFU=4.,KMRCFL=1.	11-21-79
CONSTANT KMFF2L=1.,KMFF2U=4.	
CONSTANT KMF23L=1.,KMF23U=4.	
CONSTANT KMF34L=1.,KMF34U=4.	
CONSTANT RCOR=1.,FOR=0.	
*-----CHANGE REQUIRED DUE TO SLACK IN TD-S	
CONSTANT RCOR = J.	05-27-80
CONSTANT LOOSE = .TRUE. \$*LOGICAL VALUE*	07-02-80
CONSTANT F2OR=0.	
CONSTANT F3OR =0.	
CONSTANT F4OR=0.	
---MULTIPLIER AND SWITCH TO GOVERN BENDING	
CONSTANT BENDSW=0. \$*NO BENDING WHEN 0.*	
---SPRING CONSTANTS (BENDING OF RAIL CAP)	
CONSTANT K12= .0 ,KR1 = .0 ,KF1 = .0 ,K31= .0	

```

CONSTANT K23=.0      ,KR3 = .0      ,KF3 = .0      ,KR2 = .0
CONSTANT KF2= 0.
-----DEFINITION OF DRAFT GEAR CHARACTERISTICS*
-----SPRING CONSTANTS (DRAFT GEAR)*
CONSTANT KRC=2.09E7,KF= 2.09E7
CONSTANT KCRC1=2.36E5,KCRC2=5.36E4,KCRC3=2.28E5
CONSTANT KCF1=2.36E5,KCF2=5.36E4,KCF3=2.28E5
CONSTANT KCRINF=2.0E7,KCFINF=2.E7
-----POINTS WHERE K VALUES CHANGE*
CONSTANT XURC0= 0.,XURC1= 0.984,XURC2=3.,XURC3=3.768
CONSTANT XUFD=0.,XUF1=.984,XUF2=3.,XUF3=3.768
---TIMELAG BEFORE DG ACTIVE STATE*
CONSTANT TLAGCF= .0380
CONSTANT TLAGLF= .0380
---COEFFICIENTS OF FRICTION*
CONSTANT MUC=.56,MUS=.58
CONSTANT MUPR=.58
CONSTANT MU=.58
CONSTANT MUCPL=.05,MUTR=.5,MUTF=.5,MUF=.58,MUF2=.58,MUF3=.58
CONSTANT MUF4=.58
CONSTANT MUF=.30,MUF2=.30,MUF3=.30,MUF4=.30
CONSTANT MUCPL=.5
CONSTANT MUD=.5,MUD6=.5,MUD7=.5
CONSTANT MUD6E=.2,MUD6C=.5
CONSTANT MUD7E=.2,MUD7C=.5
CONSTANT MUFF2=.5,MUFF1=.5,MUF231=.5,MUF232=.5,MUF341=.5,MUF342=.5
CONSTANT MXRCFC=0.0,MXRCFE=0.8
CONSTANT MXT12C=0.0,MXT12E=.95
CONSTANT MXT23C=0.0,MXT23E=.95
CONSTANT MXT34C=0.0,MXT34E=.95
---FRICTION FORCES ON COUPLERS*
CONSTANT FSCRC=5.E4,FSCF=5.E4
---FRICTION FORCES ON SUSPENSION SPRINGS*
CONSTANT FRACT=.50      $FRACTION OF LOAD ON A TRUCK*
---FRONT AND REAR BRAKE SWITCHES, 1. WHEN BRAKES ON, 0. OTHERWISE*
CONSTANT BRAKEF = 0.,BRAKER= 0.
---OTHER TRAIN BRAKE SET SWITCH, 1. WHEN BRAKES, 0. OTHERWISE*
CONSTANT BRKIRC = 1.      $CAUTION**BRAKER AND BRAKEF SHOULD BE 0.
CONSTANT BRKF2=1.2,BRKF3=1.2,BRKF4=1.2
CONSTANT BRKE2=1.,BRKE3=1.,BRKE4=1.
---COMMUNICATION INTERVAL*
CONSTANT CIZONE = 0,01,0,001,0,01
CONSTANT THI = 0.14,TLO = 0.03
CONSTANT EPSR=1.E-30
---SIMULATION STOP TIME*
CONSTANT TSTOP=D.5
CONSTANT TXP4 = .25
---INITIAL VALUES OF PLOT RANGES*
CONSTANT XMX=-1.E30,XMN=1.E30,YMX=-1.E30,YMN=1.E30,THMX=-1.E30
CONSTANT THMN=1.E30,DXMX=-1.E30,DXMN=1.E30,DYMX=-1.E30
CONSTANT DYMN=1.E30,DTMX=-1.E30,DTMN=1.E30,D2XMX=-1.E30
CONSTANT D2XMN=1.E30,D2YMX=-1.E30,D2YMN=1.E30,D2THMX=-1.E30
CONSTANT D2THMN=1.E30,XRMX=-1.E30,XRMN=1.E30
CONSTANT YMX2=-1.E30,YMN2=1.E30,D2YMX2=-1.E30,D2YMN2=1.E30
CONSTANT DYMX2=-1.E30,DYMN2=1.E30
CONSTANT FCPLMX=-1.E30,FCPLMN=1.E30
CONSTANT ICMX=-1.E30,ICMN=1.E30

```

CONSTANT DTMIN=1.E30,DTMAX=-1.E30 04-30-80

---LOAD-DEFLECTION CURVE FOR DRAFT GEAR--DISPL VS LOAD

TABLE XDG,1,4/0,,.984,3.,.3.768,0.,.2.32E5,3.4E5,5.15E5/	
TABLE KMFRCF,1,5/5.6,5.85,6.1,6.6,7.,1.,1.,1.,1.3,5./	11-16-79
TABLE KMFF2F,1,4/5.6,5.85,6.1,6.35,1.,1.5,2.5,4./	
TABLE KMF23F,1,4/5.6,5.85,6.1,6.35,1.,1.5,2.5,4./	
TABLE KMF34F,1,4/5.6,5.85,6.1,6.34,1.,1.5,2.5,4./	

---COUPLER FORCE-SRL EXPERIMENT-TEST 3

INST 3*	11-29-79
TABLE DUSF,1,21/0,,.048,.05,.054,.07,.075,.076,.08,.085,.095,...	11-29-79
.13,.136,.145,.185,.206,.242,.26,.27,.286,.4,...	11-29-79
1.,...	11-29-79
0.,0.,2.E4,0.,1.E5,9.E4,2.9E5,4.E4,5.E5,...	11-29-79
1.16E6,3.E5,2.E5,5.2E5,1.E5,5.E4,2.E4,1.E5,...	11-29-79
1.E5,6.E4,0.,0./	11-29-79

---LONGITUDINAL FORCE-SRL EXPERIMENT-TEST 3

TABLE DUSLFF,1,21/0,,.03,.05,.08,.09,.11,.14,.15,.164,.178,...	11-29-79
.185,.197,.21,.224,.26,.27,.274,.283,.3,.301,...	11-29-79
1.,...	11-29-79
0.,-1.E4,0.,2.8E4,1.1E5,7.6E5,1.2E4,2.E5,...	11-29-79
4.8E5,1.84E4,1.6E4,-1.4E4,4.4E4,-2.E4,-2.E4,...	11-29-79
-1.2E4,4.E4,-2.E4,4.E4,0.,0./	11-29-79

---HORIZONTAL ACCELERATION OF CASK-SRL EXP-TEST 3-INST NO. 8

INST NO. 8*	12-11-79
* FILTERED AT 100 HZ USING FFT*	03-18-80
TABLE D2XPF,1,54/0,,.0096,.0146,.0208,.0266,.0316,.0366,.042,...	03-18-80
.047,.0524,.069,.0728,.0798,.0828,.1064,.1312,...	03-18-80
.1356,.1448,.1654,.1898,.1968,.204,.2106,...	03-18-80
.2128,.2198,.2236,.2302,.2388,.2492,.2552,...	03-18-80
.262,.2692,.2758,.2824,.2898,.2958,.3026,...	03-18-80
.3106,.3168,.3238,.3344,.3428,.3488,.3568,...	03-18-80
.3626,.3708,.3798,.389,.397,.4,.407,.4094,.41,...	03-18-80
.5,...	03-18-80
-83.48,4.722,-3.15,19.15,-9.779,8.704,-12.94,...	03-18-80
17.15,-13.69,28.23,-180.3,-159.6,-265.4,...	03-18-80
-249.5,-410.3,-625.1,-718.6,177.7,-2781,...	03-18-80
405.3,-229.7,334.1,109.9,115.2,-40.37,...	03-18-80
-3.388,-161.5,162.1,-121.,-63.02,-116.5,...	03-18-80
-63.61,-140.3,19.59,-300.3,-56.94,-422.5,...	03-18-80
30.79,-139.7,40.71,-282.3,-193.4,-252.4,...	03-18-80
-17.65,-175.7,121.3,-27.77,119.7,-30.79,...	03-18-80
-21.41,-113.1,-87.29,0.,0./	03-18-80

---VERTICAL ACCELERATION OF CASK AT STRUCK END-SRL EXP-TEST 3-INST 9

INST 9*	12-11-79
* FILTERED AT 50 HZ USING FFT*	04-23-80
TABLE D2P54F,1,23/0,,.0144,.021,.0432,.057,.066,.1002,.1214,...	04-23-80
.154,.1848,.2014,.216,.237,.2606,.2682,...	04-23-80
.2902,.3334,.366,.379,.3928,.4094,.4095,...	04-23-80
.5,...	04-23-80
109.6,-21.99,-13.64,-72.46,-20.98,-53.08,...	04-23-80
1157,-1861,.1986,-431.6,-203.5,-531.4,...	04-23-80
903.2,-269.7,-234.7,-1007.7,757.2,-209,...	04-23-80
-8.948,-275.8,109.9,0.,0./	04-23-80

---HORIZONTAL ACCELERATION OF CASK-CAR - SRL EXP - TEST 3 - INST 12

INST 12*	11-29-79
* FILTERED AT 100 HZ USING FFT*	03-18-80
TABLE D2XRCF,1,47/0,,.0126,.0184,.0234,.0272,.0346,.0494,...	03-18-80
.052,.0568,.0616,.0672,.0734,.0938,.0492,...	02-08-80
.0946,.095,.1072,.1162,.1204,.1252,.1316,...	02-08-80
.1448,.1664,.1712,.172,.1736,.1744,.1762,...	02-08-80

.179,.18,.1808,.1822,.1832,.184,.1852, ...	02-08-80
.1864,.188,.1906,.1926,.1942,.1952,.197, ...	02-08-80
.1974,.1988,.1998,.2,.5, ...	03-18-80
177.2,-99.31,-7.968,-61.38,-28.9,-210.9, ...	02-08-80
100.8,11.52,-231.7,-129.,-269.8,-52.97, ...	02-08-80
-4809.,-4819.,-4809.,-4778.,1226.,-758.2, ...	02-08-80
-631.2,-802.8,-398.5,-2817.,1557.,125.2, ...	02-08-80
-211.9,-743.3,-910.9,-1049.,-892.2,-829.5, ...	02-08-80
-795.7,-769.4,-761.4,-749.7,-705.8,-618.1, ...	02-08-80
-438.2,-97.98,102.8,208.6,257.7,325.8,337.7, ...	02-08-80
366.9,370.7,0.,0./	03-18-80
---VERTICAL ACCELERATION OF CASK AT FAR END-SRL EXP-TEST 3-INST 11	11-29-79
* FILTERED AT 50 HZ USING FFT*	04-23-80
TABLE D2P12F,1,27/0.,.0124,.0222,.0332,.0414,.052,.0634,.0732, ...	04-23-80
.0978,.1178,.1534,.1888,.2018,.2102,.2336, ...	04-23-80
.2512,.267,.2896,.3044,.3146,.3364,.3612, ...	04-23-80
.3714,.3932,.4094,.4095,.5, ...	04-23-80
-165.4,52.8,-30.14,57.33,24.59,90.17,9.973, ...	04-23-80
68.97,-427.4,2464.,-2051.,601.8,370.3,427.1, ...	04-23-80
-1124.,371.1,-349.4,887.7,210.7,452.1,-696.4, ...	04-23-80
72.97,38.8,290.4,-165.7,0.,0./	04-23-80
---SPRING CONSTANTS-HORIZONTAL SPRINGS- RC TO TRUCKS	11-28-79
TABLE KS58F,1,7/-1.,-.11,-.1,0.,.1,.11,1.,.2E6,.2E6,.2E6,.2E6, ...	02-01-80
.2E6,.2E6,.2E6/	02-01-80
*---NON-LINEAR STIFFNESS COEFFICIENT FOR VERTICAL TIEDOWN AT FAR	*05-15-80
* END. LOOSE FIT AND RUBBER GASKET.	*05-15-80
TABLE KS2F,1,9/-4,0.,.5,.6,.7,.8,.9,1.,1.2, ...	05-05-80
2.5E6,0.000,0.000,0.000,0.000,0.000,0.000, ...	05-14-80
1.00E5,2.00E5/	05-14-80
*---VARIABLE DAMPING COEFFICIENT FOR VERTICAL TIEDOWN AT FAR END.	*05-15-80
* LOOSE FIT AND RUBBER GASKET.	*05-15-80
TABLE CS2F,1,9/-4,0.,.5,.6,.7,.8,.9,1.,1.2, ...	05-09-80
2000.,0.,0.,0.,0.000,0.000,0.000,1000.,2000./	05-14-80
*---VERTICAL ACCELERATION OF ---- AT CASK-CAR INTERFACE AT FE-SRL EXP	*01-08-81
* TEST 3-INST 14*	01-08-81
* FILTERED AT 50 HZ USING FFT*	01-08-81
* VERY CLOSE TO REPRESENTING D2YR12*	01-08-81
TABLE D2R12F,1,33/0.,.0088,.0192,.0302,.0406,.051,.0616,.0722, ...	01-08-81
.084,.0952,.1096,.121,.127,.1402,.1524,.1654, ...	01-08-81
.178,.1918,.209,.2258,.2446,.2718,.2858,.307, ...	01-08-81
.3234,.3338,.3448,.3598,.3608,.3734,.3858, ...	01-08-81
.3984,.4094, ...	01-08-81
77.84,-187.7,236.5,-292.5,231.2,-325.9,391.5, ...	01-08-81
-529.,972.3,-728.7,2617.,1243.,1467.,-618.4, ...	01-08-81
1862.,-1191.,1249.,-837.8,458.4,-871.6,1497., ...	01-08-81
-504.2,392.6,-683.8,645.4,175.6,620.2,45.93, ...	01-08-81
46.09,-295.6,409.,-461.5,77.65/	01-08-81
* FILTERED AT 25 HZ USING FFT*	01-12-81
TABLE D2R126,1,13/0.,.0226,.0492,.073,.116,.1586,.1756,.2098, ...	01-12-81
.2504,.2922,.3406,.3838,.4094, ...	01-12-81
7.,-115.,96.,-136.,1544.,157.,245.,-306., ...	01-12-81
923.,-326.,390.,-140.,7./	01-12-81
---VERTICAL ACCELERATION OF CAR STRUCTURE AT FE-SRL EXP-TEST 3-INST 22	01-08-81
* FILTERED AT 50 HZ USING FFT*	01-08-81
* SOMEWHERE BETWEEN FE OF CAR AND D2YR56*	01-08-81
TABLE D2R56F,1,18/0.,.0094,.0189,.0318,.0459,.0546,.0747,.097, ...	01-08-81
.1187,.1356,.1501,.1636,.1757,.1886,.2031, ...	01-08-81

.2047,.21,1., ...	01-08-81
196.6,-337.7,163.4,-645.8,99.12,-53.38, ...	01-08-81
436.9,-464.1,398.6,-1412.,667.6,-1451.,150.6,...	01-08-81
-1697.,256.6,211.5,0.,0./	01-08-81
---VERTICAL ACCELERATION OF CAR STRUCTURE AT SE-SRL EXP-TEST 3-INST 6	01-08-81
* FILTERED AT 50HZ USING FFT*	01-08-81
* SOMEWHERE BETWEEN D2YCPL AND D2YR78*	01-08-81
TABLE D2CPLF,1,18/0.,.0041,.0142,.0287,.052,.0649,.0712,.0899, ...	01-08-81
.1066,.1203,.1272,.1439,.1652,.1823,.197, ...	01-08-81
.2047,.21,1., ...	01-08-81
-171.3,-259.,-89.81,-358.,143.7,-198.4,-114.,...	01-08-81
-3181.,405.4,-983.,-791.1,-2931.,1026., ...	01-08-81
-912.2,113.6,-168.,0.,0./	01-08-81
FILTERED AT 25 HZ USING FFT*	01-12-81
TABLE D2CPL6,1,10/0.,.0109,.0452,.0845,.1126,.1425,.1842,.2047,...	01-12-81
.21,1., ...	01-12-81
-372.,-611.,326.,-1424.,-845.,-1539.,296., ...	01-12-81
-369.,0.,0./	01-12-81

---BASE CASE PARAMETERS---	03-14-80
---WEIGHTS OF SYSTEM COMPONENTS	03-14-80
CONSTANT WF = 1.75E5	\$(REF. ENSCO)* 03-14-80
CONSTANT WF2= 1.75E5	\$(REF. ENSCO)* 03-14-80
CONSTANT WF3= 1.75E5	\$(REF. ENSCO)* 03-14-80
CONSTANT WF4= 1.75E5	\$(REF. ENSCO)* 03-14-80
CONSTANT WP=8.E4 \$*40 TON CASK*	03-14-80
CONSTANT WR= 5.69E4 \$*INCLUDES 2 BULKHEADS (REF. ENSCO)*	03-14-80
CONSTANT WTF= 1.35E4	\$(REF. ENSCO)* 03-14-80
CONSTANT WTR= 1.35E4	\$(REF. ENSCO)* 03-14-80
---MOMENTS OF INERTIA	03-14-80
CONSTANT IP = 8.57E5	\$(REF. ENSCO)* 03-14-80
CONSTANT IRC= 2.8495E6	\$(REF. ENSCO)* 03-14-80
---MODULUS OF ELASTICITY OF BEAM (RAIL CAR)	03-14-80
CONSTANT E = 3.E7	\$(REF. ENSCO)* 03-14-80
---DIMENSIONS	03-14-80
CONSTANT LCPL = 341.25	\$(REF. ENSCO)* 03-14-80
CONSTANT LCF= 185.125	\$(REF. ENSCO)* 03-14-80
CONSTANT LCR= 95.125	\$(REF. ENSCO)* 03-14-80
CONSTANT LPF= 207.	\$(REF. ENSCO)* 03-14-80
CONSTANT LPR= 37.25	\$(REF. ENSCO)* 03-14-80
CONSTANT LRC= 259.5	\$(REF. ENSCO)* 03-14-80
CONSTANT ZCDG0 = 6.15	\$(REF. ENSCO)* 03- 4-80
CONSTANT ZP = 31.	03-14-80
CONSTANT ZRC = 25.2	\$(REF. ENSCO)* 03-14-80
---LIMITS ON DISPLACEMENTS	03- 4-80
CONSTANT XTL = -5.25	\$(REF. ENSCO)* 03-14-80
CONSTANT XTL1 = -2.625	\$(REF. ENSCO)* 03-14-80
CONSTANT XTL2 = -5.25	\$(REF. ENSCO)* 03-14-80
CONSTANT XTU = 5.25	\$(REF. ENSCO)* 03- 4-80
CONSTANT XTU1 = 2.625	\$(REF. ENSCO)* 03-14-80
CONSTANT XTU2 = 5.25	\$(REF. ENSCO)* 03-14-80
CONSTANT XT12L = -5.25	\$(REF. ENSCO)* 03-14-80
CONSTANT XT12U = 5.25	\$(REF. ENSCO)* 03-14-80
CONSTANT XT23L = -5.25	\$(REF. ENSCO)* 03-14-80
CONSTANT XT23U = 5.25	\$(REF. ENSCO)* 03-14-80
CONSTANT XT34L = -5.25	\$(REF. ENSCO)* 03-14-80

```

CONSTANT XT34U = 5.25                                S*(REF. ENSCO)* 03-14-80
*-----SPRING CONSTANTS*                               03-14-80
CONSTANT KSDG10 = 5.E5    S*LOWER LIMIT              (REF. ENSCO)* 03-14-80
CONSTANT KSF210 = 5.E5    S*LOWER LIMIT              (REF. ENSCO)* 03-14-80
CONSTANT KSF220 = 5.E5    S*LOWER LIMIT              (REF. ENSCO)* 03-14-80
CONSTANT KS2310 = 5.E5    S*LOWER LIMIT              (REF. ENSCO)* 03-14-80
CONSTANT KS2320 = 5.E5    S*LOWER LIMIT              (REF. ENSCO)* 03-14-80
CONSTANT KS3 = 5.E6       S*LOWER LIMIT              (REF. ENSCO)* 03-14-80
CONSTANT KS3410 = 5.E5    S*LOWER LIMIT              (REF. ENSCO)* 03-14-80
CONSTANT KS3420 = 5.E5    S*LOWER LIMIT              (REF. ENSCO)* 03-14-80
CONSTANT K55 = 5.E5       S*LOWER LIMIT              (REF. ENSCO)* 03-14-80
CONSTANT KS6INF = 3.E7    S*(REF. ENSCO)* 03-14-80
CONSTANT KS7INF = 3.E7    S*(REF. ENSCO)* 03-14-80
CONSTANT KS8 = 5.E5       S*LOWER LIMIT              (REF. ENSCO)* 03-14-80
CONSTANT K1 = 1.82E5      S*(REF. ENSCO)* 03-14-80
CONSTANT K2 = 1.82E5      S*(REF. ENSCO)* 03-14-80
CONSTANT K1F2 = 1.82E5    S*(REF. ENSCO)* 03-14-80
CONSTANT K1F2F3 = 1.82E5 S*(REF. ENSCO)* 03-14-80
CONSTANT K1F3F4 = 1.82E5 S*(REF. ENSCO)* 03-14-80
CONSTANT K2F2F3 = 1.82E5 S*(REF. ENSCO)* 03-14-80
CONSTANT K2F3F4 = 1.82E5 S*(REF. ENSCO)* 03-14-80
CONSTANT K6 = 6.4E4       S*(REF. ENSCO)* 03-14-80
CONSTANT K7 = 6.4E4       S*(REF. ENSCO)* 03-14-80
*-----COEFFICIENTS OF FRICTION*                       03-14-80
CONSTANT MUCPL = .2       S*(REF. ENSCO)* 03-14-80
CONSTANT MUF = .2         S*(REF. ENSCO)* 03-14-80
CONSTANT MUF2 = .2        S*(REF. ENSCO)* 03-14-80
CONSTANT MUF3 = .2        S*(REF. ENSCO)* 03-14-80
CONSTANT MUF4 = .2        S*(REF. ENSCO)* 03-14-80
CONSTANT MUTF = .2        S*(REF. ENSCO)* 03-14-80
CONSTANT MUTR = .2        S*(REF. ENSCO)* 03-14-80
*****
*-----DEVIATIONS FROM BASE CASE PARAMETER VALUES TO MINIMIZE 03-15-80
TIC13, TIC14, TIC53, TIC54, TIC60, TIC61, AND TMIC BY SUCCESSIVE
APPROXIMATIONS*
*-----NOTE ** WHEN USING DUSX4, ALL PARAMETERS LEADING TO DRAFT GEAR 03-15-80
BEHAVIOR HAVE NO BEARING ON THE THEILS COEFFS* 03-15-80
*****
CONSTANT LCF= 151.        S*CORRECTIONS TO ENSCO DATA* 03-21-80
CONSTANT LCR= 53.         S*CORRECTIONS TO ENSCO DATA* 03-21-80
CONSTANT LPF= 102.        S*CORRECTIONS TO ENSCO DATA* 03-21-80
CONSTANT LPR= 102.        S*CORRECTIONS TO ENSCO DATA* 03-21-80
CONSTANT LRC= 259.        S*CORRECTIONS TO ENSCO DATA* 03-21-80
CONSTANT KS1HI = 5.E5     09-16-80
CONSTANT KS1LO = 5.E4     03-24-80
CONSTANT KS4HI = 5.E5     09-16-80
CONSTANT KS4LO = 5.E4     03-24-80
CONSTANT SMPRC = 0.       04-10-80
CONSTANT SMRCP = 0.       04-07-80
CONSTANT TSTOP = 0.15    S*DATA FOR D2XRCX ONLY GOOD TO 0.15* 04-09-80
CONSTANT KTHRC = 1.E10   04-11-80
CONSTANT SKTHRC = 0.     04-11-80
CONSTANT ALFACP = 0.7    04-27-80
CONSTANT BTACPL = 1.0    04-22-80
CONSTANT CS2= 1500.,CS3=1500. 05-09-80

```

```

CONSTANT CS6 = 2000., CS7 = 2000. 05-04-80
CONSTANT KS2 = 5.E6 $'EQUAL TO KS3' 07-02-80
CONSTANT DLTY = 0.11 05-01-80
CONSTANT DLTYA = 0.22 05-02-80
CONSTANT KS2LO = 2.E5 05-01-80
CONSTANT KS2LO2 = 3.5E5 05-01-80
CONSTANT KS2HI = 5.E5 05-02-80
CONSTANT CS2L=0. 05-14-80
CONSTANT CS2H=1500. 05-14-80
CONSTANT KS2L=0. 05-14-80
CONSTANT KS2H=1.E5 05-14-80
*-----CHANGE REQUIRED DUE TO SLACK IN ID-S *05-28-80
CONSTANT KSDG10 = 5.0E4 06-03-80
CONSTANT K1 = 3.33E4 $'CHANGE REQD DUE TO SLACK IN TIEDOWNS' 06-03-80
CONSTANT KSDG20 = 5.0E4 $'CHANGE REQD DUE TO SLACK IN TIEDOWNS' 08-04-80
CONSTANT MK5=1. 10-17-80
CONSTANT MK8=1. 10-17-80
CONSTANT K2 = 3.33E4 $'CHANGE REQD DUE TO SLACK IN TIEDOWNS' 06-03-80
CONSTANT ADRCF = 10. $'CHANGE REQD DUE TO SLACK IN TIEDOWNS' 06-02-80
CONSTANT KMRCFU = 4.0 $'CHANGE REQD DUE TO SLACK IN TIEDOWNS' 06-03-80
***** 07-16-80
*****
*---LATEST CHANGES IN PARAMETERS* 07-16-80
*-----FOR PARAMETRIC AND SENSITIVITY STUDY* 07-16-80
***** 07-16-80
***** 07-16-80
*-----CONTROL VARIABLE DENOTING TYPE OF FIT *07-16-80
* AT REAR TIEDOWN, .TRUE. MEANS TD * 07-16-80
* LOOSE, .FALSE. MEANS TD TIGHT.* 07-16-80
CONSTANT LOOSE = .TRUE. 07-30-80
*-----GO TO END OF *INITIAL COMPUTATIONS* * 07-20-80
*--INITIAL COMPUTATIONS*
ZONE = 1 $'INITIALIZE ZONE TO START' 01-24-80
KS2T = KS2 07-02-80
CS2T = CS2 07-02-80
IF (TEST.EQ.3.)GO TO IT3 03-10-81
IF (TEST.EQ.3.)GO TO IT3 03-10-81
IF (TEST.EQ.10.)GO TO IT10 03-10-81
IF (TEST.EQ.11.)GO TO IT10 03-10-81
IF (TEST.EQ.13.)GO TO IT13 03-10-81
IF (TEST.EQ.16.)GO TO IT16 03-10-81
IF (TEST.EQ.17.)GO TO IT17 03-10-81
IF (TEST.EQ.18.)GO TO IT18 03-10-81
GO TO I999 03-10-81
IT3..CONTINUE 03-10-81
*---PROCEDURE FOR CASE SELECTION* 07-20-80
CONSTANT CASE = 1. 07-20-80
CONSTANT CASE = 2. 07-40-80
CONSTANT CASE = 3. 07-24-80
CONSTANT CASE = 5. 08-04-80
CONSTANT CASE = 6. 08-04-80
CONSTANT CASE = 7. 08-04-80
CONSTANT CASE = 8. 08-04-80
CONSTANT CASE = 9. 09-11-80
CONSTANT CASE = 4. 07-24-80
CONSTANT CASE = 0. 07-30-80
CONSTANT CASE = 10. 09-18-80

```

CONSTANT CASE = 11.	09-19-80
CONSTANT CASE = 12.	09-22-80
CONSTANT CASE = 13.	09-22-80
CONSTANT CASE = 14.	09-23-80
CONSTANT CASE = 15.	09-24-80
CONSTANT CASE = 16.	09-24-80
CONSTANT CASE = 17.	09-24-80
CONSTANT CASE = 18.	09-24-80
CONSTANT CASE = 19.	09-24-80
CONSTANT CASE = 21.	10-17-80
CONSTANT CASE = 23.	10-17-80
CONSTANT CASE = 21.	10-21-80
CONSTANT CASE = 1.	10-23-80
CONSTANT CASE = 2.	10-23-80
CONSTANT CASE = 0.1	10-23-80
CONSTANT CASE = 0.2	10-23-80
CONSTANT CASE = 3.	10-24-80
CONSTANT CASE = 4.	10-24-80
CONSTANT CASE = 5.	10-24-80
CONSTANT CASE = 6.	10-27-80
CONSTANT CASE = 7.	10-27-80
CONSTANT CASE = 8.	10-27-80
CONSTANT CASE = 9.	10-27-80
CONSTANT CASE = 1.1	11-19-80
CONSTANT BCASE = 0.	07-30-80
CONSTANT CASEA = 1.	07-20-80
CONSTANT CASEB = 2.	07-20-80
CONSTANT CASEC = 3.	07-20-80
CONSTANT CASED = 4.	07-20-80
CONSTANT CASE5 = 5.	08-04-80
CONSTANT CASE6 = 6.	08-04-80
CONSTANT CASE7 = 7.	08-04-80
CONSTANT CASE8 = 8.	08-04-80
CONSTANT CASE9 = 9.	09-11-80
CONSTANT CASE10 = 10.	09-18-80
CONSTANT CASE11 = 11.	09-19-80
CONSTANT CASE12 = 12.	09-22-80
CONSTANT CASE13 = 13.	09-22-80
CONSTANT CASE14 = 14.	09-23-80
CONSTANT CASE15 = 15.	09-24-80
CONSTANT CASE16 = 16.	09-24-80
CONSTANT CASE17 = 17.	09-24-80
CONSTANT CASE18 = 18.	09-24-80
CONSTANT CASE19 = 19.	09-24-80
CONSTANT CASE20 = 20.	10-17-80
CONSTANT CASE21 = 21.	10-17-80
CONSTANT CASECC = 0.1	10-23-80
CONSTANT CASEDD = 0.2	10-23-80
CONSTANT PCASE1 = 1.1	11-19-80
CONSTANT LOOSE = .FALSE. \$*NO SLACK IN REAR TIEDOWNS*	07-30-80
CONSTANT MUPR = 0. \$*ELIMINATE FRICTIONAL DAMPING*	07-20-80
CONSTANT XRPL0 = -1.E-6 \$*CHOCKS ARE TIGHT*	07-23-80
CONSTANT XRPHI = 1.E-6 \$*CHOCKS ARE TIGHT*	07-23-80
IF (CASE.EQ.CASEA)GO TO 11	07-20-80
IF (CASE.EQ.CASEB)GO TO 12	07-20-80
IF (CASE.EQ.CASEC)GO TO 13	07-20-80
IF (CASE.EQ.CASED)GO TO 14	07-20-80

IF (CASE.EQ.CASE)GO TO I6	07-30-80
IF (CASE.EQ.CASE5)GO TO I7	08-04-80
IF (CASE.EQ.CASE6)GO TO I8	08-04-80
IF (CASE.EQ.CASE7)GO TO I9	08-04-80
IF (CASE.EQ.CASE8)GO TO I10	08-04-80
IF (CASE.EQ.CASE9)GO TO I11	09-11-80
IF (CASE.EQ.CASE10)GO TO I12	09-18-80
IF (CASE.EQ.CASE11)GO TO I13	09-19-80
IF (CASE.EQ.CASE12)GO TO I14	09-22-80
IF (CASE.EQ.CASE13)GO TO I15	09-22-80
IF (CASE.EQ.CASE14)GO TO I16	09-23-80
IF (CASE.EQ.CASE15)GO TO I17	09-24-80
IF (CASE.EQ.CASE16)GO TO I18	09-24-80
IF (CASE.EQ.CASE17)GO TO I19	09-24-80
IF (CASE.EQ.CASE18)GO TO I20	09-24-80
IF (CASE.EQ.CASE19)GO TO I21	09-24-80
IF (CASE.EQ.CASE20)GO TO I22	10-17-80
IF (CASE.EQ.CASE21)GO TO I23	10-17-80
IF (CASE.EQ.CASECC)GO TO I24	10-23-80
IF (CASE.EQ.CASEDD)GO TO I25	10-23-80
IF (CASE.EQ.PCASE1)GO TO I26	11-19-80
GO TO I5	07-20-80
I1..CONTINUE \$*CASEA=CASE 1 - ITEM 3(A) IN SAFER BRIEF*	09-23-80
WP = 2.*WP	07-31-80
KS1LO = KS1LO	07-20-80
KS1HI = KS1HI	07-20-80
KS2T = KS2T	07-20-80
CS2T = CS2T	07-20-80
KS3 = KS3	07-20-80
KS4LO = KS4LO	07-20-80
KS4HI = KS4HI	07-20-80
GO TO I5	07-20-80
I2..CONTINUE \$*CASE B = CASE 2 - ITEM 3(B) IN SAFER BRIEF*	09-23-80
WP = .5*WP	07-31-80
KS1LO = KS1LO	07-20-80
KS1HI = KS1HI	07-20-80
KS2T = KS2	07-20-80
CS2T = CS2	07-20-80
KS3 = KS3	07-20-80
KS4LO = KS4LO	07-20-80
KS4HI = KS4HI	07-20-80
GO TO I5	07-20-80
I3..CONTINUE \$*CASE C = CASE 3 - ITEM 3(C) IN SAFER BRIEF*	09-23-80
WP = 2.*WP	07-31-80
KS1LO = KS1LO*2.	07-20-80
KS1HI = KS1HI*2.	07-20-80
KS2T = KS2T*2.	07-20-80
CS2T = CS2T	07-20-80
KS3 = KS3*2.	07-20-80
KS4LO = KS4LO*2.	07-20-80
KS4HI = KS4HI*2.0	07-20-80
GO TO I5	07-20-80
I4..CONTINUE \$*CASE D = CASE 4 - ITEM 3(D) IN SAFER BRIEF*	09-23-80
WP = .5*WP	07-31-80
KS1LO = KS1LO*0.5	07-20-80
KS1HI = KS1HI*0.5	07-20-80
KS2T = KS2T*0.5	07-20-80

CS2T	= CS2T	07-20-80
KS3	= KS3*0.5	07-20-80
KS4LO	= KS4LO*0.5	07-20-80
KS4HI	= KS4HI*0.5	07-20-80
GO TO I5		08-12-80
I6..CONTINUE	*BCASE = BASE CASE*	09-23-80
-----FOR ORIGINAL BASE CASE, REMOVE ALL BUT *GO TO I5**		07-30-80
WP	= WP	07-30-80
KS1LO	= KS1LO	07-30-80
KS1HI	= KS1HI	07-30-80
KS2T	= KS2T	07-30-80
CS2T	= CS2T	07-30-80
KS3	= KS3	07-30-80
KS4LO	= KS4LO	07-30-80
KS4HI	= KS4HI	07-30-80
GO TO I5		07-30-80
I7..CONTINUE	*CASE 5 - ITEM 3(G) IN SAFER BRIEF*	08-04-80
WP	= WP	08-04-80
KS1LO	= KS1LO*2.	08-04-80
KS1HI	= KS1HI*2.	08-04-80
KS2T	= KS2T	08-04-80
CS2T	= CS2T	08-04-80
KS3	= KS3	08-04-80
KS4LO	= KS4LO*2.	08-04-80
KS4HI	= KS4HI*2.	08-04-80
GO TO I5		08-04-80
I8..CONTINUE	*CASE 6 - ITEM 3(H) IN SAFER BRIEF*	08-04-80
WP	= WP	08-04-80
KS1LO	= KS1LO*0.5	08-04-80
KS1HI	= KS1HI*0.5	08-04-80
KS2T	= KS2T	08-04-80
CS2T	= CS2T	08-04-80
KS3	= KS3	08-04-80
KS4LO	= KS4LO*0.5	08-04-80
KS4HI	= KS4HI*0.5	08-04-80
GO TO I5		08-04-80
I9..CONTINUE	*CASE 7 - ITEM 3(E) IN SAFER BRIEF*	08-04-80
WP	= WP	08-04-80
KS1LO	= KS1LO	08-04-80
KS1HI	= KS1HI	08-04-80
KS2T	= KS2T*2.	08-04-80
CS2T	= CS2T	08-04-80
KS3	= KS3*2.	08-04-80
KS4LO	= KS4LO	08-04-80
KS4HI	= KS4HI	08-04-80
GO TO I5		08-04-80
I10..CONTINUE	*CASE 8 - ITEM 3(F) IN SAFER BRIEF*	08-04-80
WP	= WP	08-04-80
KS1LO	= KS1LO	08-04-80
KS1HI	= KS1HI	08-04-80
KS2T	= KS2T*.5	08-04-80
CS2T	= CS2T	08-04-80
KS3	= KS3*.5	08-04-80
KS4LO	= KS4LO	08-04-80
KS4HI	= KS4HI	08-04-80
GO TO I5		08-04-80

I11..CONTINUE	S*CASE 9 - ITEM 3(I) IN SAFER BRIEF*	09-11-80
WP	= WP	09-11-80
KS1LO	= KS1LO	09-11-80
KS1HI	= KS1HI	09-11-80
KS2T	= KS2T	09-11-80
CS2T	= CS2T	09-11-80
KS3	= KS3	09-11-80
SUMKSY	= KS2T + KS3	09-11-80
KS2T	= KS2T*0.5	09-11-80
KS3	= SUMKSY - KS2T	09-11-80
KS4LO	= KS4LO	09-11-80
KS4HI	= KS4HI	09-11-80
GO TO I5		09-11-80
I12..CONTINUE	S*CASE 10 - ITEM 3(J) OF SAFER BRIEF*	09-18-80
WP	= WP	09-18-80
KS1LO	= KS1LO	09-18-80
KS1HI	= KS1HI	09-18-80
KS2T	= KS2T	09-18-80
CS2T	= CS2T	09-18-80
KS3	= KS3	09-18-80
SUMKSY	= KS2T + KS3	09-18-80
KS3	= KS3*0.5	09-18-80
KS2T	= SUMKSY - KS3	09-18-80
KS4LO	= KS4LO	09-18-80
KS4HI	= KS4HI	09-18-80
GO TO I5		09-18-80
I13..CONTINUE	S*CASE 11 - ITEM 3(K) OF SAFER BRIEF*	09-19-80
*-----FRONT ID ATTACHMENT POINT ON CAR LOCATED		*09-19-80
* OVER CAR CG AND DIRECTLY UNDER FRONT		*09-19-80
* ATTACHMENT POINT ON CASK.		*09-19-80
WP	= WP	09-19-80
KS1LO	= KS1LO	09-19-80
KS1HI	= KS1HI	09-19-80
KS2T	= KS2T	09-19-80
CS2T	= CS2T	09-19-80
KS3	= KS3	09-19-80
KS4LO	= KS4LO	09-19-80
KS4HI	= KS4HI	09-19-80
LCTOT	= LCF + LCR	09-19-80
LCF	= 0.	09-19-80
LCR	= LCTOT - LCF	09-19-80
GO TO I5		09-19-80
I14..CONTINUE	S*CASE 12 - ITEM 3(O) OF SAFER BRIEF*	09-22-80
WP	= WP	09-22-80
KS1LO	= KS1LO	09-22-80
KS1HI	= KS1HI	09-22-80
KS2T	= KS2T	09-22-80
CS2T	= CS2T	09-22-80
KS3	= KS3	09-22-80
KS4LO	= KS4LO	09-22-80
KS4HI	= KS4HI	09-22-80
LPR	= LPR*1.5	09-22-80
LPF	= LPF*1.5	09-22-80
LOCR	= -45.	09-23-80
*-----S*BASE CASE VALUE OF LOCR*		
* WHEN		*09-19-80
* LOCR = + CASK CG AFT OF CAR CG		*09-19-80
* LOCR = 0 CASK CENTERED FORE AND AFT		*09-19-80

	GO TO I6A	LOCR = - CASK CG FORWARD OF CAR CG	*09-19-80
I15..	CONTINUE	*CASE 13 - ITEM 3(P) OF SAFER BRIEF*	09-23-80
	WP	= WP	09-22-80
	KS1LO	= KS1LO	09-22-80
	KS1HI	= KS1HI	09-22-80
	KS2T	= KS2T	09-22-80
	CS2T	= CS2T	09-22-80
	KS3	= KS3	09-22-80
	KS4LO	= KS4LO	09-22-80
	KS4HI	= KS4HI	09-22-80
	LPR	= LPR*1.5	09-22-80
	LPF	= LPF*1.5	09-22-80
	SUMLC	= LCR + LCF	09-22-80
	SUMLP	= LPR + LPF	09-22-80
	LCF	= SUMLC/2.	09-22-80
	LCR	= LCF	09-22-80
	LOCR	= 0.	*09-23-80
		*SAME AS LCR=LCF, IF CASK CENTERED	
		*FORE AND AFT ON THE RAIL CAR	*09-22-80
	GO TO I6A		09-23-80
I16..	CONTINUE	*CASE 14 - ITEM 3(Q) IN SAFER BRIEF*	09-23-80
	WP	= WP	09-23-80
	KS1LO	= KS1LO	09-23-80
	KS1HI	= KS1HI	09-23-80
	KS2T	= KS2T	09-23-80
	CS2T	= CS2T	09-23-80
	KS3	= KS3	09-23-80
	KS4LO	= KS4LO	09-23-80
	KS4HI	= KS4HI	09-23-80
	LPR	= LPR	09-23-80
	LPF	= LPF	09-23-80
	ZP	= ZP*1.5	09-23-80
	GO TO I5		09-23-80
I17..	CONTINUE	*CASE 15 - ITEM 3(R) OF SAFER BRIEF*	09-24-80
	ZP	= ZP*0.75	09-24-80
	GO TO I5		09-24-80
I18..	CONTINUE	*CASE 16 - ITEM 3(S) OF SAFER BRIEF*	09-24-80
	LOCR	= 0.	09-24-80
	KS1LO	= KS1LO*2.	09-24-80
	KS1HI	= KS1HI*2.	09-24-80
	KS4HI	= KS4HI*2.	09-24-80
	KS4LO	= KS4LO*2.	09-24-80
	GO TO I6A	*IF LOCR SET HERE*	09-24-80
I19..	CONTINUE	*CASE 17 - ITEM 3(T) OF SAFER BRIEF*	09-24-80
	KS1LO	= KS1LO*0.5	09-24-80
	KS1HI	= KS1HI*0.5	09-24-80
	KS4HI	= KS4HI*0.5	09-24-80
	KS4LO	= KS4LO*0.5	09-24-80
	LOCR	= 0.	09-24-80
	GO TO I6A	*IF LOCR SET HERE*	09-24-80
I20..	CONTINUE	*CASE 18 - ITEM 3(L) OF SAFER BRIEF*	09-24-80
		-----BASE CASE, EXCEPT LCF=LPF*	09-24-80
		* THIS IS THE SAME AS LOCR=0.	09-24-80
		* CASK CENTERED FORE AND AFT ON RAIL CAR*	09-24-80
	LCTOT	= LCF + LCR	09-24-80
	LCF	= LPF	09-24-80
	LCR	= LCTOT - LCF	09-24-80

GO TO I5		09-24-80
I21..CONTINUE	\$*CASE 19 - ITEM 3(N) OF SAFER BRIEF*	09-24-80
'	-----BASE CASE , EXCEPT LCR = C.*	09-24-80
'	REAR TD ATTACHMENT POINT ON CAR LOCATED*	09-24-80
'	OVER CAR CG AND DIRECTLY UNDER REAR*	09-24-80
'	ATTACHMENT POINT ON CASK.*	09-24-80
'	CASK LOCATED FORWARD OF CAR CG.*	09-24-80
LCTOT	= LCF + LCR	09-24-80
LCR	= 0.	09-24-80
LCF	= LCTOT - LCR	09-24-80
GO TO I5		09-24-80
I22..CONTINUE	\$*CASE 20 - POSSIBLE ALT ITEM 3(C)*	10-17-80
WP	= WP*2.	10-17-80
KS1LO	= KS1LO * 2.	10-17-80
KS1HI	= KS1HI * 2.	10-17-80
KS2T	= KS2T * 2.	10-17-80
CS2T	= CS2T	10-17-80
KS3	= KS3 *2.	10-17-80
KS4LO	= KS4LO * 2.	10-17-80
KS4HI	= KS4HI * 2.	10-17-80
MK5	= MK5 * 2.	10-17-80
MK8	= MK8 * 2.	10-17-80
K6	= K6 * 2.	10-17-80
K7	= K7 * 2.	10-17-80
GO TO I5		10-17-80
I23..CONTINUE	\$*CASE 21 - POSSIBLE ALT ITEM 3(D)*	10-17-80
WP	= WP*.5	10-17-80
KS1LO	= KS1LO * .5	10-17-80
KS1HI	= KS1HI * .5	10-17-80
KS2T	= KS2T * .5	10-17-80
CS2T	= CS2T	10-17-80
KS3	= KS3 *.5	10-17-80
KS4LO	= KS4LO * .5	10-17-80
KS4HI	= KS4HI * .5	10-17-80
MK5	= MK5 * .5	10-17-80
MK8	= MK8 * .5	10-17-80
K6	= K6 * .5	10-17-80
K7	= K7 * .5	10-17-80
GO TO I5		10-17-80
I24..CONTINUE	\$*CASECC = CASEC IN REPORT*	10-23-80
WP	= WP	10-23-80
KS1LO	= KS1LO* 2.	10-23-80
KS1HI	= KS1HI* 2.	10-23-80
KS2T	= KS2T*2.	10-23-80
CS2T	= CS2T	10-23-80
KS3	= KS3*2.	10-23-80
KS4LO	= KS4LO*2.	10-23-80
KS4HI	= KS4HI*2.	10-23-80
GO TO I5		10-23-80
I25..CONTINUE	\$*CASEDD = CASED IN REPORT*	10-23-80
WP	= WP	10-23-80
KS1LO	= KS1LO* .5	10-23-80
KS1HI	= KS1HI* .5	10-23-80
KS2T	= KS2T*.5	10-23-80
CS2T	= CS2T	10-23-80
KS3	= KS3*.5	10- 3-80
KS4LO	= KS4LO*.5	10-23-80

KS4HI = KS4HI*.5		10-23-80
GO TO I5		10-23-80
I26..CONTINUE	\$*PCASE1=PRELIMINARY CASE1 OR TRANC*	11-19-80
LOOSE = .TRUE.	\$*SLACK IN REAR TIEDOWNS*	11-19-80
EXPFRC = .TRUE.	\$*07-30-81*	
CABLES = .FALSE.	\$*06-30-81*	
WTF = 1.35E4	\$*07-08-81*	
WTR = 1.35E4	\$*07-08-81*	
XRPL0 = -0.0625		11-19-80
XRPHI = 0.0625		11-19-80
MUPR = 0.58		11-19-80
-----WP THRU KS4HI THE SAME AS BCASE		11-19-80
GO TO I5		11-19-80
I5..CONTINUE	\$*END OF CASE SELECTION*	07-20-80
LOCR = LPF - LCF		09-19-80
I6A..CONTINUE	\$*END OF CASE SELECTION*	09-23-80
-----END OF CASE SELECTION		07-23-80
GO TO ITT		03-10-81
IT10..CONTINUE		03-10-81
GO TO ITT		03-10-81
IT11..CONTINUE		
GO TO ITT		
IT13..CONTINUE	\$*05-22-81*	
GO TO ITT		
ITT..CONTINUE		03-10-81
HRCP = ZRC*ZP	\$*DISTANCE BETWEEN CASK AND RC CGS*	03-28-80
MP = WP/G		
MRC = WRC/G		
MTR = WTR/G		
MTF = WTF/G		
MF = WF/G		
MF2 = WF2/G		
MF3 = WF3/G		
MF4 = WF4/G		
WXTR = WTR+WRC/2.+(LRC+LOCR)*WP/(2.*LRC)		
WXTF = WTF+WRC/2.+(LRC-LOCR)*WP/(2.*LRC)		
RR = (LRC*WRC+(LRC+LOCR)*WP)/(2.*LRC)		
RF = (LRC*WRC+(LRC-LOCR)*WP)/(2.*LRC)		
YRC56I = 0.		
YRC78I = 0.		
YRCI = (YRC56I+YRC78I)/2.		
THRCI = (YRC56I-YRCI)/LRC		
YRC12I = YRCI+LCR*THRCI		
YP12I = YRC12I		
YRC34I = YRCI - LCF*THRCI		
YP34I = YRC34I		
THPI = THRCI		
YPI = YRCI-LOCR*THRCI		
-----INITIALIZE FOR MODEL VALIDATION USING THEILS INEQUALITY COEFFS		11-29-79
N = 0.		11-29-79
S13 = 0.		11-29-79
S14 = 0.		11-29-79
S53 = 0.		12-11-79
S54 = 0.		11-29-79
S55 = 0.		11-29-79
S60 = 0.		11-29-79
S61 = 0.		12-11-79

S13X	= 0.	11-29-79
S14X	= 0.	11-29-79
S53X	= 0.	12-11-79
S54X	= 0.	11-29-79
S55X	= 0.	11-29-79
S60X	= 0.	11-29-79
S61X	= 0.	12-11-79
SD13	= 0.	11-29-79
SD14	= 0.	11-29-79
SD53	= 0.	12-11-79
SD54	= 0.	11-29-79
SD55	= 0.	11-29-79
SD60	= 0.	11-29-79
SD61	= 0.	12-11-79
SR13	= 0.	04-14-80
SR14	= 0.	04-14-80
SR53	= 0.	04-14-80
SR54	= 0.	04-14-80
SR60	= 0.	04-14-80
SR61	= 0.	04-14-80
SR13X	= 0.	04-16-80
SR14X	= 0.	04-16-80
SR53X	= 0.	04-16-80
SR54X	= 0.	04-16-80
SR60X	= 0.	04-16-80
SR61X	= 0.	04-16-80
SVR13	= 0.	04-04-80
SVR14	= 0.	04-04-80
SVR53	= 0.	04-04-80
SVR54	= 0.	04-04-80
SVR60	= 0.	04-04-80
SVR61	= 0.	04-04-80
SVR13X	= 0.	04-16-80
SVR14X	= 0.	04-16-80
SVR53X	= 0.	04-16-80
SVR54X	= 0.	04-16-80
SVR60X	= 0.	04-16-80
SVR61X	= 0.	04-16-80
NN	= 0	04-11-80

----CALCN OF DEFLECTIONS BY AREA-MOMENT FOR EACH MASS APPLIED ONE AT...

A TIME*

I	= 0.67*WDT*RC*ZRC**3	S*AREA MOI OF EQUIV RC BEAM*
BB1	= LRC-LOCR-LP	
CC1	= LRC+LOCR+LP	
LL1	= 2.*LRC	
X21	= LRC-LOCR+LP	
X31	= LRC	
D11	= ((CC1*BB1)/(LL1)**2)/(3.*F*I)	
D21	= BB1*(LL1-X21)*(CC1*(LL1+BB1)- ... (LL1-X21)**2)/(6.*E*I*LL1)	
D31	= BB1*(LL1-X31)*(CC1*(LL1+BB1)-(LL1-X31)**2)/ ... (6.*E*I*LL1)	
BB2	= LRC-LOCR+LP	
CC2	= LRC+LOCR-LP	
LL2	= 2.*LRC	
X12	= LRC-LOCR-LP	
X32	= LRC	

```

D12 = CC2*X12*(BB2*(LL2+CC2)-X12**2)/(6.*E*I*LL2)
D22 = (CC2*BB2/LL2)**2/(3.*E*I)
D32 = (CC2*X32*(BB2*(LL2+CC2)-X32**2))/(6.*E*I*LL2)
BB3 = LRC
CC3 = LRC
LL3 = 2.*LRC
X13 = LRC-LOCR-LP
X23 = LRC-LOCR+LP
D13 = (CC3*X13*(BB3*(LL3+CC3)-X13**2))/(6.*E*I*LL3)
D23 = BB3*(LL2-X23)*(CC3*(LL3+BB3)-(LL3-X23)**2)/...
      (6.*E*I*LL3)
D33 = (CC3*BB3/LL3)**2/(3.*E*I)
DMA = D31*D12*D23+D21*D32*D13+D11*D22*D33-D11*D32*D23- ...
      D12*D21*D33-D31*D22*D13
*----CALCN OF SPRING CONSTANTS FOR BENDING OF RAIL CAR*
K11 = (D22*D33-D32*D23)/DMA
K12 = (D32*D13-D12*D33)/DMA
K21 = K12 $*BY MAXWELL RECIPROCAL THEOREM*
K31 = (D21*D32-D22*D31)/DMA
K13 = K31 $*BY MAXWELL RECIPROCAL THEOREM*
K22 = (D11*D33-D13*D31)/DMA
K23 = (D21*D13-D11*D23)/DMA
K32 = K23 $*BY MAXWELL RECIPROCAL THEOREM*
K33 = (D11*D22-D12*D21)/DMA
KF1 = ((LRC-LOCR-LP)*K11-(LRC-LOCR+LP)*K21+LRC*K31)/(2.*LRC)
KR1 = ((LOCR+LP)*K11-(LOCR-LP)*K21-LRC*KF1)/LRC
KF2 = ((LRC-LOCR-LP)*K12-(LRC-LOCR+LP)*K22+LRC*K32)/(2.*LRC)
KR2 = ((LOCR+LP)*K12-(LOCR-LP)*K22-LRC*KF2)/LRC
KF3 = ((LRC-LOCR-LP)*K13-(LRC-LOCR+LP)*K23+LRC*K33)/(2.*LRC)
KR3 = ((LRC-LOCR-LP)*K13-(LRC-LOCR+LP)*K23-LRC*KF3)/...
      (LRC-LOCR-LP)
K11 = K11 * BENDSW
K12 = K12 * BENDSW
K21 = K21 * BENDSW
K31 = K31 * BENDSW
K13 = K13 * BENDSW
K22 = K22 * BENDSW
K23 = K23 * BENDSW
K32 = K32 * BENDSW
K33 = K33 * BENDSW
KF1 = KF1 * BENDSW
KR1 = KR1 * BENDSW
KF2 = KF2 * BENDSW
KR2 = KR2 * BENDSW
KF3 = KF3 * BENDSW
KR3 = KR3 * BENDSW
END $*OF INITIAL*
DYNAMIC
      CINT = CIZONE(ZONE)
DERIVATIVE
*-----COMPUTE ZONE FOR CINT*
PROCEDURAL (ZONE=1)
      IF (T.GE.TLO.AND.T.LE.THI) ZONE=2
      IF (T.LT.TLO) ZONE=1
      IF (T.GT.THI) ZONE=3
END $*OF PROCEDURAL*
*-----MACRO FOR SIGNUM OR SIGN FUNCTION

```

```

MACRO SGNF(R,A)
  PROCEDURAL (R=A)
    IF(A.LT.O.) R= -1.
    IF(A.EQ.O.) R= -1.
    IF(A.GT.O.) R= +1.
  END S'OF PROCEDURAL'
MACRO END
-----PROCEDURAL TO SELECT TEST DATA*
PROCEDURAL(DUSLFX,DUSX4,D2XRCX,D2XPX,D2P12X,D2P34X,D2R12X,D2R12T,... 03-10-81
  D2R56X,D2CPLX,D2CPLT=TXLF, TXCF) 03-10-81
  IF(TEST.EQ.3.)GO TO A 03-10-81
  IF(TEST.EQ.10.)GO TO B 03-10-81
  IF(TEST.EQ.11.)GO TO C
  IF(TEST.EQ.13.)GO TO D
  GO TO TFIN 03-10-81
  A..CONTINUE 03-10-81
  DUSLFX = DUSLFF(TXLF)
  DUSX4 = DUSF(TXCF) S'04-07-81'
  D2XRCX = D2XPCF(TXCF) S'04-07-81'
  D2XPX = D2XPF(TXCF) S'04-07-81'
  D2P12X = D2P12F(TXCF) S'04-07-81'
  D2P34X = D2P34F(TXCF)*POL61 03-10-81
  D2R12X = D2R12F(TXCF)*PAYR12 03-10-81
  D2R12T = D2R12G(TXCF)*PAYR12 03-10-81
  D2R56X = D2R56F(TXCF)*PAYR56 03-10-81
  D2CPLX = D2CPLF(TXCF)*PAYCPL 03-10-81
  D2CPLT = D2CPLG(TXCF)*PAYCPL 03-10-81
  GO TO TFIN 03-10-81
  B..CONTINUE 03-10-81
  DUSLFX = T10I27(TXLF)*P10I27 + T10I28(TXLF)*P10I28
  DUSX4 = T10I3(TXCF)*P10I3 S'04-07-81' 03-10-81
  D2XRCX = T10I12(TXCF)*P10I12 S'04-07-81' 03-10-81
  D2XPX = T10I8(TXCF)*P10I8 S'04-07-81' 03-10-81
  D2P12X = T10I11(TXCF)*P10I11 S'04-07-81'
  D2P34X = T10I9(TXCF)*P10I9 03-10-81
  D2R12X = T0I14F(TXCF)*PAYR12 03-10-81
  D2R12T = T0I14G(TXCF)*PAYR12 03-10-81
  D2R56X = T10I22(TXCF)*P10I22 03-10-81
  D2CPLX = T10I6F(TXCF)*PAYCPL 03-10-81
  D2CPLT = T10I6G(TXCF)*PAYCPL 03-10-81
  GO TO TFIN 03-10-81
  C..CONTINUE
  DUSLFX = T11I27(TXLF)*P11I27 + T11I28(TXLF)*P11I28
  DUSX4 = T11I3(TXCF)*P11I3 S'04-09-81'
  D2XRCX = T11I12(TXCF)*P11I12 S'04-09-81'
  D2XPX = T11I8(TXCF)*P11I8 S'04-09-81'
  D2P12X = T11I11(TXCF)*P11I11 S'04-09-81'
  GO TO TFIN
  D..CONTINUE
  DUSLFX = T13I27(TXLF)*P13I27
  DUSX4 = T13I3(TXCF)*P13I3
  D2XRCX = T13I7(TXCF)*P13I7
  D2XRCI = T13I12(TXCF)*P13I12
  D2XPX = T13I8(TXCF)*P13I8
  D2P12X = T13I11(TXCF)*P13I11
  D2P34X = T13I9(TXCF)*P13I9
  GO TO TFIN

```

```

TFIN..CONTINUE
END $*OF PROCEDURAL TO SELECT TEST DATA*
-----PROCEDURAL TO CALCULATE KS1HI TO KS4LO*
PROCEDURAL(KS1HI,KS4HI,KS1LO,KS4LO = XRPRC)
IF (TEST.EQ.3.)GO TO TTFN
IF (TEST.EQ.10..OR.TEST.EQ.11.)GO TO BB
IF (TEST.EQ.13.)GO TO TTFN
GO TO TTFN
BB..CONTINUE
KS1HI = BOUND(CKS1LO,CKS1HI,KS1HF(XRPRC))
KS4HI = BOUND(CKS4LO,CKS4HI,KS1HF(XRPPC))
KS1LO = CKS1LO
KS4LO = CKS4LO
GO TO TTFN
TTFN..CONTINUE
END $*OF PROCEDURAL
*-EQUATIONS OF MOTION, INTEGRATIONS, AND SUPPORTING EQUATIONS
PROCEDURAL(YRC56,YRC78,KS6,KS7=YRC,THRC,DYRC56,DYRC78)
-----PROCEDURAL FOR CALCULATION OF SPRING CONSTANTS OF
SUSPENSION SYSTEM, AND DISPLACEMENTS OF RAIL CAR
SUPPORT POINTS WITH BOTTOMING OF SPRINGS
IF (T.LE.O.) GO TO D5
IF (YRC56.LE.YRCMAX) GO TO D1
-----YRC56.LE.YRCMAX, NOT BOTTOMED
MUD6 = RSW(DYRC56.GE.O.,MUD6E,MUD6C)
BETA6 = RSW(DYRC56.GE.O.,BETA6E,BETA6C)
KS6 = K6*(1.-MUD6*BETA6*SGNF(DYRC56))
YRC56 = YRC+LRC*THRC
GO TO D3
D5..CONTINUE $*IF T.LE.O.*
MUD6 = RSW(DYRC56.GE.O.,MUD6E,MUD6C)
BETA6 = RSW(DYRC56.GE.O.,BETA6E,BETA6C)
KS6 = K6*(1.-MUD6*BETA6*SGNF(DYRC56))
MUD7 = RSW(DYRC78.GE.O.,MUD7E,MUD7C)
BETA7 = RSW(DYRC78.GE.O.,BETA7E,BETA7C)
KS7 = K7*(1.-MUD7*BETA7*SGNF(DYRC78))
YRC56 = O.
YRC78 = O.
GO TO D4 $*GO TO END*
D3..CONTINUE
IF (YRC78.LE.YRCMAX) GO TO D2
-----YRC78.GT.YRCMAX, NOT BOTTOMED
MUD7 = RSW(DYRC78.GE.O.,MUD7E,MUD7C)
BETA7 = RSW(DYRC78.GE.O.,BETA7E,BETA7C)
KS7 = K7*(1.-MUD7*BETA7*SGNF(DYRC78))
YRC78 = YRC-LRC*THRC
GO TO D4 $* O TO END*
D1..CONTINUE $*(IF YRC56.LE.YRCMAX,BOTTOMED)*
KS6 = KS6INF
YRC56 = YRC+LRC*THRC
GO TO D3
D2..CONTINUE
KS7 = KS7INF
YRC78 = YRC-LRC*THRC
GO TO D4
D4..CONTINUE
END $*OF PROCEDURAL*

```

*-----CASK OR PACKAGE		*04-30-80
*-----EQUATION OF MOTION (HORIZONTAL ACCELERATION)		*05-15-80
D2XP	= (-DUS1-DUS4+DWS1+DWS4+DWP1+DWP4)/MP	
DUS1	= -KS1*((XRC+ZRC*THRC)-(XP-ZP*THP))	
DUS4	= -KS4*((XRC+ZRC*THRC)-(XP-ZP*THP))	
DUSLF	= DUS1 + DUS4	7-17-79
TXLF	= T + TLAGLF	7-19-79
DWS1	= CS1*((DXRC+ZRC*DTHRC)-(DXP-ZP*DTHP))	
DWS4	= CS4*((DXRC+ZRC*DTHRC)-(DXP-ZP*DTHP))	
DWP1	= -MUPR*WP1*SGNF(DXRPRC)	
DWP4	= -MUPR*WP4*SGNF(DXRPRC)	
*-----EQUATION OF MOTION (VERTICAL ACCELERATION)		*05-15-80
D2YP	= (-DUS2-DUS3 +DWS2+DWS3)/MP	
DJS2	= -KS2*((YRC+LCR*THRC)-(YP+LPR*THP))	
DUS3	= -KS3*((YRC+LCR*THRC)-(YP+LPR*THP))	
*-----VERTICAL TIEDOWN AT FAR END INCLUDES A RUBBER GASKET UNDER COLLAR, AND THERE IS APPARENT SLACK IN TIEDOWN STRUCTURE, SO KS2 AND CS2 CALCULATED USING BOUNDED TABLE FUNCTIONS.		*05-15-80
KS2	= RS _b (LOOSE,BOUND(KS2L,KS2H,KS2F(DLTY12)),KS2T)	*05-15-80
CS2	= RS _b (LOOSE,BOUND(CS2L,CS2H,CS2F(DLTY12)),CS2T)	*05-15-80
*-----KS2T AND CS2T ARE COMPUTED IN INITIAL		*05-15-80
DLTY12	= YP12 - YRC12	*07-02-80
*-----		*04-30-80
DUWP	= -W	*05-15-80
DWS2	= CS2*((DYRC+LCR*DTHRC)-(DYP+LPR*DTHP))	
DWS3	= CS3*((DYRC+LCR*DTHRC)-(DYP+LPR*DTHP))	
DXRPRC	= DXP-DXRC	
WP1	= WP/2.	
WP4	= WP/2.	
*-----FREQUENCIES		*05-28-80
OMY12	= SQRT(KS2/MP)	05-28-80
OMY34	= SQRT(KS3/MP)	05-28-80
*-----		*05-28-80
DY12	= YP12 - YRC12	05-28-80
DY12	= DYP12 - DYRC12	05-28-80
D2DY12	= D2YP12 - D2YR12	05-28-80
DY34	= YP34 - YRC34	05-28-80
DDY34	= DYP34 - DYRC34	05-28-80
D2DY34	= D2YP34 - D2YR34	05-28-80
*-----PROCEDURAL TO CALCULATE KS1 AND KS4		*04-30-80
PROCEDURAL(KS1,KS4,MP,MRC=XRPRC,DXRPRC)		*06-26-81
IF (XRPRC.GT.0..AND.XRPRC.LT.XRPHI) GO TO 10		8-01-79
IF (XRPRC.GE.XRPHI) GO TO 20		8-01-79
IF (XRPRC.EQ.0.) GO TO 30		8-01-79
IF (XRPRC.GT.XRPLO..AND.XRPRC.LT.0.) GO TO 40		8-01-79
-----IF XRPRC.LE.XRPLO, CASK MOVES TO REAR		09-16-80
KS1 = 0.		8-01-79
KS1	= 0. + KS1HI	*CABLES SLACK, BUT CONTACTS CHOCKS*
MKS1	= RS _b (XRPRC.GT.XRPLO..AND.XRPRC.LT.XRPHI....AND.DXRPRC.LT.0.,MKS1F,0.)	*06-25-81
MKS1	= RS _b (DXRPRC.LT.0..AND.CABLES,MKS1F,0.)	*06-29-81
KS1	= KS1*(1. + MKS1*SGNF(DXRPRC))	*06-25-81
CS1	= CS1	09-17-80
KS4	= KS4LO + KS4HI	*CABLES TAUT, AND CONTACTS CHOCKS*
MKS4	= RS _b (XRPRC.GT.XRPLO..AND.XRPRC.LT.XRPHI....	09-16-80

	AND.DXRPRC.LT.O.,MKS4F,O.)	\$*06-25-81*	
MKS4	= RSW(DXRPRC.LT.O.,AND,CABLES,MKS4F,O.)	\$*06-29-81*	
KS4	= KS4*(1. + MKS4*SGNF(DXRPRC))	\$*06-25-81*	
CS4	= CS4		09-17-80
MP	= WP*(1.-FRMP)/G		8-28-79
MRC	= (MRC+WP*FRMP)/G		8-28-79
	GO TO 50		8-01-79
1G..	CONTINUE \$*CASK MOVES TOWARD FRONT OF CAR*		09-16-80
KS1	= KS1LO \$*CABLES TAUT, BUT NO CONTACT WITH CHOCKS*		09-16-80
MKS1	= RSW(XRPRC.GT.XRPLO,AND,XRPRC.LT.XRPHI,....		
	AND.DXRPRC.LT.O.,MKS1F,O.)	\$*06-25-81*	
MKS1	= RSW(DXRPRC.LT.O.,AND,CABLES,MKS1F,O.)	\$*06-29-81*	
KS1	= KS1*(1. + MKS1*SGNF(DXRPRC))	\$*06-25-81*	
CS1	= CS1		09-17-80
	IF(TEST.EQ.10..OR.TEST.EQ.11.)GO TO A10A	\$*03-30-81*	
KS4	= O. \$*CABLES SLACK, AND NO CONTACT WITH CHOCKS*		09-16-80
MKS4	= RSW(XRPRC.GT.XRPLO,AND,XRPRC.LT.XRPHI,....		
	AND.DXRPRC.LT.O.,MKS4F,O.)	\$*06-25-81*	
MKS4	= RSW(DXRPRC.LT.O.,AND,CABLES,MKS4F,O.)	\$*06-29-81*	
KS4	= KS4*(1. + MKS4*SGNF(DXRPRC))	\$*06-25-81*	
CS4	= O.		09-17-80
	GO TO A10B	\$*03-30-81*	
A10A..	CONTINUE \$*03-30-81*		
KS4	= KS4LO		
CS4	= CS4		
	GO TO A10B		
A10B..	CONTINUE		
MP	= WP/G		8-28-79
MRC	= MRC/G		8-28-79
	GO TO 50		8-01-79
20..	CONTINUE \$*CASK MOVES TOWARD FRONT OF CAR*		09-16-80
KS1	= KS1LO + KS1HI \$*CABLES TAUT, AND CONTACTS CHOCKS*		09-16-80
MKS1	= RSW(DXRPRC.LT.O.,AND,CABLES,MKS1F,O.)	\$*06-29-81*	
KS1	= KS1*(1. + MKS1*SGNF(DXRPRC))	\$*06-25-81*	
CS1	= CS1		09-17-80
	IF(TEST.EQ.10..OR.TEST.EQ.11.)GO TO A20A	\$*03-30-81*	
KS4	= O. + KS4HI \$*CABLES SLACK, BUT CONTACTS CHOCKS*		09-16-80
MKS4	= RSW(DXRPRC.LT.O.,AND,CABLES,MKS4F,O.)	\$*06-29-81*	
KS4	= KS4*(1. + MKS4*SGNF(DXRPRC))	\$*06-25-81*	
CS4	= CS4		09-17-80
	GO TO A20B		
A20A..	CONTINUE		
KS4	= KS4LO + KS4HI		
CS4	= CS4		
	GO TO A20B	\$*03-30-81*	
A20B..	CONTINUE		
MP	= WP*(1.-FRMP)/G		8-28-79
MRC	= (MRC+WP*FRMP)/G		8-28-79
	GO TO 50		8-01-79
30..	CONTINUE \$*NO MOVEMENT OF CASK ON CAR*		09-16-80
KS1	= KS1LO \$*CABLES TAUT, BUT NO CONTACT WITH CHOCKS*		09-16-80
MKS1	= RSW(XRPRC.GT.XRPLO,AND,XRPRC.LT.XRPHI,....		
	AND.DXRPRC.LT.O.,MKS1F,O.)	\$*06-25-81*	
MKS1	= RSW(DXRPRC.LT.O.,AND,CABLES,MKS1F,O.)	\$*06-29-81*	
KS1	= KS1*(1. + MKS1*SGNF(DXRPRC))	\$*06-25-81*	
CS1	= CS1		09-17-80
KS4	= KS4LO \$*CABLES TAUT, BUT NO CONTACT WITH CHOCKS*		09-16-80

```

MKS4 = RSW(XRPRC.GT.XRPLO.AND.XRPRC.LT.XRPHI....
      AND.DXRPRC.LT.O.,MKS4F,O.) $'06-25-81'
-----
MKS4 = RSW(DXRPRC.LT.O..AND.CABLES,MKS4F,O.) $'06-29-81'
KS4 = KS4*(1. + MKS4*SGNF(DXRPRC)) $'06-25-81'
-----
CS4 = CS4 09-17-80
MP = WP/G 8-28-79
MRC = WRC/G 8-26-79
GO TO 50 8-01-79
4C..CONTINUE $'CASK MOVES TOWARD REAR OF CAP' 09-16-80
IF (TEST.EQ.10..OR.TEST.EQ.11.)GO TO A40A $'03-30-81'
KS1 = O. $'CABLES SLACK, BUT NO CONTACT WITH CHOCKS' 09-16-80
MKS1 = RSW(XRPRC.GT.XRPLO.AND.XRPRC.LT.XRPHI....
      AND.DXRPRC.LT.O.,MKS1F,O.) $'06-25-81'
-----
MKS1 = RSW(DXRPRC.LT.O..AND.CABLES,MKS1F,O.) $'06-29-81'
KS1 = KS1*(1. + MKS1*SGNF(DXRPRC)) $'06-25-81'
-----
CS1 = O. 09-17-80
GO TO A40B
A40A..CONTINUE
KS1 = KS1O
CS1 = CS1
GO TO A40B
A40B..CONTINUE
KS4 = KS4LG $'CABLES TAUT,BUT NO CONTACT WITH CHOCKS' 09-16-80
MKS4 = RSW(XRPRC.GT.XRPLO.AND.XRPRC.LT.XRPHI....
      AND.DXRPRC.LT.O.,MKS4F,O.) $'06-25-81'
-----
MKS4 = RSW(DXRPRC.LT.O..AND.CABLES,MKS4F,O.) $'06-29-81'
KS4 = KS4*(1. + MKS4*SGNF(DXRPRC)) $'06-25-81'
-----
CS4 = CS4 09-17-80
MP = WP/G 8-28-79
MRC = WRC/G 8-28-79
5C..CONTINUE 8-01-79
END $'OF PROCEDURAL' 8-01-79
*-----EQUATION OF MOTION (ROTATIONAL ACCELERATION) $'05-15-80
D2THP = (+DUS1*ZP+DUS4*ZP-DUS2*LPR+DUS3*LPF-DWS1*ZP- ...
      DWS4*ZP+DWS2*LPR-DWS3*LPF+4*OMRCP)/IP 03-31-80
MOMRCP = MRC*D2XRC*HRC*SMRCP 04-07-80
*-----VELOCITIES $'05-15-80
DXP = INTEG(D2XP,VXPI)
DYP = INTEG(D2YP,VYPI)
DTHP = INTEG(D2THP,VTHPI)
*-----DISPLACEMENTS $'05-15-80
XP = INTEG(DXP,XPI)
YP = INTEG(DYP,YPI)
THP = INTEG(DTHP,THPI)
*-----PARAMETERS NEEDED FOR RESPONSE SPECTRA COMPUTATIONS $'06-26-80
USING THE *CARRS* MODEL $'06-26-80
*-----RHS FORCING FUNCTIONS $'06-26-80
RHSX = D2XRC - (ZRC*THRC + ZP*THP)*OMX**2 - (CS1 + CS4)*... 06-26-80
      (ZRC*DTHRC + ZP*DTHP)/MP 06-26-80
RHSY = D2YRC + (KS3*LCF-KS2*LCR)*THRC/MP+(KS2*LPR-KS3*LPF)...07-10-80
      *THP/MP+(CS3*LCF-CS2*LCR)*DTHRC/MP+... 07-10-80
      (CS2*LPR-CS3*LPF)*DTHP/MP 07-10-80
RHSTH = D2THRC+THRC*OMTH**2+ZTATH*DTHRC-RHSTHB 06-26-80
ZTATH = ((CS1+CS4)*ZP**2+CS2*LPR**2+CS3*LPF**2)/IP 06-26-80
RHSTHB = -(KS1+KS4)*ZP*((XRC+ZRC*THRC)-XP)+KS2*LPR*((YRC+... 06-26-80
      LRC*THRC)-YP)-KS3*LPF*((YRC-LCF*THRC)-YP)... 06-26-80
      -(CS1+CS4)*ZP*((DXRC+ZRC*DTHRC)-DXP)+CS2*LPR*((DYRC+...07-15-80

```

```

LCR*(LTHRC)-DYP)-CS3*LPF*((DYRC-LCF*DTHRC)-DYP))/IP 06-26-80
-----FREQUENCIES 06-26-80
O4X = SQRT((KS1+KS4)/MP) 06-26-80
OMY = SQRT((KS2+KS3)/MP) 06-26-80
OMTH = SQRT(((KS1+KS4)*ZP**2+KS2*LPR**2+KS3*LPF**2)/IP) 06-26-80
-----COMPARISONS OF ACCELERATIONS OF RAIL CAR 06-26-80
-----TO RHS FUNCIONS 06-26-80
RHSXA = RHSX-D2XRC 06-26-80
RHSYA = RHSY-D2YRC 06-26-80
RHSTA = RHSTH-D2THRC 06-26-80
FRHSX = D2XRC/RHSX 06-26-80
FRHSY = D2YRC/RHSY 06-26-80
FRHSTH = D2THRC/RHSTH 06-26-80
FRHSXA = 1.-FRHSX 06-26-80
FRHSYA = 1.-FRHSY 06-26-80
FRHSTA = 1.-FRHSTH 06-26-80
-----RELATIVE ACCELERATIONS 07-02-80
D2XD = D2XRC-D2XP 07-02-80
D2YD = D2YRC-D2YP 07-02-80
D2TD = D2THRC-D2THP 07-02-80
-----RAIL CAR OR TRANSPORTER 04-30-80
-----EQUATION OF MOTION (HORIZONTAL ACCELERATION) 05-15-80
D2XRC = (DUS1+DUS4-DUS5-DUS8-DUSCAR-DWS1-DWS4+DWS5+DWS8-...
DWP1-DWP4)/MRC
DUSCAR = RSW(EXPFRFC,DUSX4,KSCARS*(XRC-XF)) 11-13-79
TXCF = T + TLAGCF 7-19-79
D2XRCM = -DUSX4/MRC $*CASK AND TRUCKS DISCONNECTED FROM CAR 02-05-80
DUS5 = KS5*((XRC-ZRC*THRC)-XTR)
DUS8 = KS8*((XRC-ZRC*THRC)-XTF)
DWS5 = -CS5*((DXRC-ZRC*DTHRC)-DXTR)
DWS8 = -CS8*((DXRC-ZRC*DTHRC)-DXTF)
TDUSCR = INTEG(DUSCAR,0.) 9-06-79
TDUSX4 = INTEG(DUSX4,0.) 9-06-79
-----PROCEDURAL TO CALCULATE KSDG 04-30-80
PROCEDURAL (KMRCF,KSDG1,KSDG2,MUXT,ADXT=XT,DXT,KSDG10,KSDG20) 08-04-80
KMRCF = BOUND(KMRCFL,KMRCFU,KMFPCF(XT))
ADXT = RSW(XT,LT,XTU2,AND,XT,GT,XTL2,DXT,DXT-ADRCF) 8-17-79
MUXT = RSW(ADXT,GT,D.,MXRCFC,MXRCFE) 8-15-79
KSDG1 = KSDG10*KMRCF
KSDG1 = KSDG1*(1.+MUXT*SGNF(ADXT)) 8-15-79
KSDG2 = KSDG20*KMRCF
KSDG2 = KSDG2*(1.+MUXT*SGNF(ADXT)) 8-15-79
KSDG1 = RSW(RCOR,EQ.1.,KSDG10,KSDG1)
KSDG2 = RSW(FOR,EQ.1.,KSDG20,KSDG2)
END $ OF PROCEDURAL KSDG - RC TO F1
-----PROCEDURAL TO CALCULATE KSCARS 04-30-80
PROCEDURAL (KSCARS,KRCDG,KFDG = XT,DXT,KSDG2,KSDG1,ADXT) 8-15-79
IF (XT,LT,XTU1,AND,XT,GT,XTL1) GO TO 60 8-6-79
IF ((XT,LT,XTU2,AND,XT,GT,XTU1),OR,... 8-08-79
(XT,LT,XTL1,AND,XT,GT,XTL2)) GO TO 70 8-6-79
-----BOTH DRAFT GEARS BOTTOMED 05-29-80
KRCDG = KSDG1 8-6-79
-----CHANGE REQUIRED DUE TO SLACK IN TD-S 05-27-80
KRCDG = KSDG1 05-27-80
KFDG = KSDG2 8-6-79
KSCARS = KRCDG*KFDG/(KRCDG + KFDG) 8-6-79
GO TO 80 8-6-79

```

60..CONTINUE	\$*BOTH DRAFT GEARS ACTIVE*	C5-29-80
KRC DG	= K1*(1. + MUD*SGNF(ADXT))	8-15-79
KFDG	= KSDG20	8-6-79
KFDG	= K2*(1.+MUD*SGNF(ADXT))	11-16-79
KSCARS	= KRC DG	8-6-79
KSCARS	= KRC DG*KFDG/(KRC DG+KFDG)	11-16-79
GO TO 80		8-6-79
70..CONTINUE	\$*HAMMER CAR DG BOTTOMED. ANVIL CAR DG ACTIVE*	05-29-80
KRC DG	= KSDG10	8-6-79
	*-----CHANGE REQUIRED DUE TO SLACK IN ID-S	*05-27-80
KRC DG	= KSDG1	05-27-80
KFDG	= K2*(1. + MUD*SGNF(ADXT))	8-15-79
KSCARS	= KRC DG*KFDG/(KRC DG + KFDG)	8-6-79
80..CONTINUE		8-6-79
END \$*OF PROCEDURAL*		8-07-79
XT	= XPC-XF	
DXT	= DXRC-DXF	
	*-----EQUATION OF MOTION (VERTICAL ACCELERATION)	*05-15-80
D2YRC	= (DUS2+DUS3-DUS6-DUS7 -DWS2-DWS3-DWS6-DWS7+... DwCRF)/MRC	
DUS6	= KS6*(YRC+LRC*THRC)	
DUS7	= KS7*(YRC-LRC*THRC)	
DWRC	= WRC	
DWS6	= CS6*(DYRC+LRC*DTHRC)	
DWS7	= CS7*(DYRC-LRC*DTHRC)	
DwCRF	= FYRF	
	-----VERTICAL DISPLACEMENT OF COUPLER FACE AT STRUCK END	05-15-80
FYRF	= -WUCPL*SGNF(DYCPCL)*BTACPL*ABS(FCPL)**ALFACP	9-06-79
YCPCL	= YPC-LCPL*THRC	
DYCPCL	= DYRC-LCPL*DTHRC	
D2YCPCL	= D2YRC - LCPL*D2THRC	81-08-81
FCPL	= RSW(EX>FRC,DUS4,KSCARS*(XRC-XF))	11-13-79
	*-----	*05-15-80
	*-----EQUATION OF MOTION (ROTATIONAL ACCELERATION)	*05-15-80
D2THRC	= (DUS1*ZRC+DUS4*ZRC+DUS5*ZRC+DUS2*LCR-DUS3*LCF-... DUS6*LRC+DUS7*LRC+DUS8*ZPC-DWS1*ZRC-DWS2*LRC+... DWS3*LCF-DWS4*ZRC-DWS5*ZRC-DWS6*LRC+... DWS7*LRC-DWS8*ZRC-DwCRF*LCPL+MRCCG+MOMPRC)/IRC	83-28-80
MOMPRC	= MP*D2XP*HRC*SMPRC + KTHRC*THRC*SKTHRC	04-10-80
D2XRPC	= D2XP-D2XRC \$*RELATIVE ACCELERATION , PKG WRT CAR*	03-27-80
MRCCG	= (ZCDG0+LCPL*THRC)*DUSCAR	2-23-79
	*-----BENDING TERMS	*05-15-80
DUS12	= K12*THRC*(LCR+LCF)**2	
DUSR1	= KR1 *THRC*(LRC-LCR)**2	
DUSF1	= KF1 *THRC*(LRC+LCR)**2	
DUS31	= K31*THRC*LCR**2	
DUS23	= K23*THRC*LCF**2	
DUSR3	= KR3 *THRC*LRC**2	
DUSF3	= KF3 *THRC*LRC**2	
DUSR2	= KR2 *THRC*(LRC+LCF)**2	
DUSF2	= KF2 *THRC*(LRC+LCF)**2	
DWS12	= -CS12*DTHRC*(LCR+LCF)**2	
DWSR1	= -CSR1 *DTHRC*(LRC-LCR)**2	
DWSF1	= -CSF1 *DTHRC*(LRC+LCR)**2	
DWS31	= -CS31*DTHRC*LCR**2	
DWS23	= -CS23*DTHRC*LCF**2	
DWSR3	= -CSR3 *DTHRC*LRC**2	

```

D1SF3 = -CSF3 *DTHRC*LRC**2
D1SR2 = -CSR2 *DTHRC*(LRC+LCF)**2
D1SF2 = -CSF2 *DTHRC*(LRC-LCF)**2
-----*05-15-80
*-----INTEGRATED VELOCITIES AND DISPLACEMENTS *05-15-80
DXRC = INTEG(D2XRC,VXRCI)
XRC = INTEG(DXRC,XRCI)
DBLINT(YRC,DYRC=YRCI,D2YRC,VYRCI,YRCMAX,100.)
DBLINT(THRC,DTHRC=THRCI,D2THRC,VTHRCI,THRCLO,THRCI)
THRCI = (YRC-YRCMAX)/LRC
THRCLO = -THRCI
*-----REAR TRUCKS ON RAIL CAR OR TRANSPORTER *04-30-80
*-----EQUATION OF MOTION (HORIZONTAL ACCELERATION) *05-15-80
D2XTR = (DUS5-DWS5+DWCTR)/MTR
DWCTR = FXTR
FXTR = -MUTR*WXTR*SGNF(DXTR)*BRAKER
*-----PROCEDURAL TO CALCULATE KS5 * 10-17-80
PROCEDURAL(KS5=MK5) 10-17-80
KS5 = KS58F(XRCTR) 11-28-79
KS5 = KS58F(XRCTR)*MK5 10-17-80
END $ OF PROCEDURAL TO CALCULATE KS5 * 10-17-80
XRCTR = XRC-XTR+XTINIT 02-01-80
*-----INTEGRATED VELOCITIES AND DISPLACEMENTS *05-15-80
DXTR = INTEG(D2XTR,VXTRI)
XTR = INTEG(DXTR,XTRI)
*-----FRONT TRUCKS ON RAIL CAR OR TRANSPORTER *04-30-80
*-----EQUATION OF MOTION (HORIZONTAL ACCELERATION) *05-15-80
D2XTF = (DUS8-DWS8+DWCIF)/MIF
FXTF = -MUTF*WXTF*SGNF(DXTF)*BRAKEF
DWCIF = FXTF
*-----PROCEDURAL TO CALCULATE KS8 * 10-17-80
PROCEDURAL(KS8=MK8) 10-17-80
KS8 = KS58F(XRCTF) 11-28-79
KS8 = KS58F(XRCTF)*MK8 10-17-80
END $ OF PROCEDURAL TO CALCULATE KS8 * 10-17-80
XRCTF = XRC-XTF+XTINIT 02-01-80
*-----INTEGRATED VELOCITIES AND DISPLACEMENTS *05-15-80
DXTF = INTEG(D2XTF,VXTFI)
XTF = INTEG(DXTF,XTFI)
*-----FIRST ANVIL CAR *04-30-80
*-----EQUATION OF MOTION (HORIZONTAL ACCELERATION) *05-15-80
D2XF = (DUSCAR-DUFF2+DWCFF)/MFF
DWCFF = -MUFF*WFF*SGNF(DXF)*BRKIRC
DUFF2 = KFF2*(XF-XF2)
KFF2 = KFDGR*KF2DGF/(KF2DGF+KFDGR)
*-----PROCEDURAL TO CALCULATE KSFF2 *04-30-80
PROCEDURAL(KMFF2,KSFF21,KSFF22,MUXT12,ADXT12=XT12,DXT12,KSF210,KSF220) 08-04-80
KMFF2 = BOUND(KMFF2L,KMFF2U,KMFF2F(XT12))
ADXT12 = DXT12 - AD12 8-15-79
ADXT12 = RSW(XT12,LT,XT12U,AND,XT12,GT,XT12L,DXT12,DXT12-AD12) 8-17-79
MUXT12 = RSW(ADXT12,GT,0.,MXT12C,MXT12E) 8-15-79
KSFF21 = KSF210*KMFF2
KSFF21 = KSFF21*(1.+MUXT12*SGNF(ADXT12)) 8-15-79
KSFF22 = KSF220*KMFF2
KSFF22 = KSFF22*(1.+MUXT12*SGNF(ADXT12)) 8-15-79
KSFF21 = RSW(FOR,EQ,1.,KSF210,KSFF21)
KSFF22 = RSW(F2OR,EQ,1.,KSF220,KSFF22)

```

```

END 5*OF PROCEDURAL KSFF2 - F1 TO F2*
KF2DGF = RSW(XT12.LT.XT12U.AND.XT12.GT.XT12L,K2FF2*(1.+...
MUFF2*SGNF(ADXT12)),KSFF22) 8-15-79
XT12 = XF-XF2
DXF2 = DXF-DXF2
KFDGR = RSW(XT12.LT.XT12U.AND.XT12.GT.XT12L,K1FF2*(1.+...
MUFF1*SGNF(ADXT12)),KSFF21) 8-15-79
*-----INTEGRATED VELOCITIES AND DISPLACEMENTS *05-15-80
DXF = INTEG(D2XF,VXF1)
XF = INTEG(DXF,XF1)
*-----SECOND ANVIL CAR *04-30-80
*-----EQUATION OF MOTION (HORIZONTAL ACCELERATION) *05-15-80
D2XF2 = (DUFF2-DUF2F3+DWFF2)/MF2
DUF2F3 = KF2F3*(XF2-XF3)
DWFF2 = -MUF2*WF2*SGNF(DXF2)*BRKF2
KF2F3 = KF2DGR*KF3DGF/(KF3DGF+KF2DGR)
*-----PROCEDURAL TO CALCULATE KSF23 *04-30-80
PROCEDURAL(KMF23,KSF231,KSF232,MUXT23,ADXT23=XT23,DXT23,KS2310,KS2320) 08-04-80
KMF23 = BOUND(KMF23L,KMF23U,KMF23F(XT23))
ADXT23 = DXT23-AD23
ADXT23 = RSW(XT23.LT.XT23U.AND.XT23.GT.XT23L,DXT23,DXT23-AD23) 8-17-79
MUXT23 = RSW(ADXT23.GT.0.,MXT23C,MXT23E) 8-15-79
KSF231 = KS2310*KMF23
KSF231 = KSF231*(1.+MUXT23*SGNF(ADXT23)) 8-15-79
KSF232 = KS2320*KMF23
KSF232 = KSF232*(1.+MUXT23*SGNF(ADXT23)) 8-15-79
KSF231 = RSW(F2OR.EQ.1.,KS2310,KSF231)
KSF232 = RSW(F3OR.EQ.1.,KS2320,KSF232)
END 5*OF PROCEDURAL KSF23 - F2 TO F3*
KF3DGF = RSW(XT23.LT.XT23U.AND.XT23.GT.XT23L,K2F2F3*(1.+...
MUF232*SGNF(ADXT23)),KSF232) 8-16-79
XT23 = XF2-XF3
DXT23 = DXF2-DXF3
KF2DGR = RSW(XT23.LT.XT23U.AND.XT23.GT.XT23L,K1F2F3*(1.+...
MUF231*SGNF(ADXT23)),KSF231) 8-16-79
*-----INTEGRATED VELOCITIES AND DISPLACEMENTS *05-15-80
DXF2 = INTEG(D2XF2,VXF21)
XF2 = INTEG(DXF2,XF21)
*-----THIRD ANVIL CAR *04-30-80
*-----EQUATION OF MOTION (HORIZONTAL ACCELERATION) *05-15-80
D2XF3 = (DUF2F3-DUF3F4+DWFF2F3)/MF3
DUF3F4 = KF3F4*(XF3-XF4)
DWFF2F3 = -MUF3*WF3*SGNF(DXF3)*BRKF3
KF3F4 = KF3DGR*KF4DGF/(KF4DGF+KF3DGR)
*-----PROCEDURAL TO CALCULATE KSF34 *04-30-80
PROCEDURAL(KMF34,KSF341,KSF342,MUXT34,ADXT34=XT34,DXT34,KS3410,KS3420) 08-04-80
KMF34 = BOUND(KMF34L,KMF34U,KMF34F(XT34))
ADXT34 = DXT34-AD34
ADXT34 = RSW(XT34.LT.XT34U.AND.XT34.GT.XT34L,DXT34,DXT34-AD34) 8-17-79
MUXT34 = RSW(ADXT34.GT.0.,MXT34C,MXT34E) 8-15-79
KSF341 = KS3410*KMF34
KSF341 = KSF341*(1.+MUXT34*SGNF(ADXT34)) 8-15-79
KSF342 = KS3420*KMF34
KSF342 = KSF342*(1.+MUXT34*SGNF(ADXT34)) 8-15-79
KSF341 = RSW(F3OR.EQ.1.,KS3410,KSF341)
KSF342 = RSW(F4OR.EQ.1.,KS3420,KSF342)
END 5*OF PROCEDURAL KSF34 - F3 TO F4*

```

KF3DGR = RSW(XT34.LT.XT34U.AND.XT34.GT.XT34L,K1F3F4*(1.+... MUF341*SGNF(ADXT34)),KSF341)	8-15-79
KF4DGF = RSW(XT34.LT.XT34U.AND.XT34.GT.XT34L,K2F3F4*(1.+... MUF342*SGNF(ADXT34)),KSF342)	8-15-79
XT34 = XF3-XF4	
DXT34 = DXF3-DXF4	
*-----INTEGRATED VELOCITIES AND DISPLACEMENTS	
DXF3 = INTEG(D2XF3,VXF3I)	*05-15-80
XF3 = INTEG(DXF3,XF3I)	
*-----FOURTH ANVIL CAR	
*-----EQUATION OF MOTION (HORIZONTAL ACCELERATION)	
D2XF4 = (DUF3F4+DWF3F4)/MF4	*05-15-80
DWF3F4 = -MUF4*WF4*SGNF(DXF4)*BRKF4	
*-----INTEGRATED VELOCITIES AND DISPLACEMENTS	
DXF4 = INTEG(D2XF4,VXF4I)	*05-15-80
XF4 = INTEG(DXF4,XF4I)	
*-----PARAMETER INFLUENCE COEFFICIENTS	
*-----AUXILIARY EQUATIONS	
X2PRC = XP-XRC	
THRPRC = THRC - THP	12-1-77
YP12 = YP+LPR*THP \$*REAR PKG TO POINT*	
DYP12 = YP+LPR*DTHP	
D2YP12 = D2YP+LPR*D2THP	
DYP12X = INTEG(D2P12X,0.)	04-21-80
YP12X = INTEG(DYP12X,0.)	04-21-80
DYP34X = INTEG(D2P34X,0.)	04-21-80
YP34X = INTEG(DYP34X,0.)	04-21-80
YP34 = YP-LPF*THP \$*FRONT PKG TO POINT*	
DYP34 = DYP-LPF*DTHP	
D2YP34 = D2YP-LPF*D2THP	
YRC12 = YRC+LCR*THRC \$*REAR RAIL CAR TO POINT*	
DYRC12 = YRC+LCR*DTHRC	
D2YR12 = D2YRC+LCR*D2THRC	
DYR12X = INTEG(D2R12X,0.)	01-08-81
YR12X = INTEG(DYR12X,0.)	01-08-81
DYR12T = INTEG(D2R12T,0.)	01-12-81
YR12T = INTEG(DYR12T,0.)	01-12-81
YRC34 = YRC-LCF*THRC \$*FRONT RAIL CAR TO POINT*	
DYRC34 = DYRC-LCF*DTHRC	
D2YR34 = D2YRC-LCF*D2THRC	
DYRC56 = DYRC+LRC*DTHRC	
D2YR56 = D2YRC+LRC*D2THRC	
DYR56X = INTEG(D2R56X,0.)	01-08-81
YR56X = INTEG(DYR56X,0.)	01-08-81
DYCPLX = INTEG(D2CPLX,0.)	01-08-81
YCPLX = INTEG(DYCPLX,0.)	01-08-81
DYCPLT = INTEG(D2CPLT,0.)	01-12-81
YCPLT = INTEG(DYCPLT,0.)	01-12-81
DYRC78 = DYRC-LRC*DTHRC	
D2YR78 = D2YRC-LRC*D2THRC	
-----INTEGRATION STEP SIZE	
DT = .AMAX1(HINT,AMIN1(MAXT,CINT/NSTP))	04-28-80
-----STABILITY CRITERION, EOM FOR D2YRC	
SUMKY = KS2 + KS3 + KS6 + KS7	04-28-80
DTYRC = SQRT(2.*MRC/SUMKY)	04-28-80
SUMC1 = CS2 + CS3 + CS6 + CS7	04-30-80
DTYRC2 = 2.*MRC/SUMC1	04-30-80

```

-----STABILITY CRITERION, EOM FOR D2THRC*      04-28-80
SUMKTH = ((KS1 + KS4 + KS5 + KS8)*ZRC**2) + (KS2 *LCR**2) + ... 04-28-80
          (KS3*LCF**2) + ((KS6 + KS7)*LRC**2) - (LCPL*DUSCAR) 04-28-80
DTHRC = SORT(2.*IRC/SUMKTH)                          04-28-80
SUMC2 = ((CS1+CS4+CS5+CS8)*ZRC**2) + (CS2*LCR**2) + ... 04-30-80
          (CS3*LCF**2) + ((CS6+CS7)*LRC**2)              04-30-80
DTHC2 = 2.*IRC/SUMC2                                  04-30-80
MAXTERVAL MAXT=.001
END $ OF DERIVATIVE*
*-MODEL VALIDATION                                     *04-30-80
-----CALCULATION OF THEILS COEFFICIENTS          *04-30-80
N          = N+1.                                     11-29-79
S13        = S13 + DUSCAR**2                          11-29-79
S13X       = S13X + DUSX4**2                          11-29-79
SD13       = SD13 + (DUSCAR-DUSX4)**2                 11-29-79
TIC13      = SORT(SD13/N)/(SQRT(S13/N)+SQRT(S13X/N)) 11-29-79
S14        = S14 + DUSLF**2                          11-29-79
S14X       = S14X + DUSLFX**2                        11-29-79
SD14       = SD14 + (DUSLF-DUSLFX)**2                 11-29-79
TIC14      = SORT(SD14/N)/(SQRT(S14/N)+SQRT(S14X/N)) 11-30-79
S53        = S53 + D2XP**2                            12-11-79
S53X       = S53X + D2XPX**2                         12-11-79
SD53       = SD53 + (D2XP-D2XPX)**2                  12-11-79
TIC53      = SORT(SD53/N)/(SQRT(S53/N)+SQRT(S53X/N)) 12-11-79
S54        = S54 + D2XRC**2                          11-29-79
S54X       = S54X + D2XRCX**2                       11-29-79
SD54       = SD54 + (D2XRC-D2XRCX)**2                 11-29-79
TIC54      = SORT(SD54/N)/(SQRT(S54/N)+SQRT(S54X/N)) 11-29-79
S60        = S60 + D2YP12**2                          11-29-79
S60X       = S60X + D2P12X**2                       11-29-79
SD60       = SD60 + (D2YP12-D2P12X)**2               11-29-79
TIC60      = SORT(SD60/N)/(SQRT(S60/N)+SQRT(S60X/N)) 11-29-79
S61        = S61 + D2YP34**2                          12-11-79
S61X       = S61X + D2P34X**2                       12-11-79
SD61       = SD61 + (D2YP34-D2P34X)**2               12-11-79
TIC61      = SORT(SD61/N)/(SQRT(S61/N)+SQRT(S61X/N)) 12-11-79
PP13       = SORT(S13/N)                              11-29-79
PX13       = SORT(S13X/N)                            11-29-79
PP14       = SORT(S14/N)                              11-29-79
PX14       = SORT(S14X/N)                            11-29-79
PP53       = SORT(S53/N)                              12-11-79
PX53       = SORT(S53X/N)                            12-11-79
PP54       = SORT(S54/N)                              11-29-79
PX54       = SORT(S54X/N)                            11-29-79
PP60       = SORT(S60/N)                              11-29-79
PX60       = SORT(S60X/N)                            11-29-79
PP61       = SORT(S61/N)                              12-11-79
PX61       = SORT(S61X/N)                            12-11-79
DEN        = (PP13+PX13+...                          12-11-79
             PP14+PX14+...                          12-11-79
             PP53+PX53+...                          12-11-79
             PP54+PX54+...                          12-11-79
             PP61+PX61+...                          12-11-79
             PP60+PX60)                              12-11-79
NUM        = (PP13+PX13)*TIC13+...                  12-11-79
             (PP14+PX14)*TIC14+...                  12-11-79
             (PP53+PX53)*TIC53+...                  12-11-79

```

(PP54+PX54)*TIC54+...	12-11-79
(PP60+PX60)*TIC60+...	12-11-79
(PP61+PX61)*TIC61	12-11-79
TMIC = NUM/DEN	11-29-79
*-----CALCULATION OF PROBABILITIES	
THE FOLLOWING R VALUES MAY BE ANY SUITABLE COMPARISON FUNCTION	*04-30-80
R13 = DUSCAR	04-16-80
R14 = DUSLF	04-16-80
R53 = D2XP	04-16-80
R54 = D2XRC	04-16-80
R60 = D2YP12	04-16-80
R61 = D2YP34	04-16-80
R13X = DUSX4	04-16-80
R14X = DUSLFX	04-16-80
R53X = D2XPX	04-16-80
R54X = D2XRCX	04-16-80
R60X = D2P12X	04-16-80
R61X = D2P34X	04-16-80
SR13 = SR13 + R13	04-14-80
SR14 = SR14 + R14	04-14-80
SR53 = SR53 + R53	04-14-80
SR54 = SR54 + R54	04-14-80
SR60 = SR60 + R60	04-14-80
SR61 = SR61 + R61	04-14-80
SR13X = SR13X + R13X	04-16-80
SR14X = SR14X + R14X	04-16-80
SR53X = SR53X + R53X	04-16-80
SR54X = SR54X + R54X	04-16-80
SR60X = SR60X + R60X	04-16-80
SR61X = SR61X + R61X	04-16-80
*-----EXPECTED VALUE, MEAN OR MU	
ER13 = SR13/N	*04-30-80
ER14 = SR14/N	04-14-80
ER53 = SR53/N	04-14-80
ER54 = SR54/N	04-14-80
ER60 = SR60/N	04-14-80
ER61 = SR61/N	04-14-80
ER13X = SR13X/N	04-16-80
ER14X = SR14X/N	04-16-80
ER53X = SR53X/N	04-16-80
ER54X = SR54X/N	04-16-80
ER60X = SR60X/N	04-16-80
ER61X = SR61X/N	04-16-80
NNH = INT(N)	04-11-80
NN = NN+1	04-11-80
XR13(NN) = R13	04-11-80
XR14(NN) = R14	04-11-80
XR53(NN) = R53	04-11-80
XR54(NN) = R54	04-11-80
XR60(NN) = R60	04-11-80
XR61(NN) = R61	04-11-80
XR13X(NN) = R13X	04-16-80
XR14X(NN) = R14X	04-16-80
XR53X(NN) = R53X	04-16-80
XR54X(NN) = R54X	04-16-80
XR60X(NN) = R60X	04-16-80
XR61X(NN) = R61X	04-16-80

-----RHS FORCING FUNCTIONS FOR RESPONSE SPECTRA CALCNS		*06-26-80
ACS2(NN)	= CS2	07-01-80
ARHSX(NN)	= RHSX	06-26-80
ARHSY(NN)	= RHSY	06-26-80
ARHSTH(NN)	= RHSTH	06-26-80
ATH(NN)	= T	06-26-80
ADUS1(NN)	= DUS1	09-11-80
ADUS2(NN)	= DUS2	09-11-80
ADUS3(NN)	= DUS3	09-11-80
ADUS4(NN)	= DUS4	09-11-80
XXM	= AMAX1(XXM,XP,XRC,XTR,XTF,XF)	
XMN	= AMIN1(XMN,XP,XRC,XTR,XTF,XF)	
YMX	= AMAX1(YMX,YP,YRC)	
YMN	= AMIN1(YMN,YP,YRC)	
THMX	= AMAX1(THMX,THP,THRC)	
THMN	= AMIN1(THMN,THP,THRC)	
DXMX	= AMAX1(DXMX,DXP,DXRC,DXTR,DXTF,DXF)	
DXMN	= AMIN1(DXMN,DXP,DXRC,DXTR,DXTF,DXF)	
DYMX	= AMAX1(DYMX,DYP,DYRC)	
DYMN	= AMIN1(DYMN,DYP,DYRC)	
DTHMX	= AMAX1(DTHMX,DTHP,DTHRC)	
DTHMN	= AMIN1(DTHMN,DTHP,DTHRC)	
D2XXM	= AMAX1(D2XXM,D2XP,D2XRC,D2XTR,D2XTF,D2XF,... D2XRCX,D2XPX)	01-25-80 01-25-80
D2XMN	= AMIN1(D2XMN,D2XP,D2XRC,D2XTR,D2XTF,D2XF,... D2XRCX,D2XPX)	01-25-80 01-25-80
D2YMX	= AMAX1(D2YMX,D2YP,D2YRC)	
D2YMN	= AMIN1(D2YMN,D2YP,D2YRC)	
D2THMX	= AMAX1(D2THMX,D2THP,D2THRC)	
D2THMN	= AMIN1(D2THMN,D2THP,D2THRC)	
XXRMX	= AMAX1(XXRMX,XXRPRC,XXRRCF,XXRCTR,XXRCTF)	
XXRMN	= AMIN1(XXRMN,XXRPRC,XXRRCF,XXRCTR,XXRCTF)	
YMX2	= AMAX1(YMX2,YP12,YP12X,YP34,YP34X,YRC12,YRC34,YRC56,... YRC78,YCPLX,YCPL,YR12X,YR56X)	05-08-80 01-08-81
YMN2	= AMIN1(YMN2,YP12,YP12X,YP34,YP34X,YRC12,YRC34,YRC56,... YRC78,YCPLX,YCPL,YR12X,YR56X)	05-08-80 01-08-81
DYMX2	= AMAX1(DYMX2,DYP12,DYP12X,DYP34,DYP34X,DYRC12,... DYRC34,DYRC56,DYRC78)	05-08-80 05-08-80
DYMN2	= AMIN1(DYMN2,DYP12,DYP12X,DYP34,DYP34X,DYRC12,... DYRC34,DYRC56,DYRC78)	05-08-80 05-08-80
D2YMX2	= AMAX1(D2YMX2,D2YP12,D2YP34,D2YR12,D2YR34,D2YR56,... D2YR78,D2P12X,D2P34X,D2CPLX,D2YCPL,... D2R12X,D2R56X)	01-08-81 01-08-81
D2YMN2	= AMIN1(D2YMN2,D2YP12,D2YP34,D2YR12,D2YR34,D2YR56,... D2YR78,D2P12X,D2P34X,D2CPLX,D2YCPL,... D2R12X,D2R56X)	01-08-81 01-08-81
DTMAX	= AMAX1(DTMAX,DT,DTYRC,DTTHRC)	
DTMIN	= AMIN1(DTMIN,DT,DTYRC,DTTHRC)	04-30-80
FCPLMX	= AMAX1(FCPLMX,DUSCAR,DUFF2,DUF2F3,DUF3F4)	
FCPLMN	= AMIN1(FCPLMN,DUSCAR,DUFF2,DUF2F3,DUF3F4)	
TERMT(T,GE,TSTOP)		04-15-80
END 5 OF DYNAMIC TERMINAL		
-----ROUNDING OFF MAX AND MIN VALUES FOR USE		*04-30-80
ON PLOTS SCALES		*04-30-80
SCALE(XMN,XXM=XMN,XXM)		
SCALE(YMN,YYM=YMN,YYM)		

```

SCALE (THMN,THMX=THMN,THMX)
SCALE (DXMN,DXMX=DXMN,DXMX)
SCALE (DYMN,DYMX=DYMN,DYMX)
SCALE (DTHMN,DTHMX=DTHMN,DTHMX)
SCALE (DZXMN,DZMX=DZXMN,DZMX)
SCALE (DZYMN,DZYM=DZYMN,DZYM)
SCALE (D2THMN,D2THMX=D2THMN,D2THMX)
SCALE (XRMN,XRMX=XRMN,XRMX)
SCALE (YMN2,YMX2=YMN2,YMX2)
SCALE (DYMN2,DYMX2=DYMN2,DYMX2)
SCALE (D2YMN2,D2YMX2=D2YMN2,D2YMX2)
SCALE (DTMIN,DTMAX=DTMIN,DTMAX)
SCALE (FCPLMN,FCPLMX=FCPLMN,FCPLMX)
*-----CALCULATION OF PROBABILITIES
*-----CALCULATION OF VARIANCE
VN = 0
T2..CONTINUE
NN = NN + 1
SVR13 = SVR13 + (XR13(NN)-ER13)**2
SVR14 = SVR14 + (XR14(NN)-ER14)**2
SVR53 = SVR53 + (XR53(NN)-ER53)**2
SVR54 = SVR54 + (XR54(NN)-ER54)**2
SVR61 = SVR61 + (XR61(NN)-ER61)**2
SVR13X = SVR13X + (XR13X(NN)-ER13X)**2
SVR14X = SVR14X + (XR14X(NN)-ER14X)**2
SVR53X = SVR53X + (XR53X(NN)-ER53X)**2
SVR54X = SVR54X + (XR54X(NN)-ER54X)**2
SVR60X = SVR60X + (XR60X(NN)-ER60X)**2
SVR61X = SVR61X + (XR61X(NN)-ER61X)**2
*-----THE VARIANCE IS THE SQUARE OF THE STD DEVIATION, SIGMA**2*
*-----VRXX = SIGMA**2*
VR13 = RSW(SVR13.EQ.0.,EPSR,SVR13/NN)
VR14 = RSW(SVR14.EQ.0.,EPSR,SVR14/NN)
VR53 = RSW(SVR53.EQ.0.,EPSR,SVR53/NN)
VR54 = RSW(SVR54.EQ.0.,EPSR,SVR54/NN)
VR60 = RSW(SVR60.EQ.0.,EPSR,SVR60/NN)
VR61 = RSW(SVR61.EQ.0.,EPSR,SVR61/NN)
VR13X = RSW(SVR13X.EQ.0.,EPSR,SVR13X/NN)
VR14X = RSW(SVR14X.EQ.0.,EPSR,SVR14X/NN)
VR53X = RSW(SVR53X.EQ.0.,EPSR,SVR53X/NN)
VR54X = RSW(SVR54X.EQ.0.,EPSR,SVR54X/NN)
VR60X = RSW(SVR60X.EQ.0.,EPSR,SVR60X/NN)
VR61X = RSW(SVR61X.EQ.0.,EPSR,SVR61X/NN)
IF (NN.LT.NNH) GO TO T2
NN = 0
AR13 = 1./SQRT(2.*PI*VR13)
AR14 = 1./SQRT(2.*PI*VR14)
AR53 = 1./SQRT(2.*PI*VR53)
AR54 = 1./SQRT(2.*PI*VR54)
AR60 = 1./SQRT(2.*PI*VR60)
AR61 = 1./SQRT(2.*PI*VR61)
AR13X = 1./SQRT(2.*PI*VR13X)
AR14X = 1./SQRT(2.*PI*VR14X)
AR53X = 1./SQRT(2.*PI*VR53X)
AR54X = 1./SQRT(2.*PI*VR54X)
AR60X = 1./SQRT(2.*PI*VR60X)
AR61X = 1./SQRT(2.*PI*VR61X)

```

LINES(7) 5*INFORMS SYSTEM ABOUT TO PRINT 7 LINES*	04-17-80
PRINT 98,ER13,ER14,ER53,ER54,ER60,ER61,VR13,VR14,VR53,...	04-15-80
VR54,VR60,VR61,AR13,AR14,AR53,AR54,AR60,AR61,...	04-16-80
ER13X,ER14X,ER53X,ER54X,ER60X,ER61X,...	04-16-80
VR13X,VR14X,VR53X,VR54X,VR60X,VR61X,...	04-16-80
AR13X,AR14X,AR53X,AR54X,AR60X,AR61X	04-16-80
96..FORMAT(3X,'ER13=',E12.4,3X,'ER14=',E12.4,3X,'ER53=',E12.4,...	04-17-80
3X,'ER54=',E12.4,3X,'ER60=',E12.4,3X,'ER61=',E12.4/...	04-17-80
3X,'VR13=',E12.4,3X,'VR14=',E12.4,3X,'VR53=',E12.4,3X,...	04-17-80
'VR54=',E12.4,3X,'VR60=',E12.4,3X,'VR61=',E12.4/...	04-17-80
3X,'AR13=',E12.4,3X,'AR14=',E12.4,3X,'AR53=',E12.4,3X,...	04-17-80
'AR54=',E12.4,3X,'AR60=',E12.4,3X,'AR61=',E12.4/...	04-17-80
3X,'ER13X=',E12.4,3X,'ER14X=',E12.4,3X,'ER53X=',E12.4,3X,...	04-17-80
'ER54X=',E12.4,3X,'ER60X=',E12.4,3X,'ER61X=',E12.4/...	04-17-80
3X,'VR13X=',E12.4,3X,'VR14X=',E12.4,3X,'VR53X=',E12.4,3X,...	04-17-80
'VR54X=',E12.4,3X,'VR60X=',E12.4,3X,'VR61X=',E12.4/...	04-17-80
3X,'AR13X=',E12.4,3X,'AR14X=',E12.4,3X,'AR53X=',E12.4,3X,...	04-17-80
'AR54X=',E12.4,3X,'AR60X=',E12.4,3X,'AR61X=',E12.4/...	04-18-80
T1..CONTINUE	04-11-80
NN = NN + 1	04-11-80
-----PROBABILITIES	04-15-80
FXR13(NN) = AR13*EXP((-1.*(XR13(NN)-ER13)**2)/(2.*VR13))	04-15-80
FXR14(NN) = AR14*EXP((-1.*(XR14(NN)-ER14)**2)/(2.*VR14))	04-15-80
FXR53(NN) = AR53*EXP((-1.*(XR53(NN)-ER53)**2)/(2.*VR53))	04-15-80
FXR54(NN) = AR54*EXP((-1.*(XR54(NN)-ER54)**2)/(2.*VR54))	04-15-80
FXR60(NN) = AR60*EXP((-1.*(XR60(NN)-ER60)**2)/(2.*VR60))	04-15-80
FXR61(NN) = AR61*EXP((-1.*(XR61(NN)-ER61)**2)/(2.*VR61))	04-15-80
FXR13X(NN) = AR13X*EXP((-1.*(XR13X(NN)-ER13X)**2)/(2.*VR13X))	04-16-80
FXR14X(NN) = AR14X*EXP((-1.*(XR14X(NN)-ER14X)**2)/(2.*VR14X))	04-16-80
FXR53X(NN) = AR53X*EXP((-1.*(XR53X(NN)-ER53X)**2)/(2.*VR53X))	04-16-80
FXR54X(NN) = AR54X*EXP((-1.*(XR54X(NN)-ER54X)**2)/(2.*VR54X))	04-16-80
FXR60X(NN) = AR60X*EXP((-1.*(XR60X(NN)-ER60X)**2)/(2.*VR60X))	04-16-80
FXR61X(NN) = AR61X*EXP((-1.*(XR61X(NN)-ER61X)**2)/(2.*VR61X))	04-16-80
R13 = XR13(NN)	04-11-80
R14 = XR14(NN)	04-11-80
R53 = XR53(NN)	04-11-80
R54 = XR54(NN)	04-11-80
R60 = XR60(NN)	04-11-80
R61 = XR61(NN)	04-11-80
R13X = XR13X(NN)	04-16-80
R14X = XR14X(NN)	04-16-80
R53X = XR53X(NN)	04-16-80
R54X = XR54X(NN)	04-16-80
R60X = XR60X(NN)	04-16-80
R61X = XR61X(NN)	04-16-80
FR13 = FXR13(NN)	04-11-80
FR14 = FXR14(NN)	04-11-80
FR53 = FXR53(NN)	04-11-80
FR54 = FXR54(NN)	04-11-80
FR60 = FXR60(NN)	04-11-80
FR61 = FXR61(NN)	04-11-80
FR13X = FXR13X(NN)	04-16-80
FR14X = FXR14X(NN)	04-16-80
FR53X = FXR53X(NN)	04-16-80
FR54X = FXR54X(NN)	04-16-80
FR60X = FXR60X(NN)	04-16-80
FR61X = FXR61X(NN)	04-16-80

```

*-----PRINT FINAL INFO ON PROBABILITIES *04-30-80
LINES(7) $*INFORMS SYSTEM ABOUT TO PRINT 7 LINES* 04-17-80
PRINT 99,NN,R13,FR13,R13X,FR13X,... 04-16-80
      R14,FR14,R14X,FR14X,... 04-16-80
      R53,FR53,R53X,FR53X,... 04-16-80
      R54,FR54,R54X,FR54X,... 04-16-80
      R60,FR60,R60X,FR60X,... 04-16-80
      R61,FR61,R61X,FR61X 04-16-80
99..FORMAT(5X,'NN=',I4,5X,'R13=',E12.4,5X,'FR13=',E12.4,5X,'R13X=',...04-16-80
      E12.4,5X,'FR13X=',E12.4//... 04-16-80
      17X,'R14=',E12.4,5X,'FR14=',E12.4,5X,'R14X=',E12.4,5X,... 04-16-80
      'FR14X=',E12.4//... 04-16-80
      17X,'R53=',E12.4,5X,'FR53=',E12.4,5X,'R53X=',E12.4,5X,... 04-16-80
      'FR53X=',E12.4//... 04-16-80
      17X,'R54=',E12.4,5X,'FR54=',E12.4,5X,'R54X=',E12.4,5X,... 04-16-80
      'FR54X=',E12.4//... 04-16-80
      17X,'R60=',E12.4,5X,'FR60=',E12.4,5X,'R60X=',E12.4,5X,... 04-16-80
      'FR60X=',E12.4//... 04-16-80
      17X,'R61=',E12.4,5X,'FR61=',E12.4,5X,'R61X=',E12.4,5X,... 04-16-80
      'FR61X=',E12.4//) 04-16-80
*-----FORCING FUNCTIONS FOR RESPONSE SPECTRA CALCs *06-26-80
CS2 = ACS2(NN) 07-01-80
RHSX = ARHSX(NN) 06-26-80
RHSY = ARHSY(NN) 06-26-80
RHSTH = ARHSTH(NN) 06-26-80
T = ATM(NN) 06-26-80
DUS1 = ADUS1(NN) 09-11-80
DUS2 = ADUS2(NN) 09-11-80
DUS3 = ADUS3(NN) 09-11-80
DUS4 = ADUS4(NN) 09-11-80
LINES(2) $*INFORMS SYSTEM ABOUT TO WRITE 2 LINES* 06-26-80
WRITE(26,100) T,RHSX,RHSY,RHSTH,CS2,DUS1,DUS2,DUS3,DUS4 09-11-80
100..FORMAT(5E12.4/4E12.4) 09-11-80
      IF(NN.LT.NNH)GO TO T1 04-14-80
      GO TO T998 03-11-81
T998..CONTINUE 03-10-81
      LINES(1) $*PRINT 1 LINE* 03-11-81
      WRITE(6,101) 03-11-81
101..FORMAT(1X,26HINDICATED TEST NOT ON LIST) 03-11-81
T998..CONTINUE 03-11-81
END $*OF TERMINAL*
END $*OF PROGRAM*

```

```

SET TITLE = 'PRELIMINARY DYNAMIC MODEL OF CASK-RAILCAR SYSTEM'
SET RRR = 98
*SET UP FOR DEBUG LIST OF ALL VARIABLES WHEN T=0.02*
ACTION 'VAR'=0.02,'VAL'=1,'LOC'=NDEBUG
OUTPUT T,...
ADXT,...
ADXT12,...
ADXT23,...
..
..
..
* SET OF VARIABLES TO BE PRINTED OUT*
..
..
..
YRPRC,...
YR12T ,...
YR12X , ...
YR56X , ...
ZTATH ,...
ZEND
PREPAR T,...
ADXT,...
ADXT12,...
ADXT23,...
ADXT34,...
DTHMN,...
..
..
..
* SET OF VARIABLES TO BE PLOTTED*
..
..
..
ZTATH ,...
KS1,...
KS4,...
DXRPRC,...
ZNDCRD
START
RANGE XP,XRC,XTR,XTF,XF,YP,YRC,THP,THRC
RANGE XRPRC,XRRCF,XRCTR,XRCTF,YRPRC,THPPRC
RANGE DXP,DXRC,DXTR,DXTF,DXF,DYP,DYRC,DTHP,DTHRC
RANGE D2XP,D2XRC,D2XTR,D2XTF,D2XF,D2YP,D2YRC,D2THP,D2THRC,...
D2XRCX,D2XPX
RANGE YP12,YP34,YRC12,YRC34,YRC56,YRC78
RANGE YCPL
RANGE D2XRCH,DLTY12
RANGE D2DY12,D2DY34
RANGE OMY12,OMY34
RANGE YP12,YP12X,YP34,YP34X
RANGE DYP12,DYP34,DYRC12,DYRC34,DYRC56,DYRC78
RANGE D2YP12,D2YP34,D2YR12,D2YR56,D2YR78,D2P12X,D2P34X,D2YR34
RANGE D2X,D2YD,D2THD
RANGE XF2,XF3,XF4,XT,XT12,XT23,XT34

```

```

08-04-80
08-04-80
8-15-79
8-15-79
8-15-79
01-12-81
01-08-81
01-08-81
06-26-80
8-17-79
8-17-79
8-17-79
8-17-79
06-26-80
01-25-80
01-25-80
9-02-79
05-05-80
06-02-80
06-02-80
05-05-80
01-25-80
07-02-80

```

RANGE DXF2,DXF3,D7F4,DXT,DXT12,DXT23,DXT34	
RANGE D2XF2,D2XF3,D2XF4	
RANGE DUSCAR,DUFF2,DUF2F3,DUF3F4	
RANGE DUS1,DUS4	10-23-80
RANGE DUS2,DUS3	9-03-79
RANGE RHSX,RHSY,RHSTH	08-01-80
RANGE D2YCPL,D2CPLX,D2R12X,D2R56X	01-08-81
RANGE DYCPL,DYCPLX,DYR12X,DYR56X	01-08-81
RANGE YCPL,YCPLX,YR12X,YR56X	01-08-81
CHANGE PLOT SIZE FOR PUBLICATION	
SET NPXPPL=40,NPYPPL=50,NGXPPL=10,NGYPPL=10	
PLOT *XAXIS*=T, *XLO*=0., *XHI*=TSTOP	
PLOT XT,XT12,XT23,XT34	
PLOT DXT,DXT12,DXT23,DXT34	8-17-79
PLOT ADXT,ADXT12,ADXT23,ADXT34	8-17-79
PLOT DXRC,DXF,DXF2,DXF3,DXF4	
PLOT D2XRC,D2XF,D2XF2,D2XF3,D2XF4	
PLOT XURC,XUF,XRC1,XCP,XF1,XFA	
PLOT FXTF,FXTR,FDCRC,FDCF	
SET CALPLT = .FALSE.	
CHANGE PLOT SIZE FOR PUBLICATION	
SET XINCPL = 7., YINCPL = 5., CHRCPL=0	
PLOT *XAXIS*=T, *XLO*=0., *XHI*=TSTOP	
PLOT XP,*LO*=XMN,*HI*=XMX,*CHAR*='A',XRC,*CHAR*='B',...	
XTR,*CHAR*='C',XTF,*CHAR*='D',XF,*CHAR*='E',*SAME*	
PLOT XRC,*LO*=XMN,*HI*=XMX,*CHAR*='A',XF,*CHAR*='B',XF2,*CHAR*='C',...	
XF3,*CHAR*='D',XF4,*CHAR*='E',*SAME*	
PLOT DUSCAR,*LO*=FCPLMN,*HI*=FCPLMX,*CHAR*='A',DUFF2,*CHAR*='...	
'B',DUF2F3,*CHAR*='C',DUF3F4,*CHAR*='D',*SAME*	
PLOT *XAXIS* = T,*XLO* = 0.,*XHI* = TXP4	
PLOT DUSCAR,DUSX4,*SAME*	7-2-79
PLOT TDUSCR,TDUSX4,*SAME*	11-20-79
PLOT DUSLF,*LO*=-1.E5,*HI*=8.E5,DUSLFX,*SAME*	
PLOT KS1,KS4,*SAME*	
PLOT D2XRC,*LO*=-8.E3,*HI*=4.E3,D2XRCX,D2XRCM,*SAME*	02-01-80
PLOT D2XP,*Q*=-6.E3,*HI*=1.E3,D2XPX,*SAME*	01-29-80
PLOT D2YR12,*LO*=-4.E3,*HI*=4.E3,D2P12X,D2YR56,*SAME*	04-17-80
PLOT D2YP34,*LO*=-3.E3,*HI*=3.E3,D2P34X,D2YR78,*SAME*	04-17-80
PLOT YCPLX,*LO*=YMN2,*HI*=YMX2,YCPL,YRC78,YCPLT,*SAME*	01-12-81
PLOT YR12X,*LO*=YMN2,*HI*=YMX2,YRC12,YR12T,*SAME*	01-12-81
PLOT YR56X,*LO*=YMN2,*HI*=YMX2,YRC56,*SAME*	01-08-81
PLOT D2CPLX,*LO*=D2YMN2,*HI*=D2YMX2,D2YCPL,D2YR78,D2CPLT,*SAME*	01-12-81
PLOT D2R12X,*LO*=D2YMN2,*HI*=D2YMX2,D2YR12,D2R12T,*SAME*	01-12-81
PLOT D2R56X,*LO*=D2YMN2,*HI*=D2YMX2,D2YR56,*SAME*	
PLOT DT,*LO*=0.,*HI*=DTMAX,DTYRC,DTYRC2,DTTHRC,DTTHC2,*SAME*	04-30-80
PLOT DLTY12	05-05-80
PLOT OMY34,OMY12,*SAME*	06-02-80
PLOT D2DY12,D2DY34,*SAME*	06-02-80
PLOT D2XD,D2YD,D2THD	07-02-80
PLOT RHSX,D2XRC,*SAME*	07-02-80
PLOT RHSY,D2YRC,*SAME*	07-02-80
PLOT RHSTH,D2THRC,*SAME*	07-02-80
PLOT RHSX,RHSXA	06-26-80
PLOT RHSY,RHSYA	06-26-80
PLOT RHSTH,RHSTHA	06-26-80
PLOT OMX,OMY,OMTH	06-26-80
PLOT ZTATH	06-26-80

```

PLOT DUS1,DUS4,*SAME*
PLOT DUS2,DUS3
-----
PLOT *XAXIS* = T,*XLO* =D.,*XHI* = TSTOP
PLOT YP,*LO*=YMN,*HI*=YMX,*CHAR*='A',YRC,*CHAR*='B',*SAME*
PLOT THP,*LO*=THMN,*HI*=THMX,*CHAR*='A',THRC,*CHAR*='B',*SAME*
PLOT DXP,*LO*=DXMN,*HI*=DXMX,*CHAR*='A',DXRC,*CHAR*='B',...
DXTR,*CHAR*='C',DXTF,*CHAR*='D',DXF,*CHAR*='E',*SAME*
PLOT DYP,*LO*=DYMN,*HI*=DYMx,*CHAR*='A',DYRC,*CHAR*='B',*SAME*
PLOT DTHP,*LO*=DTHMN,*HI*=DTHMX,*CHAR*='A',DTHRC,*CHAR*='B',...
*SAME*
PLOT D2XRC,*LO*=D2XMN,*HI*=D2MX,*CHAR*='A',D2XP,*CHAR*='B',...
D2XTR,*CHAR*='C',D2XTF,*CHAR*='D',D2XF,*CHAR*='E',*SAME*
PLOT D2YP,*LO*=D2YMN,*HI*=D2YMX,*CHAR*='A',D2YRC,*CHAR*='B',...
*SAME*
PLOT D2THP,*LO*=D2THMN,*HI*=D2THMX,*CHAR*='A',D2THRC, ...
*CHAR*='B',*SAME*
PLOT XRPRC,*LO*=XRMN,*HI*=XRMx,*CHAR*='A',XRRCF,*CHAR*='B',...
XRCTR,*CHAR*='C',XRCTF,*CHAR*='D',*SAME*
PLOT DXRPRC
PLOT YRPRC,*CHAR*='A',THRPRC,*CHAR*='B'
PLOT YP12X,*LO*=YMN2,*HI*=YMX2,YP34,YRC12,YRC34,YP12,... 05-06-80
YP34X,*SAME* 05-06-80
PLOT TIC13,*LO*=D.,*HI*=1.,*CHAR*='*' 05-06-80
PLOT TIC14,*LO*=D.,*HI*=1.,*CHAR*='*' 05-06-80
PLOT TIC53,*LO*=D.,*HI*=1.,*CHAR*='*' 05-06-80
PLOT TIC54,*LO*=D.,*HI*=1.,*CHAR*='*' 05-06-80
PLOT TIC60,*LO*=D.,*HI*=1.,*CHAR*='*' 05-06-80
PLOT TIC61,*LO*=D.,*HI*=1.,*CHAR*='*' 05-06-80
PLOT TMIC,*LO*=D.,*HI*=1.,*CHAR*='*' 05-06-80
PLOT YRC56,*LO*=YMN2,*HI*=YMX2,*CHAR*='A',YRC78,*CHAR*='B',...
YRC12,*CHAR*='C',YRC34,*CHAR*='D',*SAME* 09-12-80
PLOT DYP12,*LO*=DYMN2,*HI*=DYMx2,*CHAR*='A',DYP34, ...
*CHAR*='B',DYRC12,*CHAR*='C',DYRC34,*CHAR*='D',... 04-22-80
DYP12X,*CHAR*='X',DYP34X,*CHAR*='Y',*SAME* 04-21-80
PLOT DYRC56,*LO*=DYMN2,*HI*=DYMx2,*CHAR*='A',DYRC78, ...
*CHAR*='B',*SAME*
PLOT D2YP12,*LO*=D2YMN2,*HI*=D2YMX2,*CHAR*='A',D2YP34, ...
*CHAR*='B',D2YR12,*CHAR*='C',D2YR34,*CHAR*='D',*SAME*
PLOT D2YR56,*LO*=D2YMN2,*HI*=D2YMX2,*CHAR*='A',D2YR78, ...
*CHAR*='B',*SAME*
PLOT *XAXIS*=XRPRC,KS1,KS4
PLOT *XAXIS*=XT,DUSCAR
PLOT *XAXIS*=XT12,DUFF2
PLOT *XAXIS*=XT23,DUF2F3
PLOT *XAXIS*=XT34,DUF3F4
STOP
@DELETE,C RRR03EF.
@ASG,UP RRR03EF.
@COPY 98.,RRR03EF.
@DEL TF,C TEST03EF.
@ASG,UP TEST03EF.
@COPY 26.,TEST03EF.

```

1911
1912
1913
1914
1915
1916
1917
1918
1919
1920
1921
1922
1923
1924
1925
1926
1927
1928
1929
1930
1931
1932
1933
1934
1935
1936
1937
1938
1939
1940
1941
1942
1943
1944
1945
1946
1947
1948
1949
1950
1951
1952
1953
1954
1955
1956
1957
1958
1959
1960
1961
1962
1963
1964
1965
1966
1967
1968
1969
1970
1971
1972
1973
1974
1975
1976
1977
1978
1979
1980
1981
1982
1983
1984
1985
1986
1987
1988
1989
1990
1991
1992
1993
1994
1995
1996
1997
1998
1999
2000
2001
2002
2003
2004
2005
2006
2007
2008
2009
2010
2011
2012
2013
2014
2015
2016
2017
2018
2019
2020
2021
2022
2023
2024
2025

A P P E N D I X V

LISTING OF CARRS MODEL

APPENDIX V

LIST OF TABLES

LISTING OF *CARRS* MODEL

```

PROGRAM CARRS                                06-30-80
  *--(C)A(S)M (R)AIL CAR (R)ESPONSE (S)PECTRA  *07-01-80
  *--A MODEL TO CALCULATE ACCELERATION RESPONSE SPECTRA USING *07-01-80
  * RESULTS TRANSFERRED FROM THE *CARDS* MODEL VIA FILE *TRAN----*. *07-01-80
  *--CHECK LIST                                09-12-80
  * (1) SET PRE911                              09-12-80
  * (2) CHECK CONTROL CARDS                     09-12-80
  * (2.1) ASSIGNING FILE FROM *CARDS*          09-16-80
  * (2.2) USING FILE FROM *CARDS* VIA DEVICE 26 09-16-80
  INTEGER ZONE,NN,NNH,N                       06-30-80
  INTEGER NCASE                               09-25-80
  INTEGER NSTOP                               09-25-80
  LOGICAL PRE911                              09-12-80
INITIAL                                       06-26-80
  ARRAY C1ZONE(3),ARRHSX(120),ARRHSY(120),ARRHSTH(120),ATH(120),... 07-01-80
  ACS2(120),ADUS1(120),ADUS2(120),ADUS3(120),ADUS4(120) 09-12-80
  ARRAY D2XDM(120),D2YDM(120),D2THDM(120),OM(120) 09-25-80
  *--SYSTEM INPUT PARAMETERS                 *06-26-80
  CONSTANT C1ZONE = 0.01,0.001,0.01          06-30-80
  CONSTANT CS1 = 2.E3                          07-01-80
  CONSTANT CS21 = 1500.                        07-01-80
  CONSTANT CS3 = 1500.                        07-01-80
  CONSTANT CS4 = 2.E5                          07-01-80
  CONSTANT DTHPI = 0.                          06-30-80
  CONSTANT DTHRCI = 0.                        06-30-80
  CONSTANT DYPI = 0.                          06-30-80
  CONSTANT DYRCI = 0.                          06-30-80
  CONSTANT D2THDI = 0.                        09-25-80
  CONSTANT D2XDI = 0.                         09-25-80
  CONSTANT D2YDI = 0.                         09-25-80
  CONSTANT EPS = 1.E-6                        06-30-80
  CONSTANT G = 386.4                          06-30-80
  CONSTANT IP = 8.57E5                         06-30-80
  CONSTANT LPF = 102.                          06-30-80
  CONSTANT LPR = 102.                          06-30-80
  MAXTERVAL MAXT=0.001                        06-26-80
  CONSTANT MUPR = 0.58                         06-30-80
  CONSTANT NCASE = 1                           09-25-80
  CONSTANT NSTOP = 27                          09-25-80
  CONSTANT NNH = 116 *INTEGER VALUE*          06-30-80
  CONSTANT OMH = 200.                          06-30-80
  CONSTANT OMX = 50.                           06-30-80
  CONSTANT OMY = 100.                          06-30-80
  CONSTANT PRE911 = .TRUE.                     09-12-80
  CONSTANT PRE911 = .FALSE.                   09-12-80
  CONSTANT RHSTH1 = 0.                         06-30-80
  CONSTANT RHSX1 = 0.                          06-30-80
  CONSTANT RHSY1 = 0.                          06-30-80
  *-----SWITCHES CONTROLLING DAMPING. ZERO WHEN *07-17-80
  * UNDAMPED. ONE WHEN DAMPED. *07-17-80
  CONSTANT SWDHD = 1. *SWITCH CONTROLLING DAMPING IN HD EOM* 07-02-80
  CONSTANT SWDXD = 1. *SWITCH CONTROLLING DAMPING IN XD EOM* 07-02-80
  CONSTANT SWDXF = 1. *SWITCH CONTROLLING FRICTION IN XD EOM* 07-18-80
  CONSTANT SWDYD = 1. *SWITCH CONTROLLING DAMPING IN YD EOM* 07-02-80
  CONSTANT THI = 0.14                          06-30-80

```

```

CONSTANT THPI = 0. 06-30-80
CONSTANT THFCI = 0. 06-30-80
CONSTANT TLC = 0.03 06-30-80
CONSTANT TSTOP = 0.15 06-30-80
CONSTANT VXPI = 176. 06-30-80
CONSTANT VXRCI = 176. 06-30-80
CONSTANT WP = 8.24 06-30-80
CONSTANT XPI = 0. 06-30-80
CONSTANT XRCI = 0. 06-30-80
CONSTANT YPI = 0. 06-30-80
CONSTANT YRCI = 0. 06-30-80
CONSTANT ZP = 31. 06-30-80
-----INITIAL VALUES OF PLOT RANGES----- 07-11-80
CONSTANT XMX = -1.E30,XMN = 1.E30 07-11-80
CONSTANT YMX = -1.E30,YMN = 1.E30 07-11-80
CONSTANT THMX = -1.E30,THMN = 1.E30 07-11-80
CONSTANT DXMX = -1.E30,DXMN = 1.E30 07-11-80
CONSTANT DYMx = -1.E30,DYMN = 1.E30 07-11-80
CONSTANT DTHMX = -1.E30,DTHMN = 1.E30 07-11-80
CONSTANT D2XMX = -1.E30,D2XMN = 1.E30 07-11-80
CONSTANT D2YMX = -1.E30,D2YMN = 1.E30 07-11-80
CONSTANT D2THMX = -1.E30,D2THMN = 1.E30 07-11-80
CONSTANT DUSXMX = -1.E30,DUSXMN = 1.E30 09-12-80
CONSTANT DUSYMX = -1.E30,DUSYMN = 1.E30 09-12-80
*****
*--PARAMETERS CHANGED FOR FILE *TRAN-- * 07-17-80
-----SWITCHES CONTROLLING DAMPING. ZERO WHEN 07-17-80
UNDAMPED. ONE WHEN DAMPED. 07-17-80
CONSTANT SWDTHD = 0. $*SWITCH CONTROLLING DAMPING IN THD EOM* 07-16-80
CONSTANT SWDTHD = 1. $*SWITCH CONTROLLING DAMPING IN THD EOM* 07-18-80
CONSTANT SWDXD = 0. $*SWITCH CONTROLLING DAMPING IN XD EOM* 07-16-80
CONSTANT SWDXD = 1. $*SWITCH CONTROLLING DAMPING IN XD EOM* 07-18-80
CONSTANT SWDXDF = 1. $*SWITCH CONTROLLING FRICTION IN XD EOM* 07-18-80
CONSTANT SWDXDF = 0. $*SWITCH CONTROLLING FRICTION IN XD EOM* 07-18-80
CONSTANT SWDYD = 0. $*SWITCH CONTROLLING DAMPING IN YD EOM* 07-16-80
CONSTANT SWDYD = 1. $*SWITCH CONTROLLING DAMPING IN YD EOM* 07-18-80
*****
*--INITIAL COMPUTATIONS 06-26-80
ZONE = 1 $*INITIALIZE ZONE TO START* 06-26-80
MP = WP/G 06-30-80
WP1 = WP/2. 06-30-80
WP4 = WP/2. 06-30-80
DXDI = VXRCI-VXPI 06-26-80
XDI = XRCI-XPI 06-26-80
DYDI = YRCI-YPI 06-26-80
YDI = YRCI-YPI 06-26-80
DTHDI = DTHRCI-DTHPI 06-26-80
THDI = THRCI-THPI 06-26-80
CS2 = CS2I 07-01-80
ZTATH = ((CS1+CS4)*7P**2+CS2*LPR**2+CS3*LPF**2)/IP 06-26-80
RHSX = RHSXI 06-26-80
RHSY = RHSYI 06-26-80
RHSTH = RHSTHI 06-26-80
-----READ RESULTS FROM THE *CARDS* MODEL 07-01-80
NN = 0 06-26-80
REWIND 26 $*REWIND FILE 26 AFTER PREVIOUS RUN* 07-10-80
II..CONTINUE 06-26-80

```

```

NN      = NN+1
IF(PFE911)GO TO I2
-----IF *CARDS* FILE CREATED AFTER 9-11-80
READ(26,100) ATM(NN),ARHSX(NN),ARHSY(NN),ARHSTH(NN),...
      ACS2(NN),ADUS1(NN),ADUS2(NN),ADUS3(NN),ADUS4(NN)
100..FORMAT(5E12.4/4E12.4)
GO TO I3
I2..CONTINUE      $*IF *CARDS* FILE CREATED BEFORE 9-11-80$
READ(26,200) ATM(NN),ARHSX(NN),ARHSY(NN),ARHSTH(NN),ACS2(NN)
200..FORMAT(5E12.4)
GO TO I3
I3..CONTINUE
IF(NN.LT.NNH)GO TO I1
-----ARRAYS FILLED
END $*OF INITIAL$
DYNAMIC
CINT = CIZONE(ZONE)
-----CALCULATE RHS FORCING FUNCTIONS
NN      = 0
ATM(NN) = 0.
ARHSX(NN) = 0.
ARHSY(NN) = 0.
ARHSTH(NN) = 0.
ACS2(NN) = CS2I
IF(PFE911)GO TO I
ADUS1(NN) = 0.
ADUS2(NN) = 0.
ADUS3(NN) = 0.
ADUS4(NN) = 0.
1..CONTINUE
NN      = NN+1
N      = NN
IF(ATM(NN).LT.T)GO TO 4
IF(ATM(NN).GE.T)GO TO 2
4..CONTINUE
IF(NN.LT.NNH)GO TO 1
GO TO 5
2..CONTINUE
RHSX = ARHSX(NN)
RHSY = ARHSY(NN)
RHSZ = ARHSTH(NN)
CS2 = ACS2(NN)
ZTATH = ((CS1*CS4)*ZP**2+CS2*LPR**2+CS3*LPF**2)/IP
IF(PFE911)GO TO 5
DUS1 = ADUS1(NN)
DUS2 = ADUS2(NN)
DUS3 = ADUS3(NN)
DUS4 = ADUS4(NN)
5..CONTINUE
-----END OF CALCN OF RHS FORCING FUNCTIONS
DERIVATIVE
*PROCEDURAL TO CALCULATE ZONE$
PROCFORPL(ZONE=T)
IF(T.GE.TLO.AND.T.LE.THI) ZONE=2
IF(T.LT.TLO) ZONE=1
IF(T.GT.THI) ZONE=3
END $*OF PROCEDURAL TO CALCULATE ZONE$

```

```

*MACRO TO COMPUTE SIGN FUNCTION*
MACRO SGNF(R,A)
PROCEDURAL(R=A)
  IF(A.LT.C.) R=-1.
  IF(A.EQ.C.) R=0.
  IF(A.GT.C.) R=+1.
END $*OF PROCEDURAL FOR *MACRO-SGNF*
MACRO END

*-----SINGLE DEGREE OF FREEDOM EQUATIONS OF MOTION
*   ARRANGED TO YIELD RELATIVE ACCELERATIONS
*   WITH TWO INTEGRATIONS TO GIVE VELOCITIES AND DISPLACEMENTS
D2XD = RHSX-XD*OMX**2-(CS1+CS4)*DXD*SWDXD/MP...
      *MUPR*(WPI*WP4)*SGNF(DXD)*SWDXD/MP
DXD = INTEG(D2XD,DXDI)
XD = INTEG(DXD,XDI)
D2YD = RHSY-YD*OMY**2-(CS2+CS3)*DYD*SWDYD/MP
DYD = INTEG(D2YD,DYDI)
YD = INTEG(DYD,YDI)
D2THD = RHSTH-THD*OMTH**2-ZTATH*DTHD*SWDTHD
DTHD = INTEG(D2THD,DTHDI)
THD = INTEG(DTHD,THDI)
END $*OF DERIVATIVE*

*-----MAX AND MIN VALUES FOR PLOT SCALES
XMX = AMAX1(XMX,XD)
XMN = AMIN1(XMN,XD)
YMX = AMAX1(YMX,YD)
YMN = AMIN1(YMN,YD)
THMX = AMAX1(THMX,THD)
THMN = AMIN1(THMN,THD)
DXMX = AMAX1(DXMX,DXD)
DXMN = AMIN1(DXMN,DXD)
DYMX = AMAX1(DYMX,DYD)
DYMN = AMIN1(DYMN,DYD)
DTHMX = AMAX1(DTHMX,DTHD)
DTHMN = AMIN1(DTHMN,DTHD)
D2XMX = AMAX1(D2XMX,D2XD,RHSX)
D2XMN = AMIN1(D2XMN,D2XD,RHSX)
D2YMX = AMAX1(D2YMX,D2YD,RHSY)
D2YMN = AMIN1(D2YMN,D2YD,RHSY)
D2THMX = AMAX1(D2THMX,D2THD,RHSTH)
D2THMN = AMIN1(D2THMN,D2THD,RHSTH)
IF(PRE911)GO TO D1
DUSXMX = AMAX1(DUSXMX,DUS1,DUS4)
DUSXMN = AMIN1(DUSXMN,DUS1,DUS4)
DUSYMX = AMAX1(DUSYMX,DUS2,DUS3)
DUSYMN = AMIN1(DUSYMN,DUS2,DUS3)
D1..CONTINUE
IF(T.GT.C.)GO TO DY1
*-----IF T.LF.C.
D2XDP = ABS(D2XD)
D2YDP = ABS(D2YD)
D2THDP = ABS(D2THD)
GO TO DY1
DY1..CONTINUE $*IF T.GT.C.
D2XDM(INCASE) = AMAX1(ABS(D2XD),D2XDP)
D2YDM(INCASE) = AMAX1(ABS(D2YD),D2YDP)
D2THDM(INCASE) = AMAX1(ABS(D2THD),D2THDP)

```

OM(NCASE) = DMX	09-25-80
D2XDP = ABS(D2XDM(NCASE))	09-25-80
D2YDP = ABS(D2YDM(NCASE))	09-25-80
D2THDP = ABS(D2THDM(NCASE))	09-25-80
LINE\$11	09-25-80
PRINT 300, OM(NCASE), D2XDM(NCASE), D2YDM(NCASE), D2THDM(NCASE)	09-25-80
TERMTT.GE.TSTOP)	06-26-80
END \$*OF DYNAMIC*	06-26-80
TERMINAL	07-11-80
-----ROUNDING OFF MAX AND MIN VALUES FOR USE	07-11-80
ON PLOTS SCALES	07-11-80
SCALE (XMN ,XMN = XMN ,XMN)	07-11-80
SCALE (YMN ,YMN = YMN ,YMN)	07-11-80
SCALE (THMN ,THMN = THMN ,THMN)	07-11-80
SCALE (DXMN ,DXMN = DXMN ,DXMN)	07-11-80
SCALE (DYMN ,DYMN = DYMN ,DYMN)	07-11-80
SCALE (DTHMN ,DTHMN = DTHMN ,DTHMN)	07-11-80
SCALE (D2XMN ,D2XMN = D2XMN ,D2XMN)	07-11-80
SCALE (D2YMN ,D2YMN = D2YMN ,D2YMN)	07-11-80
SCALE (D2THMN ,D2THMN = D2THMN ,D2THMN)	07-11-80
IF (PRE911) GO TO T1	09-12-80
SCALE (DUSXMN ,DUSXMN = DUSXMN ,DUSXMN)	09-12-80
SCALE (DUSYMN ,DUSYMN = DUSYMN ,DUSYMN)	09-12-80
T1..CONTINUE	09-12-80
IF (NCASE.EQ.NSTOP) GO TO T2	09-25-80
GO TO T4	09-25-80
T2..CONTINUE \$*NCASE.EQ.NSTOP*	09-25-80
NCASE = 0	09-25-80
T3..CONTINUE \$*NCASE.LT.NSTOP*	09-25-80
NCASE = NCASE + 1	09-25-80
LINE\$11	09-25-80
WRITE (27,300) OM(NCASE), D2XDM(NCASE), D2YDM(NCASE), D2THDM(NCASE)	09-25-80
300..FORMAT(4E12.4)	09-25-80
PRINT 300, OM(NCASE), D2YDM(NCASE), D2YDM(NCASE), D2THDM(NCASE)	09-25-80
IF (NCASE.LT.NSTOP) GO TO T3	09-25-80
T4..CONTINUE \$*NCASE.NE.NSTOP*	09-25-80
END \$*OF TERMINAL*	07-11-80
END \$*OF PROGRAM*	06-26-80

OUTPUT T	,...	06-26-80
CS2	,...	07-01-80
DTHD	,...	06-26-80
DUS1	,...	09-12-80
DUS2	,...	09-12-80
DUS3	,...	09-12-80
DUS4	,...	09-12-80
DXD	,...	06-26-80
DYD	,...	06-26-80
D2THD	,...	06-26-80
D2XD	,...	06-26-80
D2YD	,...	06-26-80
N	,...	06-30-80
RHSTH	,...	06-26-80
RHSX	,...	06-26-80
RHSY	,...	06-26-80
THD	,...	06-26-80
XD	,...	06-26-80
YD	,...	06-26-80
ZTATH	,...	07-01-80
ZEND		06-26-80
PREPAR T	,...	06-26-80
DTHD	,...	06-26-80
DUS1	,...	09-12-80
DUS2	,...	09-12-80
DUS3	,...	09-12-80
DUS4	,...	09-12-80
DXD	,...	06-26-80
DYD	,...	06-26-80
D2THD	,...	06-26-80
D2XD	,...	06-26-80
D2YD	,...	06-26-80
RHSTH	,...	06-26-80
RHSX	,...	06-26-80
RHSY	,...	06-26-80
THD	,...	06-26-80
XD	,...	06-26-80
YD	,...	06-26-80
ZNDCRD		06-26-80
PROCED GO		07-02-80
START		07-02-80
RANGE D2THD,D2XD,D2YD		07-01-80
RANGE DTHD,DXD,DYD		07-01-80
RANGE THD,XD,YD		07-01-80
RANGE RHSTH,RHSX,RHSY		07-01-80
RANGE DUS1,DUS2,DUS3,DUS4		09-12-80
CHANGE PLOT SIZE FOR PUBLICATION		06-26-80
SET NFXPPL=40,NPYPL=50,NGXPPL=10,NGYPPL=10		06-26-80
PLOT *XAXIS*=T,*XLO*=0,*XHI*=TSTOP		06-26-80
PLOT D2XD,*LO*=D2XMN,*HI*=D2XMX,RHSX,*SAME*		07-11-80
PLOT D2YD,*LO*=D2YMN,*HI*=D2YMX,RHSY,*SAME*		07-11-80
PLOT D2THD,*LO*=D2THMN,*HI*=D2THMX,RHSTH,*SAME*		07-11-80
PLOT DXD,DYD,DTHD		06-26-80
PLOT XD,YD,THD		06-26-80
PLOT DUS1,*LO*=DUSXMN,*HI*=DUSXMX,DUS4,*SAME*		09-12-80

PLOT DUSZ, 'LO' = DUSYMN, 'HT' = DUSYMX, DUS3, 'SAME'	09-12-80
END # OF PROCEDURE	07-02-80
SET NCASE = 1	09-25-80
SET OMX = 2.	07-11-80
SET OMY = 2.	07-11-80
SET OMTH = 2.	07-11-80
GO	07-11-80
SET NCASE = 2	09-25-80
SET OMX = 5.	07-11-80
SET OMY = 5.	07-11-80
SET OMTH = 5.	07-11-80
GO	07-11-80
SET NCASE = 3	09-25-80
SET OMX = 10.	07-11-80
SET OMY = 10.	07-11-80
SET OMTH = 10.	07-11-80
GO	07-02-80
SET NCASE = 4	09-25-80
SET OMX = 20.	07-11-80
SET OMY = 20.	07-11-80
SET OMTH = 20.	07-11-80
GO	07-11-80
SET NCASE = 5	09-25-80
SET OMX = 30.	07-11-80
SET OMY = 30.	07-11-80
SET OMTH = 30.	07-11-80
GO	07-11-80
SET NCASE = 6	09-25-80
SET OMX = 40.	07-11-80
SET OMY = 40.	07-11-80
SET OMTH = 40.	07-11-80
GO	07-11-80
SET NCASE = 7	09-25-80
SET OMX = 50.	07-11-80
SET OMY = 50.	07-11-80
SET OMTH = 50.	07-11-80
GO	07-02-80
SET NCASE = 8	09-25-80
SET OMX = 60.	07-11-80
SET OMY = 60.	07-11-80
SET OMTH = 60.	07-11-80
GO	07-11-80
SET NCASE = 9	09-25-80
SET OMX = 70.	07-11-80
SET OMY = 70.	07-11-80
SET OMTH = 70.	07-11-80
GO	07-11-80
SET NCASE = 10	09-25-80
SET OMX = 80.	07-11-80
SET OMY = 80.	07-11-80
SET OMTH = 80.	07-11-80
GO	07-11-80
SET NCASE = 11	09-25-80
SET OMX = 90.	07-11-80
SET OMY = 90.	07-11-80
SET OMTH = 90.	07-11-80
GO	07-11-80

SET NCASE = 12	09-25-80
SET OMX = 100.	07-11-80
SET OMY = 100.	07-11-80
SET OMTH = 100.	07-11-80
GO	07-11-80
SET NCASE = 13	09-25-80
SET OMX = 110.	07-14-80
SET OMY = 110.	07-14-80
SET OMTH = 110.	07-14-80
GO	07-14-80
SET NCASE = 14	09-25-80
SET OMX = 120.	07-14-80
SET OMY = 120.	07-14-80
SET OMTH = 120.	07-14-80
GO	07-14-80
SET NCASE = 15	09-25-80
SET OMX = 130.	07-14-80
SET OMY = 130.	07-14-80
SET OMTH = 130.	07-14-80
GO	07-14-80
SET NCASE = 16	09-25-80
SET OMX = 140.	07-14-80
SET OMY = 140.	07-14-80
SET OMTH = 140.	07-14-80
GO	07-14-80
SET NCASE = 17	09-25-80
SET OMX = 150.	07-14-80
SET OMY = 150.	07-14-80
SET OMTH = 150.	07-14-80
GO	07-14-80
SET NCASE = 18	09-25-80
SET OMX = 160.	07-14-80
SET OMY = 160.	07-14-80
SET OMTH = 160.	07-14-80
GO	07-14-80
SET NCASE = 19	09-25-80
SET OMX = 180.	07-15-80
SET OMY = 180.	07-15-80
SET OMTH = 180.	07-15-80
GO	07-15-80
SET NCASE = 20	09-25-80
SET OMX = 190.	07-15-80
SET OMY = 190.	07-15-80
SET OMTH = 190.	07-15-80
GO	07-15-80
SET NCASE = 21	09-25-80
SET OMX = 200.	07-15-80
SET OMY = 200.	07-15-80
SET OMTH = 200.	07-15-80
GO	07-15-80
SET NCASE = 22	09-25-80
SET OMX = 210.	07-15-80
SET OMY = 210.	07-15-80
SET OMTH = 210.	07-15-80
GO	07-15-80
SET NCASE = 23	09-25-80
SET OMX = 220.	07-15-80

SET OMY = 220.	07-15-80
SET OMTH = 220.	07-15-80
GO	07-15-80
SET NCASE = 24	09-25-80
SET OMX = 230.	07-15-80
SET OMY = 230.	07-15-80
SET OMTH = 230.	07-15-80
GO	07-15-80
SET NCASE = 25	09-25-80
SET OMX = 240.	07-15-80
SET OMY = 240.	07-15-80
SET OMTH = 240.	07-15-80
GO	07-15-80
SET NCASE = 26	09-25-80
SET OMX = 250.	07-15-80
SET OMY = 250.	07-15-80
SET OMTH = 250.	07-15-80
GO	07-15-80
SET NCASE = 27	09-25-80
SET OMX = 260.	07-15-80
SET OMY = 260.	07-15-80
SET OMTH = 260.	07-15-80
GO	07-15-80
STOP	07-02-80

A P P E N D I X VI

LISTING OF FFT PROGRAM

PLATE VI

PLATE VI

LISTING OF FFT PROGRAM

```

SUBROUTINE RFFT(XC,MM,NNN,IFLAG)
C*** SUBROUTINE RFFT.FTN ***
C*** SUBROUTINE TO TAKE THE DFT OF A REAL TIME FUNCTION ***
C*** NNN=NUMBER OF REAL POINTS=2**MM
      COMPLEX XC(1026)
      NN=NNN/2
      M=MM-1
      NV2=NN/2
      DA=3.141592654/FLOAT(NN)
      SD=SIN(DA)
      CD=COS(DA)
      S=0.0
      C=1.0
      IF(IFLAG.NE.0) GO TO 1000
      CALL FFT(XC,M,0)

```

C

```

55      CONTINUE
      XC(NN+1)=XC(1)
      DO 100 I=1,NV2
          YRE=REAL(XC(I))+PEAL(XC(NN-I+2))
          YRO=REAL(XC(I))-PEAL(XC(NN-I+2))
          YIE=AIMAG(XC(I))+AIMAG(XC(NN-I+2))
          YIO=AIMAG(XC(I))-AIMAG(XC(NN-I+2))
          A1=YRE*C+YIE-S*YRO
          A2=YIO-C*YRO-S*YIE
          XC(I)=0.5*CMPLX(A1,A2)
          A1=YRE-C*YIE+S*YRO
          A2=-YIO-C*YRO-S*YIE
          XC(NN-I+2)=0.5*CMPLX(A1,A2)
          T=C*CD-S*SD
          S=S*CD+C*SD
          C=T
100      CONTINUE
      XC(NV2+1)=CONJG(XC(NV2+1))
      RETURN
1000   DO 1100 I=1,NV2
          A1=REAL(XC(I))
          A2=AIMAG(XC(I))
          A3=REAL(XC(NN-I+2))
          A4=AIMAG(XC(NN-I+2))
          YRE=A1+A3
          YRO=-S*A1-C*A2+S*A3-C*A4
          YIE=C*A1-S*A2-C*A3-S*A4
          YIO=A2-A4
          XC(NN-I+2)=CMPLX((YRE+YRO),(YIE+YIO))/(2.*NN)
          XC(I)=CMPLX((YRE-YRO),(YIE-YIO))/(2.0*NN)
          T=C*CD-S*SD
          S=S*CD+C*SD
          C=T
1100

```

```

1100 CONTINUE
      XC(INV2+1)=CONJG(XC(INV2+1))/FLOAT(INN)
      CALL FFT(XC,M,J)
      RETURN
      END
@FTN,ISFO FILTR.FFT
      SUBROUTINE FFT(X,M,IFLG)
C*** SUPROUTINE FFT.FTN ***
C*** SUBROUTINE COMPUTES DFT ***
      COMPLEX          U,W,T,TMP
      COMPLEX X(1026)
      N=2**M
      NV2=N/2
      NM1=N-1
      J=1
      D=-1.
      IF(IFLG.EQ.0) GO TO 55
      D=1.
      DO 50 I=1,N
          X(I)=X(I)/N
50    CONTINUE
55    DO 7 I=1,NM1
          IF(I.GE.J) GO TO 5
          T=X(J)
          X(J)=X(I)
          X(I)=T
          K=NV2
          IF(K.GE.J) GO TO 7
          J=J-K
          K=K/2
          GO TO 6
          J=J+K
          PI=3.14159265368979
          DO 20 L=1,M
              LE=2**L
              LF1=LE/2
              U=(1.0,0.0)
              W=CMPLX(COS(PI/FLOAT(LE1)),D*SIN(PI/FLOAT(LE1)))
              DO 10 J=1,LF1
                  DO 10 I=J,N,LE
                      IP=I+LE1
                      T=X(IP)*U
                      X(IP)=X(I)-T
10                     X(I)=X(I)+T
20                     U=U*W
61    FORMAT(1H1 , 'X ARRAY FREQUENCY DOMAIN DATA APDIL 10 TEST')
62    FORMAT(1X, 10G12.5)
      RETURN
      END

```

DISTRIBUTION

RT

DOE-RL/Office of Asst Manager
for Advanced Reactor Programs
P.O. Box 550
Richland, WA 99352

EC Norman, Director, Technology
Development Division
JJ Keating, Director, Breeder
Technology Division

DOE/Chicago Patent Group
9800 South Cass Avenue
Argonne, IL 60439

AA Churm

DOE-HQ/Office of Operational Safety
EP-32
Washington, DC 20545

J. Counts

HEDL (27)

HJ Anderson	W/C-28
JD Berger	W/E-12
HA Carlson	W/C-28
MCJ Carlson	W/C-28
RE Dahl	W/C-22
SR Fields (14)	W/C-28

E. I. Du Pont DeNemours and Company
Savannah River Laboratory
Aiken, SC 29801

RH Towell

Los Alamos National Laboratory
P.O. Box 1663
Los Alamos, NM 87545

TD Butler

Battelle
Pacific Northwest Laboratory
P.O. Box 999
Richland, WA 99352

LD Williams

Sandia Laboratories
P.O. Box 5800
Albuquerque, NM 87185

CF Magnuson

SJ Mech	W/A-132
LH Rice	W/C-5
Central Files (3)	W/C-110
Publ Services (2)	W/C-115
Microfilm Services	W/C-123

DISTRIBUTION

E. J. J. Post Laboratory and
Treatment Plant Laboratory
Arling, VA 22001

101 Tenth

U.S. Geological Survey
Box 100
Fort Belknap, MT 59701

70 Butler

Palmer
Public Health Laboratory
P.O. Box 88
Rochester, NY 14602

10 Willow

Central Laboratory
P.O. Box 600
Arling, VA 22001

11 Madison

WA-100
WC-2
WC-110
WC-112
WC-113

28 West
11 West
Central (110)
Public Health (112)
Rochester (113)

U.S. Office of Water
U.S. Environmental Protection Agency
1200 Pennsylvania Ave.
N.W.
Washington, D.C. 20460

U.S. Environmental Protection Agency
U.S. Office of Water
1200 Pennsylvania Ave.
N.W.
Washington, D.C. 20460

U.S. Environmental Protection Agency
U.S. Office of Water
1200 Pennsylvania Ave.
N.W.
Washington, D.C. 20460

1000

U.S. Environmental Protection Agency
U.S. Office of Water
1200 Pennsylvania Ave.
N.W.
Washington, D.C. 20460

1000

1000

WC-10
WC-11
WC-12
WC-13
WC-14
WC-15

U.S. Environmental Protection Agency
U.S. Office of Water
1200 Pennsylvania Ave.
N.W.
Washington, D.C. 20460

NRC FORM 335 (7-77)		U.S. NUCLEAR REGULATORY COMMISSION BIBLIOGRAPHIC DATA SHEET		1. REPORT NUMBER (Assigned by DDC) NUREG/CR-2146, Vol. 3 HEDL-TME 83-18	
4. TITLE AND SUBTITLE (Add Volume No., if appropriate) DYNAMIC ANALYSIS TO ESTABLISH NORMAL SHOCK AND VIBRATION OF RADIOACTIVE MATERIAL SHIPPING PACKAGES FINAL SUMMARY REPORT				2. (Leave blank)	
7. AUTHOR(S) S. R. Fields				3. RECIPIENT'S ACCESSION NO.	
9. PERFORMING ORGANIZATION NAME AND MAILING ADDRESS (Include Zip Code) Hanford Engineering Development Laboratory P.O. Box 1970 Richland, WA 99352				5. DATE REPORT COMPLETED MONTH August YEAR 1983	
12. SPONSORING ORGANIZATION NAME AND MAILING ADDRESS (Include Zip Code) Division of Engineering Technology Office of Nuclear Regulatory Research U.S. Nuclear Regulatory Commission Washington, DC 20555				6. (Leave blank)	
13. TYPE OF REPORT FINAL SUMMARY REPORT				7. (Leave blank)	
15. SUPPLEMENTARY NOTES				10. PROJECT/TASK/WORK UNIT NO.	
16. ABSTRACT (200 words or less) <p>A model to simulate the dynamic behavior of shipping packages (casks) and their rail car transporters during normal transport conditions was developed. This model, CARDS (Cask-Rail Car Dynamic Simulator), was used to simulate the cask-rail car systems used in Tests 3, 10, 11, 13, 16 and 18 of the series of rail car coupling tests conducted at the Savannah River Laboratories in 1978. On the basis of good agreement between calculated and measured results for these tests, it was concluded that the model has been validated as an acceptable tool for the simulation of similar systems.</p> <p>A companion model, CARRS (Cask-Rail Car Response Spectrum Generator), consisting of single-degree-of-freedom representations of the equations of motion in CARDS, was developed to generate frequency response spectra.</p> <p>A parametric and sensitivity analysis was conducted that identified the most influential of a selected set of parameters and the response variables that are the most sensitive to changes in the parameters.</p>				11. CONTRACT NO. FIN B2283	
17. KEY WORDS AND DOCUMENT ANALYSIS				14. (Leave blank)	
17a. DESCRIPTORS				17b. IDENTIFIERS/OPEN-ENDED TERMS	
18. AVAILABILITY STATEMENT Unlimited				19. SECURITY CLASS (This report) Unclassified	
20. SECURITY CLASS (This page)				21. NO. OF PAGES	
22. PRICE S					

REPORT NUMBER: 100-10000 DATE OF THIS REPORT: 1954-10-15	U.S. BUREAU OF CHEMISTRY BIBLIOGRAPHIC DATA SHEET
1. TITLE	ORGANIC ANALYSIS TO ESTABLISH SOURCE OF A DEGRADATIVE METAL SULFIDE PRODUCT
2. AUTHOR(S)	[Faint text, possibly: J. H. ...]
3. DATE OF PUBLICATION	[Faint text, possibly: 1954]
4. SOURCE OF PUBLICATION	[Faint text, possibly: ...]
5. SUBJECT TERMS	[Faint text, possibly: ...]
6. DISTRIBUTION STATEMENT	[Faint text, possibly: ...]
7. AUTHOR(S)	[Faint text, possibly: ...]
8. TITLE	[Faint text, possibly: ...]
9. AUTHOR(S)	[Faint text, possibly: ...]
10. DATE OF PUBLICATION	[Faint text, possibly: ...]
11. SOURCE OF PUBLICATION	[Faint text, possibly: ...]
12. DISTRIBUTION STATEMENT	[Faint text, possibly: ...]
[Faint text, possibly: ...]	[Faint text, possibly: ...]
[Faint text, possibly: ...]	[Faint text, possibly: ...]
[Faint text, possibly: ...]	[Faint text, possibly: ...]
[Faint text, possibly: ...]	[Faint text, possibly: ...]
[Faint text, possibly: ...]	[Faint text, possibly: ...]
[Faint text, possibly: ...]	[Faint text, possibly: ...]
[Faint text, possibly: ...]	[Faint text, possibly: ...]
[Faint text, possibly: ...]	[Faint text, possibly: ...]
[Faint text, possibly: ...]	[Faint text, possibly: ...]